

DEUTSCHE GEODÄTISCHE KOMMISSION
bei der Bayerischen Akademie der Wissenschaften

Reihe B: Angewandte Geodäsie · Heft Nr. 214

INTERNATIONAL SOCIETY OF PHOTOGRAMMETRY
COMMISSION III

PROCEEDINGS OF THE SYMPOSIUM
held in Stuttgart, Federal Republic of Germany
September 2nd to 6th 1974

München 1975

Verlag der Bayerischen Akademie der Wissenschaften
in Kommission bei der C. H. Beck'schen Verlagsbuchhandlung München

ISBN 3 7696 8519 9

DEUTSCHE GEODÄTISCHE KOMMISSION
bei der Bayerischen Akademie der Wissenschaften

Reihe B: Angewandte Geodäsie · Heft Nr. 214

INTERNATIONAL SOCIETY OF PHOTOGRAMMETRY
COMMISSION III

PROCEEDINGS OF THE SYMPOSIUM
held in Stuttgart, Federal Republic of Germany
September 2nd to 6th 1974

München 1975

Verlag der Bayerischen Akademie der Wissenschaften
in Kommission bei der C. H. Beck'schen Verlagsbuchhandlung München

ISBN 3 7696 8519 9

Adresse der Deutschen Geodätischen Kommission:

DEUTSCHE GEODÄTISCHE KOMMISSION

D-8 München 22, Marstallplatz 8

Copyright 1975 by Deutsche Geodätische Kommission München

Alle Rechte vorbehalten. Ohne Genehmigung der Herausgeber ist es auch nicht gestattet, die Veröffentlichung oder Teile daraus auf photomechanischem Wege (Photokopie, Mikrokopie) zu vervielfältigen.

Druck: Gebr. Brunner, München

ISBN 3 7696 8519 9

FOREWORD

1. This symposium of ISP-Commission III, hosted by the Federal Republic of Germany during the period 1972-76, was held at the University of Stuttgart, from September 2nd to 6th, 1974. It was open, free of charge, to all individuals with an interest in aerial triangulation and mathematical methods in photogrammetry. There were 120 participants, from 22 countries.

During the opening session welcome, addresses were delivered by Prof. Linkwitz, on behalf of the rector of Stuttgart University, by Min. Rat Knäble, on behalf of the government and the survey administration of the state of Baden-Württemberg, and by Prof. Konecny, on behalf of the German Society of Photogrammetry.

Financial reasons prevented provision of translation of papers and communications. Therefore it was decided that all presentations and discussions would be in English. The use of English as sole language greatly contributed to the efficient performance of the symposium and caused no apparent difficulties.

The social events were restricted to an evening reception and a one-day excursion to the Zeiss factory at Oberkochen.

2. We received altogether 55 papers of which 35 were selected for presentation. The technical programme comprised 9 half-day sessions (5 on aerial triangulation and accuracy, 1 on digital terrain models and contour interpolation, 2 on geometry of remote sensing, 1 closing session).

As each participant did receive in print one set of the papers most of the presentations could be kept within 20 to 30 minutes. Nevertheless the time schedule was very tight, also because of extended and thorough discussions. The active and untiring engagement of participants and speakers is highly appreciated. It made it a working symposium indeed, meeting, it is felt, the purpose of effective exchange amongst experts of detailed technical information, ideas, and experience.

3. During the opening session the board of Commission III proposed to dedicate the symposium to Prof. Dr. Willem Schermerhorn, in view of his 80th birthday in 1974. The participants adopted the move unanimously, recognizing and appreciating the personal contribution, the enthusiastic support, and the effective stimulation by which Prof. Schermerhorn has promoted the development and application of aerial triangulation. The following cable was sent:

"DEAR PROF SCHERMERHORN

I HAVE THE HONOUR AND THE PLEASURE TO INFORM YOU THAT THE PARTICIPANTS UNANIMOUSLY AGREED TO DEDICATE THE SYMPOSIUM TO YOU AT THE OCCASION OF YOUR 80TH BIRTHDAY THIS YEAR IN APPRECIATION OF YOUR STIMULATION AND PROMOTION OF AERIAL TRIANGULATION"

Prof. Schermerhorn thanked also by cable, expressing that he was "deeply touched by the generous gesture" and wishing good success to the meeting.

4. Hereafter the proceedings of the symposium are presented. The first part contains the papers, somewhat abbreviated, which were to be presented during the technical sessions. The second part includes all other submitted papers which represent equally valuable contributions. In some cases of previously published papers only abstracts are given.

We thank all participants and speakers for their active contributions and engaged discussions which not only made the symposium a very pleasant, informative and successful meeting but also reflected important and considerable technical development.

We also thank all who helped prepare the symposium and carry it through.

F. Ackermann, President of Comm. III

H. Bauer, Secretary of Comm. III

TABLE OF CONTENTS

paper no.		page
	FOREWORD	3
1	F. Ackermann Introduction to the Symposium	9
	<u>1st session, Sept. 2nd</u>	
	COMPARISON OF BLOCK-ADJUSTMENT METHODS, TEST RESULTS	
2	J.M. Anderson, George Erio and Clement Lee Analytical Bundle Triangulation with Large Scale Photography: Comparison with Polynomial Adjustment and Experiments Using Added Parameters	12
3	G.W. Marks and E.M. Mikhail Experimental Results from Block Triangulation by Bundles, Pairs and Triplets	19
4	G. Otepka Investigation on the Applicability of Block Adjustment in Austria	24
	<u>2nd session, Sept. 2nd</u>	
	COMPARISON OF METHODS, TEST RESULTS, APPLICATION	
5	H.S. Williams On the Influence of a Minimum Metrical Precision Threshold on Absolute Accuracy in Analytical Aerial Triangulation	29
6	R.-P. Mark Systematic Comparator Errors - Mathematical Description and Influence on Block Triangulation	38
7	F. Ackermann Photogrammetric Densification of Trigonometric Networks The Project Appenweier	43
8	Jonna Hvidegaard Densification of Trigonometric Nets Practical experiences with bundle-adjustment	49
	<u>3rd session, Sept. 3rd</u>	
	SYSTEMATIC ERRORS; ADJUSTMENT WITH ADDITIONAL PARAMETERS	
9	D.C. Brown Bundle Adjustment with Strip- and Block-Invariant Parameters	54
10	H. Salmenperä, J.M. Anderson, A. Savolainen Efficiency of the Extended Mathematical Model in Bundle Adjustment	66
11	G.H. Schut On Correction Terms for Systematic Errors in Bundle Adjustment	76
12	H. Bauer Bundle Adjustment with Additional Parameters - Practical Experiences	83
13	H. Ebner and W. Schneider Simultaneous Compensation of Systematic Errors with Block Adjustment by Independent Models	90

4th session, Sept. 3rd

SYSTEMATIC ERRORS, AUXILIARY DATA, THEORETICAL DEVELOPMENTS

14	H. Klein Results from the South-Western Ontario APR-Test Block	97
15	J. Albertz, W. Kreiling, J. Wiesel Block Triangulation without Point Transfer	104
16	H. Ebner Analysis of Covariance Matrices	111
17	Gy. Alpár Comparison of Adjustment Methods of the Aerotriangulation by Numerical Filtering Technics	122

5th session, Sept. 4th

METHODICAL DEVELOPMENTS, CALIBRATION

18	E. Dorrer Contribution to a General Stereoscopic Block Analytical Aerotriangulation	125
19	H.G. Jerie Development of a Computer Simulation System Concerning the Accuracy of Photogrammetric Operations	137
20	I. Hadem Camera Calibration by Photographing Test Fields	145
21	O. Kölbl Tangential and Asymmetric Lens Distortion, Determined by Self-Calibration	153

6th session, Sept. 5th

22	G.H. Schut Evaluation of Some Interpolation Methods	160
23	E. Aßmus Extension of Stuttgart Contour Program to Treating Terrain Break-Lines	171
24	E. Clerici and K. Kubik The Theoretical Accuracy of Point Interpolation on Topographic Surfaces	179
25	G. Konecny Approach and Status of Geometric Restitution for Remote Sensing Imagery (Remote Sensing)	188

7th session, Sept. 5th

REMOTE SENSING; RADAR

26	L.C. Graham Geometric Problems in Side-Looking Radar Imaging	199
27	F. Leberl Radargrammetric Point Determination "PRORADAM"	207
28	G. Dowideit A Simulation System for Theoretical Analysis of Radar Restitution and a Test by Adjustment	216

29	H. Jensen Deformations of Star Imagery - Results from Actual Surveys	230
	<u>8th session, Sept. 6th</u>	
30	H.P. Bähr Interpolation and Filtering of ERTS-Imagery	235
31	E.E. Derenyi Topographic Accuracy of Side-Looking Radar Imagery	244
32	E.M. Mikhail, J.R. Baker and G.W. Marks Analysis of Digital Multispectral Scanner (MSS) Data	251
33	A.P. Colvocoresses Space Oblique Mercator - A New Map Projection of the Earth	259
34	V. Kratky Geometric Calibration of Canada ERTS Photoreproduction System	266
	<u>Closing session, Sept. 6th</u>	
35	F. Ackermann Conclusion of the Symposium	273
	<u>Additional submitted papers</u>	
36	Gherasim Marton Some Results Concerning the Use of Aerial Triangulation with Independent Model, in Production	275
37	F. Ackermann Accuracy of Staloscope-Data - Results from the OEEPE-Test "Oberschwaben"	280
38	M. Schilcher and E. Wild Systematic Model Deformation of the OEEPE-Testblock "Oberschwaben"	287
39	P. Waldhäusl On Polynomial Methods for Strip Adjustment	296
40	E. Clerici, K. Kubik and J. van Kuilenburg Experience with Photogrammetric Triangulation in Astronomy	306
41	K.C. Saxena Analytical Triangulation - A Suggested Method	309
42	P.R. Datta Block Adjustment with Programmable Desk Calculators	314
43	P.R. Datta Comparative Accuracy of Point Determination by Absolute Orientation and Block Adjustments - A Theoretical Analysis	320
44	G.B. Das, V. Ramakrishnan, B.K. ManjappaRai Aerotriangulation with Independent Models and Adjustment Using Affine Transformations	328
45	A. Verdin Bundle Block Adjustment for Blocks of Limited Size in Order to Densify Trigonometric Nets	332
46	R.C. Badjatia Independent Model Triangulation without Using Perspective Centres Coordinates	338

47	R.B. Forrest Geometric Correction of ERTS-1 MSS Images	340
48	E. Clerici, D. Eckhart and K. Kubik MARS - A Processing System for the Mapping of Remote	358

Abstracts

	K. Tempfli Film Flatness in Aerial Cameras - A Model for its Computer Simulation	362
	H.G. Jerie Determination of Stochastic Models for Observation and Point Transfer Errors	362
	B. Makarovič Instrumental Error Analysis and Generation	362
	K. Tempfli Analysis and Simulation of Deformation	363

INTRODUCTION to the Symposium (condensed)

F. Ackermann, Stuttgart

1. Aerial triangulation has been the traditional subject of ISP-Commission III. It included all practical and theoretical aspects of what we prefer now to call photogrammetric determination of points. The redefinition of the Commissions at the XIIth International Congress of ISP in Ottawa, 1972, has considerably extended the field of interest of Commission III. It is outlined as "Mathematical Analysis of Data", a formulation which I personally do not consider well chosen. Nevertheless, the clear intention has been that Commission III is to be concerned with all aspects of photogrammetry as far as mathematical and statistical methods, accuracy, processing and assessment of photogrammetric and derived or related data are concerned. It takes into account the increased importance of mathematical methods, of data processing, of digital technology, and recognizes the increased and general influence of such techniques on the performance and application of photogrammetry.

I do not intend to speculate on the implications of the redefined tasks of Commission III. Certainly new problems of delineation against other Commissions will arise. However, we can trust that the activities of Commission III will cover the extended field of interest and shift emphasis to the various subjects in due course.

At present, we can clearly distinguish 4 different fields on which Commission III has to concentrate:

- Aerial triangulation, photogrammetric point determination, including theory (mathematical models), computation, software, accuracy, procedures, and application. It is still the main topic within the Commission. The bulk of the papers submitted to this symposium refer to it.
- Digital mapping and digital terrain models, including automatic contour interpolation. Commission III is concerned with the mathematical methods and digital techniques, whilst the applications will remain with Commission IV. The subject is related to the more general areas of automation in cartography and of digital data banks.
- Geometrical aspects of remote sensing, mathematical models of the geometric performance of various sensors, related theory, restitution techniques and accuracy questions. As remote sensing covers a very large field and the organisations dealing with it are widely spread a working group has been established under the chairmanship of Prof. Konecny. It's task is to study and clarify the geometric performance of various sensors by theory and experiment.

A considerable number of papers on remote sensing have been submitted to the symposium, to be dealt with in 2 technical sessions.

- Digital image processing, including digital image correlation, and problems of pattern recognition.

There are applications within the conventional range of aerial triangulation, such as automatic point transfer. However, the developments are eventually directed towards automatic image restitution and photo-interpretation.

This subject seems to be in a preliminary stage of development. As no papers have been submitted it will not be treated during this symposium.

2. The majority of the submitted papers concern aerial triangulation, the traditional topic of Commission III. Accordingly, it will be the subject of 5 technical sessions.

In the past decade there has been striking progress in aerial triangulation, mainly by the development of numerical methods of blockadjustment. Computer programs have been developed which have removed most previous limitations and have raised the aerial triangulation performance to a new level of effectiveness, accuracy and economy. Theoretical and empirical accuracy studies allow fair assessment of the accuracy capabilities of strip- and block-triangulation. Practical application has been considerably increased and has recovered new areas: Very large blocks with minimum control for small scale mapping, and high precision aerial triangulation for large scale mapping, cadastral application, and geodetic application (densification of networks).

There is not doubt that the development has been highly successful. It also has, by the way, revived general interest in aerial triangulation matters. It is not surprising that the development has solved a number of problems, it has also opened the approach to many new problems. Reviewing the situation briefly the following statements may point to the present problem areas of aerial triangulation which deserve attention:

- Little attention has been given to the data gathering phase of aerial triangulation, i.e. preparation and measurement. The relative merits of mono- and stereocomparators and of analogue precision instruments have not been sufficiently assessed. Investigations and better solutions are needed for point-marking and point-transfer, or rather for avoiding it. Analytical plotters may change the present practice of preparation and measurements of aerial triangulation.
 - Computer programs for block-adjustment should be extended to self-calibration; also extensions to auxiliary data are due, and to hybrid adjustment systems combining photogrammetric and terrestrial or other measurements.
 - Although the computational problems of block triangulation have been satisfactorily solved in a number of cases, there is still no general agreement on the best strategy of computation (en bloc or stepwise, approximate values), on the required degree of generality and of optimization of a software package, and on the computer requirements (core size, speed). There are no rules for the assessment and comparison of the data-handling and data-editing qualities of computer programs.
 - The accuracy performance of the various computational methods of block-adjustment (bundle method, independent spatial units, polynomials) has not been sufficiently assessed, especially in view of systematic image errors.
 - Accuracy investigations should primarily assess systematic and correlated image errors, based on empirical data, and study their effects on adjusted strips and blocks. The intention is to establish refined mathematical models of the geometry of aerial photographs. The results are needed for designing self-calibrating methods of block-adjustment.
- Empirical and theoretical accuracy studies are also suggested for auxiliary camera orientation data, especially for those affecting height accuracy.
- More fundamental research seems to be required concerning the mathematical and statistical problems of self-calibration. Related to it are fundamental problems of generalized least squares methods, including collocation and filtering techniques.
 - Theoretical and practical solutions are needed for automatic blunder detection in block-adjustment. Can one-line computations reduce the percentage of gross errors ?
 - Practical research and experimentation into the applicability of aerial triangulation for geodetic purposes (network densification) is suggested, besides the general promotion of aerial triangulation methods in every-day practice of photogrammetry. Extensions to special applications, such as architectural photogrammetry are highly recommended.

The above list demonstrates that in aerial triangulation the theoretical investigations and developments are at present concerned with the further refinement of the mathematical model of image coordinates, with the reliability and predictability of accuracy results, and also with generalized methods of adjustment and data processing. The practical side of aerial triangulation is concerned with improving the preparation and measuring phase, with computers and computer software, and with extending the fields of application.

The papers on aerial triangulation which have been submitted to this symposium do not cover the full range of the problem areas as quoted above. There are some papers on practical application of block-triangulation; one paper deals with the possibility of avoiding point transfer. Basic theoretical and methodical questions, and also computational problems receive some attention. A special highlight is D. Brown's paper on the evolution of the algorithmus to solve the computational problems of large and hybrid adjustment systems. Most papers, however, deal with accuracy investigations, amongst which the attention is focused on the comparison of adjustment methods, the analysis of systematic image errors, and the effectiveness of self-calibrating adjustment procedures.

The submitted papers reflect rather well the present research activities in aerial triangulation. In particular, the analysis and compensation of systematic image errors is obviously a major topic of investigation and development. It is a most demanding and rewarding field of research, of which great effects on practical aerial triangulation are expected, concerning especially still considerably increased accuracy and extended application.

ANALYTICAL BUNDLE TRIANGULATION WITH LARGE SCALE PHOTOGRAPHY: COMPARISONS WITH POLYNOMIAL ADJUSTMENTS AND EXPERIMENTS USING ADDED PARAMETERS

by James M. Anderson, George Erio and Clement Lee, Berkeley, California

Abstract

A bundle adjustment for simultaneous triangulation and for camera calibration has been used to triangulate a 1 km x 2 km test field. Photography (approximate scale 1 : 3000) was taken from an altitude of about 460 m over a test array containing 88 premarked control points. Relief in the test area constitutes about 20 % of the flight altitude. Comparisons of the bundle and polynomial adjustments were made with photographic coordinates observed with a Zeiss PSK Stereo comparator and using 3 control point configurations. Evaluation of the effects of added parameters was performed with photo coordinates measured on a Mann monocular comparator and using 20 and 60 % sidelap with two control point configurations. Results indicate that no real advantage is achieved by using the block adjustment for small blocks of large scale photography when 11 control points are fixed in the 14 photo block. For sparse control (5 fixed points) configurations, RMSE in planimetry and elevation are reduced by about 30 % and 60 %, respectively, by use of the bundle method. Use of three combinations of added parameters in the bundle adjustments yielded an improvement in planimetric position and elevation of about 30 %.

This investigation represents a joint effort between the University of California Department of Civil Engineering in Berkeley, California and the California Division of Highways Surveying and Photogrammetry Department in Sacramento, California. The Department of Civil Engineering recently completed development of a simultaneous bundle adjustment program for analytical aerial triangulation and/or camera calibration. Research related to development of this program was supported by National Science Foundation Grant, NSF GK 24017, "Analytical Calibration of Terrestrial and Aerial Camera Systems". Although the primary emphasis in this program was on utilization of added parameters for camera calibration of terrestrial or aerial systems, it is equally adaptable to ordinary aerial triangulation. Aerial camera calibration and the effects of added parameters on accuracies attainable in block triangulation were of primary interest in the research at the University of California.

The California Division of Highways Surveying and Photogrammetry Department has been using fully analytical, sequential control extensions since 1966 and was interested in studying the relative merits of the bundle adjustments for these tasks.

Thus, the major objectives of this investigation were to: (1) compare fully analytical sequential triangulation and adjustment by polynomials with simultaneous bundle adjustment of small blocks of large scale aerial photography; and (2) evaluate the effects of using various combinations of added parameters on the accuracies achievable in the triangulation of small blocks of large scale photography. Practical tests with real photography were employed to study these two problems.

TRIANGULATION PROCEDURES

Bundle adjustment

The photogrammetric triangulation procedure developed at the University of California is a simultaneous bundle adjustment of photographs. The computational procedure is based on the collinearity condition with parameters added for camera calibration where the calibration model is similar to the method developed by Brown [1]. The basic collinearity equations with added calibration parameters

$$\begin{aligned}
x_{ij} &= x_p - x'_{ij} - \bar{x}_{ij} \Delta r_{ij} / r_{ij} - p_1 (r_{ij}^2 + 2\bar{x}_{ij}^2) - 2p_2 \bar{x}_{ij} \bar{y}_{ij} \\
y_{ij} &= y_p - y'_{ij} - \bar{y}_{ij} \Delta r_{ij} / r_{ij} - 2p_1 \bar{x}_{ij} \bar{y}_{ij} - p_2 (r_{ij}^2 + 2\bar{y}_{ij}^2)
\end{aligned}
\tag{1}$$

in which

- x_{ij}, y_{ij} = image coordinates of point j on photograph i ;
- x_p, y_p = principal point coordinates;

x'_{ij} , y'_{ij} are functions of: camera focal length, f ; coordinates of exposure stations and orientation angles of exposure station i , $(X Y Z, \omega \phi \kappa)_{0i}$; object point coordinates of point j $(X Y Z)_j$; and

$$\Delta r_{ij} = k_0 r_{ij} + k_1 r_{ij}^3 + k_2 r_{ij}^5 + k_3 r_{ij}^7 \quad (2)$$

$$\bar{x}_{ij} = (x_{ij} - x_p); \quad \bar{y}_{ij} = (y_{ij} - y_p); \quad r_{ij} = (x_{ij}^2 + y_{ij}^2)^{1/2} \quad (3)$$

p_1 and p_2 = decentering distortion coefficients.

Each adjustment problem involves forming the linearized form of Equations (1) for all images in the block to be solved. Redundant points are utilized and the method of least squares is used to solve the resulting system of equations. All exposure station, ground point and calibration parameters can be considered as unknowns in this adjustment. Any parameter can be treated as a fixed value or as a free parameter.

Final results from adjustment computations are: 1) camera calibration data, if desired, including all or/and any combination of these parameters; 2) exterior orientation parameters for all photographs used in the adjustment; 3) object point coordinates for triangulation and check points; and 4) propagated variances for all parameters specified as unknowns in the adjustment.

Fully Analytical Sequential Procedure with Polynomial Adjustment

The Division of Highways Surveying and Photogrammetry Department sequential procedure consists of: a) relative orientation using a three photograph basic unit; and b) a polynomial block adjustment. A modification of the three photograph program developed by the National Ocean Survey is used for relative orientation and is followed by the iterative block adjustment with polynomials as developed by G. H. Schut at the National Research Council of Canada [2][3].

CALIBRATION TEST SITE AND PHOTOGRAPHY

The California Division of Highways Surveying and Photogrammetry Department's photogrammetric test area is located east of Bishop, California [4] and contains 33 horizontal and vertical (H+V) and 55 vertical (V) premarked control points. Test photography consists of three strips of eight photographs taken with a Wild RC 8 camera (Aviogon lens cone 15 Uag. 312, $f = 153.01$ mm, calibrated November 11, 66) from approximately 460 meters above terrain containing 90 meters of relief. Arrangements of photographs and control points in the test block are illustrated in Figure 1.

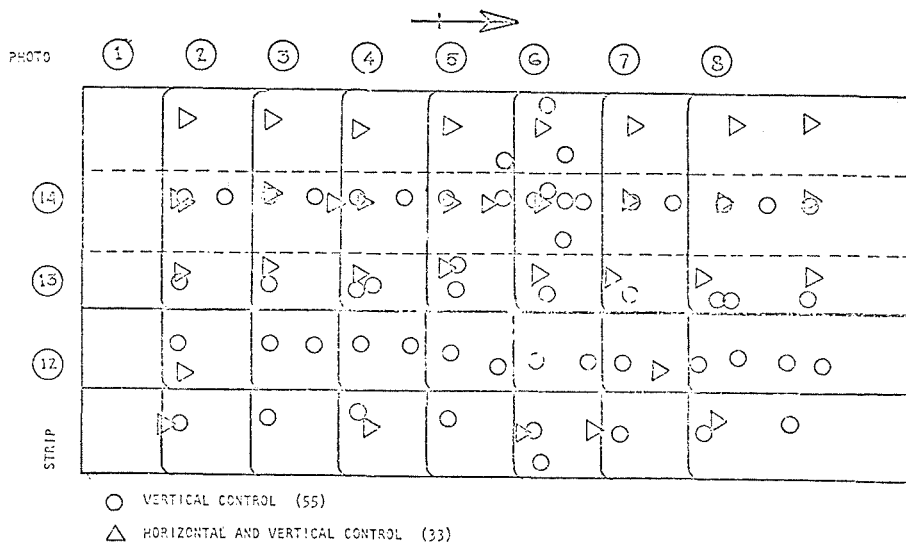


FIGURE 1.
24 PHOTO BLOCK-BISHOP TEST
SITE, CALIFORNIA

PHOTOGRAPHIC COORDINATE MEASUREMENT AND REFINEMENT

Photographic coordinate measurements can be divided into two major groups, those made for 1) comparison of the bundle and polynomial adjustment; and 2) evaluation of the effects of added parameters in the bundle adjustment.

Measurements for group 1) above were made with the Zeiss PSK stereocomparator in the Office of the Surveys and Photogrammetry Department of the Division of Highways in Sacramento, California. Observed coordinates were corrected for: affine film deformation; atmospheric refraction and earth curvature; and radial and asymmetric lens distortion.

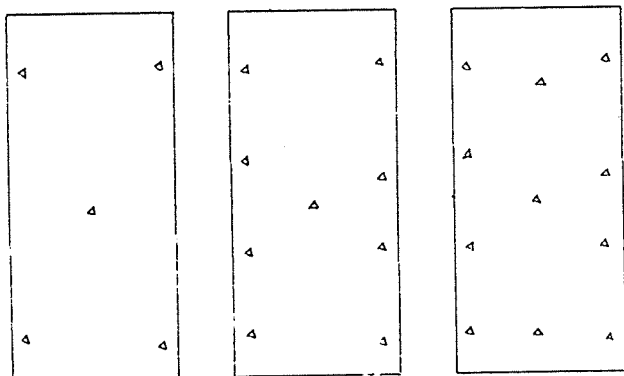
Measurements for group 2) above were made on a Mann monocular comparator at the US Geological Survey in Menlo Park, California. Two sets of refined image coordinates were prepared for this group of measurements. Set 1 was for triangulation using added parameters and observed image coordinates were corrected for; a) affine film deformation; b) atmospheric refraction. Set 2 was for block triangulation adjustment, only, so that observed image coordinates were corrected for: (a) and (b) of set 1 plus (c) radial and asymmetric lens distortion.

TEST CASES

Test cases can be divided into two separate groups. Those made for: 1) comparison of bundle polynomial adjustments; and 2) evaluation of effects of added parameters.

Bundle vs. Polynomial

Bundle block adjustments were run with three control configurations I, II and III containing 5, 9 and 11 horizontal and vertical fixed control points, resp., as illustrated in Figure 2. Test cases with each of these configurations were run using 60 % and 20 % sidelap and are labeled A and B, respectively.



I 5 H&V II 9 H&V III 11 H&V

FIGURE 2

GROUND CONTROL ARRAYS: BUNDLE VS POLYNOMIAL

The polynomial adjustments were also performed with each of these control configurations utilizing 20 % sidelap, only (test cases IB IIB, IIIB). Plate coordinates of Group 1 were used for these tests.

Estimated standard deviations of unit weight for bundle adjustments and root mean square errors (RMSE) of discrepancies in check points for bundle and polynomial adjustments are given in Table 1.

Percent changes resulting from use of bundle adjustments in the block are:

Control Points	% Change in RMSE by Use of Bundle Adj.	
	XY	Z
5	- 33	- 60 %
9	- 15	0
11	+ 17	0

On the basis of these results, use of the bundle adjustment would be justified in small blocks for cases where only the minimum number of control points is available. However, for moderately dense control points configurations, the polynomial adjustment requires less central processor unit time (by a factor of about 2) and provides comparable accuracies.

Bundle Block Adjustments with Added Parameters

A total of 12 adjustments using two control configurations and three different combinations of added parameters, with 20 and 60 % sidelap were run using photographic coordinates of Group 2, Set 1. Four additional adjustments were performed

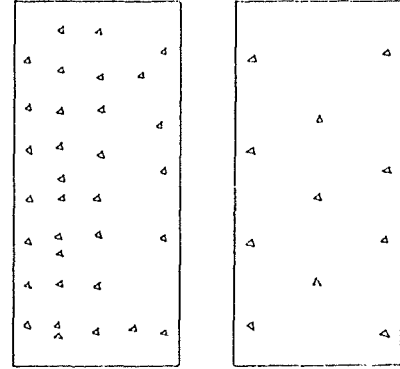
for triangulation only (no added parameters), using photo coordinates of Group 2 Set 2). The two control configurations IV and V are illustrated in Figure 3.

△ = HORIZONTAL & VERTICAL
GROUND CONTROL POINT

Combinations of added parameters utilized are:

- 1 f, x_p , y_p , k_1 , k_2 , k_3 , p_1 , p_2
- 2 f, k_1 , k_2 , k_3 , p_1 , p_2
- 3 k_1 , k_2 , k_3 , p_1 , p_2
- 4 Triangulation only.

Tests with 60 and 20 % sidelap are labeled A + B, respectively. Each test is designated by control configuration, parameter set, and sidelap condition. For example Test V 3 A is an adjustment using 11 H/V, control points, added parameters k_1 , k_2 , k_3 , p_1 , p_2 and 21 photographs. These sixteen tests with numbers of control points, photographs, added parameters and adjustment standard deviations of unit weight are given in Table 3.



IV. 33 H&V
V. 11 H&V

FIGURE 3
GROUND CONTROL ARRAYS: ADDED PARAMETERS VS. TRIANGULATION ONLY

Bartlett's test was applied to the adjustment unit variances. When the 16 cases were tested simultaneously a significant difference was indicated at the 90 % level. Bartlett's test applied to the four triangulation runs (IV 4 A+B, V 4 A+B) and the twelve calibration runs (IV + V 1, 2, 3 - A+B) separately, showed no significant differences. On the basis of these analyses it was obvious that the laboratory and in flight calibrations were providing significantly different corrections for systematic errors in the camera system. In order to deduce which method was providing the more accurate results, the root mean square errors (RMSE) in check points were analyzed, and radial symmetric lens distortion curves were plotted vs. the laboratory calibration curve.

Test case	BUNDLE				POLYNOMIAL						
	No cont. pts.	Side lap %	m μ m	RMSE, μ m.		Deg. Adj.			Iterations	RMSE, μ m	
				XY	Z	H	V_L	V_T		XY	Z
I B	5	20	6-	.042	.110	2	1	1	5	.064	.274
I A	5	60	6-	.040	.046						
II B	9	20	6+	.046	.036	2	2	1	5	.040	.046
II A	9	60	6-	.034	.040						
III B	11	20	6+	.030	.040	2	2	2	5	.036	.040
III A	11	60	6-	.027	.040						

^{x)} RMSE in discrepancies

V_L = Longitudinal correction

V_T = Transverse correction

TABLE 1 Test Case Discrepancies in Check points Bundle vs. Polynomial Block Adjustment

Test Number	No. Control Pts		No Photos	Parameters Added								m μm
	H&V	V		f	x _p	y _p	k ₁	k ₂	k ₃	p ₁	p ₂	
IV 1 A	33		21	x	x	x	x	x	x	x	x	4,5
IV 1 B	33		14	x	x	x	x	x	x	x	x	4,5
IV 2 A	33		21	x			x	x	x	x	x	4,7
IV 2 B	33		14	x			x	x	x	x	x	4,7
IV 3 A	33		21				x	x	x	x	x	4,8
IV 3 B	33		14				x	x	x	x	x	4,7
IV 4 A	33		21				Triangulation only					5,9
IV 4 B	33		14				Triangulation only					6,3
V 1 A	11		21	x	x	x	x	x	x	x	x	4,0
V 1 B	11		14	x	x	x	x	x	x	x	x	3,7
V 2 A	11		21	x			x	x	x	x	x	4,1
V 2 B	11		14	x			x	x	x	x	x	3,9
V 3 A	11		21				x	x	x	x	x	4,1
V 3 B	11		14				x	x	x	x	x	3,9
V 4 A	11		21				Triangulation only					5,3
V 4 B	11		14				Triangulation only					6,2

TABLE 3 Test Case Designations Added Parameters

Tests IV 1 A+B - - - - IV 4 A+B permitted evaluation of the effects of added parameters on elevation (all H points were used in the adjustment). RMSE's in discrepancies of elevation and % change by use of added parameters are given for each test case in Table 4.

Test Case	RMSE Z m	% Change by Use of Added Parameters	Parameters Added
21 Photographs 60 % All Around Overlap			
IV 4 A	.042		Triangulation only
IV 1 A	.037	- 11 %	All parameters
IV 2 A	.037	- 11 %	f, k ₁ , k ₂ , k ₃ , p ₁ , p ₂
IV 3 A	.037	- 11 %	k ₁ , k ₂ , k ₃ , p ₁ , p ₂
14 Photographs 20 - 25 % Sidelap			
IV 4 B	.048		Triangulation only
IV 1 B	.048		All parameters
IV 2 B	.048		f, k ₁ , k ₂ , k ₃ , p ₁ , p ₂
IV 3 B	.038	- 21 %	k ₁ , k ₂ , k ₃ , p ₁ , p ₂

When 60 % sidelap is present the RMSE in elevation decreases 11 % for each parameter set. For 20 % sidelap, parameter sets 1 and 2 yield no decrease while set 3 results in a 21 % decrease in the RMSE.

Tests V 1 A+B - - - - V 4 A+B allow evaluation of the effects of the various combinations of added parameters on accuracies of position and elevation using 11 fixed control points. RMS errors and percent changes in RMSE's are also listed in Table 5. When 60 % (21 photos) all around overlap is present the reduction in the RMSE of check points is approximately 30 % for both planimetric position and elevations. When 20 % sidelap (14 photographs) is present the RMSE in planimetric position decreases 14 to 28 % and increases 28 % in elevation. Note that results achieved by triangulation only (V 4 A vs. V 4 B) using 20 % sidelap show RMSE values about 30 % less than when the 60 % sidelap was present. This result verifies conclusions reached by Kenefick that accuracies are not increased in small blocks by use of 60 % sidelap [5].

TABLE 5
RMSE in Discrepancies-Position and Elevation

Test Case	RMSE, m		% Change by Added Parameters		Parameters Added
	XY	Z	XY	Z	
21 Photographs, 60 % All Around Overlap					
V 4 A	.032	.058			Triang. only
V 1 A	.021	.040	- 34	- 31	All parameters
V 2 A	.022	.038	- 31	- 34	f, k ₁ ,k ₂ ,k ₃ , P ₁ ,P ₂
V 3 A	.023	.038	- 28	- 34	k ₁ ,k ₂ , k ₃ ,P ₁ ,P ₂
14 Photographs, 20 % Sidelap					
V 4 B	.021	.043			Triang. only
V 1 B	.016	.055	- 24	+ 28	All parameters
V 2 B	.018	.055	- 14	+ 28	f, k ₁ ,k ₂ , k ₃ , P ₁ , P ₂
V 3 B	.018	.055	- 14	+ 28	k ₁ ,k ₂ ,k ₃ , P ₁ , P ₂

Radial symmetric lens distortion curves for Test Cases IV 1 A, IV 3 A, V 1 A, V 3 A and the laboratory calibration curve are plotted in Figure 4.

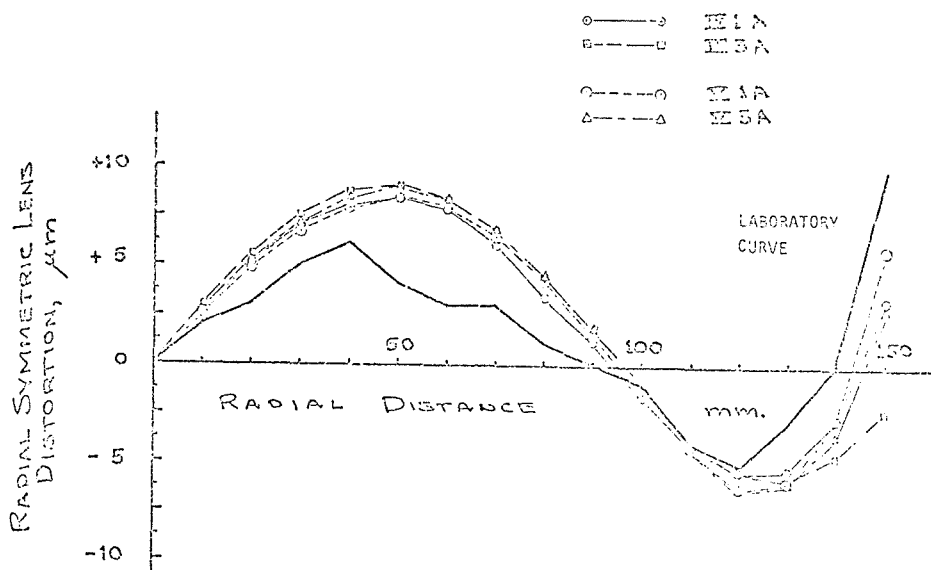


FIGURE 4 : Radial Symmetric Lens Distortion Curves

Note that the four in-flight calibration curves fall within a $- 7 \mu\text{m}$ band, the center of which fails to coincide with the laboratory curve with a RMSE in discrepancies of $2 \mu\text{m}$. The consistency of these curves in conjunction with the RMS errors in discrepancies of check points, indicates that for this camera and flight, the in-flight calibration using added parameters is providing the better results.

CONCLUSIONS

Small blocks of photographs as typified by the test area and photography of this study (1 km x 2 km, 1 : 3000 scale) are more effectively adjusted by the bundle method when fixed ground control points are sparsely distributed (figure 2, 1). RMS errors in planimetry and elevation were reduced 30 and 60 % respectively by applying the bundle adjustment. With control arrays of moderate density (figure 2 II and III) the polynomial adjustment yielded accuracies in planimetric position and elevation equal to and in one case surpassing that achieved by the bundle method. Thus, an organization having a substantial number of small blocks to adjust, would have difficulty justifying development costs for a bundle adjustment on the basis of improved accuracies for the average job. If a bundle adjustment is operational then the problem becomes one of applying the procedure which is more appropriate in view of the available control point distribution.

Use of additional parameters for in-flight camera calibration yielded accuracies in planimetric positions and elevations improved by about 30 % when compared to triangulation with no added parameters and using coordinates refined with laboratory camera calibration data. No significant differences existed among accuracies in check points attained using three different combinations of added parameters. Symmetric radial lens distortion curves from 4 in-flight calibrations are quite consistent but deviate from the laboratory curve with an RMSE of $2 \mu\text{m}$. As a consequence one can conclude that laboratory calibration data for lens distortions are somewhat in error for this particular camera.

In general one can say that for small blocks containing 60 % sidelap use of added parameters with the bundle adjustment is an effective procedure to compensate for residual systematic errors not corrected in the coordinate refinement procedure. This effectiveness would be especially pertinent for older cameras in which laboratory calibration data would be more likely to be erroneous.

REFERENCES

- |1| Brown, D. C.: "Advanced Methods for Calibration of Metric Cameras", Symposium on Computational Photogrammetry, State University of New York, Syracuse University, January 1969
- |2| Tewinkel, G. C.: "Three-Photo Analytics", paper presented at Semi Annual Convention of ASP, Dayton, Ohio, September 1965
- |3| Schut, G. H.: "Development of Programs for Strip and Block Adjustment at The National Research Council of Canada", NRC AP-PR 25, NRC 7632, Ottawa 1963
- |4| Mori, J.: "Development of Photogrammetric Testing and Evaluation Procedures, Phase 1, Establishment of a Photogrammetric Test Area", Research Report 627 105, Surveys and Photogrammetry Department, State of California Division of Highways, Sacramento, 1972
- |5| Kenefick, J. F.: "60 Percent vs. 20 Percent Sidelap", Photogrammetric Engineering, p. 583, June 1968

EXPERIMENTAL RESULTS FROM BLOCK TRIANGULATION BY BUNDLES, PAIRS AND TRIPLETS

by E. M. Mikhail and G.W. Marks, West Lafayette, In.

ABSTRACT

Block triangulation by bundles is known to theoretically yield the best accuracy. Recent results, however, imply that in the presence of residual correlated random (systematic) components, block triangulation by pairs may be as accurate as, and sometimes more accurate than, by bundles.

In order to gain more experience in block triangulation by independent units, the ISP simulated block was used to test three block triangulation techniques. In addition to bundles and pairs used so far, the method of independent triplets is also included. Tests are performed using data with both uncorrelated and correlated random errors. The results obtained are compared and characterized relative to the expended effort. This may aid in the selection of technique suitable for meeting the accuracy required within the available effort level.

INTRODUCTION

Numerical block triangulation schemes have reached a stage such that their application in practice is now a reality. It is generally recognized that there are basically three procedures of block triangulation: (1) the so-called fully analytical method which is also referred to as triangulation by bundles; (2) the independent model method; and (3) the polynomial method (Schut's program). This paper is concerned with the first two procedures only.

There has been several efforts to determine the relative accuracy of the three techniques of block triangulation. Some of these efforts relied on theoretical derivation [1][2][3][4] others made use of simulated test data [5], and yet others applied actual photography of test fields [6]. On the basis of theory alone (which usually assumes uncorrelated random components) it has been stated that analytical block triangulation by bundles should give the best accuracy results. This is mentioned in reference [4] where it is said that "fully analytical blocks evidently are more accurate than blocks with independent models". The same reference [4] cites preliminary results of unpublished work by Krack where σ_x and σ_y for bundle triangulation are said to be better by a factor of 1.6 over the independent model method. The cases investigated considered a 200 model block with 20 % and 60 % sidelaps and dense perimeter control. For σ_z the bundle adjustment is said to show factors of improvement ranging from 1.1 to 1.8.

On the basis of test results with actual photography, Ackermann [6] gives the following conclusions with respect to the Oberschwaben test block of OEEPE : "The independent model results show consistently better accuracy than the results from bundle adjustments which is quite contrary to general expectation and to theoretical studies." He goes further to point out, however, that "the results of the bundle adjustments as such differ very considerably from theoretical expectation, in terms of multiples of the standard error of unit weight."

It is apparent from the above statements that theoretical predictions on the basis of uncorrelated random variables are not quite adequate when dealing with actual photography which seems to include residual correlated random (or systematic) effects. However, the indications arrived at so far are on the basis of limited amounts of data from the statistical standpoint. Consequently, as more test results become available, more reliable statistical inferences can be made.

While the tendency is, at present, to seek extended mathematical models to accommodate correlated components in the case of bundle triangulation, the method of independent models appears to have established itself as a viable alternative. It is not unrealistic to assume that extended mathematical models will similarly be investigated for the independent model method in order to increase its potential. With this aim in mind, it is deemed worthy of consideration to use basic units other than the single stereopair. It is the purpose of this paper to look into the use of one such unit, the triplet, and to compare results from its utilization to those from other methods, notably the single bundle, and the stereopair.

BLOCK TRIANGULATION BY TRIPLETS

The idea of the triplet was introduced over a decade ago [7] within the prevailing practice at that time of sequential triangulation, where separate units are relatively oriented, assembled in strips, then in blocks. Many researchers since then have analyzed the use of triplets as regards any attendant advantages, particularly in the context of strip triangulation. In this respect, the scheme is to proceed from one triplet to another such that they overlap by two photographs. This practice becomes unnecessary when the triplet is to be used as a basic unit in block triangulation. Here, an overlap by one photograph between triplets is all that is required.

For the purpose of the tests reported in this paper, both pairs and triplets were formed using a general program called URELO (Unit Relative Orientation) available at Purdue University. This program is capable of performing relative orientation of units of variable size (up to a maximum of 8 photographs each) and assembling the units into one integral strip with a variable number of photographs as overlap between successive units. URELO was utilized to form both pairs and triplets (overlapping by one photograph) and only the separate unit coordinates were used, and not the assembled strip coordinates. Consequently all units, for both pairs and triplets, were independent and could therefore be used in a program for block triangulation by independent models (units).

Before proceeding to the actual results, it is perhaps pertinent to discuss why one should be interested in using the triplet as a unit in block triangulation. The obvious reason is the reduction in the number of units, and hence the number of parameters. For instance, if n is the number of photographs in each of s strips forming a block, and assuming that no additional parameters are used, then:

number of parameters in the bundle method	=	$6ns$	
number of parameters in the method of pairs	=	$7(n-1)s$	
number of parameters in the method of triplets	=	$3.5(n-1)s$	for n odd
	=	$3.5ns$	for n even

Therefore, for a block of $s = 20$ strips, each of $n = 30$ photographs, the bundle method would involve 3600 camera parameters; the method of independent pairs 4060 parameters; and the method of independent triplets 2100 parameters.

There is clearly a significant reduction in the number of parameters in the case of triplets. Such a reduction may be viewed either as for increasing the maximum size of the block to be handled by a given computer system.

Having pointed out what appears to be an advantage in using the triplets, it is important to discuss any possible disadvantages. After all, one cannot usually get something for nothing. In fact, when the idea of its use came to mind, it was not so much a question of whether it is better or more accurate, but of whether any gain in the use of triplets outweighs whatever reduction in accuracy that may occur. The first point concerns the internal accuracy of the triplet versus that of a stereopair. From the results of URELO, and limiting the number of iterations per unit to a maximum of 5, the difference in the value of the reference variance between pairs and triplets was not excessive. The actual values will be given in the section on test results. The second, and perhaps more important, point is how well the triplets as units would adjust amongst themselves in the block. Since it has been surmised that the reason for block triangulation by pairs yielding better results than by bundles is due to the increase in number of parameters, one would expect triangulation by triplets to be inferior. The question is not whether or not this could occur, but rather how much inferior. Test results given in a later section will concern this point.

The International Society of Photogrammetry (ISP) through the Commission III Working Group, has recognized that a simulated block of photographs is a suitable means for comparative studies, since it is standardized for use by all participants. A very brief summary of the ISP test block therefore follows.

ISP SIMULATED TEST BLOCK

As reported in detail by Anderson [5], the test block was generated by the Topographic Center of the Defense Mapping Agency. It consisted of 9 strips of 20 photographs each, with 60 % forward- and side-lap taken at a nominal altitude of 11 000 m. Camera focal length is 152 mm and the format is 23 x 23 cm. The principal point was offset +10 μ m in x and -10 μ m in y . A regular array of 5 x 5 image points was generated for each photograph. The image coordinates were perturbed

bed in a random manner in onest (with a standard deviation of 6 μm) and random plus systematic in another.

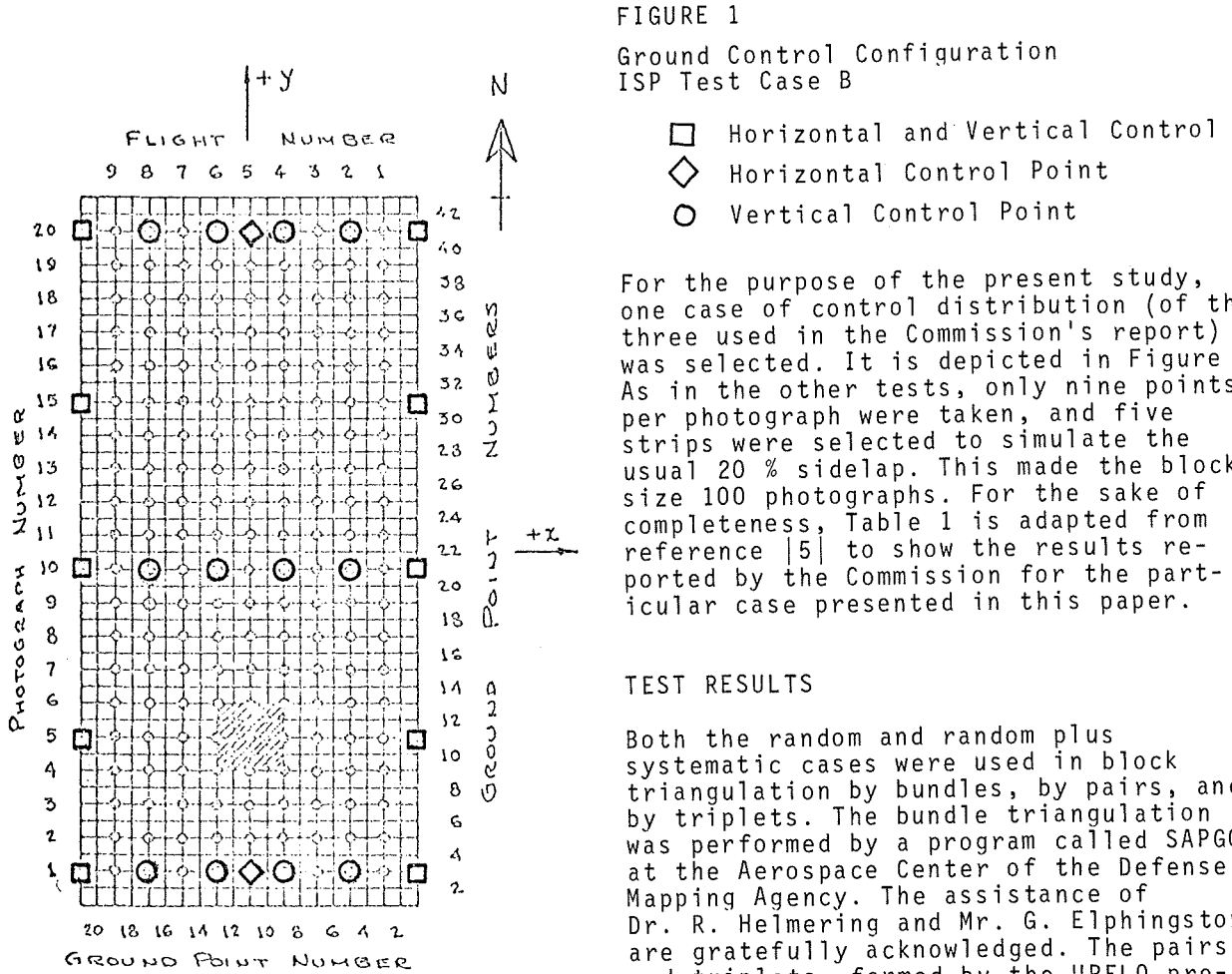


FIGURE 1
Ground Control Configuration
ISP Test Case B

For the purpose of the present study, one case of control distribution (of the three used in the Commission's report) was selected. It is depicted in Figure 1. As in the other tests, only nine points per photograph were taken, and five strips were selected to simulate the usual 20 % sidelap. This made the block size 100 photographs. For the sake of completeness, Table 1 is adapted from reference [5] to show the results reported by the Commission for the particular case presented in this paper.

TEST RESULTS

Both the random and random plus systematic cases were used in block triangulation by bundles, by pairs, and by triplets. The bundle triangulation was performed by a program called SAPGO at the Aerospace Center of the Defense Mapping Agency. The assistance of Dr. R. Helmering and Mr. G. Elphingstone are gratefully acknowledged. The pairs and triplets, formed by the URELO program at Purdue, were adjusted as blocks through the program PAT-M-43 at the Photogrammetric Institute in Stuttgart.

	Participant	Random Only		Random + Sys.	
		m_{xy}	m_z	m_{xy}	m_z
Sequential	1	1.4	2.1	1.5	2.4
	2	1.74	2.24	2.54	2.53
	3	4.67	2.99	10.02	8.66
		1.94	2.99	2.24	8.06*
	4	2.67	2.89	--	--
	5	3.04	3.52	2.71	6.93
	6	2.57	3.33	2.90	3.33
7	6.82	13.51			
Σ**		1.09	1.82	1.92	2.45
Simultaneous	9	0.67	1.66	1.31	2.03
	10	0.68	1.54	--	--
	11	0.74	1.66	2.12	2.25
	12			1.41	1.86

TABLE 1
Reported ISP Results-Test Case B
RMS (in meters) Discrepancies in
Planimetry and Elevations of
Check Points

* 3 sections per strip
** simultaneous adjustment of independent models

Bundle Triangulation

The program SAPGO used for the bundle method applied the following a priori standard deviations: 0.01 m in X, Y and Z for the control points; 100 m in X, Y and Z for pass points and exposure station positions; and 10° in ω, φ and κ for each camera station. The a priori standard deviation in x and y image coordinates was taken equal to the 6 μm value used in generating the data. These values were applied for both the random as well as the random plus systematic cases. The a posteriori reference standard deviation obtained was 4.2 μm for the random case, and 6.6 μm for the case of random plus systematic components.

Triangulation By Pairs and Triplets

The average reference standard deviation for all the pairs, obtained from relative orientation, was a little less than 7 μm for both random and random plus systematic cases. For the triplet relative orientation the corresponding values were about 7 μm for the random and about 10 μm for the random plus systematic cases.

After block triangulation, one reference standard deviation is obtained for position and another for elevation from the program PAT-M-43. The values in meters are:

	Random		Random + Systematic	
	Position	Elevation	Position	Elevation
Pairs	0.608	1.104	1.001	2.029
Triplets	0.653	1.108	1.067	1.983

The results on the check points are summarized in Table 2. The value m_{xy} was evaluated from

$$m_{xy} = \sqrt{m_x^2 + m_y^2}$$

which is the same expression used in the ISP results given in Table 1. The reason for the difference in values for the base of pairs between Table 2 and Table 1 (participant number 8) is due to the fact that a different number of check points was used in each of the tests.

TABLE 2

		m_x	m_y	m_{xy}	m_z
Test Results RMS (in meters) Discrepancies in Planimetry and Elevations of Check Points	Random				
	Bundles	.521	.456	.692	1.576
	Pairs	.775	.809	1.120	2.663
	Triplets	.867	.817	1.191	2.561
	Random + Systematic				
	Bundles	1.074	1.139	1.566	2.078
Pairs	.922	1.590	1.837	2.612	
Triplets	.993	1.274	1.615	2.518	

Several remarks may be made on the basis of the results given in Table 2.

- (1) At least for this particular experiment, the results from bundle triangulation are for the most part better than those from triangulation by pairs and triplets. This is true for both the random as well as the random plus systematic cases.
- (2) For the case of random perturbations only, the check standard deviation value for triangulation by triplets is only slightly different from that for triangulation by pairs. It is marginally higher in the X and Y, and lower in the Z to the extent that one may assume that the difference is insignificant.
- (3) It is somewhat surprising that in the case of random plus systematic components, both m_{xy} and m_z were lower for the triplets than for pairs. Realistically speaking, the difference should still not be considered significant. Even if there were no differences, it is rather encouraging to see that reducing the number of parameters by almost 50 % when using triplets did not

seem to affect the accuracy of block triangulation. One must emphasize, however, that this is only one test and much more experimentation is needed.

- (4) If one refers to the total results from sequential triangulation in Table 1, it is worth noting that the results from triangulation by independent triplets is better than almost all of the sequential methods.

CONCLUSIONS

Although only one experiment with simulated data was performed, the results from the triplet method were rather encouraging. Instead of obtaining significantly inferior results, the numbers indicated insignificant differences at least for this test. This is particularly interesting for the base of residual systematic components because it contradicts the hypotheses that the increased number of parameters better accommodates such components. For triplets, the number of parameters was actually reduced drastically.

On the basis of these preliminary results, it is recommended that comparison block triangulations by triplets and pairs be performed on other sets of test data, not only simulated, but also actual project data such as those from Oberschwaben [6].

REFERENCES

- |1| Gyer, M. S., Kenefick, J. F., "Propagation of error in Blocks",
Photogrammetric Engineering, September 1970
- |2| Ackermann, F. "On the Theoretical Accuracy of Planimetric Block Triangulation",
Photogrammetria 21, 1966
- |3| Ebner, H. "The Theoretical Horizontal Accuracy of Adjusted Blocks of
up to 10 000 Independent Models", Translation from Bild-
messung und Luftbildwesen 39, 1971
- |4| Ebner, H. "Theoretical Accuracy Models for Block Triangulation",
Translation from Bildmessung und Luftbildwesen 40, 1972
- |5| Anderson, J. M. and Ramey, E. H., "Analytic Block Adjustment", Photogram-
metric Engineering, October 1973
- |6| Ackermann, F. "Results of Recent Experimental Investigations in Aerial
Triangulation", Proceedings of March 1974 ASP Annual Meeting,
St. Louis, Missouri
- |7| Mikhail, E. M. "Use of Triplets for Analytical Aero-triangulation", Pho-
togrammetric Engineering, September 1962.

Investigation on the applicability of block adjustment
in Austria +)

G. Otepka, Vienna.

1. Introduction

The performed investigation is limited to two problems of the Austrian Federal Bureau of Standards and Surveying (BAfEuV) and conditions which are present in this organisation and in Austria. The two problems mentioned are :

- a) to produce control points for the plotting of Austria in the topographic map "Österreichische Karte (ÖK) 1:50 000"
- b) to intercalate points between the existing Fifth-Order Trigonometric-Network. These points are called "Einschaltpunkte (EP)".

For years the BAfEuV has used photogrammetric methods for both problems. Previously the advantages of block adjustment never had been used though general computer programs are available and a suitable computer exists.

In the first part of this investigation two typical routine projects of the BAfEuV are used for block adjustment to show its efficiency. In the second part, the costs of different methods for solving the two above mentioned problems are compared, methods which are used by the BAfEuV on one hand and block adjustment on the other. The results of these computations and comparisons are reported.

2. Block adjustment

All the blocks have been adjusted by a CDC 6600 computer using the well known program for aerial triangulation with independent models - PAT-M 43 - developed by ACKERMANN, EBNER and KLEIN /2/.

2.1 Block ÖK 161

The Austrian map (ÖK) 1:50 000 consists of 213 map sheets. Sheet number ÖK 161 was chosen for this test. The block adjustment was performed using the same photogrammetric measurements which were the base for the strip adjustment of the BAfEuV. These measurements were carried out on a Wild A 7. All control and tie points are non signalized natural points. The most important technical data of this project are: 6 strips with a total of 55 models, wide angle camera, negative scale 1:20 100 - 31 800, end lap 60 %, side lap 8 - 37 %, block area 530 km², terrain heights 600 - 2 200 m.

The block was adjusted twice: Version a 1 using all existing control points, which have been determined by the BAfEuV for their strip adjustment. This version has no importance for production. It was carried out merely to check the data. Version b 1 uses only 4 planimetric and 16 vertical perimeter control points. This control point pattern is a very economic aerial-triangulation possibility. The weight of the terrestrial and photogrammetric coordinates was assumed to be equal and to be "1" for the adjustment of both versions.

+) outline of a paper /1/ presented to the I.S.P. Commission III, Symposium in Stuttgart, 1974.

2.2 Block EP Rev. Altenfelden

The density of the Austrian Fifth-Order Triangulation-Network is one point on each square kilometer. It is provided by law, that any kind of cadastral surveying has to use the State Coordinate System. The distances between the triangulation stations normally would be too large, therefore a densification of the trigonometric net is necessary. The result of this intercalation is a density of 8 to 10 points on each square kilometer. The control and tie points were targetted before the flight. The photogrammetric measurements were carried out using a Wild STK-1 stereocomparator. To get a dense perimeter controlled block, the original project EP Rev. Altenfelden was enlarged by 8 models of 2 neighbouring EP projects. The most important technical details of this block are: an irregular flight pattern caused by the single model orientation method of the BAfEuV, 105 models, wide angle camera, negative scale 1:6 200 - 10 500, block size 9 x 8 km², terrain heights 335 - 620 m.

The block adjustment was repeated several times with 2 different weights and 4 different control assumptions. The weight assumption of Version b 1 is equal to that of the ÖK blocks (2.1). This weight relation enables a detection of any existing inhomogeneity in the survey controlled stations. Such an assumption is impossible for practical EP projects. Once determined, the coordinates of the trigonometric points and EP's must remain constant. Therefore the weight of the terrain coordinates has to be infinite for the control points. The Versions b 2, c 2, d 2 and e 2 use this mentioned weight.

The different control point density for the adjustment versions is indicated by the letters b, c, d and e. Version b 1 and b 2 use all existing control points. Version c 2 uses all trigonometric points plus a dense terrestrial EP perimeter control. Version d 2 uses all triangulation points plus 8 terrestrial determined EP's at the "open" places of the block perimeter for control purposes. In Version e 2 the triangulation points only are applied for control within the block adjustment. This version is computed only as a necessity for Version \bar{e} 2, which has been derived from e 2 in such a way that the 49 perimeter models were cancelled after the adjustment.

3. Results of the block adjustment

Table 1 shows the results of the different block adjustments of the two projects.

4. Comparison of economy

The comparison of costs shows that block triangulation is about 30 % cheaper than strip adjustment for the ÖK-project of the same size (for further informations see /1/).

At the moment the BAfEuV uses the following 3 methods for the determination of EP's :

- a. trigonometric intersection method
- b. radiation method
- c. single model orientation method.

Block		OK 161		EP Rev. Altenfelden					e 2	
Version		a 1	b 1	b 1	b 2	c 2	d 2	e 2		
planimetric adjustment	number of measurements	1148	954	3078	3078	2996	2924	2896	no proper adjustment; the results are derived from Version e 2 by cancelling the perimeter models	
	number of unknowns	652	602	1468	1468	1460	1436	1424		
	redundancy	496	352	1610	1610	1536	1488	1472		
vertical adjustment	number of measurements	877	786	1970	1970	1929	1893	1893		
	number of unknowns	530	506	1055	1055	1051	1039	1033		
	redundancy	347	280	915	915	878	854	846		
number of planimetric control-points		76	4	127	127	89	65	57		
number of vertical control-points		83	16	126	126	88	64	56		
QMV MPX } QMV MPY } QMV MPZ }	r.m.s.value of residuals at tie points	0,176 m 0,217 0,240	0,163 m 0,193 0,232	0,023 m 0,027 0,044	0,027 m 0,031 0,050	0,026 m 0,029 0,048	0,024 m 0,028 0,047	0,023 m 0,028 0,047		
	QMV PZX } QMV PZY } QMV PZZ }	r.m.s.value of residuals at projection centres	0,503 m 0,632 0,258	0,444 m 0,612 0,242	0,108 m 0,081 0,032	0,109 m 0,081 0,022	0,107 m 0,081 0,023	0,110 m 0,079 0,022		0,111 m 0,079 0,023
		QMV PPX } QMV PPY } QMV PPZ }	r.m.s.value of residuals at control points (terrain coordinates)	0,182 m 0,236 0,190	0,077 m 0,112 0,130	0,026 m 0,023 0,036	- - -	- - -	- - -	- - -
QMV PPP X } QMV PPP Y } QMV PPP Z }			r.m.s.value of residuals at control points (model coordinates)	0,193 m 0,213 0,220	0,077 m 0,112 0,204	0,023 m 0,028 0,043	0,035 m 0,038 0,061	0,036 m 0,036 0,059	0,033 m 0,035 0,056	0,030 m 0,035 0,056
	σ_o of the planimetric adjustment (referred to photo scale)		12 μ m	11 μ m	4 μ m	4 μ m	4 μ m	4 μ m	4 μ m	4 μ m
		σ_o of the vertical adjustment (in‰ of flying altitude above ground)	0,396 m 0,07 ‰	0,404 m 0,07 ‰	0,064 m 0,05 ‰	0,070 m 0,05 ‰	0,069 m 0,05 ‰	0,069 m 0,05 ‰	0,069 m 0,05 ‰	
number of planimetric check-points		-	72	-	-	37	61	69		
number of vertical check-points		-	67	-	-	37	61	69		
\bar{m}_X } \bar{m}_Y } \bar{m}_Z }	= σ check	- - -	1,180 m 0,984 +) 1,104	- - -	- - -	0,041 m 0,042 0,072	0,054 m 0,055 0,091	0,095 m 0,079 0,105	0,044 m 0,045 0,082	
	$\bar{m}_{max.X}$ } $\bar{m}_{max.Y}$ } $\bar{m}_{max.Z}$ }	maximum residuals at the check-points	- - -	3,313 m 1,302 +) 3,318 m	- - -	- - -	0,098 m 0,149 0,221 m	0,188 m 0,142 0,228 m	0,426 m 0,401 0,296 m	0,102 m 0,138 0,222 m
		\bar{m}_X / σ_o \bar{m}_Y / σ_o \bar{m}_Z / σ_o		- - -	4,0 3,3 +) 2,7	- - -	- - -	1,1 1,1 1,0	1,5 1,5 1,5	2,6 2,2 1,5

Table 1

+) = flight direction, ++) = with σ_o of Version e 2, σ_o = standard error of unit weight = accuracy of model coordinates.

Table 1: Results of the different spatial block adjustments.

Figure 1 shows the total costs which are necessary to determine one EP by the 3 methods of the BAfEuV and by block adjustment with two possible photo scales.

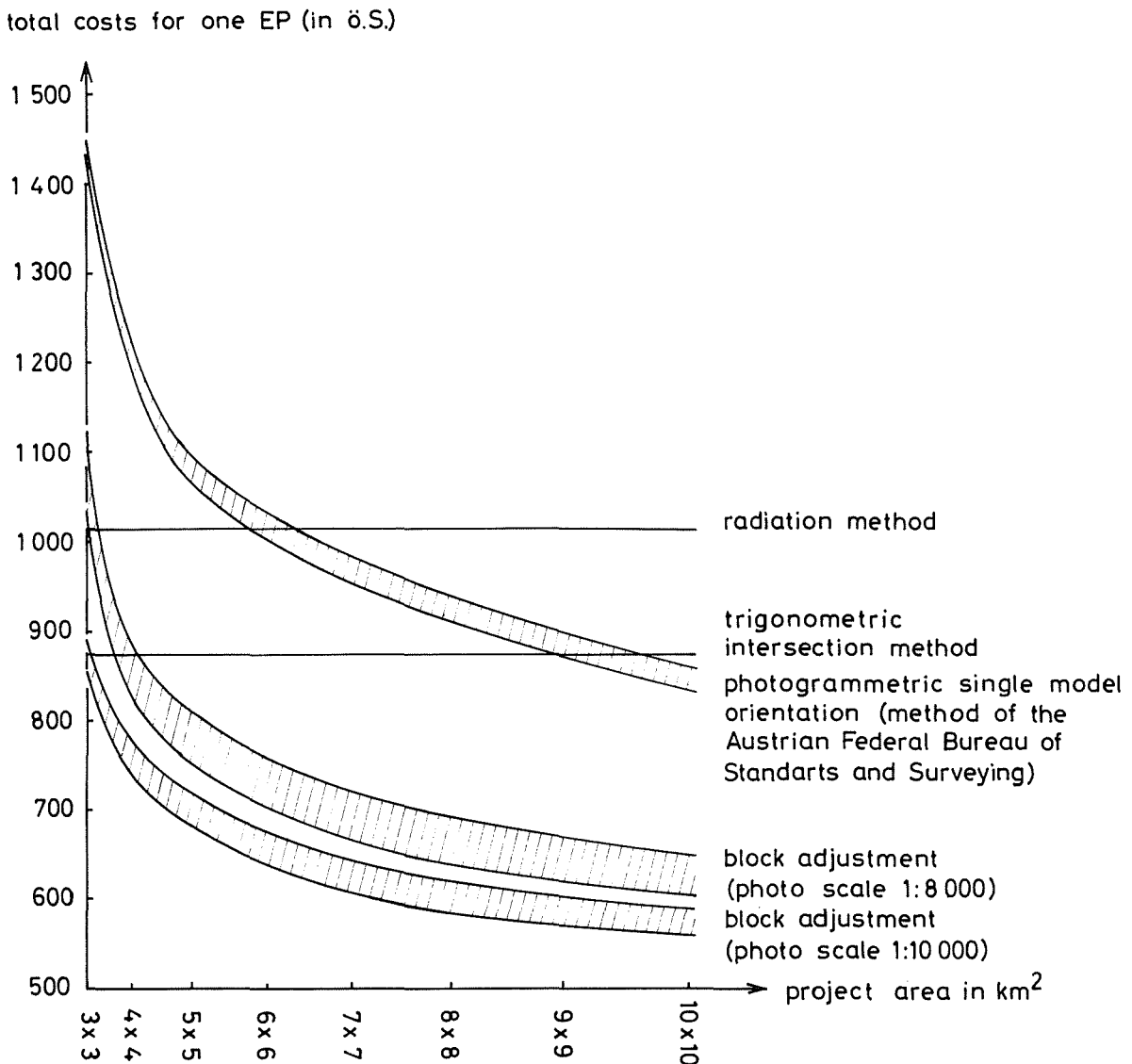


Fig. 1: Total costs of one EP

Summary :

Two problems of the Austrian Federal Bureau of Standards and Surveying are used to investigate the applicability of photogrammetric block adjustment. Using this method different versions of two typical routine projects of this organisation have been adjusted. The results were reported. The last part of the paper shows the expenditure of competitive methods and the superiority of block adjustment for the two investigated problems.

Zusammenfassung :

An Hand zweier Vermessungsaufgaben des Bundesamtes für Eich- und Vermessungswesen (BAfEuV) wird die Einsatzmöglichkeit der photogrammetrischen Blockausgleichung in

Österreich untersucht. Dazu wurden 2 typische Routineoperate dieser Organisation mit verschiedenen Gewichts- und Paßpunktannahmen als Blöcke berechnet und ihre Ergebnisse angegeben. Ein Kostenvergleich mit den konkurrenzierenden Verfahren liefert konkrete Werte für die Überlegenheit der Blockausgleichung.

References

- /1/ OTEPKA G.: Untersuchung über die Einsatzmöglichkeit der Blockausgleichung in Österreich. Paper will be printed in Österreichische Zeitschrift für Vermessungswesen und Photogrammetrie, 63, 1975.
- /2/ ACKERMANN F., EBNER H., KLEIN H.: Ein Programm-Paket für die Aerotriangulation mit unabhängigen Modellen. Bildmessung und Luftbildwesen 38, 218-224, 1970.

ON THE INFLUENCE OF A MINIMUM METRICAL PRECISION THRESHOLD ON ABSOLUTE ACCURACY IN ANALYTICAL AERIAL TRIANGULATION

by H. S. Williams, Johannesburg, South-Africa

ABSTRACT

Metrical requirements of analytical photogrammetry are examined in relation to currently attainable standards of absolute accuracy of digital aerial triangulation. A series of controlled experiments is used in the study involving three test areas and five comparators in different precision classes.

INTRODUCTION

Little has been done in the past to map a minimum precision threshold for analytical photogrammetry. Random and unrelated experiments by T. J. Blachut (1963), P. R. J. Boniface (1967), H. Salmenperä (1970) and H. S. Williams (1973a, 1973b) have shown that single-micron measuring precision of photo coordinates is not essential for accurate point fixation in the terrain by digital aerial triangulation. These experiments, however, shed no light on any minimum metrical criterion. In the present study a series of controlled experiments has been used in an endeavour to find an approximation to this important quantity.

THE CONTROLLED EXPERIMENTS

For present purposes, a "minimum metrical precision threshold" is defined as the lowest measuring precision that can be mapped empirically using a number of comparator apparatuses of different accuracy capabilities for the measurement, or determination, of plate coordinates adequate for digital aerial triangulation to currently attainable standards of absolute accuracy.

Five categories of comparators were used in the controlled investigation. These were:

- 1) a standard comparator, which for all practical purposes could be assumed to be free of the errors normally associated with cartesian comparators;
- 2) a comparison comparator, of similar metrical accuracy to that of the standard comparator, which was used to compare the relative accuracies of stereoscopic and non-stereoscopic measurements;
- 3) plotter-monocomparators of moderate accuracy - stereoplotters which could be used efficiently as monocomparators;
- 4) a crude trilaterative comparator, which was capable of a metrical accuracy nominally lower than that of the class (3) instruments, and
- 5) a plotter-monocomparator of low accuracy, a stereoplotter with a lower measuring accuracy than any of the other comparators.

The Trilateration Microscope (TM), H. S. Williams (1971), was used as the standard comparator. This instrument had a $\sigma_{x,y}$ (standard deviation of a photo-point coordinate) of 0.96 micron. A magnification of 60 times was used with the TM.

A Wild STK 1 stereocomparator was used as the comparison comparator and was confined to an air-conditioned room at all times. The standard deviation of photo-point coordinate for this instrument was 2.8 microns. The STK 1 was fitted with x 20 eyepieces.

Two Wild A7 Autographs, both equipped with x 10 eyepieces, served as the plotter-monocomparators of moderate accuracy.

The TM main scale was used alone as the crude trilaterative comparator. It was fitted with x 10 magnification readers which enabled it to have a measuring accuracy of approximately 30 microns in distances of up to 320 mm.

A Wild A8 Autograph, fitted with x 6 eyepieces, was used as the plotter-mono-comparator of low accuracy. Neither of the Wild A7's nor the Wild A8 were used in a humidity and temperature controlled environment.

The test areas used in the controlled experiments were:

- the AOC Test Area (H. S. Williams, 1971, 1974);
- the St. Faith's Test Area (Urban 1966), and
- the Durban Test Area (H. S. Williams 1974).

A schedule of the measurements made of the diapositives of the various test areas is given in Table I below.

Table I : Schedule of Measurements made of the Test Areas which were used in the Controlled Experiments

Comparator	AOC Models			St. Faith's Test Area	Durban Test Area
	3058/3059	309/310	1/2		
TM	x	x	x1 x2	x3 x5	x4 x5
STK 1	x	x	x	x	x
A7U (i)	x	x	-	x	x
A7U(ii)	-	-	-	x	-
A7R	-	-	-	x	-
A8P	x	-	-	x	-
TMMS	x	x	-	x	-
A7U+CR	-	-	-	x	x
Diapositives	glass/7*	glass/10	film/4	glass/11	glass/3

- x1 - measured in controlled environment
- x2 - measured in uncontrolled environment
- x3 - premarked points and/or transfer points
- x4 - PUG marked transfer points, on the basis of 9 points per diapositive
- x5 - points of natural detail used as transfer points
- TMMS - TM main scale only
- CR - camera reseau
- * - age of diapositive plates in years

Measurement with the three plotter comparators was carried out in single projection planes, that is, once a suitable photo-plane to projection-plane enlargement had been decided on, and pre-set, the foot-disc was taped or otherwise immobilized. No Z-drum readings, therefore, were ever recorded. All rotation and translation orientation elements of the plotter projections were zeroed before any measurements were made. Three mathematical models were used for deriving plate coordinates from the projection plane measurements, namely, (1) central perspective transformation, (2) two-dimensional similarity transformation, and (3) use of the projection plane coordinates themselves, treating the projection plane as a pseudo-photo-plane. In the tables of aerial triangulation results that appear later in the paper, the use of these models is shown by (1), (2) and (3), respectively, after the plotter name, for example, Wild A7U (3), where Wild A7U is the Wild A7 of the University of the Witwatersrand, Johannesburg, and (3) is the third transformation model. Abbreviations used for the other plotters which feature in the investigations are Wild A7R - the Wild A7 of the Roads Department, Pretoria and Wild A8P - a Wild A8 of Photosurveys (Pty) Ltd., Johannesburg. Essentially, models (2) and (3) lead to the same result. By using model (3) the similarity transformation between projection-plane and photo-plane is avoided.

All model restitutions, aerial triangulations and adjustments were carried out with the IBM System 360/50 and 370/145 computers of the University of the Witwatersrand, Johannesburg using the photogrammetric programme set developed by the writer. The Wild STK 1 measured plate coordinates were also processed with the IBM 1140 computer of Aircraft Operating Company (Pty) Ltd. Johannesburg, by courtesy of that Company.

ESTIMATES OF THE INTERNAL ACCURACY CAPABILITIES OF THE COMPARATOR APPARATUSES

Calibration of the five classes of comparators was carried out by means of measurements made of high precision grid plates. Results of the respective calibrations are tabulated in Table II below. These results contain the errors of the reseau plates themselves.

Examples of the internal accuracy capabilities of the TM, TM main scale alone, Wild A7U and Wild A8P are given for the measurement of glass diapositives in Table III below. Estimates of the internal accuracies of the TM measurements of film diapositives in an uncontrolled environment are also included in the Table. The internal accuracies of the TM measurements of film diapositives in a controlled environment compare with those obtainable with glass diapositives in an uncontrolled environment.

Table II : Standard Deviations of Observations of Unit Weight, of Plate Point Position and Maximum Residuals in Plate x and y coordinates (in microns) from Grid Plate Calibrations of the Comparator Apparatuses

Instrument	σ_o	σ_p	$v_x(\text{max})$	$v_y(\text{max})$	n-r	A
TM	1.14	1.36	2.1	1.9	21	1
STKI	2.8	4.0	6	8	26	2
A7U	5.0	7.0	31.5	17.8	238	2
A7R	9.6	13.5	24.7	20.1	14	2
A8P	10.6	15.0	22.3	24.6	128	2
TMMS	8.2	8.4	18.2	16.5	21	1

- (n-r) - number of degrees of freedom of the adjustment
- A - method of computation and adjustment
- 1 - trilateration adjustment using a defect free solution + a linear conformal two-dimensional transformation
- 2 - linear conformal transformation between projection plane and photo-plane

Table III: Precision Estimators for Co-ordination of Photo-Details Using Unconventional Comparator Apparatuses (in microns)

Instrument	σ_o	σ_p	$v_x(\text{max})$	$v_y(\text{max})$	Diapositive
TM	2.6	3.1	3.2	2.8	glass
TM*	4.6	5.1	8.8	7.2	film
TMMS*	7.2	11.5	17.2	19.6	glass
Wild A7U (1)	4.3	6.1	9.2	9.3	glass
Wild A7U (2)	8.3	11.7	15.7	16.2	glass
Wild A7U(2)+CR	11.3	16.0	13.2	13.3	glass
Wild A8P*	12.4	17.5	22.5	25.0	glass

* - precision estimators based on transformations to TM determined plate coordinates

In Tables II and III the following symbols are used:

- σ_o - The standard deviation of the observation of unit weight
- σ_x, σ_y - standard deviations in x and y plate coordinates, respectively
- σ_p - standard deviation in point position, $\sigma_p = \sigma_x^2 + \sigma_y^2$

$v_x(\max)$, $v_y(\max)$ - maximum residuals in x and y coordinates, respectively.

The results summarized in Table III for the Wild A7U are interesting but in themselves are no indication whatsoever of the accuracy that can be achieved in block aerial triangulation using the transformation models (1) and (2). For example, plate coordinates derived via a perspective transformation, that is transformation (1), of the projection plane coordinates will not produce point positions in the terrain that will be twice as accurate as could be obtained with plate coordinates derived through a linear conformal transformation. It will be seen from an examination of the tables of aerial triangulation results for the St. Faith's and Durban Test Areas, namely Tables V and VI, that the three transformation models do, in fact, lead to the same results in the terrain for all practical purposes.

ACCURACIES OBTAINED IN THE DIGITAL AERIAL TRIANGULATION EXPERIMENTS WITH SINGLE MODELS AND BLOCKS

In Table IV, results are given for the single model tests which involve the three models of the AOC test Area. In these tests it was always assumed that the weight matrix reduced to a unit matrix of like order.

Table IV : Results from Tests with Models of the AOC Test Area

Model Comparator	3058/3059							
	TM	TM	STKI	TM Main Scale	TM Main Scale	Wild A7U(3)	Wild A8P(3)	Wild A8P(2)
Computation Method	A	B	A	A	B	A	A	A
$\sigma_{py}(\mu\text{m})$	3.4	-	4.5	7.2	-	6.2	4.7	4.7
$\sigma_H(\mu\text{m})$	15.2	13.5	11.3	14.1	15.9	10.4	13.2	13.2
$\sigma_H(o/oOH)$	0.10	0.09	0.07	0.09	0.10	0.07	0.09	0.09
$\sigma_X(\mu\text{m})$	9.0	9.7	9.8	10.1	11.6	10.2	9.8	9.8
$\sigma_Y(\mu\text{m})$	11.0	8.8	9.7	10.7	10.4	9.8	10.2	10.2
$\sigma_P(\mu\text{m})$	14.6	13.1	14.0	14.7	15.6	14.1	14.2	14.2
$\sigma_o(\mu\text{m})$	3.4	9.3	4.5	7.2	10.6	6.2	4.7	4.7

Model Comparator	309/310				1/2		
	TM	STKI	TMMS	Wild A7U(3)	TMx1	TMx2	STKix1
Computation Method	A	A	A	A	A	A	A
$\sigma_{py}(\mu\text{m})$	7.2	8.6	5.9	3.4	6.2	4.7	4.5
$\sigma_H(\mu\text{m})$	20.7	23.2	16.8	16.8	21.0	19.7	18.3
$\sigma_H(o/oOH)$	0.13	0.15	0.11	0.11	0.13	0.13	0.12
$\sigma_X(\mu\text{m})$	9.4	11.6	11.0	10.4	8.2	10.3	13.1
$\sigma_Y(\mu\text{m})$	13.6	14.6	12.9	9.3	8.2	8.5	9.2
$\sigma_P(\mu\text{m})$	16.5	18.6	16.9	14.0	11.6	13.4	16.6
$\sigma_o(\mu\text{m})$	7.2	8.6	5.9	3.4	6.2	4.7	4.5

- A - relative and absolute orientations
- B - Schmid's Bundle adjustment
- TMMS - TM Main Scale
- TMx1 - measured with the TM in a controlled environment
- TMx2 - measured with the TM in an uncontrolled environment
- STKix1 - measured with the Wild STKI Stereocomparator in a controlled environment

The results of the experimental aerial triangulations which involved the St. Faith's Test Area, and other relevant information, are shown in Table V. Those for the Durban Test Area are shown in Table VI.

Table V : Summary of Experimental Aerial Triangulation Results after Block Adjustment for the St. Faith's Test Area

Comparator	Adjustment	Weights		σ_0	1 P/Z	2 P/Z	3 P/Z	σ_p			σ_z			Pass Pts.	I.D &R
		C/T/P	C/T/P					A	B	C	A	B	C		
TM	Amer (X,Y & Z separate)	1/1/0	1/1/1	4.6	20	6/12	79/9	5.9	6.4	9.8	5.8	7.8	8.8	PM	Yes
TM	Amer (X,Y & Z separate)	1/1/0	4/2/1	4.6	50	6/12	75/12	6.4	6.4	12.3	4.4	7.8	13.4	PM	Yes
TM	Amer (X,Y & Z separate)	3/1/0	3/3/1	5.0	50	6/12	75/12	5.0	7.0	13.4	6.2	7.4	13.4	PM	Yes
TM	Amer (X,Y,Z simultaneous)	4/2/0	4/2/1	7.2	50	6/12	66/6	5.0	10.0	12.6	9.7	6.6	18.8	PM	Yes
TM	Bundle	$w = 1$		6.8	1	6/12	75/12	10.4	-	14.2	11.2	-	23.2	PM	Yes
TM	ANBLOCK x1	1/1/1	1/1/1	4.9	1/3	6/12	75/12	6.4	6.9	15.4	10.0	12.0	20.7	PM	Yes
TM	ANBLOCK x2	1/1/1	1/1/1	4.9	1/3	6/12	75/12	6.4	6.9	13.3	10.0	12.0	26.0	PM	Yes
STK1	ANBLOCK (Plan Only)	1/1/-	-/-/-	8.8	1	111/-	-/-	4.2	12.3	-	-	-	-	PM	Yes
STK1	Amer (X,Y & Z separate)	1/1/0	4/2/1	7.6	50	6/12	75/10	9.8	10.6	13.1	3.2	8.4	16.6	PM	Yes
TM Scale Only	Bundle	$w = 1$		9.9	1	6/12	79/12	12.2	-	15.7	10.2	-	28.4	PM	No
Wild A7U (2)+ CR	Amer (X,Y & Z separate)	1/1/0	4/2/1	3.6	20	6/12	67/9	5.1	7.4	10.2	11.0	13.0	32.5	PM	No
Wild A7U (3)	Amer (X,Y & Z separate)	1/1/0	4/2/1	4.8	20	6/12	67/9	6.8	8.8	13.3	11.0	15.0	13.6	PM	No
Wild A7R (2)	Amer (X,Y & Z separate)	1/1/0	4/2/1	4.7	20	6/12	85/12	5.7	7.4	15.7	9.3	11.7	17.1	PM	No
Wild A7U (2)	Amer (X,Y & Z separate)	1/1/0	4/2/1	5.0	20	6/12	67/9	6.2	7.9	14.2	10.4	14.2	15.1	PM	No
Wild A8P (3)	Amer (X,Y & Z separate)	1/1/0	4/2/1	5.7	20	6/12	67/9	5.9	9.7	14.1	9.8	13.2	16.2	PM	No
TM	Amer (X,Y & Z separate)	1/1/0	4/2/1	6.2	15	6/11	75/8	8.7	9.8	15.3	6.8	10.2	20.4	ND	No
TM	Bundle	$w = 1$		7.5	2	6/11	75/8	13.4	-	15.7	19.0	-	23.6	ND	No
TM	ANBLOCK x2	1/1/1	1/1/1	6.5	1/1	6/11	75/8	9.2	7.9	16.9	9.8	12.4	24.2	ND	No

- x1 - ANBLOCK adjustment with three-dimensional transformation after each iteration of the height adjustment phase
- x2 - ANBLOCK adjustment without three-dimensional transformation after each iteration of the height adjustment phase
- C/T/P - control points/tie points/perspective centres
- 1 - number of iterations used in the adjustment
- 2 - number of control points
- 3 - number of check points
- P/Z - planimetry/height
- A - control points
- B - tie points
- C - check points
- LD&R - Was lens distortion and refraction corrected for?
- PM - pre-marked points used as model pass points
- ND - natural points of detail used as model pass points
- CR - camera reseau
- (1) - perspective transformation carried out between plotter projection plane measurement and photo-plane
- (2) - two-dimensional linear conformal transformation carried out between projection plane and photo-plane
- (3) - projection plane measurements used as pseudo-photo-plane coordinates

Table VI : Summary of Experimental Aerial Triangulation Results after Block Adjustment for the Durban Test Area

Comparator	Adjustment	Weights		σ_o	1	2	3	σ_p			σ_z			Pass Pts.	LD & R
		Plan.	Height					A	B	C	A	B	C		
		C/T/P	C/T/P												
TM	Amer (X, Y & Z separate)	1/1/0	1/1/1	7.6	30	11/14	26/23	10.7	11.8	23.0	3.6	7.8	23.8	AT	Yes
TM	Amer (X, Y & Z separate)	1/1/0	4/2/1	8.0	80	36/36	-/-	12.0	12.0	-	9.1	15.8	-	AT	Yes
TM	Amer (X, Y & Z separate)	1/1/0	3/3/1	6.2	20	10/13	26/23	8.7	8.7	19.3	5.0	13.8	27.5	AT	Yes
TM	Bundle	$w = 1$		8.4	1	10/13	26/23	10.5	-	22.8	13.8	-	21.3	AT	Yes
TM	ANBLOCK x2	1/1/1	1/1/1	6.7	1/1	10/13	26/23	9.4	6.4	19.8	8.4	16.9	26.3	AT	Yes
STK1	Amer (X, Y & Z separate)	2/1/0	3/1/1	4.5	50	6/34	15/36	5.0	6.3	23.7	5.0	7.4	17.5	AT +S	Yes
Wild A7 U(3)	Amer (X, Y & Z separate)	1/1/0	4/2/1	7.3	30	11/14	26/22	10.3	11.0	24.7	3.5	12.0	20.0	AT	No
Wild A7 U(2) + CR	Amer (X, Y & Z separate)	1/1/0	4/2/1	7.1	20	11/14	26/22	8.5	9.9	20.3	5.4	9.6	28.0	AT	No
Wild A7 U(1)	Amer (X, Y & Z separate)	1/1/0	4/2/1	7.1	30	11/14	26/22	9.8	11.2	23.6	4.2	11.0	18.7	AT	No
TM	Amer (X, Y & Z separate)	1/1/0	4/2/1	7.2	10	10/13	27/24	10.1	8.3	14.4	4.0	8.3	25.1	ND	No
TM	Bundle	$w = 1$		6.7	1	10/13	27/24	9.9	-	16.9	16.6	-	29.8	ND	No
TM	ANBLOCK x2	1/1/1	1/1/1	7.5	1/1	10/13	27/24	10.6	6.3	19.0	8.8	9.7	21.8	ND	No

- PM+S - pre-marked points used as model pass points + stereo-measurement
 - AT - artificial marks used as model pass points, that is, artificial transfer points were marked on every diapositive
 - AT+S - pass points between models PUG-marked for stereo-measurement
- See footnotes to Table V as well.

The following precision criteria, expressed in microns in the photo-plane, are used to describe the results obtained in the various single model tests:

- | <u>Notation</u> | <u>Meaning</u> |
|-----------------------|--|
| σ_{py} | Standard deviation in y-parallax calculated with (n-5) degrees of freedom, where n is the number of points used in the adjustment solution of the model's relative orientation |
| $\sigma_z = \sigma_H$ | Standard deviation in height calculated with (n-3) degrees of freedom following the absolute orientation of the model, where n is the number of points known in Z used in the absolute orientation |
| σ_x, σ_y | Standard deviation in X and Y, respectively, each determined with (n-2) degrees of freedom, where n is the number of points with X, Y coordinates used in the absolute orientation |
| σ_p | Standard deviation in planimetry calculated from $\sigma_p^2 = \sigma_x^2 + \sigma_y^2$ |

The following precision criteria, expressed in microns in the photo-plane, are used to describe the results obtained in the aerial triangulation experiments of the St. Faith's and Durban Test Areas:

- | <u>Notation</u> | <u>Meaning</u> |
|------------------------|--|
| σ_o | Standard deviation of the observation of unit weight, for example, that for an x or y plate coordinate in the Schmid Bundle Adjustment |
| $\sigma_p(\text{tie})$ | Standard deviations in planimetry and height, respectively, calculated at tie points. Estimators which apply to the Amer and ANBLOCK adjustment procedures |
| $\sigma_z(\text{tie})$ | |

<u>Notation</u>	<u>Meaning</u>
$\sigma_p(\text{control})$ $\sigma_z(\text{control})$	Standard deviations in planimetry and height, respectively, calculated at control points only. This estimator is applicable to all block adjustment procedures
$\sigma_p(\text{check})$ $\sigma_z(\text{check})$	Standard deviations in planimetry and height, respectively, calculated with (n-1) degrees of freedom at check points only, that is, at points not used in the block adjustment as control.

The estimator σ_0 used in the triangulation adjustment processes is the reference standard deviation and is generally different for each adjustment method. It may, for example, be the standard deviation of a y-parallax, a model coordinate or a plate coordinate depending on which of these quantities was considered to be the observation at the parametric adjustment stage. σ_0 used exclusively as an accuracy criterion for judging the performances of different block adjustment methods would therefore be unsatisfactory.

SOME COMPARISONS WITH PREVIOUS EXPERIMENTS WITH UNCONVENTIONAL COMPARATOR APPARATUSES

Before any conclusions are drawn from the experiments of the present study it is appropriate that some of the significant findings of previous investigations should be emphasised.

Comparison between the results of experiments 4 and 6 of Table VI and experiment 10 of the same Table shows that, for all practical purposes, aerial triangulation using mono-measurement and artificial transfer points or small points of natural detail as transfer points produces the same order of absolute accuracy in the terrain as aerial triangulation based on stereo-measurement. These experiments extend the conclusions of T. J. Blachut (1963) for single models to blocks.

Experiments 11 to 14, inclusive, of Table V and experiments 7 and 9 of Table VI show that aerial triangulation absolute accuracies after block adjustment using the Wild A7 as a monocomparator compare very well with the absolute accuracies obtainable with single-micron reading mono- or stereocomparators. These experiments extend the results obtained by H. Salmenperä (1970).

It is apparent from the writer's experiment Wild A8P(3) that the precision plotter is quite capable of attaining the absolute accuracy performance of the single micron reading comparators in block adjusted digital aerial triangulation. The uncertainty raised by Boniface's (1967), experiment with the St. Faith's Test Area using a Thompson Watts (Model 2) plotter with "reseau plate holders" as a stereo-comparator is now removed.

Experiments 11 and 16 in Table V confirm the 5 microns of difference between the check standard deviations in planimetry obtained by Boniface (1967) and Eden (1967), in their experiments with the St. Faith's Test Area. In passing, the 10.2 micron result of experiment 11 which was based on a sample of 67 check points confirms Boniface's small sample result and supports F. Ackermann's contention concerning the minimum number of check points needed for obtaining a reliable estimate of absolute accuracy from block adjustment (Ackermann 1973).

The experiments summarized in Tables V and VI confirm that the stereocomparator enjoys no accuracy advantage over the monocomparator when premarked or points of natural detail are used as transfer points. Even when artificial transfer points are used the absolute accuracies in the terrain are comparable for all practical purposes.

Some small improvement in the absolute accuracies in planimetry was possible using the camera reseau (as distinct from the overlaid reseau) in conjunction with the Wild A7 of the University of the Witwatersrand, Johannesburg, for both the St. Faith's and Durban Test Areas. However, some deterioration in absolute accuracy in height was experienced.

It is significant that even with the two small blocks that have featured in the tests summarized in this paper that check standard deviations in both planimetry and height using the Bundle adjustment have been inferior to those obtained with the iterative Amer adjustment. Ackermann (1973) comments on this interesting phenomenon as well.

Previous attempts to introduce the universal and precision stereoplotters into analytical aerial triangulation practice as stereocomparators (cf. Boniface 1967) have not been very successful, primarily because these instruments are too tedious to use in this way, or even more so if they are used with the overlaid reseau. It has become evident during the writer's investigations that the stereoplotter is best used as a monocomparator in analytical aerial triangulation. When used in this way the diapositive through-put rate is very high, operators without any previous photogrammetric experience can be used and, as has been demonstrated by the results of this integrated series of experiments there is no loss of absolute accuracy.

CONCLUSIONS

In the previous Section of this paper while making a number of comments on past experience with unconventional comparator apparatuses in analytical aerial triangulation it has been opportune to record many of the conclusions that can be drawn from the writer's studies. No attempt has been made to draw all possible conclusions from these studies however.

Since it is shown in Tables IV, V and VI that aerial triangulations using the five classes of comparator apparatuses all lead to the same orders of absolute accuracy for the three test areas involved the worst precision estimator recorded in Table II is, in fact, an adequate estimate of "a minimum metrical precision threshold" for analytical aerial triangulation purposes. This conclusion may be summarized as follows: Any comparator apparatus which is capable of determining x and y plate coordinates with a standard deviation of 11 microns and maximum residuals in x and y of approximately 25 microns may be used with confidence in analytical aerial triangulation. The standard deviation of 11 microns corresponds to one of approximately 15 microns in point position.

Using the TM main scale alone as a crude comparator it is possible to produce plate coordinates with a standard deviation of 8 microns and maximum residuals in x and y of the order of 15 microns.

There appears to be no practical advantage to be gained by using a central perspective transformation between the projection and photo-planes of the plotter-comparators as the absolute accuracies of the Wild A7U(1) and Wild A7U(3) tests with the Durban Test Area agree almost exactly. This is a very important conclusion because if it is not necessary to use the central perspective transformation mapping of the plotter perspective centres ceases to be of much interest.

Finally, it is possible that had a sixth class of comparators been used in the writer's investigations, which had a measuring accuracy lower than that of the class (5) comparator, it might still have been feasible to match the absolute accuracy performance of the TM in digital aerial triangulation.

REFERENCES

- Ackermann, F.: "Results of controlled strip and block adjustment", S.A. Journal of Photogrammetry 5,1, p. 3 - 21
1973
- Blachut, T. J.: "Monomeasurements in photogrammetric operations", paper No 49, Proc. Comm. Survey Officers' Conf. 1963, p. 213 - 218
1963
- Boniface, P.R.J.: "The use of the reseau for analytical photogrammetry", Ph. D. thesis, University College, London
1967
- Eden, J. A.: "A new fast working approach to analytical photogrammetry" Photogrammetric Record V,3, p. 474-491
1967
- Salmenperä, H.: "Use of the Wild A7 in measuring image coordinates for analytical aerotriangulation", Phot. Journal of Finland 4,1, p.10-14
1970
- Urban, V. F.: "The St. Faith's Photogrammetric Experiments", Tech.Pub.No. 4 Department of the Surveyor General, Rhodesia
1966
- Williams, H. S.: "Analytical aerial triangulation by trilateration microscope" S.A.Jour. Of Photogrammetry 3,5, p. 351-368
1971
- Williams, H. S.: "A new method for the use of universal stereoplotters in analytical photogrammetry", S.A. Survey Jour. XVI,1, p.16 - 32
1973a
- Williams, H. S.: "Further thoughts about the use of plotters as monocomparators" S.A. Survey Jour. XIV,2,83, p. 48-49
1973b
- Williams, H.S.: "A controlled investigation of the metrical requirements and practical accuracies of analytical photogrammetry", Ph.D.thesis University of the Witwatersrand, Johannesburg
1974

SYSTEMATIC COMPARATOR ERRORS - MATHEMATICAL DESCRIPTION AND INFLUENCE ON BLOCK TRIANGULATION

by R.-P. Mark, Jena, GDR

SYSTEMATIC COMPARATOR ERRORS

Systematic errors influencing the results of block triangulations also include the systematic errors of the comparators which provide the basic data for the calculations, the image coordinates.

Measuring instruments of any types are physical implementations of a theoretical principle, but in no case can the mechanical, optical and electrical components contained in the measuring instruments be produced completely free of errors. The sum of their errors falsifies the measuring result both accidentally and systematically. This depends on the constructional principle as well as the function, a component has in the practical realization of the theoretical principle.

In the practice of instrument manufacture experience has shown that for the investigation of systematic errors of comparators it will suffice to concentrate upon the scale errors of the spindles, glass scales and the like and the positional errors of guides (orthogonality, parallelism). Generally, these errors are smaller than $2.5 \cdot 10^{-5}$. This means that for a length of 200 mm a scale error of no more than 5 μm and an error of orthogonality of 15'' will occur. Any other systematic errors can be neglected due to their small amounts.

A prerequisite for the investigation of the influence of systematic comparator errors is the derivation of a mathematical functional model for each instrument type.

The way of procedure shall be exemplified for the Stecometer from Jena. In its design the Stecometer is based on the Pulfrich comparator principle, i.e. coordinates and parallaxes are measured. The necessary movements are performed by the photo carriers (x' , p_x and p_y) and the optics (y''), Fig. 1. With a coordinate system parallel to the y guide the following positional errors on guides are possible:

left x guide ($\alpha_{x'}$), right x guide ($\alpha_{x''}$), p_x guide (α_{p_x}), p_y guide (α_{p_y}).

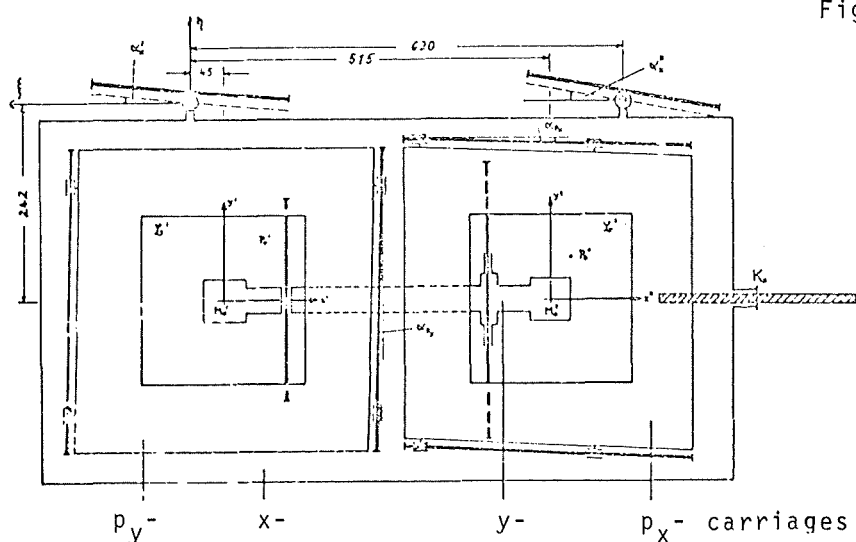


Fig.1: coordinate system of Stecometer

Motion equations are derived for the moveable carriages in the Stecometer. The coincidence of the measuring marks with the homologous image points (measuring procedure) is described as coincidence of the carriage motions in the different directions. The transfer of the carriage motion to the spindles and the consideration of their errors lead to the measured image coordinates as a function of the introduced instrument errors.

For the Stecometer the application of this principle led to the following equations:

$$\begin{aligned} x'_m &= x' - x' dm_x && - p_y \alpha_{py} \\ y''_m &= y'' - y'' dm_y + x' \frac{105 \alpha_{x'} + 515 \alpha_{x''}}{620} - p_x \alpha_{px} \\ p_{xm} &= p_x - p_x dm_{px} && - p_y \alpha_{py} \\ p_{ym} &= p_y - p_y dm_{py} + x' \frac{470(\alpha_{x'} - \alpha_{x''})}{620} + p_x \alpha_{px} \end{aligned}$$

In these relations quadratic terms with maximum values of 0.4 μm were neglected.

If image coordinates are used in the triangulation technique, then also the influence of the measuring procedure has additionally to be considered, because on the Stecometer measurements are exclusively made with "common area inward". This fact involves the great advantage, that the same mathematical model applies for all photographs of a strip, except for the first and the last.

CORRECTION OF IMAGE ERRORS

It is common practice in analytical restitutions to make corrections of image errors in order to eliminate systematic errors of the photographic material. The mathematical statement always includes also terms which at the same time cover the instrumental errors. Good results of a correction of image errors can be expected when using at least 8 fiducial marks. Even more favourable preconditions for the correction of image errors are offered by the marginal glass scales (external reseau) provided in the photogrammetric cameras from Jena. With these glass scales systematic image errors can be determined just as well as with a complete reseau, with the added advantage of avoiding all drawbacks of the reseau.

From an affine transformation

$$\begin{aligned} x'_{mk} &= x'_m + a_1 + a_2 x'_m + a_3 y'_m + a_4 x'_m y'_m \\ y'_{mk} &= y'_m + b_1 + b_2 x'_m + b_3 y'_m + b_4 x'_m y'_m \end{aligned}$$

(neglecting those terms which do not exceed a maximum amount of 0.5 μm) it follows for the Stecometer that only terms depending on p_x are not covered by the given polynomial. However, these terms are constant practically over the entire image and thus give rise only to an error of the origin.

SYSTEMATIC ERRORS IN BLOCK TRIANGULATION

The influence of the systematic comparator errors was investigated both theoretically and by practical examples. For the theoretical investigation the bundle method was used in the form of the block triangulation with single photographs suggested by ALBERTZ. For practical work the convergence properties of this iterative procedure are not particularly favourable. It is, however, very well suited for a theoretical investigation, because it results in an alternating computation of space resections and space intersections. The normal equation systems for these two tasks can easily be solved. In view of the minuteness of the systematic errors a sufficiently clear picture of the effects of the systematic errors can be obtained by an iteration. For a side overlap of less than 50 % and an ideal position of points there exist, as is apparent from Fig. 2 and 3, three types of resections and 20 types of intersections caused by the fact that each point is imaged in a different number of photographs, for which apply different types of resection.

The following conclusions may be drawn from the investigations:

A) GENERAL

- Plane coordinate errors are proportional to the base, height errors to the flying height.
- Errors are caused by affinity errors ($dm_x - dm_y$, $dm_{px} - dm_{py}$) and errors of orthogonality or parallelism. The amount of the scale errors has no influence on the size of the point coordinate errors.

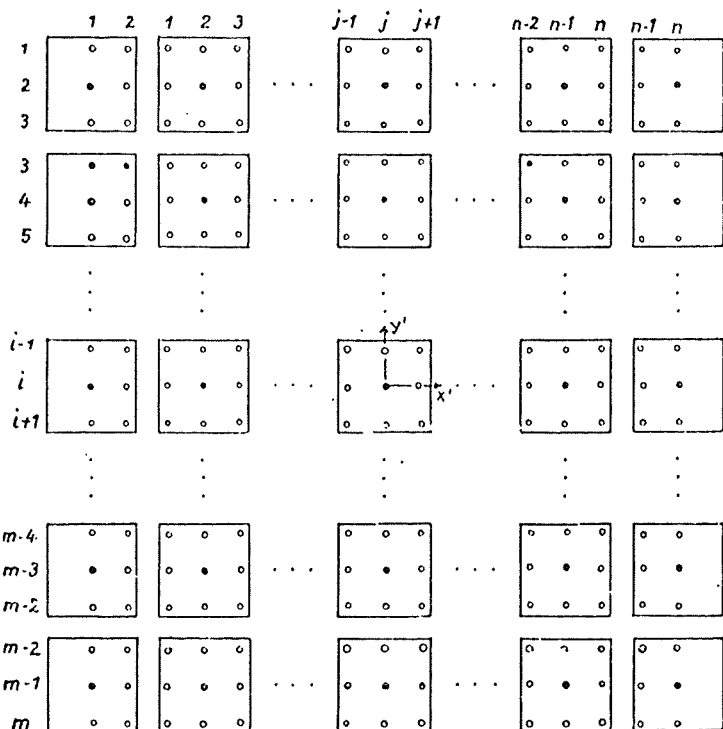


Fig. 2: images on block triangulation

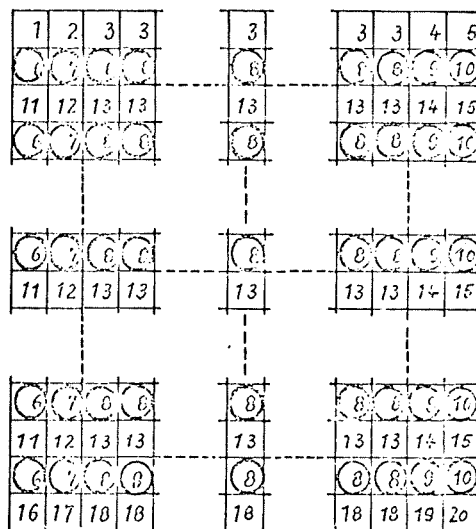


Fig. 3: intersections on block triangulation

B) PLANE COORDINATE ERRORS

- The systematic Stecometer errors practically affect only the block edges.
- In the y-direction a periodicity of the x and y errors is found at the block edge, which is attributed to the number of the rays taking part in the intersection (4 rays in the area of the side overlap, 2 rays outside this area).

C) HEIGHT ERRORS

- The affinity errors of the comparators have consequences within the whole block the errors of orthogonality and parallelism only at the block edges.

The following two paragraphs merely refer to the height errors caused by affinity errors:

- In the y-direction a periodicity of the height errors is found, which is attributed to the number of the rays taking part in the intersection (4 or 6 rays in the area of side overlap, 2 or 3 rays outside this area).
- In the x-direction a warping is found at the block edge, which is attributed to the rays taking part in resection (6 rays in the outer photos, 9 in the inner photos).

To corroborate the conclusive force of the theoretical investigations a practical example was calculated, for comparison, on the basis of the same block triangulation technique. The block was calculated without control points (Fig. 6), with 4 control points (Fig. 7) and with 8 control points (Fig. 8).

It becomes apparent that the effect of the systematic errors is correctly described in their typical behaviour. The amount deviates by about 30 % especially at the block edge, which is attributable to the iterative character of the technique.

From the error illustrations with 4 and 8 control points we can see without exception that the control points have predominantly a local effect. In all remaining points the errors are only slightly affected, partly reduced but partly also increased. Thus, even when there is a great density of control points at the block edges it cannot be expected that the errors in the block interior will disappear.

The investigations have shown that the bundle adjustment is not in the position to suppress the influence of systematic comparator errors. One has of course to bear in mind that only small amounts are concerned in the case of the systematic errors of the Stecometer, whose influence is scarcely traceable in practice. On the other hand, however, it cannot be expected that other systematic errors will basically behave differently than the discussed comparator errors. Therefore, it is justified to draw the conclusion that for the bundle adjustment systematic errors can only be eliminated, when proper measures are taken against them at their places of origin (e.g. by adjustment with additional parameters).

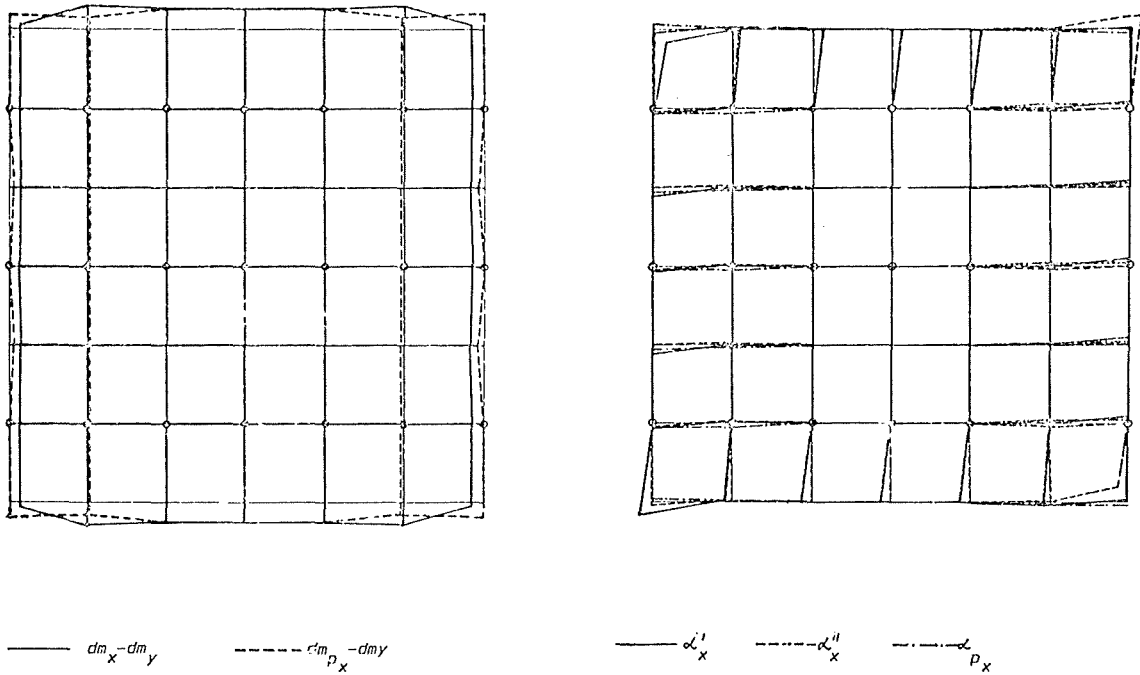


Fig. 4: Planimetric errors issued from systematic Stecometer errors

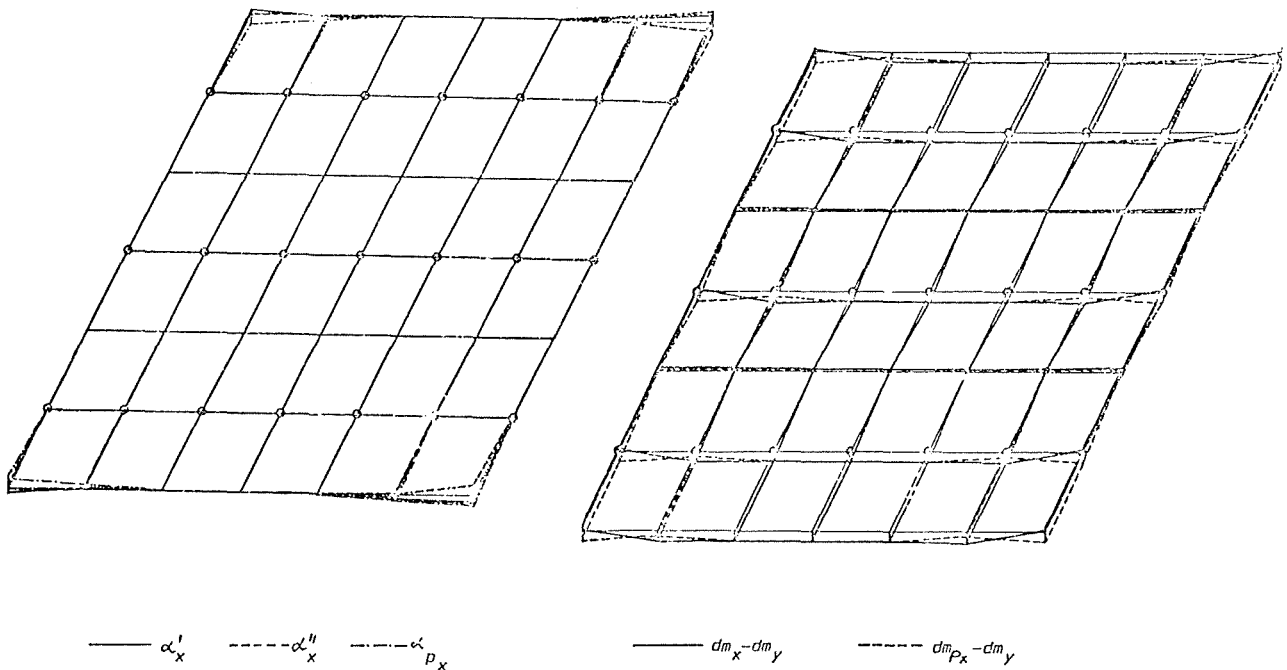
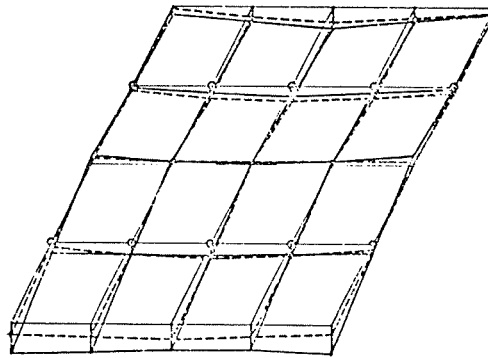
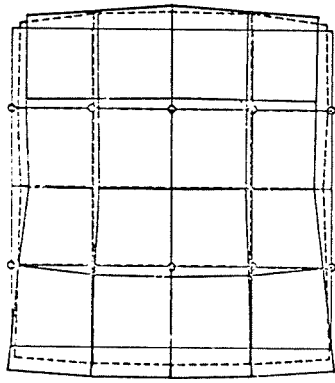


Fig. 5: Height errors issued from systematic Stecometer errors

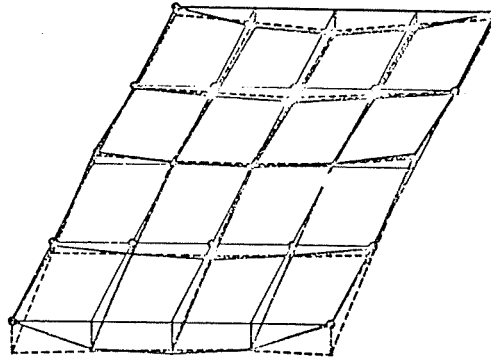
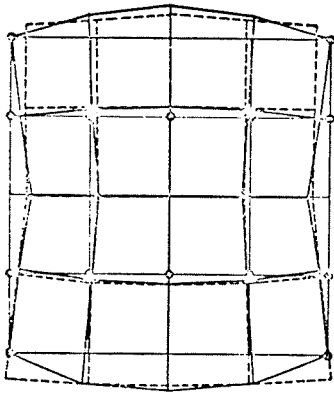


planimetric errors

height errors

— practical results - - - - - theoretical results o projection centre

Fig. 6: Influence of systematical Stecometer errors on point coordinates comparison of a theoretical example with a practical triangulation

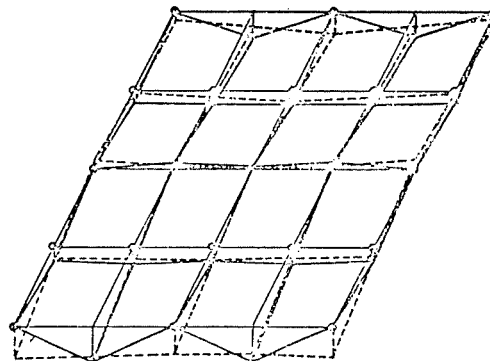
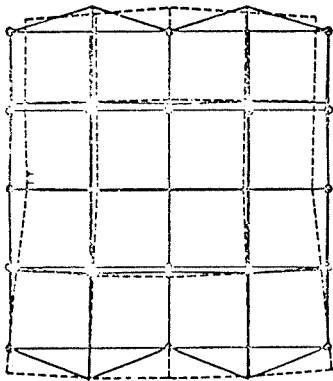


planimetric errors

height errors

— triangulation with 4 pass points - - - - - triangulation with- o projection centre
out pass points ● pass points
from Fig. 6

Fig. 7: Influence of systematical Stecometer errors on point coordinates by use of 4 pass points



planimetric errors

height errors

— triangulation with 8 pass points - - - - - triangulation with- o projection centre
out pass points ● pass points
from Fig. 6

Fig. 8: Influence of systematical Stecometer errors on point coordinates by use of 8 pass points Mark 5

PHOTOGRAMMETRIC DENSIFICATION OF TRIGONOMETRIC NETWORKS THE PROJECT APPENWEIER

by F. Ackermann, Stuttgart, Fed.Rep, Germany

1. Introduction

Photogrammetric point determination has reached a level of accuracy, which makes practical application to geodetic problems feasible. In particular photogrammetric determination of low order trigonometric nets or of traverse nets seems possible, meeting accuracy and economy requirements.

Theoretical basis is the property of aerial triangulation, repeatedly confirmed, that fairly well controlled blocks of moderate size reach planimetric coordinate accuracies of around 10 μ m or better, referred to photo-scale, provided the points are well signalized. This accuracy-figure is valid for photo scales up to about 1 : 2000, and is very little dependent on block-size. Thus, the accuracy of points, referred to the terrain, depends mainly on photo-scale and on the signalisation of points. It depends, to a lesser degree, also on distribution and density of planimetric ground control.

The inherent accuracy of conventional photogrammetric block triangulation has been sufficiently established. It is being considerably increased by the application of additional parameters for systematic image- or model-deformation. Nevertheless, it is advisable, to confirm by controlled tests, that the high accuracy requirements of geodesists can be met in practice. Such tests give, in addition, experience about circumstantial conditions, such as signalisation, photo-scales, and ground control.

2. The pilot project "Appenweier"

2.1 The state survey authorities of the state of Baden-Württemberg have decided in 1973 to try the applicability of the photogrammetric method for the densification of an existing trigonometric net of 3rd order into 4th order. The photogrammetric part of the test was handled by the Photogrammetric Institute of Stuttgart University. The test area Appenweier (in Badenia) covers 9.1 x 10.4 km². In it 24 targetted trigonometric points of 3rd and 2nd order are given (some of them targetted excentrically by subsidiary points), see fig. 1. 85 rather evenly distributed points were to be determined. They are check points for the test, their known terrestrial coordinates being withheld. The accuracy of the terrestrial coordinates is supposed to be about 1 cm, direct confirmation is lacking, however.

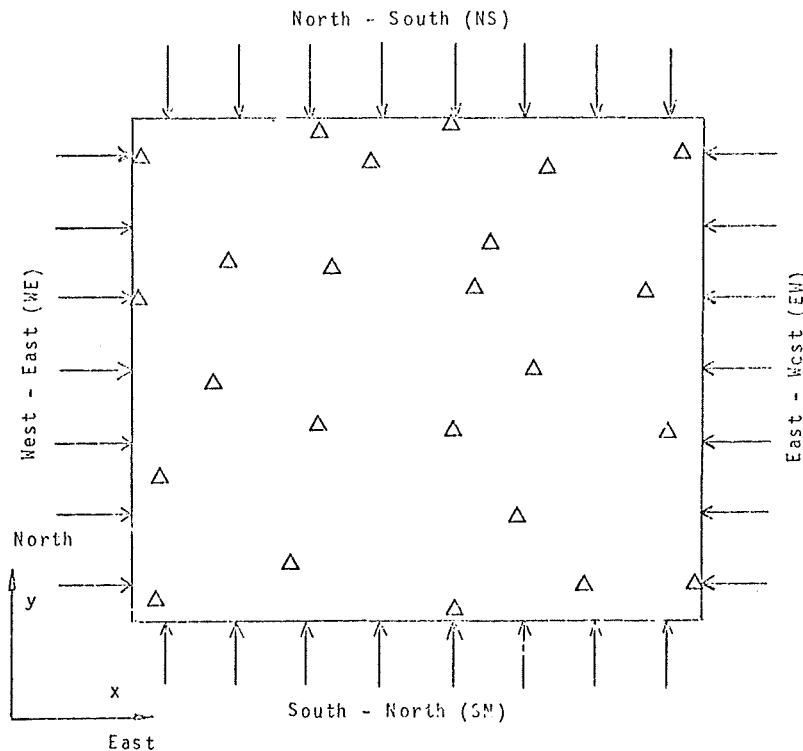


FIGURE 1
Appenweier
flight plan and
planimetric control

The planning of the project aimed at a resultant planimetric coordinate accuracy of 3 cm in the terrain, which implies a photo-scale of about 1 : 3000 to 1 : 4000 equivalent to a required accuracy of 10 μm to 7.5 μm at photo-scale.

Because of expected difficulties with point transfer in very large photo-scales, the photo-scale of 1 : 7800 was applied, instead, with 4-fold flying, in 4 directions, see fig. 1. 4-fold photo-overlap, with simultaneous block-adjustment, is expected to improve accuracy by at least a factor of 2, compared with single coverage at the same scale. The 4-fold overlap of 1 : 7800 scale gave altogether 448 models, which is about the same number of models as the single coverage of photo-scale 1 : 4000 would have implied.

All 24 control- and 85 check-points were targetted, by 20 cm x 20 cm size signals, 35 of them by excentric subsidiary points. Each of the points had attached 2 or 4 auxiliary points, also targetted, forming a straight line or a cross, according to fig. 2. They are to ascertain (and adjust) the position of the signals by straight-line and distance conditions. In addition, for special test purposes, all standard tie-points (6 per model) were targetted with triple signals each. It was to be investigated how transfer of natural and/or artificial tie-points would compare with ideally targetted points.

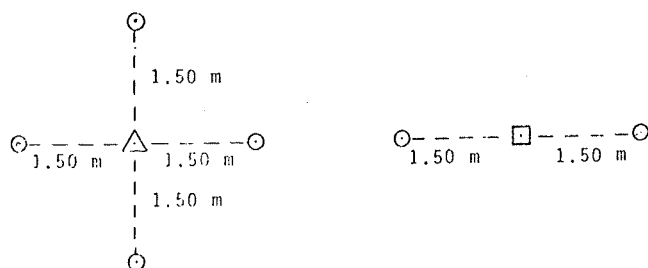


FIGURE 2
Auxiliary signals, for
straight line- and
distance-conditions

The Appenweier test has been set up to investigate the accuracy performance of the photogrammetric method. According to experience the accuracy and the economy of a method cannot be tested jointly. Therefore, optimization of economy will have to be studied seperately, once the accuracy capability is established.

Aerial photography was taken in two missions on April 24th and May 12th, 1973, with the Zeiss RMK A 15/23 wide-angle camera, by Rheinische Braunkohle AG. The first flight mission was discontinued due to turbulence. Due to bad weather conditions the targets in the field had to be maintained for about 2 months, which caused some difficulties.

2.2 The film-diaositives of the aerial photographs were measured with the Zeiss Stereocomparator PSK. Each photograph was measured twice. Some photographs showed noticeably blurred signals due to image movement. The standard measuring accuracy of the mean of the double plate-coordinate-measurements, was established from all recordings to be about 1.5 μm . The total measuring time amounted to about 600 h (for 448 models, double measurements of about 20 points/model and 4 fiducials per plate).

The machine coordinates were transformed into the image coordinates via the fiducial marks by applying similarity transformation ¹⁾. After correction of image coordinates for lens distortion ²⁾, earth curvature, and refraction independent models were computed by analytical relative orientation. The average residual y-parallax of about 4.5 μm confirms the good overall quality of the material.

- 1) A first attempt with affine transformation was abandoned. Presumably due to disagreement between calibrated and actual fiducial marks the resulting block still showed overall affinity. Block-accuracy results turned out to be slightly inferior to the ones based on similarity transformation.
- 2) According to the procedure of double linear sector interpolation, described by K. Kraus and E. Stark in "Flächenhafte Verzeichnungskorrektur in der numerischen Photogrammetrie", Bildmessung und Luftbildwesen 2/1973, 50 ... 56.

The computed model-coordinates formed the input for the block-adjustment by the method of independent models.

3. Block-Adjustments

3.1 The data allowed several investigations with regard to different points of view. Several series of adjustments were performed. Here only the results concerning planimetry are reported. The adjustments can be classified according to 3 main features :

- Control: Version 1, utilizing all given control points (perimeter point + 8 points inside the block); Version 2, dense perimeter-control (omitting the control points inside the block and adding a few perimeter points in order to avoid large spacings).
- Combined adjustment of the 4-fold block; adjustment of the 2 double blocks of crossing flight directions; separate adjustment of the 4 single blocks, labeled according to their flight directions (EW - WE - NS - SN, see Fig. 1).
- Post treatment of the adjusted blocks by the method of least squares interpolation.

Remark: The adjustments used up to 30 control points, as some of the 24 given points had subsidiary signals close by which were also treated as control points. Some additional investigations have not been completed, as yet, concerning height accuracy, point transfer, adjustment of auxiliary points (by the additional conditions implied), bundle adjustment, systematic errors, and adjustment with additional parameters.

3.2 Presentation of results

The test results of the various block-adjustments are summarized in tables 1 + 2. The accuracy figures are given in cm and in μm . They refer to the 3 main series of computation: (1) single, double and 4-fold overlap; (2) area-distributed control and perimeter control ; (3) standard block-adjustment and additional least squares interpolation¹⁾.

4. Evaluation of the results ; comments

4.1 Four-fold overlap

The first comment should refer to the actual case on test, the 4-fold block, with the given control, table 1.

The resulting planimetric coordinate accuracy figures are

$$\begin{aligned}\mu_{xy} &= 3,5 \text{ cm} = 4,5 \mu\text{m} \text{ after block adjustment} \\ \mu_{xy} &= 2,7 \text{ cm} = 3,4 \mu\text{m} \text{ after least squares interpolation.}\end{aligned}$$

Such results are, generally speaking, highly satisfactory and meet the planning specifications. of 3 cm.

The vector diagrams of residual errors at the check points are not presented in this paper. They show the familiar trend effects within local areas. 4 such areas of high correlation of residuals can be distinguished, each extending over about 1/4 of the block area. By the least squares interpolation the local systematic trends have been considerably reduced. They are, however, still discernible. Thus there are still some systematic error effects left uncompensated.

The magnitudes of the maximum residual coordinate errors of 10.6 cm and 9.4 cm, respectively, are in general agreement with expectation. The large errors have some relationship with the trendfields of the vectors. Nevertheless, they occur in first instance independently, sometimes rather close to control points. Most likely they are caused by disturbed signals. It remains to be seen whether the additional adjustment of the auxiliary signals by straight-line and distance-conditions will be able to reduce the magnitudes of the maximum residual errors.

¹⁾ Empirical determination of the covariance function was effective only with the 4-fold block. In all other cases a priori covariance functions had to be used.

Table 1 APPENWEIER, Planimetric results of block-adjustment with independent models (wide angle, photoscale 1:7800)
All given control points used (perimeter + points inside)¹⁾

Block	after block-adjustment					after least squares interpolation												
	σ_0	μ_x	μ_y	μ_{xy}	ϵ_{max}	σ_0	μ_x	μ_y	μ_{xy}	ϵ_{max}	μ_x	μ_y	μ_{xy}	ϵ_{max}				
		cm					μm				cm							
Single blocks (112 models, 27 control points, 77 check points)																		
EW	3.5	4.0	5.3	4.7	12.8	4.5	5.1	6.8	6.0	16.4	3.2	4.7	4.0	13.3	4.1	6.0	5.1	17.1
WE	3.8	5.4	6.5	6.0	19.1	4.9	6.9	8.3	7.6	24.5	4.5	5.3	4.9	16.3	5.8	6.8	6.3	20.9
NS	3.4	4.7	3.5	4.1	12.8	4.4	6.0	4.5	5.3	15.4	4.0	3.1	3.6	9.9	5.1	4.0	4.6	12.7
SN	3.8	6.0	6.1	6.1	20.3	4.9	7.7	7.8	7.8	26.0	5.1	4.2	4.7	19.7	6.5	5.4	6.0	25.3
mean	3.6	5.1	5.5	5.3	20.3	4.7	6.5	7.1	6.8	26.0	4.3	4.4	4.4	19.7	5.5	5.6	5.6	25.3
Double blocks (224 models, 30 control points, 82 check points)																		
WE/NS	3.8	3.8	4.1	4.0	12.6	4.9	4.9	5.3	5.1	16.2	3.1	3.3	3.2	13.1	4.0	4.2	4.1	16.8
EW/SN	3.7	4.2	5.1	4.7	14.3	4.7	5.4	6.5	6.0	18.3	3.6	3.7	3.7	12.2	4.6	4.7	4.7	15.6
mean	3.8	4.0	4.6	4.3	14.3	4.9	5.1	5.9	5.5	18.3	3.4	3.5	3.5	13.1	4.3	4.5	4.4	16.8
4-fold block (WE/EW/NS/SN 448 models, 30 control points, 83 check points)																		
)	3.3	3.4	3.6	3.5	10.6	4.9	4.4	4.6	4.5	13.6	2.7	2.6	2.7	9.4	3.5	3.3	3.4	12.1
	3.3	3.3	3.2	3.3	10.6	4.9	4.2	4.1	4.2	13.6	2.6	2.4	2.5	9.2	3.3	3.1	3.2	11.8

μ_x, μ_y = r.m.s. values of residual errors at check points ; $\mu_{xy} = \sqrt{(\mu_x^2 + \mu_y^2)}/2$; ϵ_{max} = max. residual coordinate error of check points

¹⁾ 8 additional perimeter control points, 75 check points

4.2 Comparison of 1-, 2- and 4-fold blocks

The 4 single blocks represent conventional blocks of 20 % lateral overlap, photo scale 1 : 7800. Their summarized accuracy figures are :

$$\begin{aligned} \sigma_0 &= 3.6 \text{ cm} = 4.7 \text{ } \mu\text{m} \text{ (range } 4.4 - 4.9 \text{ } \mu\text{m)} \\ \mu_{xy} &= 5.3 \text{ cm} = 6.8 \text{ } \mu\text{m} \text{ (range } 6.0 - 7.8 \text{ } \mu\text{m) after block adjustment} \\ \mu_{xy} &= 4.4 \text{ cm} = 5.6 \text{ } \mu\text{m} \text{ (range } 4.6 - 6.3 \text{ } \mu\text{m) after least squares interpol.} \\ \mu_{xy}/\sigma_0 &= 1.5 \text{ and } 1.2, \text{ respectively} \end{aligned}$$

Such figures qualify the block-results of the independent model method as most satisfactory. They confirm the high level of accuracy which the photogrammetric system is capable of.

Compared with the single blocks the improvement of accuracy by double and 4-fold overlap does not reach expectation. The ratios of the r.m.s. values μ_{xy} of single, double, and 4-fold blocks are :

$$\begin{aligned} 1 : 0.81 : 0.66 & \left(1 : \frac{1}{1.23} : \frac{1}{1.52} \right) \text{ after block adjustment} \\ 1 : 0.80 : 0.61 & \left(1 : \frac{1}{1.25} : \frac{1}{1.63} \right) \text{ after interpolation} \end{aligned}$$

The theoretical ratio, on the basis of random errors only, is expected to be about a factor 1.5 ($>\sqrt{2}$) per step. Thus, only little more than half the expected improvement has been realized. The previous statement about the satisfactory overall results of the 4-fold block (see 4.1) can now be specified more precisely: The resulting accuracy is due to the high initial quality of the separate input blocks in first instance, whilst their combined adjustment was not as effective as expected.

The general explication of such results must refer to the presence of uncompensated systematic image errors which have been known to disturb unfavourably theoretical expectations which are based on random errors only. Nevertheless such ex-

planation still leaves some questions open. It had been anticipated, originally, that the 4-fold block would compensate systematic errors very well. Evidently such effects did not come about. Strange to say, the least squares interpolation, supposed to remove remaining systematic error effects, has been more effective with the 4-fold block than with the single or double blocks (1 : 1/1.30 against 1 : 1/1.22 and 1 : 1/1.23).

4.3 Least squares interpolation

The conclusion just drawn about the presence of systematic image errors is confirmed by the general effectiveness of the least squares interpolation after the block-adjustments. The accuracy improvement for single, double, and 4-fold blocks amount to 18 %, 19 %, and 23 %, respectively (1:0.82; 1:0.81; 1:0.77). It means that treatment of systematic errors one way or another is essential.

The maximum residual errors have been hardly reduced by least squares interpolation, which confirms their independent, local causes as stated in section 4.1.

4.4 Comparison with perimeter control

The results of table 2 refer to dense perimeter control. The control points inside the block have been removed, and a few points have been added at the perimeter. The resulting average spacing between control points along the perimeter is 2 base lengths.

Comparison of table 2 with table 1 shows that the accuracy results of both control versions are virtually identical. Therefore, the evaluation of the results and the comments, as given in sections 4.1 - 4.3, apply equally to adjustments based on perimeter control. Once more the practicability of planimetric perimeter control has been confirmed.

Table 2 APPENWEIER, Planimetric results of block-adjustment with independent models (wide angle, photoscale 1:7800)
Dense perimeter control

Block	after block adjustment					after least squares interpolation												
	σ_0	μ_x	μ_y	μ_{xy}	ϵ_{max}	σ_0	μ_x	μ_y	μ_{xy}	ϵ_{max}	μ_x	μ_y	μ_{xy}	ϵ_{max}	μ_x	μ_y	μ_{xy}	ϵ_{max}
		— cm —					— μm —				— cm —				— μm —			
Single blocks (112 models, 25 control points, 79 check points)																		
EW	3.5	3.9	4.8	4.4	12.5	4.5	5.0	6.2	5.6	16.0	3.4	4.4	3.9	12.0	4.4	5.6	5.0	15.4
WE	3.8	5.9	6.1	6.0	21.7	4.9	7.6	7.8	7.7	27.8	5.7	4.8	5.3	20.3	7.3	6.2	6.8	26.0
NS	3.4	4.2	3.8	4.0	11.6	4.4	5.4	4.9	5.2	14.9	3.6	3.3	3.5	10.1	4.6	4.2	4.4	12.9
SN	3.9	6.0	5.2	5.6	19.3	5.0	7.7	6.7	7.2	24.7	5.1	4.1	4.6	18.4	6.5	5.3	5.9	23.6
mean	3.7	5.1	5.0	5.1	21.7	4.7	6.5	6.4	6.5	27.8	4.6	4.2	4.4	20.3	5.9	5.4	5.7	26.0
Double blocks (224 models, 28 control points, 84 check points)																		
WE/NS	3.8	3.3	4.0	3.7	12.5	4.9	4.2	5.1	4.7	16.0	3.3	3.2	3.3	13.0	4.2	4.1	4.2	16.7
EW/SN	3.7	4.2	4.3	4.3	14.0	4.7	5.4	5.5	5.5	17.9	3.6	3.3	3.5	12.4	4.6	4.2	4.4	15.0
mean	3.8	3.8	4.2	4.0	14.0	4.9	4.9	5.4	5.2	17.9	3.5	3.3	3.4	13.0	4.5	4.2	4.4	16.7
4-fold block (WE/EW/NS/SN ; 448 models, 28 control points, 85 check points)																		
	3.8	3.1	3.3	3.2	10.4	4.9	4.0	4.2	4.1	13.3	2.6	2.4	2.5	7.7	3.3	3.1	3.2	9.9

5. Summary and conclusion

First of all the test has confirmed the high accuracy level of photogrammetric point determination, indicated by the mean planimetric coordinate accuracy of single blocks of 4.4 cm or 5.6 μm , from the photo-scale 1 : 7800.

With double and 4-fold overlap the accuracies improved to r.m.s. values of planimetric coordinate errors of 3.5 cm (= 4.4 μm) and 2.7 cm (= 3.4 μm). Such results are highly satisfactory in absolute terms. Nevertheless the double and 4-fold coverage has not been as effective as expected.

The results indicate the presence of systematic image errors. Research into their more effective compensation is continued and further improvement of accuracy is expected.

DENSIFICATION OF TRIGONOMETRIC NETS
Practical experiences with bundle-adjustment

by Jonna Hvidegaard, Kobenhavn, Denmark

ABSTRACT

Fixed-points for cadastral measurements have been coordinated by use of the bundle adjustment method. The coordination was done by densification of an existing 2 km net of triangulated points down to a density of approx. 400 m. The photo scale was 1 : 8000 - 1 : 10 000 and the overlap 60/30.

The accuracy of 8 blocks, covering an area of 448 km², has been tested in the field by measuring distances between coordinated points. More than 700 points were checked and gave a standard error of 5 cm on a photogrammetric coordinated point.

The investigation was done as a cooperation between the Cadastral Service and the Royal Veterinary and Agricultural University.

BACKGROUND

Photogrammetry has already for some years been used for cadastral purposes in Denmark. To a certain degree photogrammetric plans have formed the basis of new cadastral maps. Perhaps more interesting in this connection is the fact that photogrammetrically coordinated fixed-points are being used for cadastral measurements.

The Geodetic Institute of Denmark is responsible for the triangulation of higher order. The Institute establishes points down to a density of approx. 2 km. Further densification is left to the Cadastral Service and the private surveyors. According to official regulations the surveyors have to tie new cadastral measurements to fixed-points when these are located within a distance of 200 m (for measuring of roads the limit is 500 m). This means in practice that unless you have a net of points with a density of approx. 400 m problems may arise especially in the developing areas of larger towns.

Also the local authorities have a professional interest in the developing areas of the towns. One of the main jobs for the photogrammetric firms is to produce technical plans in the scale of 1 : 1000 to the municipalities. The need for ground control for the compiling of these plans corresponds very well with the earlier mentioned 400 m net. The net is furthermore useful for the local technical administration for map revision and setting out purposes.

The jobs that will be presented in this paper are all the result of a cooperation between a state authority, namely the Cadastral Service, a private photogrammetric firm, the local municipality, and the local private surveyor. Such a cooperation implies of course both advantages and difficulties.

THE PHOTOGRAMMETRIC TRIANGULATION

Up to 1970 the only photogrammetric triangulation method used for the described kind of jobs was the Anblock with models measured in analogue instruments such as A8, A7 and Simplex III. This method is still in use for smaller blocks and gives sufficiently good results with a photo scale of 1 : 4000 or 1 : 5000.

In 1970 the first test block in Denmark using "bundle adjustment" was made. The measuring and the calculations were done in Finland at the Technical University of Helsinki. The results were promising, and since then some 40 jobs covering approx. 1400 km² have been performed mainly in Finland but lately also in Denmark.

All the jobs mentioned in this report were carried out in Finland. The pictures were measured on Zeiss PSK comparator using glass-diaositives and the calculations were made with the Finnish triangulation programme.

Prior to the adjustment the pictures were corrected for

- 1 - film distortion (using affine transformation on the fiducial marks),
- 2 - lens distortion (radial),
- 3 - refraction, and
- 4 - earth curvature.

Criteria had to be established for the practical execution. Up till now only very little has been published about bundle adjustment used on practical jobs where the results have been tested in the field. Most papers seem to deal with simulated blocks or test blocks.

The intention was to end up with a standard point error ($\sqrt{m_x^2 + m_y^2}$) of 5 cm on the ground, and after many considerations the following lines of direction were proposed :

1) - Photoscale between 1 : 8000 and 1 : 10 000. The predicted accuracies of the bundle adjustment were 4 - 6 μ in photo scale.

2) - The cameras had to be the ordinary wide-angle cameras of the photogrammetric firms ($c = 15$ cm) and the film: panchromatic, which is the film normally used in Denmark.

3) - Overlap 60/30 was chosen. Certainly 60/60 would form a stronger block (|1| and 3), but as the improvement is mainly on the Z-coordinate, and considering the increase in number of photographs in a block, 60/30 was agreed upon. In some cases 80 % forward overlap was photographed. Not all the pictures were used in the block, but selections were done in order to "get down" into streets, to get pictures in a good position in one strip compared to the next strip, or to fortify the block in weak areas by including extra pictures.

4) - The distribution of ground control points was chosen after the scheme :
 Planimetric control along the perimeter of the block with a mutual distance of 4 x base.
 Height control as a net covering the whole block, the density being 2 x base.
 These figures are recommended by Dr. Kilpelä from the Technical University of Finland in his investigation using simulated blocks [2].

Remembering the 2 km net of triangulated points already existing in Denmark the figures outlined the prospect of never having to measure anything but vertical control points in the field. These expectations have only been fulfilled to a certain extent. In a block of for instance 100 pictures it will normally be necessary to measure 2 - 3 horizontal control points. As to the vertical controls these all have to be measured and in spite of the fact that the Z-coordinate is only of minor interest, at least from a cadastral point of view, it was agreed to use the recommended net.

5) - The accuracy of the triangulated points was stated by the Geodetic Institute in the following way: The maximum error on a distance between two neighbouring points is 10 cm. As to the accuracy of the vertical control points the standard error was predicted to be 2 - 3 cm.

6) - For targets were chosen white plates 40 x 40 cm, and a black contrast of at least 15 cm around the signal was recommended. All ground control points should have extra signals (fig. 1) first of all to ensure the identification in the pictures.

7) - Artificial points (marked in the emulsion) were abandoned mainly because of unfavorable experiences from Anblock-jobs. Where extra pass-points were needed either signals were set out in advance in the predicted side-lap and perimeter, or natural points were measured in the comparator.

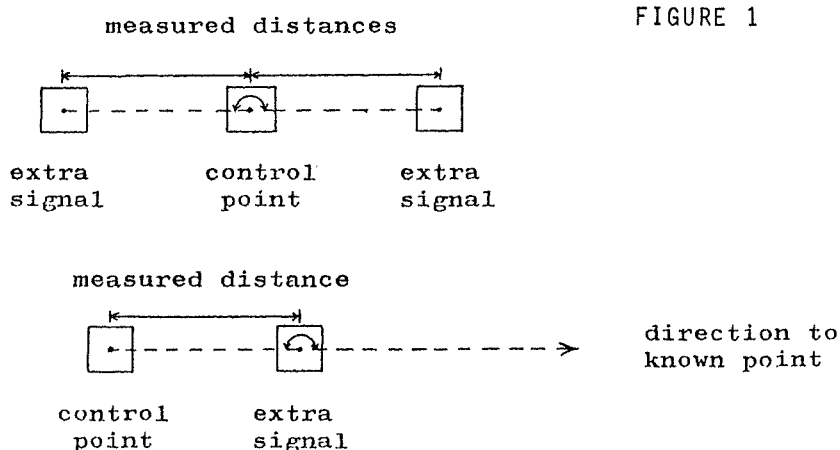


FIGURE 1

Broadly speaking these lines have been followed in the reported jobs.

TEST

Having made a number of blocks with the new method it seemed natural to check whether the results were in accordance with the expectations. During the last year the possibility of reaching the goal of 5 cm in standard error had been questioned. In order to certify an accuracy of 5 cm a very exact geodetic measurement is required.

At the same time the test should be fairly easy to carry out since a secondary aim of the investigation was to see whether a test could be done in a way that would make it reasonable to include it as a permanent part of future densification jobs.

As the standard error of a distance can be shown to be equal to the standard error of a point, under the assumption of independence between the coordinates, measurement of distances would give the wanted result directly. Furthermore, the very simple geodetic "net" would give no error-propagation, and by using electronic distance measuring equipment (EDM) the measurement could be of high accuracy. The standard error you get by using distances is the relative one, but that is precisely the error of major interest here, as the coordinated points are going to be used for cadastral measurements in the classical way.

Having decided to use distances the next problem was how to plan the field work. To allow the use of the normal distribution the elements (here being the difference between the measured distance and the same distance calculated from the photogrammetric coordinates) must be independent. If you use EDM the easiest way to get many controls would be to measure several distances from the same station, but then the elements are not independent. However, measuring only one distance from each point would increase the control work and the costs considerably.

The actual work was done as a compromise between these two extremes, and calculations afterwards showed that the correlation was hardly ever significant.

In all the jobs but one, the measured distances have been regarded as error-free. This is of course a point where you have to be careful. In the start of the collection of controls we also intended to use distances measured by the local surveyors during their normal work. It appeared later that the standard error here (based on the remeasurement of 118 distances) was approx. 5 cm, which is the same as the expected error to be controlled. Out of 40 double measurements (never from the same station) the standard error on a distance measured by the testing group is computed to be just under 1 cm.

It has to be mentioned that quite a few of the distances were in fact measured with steel-tape but as it appears from table 2 they were all under 10 m. These short distances date from double-signalized points where both the point itself and the extra signal have been coordinated.

RESULTS

The results are presented in tables 1 and 2, the first one dealing with the actual flight mission and the calculations, the second with the control measurement. As can be seen from table 1 the side-lap and the photo scale vary to some extent. If a contract is set up for a flying a variation of $\pm 10\%$ is usually allowed in the side-lap. Nevertheless the last block on the list seems to have been photographed in rough weather. As to the photo scale it has to be mentioned that one of the photogrammetric firms right from the start wanted to use 1 : 8000 instead of 1 : 10 000. The same firm uses 1 : 4000 for low flying where the others prefer 1 : 5000. Therefore, the figures in the table should not solely be expounded as a growing confidence in the method.

The table does not tell anything about the distribution of the ground control points. An investigation showed that compared with the recommended distribution, there were more horizontal controls (mainly points inside the blocks) but less vertical controls (the net being closer to 3 x base than to 2 x base).

In table 2 it has to be noticed that the standard error of the last test includes a standard error on the control measurement of 2.5 cm. If that is deducted it leaves 5.2 cm for the photogrammetry.

In all blocks but one the aim of a standard point error of 5 cm seems to have been reached. As to the Jersie-block a closer study revealed errors in the ground control. At the time of writing the recomputing is just about to start and it is hoped that the results will be ready for the symposium.

TABLE 1 - Photogrammetric information

Block	km ²	number of pictures	number of coordinated points	end-lap %	side-lap %	photo-scale	in the photo μ	σ_0 on the ground cm
Aarhus (B) 1971	20	27	570	60	20	1:8000	6.2	5.0
Aalborg 1971	104	85	1289	60	30	1:8000	6.1	4.8
Jersie 1971	20	22	185	60	30	1:8000	6.1	4.9
Aarhus 1972	85	84	738	60	30	1:8000	5.9	4.7
Aalborg 1972 Gistrup øst	36	59	736	60	40	1:10000	6.8	6.8
Aarhus 1973	50	73	1450	60	20-30	1:8500	5.4	4.6
Aalborg 1973 Ajstrup	55	40	550	60	25	1:10000	5.0	5.0
Hoje-Tåstrup 1973	65	41	572	60	10-40	1:9500	5.9	5.6

In two of the blocks the geodetic control also included measurement of angles. This gave the possibility of computing ground coordinates, and a transformation (Helmert) on the photogrammetric coordinates gave the standard point error shown in the table. Although this error theoretically should be of the same size as the standard error computed from the distances it turned out to be larger. The error propagation when building a geodetic net certainly has to be taken into consideration.

TABLE 2 - Control-measurement

Block	control-instrument	number of points p	number of distances d	quotient P/d	mean (cm)	standard error (cm)	rms (cm)	max. discrepancies		min.-max distance (m)	point standard error (cm)	error number of points
								+	+			
Aarhus (B) 1971	DI 10 (1974)	54	62	0.87	-1.9	3.9	4.3	-10	+6	42-786	4.9	50
	DI 10 (1971)	61	64	0.95	-0.7	4.9	4.9	-13	+11	31-655		
Aalborg 1971	DI 10	72	67	1.07	-0.6	4.1	4.1	-10	+12	17-480		
Jersie 1971	DI 10	58	49	1.18	-0.2	6.2	6.2	-17	+18	64-610		
Aarhus 1972	steel-tape	191	100	1.91	0.0	4.2	4.2	-13	+12	≤ 10		
Aalborg 1972 Gistrup øst	DI 10 T16	34	28	1.21	-1.3	4.7	4.8	-10	+7	48-508		
Aarhus 1973	DI 10	22	21	1.05	+0.4	3.7	3.7	-10	+7	123-1409	4.2	27
	steel-tape	155	78	1.99	-0.3	4.2	4.2	-15	+19	≤ 10		
Aalborg 1973 Ajstrup	DI 10	36	30	1.20	+0.1	4.9	4.8	-10	+14	48-470		
Hoje-Tåstrup 1973	AGA 700	68	115	0.59	+0.2	5.8 ^{x)}	5.8 ^{x)}	-14	+14	2-1075		

x) 2.5 cm standard error on control included

Finally I have set up a small table to compare σ_0 of the adjustment with RMS from the test. The quotient RMS/σ_0 stays fairly steady on 0.9. The two blocks that vary most from this value are: 1. Jersie which has already been mentioned above, and 2. Aalborg 1972. The last one should be noticed for another reason also: σ_0 is unexpectedly large. The block is in fact the one half of a job where the other half was rejected due to bad photographing. Certainly there have been problems during the photo-flight of the accepted part too.

When judging the quotient RMS/σ_0 you of course have to remember that the blocks were performed after the same scheme, but bearing that in mind σ_0 gives a good idea of the size of the standard error to be expected in the field.

TABLE 3

Block	adjustment σ_0 cm	control rms cm	rms/ σ_0	remarks
Aarhus 1971	5.0	4.6	0.92	
Aalborg 1971	4.8	4.1	0.85	
Jersie 1971	4.9	6.2	1.27	gross errors in ground control
Aarhus 1972	4.7	4.2	0.89	
Aalborg 1972	6.8	4.8	0.71	problems during photo-flight, lack of vacuum?
Aarhus 1973	4.6	4.1	0.89	
Aalborg 1973	5.0	4.8	0.96	
Høje-Taastrup 1973	5.6	5.2	0.93	
			mean: 0.93	

CONCLUSION

As a whole the testing has been successful. The results correspond very well with the expectations, and the test have been quite easy to carry out. It was for instance possible to check 3 blocks (Aalborg) in one week.

For the Cadastral Service as the supervising authority the field work gave in addition valuable information about the quality of the work done by the private surveyors, e.g. the marking of the points and the identification in the pictures.

It is, therefore, the intention to make similar tests in future densification jobs.

REFERENCES

- [1] Malinen, R. P. Simulation in photogrammetry
Helsingfors 1969
- [2] Kilpelä, E. Theoretische Genauigkeitsuntersuchungen der in Finland angewandten analytischen Bündelausgleichungsmethode
Helsingfors 1970
- [3] Tewinkel, G. C. Photogrammetric geodesy
Commission III, I.S.P. Symposium London 1971

BUNDLE ADJUSTMENT WITH STRIP- AND BLOCK-INVARIANT PARAMETERS

by D. C. Brown, Melbourne, Florida

INTRODUCTION

At the 1974 Symposium of Commission III at Stuttgart I presented a fairly lengthy review paper entitled: "Evolution, Application and Potential of the Bundle Method of Photogrammetric Triangulation" (Brown 1974). The present paper has been extracted from this review and is concerned with methods for taking effective advantage of the potential availability of the border of the banded-bordered system of normal equations associated with certain formulations of the bundle adjustment. Several examples will be provided showing how through judicious use of the border one can develop simple solutions to problems that would otherwise be computationally awkward or difficult.

BACKGROUND

As was shown in the earlier sections of my review paper, the general system of normal equations for the basic bundle adjustment are of the form

$$(1) \begin{bmatrix} \dot{N} + \dot{W} & \bar{N} \\ \bar{N}^T & \ddot{N} + \ddot{W} \end{bmatrix} \begin{bmatrix} \delta \\ \ddot{\delta} \end{bmatrix} = \begin{bmatrix} \dot{c} - \dot{W}\epsilon \\ \ddot{c} - \ddot{W}\epsilon \end{bmatrix}$$

in which δ and $\ddot{\delta}$ represent the vectors of unknown elements of orientation and unknown coordinates of ground points, respectively. The matrices \dot{N} and \ddot{N} consist of block-diagonal matrices of 6×5 and 3×3 submatrices. When decomposed into conformable 6×3 submatrices \bar{N}_{ij} , the matrix \bar{N} generated by a typical aerial block is also sparse (though not block-diagonal), for each \bar{N}_{ij} is a null matrix except when the j th point appears on the i th photo. The elimination of δ from (1) yields the reduced system

$$(2) S\delta = c, \text{ in which}$$

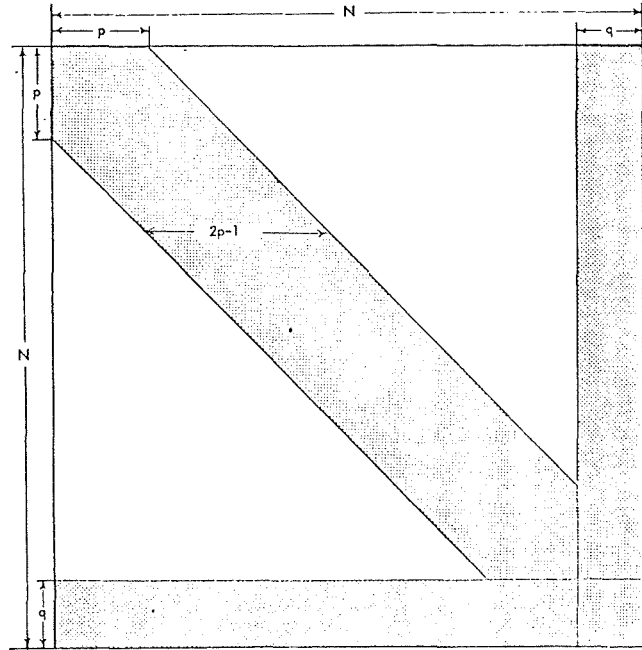
$$(3) S = \dot{N} + \dot{W} - \bar{N}(\ddot{N} + \ddot{W})^{-1}\bar{N}^T$$

$$(4) c = \dot{c} - \dot{W}\epsilon - \bar{N}(\ddot{N} + \ddot{W})^{-1}(\ddot{c} - \ddot{W}\epsilon)$$

When \dot{W} and \ddot{W} (the a priori weight matrices for elements of orientation and coordinates of control, respectively) are regarded a block diagonal conformably with \dot{N} and \ddot{N} , it turns out that with suitable ordering of the photos the coefficient matrix S of the reduced system of normal equations can be made to assume a banded form. This is a direct consequence of the sparseness of the matrix \bar{N} associated with the typical aerial block. Such banded systems can be solved efficiently by a method referred to as "recursive partitioning" (Gyer 1967). Recursive partitioning is equally applicable to banded systems that are accompanied by a border as indicated in Figure 1. The number of arithmetic operations required in the reduction of a banded-bordered system of bandwidth p and borderwidth q is approx. proportional to $(p+q)^2N$ (for $p \gg q$) as compared with a number proportional to N^3 for a conventional reduction. It follows that when a problem can be so structured that $(p+q) \ll N$, great computational savings can be realized through the exercise of recursive partitioning.

The first applications of recursive partitioning to the bundle adjustment were effected in 1967 in the programs COMBAT and SURBAT developed by DBA Systems (Gyer 1967; Gyer, Lewis, Saliba 1967; Brown 1968a; Callancer, Brown, Gyer 1969; Gyer, Kenefick 1969). In these early programs only banded systems of normal equations were generated. In the more recent developments to be discussed in this paper, the potential availability of the border has been extensively exploited in order to accomodate parameters that may be common to significantly large subsets of observational equations.

FIGURE 1 - Illustrating form of $N \times N$ banded-bordered coefficient matrix with bandwidth p and borderwidth q



GENERAL ADJUSTMENT WITH BLOCK-INVARIANT PARAMETERS

The general formulation of the process of self-calibration within the bundle adjustment was originally stated in the broadest possible terms in Brown, Davis, Johnson (1964). Here, the problem was addressed from the point of view of the possible existence of an unspecified number of biased "auxiliary sensors" that were considered to generate observations relating to any conceivable combination of the parameters involved in the bundle adjustment. Examples of such sensors could include: stascopes, inertial navigational systems, aircraft tracking systems, horizon cameras, solar periscopes, auxiliary stellar cameras (as in the Apollo mapping system), laser or radar altimeters, any surveying instruments serving to interrelate positions of ground points etc. I would hasten to point out that the general bundle adjustment as had been developed earlier (Brown 1958+1959) was already fully capable of coping with virtually any combination of auxiliary sensors provided only that they were considered to generate sensibly unbiased observations. Pertinent information from such sensors could, in principle, be introduced through the imposition of a priori statistical constraints in combination, where needed, with the method of dummy observations. Several examples of this process are to be found in Brown (1959). When the auxiliary sensors are considered to be affected by a significant degree of systematic error, however, this earlier development is no longer strictly valid.

To overcome the problem of biased auxiliary sensors, I turned to a reduction that I had developed several years earlier to solve the problem of determining accurate rocket trajectories from optical and electronic tracking observations that were considered to be significantly biased. This reduction was named EMBET, short for Error Model Best Estimate of Trajectory, and it depended on the presumption that the systematic errors affecting any given observational channel could be represented accurately by a specified mathematical error model involving a set of parameters (the error model coefficients) that were subject to specified a priori statistical constraints (this, of course, did not preclude the possibility that some or all of the parameters might be totally unknown). The EMBET reduction itself consisted of a least squares adjustment in which the coordinates of all observed trajectory points were recovered simultaneously along with the error model coefficients of all participating tracking systems. The structure of the general normal equations turned out to be of precisely the same form as in the bundle adjustment (equation (1)) with the \dot{N} portion of the matrix corresponding to error model coefficients and the \ddot{N} portion corresponding to coordinates of trajectory points. With the exercise of appropriate geometry and observational redundancy, an EMBET reduction was found capable of generating estimates of the error coefficients sufficiently accurate to suppress the effects of systematic errors in the observations to a level significantly below that of the purely random errors. Because no absolute control of any sort is required in the reduction, EMBET is

said to constitute a process of self-calibration. Details concerning EMBET and its application to rocket and satellite tracking are to be found in Brown, Bush, Sibol (1963) (1964) and in Brown (1964) (1966). The multilaterative comparator described in Brown (1967) was based entirely on principles of self-calibration made possible by EMBET.

The application of the principles of EMBET to the bundle adjustment requires that an appropriate error model be specified for each type of observation considered subject to a significant degree of systematic error. An example cited in Brown, Davis, Johnson (1964) is provided by the following equation applying to the stastoscopic observation h_{ij}^0 of the flying height at the i th exposure along the j th strip:

$$(5) \quad h_{ij} = h_{ij}^0 + v_{h_{ij}} + \underbrace{a_{0i} + a_{1i} s_{ij} + a_{2i} s_{ij}^2 + \dots}_{\text{(equation defining departure of isobaric surface from reference spheroid along } i \text{th flight line)}}$$

(true altitude) (measured altitude) (residual)

In this equation s_{ij} denotes the distance of the i th exposure on the j th flight line from the initial exposure on that line ($s_{ij} = 0$) and the a 's are the appropriate unknown error model coefficients needed to account for the slowly varying separation between the isobaric surface being utilized and the adopted reference spheroid.

Stated in the most general possible terms (as in the above reference an arbitrary set of biased auxiliary sensors will introduce into the bundle adjustment a set of observational equations of the following functional form :

$$(6) \quad f_k(\theta_1, \theta_2, \dots, \theta_p; \dot{U}_1, \dot{U}_2, \dots, \dot{U}_{6m}; \ddot{U}_1, \ddot{U}_2, \dots, \ddot{U}_{3n}; \dddot{U}_1, \dddot{U}_2, \dots, \dddot{U}_q) = 0$$

in which k , the number of equations, can be indefinitely large and

- $\theta_1, \theta_2, \dots, \theta_p$ = quantities observed by the sensors;
- $\dot{U}_1, \dot{U}_2, \dots, \dot{U}_{6m}$ = elements of orientation of the m exposure stations;
- $\ddot{U}_1, \ddot{U}_2, \dots, \ddot{U}_{3n}$ = coordinates of the n control points;
- $\dddot{U}_1, \dddot{U}_2, \dots, \dddot{U}_q$ = error coefficients and any other parameters associated with the auxiliary sensors.

In the event that the plate coordinates themselves are considered to be subject to systematic errors governed by specified error models, the above system of equations can, of course, be interpreted to be sufficiently broad to embrace the projective equations as well (i.e., the camera loses its special status and becomes merely another biased sensor with a subset of the \dot{U} 's serving as error coefficients).

The strictly formal introduction of the general observational equations (6) into the bundle adjustment is a straightforward chore that was carried out in the above reference. In principle, it leads to the complete generalization of the bundle adjustment to embrace any conceivable set of (possibly) biased observations that in any way may be pertinent to the adjustment. In practice, of course, for any particular circumstance the computational feasibility of the bundle adjustment as thus extended will depend on the specific structure of the resulting system of normal equations. Fortunately, it turns out that in most concrete situations of practical interest, the specialization of the foregoing general theory leads directly to a banded-bordered system of normal equations wherein the border accommodates the coefficients of the error models along with any other block-invariant parameters. Hence, the development of recursive partitioning in its more general form provided the sought-after key to the practical implementation (in most instances) of the generalized theory of bundle adjustment with block-invariant parameters.

BUNDLE ADJUSTMENT FOR ORBITAL PHOTOGRAMMETRY

At the time of the discovery of recursive partitioning, DBA was well along in a contract with RADC to perform the analysis and computer programming appropriate to the reduction of photographs taken by the Lunar Orbiter satellite. This led

ultimately to the development of the programs LOSAT and LOBAT (Lunar Orbiter Strip Analytical Triangulation and Lunar Orbiter Block Analytical Triangulation). Both of these reductions consisted of rigorous bundle adjustments subject, however, to the imposition of orbital constraints governing the locations of the exposure stations. In both LOSAT and LOBAT the reduced system of normal equations (2) was solved directly by Gauss Elimination; the finer, banded-bordered structure was not exploited. This, of course, placed significant limitations on the capacities of the programs. The detailed development of LOSAT and LOBAT is given by Davis and Riding (1970).

By the time recursive partitioning had been discovered and fully implemented in COMBAT and SURBAT, the development of LOSAT/LOBAT was too far advanced to admit alteration. However, a new opportunity presented itself with the anticipated Apollo photographic missions. Here, an obvious need existed for a more advanced version of LOSAT/LOBAT that would rigorously accommodate data from auxiliary sensors (a laser altimeter and a pair of stellar cameras synchronized with the mapping camera) and would, in addition, have the capacity for the adjustment of blocks embracing many hundreds of photos. Accordingly, in mid 1969 we submitted an unsolicited proposal to the U.S. Army Engineer Topographic Laboratories (ETL) to develop an advanced program for orbital photogrammetry (NASA, not having a sufficient photogrammetric capability of its own, had delegated a major part of the responsibility for the photogrammetric reduction of Apollo observations to the U.S. Army). The key to our proposed approach lay in the exploitation of the banded-bordered form of recursive partitioning to solve the normal equations (at that time we still regarded the more general form of recursive partitioning to be a proprietary development). The border would not only accommodate the orbital parameters for the various strips comprising the block, but it would also accommodate additional parameters including: (a) coefficients of radial and decentering distortion, (b) elements of interior orientation x_p , y_p , c , (c) biases in precalibrated interlock angles between stellar cameras and mapping camera, (d) selenodetic datum shifts. In addition, by virtue of the implementation of a still newer concept called "augmented bordering" (which will be discussed in a later section), we proposed to solve the problem of introducing various possible geodetic constraints (distances, azimuths, height differentials) between ground points without disturbing the bandwidth of the reduced normal equations no matter what the spacing or ordering of such interrelated points.

In late 1969 we received a contract from ETL to implement our proposal. The resulting computer program for the reduction was named PLODS (Photogrammetric Lunar Orbital Data Processing System). By late 1971 PLODS had been developed and checked out on DBA's Sigma 5 computer and by June 1972 it had been installed on the Univac 1108 systems at both TOPOCOM and ACIC. On these latter systems PLODS was designed to accommodate blocks of up to 500 photos in as many as 30 different orbital strips. Any surface point could be measured in up to 30 different photos. Provisions were made for the inclusion of up to 100 parameters in the border of the normal equations (in addition to the 180 parameters reserved for the orbital parameters of up to 30 strips). Because different cameras would be used on different Apollo Missions, the process of self-calibration of camera parameters admitted participation of up to six independent camera systems in the overall block. The analysis underlying the reduction was published in August 1972 in a report entitled: "Analysis for the Photographic Lunar Orbital Data Processing System" (Haag, Hodge 1972).

PLODS provides a good example of a bundle adjustment with block-invariant parameters. Such parameters are distinguished by being common to a sufficiently large subset of observational equations to make their assignment to the border of the normal equations computationally worthwhile. Within the purview of block-invariant parameters we include parameters that are common only to photos within a given strip (e.g., orbital parameters) and which may be referred to as strip-invariant parameters.

IMPLEMENTATION OF SELF CALIBRATION IN COMBAT

With the delivery of SURBAT in November 1967, it was clear that the next logical step in the development of the general bundle method would consist of the practical implementation of the process of self calibration as made feasible by the more general form of recursive partitioning. I expressed this view in two separate papers delivered in March 1968 (Brown 1968a, 1968b). In the latter paper which was concerned with an astrometric application of the bundle adjustment (i.e., the adjustment of a block of plates uniformly covering the celestial sphere) I stated :

"The border in a banded-bordered system allows one to accomodate unknowns that may be common to many plates - parameters for distortion, for example (perhaps with temperature dependent coefficients). Another possibility is to employ the border for the coefficients of a tentative, empirical error model intended to account for unknown systematic errors that are regarded as common to all plates or to large subsets of plates. For example, one might postulate that systematic errors common to all plates can be described empirically by selected terms of general polynomials such as :

$$\Delta x = \sum_{i=2}^r \sum_{j=0}^i \sum_{k=0}^j a_{i,j,k} x^{i-j} y^{j-k} z^k$$

$$\Delta y = \sum_{i=2}^r \sum_{j=0}^i \sum_{k=0}^j b_{i,j,k} x^{i-j} y^{j-k} z^k$$

where x,y denote plate coordinates and z denotes either image diameter or stellar magnitude. The unknown coefficients a_{ijk} , b_{ijk} would be determined within the adjustment (note: zero and first order terms are not included in the above expression because they would ordinarily be equivalent to the parameters in the banded portion of the matrix). When all plates contribute to a common empirical model, the result is far more deterministic than when independent empirical models are postulated for each plate. For this reason, one can accommodate rather extensive empirical models in the border without serious risk of inducing ill-conditioning. The border can also serve as a convenient place to assign occasional portion of the matrix. Thus one sometimes finds that a logical ordering scheme leads to a very narrow bandwidth except for a few outlying blocks requiring a significantly wider bandwidth for their accommodation. One easily overcomes this problem by re-ordering the offending parameters so that they become relegated to the border."

As is our usual practice with what we consider to be marketable innovations, we attempted through unsolicited proposals put forward repeatedly in 1968 through 1972 to gain sponsorship for the extension of SURBAT to incorporate self-calibration. In this we were consistently unsuccessful for a variety of reasons: governmental research budgets were declining; SURBAT appeared to be sufficient as it was to satisfy current and anticipated governmental requirements (it was, after all, considered to be a major advance); available resources and research interest were increasingly gravitating towards more glamorous extra-terrestrial applications (Apollo, Mariner). As I have already mentioned, we did meet with success by late 1969 in proposing to implement recursive partitioning and self-calibration (along with other special features) in LOSAT/LOBAT, thereby generating PLODS. Although PLODS could be "tricked" into correctly processing conventional blocks of aerial photos (by simply treating each photo as an individual orbital strip and constraining the velocity components of the associated state vector to zero), this would be an inefficient utilization of the program.

Having failed over an undue period of time to gain outside sponsorship for the implementation of self-calibration in a conventional bundle adjustment, we proceeded in early 1972 with a company-sponsored project to extend our program COMBAT to embrace self-calibration. The error models adopted for the plate coordinates involve a combination of physically interpretable expressions along with strictly empirical expressions. Specifically the models involve a total of 29 parameters and are of the form:

$$(7) \quad \Delta x = a_1 x + a_2 y + a_3 x^2 + a_4 xy + a_5 y^2 + a_6 x^2 y + a_7 xy^2$$

$$+ \frac{x}{r} (c_1 x^2 + c_2 xy + c_3 y^2 + c_4 x^3 + c_5 x^2 y + c_6 xy^2 + c_7 y^3)$$

$$+ x (K_1 r^2 + K_2 r^4 + K_3 r^6) + P_1 (y^2 + 3x^2) + 2P_2 xy + \delta x_p + \left(\frac{x}{c}\right) \delta c$$

$$(8) \quad \Delta y = b_1 x + b_2 y + b_3 x^2 + b_4 xy + b_5 y^2 + b_6 x^2 y + b_7 xy^2$$

$$+ \frac{y}{r} (c_1 x^2 + c_2 xy + c_3 y^2 + c_4 x^3 + c_5 x^2 y + c_6 xy^2 + c_7 y^3)$$

$$+ y (K_1 r^2 + K_2 r^4 + K_3 r^6) + 2P_1 xy + P_2 (x^2 + 3y^2) - \delta y_p + \left(\frac{y}{c}\right) \delta c.$$

The various coefficients are subject to the following interpretation:

- (a) $a_1, a_2, \dots, a_7 =$ coefficients defining mean uncompensated film deformation;
 b_1, b_2, \dots, b_7
- (b) $c_1, c_2, \dots, c_7 =$ coefficients defining curvature of camera platen;
- (c) $K_1, K_2, K_3 =$ coefficients of radial distortion;
- (d) $P_1, P_2 =$ coefficients of decentering distortion;
- (e) $\delta x, \delta y, \delta c =$ biases in enforced elements of interior orientation.

The terms in groups (a) and (b), being strictly empirical in nature, may also be regarded together as accounting (in part at least) for anomalous distortion as well for any other persistent source of otherwise unmodeled systematic error. All error coefficients are, of course, subject to the imposition of appropriate a priori statistical constraints.

COMBAT II has been designed so that the error model can readily be altered or extended. As it is, we have found several coefficients in the above model to be superfluous because of strong coupling effects. When any two coefficients are highly correlated, both tend to perform the same function in the model; hence one or the other can be suppressed without ill effect. Some of the more strongly coupled coefficients are $(a_1, b_2), (a_2, b_1), (a_3, c_4), (a_6, c_7), (c_3, P_2)$.

Of course, with vertical photos over relatively flat terrain the elements of interior orientation are almost perfectly coupled with the coordinates of the exposure stations. Accordingly, they are carried in the reduction (with appropriately tight constraints) mainly for purposes of error propagation. This makes them available also for potential special situations where they might be needed (e.g., operations over very rugged terrain, operations with convergent photography).

THE METHOD OF AUGMENTED BORDERING

Before proceeding with further examples of the practical use of the border of banded-bordered systems, we shall next consider a useful technique for preserving the bandwidth of an already banded system when potentially disruptive fresh information is brought to bear on an adjustment. Our starting point is the arbitrary system of normal equations.

$$(9) \quad N\delta = c$$

which is assumed to be of banded-bordered form. We now assume that new and independent information is to be brought to bear on the adjustment. This new information is represented by the system of s observational equations given by the matrix expression

$$(10) \quad \tilde{A}\tilde{v} + \tilde{B}\delta = \tilde{\epsilon}.$$

The covariance matrix of the new observational vector is denoted by \tilde{A} . The coefficient matrix \tilde{B} is assumed to have been appropriately augmented with zeros in the event that the new information interrelates only a subvector of the vector δ appearing in (9). The system of normal equations resulting from the independent adjustment of the observations giving rise to (10) is given by

$$(11) \quad [\tilde{B}^T (\tilde{A}\tilde{A}^T)^{-1} \tilde{B}] \delta = \tilde{B}^T (\tilde{A}\tilde{A}^T)^{-1} \tilde{\epsilon}.$$

Because the observations generating (10) are independent of those generating (9), it follows immediately that the normal equations resulting from the simultaneous adjustment of both sets of observations are to be obtained by simply adding the two systems together to get

$$(12) \quad [N + \tilde{B}^T (\tilde{A}\tilde{A}^T)^{-1} \tilde{B}] \delta = c + \tilde{B}^T (\tilde{A}\tilde{A}^T)^{-1} \tilde{\epsilon}.$$

But the difficulty with this system is that, in general, it can be expected to destroy the postulated banded-bordered character of the matrix N from original system (9). To get around this difficulty we employ the following artifice. We form the new system of equations

$$(13) \quad \begin{bmatrix} N & \tilde{B}^T \\ \tilde{B} & -(\tilde{A}\tilde{A}^T) \end{bmatrix} \begin{bmatrix} \delta \\ \tilde{\delta} \end{bmatrix} = \begin{bmatrix} c \\ \tilde{\epsilon} \end{bmatrix}$$

in which $\tilde{\delta}$ is a presently unspecified vector of parameters equal in number to s , the number of equations generated by the new observations. From the structure of (13) it is apparent that the elimination of the vector δ will lead precisely to the system (12). Hence the vector δ obtained from the solution of (13) will be identical with the δ obtained from the solution of (12). But by virtue of our assumption that N is of banded-bordered form, it follows that the new system (13) is also of such form with the borderwidth of N being augmented by s new elements. It follows that by introducing the new information by means of (13) rather than (12), one preserves the original system totally in tact and merely adds to its border. Hence, the name, the "method of augmented bordering".

SIMULTANEOUS ADJUSTMENT OF PHOTOGRAMMETRIC AND GEODETIC OBSERVATIONS

The extension of recursive partitioning to accommodate banded-bordered systems served not only to make the bundle adjustment with block-invariant parameters computationally feasible, but, as we shall now see, it also opened a new avenue for the solution of other problems. A good example is provided by the problem of executing the adjustment of the photogrammetric observations simultaneously with the adjustment of the geodetic observations defining the survey of the control net. In principle, this is taken care of immediately in the general normal equations (1) by virtue of the imposition of a priori statistical constraints implicit in the matrices \bar{W} and \bar{W}_ϵ . The practical difficulty with this is that, in the problem at hand, \bar{W} is not a block diagonal matrix of 3x3 submatrices as in the development following (1). Instead \bar{W} represents the zero-augmented coefficient matrix of the system of normal equations arising from the separate adjustment of the geodetic observations of the control points (the zero augmentation makes the matrix suitably conformable with the total vector δ). Thus the inversion of $N+\bar{W}$ is no longer a simple matter, for nonzero submatrices are scattered throughout the matrix.

In addressing this problem in the development of their program SAPGO (Simultaneous Adjustment of Photogrammetric and Geodetic Observations) Wong and Elphinstone (1971) adopted the following approach (slightly paraphrased here). The total set of control points was reordered so that those points that were interrelated by geodetic observations were numbered first. This caused the general system of normal equations to assume the form

$$(14) \quad \begin{bmatrix} \dot{N}+\dot{W} & \bar{N}_s & \bar{N}_r \\ \bar{N}_s^T & \ddot{N}_s+\ddot{W}_s & 0 \\ \bar{N}_r^T & 0 & \ddot{N}_r+\ddot{W}_r \end{bmatrix} \begin{bmatrix} \dot{\delta} \\ \ddot{\delta}_s \\ \ddot{\delta}_r \end{bmatrix} = \begin{bmatrix} \dot{c} - \dot{W}\dot{\epsilon} \\ \ddot{c}_s - \ddot{W}_s\ddot{\epsilon}_s \\ \ddot{c}_r - \ddot{W}_r\ddot{\epsilon}_r \end{bmatrix}$$

in which

- $\ddot{\delta}_g = 3g \times 1$ vector corresponding to subset of g points interrelated by geodetic observations;
- $\ddot{\delta}_r = 3(n-g) \times 1$ vector corresponding to all remaining points;
- $\ddot{W}_g = 3g \times 3g$ coefficient matrix of normal equations from the independent geodetic adjustment (a filled matrix);
- $\ddot{W}_r =$ block diagonal $3(n-g) \times 3(n-g)$ weight matrix of points not geodetically observed;

and in which the remaining quantities are essentially self-explanatory. The system of reduced normal equations (2) resulting from the elimination of $\dot{\delta}_g$ and $\ddot{\delta}_r$ then became

$$(15) \quad [\dot{N}+\dot{W} - \bar{N}_s(\ddot{N}_s+\ddot{W}_s)^{-1}\bar{N}_s^T - \bar{N}_r(\ddot{N}_r+\ddot{W}_r)^{-1}\bar{N}_r^T] \dot{\delta} \\ = \dot{c} - \dot{W}\dot{\epsilon} - \bar{N}_s(\ddot{N}_s+\ddot{W}_s)^{-1}(\ddot{c}_s - \ddot{W}_s\ddot{\epsilon}_s) \\ - \bar{N}_r(\ddot{N}_r+\ddot{W}_r)^{-1}(\ddot{c}_r - \ddot{W}_r\ddot{\epsilon}_r).$$

Because $\ddot{N}_r + \ddot{W}_r$ is a block diagonal matrix of 3x3 submatrices its inversion presents no problems. Hence, the largest intermediate matrix to be inverted in the process of forming the reduced normal equations is the 3gx3g matrix $\ddot{N}_g + \ddot{W}_g$.

This approach does get around the difficulty of having to invert the 3nx3n matrix $\ddot{N}+\ddot{W}$. However, it also engenders some alternative difficulties when the solution of the reduced normal equations by recursive partitioning is considered. These are recognized by Wong and Elphinstone. They state :

"The present version of SAPGO does not take advantage of the potential banded-structure of the N matrix of equation (30). It is recognized that if no restriction were placed on the locations of the geodetic measurements in the block, the banded structure would be destroyed and the N matrix must be treated as a compact matrix. In order to maintain maximum flexibility in our research experimentations, the present version of SAPGO does not impose restriction on the locations of the geodetic measurements. However, the banded structure can easily be restored by stipulating that no geodetic measurement should span across more than two strips. A second version of SAPGO is being prepared to include this feature."

From this it is clear that SAPGO and recursive partitioning are incompatible unless rather severe geometric limitations are imposed on the geodetic survey.

The difficulties raised by Wong and Elphinstone's approach disappear when the banded-bordered form of recursive partitioning is applied. Thus when only the vector $\dot{\delta}_r$ is eliminated from (14), one has

$$(16) \quad \begin{bmatrix} S & \bar{N}_g \\ \bar{N}_g^T & \ddot{N}_g + \ddot{W}_g \end{bmatrix} \begin{bmatrix} \dot{\delta} \\ \ddot{\delta}_g \end{bmatrix} = \begin{bmatrix} \bar{c} \\ \ddot{c}_g - \ddot{W}_g \ddot{\epsilon}_g \end{bmatrix}$$

in which

$$(17) \quad S = \dot{N} + \dot{W} - \bar{N}_r (\ddot{N}_r + \ddot{W}_r)^{-1} \bar{N}_r^T$$

$$\bar{c} = \dot{c} - \dot{W} \dot{\epsilon} - \bar{N}_r (\ddot{N}_r + \ddot{W}_r)^{-1} (\ddot{c}_r - \ddot{W}_r \ddot{\epsilon}_r).$$

But for a properly ordered aerial block, S is, as we have seen, a banded matrix. Hence by leaving (16) as it is, one has a banded-bordered system (with border-width 3g) that is amenable to an efficient reduction by the more general form of recursive partitioning. This, in turn, obviates the need for any geometric restrictions on the geodetic observations.

Still another approach to the use of the border for solving the above problem results from the application of the method of augmented bordering and proceeds as follows. The geodetic observation equations may be written

$$(18) \quad v_g + B_g \ddot{\delta} = \epsilon_g.$$

By zero augmentation this can be enlarged to include the vector $\dot{\delta}$ of projective parameters :

$$(19) \quad v_s + (0 \ B_r) \begin{bmatrix} \dot{\delta} \\ \ddot{\delta} \end{bmatrix} = \epsilon_s.$$

The general normal equations for the bundle adjustment (1) with augmented bordering to accommodate geodetic observations then become

$$(20) \quad \begin{bmatrix} \dot{N} + \dot{W} & \bar{N} & 0 \\ \bar{N}^T & \ddot{N} + \ddot{W} & B_r^T \\ 0 & B_r & -\Lambda_s \end{bmatrix} \begin{bmatrix} \dot{\delta} \\ \ddot{\delta} \\ \ddot{\delta} \end{bmatrix} = \begin{bmatrix} \dot{c} - \dot{W} \dot{\epsilon} \\ \ddot{c} - \ddot{W} \ddot{\epsilon} \\ \epsilon_s \end{bmatrix}.$$

The matrix \dot{W} as carried in this particular system is considered to be block diagonal and independent of any geodetic information implicit in equation (18). The elimination of δ from this system yields

$$(21) \quad \begin{bmatrix} \dot{N} + \dot{W} - \bar{N}(\ddot{N} + \ddot{W})^{-1} \bar{N}^T & \bar{N}(\ddot{N} + \ddot{W})^{-1} B_z^T \\ -B_z(\ddot{N} + \ddot{W})^{-1} \bar{N}^T & -A_z - B_z(\ddot{N} + \ddot{W})^{-1} B_z^T \end{bmatrix} \begin{bmatrix} \delta \\ \tilde{\delta} \end{bmatrix} = \begin{bmatrix} \dot{c} - \dot{W}\dot{c} - \bar{N}(\ddot{N} + \ddot{W})^{-1} \ddot{c} \\ \epsilon_z - B_z(\ddot{N} + \ddot{W})^{-1} \ddot{c} \end{bmatrix}.$$

The upper right hand portion of this matrix represents the banded system one would obtain independently of the geodetic observations. Hence the introduction of geodetic observations by the method just indicated leaves the photogrammetric system of normal equations unaltered and simply adds a border to that system.

Either of the two banded-bordered systems (16) and (21) provides a practical means for the simultaneous adjustment of photogrammetric and geodetic observations. Neither entails a compromise of the bandwidth of the photogrammetric system and neither requires the imposition of special geometric restrictions on the geodetic net. The one to be preferred depends mainly on considerations of borderwidth. In equation (86) the borderwidth is equal to the number of geodetic observational equations that are to be used. Accordingly, this form is particularly advantageous when incomplete or relatively limited sets of geodetic observations are to be introduced - miscellaneous distances between various pairs of control points, for example. When the number of geodetic observations becomes sufficient for the complete determination (or overdetermination) of a set of control points, the advantage swings to the use of equation (16). A synthesis of the two approaches may be appropriate in a mixed situation involving some points that are completely determinable from the geodetic observations alone and other geodetically observed points that are not (typically, these would consist of isolated pairs of points). Here, one would include in \dot{N}_G in (14) only points of the first type; the method of augmented bordering would then be used in (14) to introduce the remaining geodetic information pertinent to points of the second type. Elimination of δ from this system would then lead to a system of the form (16) with an additional border similar to that in (21) (but with a block of zeros interposed in positions (2,3) and (3,2) of the matrix). This hybrid approach would admit the rigorous processing of the geodetic observations in such a manner as to produce the minimum possible borderwidth.

BUNDLE ADJUSTMENT WITH EQUAL-ELEVATION CONSTRAINTS

As a further (and final) example of the flexibility afforded by the appropriate utilization of the banded-bordered form of recursive partitioning, I shall briefly touch on one of a number of possible ways that the border can be exploited to impose equal-elevation constraints on measured points on the shorelines of lakes of unknown elevation.

For those particular points falling on the shores of the k^{th} lake, the linearized projective equations assume the form

$$(22) \quad v_{i,j} + \dot{B}_{i,j} \delta_i + \ddot{B}_{i,j} \delta_{i,j} + \ddot{B}_{i,j} \delta_{i,j} + \ddot{B}_{i,j} \delta_x = \epsilon_{i,j}$$

$$\begin{matrix} (\varrho, 1) & (\varrho, \varrho) & (\varrho, 1) & (\varrho, \varrho) & (\varrho, 1) & (\varrho, 1) & (1, 1) & (1, 1) \end{matrix}$$

in which $\delta_{i,j}^{\varrho}$ now refers to the corrections $\delta\phi_{ij}$, $\delta\lambda_{ij}$ to the geographic coordinates of the point and δh_k is the correction δh_k to the approximation used for the unknown height of the k^{th} lake.

The general system of normal equations arising from consideration of these equations in combination with the regular system of observational equations can be shown to assume the form

$$(23) \begin{bmatrix} \dot{N} + \dot{W} & \bar{N} & \bar{N}_l & \dot{H} \\ (\dot{m}, \dot{n}) & (\bar{m}, \bar{n}) & (\bar{m}_l, \bar{n}_l) & (\dot{m}, \dot{q}) \\ \bar{N}^T & \ddot{N} + \ddot{W} & 0 & 0 \\ (\bar{m}, \bar{m}) & (\bar{m}, \bar{n}) & (\bar{m}, \bar{n}_l) & (\bar{m}, \dot{q}) \\ \bar{N}_l^T & 0 & \ddot{N}_l + \ddot{W}_l & \bar{H} \\ (\bar{m}_l, \bar{m}) & (\bar{m}_l, \bar{n}) & (\bar{m}_l, \bar{n}_l) & (\bar{m}_l, \dot{q}) \\ \dot{H}^T & 0 & \bar{H}^T & \ddot{N} + \ddot{W} \\ (\dot{m}, \dot{m}) & (\dot{m}, \bar{n}) & (\dot{m}, \bar{n}_l) & (\dot{m}, \dot{q}) \end{bmatrix} \begin{bmatrix} \dot{\delta} \\ (\dot{m}, \dot{q}) \\ \ddot{\delta} \\ (\bar{m}, \dot{q}) \\ \ddot{\delta}_l \\ (\bar{m}_l, \dot{q}) \\ \ddot{\delta} \\ (\dot{m}, \dot{q}) \end{bmatrix} = \begin{bmatrix} \dot{c} - \dot{W}\dot{\epsilon} \\ (\dot{m}, \dot{q}) \\ \ddot{c} - \ddot{W}\ddot{\epsilon} \\ (\bar{m}, \dot{q}) \\ \ddot{c}_l - \ddot{W}_l\ddot{\epsilon}_l \\ (\bar{m}_l, \dot{q}) \\ \ddot{c} - \ddot{W}\ddot{\epsilon} \\ (\dot{m}, \dot{q}) \end{bmatrix},$$

wherein m, n, p, q denote respectively, the number of photos, the number of points not on shorelines, the number of points on shorelines, and the number of lakes. The elimination of $\dot{\delta}$ and $\ddot{\delta}_l$ from these equations leads to the reduced system

$$(24) \begin{bmatrix} S & P \\ (\dot{m}, \bar{n}) & (\bar{m}, \dot{q}) \\ P^T & Q \\ (\dot{m}, \bar{m}) & (\dot{m}, \dot{q}) \end{bmatrix} \begin{bmatrix} \dot{\delta} \\ (\dot{m}, \dot{q}) \\ \ddot{\delta} \\ (\bar{m}, \dot{q}) \end{bmatrix} = \begin{bmatrix} \bar{c} \\ (\bar{m}, \dot{q}) \\ c_l \\ (\dot{m}, \dot{q}) \end{bmatrix},$$

in which

$$(25) \begin{aligned} S &= \dot{N} + \dot{W} - [\bar{N}(\ddot{N} + \ddot{W})^{-1} \bar{N}^T + \bar{N}_l(\ddot{N}_l + \ddot{W}_l)^{-1} \bar{N}_l^T], \\ P &= \dot{H} - \bar{N}_l(\ddot{N}_l + \ddot{W}_l)^{-1} \bar{H}, \\ Q &= \ddot{N} + \ddot{W} - \bar{H}^T(\ddot{N}_l + \ddot{W}_l)^{-1} \bar{H}, \\ \bar{c} &= \dot{c} - \dot{W}\dot{\epsilon} - \bar{N}(\ddot{N} + \ddot{W})^{-1}(\ddot{c} - \ddot{W}\ddot{\epsilon}) - \bar{N}_l(\ddot{N}_l + \ddot{W}_l)^{-1}(\ddot{c}_l - \ddot{W}_l\ddot{\epsilon}_l), \\ c_l &= \ddot{c} - \ddot{W}\ddot{\epsilon} - \bar{H}^T(\ddot{N}_l + \ddot{W}_l)^{-1}(\ddot{c}_l - \ddot{W}_l\ddot{\epsilon}_l). \end{aligned}$$

Once again, with a properly ordered aerial block, the matrix S will be of banded form. Thus the reduced system (24) is of banded-bordered form with borderwidth equal to q, the number of lakes being used.

In the approach just outlined, lakes may stretch across several strips and across several models within strips without damaging consequences to the bandwidth of the normal equations, for the bandwidth is unaffected by such considerations. This is in contrast with the method proposed by Ackermann, Ebner and Klein (1972) in their extension of the PAT-M 43 program to accommodate equal-elevation constraints. In order to avoid undue widening of the bandwidth, they adopted an approach wherein large lakes spanning several models were broken up into a number of "sublakes", each being assigned an independent unknown height. Such restrictions, of course, severely vitiate the desired stabilizing effects of lakes. As the above development shown, with the proper exercise of the border such restrictions become unnecessary.

CONCLUSIONS

The feasibility of the bundle adjustment for large blocks of aerial photographs depends on the fact that the reduced normal equations can be made to assume a banded form amenable to an efficient reduction by recursive partitioning. The more general form of recursive partitioning accommodating banded-bordered systems makes practical the extension of the basic bundle adjustment to embrace a variety of ad-

vances including: self-calibration of the camera system itself along with any biased auxiliary sensors, utilization of orbital constraints, simultaneous adjustment of photogrammetric and geodetic observations, utilization of equal-elevation constraints. Doubtless other applications will emerge as the photogrammetric community becomes more widely aware of techniques for exploiting the border of banded-bordered systems.

REFERENCES

- Ackermann, Ebner, Klein (1972) - "Combined Block Adjustment of APR-Data and Independent Photogrammetric Models", presented at the 12th Congress of the ISP, Ottawa 1972
- Brown, D.C., 1958 - "A Solution to the General Problem of Multiple Station Analytical Stereotriangulation", RCA-MTP Data Reduction Technical Report No. 43, Patrick Air Force Base, Florida (also designated as AFMTC TR 58)
- Brown, D.C., 1959 - "Results in Geodetic Photogrammetry I: The Precise Determination of the Location of Bermuda from Photogrammetric Observations of Flares Elected from Juno 11", RCA-MTP Data Reduction Technical Report No 54, Patrick Air Force Base, Florida (also designated as AFMTC TR 59)
- Brown, D.C., 1960 - "Introduction of Orbital Constraints into an Adjustment of a Satellite Photogrammetric Net", unpublished, privately circulated paper
- Brown, D.C., 1964 - "A Calibration Satellite as a Means for the Evaluation of the Concept of Self-Calibration of Tracking Systems", Air Force Cambridge Research Laboratories, Report No. 64-1004
- Brown, D.C., 1966 - "Advanced Techniques for the Reduction of Geodetic Secor Observations", final Report prepared for GIMRADA, Fort Belvoir, Va. under U.S. Army Contract No. DA-44-009-AMC-937(X)
- Brown, D.C., 1967 - "Computational Tradeoffs in the Design of a Comparator", presented at the Semi-Annual Convention of the ASP St. Louis, October 1967 also published in Photogrammetric Engineering February 1969
- Brown, D.C., 1968a- "A Unified Lunar Control Network", presented at the 34th Annual Convention of the ASP Washington, March 1968 also published in Photogrammetric Engineering, December 1968
- Brown, D.C., 1968b- "Inversion of Very Large Matrices Encountered in Large Scale Problems of Photogrammetry and Photographic Astrometry", presented at the Conference of Photographic Astrometric Technique, University of South Florida, Tampa, March 1968; also published in NASA CR-1825: Conference on Photographic Astronomic Technique, November 1971
- Brown, Bush, Sibol, 1963 - "Study of the Feasibility of Rocket and Satellite Approaches to the Calibration of Tracking Systems", Air Force Cambridge Research Center Report No. 63-789.
- Brown, Bush, Sibol, 1964 - "Investigation of the Feasibility of Self-Calibration of Tracking Systems", Air Force Cambridge Research Laboratories Report No. 64-441
- Brown, Davis, Johnson, 1964 - "The Practical and Rigorous Adjustment of Large Photogrammetric Nets", RADC TRD 64-092, Rome Air Development Center
- Callander, Brown, Gyer, 1969 - "The Analytical Aerotriangulation of a Block of 1000 Aerial Photographs on a Large Scale Digital Computer", presented at the 35th Annual Meeting of the American Society of Photogrammetry, Washington, March 1969
- Case, J.B., 1961 - "The Utilization of Constraints in Photogrammetry", Photogrammetric Engineering, Vol. XXVII, No. 5, Dezember 1961

- Davis, Riding, 1970 - "The Rigorous and Simultaneous Adjustment of Lunar Orbiter Photography Considering Orbital Constraints", RADC-TR-70-274. Rome Air Force Base, Rome-New York
- Gyer, M.S., 1967 - "The Inversion of the Normal Equations of Analytical Aerotriangulation by the Method of Recursive Partitioning", RADC-TR-67-69. Rome Air Development Center, Rome-New York
- Gyer, Kenefick, 1969- "Block Analytical Aerotriangulation for Commercial Mapping on a Medium Scale Computer", presented at the 1969 Symposium on Computational Photogrammetry, University of Syracuse, January 1969
- Gyer, Lewis, Saliba, 1967 - "Mathematical Targeting III", RADC-TR-67-562. Rome Air Development Center, Rome-New York
- Haag, Hodge, 1972 - "Analysis for the Photogrammetric Lunar Orbital Data Processing System", Final Report prepared for the US Army Engineer Topographic Laboratories, Fort Belvoir, Virginia, under US Army Contract Nos DACA 76-70-C-0003 and -0004
- Wong, Elphinstone, 1971 - "Aerotriangulation by SAPGO", presented at the 37th Annual Meeting of the ASP, Washington, March 1971

EFFICIENCY OF THE EXTENDED MATHEMATICAL MODEL IN BUNDLE ADJUSTMENT

by H. Salmenperä, J. M. Anderson, A. Savolainen, Otaniemi, Finland

ABSTRACT

A bundle block adjustment containing up to 7 added parameters is used to triangulate a block of 48, 1 : 4000 scale photographs taken with a Zeiss RMK A 15/23 camera. Three sets of photographic coordinates are employed: refined; partially refined (affine transformation); and unrefined. The effects of the added parameters are positive. However, results indicate that photographic coordinates can be refined using laboratory calibration data so that the added parameters would have minimal effects. The critical phase in this refinement is the fiducial transformation with four fiducial marks.

EFFICIENCY OF THE EXTENDED MATHEMATICAL MODEL IN BUNDLE ADJUSTMENT

Proper application of analytical photogrammetry to practical mapping problems requires that all known systematic differences between the geometrical central projection and the actual projection be taken into account by correction of the image coordinates. Corrections normally applied to these image coordinates are those which compensate for: refraction and earth curvature; radial lens distortion; and film deformation. The remaining part of the systematic error together with the random error affects the final results of the adjustment.

The most efficient way to achieve better results in analytical photogrammetry is to obtain more information concerning the characteristics of these systematic errors. Laboratory calibration has long been the primary source of this information. However, during the past six years, in flight calibration using a test field has gained some favour as method for providing not only camera calibration parameters but also improved triangulation results. One should recognize that in flight calibration provides at best only an estimate of the true systematic errors for the specific set of conditions which affected the flight. In practice, if the geometric and environmental conditions are similar to the test field calibration, the results should be the same. In any event one part of the systematic error changes from flight to flight, and photograph to photograph.

Recent experiments for increasing the accuracy of photogrammetric adjustments have been performed using an extended mathematical model in the solution of the aerial triangulation [1], [2]. In these procedures, additional parameters, which are common to all photographs, have been added to the observation equations used in the triangulation adjustment. From a theoretical standpoint, it would be equally logical to introduce separate parameters for each photograph. However, in such a case the computational burden of the adjustment would be increased by an impractical amount.

In this investigation the effects of common additional parameters on the final accuracy achieved in bundle adjustment of a 48 photograph block are studied. Testing is performed with large scale photography (1 : 4000) of an accurately surveyed array of premarked object points. Triangulation using only six exterior orientation parameters for each picture and coordinate unknowns for ground points is used as a basis for comparison. The accuracy of final calculated ground coordinates when compared with known geodetic positions is used as the most reasonable criterion in judging the effectiveness of various combinations of added parameters.

TEST FIELD AND PHOTOGRAPHY [3]

The Jämijärvi test field, located about 200 km northwest of Helsinki, was established by the National Board of Survey in Finland. The test site covers an area 2 km x 2 km provided with signalized ground points of known positions. A set of 136 points has been used for the present study. The adjustment of geodetic network shows a standard coordinate error of less than ± 5 mm. Elevations have been determined with an internal precision of ± 0.6 mm/km.

Photography consists of 7 strips of photography taken with a Zeiss Pleogon RMK A 15/23 ($f = 152.36$ mm) from about 600 m over average terrain which contains about 60 m of relief. The resulting photography has an approximate scale of 1:4000. All strips are flown in the same direction with 80 % forward overlap and 60 % sidelap.

Leaving out every other photograph a total of 48 photographs containing a minimum of 8, a maximum of 30 and an average of ~15 points per photograph make up the block triangulated. Every other strip can be removed to yield a 28 photograph block with ~25 % sidelap. Contact diapositives were printed on 6 mm Ilford diapositive plates.

COMPARATOR OBSERVATIONS AND CORRECTIONS TO COORDINATES

Image coordinates were measured on a Zeiss PSK Stereocomparator. Five observations were made to the 4 fiducials on the sides of the photographs and three observations to images of ground points.

Three sets of coordinates were prepared according to the procedure outlined by Kilpelä and Savolainen [3]. Corrections applied in these sets were:

- 1 - Atmospheric refraction and earth curvature, radial symmetric lens distortion using camera calibration data and affine film deformation with

$$\begin{aligned} x &= a_0 + a_1x' + a_2y' \\ y &= b_0 + b_1x' + b_2y' \end{aligned} \quad (1)$$

- 2 - Affine film deformation with equations (1).

- 3 - Comparator coordinates are transformed to the fiducial system using the Helmert transformation

$$\begin{aligned} x &= a_0 + a_1x' - a_2y' \\ y &= b_0 + a_2x' + a_1y' \end{aligned} \quad (2)$$

These three sets of coordinates are designated: refined, partially refined, and unrefined coordinates, respectively.

EXTENDED MATHEMATICAL MODEL

The triangulation procedure utilized is a bundle adjustment in which the collinearity equation is the geometric condition to be satisfied. The basic collinearity equation for an image of object point j as seen from exposure station i is

$$\begin{aligned} x_{ij} &= f[U/W]_{ij} \\ y_{ij} &= f[V/W]_{ij} \end{aligned} \quad (1)$$

in which U, V, W are functions of $[(X, Y, Z, \omega, \phi, \kappa)_i (XYZ)_j]$, the exposure station coordinates and elements of orientation and object point coordinates; and f is the estimated camera focal length. Equations (1) with parameters added are:

$$\begin{aligned} (x + x_p + dx_1 + dx_2 + dx_3)_{ij} &= f[U/W]_{ij} \\ (y + y_p + dy_1 + dy_2 + dy_3)_{ij} &= f[V/W]_{ij} \end{aligned} \quad (2)$$

where

x_{ij}, y_{ij} = image coordinates of point j on photo i

x_p, y_p = estimated principal point coordinates

dx_1 and dy_1 errors due to radial symmetric distortion approximated by

$$dx_{1ij} = \bar{x}_{ij}(1 - r_0/r)_{ij}(a_1 + a_3r^2 + a_5r^4 + a_7r^6)$$

$$dy_{1ij} = \bar{y}_{ij}(1 - r_0/r)_{ij}(a_1 + a_3r^2 + a_5r^4 + a_7r^6)$$

in which r = radial distance to image of j

r_0 = a given constant

$\bar{x}_{ij} = x_{ij} - x_p$; $\bar{y}_{ij} = y_{ij} - y_p$

$a_1 \dots a_7$ = unknown coefficients,

dx_2 and dy_2 are errors due to lens decentering

$$dx_2 = p_1(r^2 + 2\bar{x}^2) + p_2 2\bar{x}\bar{y}$$

$$dy_2 = p_1 2\bar{x}\bar{y} + p_2(r^2 + 2\bar{y}^2)$$

in which p_1 and p_2 are unknown parameters, and dx_3 and dy_3 are af-fine corrections

$$dx_3 = 0$$

$$dy_3 = m_1\bar{y} + m_2\bar{x}$$

in which m_1 = unknown parameter for scale difference between x and y axis

m_2 = unknown parameter for lack of orthogonality.

All parameters are common to all photographs. Linearized equations (2) are solved in a bundle adjustment program developed by Haljala at the National Board of Survey in Finland [4]. In this procedure, solution of the system of equations is by the method of conjugate gradients. All observations are assumed of equal weight and any combination of the eleven added parameters can be enforced in the solution. Ground control points are considered errorless.

TEST ADJUSTMENT

A total of 26 test cases were performed using the three sets of photographic coordinates, various combinations of added parameters, and 60 and 25 % sidelap. Test case designations and characteristics are listed in Table 1.

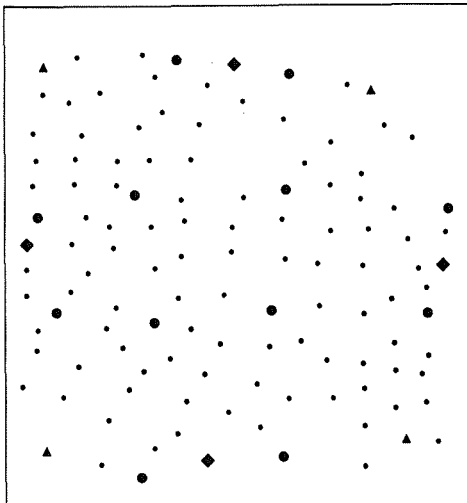


FIGURE 1

Test block control configuration

- ▲ COMBINED PLANIMETRIC AND HEIGHT CONTROL
- ◆ PLANIMETRIC CONTROL
- HEIGHT CONTROL
- CHECK POINT

Fixed ground control point configuration for the tests is illustrated in Figure 1. The numbers of fixed control points, check points, unknowns, and observations for the 60 % and 25 % sidelap tests are as shown here :

	60 %/60 %	60 %/25 %
Control	Number	Number
X,Y,Z	4	4
X,Y	4	4
Z	12	12
Check		
X,Y,Z	100	98
X,Y	12	12
Z	4	4
Unknowns	757+added parameters	613+added parameters
Observations	1672	922

An additional 47 natural points outside the ground control perimeter are taken into the adjustment as normal triangulation points.

TEST DESIGNATION	PHOTO COORDINATES	ADDED PARAMETERS	SIDE LAP	
A 1	Refined (1) Radial Distortions, Affine Transf.	Without added par.	60% ↑	
A 2		a_3		
A 3		a_5		
A 4		a_7		
A 5		$a_3 a_5$		
A 6		$a_3 a_5 a_7$		
A 7		$p_1 p_2$		
A 8		$a_3 a_5 p_1 p_2$		
A 9		m_1		
A 10		m_2		
A 11		$m_1 m_2$		
A 12		f		
A 13		$a_3 a_5 a_7 m_1 m_2$		
A 14		$a_3 a_5 p_1 p_2 m_1 m_2$		
B 1	Unrefined (2) Affine Transformation	$a_3 a_5 a_7 m_1 m_2$	60% ↓	
B 2		$a_3 a_5 p_1 p_2 m_1 m_2$		
B 3		$a_3 a_5 a_7 p_1 p_2$		
B 4		$a_3 a_5 a_7$		
C 1	Unrefined (3) Helmert Transformation	Without added par.		25%
C 2		$a_3 a_5$		
C 3		m_1		
C 4		m_2		
C 5		$a_3 a_5 a_7 m_1 m_2$		
C 6		$a_3 a_5 a_7 p_1 p_2 m_1 m_2$		
D 1	Re-fined	Without added par.		25%
D 2		$m_1 m_2$		

TABLE 1
Test Designations

TESTS RESULTS

Estimated standard errors of unit weight for the adjustments, and root mean square (RMS) values of discrepancies at check points at photo scale and on the terrain are listed in Table 2.

ADJUST- MENT	STD. ERROR $\frac{\mu\text{m}}{m_0}$	RMS VALUES OF DISCREPANCIES AT THE CHECK POINTS							
		at photo scale (μm)				on the terrain (mm)			
		m_x	m_y	m_z	m_{xy}	m_x	m_y	m_z	m_{xy}
A 1	5.40	4.3	4.7	8.2	6.4	17	19	33	26
A 2	5.40	4.3	4.7	8.1	6.4	17	19	32	26
A 3	5.40	4.4	4.7	8.2	6.4	18	19	33	26
A 4	5.40	4.3	4.7	8.3	6.4	17	19	33	26
A 5	5.39	4.3	4.8	8.1	6.4	17	19	32	26
A 6	5.37	4.3	4.7	7.9	6.4	17	19	32	26
A 7	5.25	3.9	4.7	8.2	6.1	16	19	33	25
A 8	5.25	3.9	4.7	8.1	6.1	16	19	32	24
A 9	5.39	4.1	4.8	8.1	6.3	17	19	33	25
A 10	5.28	3.4	3.4	8.0	4.9	14	14	32	20
A 11	5.28	3.4	3.4	7.9	4.8	14	14	32	19
A 12	5.40	4.4	4.7	8.2	6.4	18	19	33	26
A 13	5.25	3.5	3.3	7.6	4.8	14	13	30	19
A 14	5.14	3.3	3.4	7.8	4.7	13	14	31	19
B 1	5.23	3.5	3.3	7.5	4.8	14	13	30	19
B 2	5.32	3.2	3.5	8.1	4.7	13	14	33	19
B 3	5.20	3.8	4.5	8.0	5.9	15	18	32	24
B 4	5.34	4.2	4.6	8.0	6.3	17	18	32	25
C 1	6.82	9.5	11.9	10.7	15.2	38	47	43	61
C 2	6.67	9.5	11.7	8.2	15.1	38	47	33	60
C 3	5.67	4.6	3.8	10.4	6.0	18	15	42	24
C 4	6.81	10.1	11.5	10.6	15.3	41	46	42	61
C 5	5.23	5.2	3.2	7.3	6.1	21	13	29	24
C 6	5.16	4.9	3.2	7.3	5.9	20	13	29	23
D 1	5.85	6.2	4.2	14.5	7.5	25	17	58	30
D 2	5.74	6.0	4.4	14.1	7.4	24	18	56	30

TABLE 2
Test Results

SAMPLE GROUP	NO.OF ADJUSTMENTS IN GROUP	POOLED m_o μm	RESULTS OF BARTLETTS TEST COMMENTS
ABCD	26	5.53	Significant Diff.
ABC	24	5.52	Significant Diff.
AB	18	5.32	No Sign.Diff. 99.9% Conf.Interval
A	14	5.33	No Sign.Diff. 99.9% Conf.Interval
B	4	5.27	No Sign.Diff. 99.9% Conf. Interval
C	6	6.10	Significant Diff.
ABD	20	5.33	No Sign.Diff. 99.9% Conf.Interval
ABD (C5,C6)	22	5.32	No Sign.Diff. 99.9% Conf.Interval

TABLE 3
Results of Significance Tests

In order to check the homogeneity of the data, Bartlett's test was applied to eight sample groups of the results. Sample groups and results of the Bartlett tests are shown in Table 3. Note that when tests of Group C (unrefined coordinates, Helmert Transformation) are included, a significant difference is indicated by applying the Bartlett test. However, individual Groups A, B and D and sample groups in which tests C1, C2, C3, C4 are eliminated show no significant differences. On the basis of these tests one can conclude that the data are homogeneous and a significant amount of uncorrected systematic error is present in tests C1, C2, C3 and C4. This result indicates that in block triangulation a correction of film deformation is necessary either before the adjustment or in connection with adjustment with additional parameters.

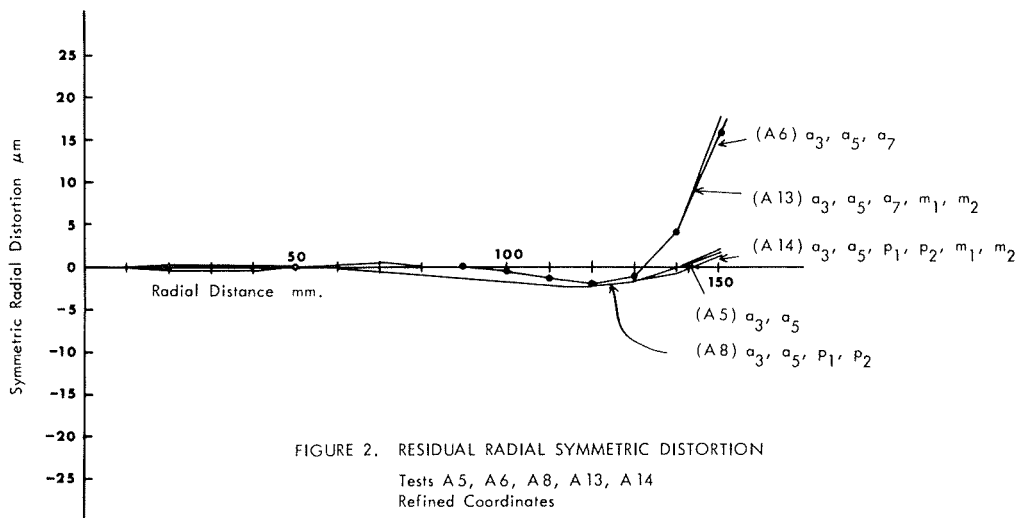
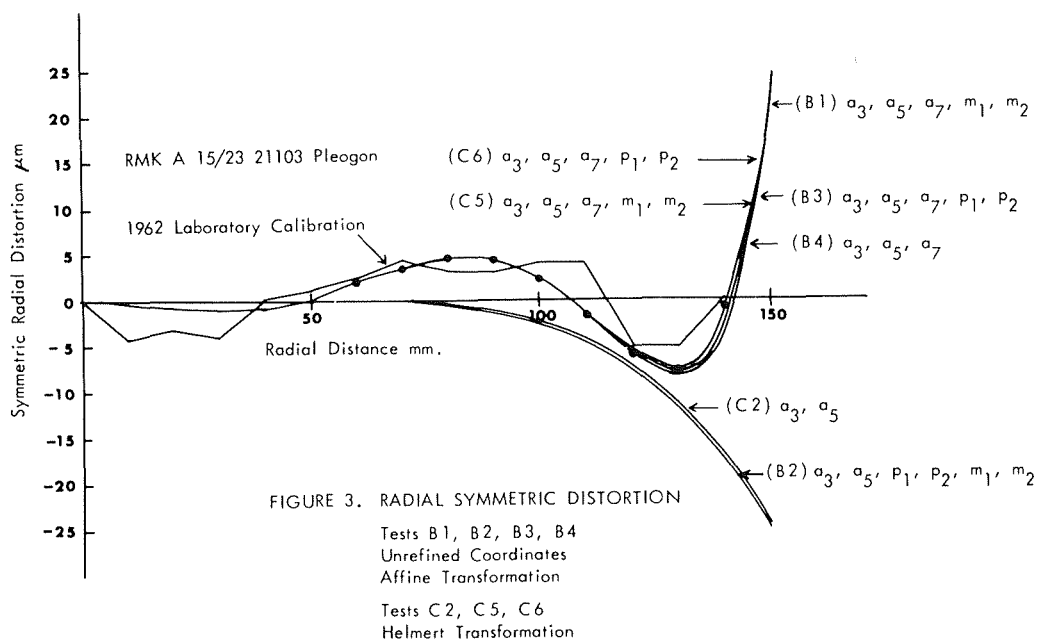


FIGURE 2. RESIDUAL RADIAL SYMMETRIC DISTORTION
Tests A5, A6, A8, A13, A14
Refined Coordinates



The basis for evaluating the effects of various combinations of added parameters is a comparison of all tests with Test A 1 (refined coordinates with affine transformation and no added parameters) and analysis of the adjustment radial distortion curves. The per cent changes in RMSE at check points for all tests, when compared with Test A 1, are listed in Table 4. Radial symmetric distortion curves for Tests A5, A8, A13, A14 and Tests B1, B2, B3, B4, C2, C5, C6 are illustrated in Figures 2 and 3 respectively. The effects of the parameters for scale difference between x- and y-axes and for lack of orthogonality are shown in Table 5.

Examination of tests in Group A permit an evaluation of the goodness of the laboratory calibration data and effects of added parameters used with refined coordinates. The most effective individual added parameter is m_2 (correction for lack of orthogonality) which yields reductions in the RMSE in position and elevation of 23 and 03 percent, respectively. The most effective combinations of added parameters are those of Tests A13 and A14 which resulted in reductions of the RMSE in position and elevation of 25 and 08 percent and 27 and 05 percent, respectively. Figure 2 which is a plot of the uncorrected radial symmetric distortion, still in the system, shows that these residuals are indeed quite small.

Tests of Group B permit evaluation of the utility of substituting in a flight calibration for application of laboratory calibration lens distortion data in the coordinate refinement. Maximum reductions in RMSE in position and elevation are 25 and 9 %, respectively, when a_3, a_5, a_7, m_1, m_2 are added. Note that when m_1 and m_2 are not included with the added parameters the reductions in RMSE are relatively insignificant.

Tests of Group C allow evaluating the effects of trying to compensate for film deformation when no affine correction is made and only a first degree conformal transformation is used. Here the most effective single parameter is m_1 , scale difference in x- and y-coordinate axes which yields a reduction of 7 % but an increase of 27 % in the RMSE of elevation and position, respectively. Addition of term m_2 has no effect. The most effective combination of added parameters is $a_3, a_5, a_7, p_1, p_2, m_1, m_2$ yielding decreases in RMSE of position and elevation of 11 and 9 percent, respectively. However, note that in this test the RMSE in X is increased by 14 %.

Examination of distortion curves in Figure 3 for Test Groups B and C shows that the 7th order polynomial curves are remarkably consistent and compare well with the laboratory calibration curve. The 5th order polynomial obviously is not suitable to approximate the lens distortion for this lens.

TEST	% CHANGE IN RMS ERRORS AT CHECK POINTS					ADDED PARAMETERS
	m _x	m _y	m _z	m _{xy}		
A 2	+01	0	- 02	0	Refined, Affine transformation	a ₃
A 3	+01	+01	- 01	0		a ₅
A 4	+01	+01	+ 01	0		a ₇
A 5	0	+01	- 02	0		a ₃ a ₅
A 6	-01	+01	- 04	0		a ₃ a ₅ a ₇
A 7	-08	-01	0	-04		p ₁ p ₂
A 8	-09	-01	- 02	-05		a ₃ a ₅ p ₁ p ₂
A 9	-04	+02	- 01	-01		m ₁
A 10	-18	-27	- 03	-23		m ₂
A 11	21	-28	- 04	-25		m ₁ m ₂
A 12	+01	+01	- 01	0		f
A 13	-19	-29	- 08	-25		a ₃ a ₅ a ₇ m ₁ m ₂
A 14	-25	-28	- 05	-27		a ₃ a ₅ p ₁ p ₂ m ₁ m ₂
B 1	-19	-31	- 09	-25		Partially refined
B 2	-25	-26	- 01	-26	a ₃ a ₅ p ₁ p ₂ m ₁ m ₂	
B 3	-12	-04	- 03	-08	a ₃ a ₅ a ₇ p ₁ p ₂	
B 4	-02	-02	- 03	-02	a ₃ a ₅ a ₇	
C 1	+119	+152	+ 30	+136	Unrefined Helmert	No added parameters
C 2	+119	+149	- 01	+136		a ₃ a ₅
C 3	+ 06	- 19	+ 27	- 07		m ₁
C 4	+134	+144	+ 28	+139		m ₂
C 5	+ 21	- 32	- 11	- 05		a ₃ a ₅ a ₇ m ₁ m ₂
C 6	+ 14	- 33	- 11	- 09		a ₃ a ₅ a ₇ p ₁ p ₂ m ₁ m ₂
D 1	+ 42	- 11	+ 76	+ 17	Re-fined	No added parameters
D 2	+ 38	- 7	+ 71	+ 16		m ₁ m ₂

TABLE 4
Per cent changes of RMSE in check points when compared with Test A 1.

Table 5, which presents the effect of scale difference between x- and y-coordinate axes and of lack of orthogonality at a distance of 100 mm, reveals that in Groups A and B (affine transformation) the effect of parameter m₂ (lack of orthogonality) at the distance of 100 mm on the photograph is considerable, 5 - 6 μm. The effect of parameter m₁, again, is slight in these tests, 1 μm. On the contrary, in group C the effect of m₁ is considerable, 20 μm, and the effect of m₂ half of what it is in groups A and B, i. e. 3 μm.

The limited number of tests with 25 % sidelap using refined photographic coordinates, verifies the superiority of 60 % all around overlap with this scale of photograph and size of block. It must be stated, however, that although the RMS errors in these cases have increased both in planimetric position and in elevation by 17 % and 76 % and 16 % and 71 % respectively, the planimetric accuracy, in particular, is sufficient for various practical purposes.

TEST	EFFECT OF		ADDED PARAMETERS
	scale difference	lack of orthogonality	
	at the distance of 100 mm on photo (μm)		
A 9	1	-	m_1
A 10	-	6	m_2
A 11	1	6	m_1 m_2
A 13	1	6	a_3 a_5 a_7 m_1 m_2
A 14	1	6	a_3 a_5 p_1 p_2 m_1 m_2
B 1	1	6	a_3 a_5 a_7 m_1 m_2
B 2	1	5	a_3 a_5 p_1 p_2 m_1 m_2
C 3	20	-	m_1
C 4	-	3	m_2
C 5	20	3	a_3 a_5 a_7 m_1 m_2
C 6	20	3	a_3 a_5 a_7 p_1 p_2 m_1 m_2
D 2	1	7	m_1 m_2

TABLE 5
Effect of scale difference and lack of orthogonality.

Using a 25 - 30 % sidelap would mean a saving of approximately 50 % in measuring the image coordinates; consequently, the amount of sidelap must be determined individually for each work. The effects of added parameters m_1 and m_2 are minimal for these tests.

CONCLUSIONS

The added parameters have been used in adjustments with three sets of photographic coordinates which were 1) completely refined; 2) partially refined with affine transformation; and 3) unrefined with a first degree conformal transformation.

The results of block triangulation obtained in using the Jämijärvi test field agree well with the corresponding results of theoretical investigations of accuracy [5]. This is probably due to the high accuracy of the points on the test field and to a successful photography of the test field. Consequently, even the accuracy of Test A1 (no added parameters) is remarkably good as compared to some other investigations of accuracy performed by using test fields. Utilization of added parameters does yield improved accuracies (25% in planimetry, 5 to 8 % in elevation) with refined and partially refined (film deformation only) image coordinates. Added parameters included in the adjustment with unrefined coordinates provide comparable improvement in elevation but less improvement to deterioration of accuracies in planimetric position.

Added parameters m_1 (scale difference) and m_2 (lack of orthogonality) have more pronounced individual effects on the accuracies of results with refined and partially refined data, than any other single parameter. However, with unrefined data m_2 virtually no effect. This indicates that the original photographs have only slight non-orthogonality and that most of this deformation was induced by the six parameter transformation used to compensate for film deformation. Consequently, a five parameter transformation with one rotation, two translations, and two scale changes would be more effective to compensate for film deformation when four fiducial marks are available. If one assumes up-to-date reliable, laboratory calibration data and use of such a five parameter transformation for film distortion compensation, then the effect of m_2 would be minimal and the results obtainable with refined data, only, would be comparable with results achieved by use of the added parameters.

REFERENCES

- |1| Bauer and Müller "Height Accuracy of Blocks and Bundle Adjustment with Additional Parameters", presented to the 12th Congress of the International Society for Photogrammetry, Ottawa, July - August 1972
- |2| Brown, D.C. "Advanced Methods for the Calibration of Metric Cameras" Final Report Contract DA-44-009-AMC-1457 (x) with U.S.Army Topographic Laboratories, Fort Belvoir, Va., 1968
- |3| Kilpelä, E. and Savolainen, A. "On the Effect of Some Error Sources in Bundle Adjustment" The Photogrammetric Journal of Finland, Vol. 6, No. 1-1972 pp. 31 - 54
- |4| Haljala, Sakari "Method of Conjugate Gradients for the Solution of Normal Equations in the Analytical Block Adjustment", The Photogrammetric Journal of Finland, Vol. 6, No. 2-1974, pp. 160 - 165
- |5| Kilpelä, E. "Theoretische Genauigkeitsuntersuchungen der in Finnland angewandten analytischen Bündelausgleichungsmethode" Diss. at Helsinki University of Technology, 1970

ON CORRECTION TERMS FOR SYSTEMATIC ERRORS IN BUNDLE ADJUSTMENT

by G. H. Schut, Ottawa, Canada

ABSTRACT

An investigation is made of correction terms which should be added to the photograph coordinates to eliminate systematic image deformation during bundle adjustment. The effect of all terms of polynomials of the third degree with respect to the photograph coordinates is evaluated and suitable selections are made which can correct standard strip deformations. The use of these terms does not affect the photograph residuals in the case of level terrain and exactly vertical photographs. Other terms in which occurs the absolute value of a photograph coordinate or the radial distance from image point to principal point may be useful also and deserve to be investigated further.

INTRODUCTION

Correction terms applied to the photograph coordinates for the purpose of eliminating systematic deformation during the bundle adjustment of a block of photographs were first proposed by G. de Masson d'Autume, in a paper presented at the International Symposium on Spatial Aerotriangulation in Urbana, Illinois, in 1966. The same terms appear, unaltered in a paper presented at the XIIth Congress of the International Society for Photogrammetry at Ottawa, Canada, in 1972 (De Masson d'Autume 1968, 1972). These terms were derived from the effect upon the photograph coordinates of changes in orientation given to the perspective bundles of a strip. The changes correspond to four general types of strip deformation: torsion, longitudinal height curvature, planimetric curvature, and variation of scale.

To analyze the effect of these correction terms, one can add the corrections which they produce to the coordinates of a perfect grid and perform an analytical triangulation with the modified grid coordinates. The present writer did this upon his return from the Symposium, using analytical strip triangulation by separate relative orientation and scaling of models. This triangulation showed that the correction terms for torsion leave residual y-parallaxes and those for height curvature produce a curvature correction of each model that is very different from the correction applied to the strip. This is unsatisfactory because the correction terms were not designed to correct such errors.

Subsequently, this writer derived correction terms which were based upon the placing of each photograph in a suitable position above a strip of terrain which was given each of the four types of deformation and he showed these in a short presentation during a panel discussion at the XIIth Congress of the ISP. These terms are different from and somewhat simpler than those presented by De Masson d'Autume - and by the nature of their derivation they produce no side-effects in analytical triangulation.

In both formulations, the correction terms are polynomials in the photograph coordinates. The differences between the two formulations and the possibility that systematic image deformations exist which do not cause the standard strip deformations make it of interest to investigate the effect of all polynomial correction terms separately. This will give information on which terms promise to be useful which ones are not, and how the useful ones should be combined.

Such an investigation is the subject of this paper. It has been limited to the polynomial terms of the third and lower degrees in the photograph coordinates. The computations have been performed by the bundle adjustment, assuming level terrain and a strip of ten exactly vertical photographs, each with 25 measured points in a square grid.

Other writers have recently experimented with the radial distance to the principal point and with the absolute value of a photograph coordinate as a parameter in specific polynomial correction terms. Such terms are here discussed only very briefly, but they deserve further investigation.

LINEAR CORRECTIONS

The simplest but also the least interesting corrections which can be given to the photograph coordinates are the linear ones :

$$\begin{aligned} dx &= a_{11} + a_{12}x + a_{13}y \\ dy &= a_{21} + a_{22}x + a_{23}y \end{aligned} \tag{1}$$

The constant terms in these corrections represent shifts of the position of the projection centre of a photograph in either the interior or the exterior orientation. Except in very exceptional circumstances, these shifts cannot be computed during the bundle adjustment.

The terms with coefficients a_{12} and a_{23} represent scale corrections to the x- and y-coordinates, respectively. These terms are not greatly needed because scale corrections can be computed in advance of the adjustment from distances of fiducial marks or, possibly, reseau marks in the photographs. The two coefficients cannot even be computed during the adjustment, except in exceptional circumstances such as extremely accidented terrain with suitably located ground control points or very accurately known heights of the projection centres. However, if desired, a differential scale change can be computed during the adjustment. This is achieved by using only one of these terms in the adjustment.

If $a_{13} = -a_{22}$, the terms with these coefficients represent a rotation of the photograph axes. This is of no interest in the adjustment. If one of these terms is eliminated, the remaining one represents a correction for non-orthogonality of the x,y axes. This may be of interest. This leaves the linear corrections:

$$dx = a_1x + a_2y \tag{1a}$$

or, alternatively

$$dy = a_1x + a_2y \tag{1b}$$

SECOND DEGREE CORRECTIONS

The second degree corrections

$$\begin{aligned} dx &= a_{11}x^2 + a_{12}xy + a_{13}y^2 \\ dy &= a_{21}x^2 + a_{22}xy + a_{23}y^2 \end{aligned} \tag{2}$$

affect primarily the planimetry of a triangulated strip. If the terrain is level and the photographs are exactly vertical, they have no effect at all upon the heights of a strip.

The terms with a_{11} , a_{13} , and a_{22} may be called scale correction terms. If $a_{13} = -a_{11}$ and $a_{22} = 2a_{11}$, they cause a conformal change of scale throughout the strip. If $a_{13} = 0$ and $a_{22} = 2a_{11}$, they cause a so-called parabolic scale correction.

The effect of these three terms separately on the bundle adjustment of a strip with minimum ground control is shown in Figure 1 and Table 1. Assumed is 60 % overlap between photographs, measurement of 25 points in a square grid pattern in each photograph with 45 mm spacings between points, and a focal length of 150 mm. Again, level terrain and exactly vertical photographs are assumed. The strip coordinates are denoted by X, Y, and Z.

If $a_{22} = a_{11}$, the planimetric effects of the terms with x^2 and xy cancel each other and these terms produce only an x-shift of the projection centres with respect to the terrain points and a corresponding longitudinal tilt of each photograph. Therefore, if one has somehow solved for a_{22} and a_{11} , adding the same amount to these two parameters gives another solution which differs from the first one only in the X-coordinates of the projection centres and in the longitudinal tilts. In general, the data will not make it possible to decide which of the two solutions is the better one. As a result, only the difference between these two parameters can be a parameter in the adjustment.

Further, it is obvious also from the figure and the table that the coefficient a_{13} of the term with y^2 can be determined from the data only in the exceptional case of dense and very accurate ground control in suitable locations. Therefore in general this coefficient can be given a more or less arbitrary value.

FIGURE 1 - Planimetric corrections at the 15 points in each model, caused by the three scale correction terms

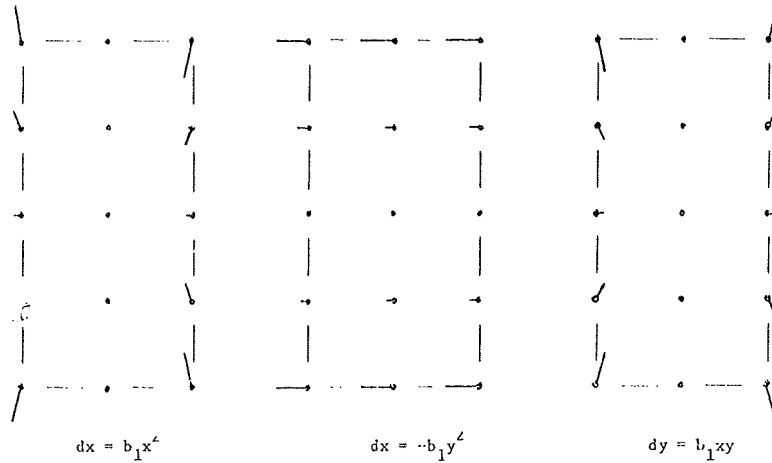


TABLE 1 - Effects upon a triangulated strip of scale correction terms which each amount to 40 μm in the corner grid points in the photographs; b₁ is positive, results are at photograph scale.

	$dx = b_1x^2$	$dx = -b_1y^2$	$dy = b_1xy$
Largest planimetric correction in each model (see Fig. 1)	0.04 mm	0.04 mm	0.04 mm
X-shift of centre of strip with respect to ends	+0.81 mm	no shift	-0.81 mm
X-shift of projection centres with respect to terrain points	+0.22 mm	no shift	-0.11 mm
corresponding tilt correction	+0.00148 rad		-0.00074 rad
Z-shifts of projection centres	+0.60 to -0.60 mm		-0.60 to +0.60 mm

Accordingly, taking $a_{22} - a_{11} = b_1$, suitable scale corrections are the conformal and the parabolic corrections:

$$\begin{aligned} dx &= b_1(x^2 - y^2) & \text{and} & & dx &= b_1x^2 \\ dy &= 2b_1xy & & & dy &= 2b_1xy \end{aligned} \quad (2a, b)$$

and also, for instance, the pairs of corrections

$$\begin{aligned} dx &= -b_1y^2 & \text{and} & & dx &= -b_1(x^2 + y^2) \\ dy &= b_1xy & & & dy &= 0 \end{aligned} \quad (2c, d)$$

and the pairs

$$\begin{aligned} dx &= 0 & \text{and} & & dx &= -b_1x^2 \\ dy &= b_1xy & & & dy &= 0 \end{aligned} \quad (2e, f)$$

The corrections (2c) and (2d) may be called pseudo-conformal scale corrections and the corrections (2e) and (2f) may be called pseudo-parabolic scale corrections because they have the same effect upon the planimetry as the corrections (2a) and (2b), respectively.

The terms with a_{21} , a_{23} , and a_{12} may be called azimuth correction terms. If $a_{23} = -a_{21}$ and $a_{12} = -2a_{21}$, they cause a conformal change of azimuth throughout a triangulated strip. If $a_{23} = 0$ and $a_{12} = -2a_{21}$, they cause a parabolic azimuth correction.

The effect of these three terms separately on the bundle adjustment of a single strip with minimum ground control is shown in Figure 2 and Table 2, under the same assumptions as before.

Here, it is obvious that only the term $a_{21}x^2$ causes an azimuth correction. Therefore, the coefficient a_{21} is here the parameter. As regards the coefficients a_{12} and a_{23} , only their difference could be determined and this only in the case of dense and very accurate planimetric ground control in suitable locations.

In general, these two coefficients cannot be free parameters in the adjustment. Each can be either made equal to zero or related to the coefficient a_{21} . Accordingly, suitable corrections are, here also, the conformal and the parabolic corrections

$$\begin{aligned} dx &= -2b_2xy & \text{and} & & dx &= 2b_2xy \\ dy &= b_2(x^2 - y^2) & & & dy &= b_2x^2 \end{aligned} \quad (2g,h)$$

and also, for instance, the pairs of corrections

$$\begin{aligned} dx &= -b_2xy, \quad dx = 0 & \text{and} & & dx &= 0 \\ dy &= b_2x^2, \quad dy = b_2(x^2 + y^2) & & & dy &= b_2x^2 \end{aligned} \quad (2i,j,k)$$

The corrections (2i) and (2j) may be called pseudo-conformal azimuth corrections. The selection of suitable pairs for correction terms with parameters b_1 and b_2 from the above or from other possible pairs appears to be rather arbitrary. Perhaps, extraneous information on the type of image deformation which can be expected may help in the choice. Otherwise, one may as well select a simple set, such as given by equations (2e) and (2k).

FIGURE 2 - Planimetric corrections at the 15 points in each triangulated model, caused by the three azimuth correction terms

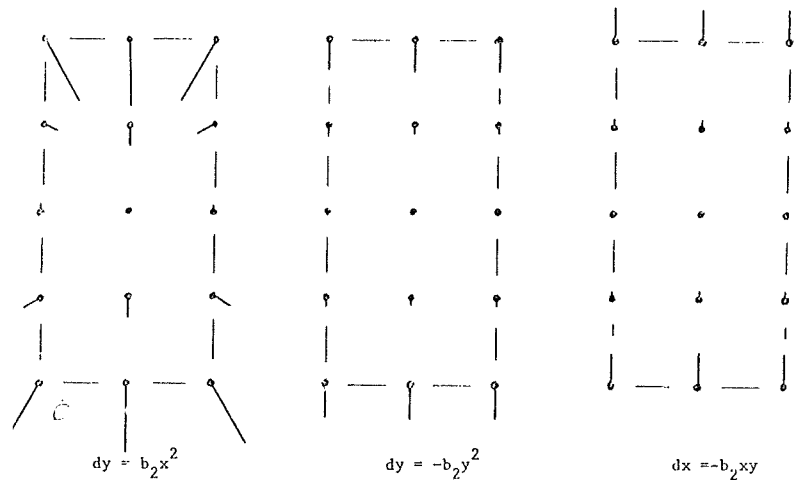


TABLE 2 - Effects upon a triangulated strip of azimuth correction terms which each amount to 40 μm in the corner grid points in the photographs; b_2 is positive, results are at photograph scale.

	$dy = b_2x^2$	$dy = -b_2y^2$	$dx = -b_2xy$
largest planimetric correction in each model (see Fig. 2)	0.08 mm	0.04 mm	0.04 mm
Y-shift of centre of strip with respect to ends	-0.81 mm	no shift	no shift
Y-shift of projection centres with respect to terrain points	+0.22 mm	no shift	-0.11 mm
corresponding tilt correction	-0.00148 rad		+0.00074 rad

THIRD DEGREE CORRECTIONS

The third degree corrections

$$\begin{aligned} dx &= c_{11}x^3 + c_{12}x^2y + c_{13}xy^2 + c_{14}y^3 \\ dy &= c_{21}x^3 + c_{22}x^2y + c_{23}xy^2 + c_{24}y^3 \end{aligned} \quad (3)$$

are useful for the correction of height deformation in a triangulated strip. Some of these terms also affect the planimetry.

If $c_{11} = c_{22}$, the terms with these coefficients apply a constant correction to

longitudinal height curvature of a triangulated strip, without causing other deformations. If $c_{11} \neq c_{22}$, the longitudinal curvature correction given to each model is different from the one given to the whole strip. For instance, the term with c_{22} alone applies a correction to each model which is twice that applied to the strip and is in the opposite direction. Each of the two terms separately also applies corrections to the scale in y-direction and these corrections are four times larger in the model overlap than in the centre line of each model.

If $c_{12} = c_{23}$, the terms with these coefficients apply a linear torsion to a triangulated strip. If $c_{12} \neq c_{23}$, the bundle adjustment leaves residuals in the x- and y-coordinates, it causes irregular height corrections at the ends of the strip, and it causes planimetric deformation.

If $c_{13} = c_{24}$, the terms with these coefficients apply a constant correction to height curvature across a triangulated strip. The term with c_{24} alone causes only a third degree variation in the y-scale as a function of y. It serves to cancel a similar variation but of opposite sign caused by the term with c_{13} alone.

The two remaining terms in Eq. (3) appear to be of little interest. The term $c_{14}y^3$ applies a correction to the strip X-coordinates which is the same as the one applied to the photograph coordinates. It can be used only in the case of an exceptionally large amount of planimetric ground control in suitable locations. The term $c_{21}x^3$ causes systematic residuals in the y-coordinates, height deformation at the ends of a triangulated strip, and skewing of the X,Y axes.

Accordingly, of interest are the following third degree corrections :

$$\begin{aligned} dx &= c_1x^3 + c_2x^2y + c_3xy^2 \\ dy &= c_1x^2y + c_2xy^2 + c_3y^3 \end{aligned} \tag{3a}$$

M. DE MASSON D'AUTUME'S CORRECTION TERMS

The preceding results can serve to analyse the terms for correction of systematic deformation proposed by De Masson d'Autume (1968, 1972). Each pair of these correction terms has two variables which are different functions of one independent parameter.

The correction terms for variation of scale can be written:

$$dx = \alpha_1 + \alpha_2x^2 ; \quad dy = -\frac{1}{12} \alpha_2xy$$

The shift α_1 can here be computed during the adjustment because, via the independent parameter, it is a function of α_2 . However, being such a function, it depends upon an arbitrary assumption regarding the relation between the shift and the required scale correction. With equal justification, it can be omitted. As the discussion of Eqs. (2) shows, the choice of a ratio -1/12 between the coefficients of x^2 and xy is also arbitrary. It makes the scale correction neither pseudo-conformal nor pseudo-parabolic. As the actual systematic deformation is unknown this ratio is equally acceptable as the ratios implied in Eqs. (2a) to (2f).

The terms for correction of curvature in the horizontal plane can be written:

$$dx = 0 ; \quad dy = \beta_1 + \beta_2x^2$$

Here, the shift β_1 may be omitted for similar reasons as the shift α_1 in the preceding equations. This reduces the equations to the equations (2k) which are neither pseudo-conformal nor pseudo-parabolic but equally acceptable.

The terms for longitudinal curvature in the vertical plane can be written:

$$dx = 0 ; \quad dy = \gamma_1y + \gamma_2x^2y$$

As stated earlier, the term γ_2x^2y without a corresponding correction γ_2x^3 for the x-coordinates applies a curvature correction to each model which is very different from that applied to the whole strip. With orientation points only in the six regular positions in each model, as used by De Masson d'Autume, this does not become apparent. The term γ_1y applies a linear correction to the y-scale of the triangulated

ated strip which is a function of the curvature correction. This correction cannot compensate for the non-linear correction to the y-scale caused by the term $\gamma_2 x^2 y$. These are by-products of the adjustment that do not serve to correct assumed strip deformation. It follows that these corrections for longitudinal curvature are a rather unfortunate choice.

The terms for torsion can be written :

$$dx = 2\delta_1 y + 2\delta_2 x^2 y ; \quad dy = \delta_1 x + \delta_2 xy^2 .$$

Because the terms with $x^2 y$ and xy^2 have different coefficients, they cause x- and y-residuals and planimetric deformation. These, also, are an unwarranted by-product of the adjustment. The two linear correction terms cause a non-orthogonality of the strip axes that is a function of the torsion correction. It follows that the torsion corrections, also, are rather unfortunately chosen.

OTHER CORRECTION TERMS

Duane C. Brown computes correction terms both in camera calibrations and in block adjustments. In one investigation (Brown 1971) polynomials of the third degree with independent coefficients were used for x- and y-corrections (10 terms each). All terms except the four with x^3 and y^3 were found to be significant. However, the elimination of small systematic errors near the edges of the photographs required the use of general polynomials of the fifth degree. In a program used for commercial block adjustment (Brown 1973), correction terms are used for radial distortion (3), decentering distortion (2), systematic film deformation (7 for x and 7 for y) and unflatness of film platen (7). Detailed information on the selected terms has not been published but, obviously, all coefficients are assumed to be independent.

Bauer and Müller (1972) also make use of correction terms in block adjustment. Two terms with coefficients r^3 and r^6 correct for symmetric radial distortion (r is the distance from image point to principal point). Thus, apart from related terms which are designed to reduce the introduced scale changes, they specify:

$$dx = a_1 x r^2 + a_2 x r^5$$
$$dy = a_1 y r^2 + a_2 y r^5$$

Bauer and Müller also use other radial corrections and tangential corrections. These corrections can be reformulated as sums of terms which are also functions of x , y , and r . Such terms occur in pairs with the same coefficient. The radial correction terms are of the form :

$$dx = b_{xx} p y^q / r^{p+q}$$
$$dy = b_{yx} p y^q / r^{p+q}$$

and the tangential correction terms are of the form

$$dx = -c_{yx} p y^q / r^{p+q}$$
$$dy = c_{xx} p y^q / r^{p+q}$$

in which p and q are positive integers. The division by a power of r serves to make the corrections for points on a line through the principal point proportional to r .

Kubik (1971, 1973) has investigated the effect of four types of corrections on triangulated strips and blocks. Three of these can be written as simple polynomial corrections to the y-coordinates :

$$dy = P_x + A_y + T_{xy}$$

The fourth type of correction introduces the novel feature of the absolute value of x or y as a factor in the correction terms. These terms can be written

$$dx = R_x |y| ; \quad dy = R_y |x| .$$

In the way this feature is used here, the derivatives of the corrected coordina-

tes with respect to the uncorrected ones show discontinuities at the coordinate axes. However, this can be avoided when the absolute values are combined in different ways with powers of x and y .

CONCLUSION

This investigation has demonstrated that certain terms and combinations of terms of polynomials in the photograph coordinates are especially suitable for the correction of systematic strip deformation during bundle adjustment.

The first degree terms (1a) or, alternatively, (1b) may be used if planimetric torsion and differential scale error were not eliminated before the adjustment and if, in addition, sufficient planimetric ground control is available.

A selection of terms may be made from the second degree terms (2a) to (2k) to correct systematic planimetric curvature and variation of scale. Because the actual image deformations are unknown, the selection can only depend upon subjective criteria.

The third degree terms (3a) are suitable for the correction of systematic height deformation. The last of these terms can be used only if either sufficient height control exists across at least one strip or the lateral overlap of the strips is large.

All these terms have no effect, or at the most very little effect upon the x - and y -residuals that the actual systematic deformations would leave after an adjustment without them. Consequently, the effectiveness of correction terms cannot be judged by their effect upon the residuals. For that purpose, one must use check points and an investigation of any remaining systematic pattern in the residuals.

The quoted investigations show that in addition to the above, terms with powers of the radial distance r and their reciprocals and terms with the absolute value of a photograph coordinate may be useful. There are here still many unexplored terms which correspond to simple deformation patterns. A systematic investigation of these terms should be made also.

REFERENCES

- Bauer, H. and Müller, J. "Height accuracy of blocks and bundle adjustment with additional parameters", presented paper for the XIIth Congress of the International Society for Photogrammetry, July 23 - August 4, 1972
Ottawa, Canada
- De Masson d'Autume, G., 1968 "The perspective bundle of rays as the basic element in aerial triangulation", *Photogrammetria* 23, pp. 55 - 66
- De Masson d'Autume, G., 1972 "Le traitement des erreurs systématiques dans l'aérotriangulation", *Bulletin de la Société Française de Photogrammetrie* No. 46
- Kubik, K., 1971 "The effects of systematic image errors in block triangulation", *I.T.C. Publication A 49*, pp.1 -143
- Kubik, K., 1973 "Systematic image errors in aerial triangulation" *Photogrammetria* 29, pp. 113 - 131

BUNDLE ADJUSTMENT WITH ADDITIONAL PARAMETERS - PRACTICAL EXPERIENCES

by H. Bauer, Hannover, Fed.Rep. Germany

THE THEORY OF THE ADDITIONAL PARAMETERS

The theory is simple. The error equations of the central perspective between the photo and the terrain are extended by additional free parameters. The equations then run :

$$v = A_1x + A_2y + A_3z -$$

x are the coordinate unknowns
 y are the orientation unknowns
 z are the unknown correction parameters.

What demands should the correction terms fulfil ?

- The terms should be effective.
- The correction terms should be simple and as short as possible.
- The terms should not be correlated with each other.
- The terms should not be correlated with orientation unknowns (coordinates of the perspective centres and orientation angles).
- The interior orientation of the photos (focal length and principal points) should not be changed.
- For practical work terms are preferable which are not affected by rotation by 180°. In this case it is not necessary to distinguish the direction in which the strips were flown, and the position of the photos in the comparator (direction of triangulation) has no influence on computation.

WE HAVE EXPERIMENTED WITH THE FOLLOWING TERMS :

1. radial and independent on direction

$$\begin{aligned} \Delta x'_1 &= a_1x'(r'^2 - r'_0{}^2); & \Delta y'_1 &= a_1y'(r'^2 - r'_0{}^2) \\ \Delta x'_2 &= a_2x'(r'^5 - r'_0{}^5); & \Delta y'_2 &= a_2y'(r'^5 - r'_0{}^5) \end{aligned}$$

$r'_0 = 100 \text{ mm}$

2. radial and dependent on direction

$$\begin{aligned} \Delta x'_3 &= a_3x'\cos 2\alpha + a_4x'\sin 2\alpha \\ \Delta y'_3 &= a_3y'\cos 2\alpha + a_4y'\sin 2\alpha \\ \Delta x'_5 &= a_5x'\cos 4\alpha + a_6x'\sin 4\alpha \\ \Delta y'_5 &= a_5y'\cos 4\alpha + a_6y'\sin 4\alpha \\ \Delta x'_7 &= a_7x'\cos \alpha + a_8x'\sin \alpha \\ \Delta y'_7 &= a_7y'\cos \alpha + a_8y'\sin \alpha \end{aligned} \left. \vphantom{\begin{aligned} \Delta x'_3 \\ \Delta y'_3 \\ \Delta x'_5 \\ \Delta y'_5 \\ \Delta x'_7 \\ \Delta y'_7 \end{aligned}} \right\} \begin{array}{l} \text{dependent} \\ \text{on flight direction} \end{array}$$

3. tangential and dependent on direction

$$\begin{aligned} \Delta x'_9 &= -a_9y'\cos 2\alpha - a_{10}y'\sin 2\alpha \\ \Delta y'_9 &= a_9x'\cos 2\alpha - a_{10}x'\sin 2\alpha \\ \Delta x'_{11} &= -a_{11}y'\cos 4\alpha - a_{12}y'\sin 4\alpha \\ \Delta y'_{11} &= a_{11}x'\cos 4\alpha + a_{12}x'\sin 4\alpha \\ \Delta x'_{13} &= -a_{13}y'\cos \alpha - a_{14}y'\sin \alpha \\ \Delta y'_{13} &= a_{13}x'\cos \alpha + a_{14}x'\sin \alpha \end{aligned} \left. \vphantom{\begin{aligned} \Delta x'_9 \\ \Delta y'_9 \\ \Delta x'_{11} \\ \Delta y'_{11} \\ \Delta x'_{13} \\ \Delta y'_{13} \end{aligned}} \right\} \begin{array}{l} \text{dependent} \\ \text{on flight direction} \end{array}$$

4. shearing

$$\begin{aligned} x' &= 0 \\ y' &= a_{19}x' \end{aligned}$$

5. affinity

$$\begin{aligned} x' &= -a_{20}x' \\ y' &= +a_{20}y' \end{aligned}$$

The program allows four terms to be computed at the same time. For this reason we combined the terms to correction groups with four unknown parameters.

- group 1: radial with r'^3 , r'^6 and $r'\cos 2(a-\epsilon_1)$
- group 2: shearing, affinity and tangential with $r'\cos 2(a-\epsilon_4)$
- group 3: radial and tangential with $r'\cos(a-\epsilon_3 - x_j)$
- group 4: radial and tangential with $r'\cos 4(a-\epsilon)$

RESULTS OF THE OBERSCHWABEN TEST

Strip 1, 3, 5, 7 and 9 of the test block were added to a subblock. In this block the effectiveness of the correction terms was checked. The following tables show the profit in accuracy of the standard deviation of an image coordinate observation (σ_o), the increase of sigma check, and also the size of the individual correction terms.

The 1. parameter group resulted radial corrections as a function of r'^3 in a size of $2\mu\text{m}$ at the maximum and pointed to a lack of orthogonality. The term r'^6 proved to be ineffective. The accuracy increase at the check points is 14 % respectively 31 % (table 1).

1. PARAMETER GROUP – Subblock Oberschwaben					
Strips 1, 3, 5, 7, 9					
parameter		max.correction of an image coordinate	increase of accuracy in relation to without add. parameter		
function	size				
$\Delta r'_1 = a_1 r' (r'^2 - 10^2)$	$a_1 = + 0,0051$	$- 2 \mu\text{m}$	11,4 %	5,13 μm	standard deviation of an image coordinate
$\Delta r'_2 = a_2 r' (r'^5 - 10^5)$	$a_2 = + 0,16 \cdot 10^{-6}$	$- 0,2 \mu\text{m}$	14,2 %	25,5 cm	
$\Delta r'_3 = a_3 r' \cos 2\alpha$	$a_3 = - 0,04$	$- 0,4 \mu\text{m}$			31,0 %
$\Delta r'_4 = a_4 r' \sin 2\alpha$	$a_4 = - 0,225$	$- 2,2 \mu\text{m}$	sigma check UTM - South		

TABLE 1

The 2. parameter group contains affine and tangential corrections. This group was charged twice :

- 1 - To the image coordinates, which have been applied to the corrections of the first parameter group (table 2).
- 2 - To the original image coordinates (table 3).

The results of both computations were about the same. The accuracy of the adjustment increases about 25 % and the accuracy of the check points even about 50 %. In the first case (table 2) the size of the shearing, affinity and tangential distortion attains equal $2,6 \mu\text{m}$ in a distance of 10 cm of the principal point.

2. PARAMETER GROUP – Subblock Oberschwaben					
1 parameter group given					
Strips 1, 3, 5, 7, 9					
parameter		max.correction of an image coordinate	increase of accuracy in relation to without add.parameter		
function	size				
$\Delta x'_{1g} = 0$ $\Delta y'_{1g} = a_{1g}x'$	$a_{1g} = -0,265$	- 2,6 μm	26,4 %	4,26 μm	standard deviation of an image coordinate
$\Delta x'_{20} = -a_{20}x'$ $\Delta y'_{20} = +a_{20}y'$	$a_{20} = -0,264$	- 2,6 μm			
$\Delta x'_g = -a_g y' \cos 2\alpha$ $\Delta y'_g = a_g x' \cos 2\alpha$	$a_g = -0,267$	- 2,7 μm	49,0 %	15,2 cm	sigma check UTM - North
$\Delta x'_{10} = -a_{10}y' \sin 2\alpha$ $\Delta y'_{10} = a_{10}x' \sin 2\alpha$	$a_{10} = -0,052$	- 0,5 μm	44,7 %	15,3 cm	sigma check UTM - South

TABLE 2

In the second case (table 3) the shearing amounts to 9,3 μm and the affinity 4,2 μm in the same distance from the principal point. The tangential distortion is insignificant. That means all radial corrections we have computed with parameter group 1 and 2 may be explained as shearing and affinity. The size of the corrections to suppose that there are no systematics with photogrammetrical origin but systematics with terrainian origin.

2. PARAMETER GROUP – Subblock Oberschwaben					
only parameter group 2					
Strips 1, 3, 5, 7, 9					
parameter		max.correction of an image coordinate	increase of accuracy in relation to without add.parameter		
function	size				
$\Delta x'_{1g} = 0$ $\Delta y'_{1g} = a_{1g}x'$	$a_{1g} = -0,928$	- 9,3 μm	24,0 %	4,40 μm	standard deviation of an image coordinate
$\Delta x'_{20} = -a_{20}x'$ $\Delta y'_{20} = +a_{20}y'$	$a_{20} = -0,425$	- 4,3 μm			
$\Delta x'_g = -a_g y' \cos 2\alpha$ $\Delta y'_g = a_g x' \cos 2\alpha$	$a_g = -0,007$	- 0,0 μm	47,9 %	15,5 μm	sigma check UTM - North
$\Delta x'_{10} = -a_{10}y' \sin 2\alpha$ $\Delta y'_{10} = -a_{10}x' \sin 2\alpha$	$a_{10} = -0,064$	- 0,6 μm	45,1 %	15,2 cm	sigma check UTM - South

TABLE 3

4. PARAMETER GROUP – Subblock Oberschwaben

only parameter group 4

Strips 1, 3, 5, 7, 9

parameter		max.correction of an image coordinate	increase of accuracy in relation to without add. parameter		
function	size				
$\Delta x'_5 = a_5 x' \cos 4\alpha$ $\Delta y'_5 = a_5 y' \cos 4\alpha$	$a_5 = -0,198$	- 2,0 μm	2,6 %	4,88	standard deviation of an image coordinate
$\Delta x'_6 = a_6 x' \sin 4\alpha$ $\Delta y'_6 = a_6 y' \sin 4\alpha$	$a_6 = -0,015$	- 0,2 μm			
$\Delta x'_{11} = a_{11} y' \cos 4\alpha$ $\Delta y'_{11} = a_{11} x' \cos 4\alpha$	$a_{11} = +0,006$	+ 0,1 μm	9,9 %	46,3 cm	sigma check UTM - North
$\Delta x'_{12} = -a_{12} y' \sin 4\alpha$ $\Delta y'_{12} = a_{12} x' \sin 4\alpha$	$a_{12} = +0,054$	+ 0,1 μm			
			1,7 %	50,8 cm	sigma check UTM - South

TABLE 4

The parameter group 4 with radial and tangential corrections as a function of the quadrupel period of the image angle should eliminate systematic errors in the corners of the images. The parameter group proved to be ineffective (table 4).

The parameter group 3 is the radial and tangential image coordinate correction with the single period of the image angle. The correction depends on an image rotation by 180° (that may be change of flight direction of the strips or the photo position in the comparator). The flight direction and the photo position in the

3. PARAMETER GROUP – Subblock Oberschwaben

1 and 2 parameter group given actual feight direction,
strips 1, 3, 5, 7 north-south, strip 9 south-north

Strips 1, 3, 5, 7, 9

parameter		max.correction of an image coordinate	increase of accuracy in relation to without add. parameter		
function	size				
$\Delta x'_7 = a_7 x' \cos \alpha$ $\Delta y'_7 = a_7 y' \cos \alpha$	$a_7 = + 0,631$	+ 6,3 μm	35 %	3,76 μm	standard deviation of an image coordinate
$\Delta x'_8 = a_8 x' \sin \alpha$ $\Delta y'_8 = a_8 y' \sin \alpha$	$a_8 = +1,392$	+ 13,9 μm			
$\Delta x'_{13} = -a_{13} y' \cos \alpha$ $\Delta y'_{13} = a_{13} x' \cos \alpha$	$a_{13} = - 0,199$	- 2,0 μm	48,3 %	15,4 μm	sigma check UTM-North
$\Delta x'_{14} = -a_{14} y' \sin \alpha$ $\Delta y'_{14} = a_{14} x' \sin \alpha$	$a_{14} = - 0,107$	- 1,1 μm			
			49,1 %	14,1 cm	sigma check UTM-South

TABLE 5

comparator were considered as additional informations at the adjustment.

The parameter group 3 effects an important increase of the standard deviation of an image coordinate and no improvement in accuracy of the check points as against the second group (table 5). The radial correction amounts to more than 15 μm in a distance of 10 cm from the principal point, but the effect upon the accuracy of the block coordinates is small. This is an indication for a large correlation between correction parameters and the elements of the interior orientation (principal point location).

The correction of a single period may have three causes: Camera errors, refraction errors due to an air stream close to the airplane and influences of the atmosphere on account of the sun light radiating from one side. Only the first two elements are connected with the airplane. It is possible to separate these parts by a combination of the parameters of one test, in which the flight direction is considered to be uniform (table 6), and another test in which the real flight direction is taken into consideration. In our case the systematic errors of the camera and of refraction of the air stream close to the airplane dominate. These are influences which are independent of the flight direction. The errors which are dependent of flight direction are insignificant.

3. PARAMETER GROUP – Subblock Oberschwaben					
1. and 2. parameter group, given assumed uniform feight direction					
Strips 1, 3, 5, 7, 9					
parameter		max.correction of an image coordinate	increase of accuracy in relation to without add. parameter		
function	size				
$\Delta x_7 = a_7 x' \cos \alpha$ $\Delta y_7 = a_7 y' \cos \alpha$	$a_7 = +0,376$	+ 3,8 μm	29, %	4,11 μm	standard deviation of an image coordinate
$\Delta x_8 = a_8 x' \sin \alpha$ $\Delta y_8 = a_8 y' \sin \alpha$	$a_8 = +0,787$	+ 7,9 μm	49,6 %	15,0 cm	sigma check UTM - North
$\Delta x_{13} = -a_{13} y' \cos \alpha$ $\Delta y_{13} = a_{13} x' \cos \alpha$	$a_{13} = -0,105$	- 1,0 μm			
$\Delta x_{14} = -a_{14} y' \sin \alpha$ $\Delta y_{14} = a_{14} x' \sin \alpha$	$a_{14} = -0,114$	- 1,1 μm	42,2 %	16,0 cm	sigma check UTM-South

TABLE 6

On the basis of the results of the explained tests we draw the following conclusion:

1. Correction terms of a single and a quadruple period prove to be ineffective, as corrections of $r^1 6$.
2. We have little effect with radial and tangential corrections with the double period.
3. Effective is the radial correction $r^1 3$, which considers refraction errors and corrections which eliminate shearing and affinity.

Based on this analysis we chose one parameter group with four terms and another with three terms, which we hoped to be very effective. The four terms are $r^1 3$, shearing and radial correction of the double period. The three terms comprehend $r^1 3$, shearing and affinity.

Both parameter groups were used regular at all aerial triangulations of the Landesvermessungsamt Hannover. About the size of the correction terms in some block

TEST AREA							CORRECTION PARAMETERS				
name	Photo-scale	camera	sidelap	strips	models	rms	radial with r^3 $\Delta x' = a_1 x' (r'^2 \cdot 10^2)$ $\Delta y' = a_1 y' (r'^2 \cdot 10^2)$	shearing $\Delta x' = 0$ $\Delta y' = a_2 x'$	radial with $ar' \cos 2(a - \epsilon)$ $\Delta x' = a_3 x' \cos 2a$ $\Delta y' = a_4 y' \cos 2a$		affinity $\Delta x' = -a_5 x'$ $\Delta y' = +a_5 y'$
						μm	a_1	a_2	a_3	a_4	a_5
Oberschwaben	1 : 28 000	15/23	20 %	8	200	4,2	0,0036	- 0,941			- 0,383
Oberschwaben	1 : 28 000	15/23	20 %	8	200	4,6	0,0048	- 0,995	0,053	0,033	
Steinbergen	1 : 8 000	15/23	60 %	10	90	5,3	0,0115	- 0,112	0,120	- 0,015	- 0,107
			20 %	5	45	5,1	0,0114	- 0,111			
Unsen	1 : 6 000	15/23	60 %	6	96	11,0	0,0111	- 1,092	- 0,144	- 0,112	
				7	81	11,0	0,0096	0,061	- 0,526	- 0,185	
				8	127	13,7	0,0132	- 2,045	- 0,432	- 0,028	
Stadtoldendorf	1 : 3 300	30/23	60 %	9	100	5,3	0,0032	- 0,212	- 0,060	+ 0,001	
Mörse	1 : 3 300	30/23	60 %	5	18	4,9	- 0,0035	+ 1,85	- 0,106	+ 0,470	
Alfeld	1 : 3 300	30/23	60 %	7	80	8,4	- 0,0047	0,82	0,255	0,139	
Brockel	1 : 6 000	30/23	20 %	5	85	6,8	- 0,0038	1,71	0,120	- 0,090	
	1 : 8 000			8	56	5,5	- 0,0057	0,70	0,316	- 0,000	

TABLE 7

adjustments for height evaluation, cadastral surveying, and fix point evaluation will be reported (table 7).

In the whole Block Oberschwaben with 8 strips and 200 models the size of the parameter corresponds to the subblock Oberschwaben, we tested before. This demonstrates the reliability of the method of additional parameters and proves that even such a large block as Oberschwaben, covering an area of 40 x 62,5 km, contains dominant systematic errors, which can be eliminated by additional parameters. In the block Oberschwaben a radial effect, shearing and affinity could be filtered out, but no radial correction with double period.

The aerial triangulations Steinbergen and Unsen served for height evaluation with an accuracy of about 1 dm. A sidelap of 60 % was used in these blocks to give them a maximum of stability. Compared to the Oberschwaben test the size of the parameters with r^3 is more than doubled. That can be interpreted, errors due to refraction have more importance than we supposed till now. In block adjustment Steinbergen with the same comparator data but a sidelap of 20 %, the parameter r^3 has only half the size. That means, the whole size of refraction errors can only be eliminated with a sidelap of 60 %. For the aerial triangulation by cadastral surveying a camera 30/23 was used. In spite of the smaller image angle the refraction parameter is rather large, and the sign of the parameter changes between plus and minus. The shearing has a different size. In areas with horizontal control points of absolutely high accuracy, like Steinbergen and Stadtoldendorf, the correction of shearing is in the maximum 1 to 2 μ m. In all cases in which the quality of the horizontal control points is unknown and probably poor, the shearing effect is large, sometimes in a magnitude which is surprising. I believe with the shearing primarily terrestrial errors are eliminated.

In most of the discussed aerial triangulations the root mean square error of an image coordinate is about 5 μ m. Without a shearing parameter you certainly don't get this, if you have no horizontal control points with high accuracy.

The correction with r^3 , shearing and affinity have approved themselves in many practical cases. It is desirable to find out a correction term which eliminates the systematics in the corners of the images.

REFERENCES

- [1] Bauer, H., Müller, J.: "Height accuracy of blocks and bundle adjustment with additional parameters", presented paper for the 12th International Congress for Photogrammetry
- [2] Bauer, H.: "Compensation of systematic errors by analytical block adjustment with common image deformation parameters", OEEPE Publication Officielle No 8, p. 319 - 334

SIMULTANEOUS COMPENSATION OF SYSTEMATIC ERRORS WITH BLOCK ADJUSTMENT BY INDEPENDENT MODELS

by H. Ebner and W. Schneider, Stuttgart, Fed.Rep. Germany

SUMMARY

An advanced concept of block adjustment by independent models is presented, allowing for a simultaneous compensation of certain types of systematic errors of model coordinates. To gain practical experience with this concept a corresponding computer program was written. The test results obtained up to now allow for the following conclusions:

- The practical application of the concept causes no problems.
- The accuracy of adjusted block coordinates is improved up to a factor 3.
- The obtained accuracy corresponds very well with the accuracy as predicted by theory.

PREFACE

In modern aerial triangulation systematic errors are of central importance again. This was so already, years ago, when the polynomial methods were introduced into strip and block triangulation. But during the following phase which was characterized by simultaneous least squares adjustment of all bundles or models of a block the interest concentrated on random errors whilst systematic errors were neglected most of the time.

The recent change of thinking was caused by the results of various practical block adjustments which indicate clearly that systematic errors of considerable size are present in photogrammetric data usually [1]. Some of the typical phenomena which can be caused by not compensated systematic deformations are:

- A reduction of control leads to a higher decrease of accuracy than predicted by theory.
- The accuracy decrease with increasing block size is higher than expected from theory.
- Replacing 20 % sideward overlap by 60 % side lap the accuracy is improved only slightly or even not at all.
- Starting from the same data a block adjustment by independent models can give more accurate results than a bundle block adjustment (see [2], [3], [4], [5], [6]).

THE MATHEMATICAL MODEL FOR COMPENSATION OF SYSTEMATIC ERRORS

Among the possibilities to compensate the inherent systematic errors of photogrammetric data the concept of selfcalibration by additional parameters is the most promising one being available today [7], [8]. In the adjustment we treat these parameters as random variables with appropriate weights [9], [10]. This approach has two essential advantages :

- It is fully general and leads to optimal accuracy results. Random variables (or observations) are the general case of parameters. Free unknowns as well as constants are special cases of observations and can be represented by weight zero and infinite weight respectively.
- Additional parameters put up as free unknowns can cause serious numerical problems. If some of the unknowns are highly correlated with each other the normal equations become ill conditioned. This problem is avoided when the additional parameters are treated as observations with proper weights.

The block adjustment can be formulated in different ways [10]. If the additional parameters generally are common to groups of models (to whole strips for instance) the following formulation is suitable :

$$\begin{aligned} v_1 &= Ax + By - f \\ v_2 &= \quad \quad \quad Iy - s \end{aligned} \quad G = \begin{bmatrix} G_{ff} & \\ & G_{ss} \end{bmatrix} \quad (1)$$

- f = vector of observations
- v₁ = vector of residuals belonging to f
- s = vector of additional observations
- v₂ = vector of residuals belonging to s
- x = vector of unknowns
- A = coefficient matrix belonging to x
- y = vector of additional unknowns
- B = coefficient matrix belonging to y
- I = unit matrix
- G_{ff} = weight coefficient matrix of the observations f
- G_{ss} = weight coefficient matrix of the additional observations s .

In equations (1) the additional parameters are put up as unknowns and these unknowns are observed. Usually the additional observations s will be zero. But if some of the additional parameters are known from a priori calibrations the corresponding amounts can be introduced into the adjustment.

The formulation presented here fits into the approach of Generalized Least Squares [11]. This approach itself is related to the concept of Bayesian Estimation [12]. Furthermore it can be shown that the present formulation according to equations (1) fits into the mathematical model of Least Squares Collocation if we set s = 0 (additional observations of amount zero) [13]. In this case we obtain :

$$Ax - v_1 + Bv_2 = f \quad (2)$$

- Ax = trend
- v₁ = noise
- Bv₂ = signal
- G_{ff} = weight coefficient matrix referring to noise
- BG_{ss}B^T = weight coefficient matrix referring to signal .

REALIZATION IN CASE OF INDEPENDENT MODEL BLOCK ADJUSTMENT

As the basic method for block adjustment by independent models we choose the planimetry height iteration used in the PAT-M43 program [14]. Concerning the additional parameters we suppose that the systematic deformations are common to a certain group of models at times but change from group to group. In addition some systematic can be common to all models.

With the formulation of identic deformations for different models a problem appears resulting from the fact that the coordinate origin is arbitrary for each model. The same formulation $\Delta x = axy, \Delta y = 0$ for instance leads to different model deformations, depending on the origin of x (see figure 1).

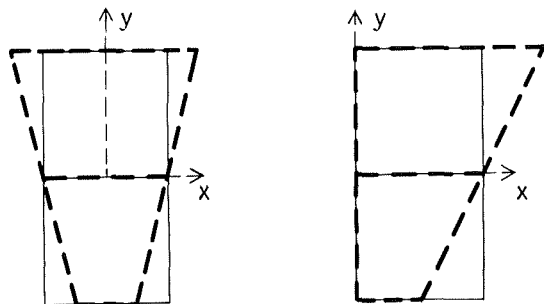


FIGURE 1

This problem doesn't appear in bundle block adjustment where the origin of each image is well defined by the centre point. To solve the problem also in case of independent models we search for parameters whose effects are not changed by shifts of the coordinate system in x and y direction. This condition leads to 4 planimetric parameters e, f, p, q and to 6 height parameters r, s, t, u, v, w. The effect of these parameters and their contributions to the observational equations for planimetry and height are shown in fig. 2 and fig. 3.

FIGURE 2

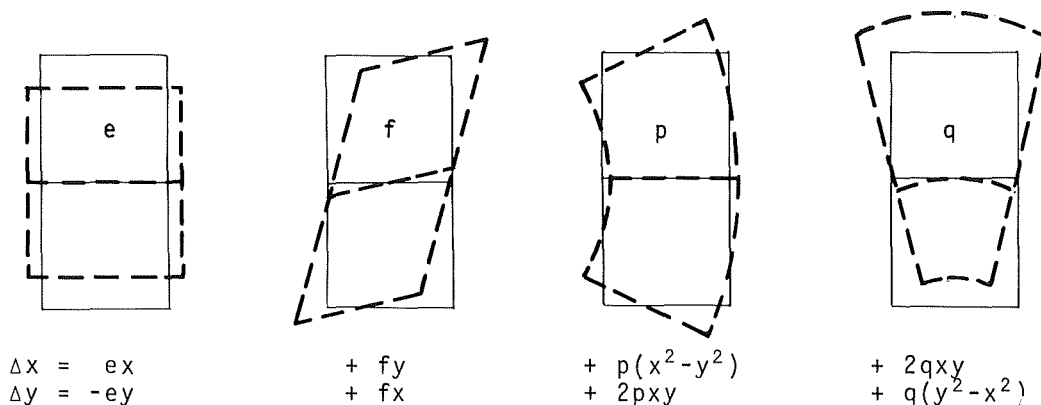
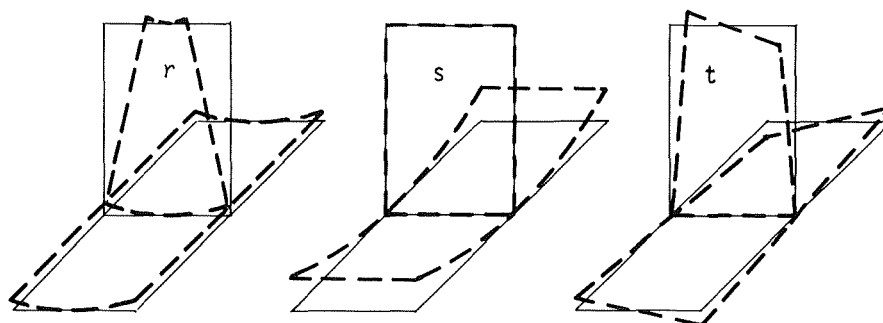


FIGURE 3



model points	$\Delta z = rx^2$	$+ sy^2$	$+ txy$
left (right)	$\Delta x = -2rxz$		$- tyz + (-) u$
hand side PC	$\Delta y = rx^2$	$- 2syz$	$- txz + (-) v$
		$+ sy^2$	$+ txy + (-) w$

The parameters e and f allow for a compensation of affine deformations of the planimetric model coordinates. The parameters p and q are the only one parameters of degree 2 whose effects are independent of coordinate shifts in x and y direction. They also appear in conformal polynomial strip adjustment and are able to compensate the trapezoid shaped model deformations gained in |1|.

The effects of the affinity terms e and f are independent of the flight direction. In contrast to that the effects of the parameters p and q change when the flight direction is turned.

The height parameters r and s compensate for quadratic z deformations in x and y direction whilst the parameter t corrects for twisted models. The terms u, v and w compensate for systematic errors of perspective centre coordinates.

TESTS RESULTS

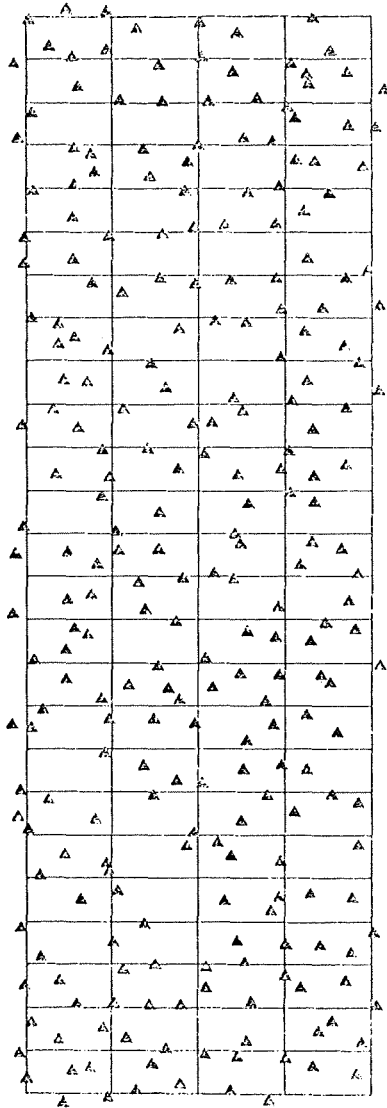
To gain practical experience with the suggested concept a preliminary computer program was written by the second author. This program is fully operational and is capable to adjust blocks of medium size with a reasonable computing time. The additional parameters may be common to any group of models or/and to all models of the block. The weight of each of those parameters can be varied separately in a range between zero and infinite. At a later time this program shall be replaced by an extended version of the PAT-M package |14|.

The practical tests were performed to get answers to the following questions:

- For which groups of models shall be put up identical additional parameters and which weights shall be used for these parameters?
- Which accuracy improvement can be attained by an extended block adjustment with additional parameters?
- Is the accuracy obtained in agreement with the corresponding theoretical accuracy predictions?

So far as the test material is concerned use could be made of the data of the OEEPE project Oberschwaben. From the comprehensive material of this project we selected a subblock consisting of strips 5, 7, 9 and 11 of the block Frankfurt. The test block and the 258 available control points are shown in figure 4.

FIGURE 4



The total number of models is 100 and the block size is 20 km x 62.5 km. All control points and tie points were signalized. The photography was taken with a Zeiss RMK A 15/23 camera at a photo scale of 1 : 28 000. The image coordinates were measured with a Zeiss PSK stereo comparator and the independent models were formed computationally.

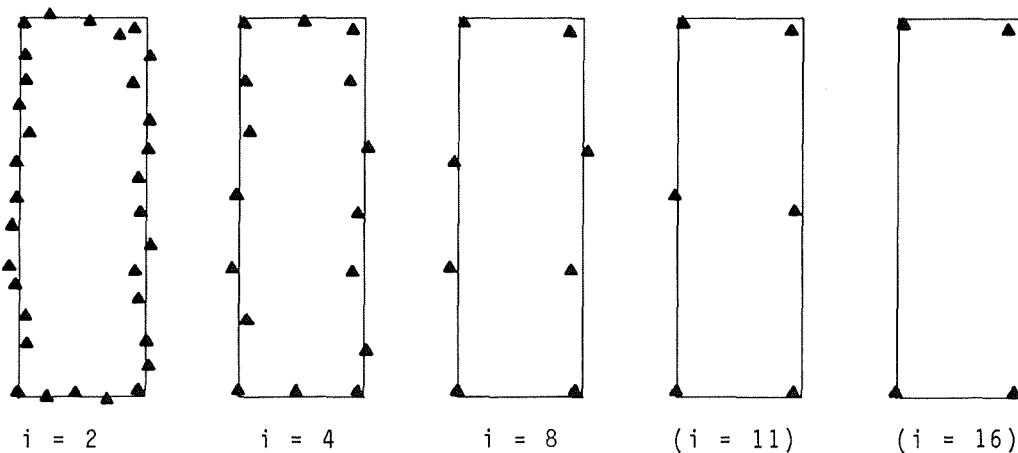
The test is not yet finished completely. In particular the investigation on height block adjustment with additional parameters is still at work. For that reason only the planimetric results are available up to now. The control distributions investigated here are represented in Figure 5.

The results obtained shall be discussed according to the questions raised at the beginning of this chapter.

IDENTICAL ADDITIONAL PARAMETERS AND PROPER WEIGHTS

At the beginning each strip was given its own set of additional parameters e , f , p and q . Considering the standard deviations σ of those parameters we have learned that the terms p and q are very well determined even if only 4 control points are used. Unfortunately the determination of the affinity terms e and f is much poorer. If only 4 control points are used the standard deviations are in the order of the amounts of the parameters themselves. However, if the affinity terms are common to all models of the block the standard deviations are reduced significantly. Respecting this it can be recommended to put up individual parameters e and f only if there is a real reason to do so. In case of our test block it was found as adequate to put up common affinity terms only.

FIGURE 5



Concerning proper weights of the additional parameters it was found that the amounts of the terms e, f, p and q, being computed in the block adjustment are only slightly dependent on their weights. This is true also in case of poor control distributions.

Therefore it can be recommended to choose the weights of the additional parameters according to their expected amounts or somewhat smaller. With that the accuracy is optimized and problems with respect to the condition of the normal equation matrix are avoided. The amounts of the additional parameters themselves are in agreement with the model deformations obtained in [1].

ACCURACY IMPROVEMENT BY ADDITIONAL PARAMETERS

Using the control distributions represented in figure 5 the test block was adjusted without and with additional parameters. The corresponding results are represented in table 1. The accuracies are related to the photo scale.

TABLE 1

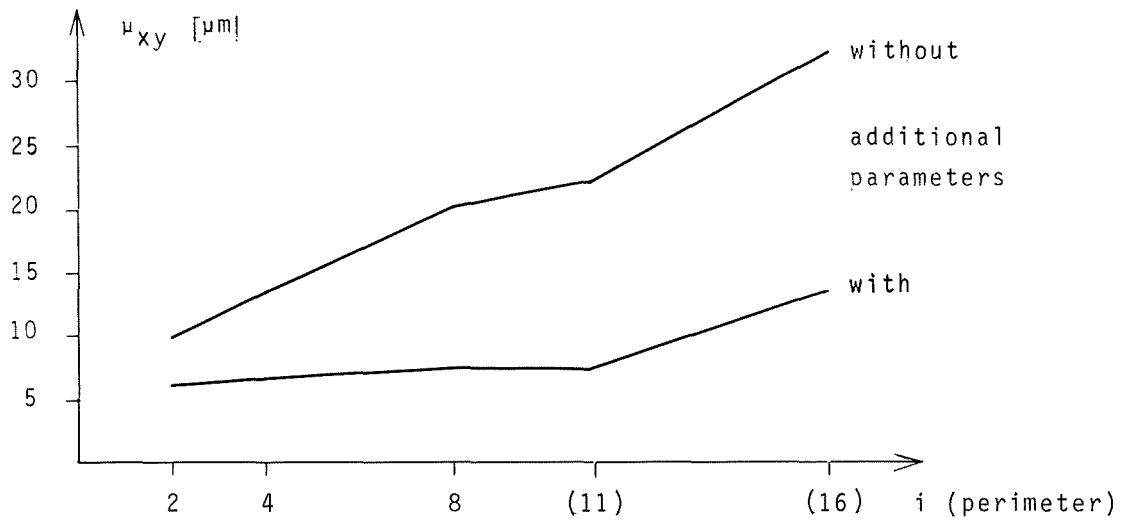
control version	control points	check points	without add. param.		with add. param.		accuracy ratios	
			σ_0 [μm]	μ_{xy} [μm]	σ_0 [μm]	μ_{xy} [μm]	σ_0	μ_{xy}
i=2	32	226	6.8	9.9	4.3	6.3	1.6	1.6
i=4	16	242	6.5	13.4	4.2	6.6	1.5	2.0
i=8	8	250	6.2	20.0	4.2	7.4	1.5	2.7
(i=11)	6	252	6.1	22.1	4.2	7.3	1.5	3.0
(i=16)	4	254	5.9	32.4	4.2	13.5	1.4	2.4

Let us start the discussion with σ_0 representing the random accuracy of model coordinates. Without additional parameters σ_0 depends significantly on the control distribution used. This is in disagreement with theory. When additional parameters are introduced into the block adjustment σ_0 becomes considerably smaller (at a factor 1.4 to 1.6) and the dependency on control distribution disappears. With 4.2 μm sigma nought is close to the noise limit we can expect from todays photogrammetry at all.

Although the discussion of σ_0 is most illuminating, the real power of the new concept is only shown by the comparison of the absolute accuracies, expressed by μ_{xy} , the RMS value of the coordinate errors at check points. We see that the additional parameters improve the accuracy the more the poorer the control distribution is. The improvement increases up to a factor 3.0 in case of 6 control points used. In figure 6 the corresponding results are represented graphically.

The test shows that absolute accuracies of about 7 μm at the photo scale can be realized today, even when the control spacing along the block perimeter is in the order of 4 to 8 base length. If we put this accuracy of 7 $\mu\text{m} \hat{=} 20 \text{ cm}$ in relation to the length of the block (62.5 km) we obtain a relative accuracy which is better than 1 : 300 000.

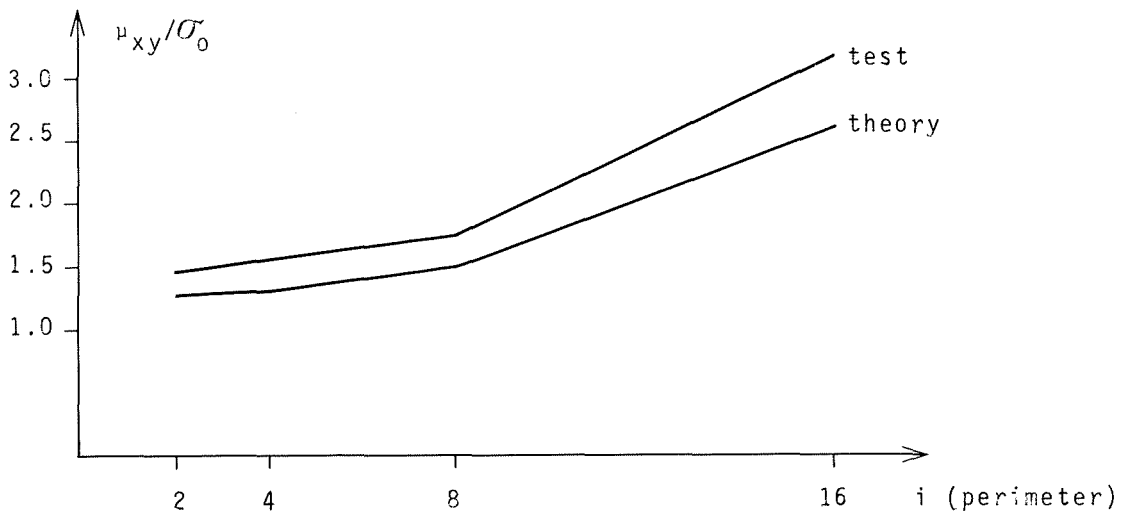
FIGURE 6



COMPARISON WITH THEORY

Now a comparison is made between the accuracy obtained by block adjustment with additional parameters and the corresponding theoretical accuracy being based on random errors only [4]. However, to allow for a correct comparison we have to consider that the check points used in the test are not error-free. Therefore the theoretical accuracy figures obtained from [4] are superposed by the random accuracy of check points which we assume with 10 cm in the terrain. This assumption can be considered as realistic. The result of the comparison is given graphically in figure 7.

FIGURE 7



The plot shows that the accuracy obtained in the test is somewhat poorer than the accuracy as predicted by theory. However, the discrepancies are less than 20 % and can be explained by the facts that our test is only one sample and doesn't meet the premises of the theory rigorously (different block shape for instance).

Considering this we can say that the accuracy results of the test are in agreement with the corresponding theoretical expectations. This agreement is most important because it indicates that the systematic errors of the model coordinates are compensated very well by the additional parameters used and that the remaining errors can be considered as random.

REFERENCES

- [1] Schilcher, M. and Wild, E.: Systematic Model Deformations of the OEEPE Testblock Oberschwaben. Presented to the Symposium of Commission III/ISP, Stuttgart 1974.
- [2] Kubik, K.: The Effect of Systematic Image Errors in Block Triangulation. ITC Publication A 49, 1971.
- [3] Ebner, H.: Die theoretische Genauigkeitsleistung der räumlichen Blockausgleichung. Sammlung Wichmann, Neue Folge, Band 5, 81 - 107, 1973.
- [4] Ebner, H.: Theoretical Accuracy Models for Block Triangulation. Bildmessung und Luftbildwesen, 214 - 221, 1972.
- [5] Ackermann, F.: Testblock Oberschwaben, Program I. Results of Block Adjustment by Independent Models. OEEPE, Official Publication N^o 8, 87 - 150, 1973.
- [6] Ebner, H.: Comparison of Different Methods of Block Adjustment. OEEPE, Official Publication N^o 8, 151 - 174, 1973.
- [7] Bauer, H.: Compensation of Systematic Errors by Analytical Block Adjustment with Common Image Deformation Parameters. OEEPE, Official Publication N^o 8, 319 - 334, 1973.
- [8] Brown, D.C.: Accuracies of Analytical Triangulation in Applications to Cadastral Surveying. Surveying and Mapping, 281 - 302, 1973.
- [9] Brown, D.C. et al.: Research in Mathematical Targeting, the Practical and Rigorous Adjustment of Large Photogrammetric Nets. Report by D. Brown Associates, Inc.
- [10] Ebner, H.: Zusätzliche Parameter in Ausgleichungen. Zeitschrift für Vermessungswesen, 385 - 391, 1973.
- [11] Schmid, H.H. and Schmid, E.: A Generalized Least Squares Solution for Hybrid Measuring Systems. The Canadian Surveyor, 27 - 41, 1965.
- [12] Bossler, J.D.: Bayesian Inference in Geodesy. Dissertation. The Ohio State University, 1972.
- [13] Moritz, H.: The Method of Least Squares Collocation in Geometrical Geodesy. Presented to the Symposium on Computational Methods in Geometric Geodesy, Oxford, 1973.
- [14] Ackermann, F., Ebner, H. and Klein, H.: Ein Programm-Paket für die Aerotriangulation mit unabhängigen Modellen. Bildmessung und Luftbildwesen, 218 - 224, 1970.

RESULTS FROM THE SOUTH-WESTERN ONTARIO APR-TEST BLOCK

by H. Klein, Stuttgart, Fed.Rep. Germany

SUMMARY

A new adjustment program has been developed at the Institute of Photogrammetry in Stuttgart: PAT-M 43-APR; a program for the combined simultaneous block adjustment of photogrammetric models with APR and/or statorscope data. As a first application the APR test block South-western Ontario was adjusted, in order to prove theory and to check handling of the program in practice.

The results of several test groups with different control distribution, different bridging distances for APR cross flights and a varied density of APR points on the profiles show the advantage of a rigorous combined adjustment.

THE APR TEST BLOCK

The APR test block South-western Ontario was provided by the Canadian Ministry of Energy, Mines and Resources for the purpose of evaluating the results of the combined block adjustment of independent photogrammetric models with APR data and of testing the APR version of the computer program PAT-M43 [1], [2]. The test area is located in Canada between Lake Huron, Lake St Clair, Lake Erie and Lake Ontario as shown on the attached map. It is a rectangle flown in 5 strips between Lake St Clair and Lake Ontario, each strip about 76 models or 250 km long.

Block description :

Date of photography	July 1972
Camera	class A, wide-angle, $f = 6''$
Flying height of photography	5250 m
Scale of photography	1/33.000
Strips with simultaneous APR	5
Number of models per line	appr. 76
Total number of models	380
Area	6750 km ²
East-west extension	250 km
North-south extension	25 km
Number of APR cross flights	10
Flying height of cross flights	appr. 2000 m
APR instrumentation	Radar APR

The area is hilly with heights above sea-level between 75 m and 370 m. The density of APR points is 1/2 base length or 5 points across a photograph in both directions, the number is 988. The total number of vertical control points is 440; they are very evenly distributed across the block.

MATHEMATICAL APPROACH

The APR block program is based on the PAT-M43 program of block adjustment with independent models [1]. The program iterates horizontal and vertical adjustments, applying 4-parameter and 3-parameter transformations in successive steps.

The 4-parameter horizontal adjustment is the wellknown "Anblock"-method. Because of the small correlation between horizontal and vertical accuracy only the vertical adjustment is discussed in this paper. As described in [1] the vertical block adjustment makes use of the following linearized observational equations for the height z_{ij} of a point i within a model j when Z_i means the unknown height of the terrain point i :

for model points:
$$\begin{bmatrix} v_z \end{bmatrix}_{ij} = \begin{bmatrix} -y & x \end{bmatrix}_{ij} \begin{bmatrix} da \\ db \end{bmatrix}_j - \begin{bmatrix} dz \end{bmatrix}_j + \begin{bmatrix} Z \end{bmatrix}_i - \begin{bmatrix} z \end{bmatrix}_{ij} \quad (1a)$$

for perspective centers:
$$\begin{bmatrix} v_x \\ v_y \\ v_z \end{bmatrix}_{ij} = \begin{bmatrix} 0 & -z \\ z & 0 \\ -y & x \end{bmatrix}_{ij} \begin{bmatrix} da \\ db \end{bmatrix}_j - \begin{bmatrix} 0 \\ 0 \\ dz \end{bmatrix}_j + \begin{bmatrix} X \\ Y \\ Z \end{bmatrix}_i - \begin{bmatrix} x \\ y \\ z \end{bmatrix}_{ij} \quad (1b)$$

for vertical control:
$$\begin{bmatrix} v_z \end{bmatrix}_i = \begin{bmatrix} Z \end{bmatrix}_i - \begin{bmatrix} z \end{bmatrix}_i^{terr} \quad (1c)$$

The increments da, db are two of the three independent rotation parameters of a modified Rodrigues-Cayley matrix [1], dz is the z-shift of the model j.

Points of APR profiles are used as observational data for the combined adjustment. They are treated, in a way, as additional vertical control with appropriate weighting. However, the isobaric surface to which the APR recordings refer is not known. Therefore additional unknown parameters are needed. We allow a constant shift and a tilt correction of the isobaric surface along each profile.

For the APR height z_{ik} of a point i in profile k we obtain the following observational equation:

for APR heights of model points:
$$\begin{bmatrix} v_z \end{bmatrix}_{ik} = - \left[a_k + b_k \cdot t_{ik} \right] + \begin{bmatrix} Z \end{bmatrix}_i - \begin{bmatrix} z \end{bmatrix}_{ik} \quad (2a)$$

for vertical control:
$$\begin{bmatrix} v_z \end{bmatrix}_i = \begin{bmatrix} Z \end{bmatrix}_i - \begin{bmatrix} z \end{bmatrix}_i^{terr} \quad (2b)$$

The coefficient t_{ik} represents the distance of APR measurement i on profile k from an arbitrary starting point, in practice the elapsed time is used.

The essential difference between (2b) and (1c) is the fact that the point i in (2b) is not necessarily measured in a photogrammetric model, for instance it can be the height of a lake level on which the APR-line closes. Therefore a connection of a photogrammetric block to control outside of the block is possible using APR profiles.

HENRY CORRECTION

The ideal situation for APR measurements would be to fly on a geopotential surface. Unfortunately the noise level is prohibitive for the delicate gravimeter instrumentation needed to measure deviations from this surface.

Another possibility is to fly on an isobaric surface and calculate the slope of the isobaric surface with respect to the geopotential surface from wind information. On the assumption of constant atmospheric pressure and a balance between the pressure force and the Coriolis force we obtain the following correction formula for APR measurements, recorded on an isobaric surface; the so called Henry-correction formula [3]:

$$\Delta z = \frac{2 \omega}{g} \int_{s_1}^{s_2} A \cdot \sin L \cdot \sin \delta \cdot ds \quad (3)$$

ω = angular velocity of the earth, g = local value of gravity ($g_{45} = 980.665 \text{ cm/sec}^2$), A = true air speed, L = latitude, δ = drift angle, ds = line element along the APR-line. In practice g , A , ω and L are assumed constant on the track, the drift angle δ is measured about every five minutes with an accuracy of 1/2 degree. Therefore the Henry correction is used as a linear correction between two changes of the drift angle. Because we allow a linear correction of

the isobaric surface in our adjustment program, we have the possibility to use non-corrected APR-measurements while cutting the profiles at the points of change of the drift angle.

THE STOCHASTICAL MODEL

In our combined adjustment program all observations can be weighted. Because it is impractical to weight all observations individually, the program allows only for different sets of weight matrices to different groups of observations. In order to obtain realistic weights the APR test block South-western Ontario was first adjusted with all given 440 vertical control points and all 988 APR measurements. The following table shows the chosen weights for the vertical adjustment and their agreement with the r.m.s. values of the residuals.

Group of observations		weights (related to the ground)	r.m.s. values of residuals
model points	z	1	0.347
perspective centers	x	0.1	1.209
	y	0.1	1.119
	z	0.0	0.469
control points in the model	z	1	0.303
APR points in the model	z	1	0.330
APR profile points (≈ 5200 m)	z	0.25	0.913
APR profile points (≈ 2000 m)	z	0.5	0.572
vertical control	z	0.5	0.521

Sigma-nought of vertical adjustment = 0.43

Because of unexplained large z-residuals of the perspective centers at the beginning and the end of each strip the weight 0 was given to the z-coordinate of the perspective centers, which is possible without detrimental effects to the adjustment.

Looking at the root mean square values of the residuals and sigma-nought we already can point out the following results:

1. The accuracy of observations before adjustment is about 0.43 m.
2. The accuracy of APR heights depends on the flying height. APR heights from profiles flown at lower altitude have a better accuracy.
3. The accuracy of APR cross profiles and the accuracy of vertical control happens to be about the same.

RESULTS OF THE COMBINED ADJUSTMENT

Up to now 10 different series of adjustments have been performed with the test-block South-western Ontario, always using minimum control. Each series consists of 7 adjustments, varying the distance between cross profiles from 76 models to 5 models.

The last 4 adjustments of each group were done only with the western half of the block because in the other part not enough cross profiles were flown. Absolute accuracy is obtained from 170 check points.

The first 4 testgroups were adjusted with 2 chains of control at the front sides of the block and without any closing of the profiles on control.

Accuracy results of the testblock Southwestern Ontario
absolute accuracy in m obtained from 170 check points.

combined adjustment:

Δb ¹⁾	full block			half block				control			sub- divided profiles	space of APR points
	76	38	19	38	19	10	5	2 chains	simult. profiles	cross profiles		
group 1	2.45	1.66	1.46	1.57	1.32	1.20	1.21	yes	no	no	no	0.5b ²⁾
group 2	4.39	3.43	2.42	2.52	1.89	1.80	1.76	yes	no	no	yes	0.5b
group 3	2.77	1.91	1.72	1.85	1.56	1.36	1.37	yes	no	no	no	1 b
group 4	3.61	3.02	1.79	2.37	1.68	1.53	1.49	yes	no	no	yes	1 b
group 5	2.05	2.67	2.11	2.67	2.11	1.90	1.96	no	yes	yes	no	0.5b
group 6	2.14	2.54	2.16	2.70	2.62	2.05	2.14	no	yes	yes	yes	0.5b
group 7	1.96	2.38	1.98	2.33	1.93	1.63	1.77	no	yes	yes	no	1 b
group 8	1.86	1.69	1.63	1.67	1.61	1.54	1.55	no	yes	no	no	1 b
group 9	1.38	2.35	1.56	2.31	1.51	1.22	1.14	no	yes	yes	no	0.5b
group 10	1.45	2.13	1.53	2.06	1.45	1.22	1.17	no	yes	yes	no	1 b

¹⁾ Δb = bridging distance of cross profiles in base length ²⁾ b = base length

two step method:

absolute accuracy with all APR points

and all closing points

3.24 m.

Test 5 - 10 used no height control points within the block. Instead 2 cross profiles were used and the longitudinal APR profiles closed on the lakes. It was anticipated that the overall absolute height accuracy of the combined block adjustment would reach about 2 m (2). The results now show that the expectation was not too optimistic.

Before going into a more detailed discussion it is perhaps expedient to point to some accuracy results first:

- Bridging the full length of the block (~ 250 km or 76 models) the height accuracy can be about 2 m.
- The accuracy is increased when cross profiles are used. When bridging 19 models or about 60 km 1.60 m is reached.
- The best results, obtained with cross profiles all 5 models or 15 km, are around 1.20 m. This is obviously the inherent limit of the test material, given by flying height, photo-scale, APR equipment, terrain and control.

Up to now the adjustment of APR profiles and their use for aerial triangulation was in most cases much simplified. The profiles starting and closing over known areas were adjusted by applying linear corrections. From the adjusted profiles, vertical control points were drawn to be used for the subsequent block adjustment.

With this two step method the absolute accuracy reached with our test material was 3.24 m. Due to the more general mathematical and stochastic approach of the combined adjustment the height accuracy has been considerable increased.

Thus, the combined adjustment has proven its effectiveness. There are a number of details to be commented upon. There is one point in particular to mention: Absolute accuracy is steadily increased with shorter distances between cross profiles up to an inherent limit (testgroup 1 - 4). This effect is disturbed when the cross profiles are closed on known water surfaces. The results become irregular and absolute accuracy is not as much increased as with free cross profiles (testgroup 5 - 7). Using less control absolute accuracy even is sometimes better (compare testgroup 7 with testgroup 8).

This results show that control is only necessary to fix in a way the isobaric surface. More control points do not result in a better accuracy.

Using control only on known water surfaces the ratio of the maximum error and the average absolute accuracy is less than 2. While using this closing points as check points the residuals on each lake are close to a certain positive value. There is obviously a systematic effect of the APR recordings on lakes. After correction of the APR measurements with this values we obtained a much better result. The absolute accuracy has been increased to 1.14 m (testgroup 9 - 10).

In the test material the density of APR points is 1/2 base length. Using APR points all 1 base length only (without the APR points in the middle of the models) absolute accuracy become sometimes better (compare testgroup 2 against 4) and sometimes worse (compare testgroup 1 against 3). Nevertheless the r.m.s. values of APR measurements of longitudinal profiles are decreasing in both cases from 91 cm to 85 cm. It seems to be a systematic effect of the APR points on the sides of the models against the points in the centers.

It is an advantage of the combined adjustment that profiles which can not be closed on known water surfaces or other vertical control can nevertheless be used very efficiently. The system automatically provides the interconnection of different profiles via the photogrammetric models. Particularly free cross profiles are controlling tilts and twists of long strips. By using free cross profiles the absolute accuracy of the testblock South-western Ontario has been increased by more than a factor 2 (testgroup 1 - 4).

Between two changes of the drift angle the Henry correction is used in practice as a linear correction. Because we allow a linear transformation of each profile we can do the combined adjustment using non-corrected profiles. The profiles have to be subdivided at the points of change of the drift angles. Each part then is treated as a separate computational profile. It has to be tested in further investigations whether it is possible to use non-subdivided profiles in a first adjustment and then cut the profiles on the strength of the obtained residuals for a second adjustment.

Also the problems which are due to local irregularities or disturbances of the isobaric surface can be solved in that way. However, in all these cases we have to take care of the geometric stability. Additional control or cross profiles could be necessary.

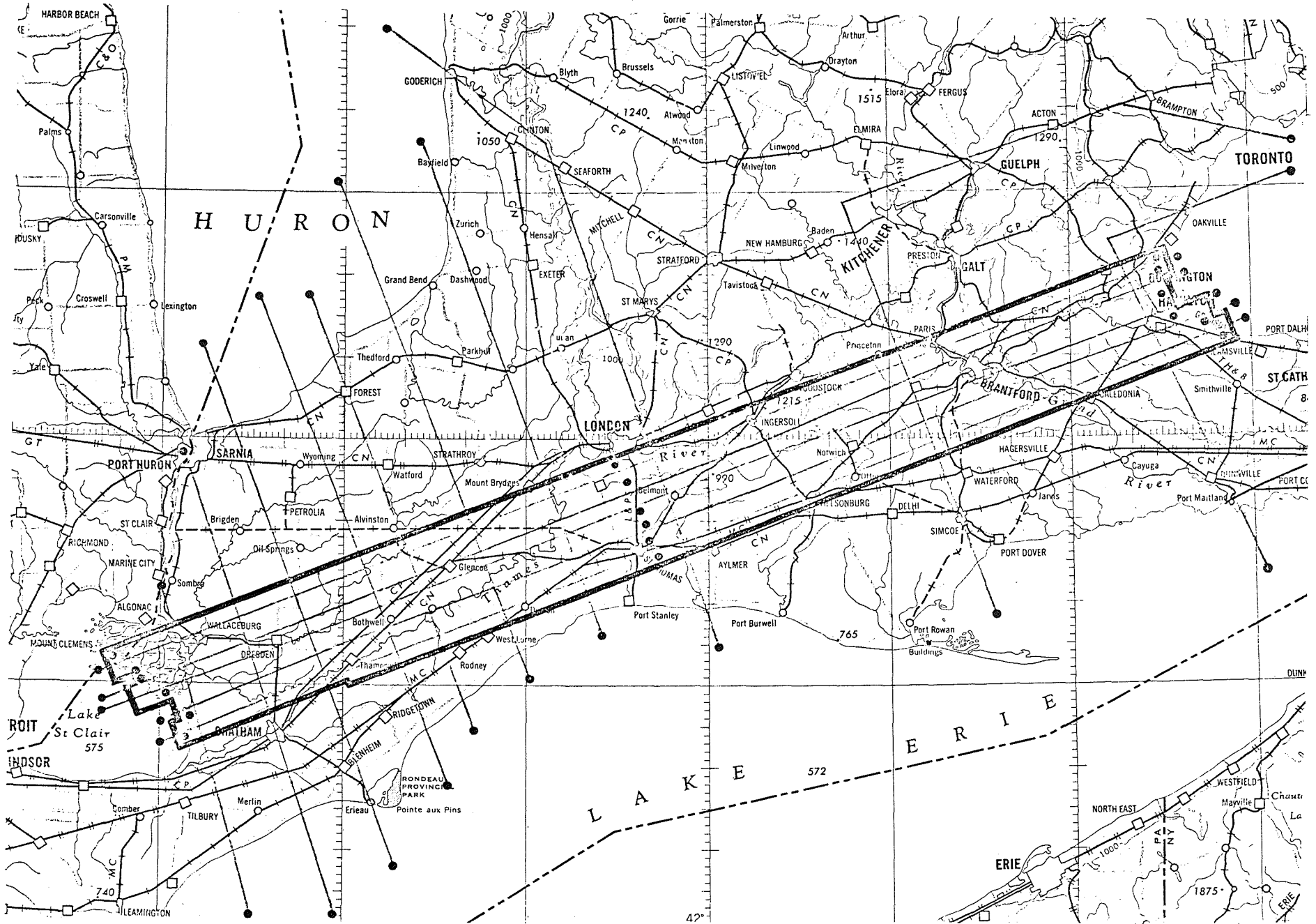
If we compare the results of testgroup 1, 3 and 5 against 2, 4 and 6 respectively we see that the non-subdivided profiles are always better. The largest differences were obtained without cross profiles, whilst the results get closer with increasing number of cross profiles and control points.

Errors of terrain coordinates or APR measurements of control points are hard to detect with the two step method. Because of the interconnection of different APR profiles via the photogrammetric models such erroneous measurements are recognized by large residuals in the combined adjustment. Within the material of the testblock South-western Ontario it was possible to detect 4 grossly erroneous APR measurements of control points. With weight zero they obtained residuals of more than 7 meters.

CONCLUSION

The results of the combined adjustments show that an absolute accuracy of 1.30 m (~ 0.25 ‰ of flying height) can be obtained even with bridging distances between control points from 125 km to 250 km at photo scale 1 : 33 000. In future the combined adjustment will give results sufficient for mapping with contour intervals of 5 m and less and very long bridging distances of control points, even with control points up to 50 km or 100 km outside the block. The use of APR measurements with simultaneous block adjustment represents a similar break through for height accuracy as perimeter control did for planimetry.

Klein 6



REFERENCES

- | 1| Ackermann, F., Ebner, H., Klein, H.: "Ein Programmpaket für die Aerotriangulation mit unabhängigen Modellen", Bildmessung und Luftbildwesen 4/1970
- | 2| Ackermann, F., Ebner, H., Klein, H.: "Combined Block Adjustment of APR Data and Independent Photogrammetric Models" The Canadian Surveyor, 26 (1972)-4, p. 384 - 396
- | 3| EMR (Department of Energy, Mines and Resources in Canada) "Errors in isobaric formula for use in APR"
- | 4| Jerie, H.G. and Kure, J.: "Data analysis and report on the investigation into the application of the airborne profil recorder to photogrammetric mapping, ITC Publications A 25/26, p. 80 1964
- | 5| Jerie, H.G.: "Theoretical height accuracy of strip and block triangulation with and without use of auxiliary data" Photogrammetria 23 (1968), p. 19 - 44.

BLOCK TRIANGULATION WITHOUT POINT TRANSFER

by J. Albertz, W. Kreiling, J. Wiesel, Karlsruhe, Fed. Rep. Germany

1. THE PROBLEM OF POINT TRANSFER

Usually the formation of strips and blocks in numerical aerotriangulation is based on the fact that coordinates of identical points (tie points) are measured in different photos or models. In order to get good results it is not sufficient to perform precision measurements, but is absolutely necessary to ensure that the same points are observed in adjacent photos or models. Any identification error is causing the same effect as a measuring error. For that reason the identification of points in overlapping photographs should be carried out with the same precision as the measurements are performed.

In practice the identification of points in various photographs is not as easy to perform as it would seem. In particular this applies to the identification of points in different strips. Therefore various methods and instruments were developed to transfer points from one photograph to another (de Masson d'Autume 1968).

The most rigorous solution of the problem is the signalization of tie points on the ground. This can be done with targets normally used for marking control points. In the photographs the images of a target relate of course to exactly the same point, misidentification is impossible and a monocomparator can be used for measurements. But this method involves a severe disadvantage: field work is increased considerably and this is just the opposite of what we want to achieve by using aerotriangulation methods. Besides, taking the photographs becomes much more difficult because pin-point flying is required in order to get the signalized points at preplanned positions in the image plane.

Another point transfer procedure is mainly propagated in Great Britain (Eden 1967). It consists in selecting small objects in overlapping photographs using a stereoscope and rather high magnification. It depends on the photo scale what types of objects are usable, e.g. stones, tufts of grass, bushes or similar objects. Stereoscopic vision is only used to guarantee identity of these small objects. But the measurements relating to their centers of gravity are performed in a monocomparator.

A third method is the marking of points in the photographic emulsion by means of a point transfer device. Many manufacturers of photogrammetric equipment offer special instruments for this purpose, e.g. Zeiss Snap Marker, Wild PUG 4, Kern PMG 1, Jenoptik Transmark. In any case stereoscopic fusion in conjunction with a floating mark is used to identify points in adjacent photos. The marking itself is accomplished by a mechanical device or by a laser beam. Unfortunately the marking results in a damage to the photographic emulsion so that stereoscopic fusion becomes more difficult.

With regard to the accuracy of transferred points Brucklacher (1961) reports that coordinate errors between $+ 4$ and $+ 7 \mu\text{m}$ were achieved with the aid of the Zeiss Snap Marker. Ackermann (1972) states that the errors lie somewhere between $+ 5$ and $+ 10 \mu\text{m}$ (vectorial error). Eden (1973) compared the accuracy of the monocular method using small objects in the photos and the point transfer by stereoscopy. Against the widely held opinion that the stereoscopic performance results in the highest accuracy, he states that it is more dependent on the observer's skill and also more prone to occasional mistakes in identification.

In any case, the transfer of points is a rather troublesome and time-consuming procedure. Some attempts have been made to overcome the difficulties by automation using an electronic or digital correlation technique (e.g. Roos 1971). But it would be unrealistic to expect from this method a practicable solution of the problem in the near future. Such a system would not directly reduce the tedious work of manipulating the photographs. Moreover, enormous costs would be involved, and the necessary equipment is at present not available.

During the International Congress of Photogrammetry in Lausanne 1968 the acquisition of data in aerotriangulation and especially the problem of point transfer were thoroughly discussed (ISP 1971). This led to a resolution proposing "that research on the problem of point transfer be encouraged", a resolution which was almost forgotten in the following years. But the problem still exists.

2. A METHOD OF BLOCK FORMATION WITHOUT POINT TRANSFER

A block triangulation method which does not require point transfer was briefly described by Albertz (1972). In contrast to the aerotriangulation methods in use, it is not based on the identity of points in adjacent models or strips.

In order to understand the procedure we can compare it to a triangulation of the perspective centers. Not only the coordinates of the perspective centers have to be determined in relation to a common coordinate system but also the angles of rotation. In a terrestrial triangulation network angle measurements are used as observations. If the photos have been oriented with respect to each other the two straight lines, connecting the perspective centers, the image points and the ground point, form an epipolar plane. In other words, the condition of coplanarity which can be established for every pair of homologous straight lines is satisfied. If this is not the case, the discrepancies can be utilized to derive corrections for the orientation parameters of the two photos.

In practice the orientation elements of all the photographs should be simultaneously determined in a least squares adjustment. For this purpose we need a sufficient number of observations appropriately distributed within the block. Such observations are easily obtainable by the stereoscopic measurement of any ground points in the overlapping area of adjacent photos. This applies not only to the photos within a flight line but also to the photos of adjacent strips. The ground points need not be signalized in the field or marked in the photographs. The measurements are performed by means of a stereocomparator and result in the image coordinates of the point in both photos. As mentioned above each measurement yields an observation equation according to the condition of coplanarity. In the least squares adjustment the orientation parameters of all the photographs are determined in such a way that the sum of squares of the remaining errors is minimized.

This adjustment procedure results of course in a block model which is not fitting to control points. In order to adjust the whole block to the geodetic coordinate system another group of observation equations must be set up and introduced into the system. For each control point whose image coordinates were measured two equations can be established according to the basic equations governing central-perspective image formation. This the adjustment will yield orientation elements related to the coordinate system defined by the control points.

3. NUMBER AND PATTERN OF OBSERVATIONS

Each photo within the block has overlapping areas with at least 8 adjacent photos. Stereoscopic measurements of the images of ground points could be carried out in all these photopairs. Let us consider an example which is shown schematically in Fig. 1. The block consists of 9 x 9 photos whose centers are plotted in the figure. Forward and side overlap are supposed to be 60 % either.

Under these conditions any photo inside the block has overlapping areas even with 24 photos. The performance of measurements in all these combinations would result in a highly overdetermined system. But of course this would be very time-consuming and uneconomic.

Investigations have shown that the measurements relating to one photograph and the photographs not directly adjoining can be omitted without difficulty. Then eight photos, adjoining directly, will remain as sketched in the upper right hand corner of Fig. 1. If all these combinations are measured for the whole block we get the pattern of observations shown in Fig. 2. Altogether, among the 81 photographs there are 272 combinations to be measured.

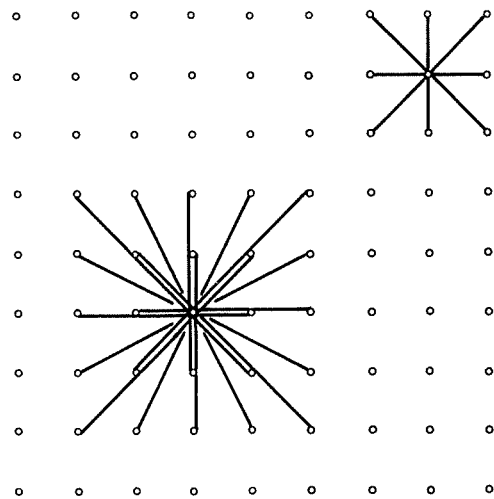


Fig. 1

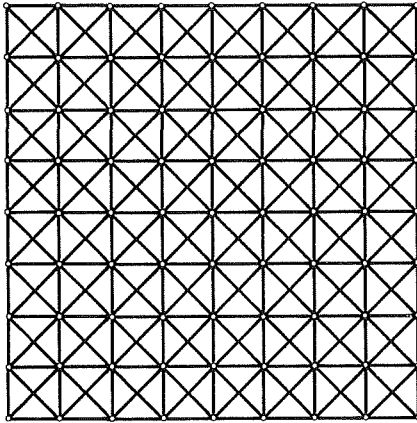


Fig. 2

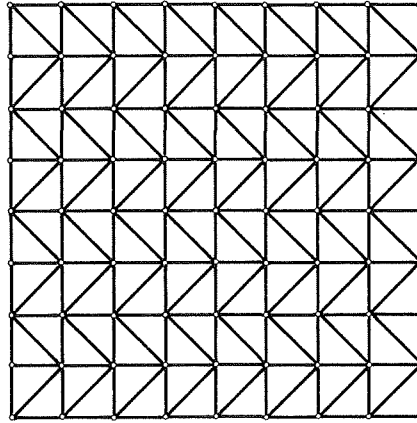


Fig. 3

This number is still reducible. In each square formed by the adjacent photo centers one diagonal can be omitted. In this case the observations could be arranged as shown in Fig. 3. This way 208 combinations are left to be measured.

The most advantageous pattern with regard to the amount of measurements follows if every second photograph along the flight line is omitted. Thus we obtain a block formed of photo strips with the unusual conditions of 20 % forward and 60 % side lap. The number of stereo pairs to be measured is reduced to 120 as shown in Fig. 4, where also a few photos are sketched to demonstrate their grouping.

The amount of measurements could be further diminished by reducing the side lap to 20 %. But this version would require a rather dense distribution of control points in order to achieve sufficient height accuracy.

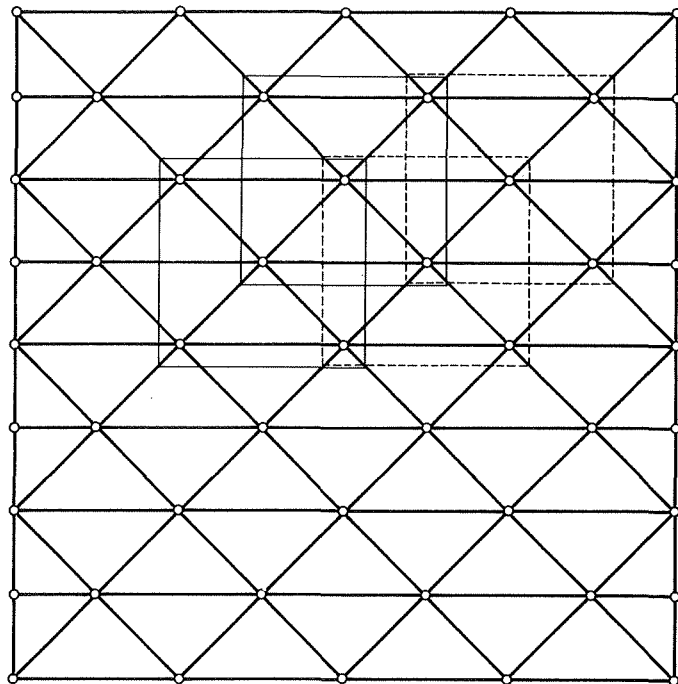


Fig. 4

4. PERFORMANCE OF THE MEASUREMENTS

The measurements described above have to be carried out by means of a stereocomparator. The operator has to choose a number of ground points in the stereogram. These points are selected in such a way that they are well distributed in the overlapping area of the photos. The number of points necessary to form a block depends on the observation pattern. But in general it is advisable to take a few more measurements than the minimum amount, e.g. to measure six points per stereogram. In doing so the loss of time becomes small since the time-consuming part of the procedure is the manipulation and set up of the photos and the measurement of the fiducial marks. Compared to that the operator can rather quickly set at any ground point.

The measurements would not be completed without measuring the image coordinates of the control points and the points whose coordinates are to be determined by the aerotriangulation. In either case the points must be identified in one stereogram but a transfer to other photos does not have to be done. In general this procedure is much the same as in other aerotriangulation methods.

Some stereocomparators do not allow the rotation of the photos. In this case the stereoscopic observation cannot be carried out in epipolar planes if the base direction is not parallel to one of the edges of the photograph. However, in experiments this fact was found to be of no disadvantage.

5. NUMERICAL SOLUTION

The computations of this aerotriangulation method consists of two parts. As the first step the block is formed by determining the orientation elements of the photos in a least squares adjustment. In the following step which is independent of the previous one the coordinates of new points are determined by intersection in space.

DETERMINATION OF THE ORIENTATION ELEMENTS

The adjustment is based on observation equations. Since there are two types of observation equations these equations are divided into two groups. The first group relates to the stereoscopic measurements and makes use of the condition of coplanarity in its general form.

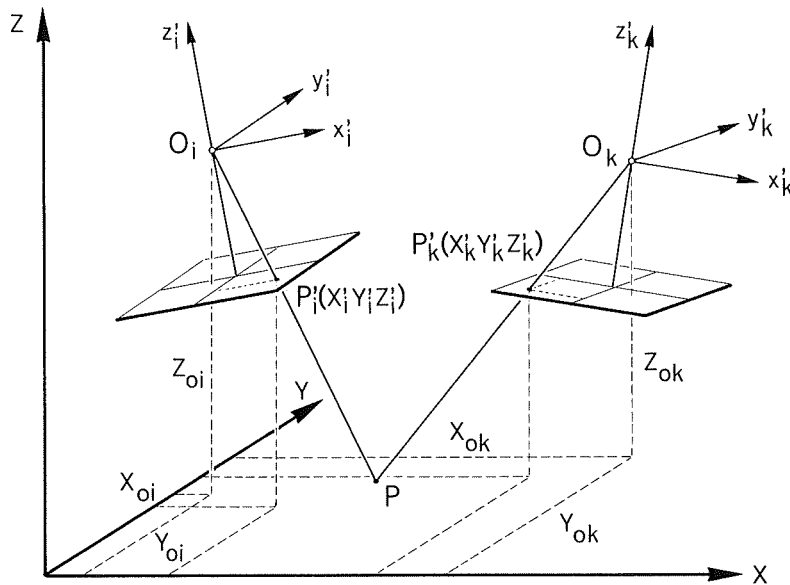


Fig. 5

Fig.5 shows any pair of photos in the block. The following condition must be satisfied for each pair of homologous rays:

$$\Delta = \begin{vmatrix} X'_i & Y'_i & Z'_i & 1 \\ X_{oi} & Y_{oi} & Z_{oi} & 1 \\ X'_k & Y'_k & Z'_k & 1 \\ X_{ok} & Y_{ok} & Z_{ok} & 1 \end{vmatrix} = 0 \qquad \begin{pmatrix} X' \\ Y' \\ Z' \end{pmatrix} = \begin{pmatrix} X_o \\ Y_o \\ Z_o \end{pmatrix} + D \begin{pmatrix} x' \\ y' \\ z' \end{pmatrix}$$

X'_i, Y'_i, Z'_i and X'_k, Y'_k, Z'_k are the coordinates of the image points after the transformation into the geodetic reference system X, Y, Z . D is the rotation matrix of the respective photo. Due to the second equation, in the first one the unknown angles of rotation ω, ϕ, κ appear in transcendental functions. Therefore this equation must be linearized after the introduction of approximate values for the unknowns. In order to simplify the computation we use the volume of the tetrahedron $O_i P'_i P'_k O_k$ as a fictitious observation. But this type of observations must be normalized before being adjusted simultaneously with other observations. Thus we obtain the following observation equation for each point measured stereoscopically (Albertz and Kreiling 1972, p. 184) :

$$v_{\Delta} = \frac{1}{N} (k_{X_i} dX_{oi} + k_{Y_i} dY_{oi} + k_{Z_i} dZ_{oi} + k_{\omega_i} d\omega_i + k_{\varphi_i} d\varphi_i + k_{x_i} dx_i + k_{X_k} dX_{ok} + k_{Y_k} dY_{ok} + k_{Z_k} dZ_{ok} + k_{\omega_k} d\omega_k + k_{\varphi_k} d\varphi_k + k_{x_k} dx_k + \Delta_o)$$

with N factor of normalization
 $k_{X_i} \dots k_{x_k}$ observation equation coefficients
 $dX_{oi} \dots dx_i$ corrections for the orientation elements (photo i)
 $dX_{ok} \dots dx_k$ corrections for the orientation elements (photo k)

The second group of observation equations relates to the measurements of the control points and is based on the equations governing central-perspective image formation:

$$\bar{x}' = c_k \frac{a_{11}(X - X_o) + a_{21}(Y - Y_o) + a_{31}(Z - Z_o)}{a_{13}(X - X_o) + a_{23}(Y - Y_o) + a_{33}(Z - Z_o)}$$

$$\bar{y}' = c_k \frac{a_{12}(X - X_o) + a_{22}(Y - Y_o) + a_{32}(Z - Z_o)}{a_{13}(X - X_o) + a_{23}(Y - Y_o) + a_{33}(Z - Z_o)}$$

with X, Y, Z control point coordinates
 $a_{11} \dots a_{33}$ coefficients of the rotation matrix D

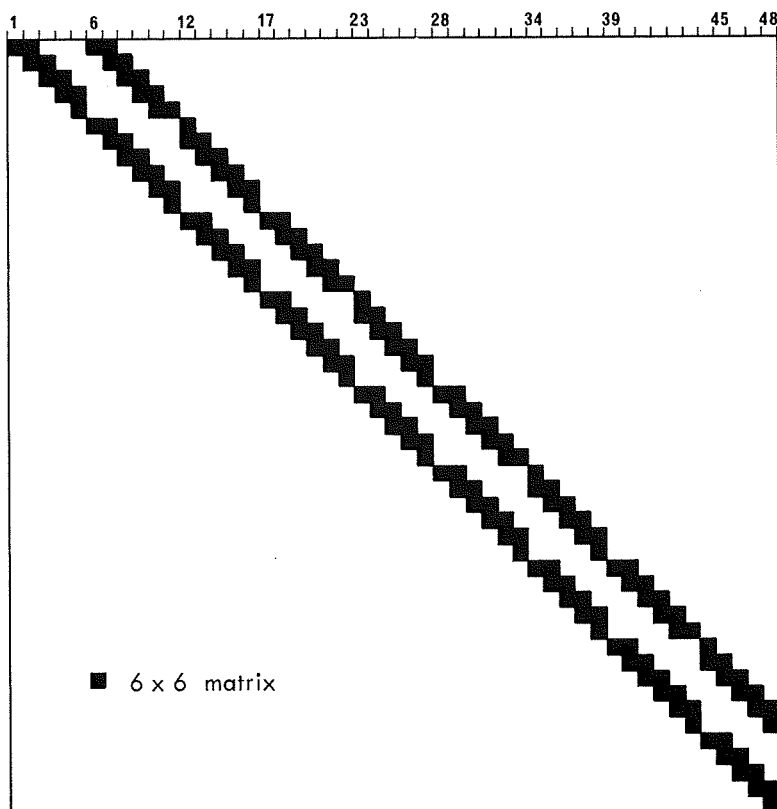
Again the equations must be linearized by the use of approximate values for the unknowns. Thus for each control point and for each photo in which it is imaged we obtain two observation equations:

$$v_{x'} = g_X dX_o + g_Y dY_o + g_Z dZ_o + g_{\omega} d\omega + g_{\varphi} d\varphi + g_x dx + \bar{x}' - x'$$

$$v_{y'} = h_X dX_o + h_Y dY_o + h_Z dZ_o + h_{\omega} d\omega + h_{\varphi} d\varphi + h_x dx + \bar{y}' - y'$$

with $g_X \dots g_x, h_X \dots h_x$ observation equation coefficients
 \bar{x}', \bar{y}' image coordinates as calculated with the approximate values of the unknowns
 x', y' measured image coordinates

Due to the fact that only the orientation elements of the photos appear as unknowns the system of normal equations has the form of a banded matrix. The block shown in Fig. 4 yields the following distribution of non-zero elements in the normal equations:



Due to the nonlinearity of the observation equations the unknowns have to be determined in an iteration procedure.

Fig. 6

DETERMINATION OF NEW POINTS

The orientation elements resulting from the adjustment are used to determine the coordinates of new points by intersection in space. In this procedure the object point has to be determined by a definition since in general the homologous rays will not really intersect. It is advisable to define the midpoint of the line segment which represents the shortest distance between the skew lines as an object point (Albertz and Kreiling 1972, p. 193).

6. PRACTICAL INVESTIGATIONS

The block triangulation method described above was programmed for the UNIVAC 1108 of the University of Karlsruhe. This program is a test version, that is to say it is not optimized. From these investigations the following results are reported.

TESTBLOCK OBERSCHWABEN

A part of the OEEPE Testblock Oberschwaben was used for a practical test. This subblock consisted of 7 strips of 11 photos each. The photos were taken with a wide angle camera ($f = 143 \text{ mm}$) at a flying height of 4300 m (photo scale 1:28000) with 60 % forward and side overlap. The material is described in detail by the OEEPE (1973).

The measurements were performed according to the configuration shown in Fig. 3. In the recording of the image coordinates occasional errors of $100 \mu\text{m}$ occurred, as a consequence of which the following computations became rather difficult. 16 control points were arranged at the perimeter of the block with average distances of two base lengths. In addition 4 vertical control points were used inside the block at nearly equal distances. The results were checked at the signalized points of the testfield, and the residual errors were found to be

in planimetry (coordinate errors) $\mu_{xy} = \pm 9 \mu\text{m} = \pm 25 \text{ cm}$

in height $\mu_z = \pm 13 \mu\text{m} = \pm 36 \text{ cm} = \pm 0.08 \text{ ‰ } h_g$

FICTITIOUS TESTBLOCK

For investigations into the accuracy of various patterns of observation and the amount of measurements involved a fictitious block was used. It consisted of 9x9 photos with 60 % forward and side overlap. To the fictitious image coordinates the normally distributed random error σ_0 was added.

The observation pattern sketched in Fig. 4 was found to be the optimum if the accuracy is compared to the number of photo pairs to be measured. Control points were arranged at the perimeter of the block. Their average distances were two base lengths ($i = 2$) as according to 16 points, and four base lengths ($i = 4$) according to 8 points. The following coordinate errors were obtained at check points:

	μ_x	μ_y	μ_z
$i = 2$	$0.9 \sigma_0$	$0.9 \sigma_0$	$2.3 \sigma_0$
$i = 4$	$1.2 \sigma_0$	$1.1 \sigma_0$	$3.1 \sigma_0$

The accuracy is nearly the same as the one resulting from the observation pattern of Fig. 3 although the number of models was reduced by 42 %. The investigation will be continued.

SUMMARY

An aerotriangulation method is described which does not need identical points in adjacent models to form a block. Compared to the method with independent models the number of models to be measured is increased, but the time-consuming point transfer procedure which is also a source of errors is eliminated. The method makes use of the condition of coplanarity which is applied to stereoscopic measurements in various combinations of photopairs. In a least squares adjustment only the orientation parameters of the photographs have to be determined. Therefore the non-zero elements in the system of normal equations coefficients form a banded matrix which is advantageous for numerical solution. A practical test confirmed the theoretical investigation.

REFERENCES

- Ackermann, F. 1972: "Die Vorbereitung der räumlichen Aerotriangulation" in Handbuch der Vermessungskunde, 10. Auflage, Band IIIa/3, p. 1658 - 1670
- Albertz, J. 1972: "Blocktriangulation ohne Punktübertragung", Bildmessung und Luftbildwesen, vol. 40, p. 38 - 40
- Albertz, J. and Kreiling, W. 1972: "Photogrammetrisches Taschenbuch/Photogrammetric Guide" Herbert Wichmann Verlag, Karlsruhe; 209 p.
- Brucklacher, W. 1961: "Geräte zur Markierung natürlicher und zur Herstellung künstlicher Punkte bei der Vorbereitung für die Aerotriangulation" Bildmessung und Luftbildwesen, vol. 29, p. 15 - 20
- Eden, J. A. 1967: "A new fast-working approach to analytical photogrammetry" Photogrammetric Record, vol. 5, no. 30, p. 474 - 491
- Eden, J. A. 1973: "Point transfer from one photograph to another" Photogrammetric Record, vol. 7, no. 41, p. 531 - 537
- ISP 1971: "Proceedings of the 11th International Congress of Photogrammetry" Lausanne 1968, Internat. Archives of Photogrammetry, ser. XVII, vol. I, p. 141
- de Masson d'Autume, G. 1968: "The acquisition of data in aerotriangulation" Photogrammetric Engineering, vol. 34, p. 452 - 456
- OEEPE 1973: "Proceedings of the OEEPE Symposium on experimental research on accuracy of aerial triangulation (results of Oberschwaben test)" Official Publication no. 8, 350 p.
- Roos, M. 1971: "Test results of the automatic point-transfer instrument (abstract)" Photogrammetric Engineering, vol. 37, p. 493 - 494

ANALYSIS OF COVARIANCE MATRICES

by H. Ebner, Stuttgart, Fed.Rep. Germany

SUMMARY

The paper starts with a representation of the concept of inner accuracy which was introduced by P. Meissl in 1962 and which is applied frequently in Geodesy. Proceeding from this concept a theory is developed, allowing for a rigorous analysis of covariance matrices. By this theory any given covariance matrix can be disintegrated into a covariance matrix of simpler structure and the effect of a set of filter parameters. An example shows how the analysis works and demonstrates the power of the theory.

THE CONCEPT OF INNER ACCURACY

In 1962 P. Meissl introduced a concept into Geodesy which allows to filter the effect of an arbitrary set of parameters out of a given covariance matrix. The accuracy remaining after filtering is called inner accuracy [1], [2], [3].

In Geodesy the filter parameters most of the time are restricted to shifts, rotations and eventually a scale factor. In this case the inner accuracy is the accuracy being liberated from the effect of shifts, rotations and scale. Moreover most of the geodetic applications of the theory of inner accuracy are related to free adjustments [4], [5], [6].

It should be emphasized, however, that the concept of inner accuracy is neither restricted to free adjustments nor to a certain number or type of filter parameters.

FORMULATION

We start from a random vector x and the associated covariance matrix M . The vector x is split into the expectation vector $E[x]$ and the increment vector dx :

$$x = E[x] + dx \tag{1}$$

From dx we separate the effect of the filter parameters dt , being represented by the filter matrix G . The remaining vector is called $d\bar{x}$. The associated covariance matrix we call Q .

$$d\bar{x} = dx - Gdt \tag{2}$$

The filter parameters dt now are determined so that the trace of Q becomes a minimum.

$$\text{tr}Q \rightarrow \text{Min} \tag{3}$$

The derivation of the vector dt and of the corresponding covariance matrix R is given in [2]. The results are:

$$dt = (G^T G)^{-1} G^T dx \tag{4}$$

$$R = (G^T G)^{-1} G^T M G (G^T G)^{-1} \tag{5}$$

Inserting (4) into (2) we get (I = unit matrix):

$$d\bar{x} = (I - G(G^T G)^{-1} G^T) dx \tag{6}$$

$$Q = (I - G(G^T G)^{-1} G^T) M (I - G(G^T G)^{-1} G^T) \tag{7}$$

The covariance matrix Q represents the inner accuracy of the random vector x which remains when the effect of the filter parameters dt is eliminated. The results (4) and (6) are identical with the results of a least squares adjustment, which fits the vector x onto the vector $E[x]$ using the parameters dt and minimizing the sum of squares of the residuals $d\bar{x}$:

$$d\bar{x}^T d\bar{x} \rightarrow \text{Min} \tag{8}$$

From there it follows that the minimum conditions (3) and (8) are equivalent. This is shown in detail in proof 1 (see appendix). At the same time Q is identified as the covariance matrix of the residuals.

GENERALIZATION

By introducing a weight matrix P the minimum conditions (8) and (3) can be generalized to:

$$d\bar{x}^T P d\bar{x} \longrightarrow \text{Min} \quad (9)$$

$$\text{tr}QP \longrightarrow \text{Min} \quad (10)$$

The conditions (9) and (10) are equivalent again (see proof 2, appendix). Analogue to the more general minimum condition (10) equations (4) to (7) are generalized to:

$$dt = (G^T P G)^{-1} G^T P dx \quad (11)$$

$$R = (G^T P G)^{-1} G^T P M P G (G^T P G)^{-1} \quad (12)$$

$$d\bar{x} = (I - G(G^T P G)^{-1} G^T P) dx \quad (13)$$

$$Q = (I - G(G^T P G)^{-1} G^T P) M (I - P G (G^T P G)^{-1} G^T) \quad (14)$$

Converting equation (2) the random vector dx now can be expressed as a linear function of the components $d\bar{x}$ and dt:

$$dx = d\bar{x} + G dt = \begin{bmatrix} I & G \end{bmatrix} \begin{bmatrix} d\bar{x} \\ dt \end{bmatrix} \quad (15)$$

Analogue to (15) the covariance matrix M of the random vector dx can be represented as:

$$M = \begin{bmatrix} I & G \end{bmatrix} \begin{bmatrix} Q & U \\ U^T & R \end{bmatrix} \begin{bmatrix} I \\ G^T \end{bmatrix} = Q + GU^T + UG^T + GRG^T \quad (16)$$

The submatrix U of the common covariance matrix of the components $d\bar{x}$ and dt can be obtained by applying the law of error propagation to equations (13) and (11):

$$U = (I - G(G^T P G)^{-1} G^T P) M P G (G^T P G)^{-1} \quad (17)$$

The existence of U demonstrates that $d\bar{x}$ and dt are correlated with each other.

A THEORY FOR ANALYSIS OF COVARIANCE MATRICES

In a previous paper a theory was presented, which proceeds from the concept of inner accuracy and allows for a rigorous analysis of a given covariance matrix [7]. In the present paper this theory is derived slightly different and the whole problem is treated more comprehensively. By analysis we understand a rigorous disintegration of M into a covariance matrix K with a structure as simple as possible and the effect of a set of filter parameters, represented by a coefficient matrix G.

DERIVATION OF THE THEORY

We search for a random vector dx_K with the associated covariance matrix K and for a filter matrix G which allow for a rigorous separation of the given random vector dx according to:

$$dx = dx_K + G \Delta t \quad (18)$$

At the same time we dispose of the weight matrix P, which was arbitrary up to now and set:

$$P \triangleq K^{-1} \quad (19)$$

The vector dx_K and the covariance matrix K can be represented analogue to equations (15) and (16)

$$dx_K = d\bar{x}_K + Gdt_K = \begin{bmatrix} I & G \end{bmatrix} \begin{bmatrix} d\bar{x}_K \\ dt_K \end{bmatrix} \quad (20)$$

$$K = \begin{bmatrix} I & G \end{bmatrix} \begin{bmatrix} Q_K & \cdot \\ \cdot & S \end{bmatrix} \begin{bmatrix} I \\ G^T \end{bmatrix} = Q_K + GSG^T \quad (21)$$

Because of (19) $d\bar{x}_K$ and dt_K are not correlated with each other.

Q_K and S follow as:

$$Q_K = K - G(G^TK^{-1}G)^{-1}G^T \quad (22)$$

$$S = (G^TK^{-1}G)^{-1} \quad (23)$$

It can be shown that the random vector dx can be separated according to (18) if and only if by use of the same filter matrix G both vectors dx and dx_K lead to the same residuals:

$$d\bar{x}_K = d\bar{x} \quad (24)$$

(see proof 3, appendix).

Equation (24) is equivalent with the condition:

$$Q_K = Q \quad (25)$$

Using equations (22) and (23) we convert the condition (25) into the more practicable form:

$$K = Q + GSG^T \quad (26)$$

Combining equation (16) and (21) and considering condition (25) the covariance matrix M now can be disintegrated analogue to the separation of dx in (18):

$$M = K + \begin{bmatrix} I & G \end{bmatrix} \begin{bmatrix} Q & U \\ U^T & R \end{bmatrix} \begin{bmatrix} Q & \cdot \\ \cdot & S \end{bmatrix} \begin{bmatrix} I \\ G^T \end{bmatrix} = K + GU^T + UG^T + GTG^T$$

with

$$T = R - S \quad (27)$$

R and S are positiv semidefinit matrices, but the difference matrix T is not necessarily positiv semidefinit. Equation (27) represents the aspired analysis of the covariance matrix M . The meaning is that M can be expressed rigorously by the covariance matrix K and the effect of filter parameters with the coefficient matrix G . As can be shown condition (26) is necessary and adequate for the validity of equation (27) (see proof 4, appendix). Therefore (26) can be used as a proper criterion regarding the choice of K and G .

CRITERION I

The given covariance matrix M can be analysed rigorously according to equation (27) if and only if the chosen matrices K and G fulfil condition (26). The performance of the analysis can be simplified essentially by replacing the choice of K by the choice of the weight matrix P which is related to K according to equation (19). Then the covariance matrix K needed in criterion I is estimated as follows:

$$E[\sigma_o^2] = E[d\bar{x}^T P d\bar{x}] / r = \text{tr}QP / r \quad (28)$$

$$K = E[\sigma_o^2] P^{-1} \quad (29)$$

$E[\sigma_o^2]$ is the expectation of the variance factor being computed from the residuals dx . The redundancy r is determined by the number n of random variables minus the number u of filter parameters. The proof of equation (28) and a discussion of equation (29) is given in the appendix (proof 5).

As soon as criterion I is fulfilled the question appears whether all filter parameters effect the analysis or whether some of them can be omitted without effecting criterion I. Therefore we look for a criterion which detects filter parameters without influence over the analysis. For that purpose we split the vector Δt into the components Δt_1 and Δt_2 and represent equation (27) accordingly as:

$$M = K + \begin{bmatrix} I & G_1 & G_2 \end{bmatrix} \begin{bmatrix} Q & U_1 & U_2 \\ U_1^T & R_{11} & R_{12} \\ U_2^T & R_{12}^T & R_{22} \end{bmatrix} - \begin{bmatrix} Q & \cdot & \cdot \\ \cdot & S_{11} & S_{12} \\ \cdot & S_{12}^T & S_{22} \end{bmatrix} \begin{bmatrix} I \\ G_1^T \\ G_2^T \end{bmatrix}$$

$$= K + G_1 U_1^T + U_1 G_1^T + G_1 T_{11} G_1^T + G_1 T_{12} G_2^T + G_2 T_{12}^T G_1^T + G_2 U_2^T + U_2 G_2^T + G_2 T_{22} G_2^T$$

with

$$T_{11} = R_{11} - S_{11}$$

$$T_{12} = R_{12} - S_{12}$$

$$T_{22} = R_{22} - S_{22}$$

(30)

The aspired criterion can be formulated as follows:

CRITERION II

The analysis (30) is not effected by the filter parameters Δt_2 and can be represented without putting up G_2 if and only if the following equations (31) are valid

$$T_{22} = 0$$

$$U_2 = 0$$

(31)

(see proof 6, appendix).

SPECIAL CASES OF THE ANALYSIS

Equation (27) represents the general case of an analysis of the given covariance matrix M. Beside this various special cases of the analysis are possible. Two of them, being of particular interest and appearing frequently shall be treated in detail.

SPECIAL CASE A : $U = 0, T = \text{positiv semidefinit}$

With that equation (27) is simplified considerably to:

$$M = K + GTG^T \tag{27a}$$

Considering (27a) together with equation (18) we see that here T is the covariance matrix of the filter parameters Δt . Moreover from (27a) it follows that dx_k and Δt are not correlated with each other. In this case equation (18) can be interpreted as a separation of the random vector dx into the independent components of noise and signal, being used in collocation [8].

SPECIAL CASE B : $U_2 = 0, T_{22} = \text{positiv semidefinit}$

With that equation (30) is simplified to:

$$M = K + G_1 U_1^T + U_1 G_1^T + G_1 T_{11} G_1^T + G_1 T_{12} G_2^T + G_2 T_{12}^T G_1^T + G_2 T_{22} G_2^T \tag{30a}$$

Equation (30a) can be split properly into

$$M = \bar{M} + G_1 U_1^T + U_1 G_1^T + G_1 T_{11} G_1^T + G_1 T_{12} G_2^T + G_2 T_{12}^T G_1^T \tag{30b}$$

$$\bar{M} = K + G_2 T_{22} G_2^T \tag{30c}$$

The covariance matrix \bar{M} differs from M due to the effect of the filter parameters Δt_1 only (see proof 7, appendix). If the filter parameters Δt_1 are of no particular interest, equation (30a) therefore can be replaced by the much simpler disintegration (30c). Considering equation (30c) we see that here T_{22} is the covariance matrix of the filter parameters Δt_2 . Moreover Δt_2 and dx_k are not correlated with each other.

PERFORMANCE OF THE ANALYSIS

The following block diagram shows the steps of the analysis and their sequence. The analysis starts with a proper choice of the weight matrix P and the filter matrix G , representing the stochastic model and the functional model of the analysis. The necessity to assume a proper mathematical model a priori we know from least squares adjustment and regression analysis respectively. Of great importance in this context is the fact that the suitability of P and G can be checked rigorously by criterion I.

Equation (26) which is used in criterion I is identical with the basic equation of a posteriori variance and covariance estimation, given in [9]. Therefore the corresponding procedures can be used successfully to estimate K . Most of the time it will be sufficient to assume uncorrelated random variables dx_k and to estimate their weights only. Concerning the choice of the filter matrix G use can be made of the fact that filter parameters without influence over the analysis are detected by criterion II. Therefore it can be recommended to start the analysis with putting up relatively many filter parameters. Of course they have to be linear independent. As filter parameters often the coefficients of regression polynomials will be used.

With the practical application frequently it will not be possible to fulfill criterion I rigorously. In this case, suitable statistical test procedures have to be applied to decide whether criterion I is fulfilled or not. If equation (26) being used in criterion I isn't valid exactly we must not apply criterion II rigorously. The question whether some of the filter parameters don't effect the analysis in this case again has to be answered by applying suitable statistical tests.

COMMENT

The analysis of a covariance matrix M according to equation (27) has to be discriminated from a decomposition of a covariance matrix Σ by factor analysis [10]. This method of multivariate analysis is characterized by:

$$\Sigma = \Lambda \Lambda^T + D \quad (32)$$

Λ is the factor loading matrix. The number of columns of Λ is fixed usually. D is a diagonal matrix. Equation (32) is less general than (27) because no covariance term corresponding with U is existing in (32). As opposed to the analysis (27) where P and G are chosen a priori and improved if necessary, in case of factor analysis Λ and D are estimated directly. The corresponding estimation procedures are relatively complicated and depend on the assumption of normal distributed variables. The estimation of Λ and D is followed by an interpretation of the factor loadings of Λ . With the analysis treated here this step is avoided completely because the meaning of the filter parameters is given a priori.

Analysis of the covariance matrix M according to (27)

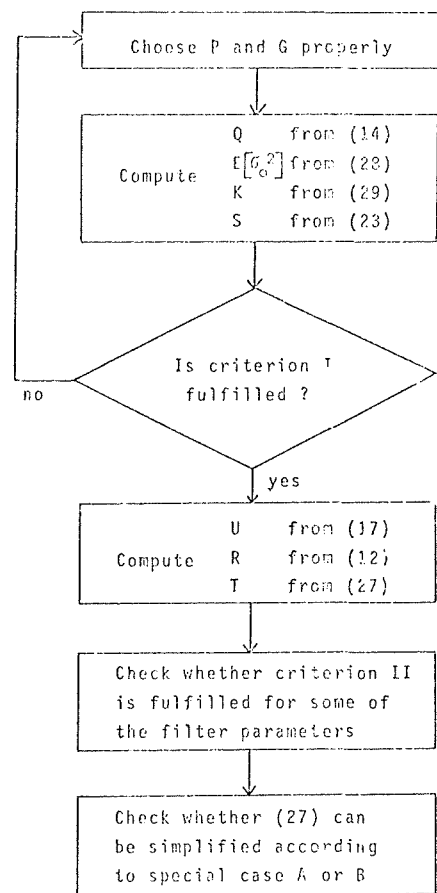


Figure 1

APPLICATIONS OF THE THEORY

The concept presented in this paper is a suitable tool to analyse any given covariance matrix, obtained theoretically or empirically. This shall be demonstrated by the following analysis of the theoretical covariance matrix of the z coordinates of a photogrammetric model.

For that purpose we suppose vertical wide angle photography. The base length we assume as $b = 1$ and the flying height as $h = 153/92$. The 8 model points have the same heights and are distributed regularly (see figure 2). Points 3 and 5 are control points in planimetry and height, point 2 is an additional height control point (free adjustment).

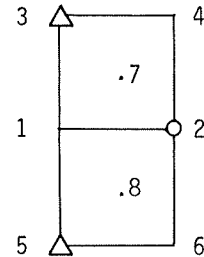


FIGURE 2

The image coordinates we assume as uncorrelated observations of variance 1. Putting up a rigorous least squares adjustment according to the bundle method we obtain the covariance matrix M of the 8 model heights as a sub-matrix of the complete inverse of the normal equation matrix:

$$M = \begin{bmatrix} 8.30 & \cdot & \cdot & \cdot & \cdot & \cdot & 1.38 & 1.38 \\ \cdot & \cdot & \cdot & \cdot & \cdot & \cdot & \cdot & \cdot \\ \cdot & \cdot & \cdot & \cdot & \cdot & \cdot & \cdot & \cdot \\ \cdot & \cdot & \cdot & 17.30 & \cdot & -0.70 & 5.02 & 0.52 \\ \cdot & \cdot & \cdot & -0.70 & \cdot & 17.30 & 0.52 & 5.02 \\ 1.38 & \cdot & \cdot & 5.02 & \cdot & 0.52 & 8.86 & 1.51 \\ 1.38 & \cdot & \cdot & 0.52 & \cdot & 0.52 & 1.51 & 8.86 \end{bmatrix}$$

The variances and covariances belonging to the height control points 2, 3 and 5 are zero of course. Due to the existing symmetry the heights 4 and 6 as well as 7 and 8 are of equal accuracy.

The analysis of the covariance matrix M we start assuming $P = I$ for the weight matrix and putting up 6 filter parameters according to a regression polynomial of degree 2 in the model coordinates x and y. With that we obtain the following filter matrix G:

$$G = \left[\begin{array}{ccc|ccc} 1 & x_1 & y_1 & x_1^2 & x_1 y_1 & y_1^2 \\ \vdots & \vdots & \vdots & \vdots & \vdots & \vdots \\ 1 & x_8 & y_8 & x_8^2 & x_8 y_8 & y_8^2 \end{array} \right]$$

The first three filter parameters allow for a shift in z and for tilts in x and y direction. These parameters are needed for levelling the model. The other three filter parameters are put up arbitrary. Performing the analysis we obtain:

$$E [\sigma_o^2] = 5.53$$

$$K = 5.53 I$$

This covariance matrix K and the chosen filter matrix G fulfil criterion I. That means that K and G allow for a rigorous disintegration of M according to equation (27). The matrices U and T follow as:

$$U = \begin{bmatrix} U_1 & U_2 \end{bmatrix} = \begin{bmatrix} 0.92 & 0.92 & \cdot & \cdot & \cdot & \cdot \\ -0.92 & -0.92 & \cdot & \cdot & \cdot & \cdot \\ -0.46 & -0.46 & -0.15 & \cdot & \cdot & \cdot \\ 0.46 & 0.46 & -0.15 & \cdot & \cdot & \cdot \\ -0.46 & -0.46 & 0.15 & \cdot & \cdot & \cdot \\ 0.46 & 0.46 & 0.15 & \cdot & \cdot & \cdot \\ \cdot & \cdot & 0.61 & \cdot & \cdot & \cdot \\ \cdot & \cdot & -0.61 & \cdot & \cdot & \cdot \end{bmatrix}$$

$$T = \begin{bmatrix} T_{11} & T_{12} \\ T_{12}^T & T_{22} \end{bmatrix} = \begin{bmatrix} 0.92 & -0.46 & \cdot & -1.38 & \cdot & -1.38 \\ -0.46 & 20.28 & \cdot & -12.45 & \cdot & 4.15 \\ \cdot & \cdot & -2.46 & \cdot & 2.77 & \cdot \\ -1.38 & -12.45 & \cdot & 5.53 & \cdot & \cdot \\ \cdot & \cdot & 2.77 & \cdot & 3.47 & \cdot \\ -1.38 & 4.15 & \cdot & \cdot & \cdot & \cdot \end{bmatrix}$$

Because criterion I is fulfilled criterion II can be applied rigorously. Doing this we see that the last filter parameter Δt_6 going with y^2 has no influence over the analysis of M ($T_{66} = 0, U_6 = 0$).

If we collect the first three levelling parameters in the vector Δt_1 and the last three in the vector Δt_2 and if we divide the matrices G, U and T correspondingly we see that the premises of special case B are given:

$$U_2 = 0, T_{22} = \text{positiv semidefinit}, \bar{M} = K + G_2 T_{22} G_2^T$$

\bar{M} differs from M due to the effect of the levelling parameters Δt_1 only. We are allowed to replace M by \bar{M} because M is arbitrary with respect to these three parameters due to the arbitrary choice of the three height control points 2, 3 and 5. If we fix three other heights, we obtain different results for U_1, T_{11} and T_{12} but we get $U_2 = 0$ again and T_{22} remains unchanged.

From these facts it follows that \bar{M} can be represented by $K = 5.53 I$ and the effect of two filter parameters, going with x^2 and xy respectively. These two parameters are uncorrelated with each other and their variances are 5.53 and 3.47 respectively.

The results of this analysis can be interpreted as follows: The covariance matrix K describes the accuracy of the model heights without the effect of the orientation parameters of the bundle adjustment. This accuracy is obtained keeping the orientation parameters of both photos fixed. Then all model heights get the same accuracy and are not correlated with each other. The variance in z is $2 \cdot c^2 / b^2 = 2 \cdot 1532 / 92^2 = 5.53$.

Among the orientation parameters of the images 1 and 2 the only one of interest here are those which lead to model deformations in z being not compensated by the filter parameters Δt_1 of model levelling. These orientation parameters are ϕ_1 or ϕ_2 causing a cylinder shaped deformation in z and ω_1 or ω_2 causing a twisted model. The filter parameters going with x^2 and xy are able to compensate those deformations rigorously. The filter parameter going with y^2 is not needed at all and gets a variance of zero accordingly.

ACKNOWLEDGMENT

The author is grateful to Prof. Meissl, Graz, to Prof. Grafarend, Bonn and to Mr. Pope, Rockville for fruitful and encouraging discussions.

REFERENCES

- [1] Meissl, P.: Die innere Genauigkeit eines Punkthaufens. Österr. Zeitschrift für Vermessungswesen, 159-165, 186-194, 1962.
- [2] Meissl, P.: Über die Verformungsfehler eines Systems von endlich vielen Punkten. Österreichische Zeitschrift für Vermessungswesen, 105-109, 1964.
- [3] Meissl, P.: Zusammenfassung und Ausbau der inneren Fehlertheorie eines Punkthaufens. Beiträge zur Theorie der geodätischen Netze im Raum. Deutsche Geodätische Kommission, A 61, 8-21, 1969.
- [4] Mittermayer, E.: A Generalization of the Least Squares Method for the Adjustment of Free Networks. Bulletin Geodesique, 139-157, 1972.
- [5] Grafarend, E. and Schaffrin, B.: Unbiased Free Net Adjustment. Presented to the Symposium on Computational Methods in Geometric Geodesy, Oxford, 1973.
- [6] Pope, A.J.: The use of the Solution Space in the Analysis of Geodetic Network Adjustments. Presented to the Symposium on Computational Methods in Geometric Geodesy. Oxford 1973.
- [7] Ebner, H.: Eine Theorie zur Analyse von Kovarianzmatrizen. Zeitschrift für Vermessungswesen, 453-461, 1974.
- [8] Moritz, H.: Advanced Least Squares Methods. Report No. 175, Dept. of Geodetic Science, Ohio State University, 1972.
- [9] Ebner, H.: A posteriori Varianzschatzungen für die Koordinaten unabhängiger Modelle. Zeitschrift für Vermessungswesen, 166-172, 1972.
- [10] Press, S.J.: Applied Multivariate Analysis. Holt, Rinehart and Winston, 303-329, 1972.

APPENDIX

Proof 1

Replacing (8) by the expectation $E [d\bar{x}^T d\bar{x}]$ and considering $E [d\bar{x}] = 0$ we get:

$$E [d\bar{x}^T d\bar{x}] = E [\text{tr}(d\bar{x}^T d\bar{x})] = E [\text{tr}(d\bar{x} d\bar{x}^T)] = \text{tr}(E [d\bar{x} d\bar{x}^T]) = \text{tr}Q$$

Proof 2

Analogue to proof 1 we obtain:

$$\begin{aligned} E [d\bar{x}^T P d\bar{x}] &= E [\text{tr}(d\bar{x}^T P d\bar{x})] = E [\text{tr}(d\bar{x} d\bar{x}^T P)] = \text{tr}(E [d\bar{x} d\bar{x}^T P]) \\ &= \text{tr}(E [d\bar{x} d\bar{x}^T] P) = \text{tr}QP \end{aligned}$$

Proof 3

From (18) follows (24):

$$d\bar{x}_K = (I - G(G^T P G)^{-1} G^T P) dx_K = (I - G(G^T P G)^{-1} G^T P)(dx - G \Delta t) = d\bar{x}$$

From (24) follows (18):

$$dx = d\bar{x} + G dt = d\bar{x}_K + G dt = dx_K + G(dt - dt_K) = dx_K + G \Delta t$$

Proof 4

(26) is identic with (25). From (25) follows (27) directly.

From (27) follows (26):

$$K = M - G U^T - U G^T - G R G^T + G S G^T = Q + G S G^T$$

Proof 5

(28) follows from proof 2:

$$E [\bar{\sigma}_o^2] = E [d\bar{x}^T P d\bar{x}] / r = \text{tr}QP / r$$

(29) is an approximate estimation of K. The rigorous relation between K and P should be:

$$K = E [\bar{\sigma}_o^2]_K P^{-1}$$

with $E [\bar{\sigma}_o^2]_K$ being computed analogue to above as:

$$E [\bar{\sigma}_o^2]_K = E [d\bar{x}_K^T P d\bar{x}_K] / r = \text{tr}Q_K P / r$$

A rigorous estimation of K using $E [\sigma_o^2]_K$ is impossible because K itself is needed for the determination of $E [\sigma_o^2]_K$. Therefore $E [\sigma_o^2]$, being determinable replaces $E [\sigma_o^2]_K$ in (29). The better the choice of P and G the closer is $E [\sigma_o^2]$ to $E [\sigma_o^2]_K$. As soon as K, computed from (29) fulfils criterion I we obtain:

$$E [\sigma_o^2] = \text{tr}QP / r = \text{tr}Q_K P / r = E [\sigma_o^2]_K$$

The rigorous validity of

$$K = E \left[\sigma_o^2 \right]_K P^{-1}$$

can be shown starting from $K = cP^{-1}$ and proving $c = E \left[\sigma_o^2 \right]_K$

$$\begin{aligned} E \left[\sigma_o^2 \right]_K &= \text{tr} Q_K P / r = \text{tr} (K P - G (G^T K^{-1} G)^{-1} G^T P) / r \\ &= (\text{tr} K P - \text{tr} (G^T K^{-1} G)^{-1} G^T P G) / r = c(n-u) / r = c \end{aligned}$$

Proof 6

From (30) and (31) follows $(Q-Q_K)_1 = 0$, which is necessary and adequate for the validity of (30) using G_1 only

$$\begin{aligned} (Q-Q_K)_1 &= (I - G_1 (G_1^T P G_1)^{-1} G_1^T P) (M-K) (I - P G_1 (G_1^T P G_1)^{-1} G_1^T) \\ &= (I - G_1 (G_1^T P G_1)^{-1} G_1^T P) (G_1 U_1^T + U_1 G_1^T + G_1 T_{11} G_1^T + G_1 T_{12} G_2^T + G_2 T_{12}^T G_1^T) \\ &\quad (I - P G_1 (G_1^T P G_1)^{-1} G_1^T) = 0 \end{aligned}$$

For proving that (31) follows from (30) and $(Q-Q_K)_1 = 0$ we separate $(G^T P G)^{-1}$ into:

$$(G^T P G)^{-1} = \begin{bmatrix} A_{11} & A_{12} \\ A_{12}^T & A_{22} \end{bmatrix}$$

U_2 and T_{22} , appearing in (30) we represent explicitly as:

$$\begin{aligned} U_2 &= (I - G (G^T P G)^{-1} G^T P) (M-K) P (G_1 A_{12} + G_2 A_{22}) \\ &= (I - G_1 A_{11} G_1^T P - G_2 A_{12}^T G_1^T P - G_1 A_{12} G_2^T P - G_2 A_{22} G_2^T P) (M-K) (P G_1 A_{12} + P G_2 A_{22}) \\ T_{22} &= (A_{12}^T G_1^T P + A_{22} G_2^T P) (M-K) (P G_1 A_{12} + P G_2 A_{22}) \end{aligned}$$

In the following proofs we consider:

$$\begin{bmatrix} A_{11} & A_{12} \\ A_{12}^T & A_{22} \end{bmatrix} \begin{bmatrix} G_1^T P G_1 & G_1^T P G_2 \\ G_2^T P G_1 & G_2^T P G_2 \end{bmatrix} = \begin{bmatrix} I & \cdot \\ \cdot & I \end{bmatrix}$$

From $0 = (Q-Q_K)_1$ follows $U_2 = 0$:

$$\begin{aligned} 0 &= (I - G_1 A_{11} G_1^T P - G_2 A_{12}^T G_1^T P - G_1 A_{12} G_2^T P - G_2 A_{22} G_2^T P) \\ &\quad (Q-Q_K)_1 (P G_1 A_{12} + P G_2 A_{22}) \\ &= (I - G_1 A_{11} G_1^T P - G_2 A_{12}^T G_1^T P - G_1 A_{12} G_2^T P - G_2 A_{22} G_2^T P) (I - G_1 (G_1^T P G_1)^{-1} G_1^T P) \\ &\quad (M-K) (I - P G_1 (G_1^T P G_1)^{-1} G_1^T) (P G_1 A_{12} + P G_2 A_{22}) \\ &= (I - G_1 A_{11} G_1^T P - G_2 A_{12}^T G_1^T P - G_1 A_{12} G_2^T P - G_2 A_{22} G_2^T P) (M-K) \\ &\quad (P G_1 A_{12} + P G_2 A_{22}) = U_2 \end{aligned}$$

From $0 = (Q-Q_K)_1$ follows $T_{22} = 0$:

$$\begin{aligned} 0 &= (A_{12}^T G_1^T P + A_{22} G_2^T P)(Q-Q_K)_1 (PG_1 A_{12} + PG_2 A_{22}) \\ &= (A_{12}^T G_1^T P + A_{22} G_2^T P)(I - G_1 (G_1^T P G_1)^{-1} G_1^T P) \\ &\quad (M-K)(I - PG_1 (G_1^T P G_1)^{-1} G_1^T)(PG_1 A_{12} + PG_2 A_{22}) \\ &= (A_{12}^T G_1^T P + A_{22} G_2^T P)(M-K)(PG_1 A_{12} + PG_2 A_{22}) = T_{22} \end{aligned}$$

Proof 7

We put up G_1 only and prove that M and \bar{M} lead to the same covariance matrix of residuals:

$$\begin{aligned} (Q-\bar{Q})_1 &= (I - G_1 (G_1^T P G_1)^{-1} G_1^T P)(M-\bar{M})(I - PG_1 (G_1^T P G_1)^{-1} G_1^T) \\ &= (I - G_1 (G_1^T P G_1)^{-1} G_1^T P)(G_1 U_1^T + U_1 G_1^T + G_1 T_{11} G_1^T + G_1 T_{12} G_2^T + G_2 T_{12}^T G_1^T) \\ &\quad (I - PG_1 (G_1^T P G_1)^{-1} G_1^T) = 0 \end{aligned}$$

From $(Q-\bar{Q})_1 = 0$ follows that M and \bar{M} differ due to the effect of Δt_1 only.

COMPARISON OF ADJUSTMENT METHODS OF THE AEROTRIANGULATION BY NUMERICAL FILTERING TECHNIQS

by Gy. Alpár, Sopron, Ungarn

Aerotriangulation is a complex process involving sophisticated recording, measuring and computing technics. Generally two kinds of comparison are practised for the test of aerotriangulation methods.

The first of them starts with aerial photographs taken of a test area with precise geodetic control. The second one operates with computer simulation of the previous items. Both are concerned with the whole complexity of the aerotriangulation and the "goodness of fit" is judged by average coordinate discrepancies determined at check points.

The adjustment of an aerotriangulation is, however, a purely mathematical procedure even if it anticipates profound knowledge of the preceding processes. So, we can split the problems if the comparison of the different adjustment methods is restricted only to the different mathematical formulation of the same aerotriangulation problem. It is not a new, but a scarcely appreciated fact namely that the coefficient matrix of the (linearised) observation equations A , together with the appropriate weight matrix Q^{-1} widely determine the outcomes of an adjustment. From these matrices we can compute always a third one, which gives the inverse relationship expressing explicitly the unknowns parameters of the adjustment problem:

$$x_{m,1} = B_{m,n} L_{n,1} \quad (1)$$

Here, x is the vector of the unknowns, B is a m,n -matrix ($m < n$) and L stands for the residuals (containing also the observations).

At this point we get in touch with numerical filtering technics, because the linear combination BL in equation (1) represents - no doubt - a simple linear filter stock. Numerical filtering is, however, a much more general and very powerful estimation method. With knowledge of some criticism related to "least squares filtering" (see e.g. A. H. Jazwinski, 1970), mention must be made here that linear combinations in the sense of equation (1) are practical filters for our simple stationary case.

In the following, the B matrix will be called the "Filter Matrix" and we will show how to perform a comparison with its help.

In the case of a least squares adjustment the B matrix is given by the matrix product:

$$B = (A^T Q^{-1} A)^{-1} A^T Q^{-1} \quad (2)$$

Here, the B matrix is a special type of the generalized (or pseudo) inverses of A (see e.g. A. Bjerhammar, 1973). Each row of such an inverse matrix is a linear filter, which enhances just the unknown to be determined while suppressing all the other ones with the help of appropriate linear combinations of all measurements. It is also possible - even if it is not practical - to compute a B matrix for the non least squares adjustment methods; however not only these filter matrices but also the x and L vectors in equation (1) can be considerably different for the same aerotriangulation problem. Supposing always identical geometric situation for a test case only the coordinate unknowns of the different adjustment procedures can be regarded as common elements. For this reason we split equation (1) :

$$\begin{pmatrix} x_1 \\ x_2 \end{pmatrix} = \begin{pmatrix} B_1 \\ B_2 \end{pmatrix} L, \quad (1a)$$

where x_1 stands for the coordinate unknowns and B_1 is the appropriate filter matrix while x_2 denotes the orientation parameters and B_2 is the related filter matrix.

Now, we can compare two different adjustment methods applied to the same test case computing the difference of their B_1 matrices under the constraints, that they are of equal size and the L vector is common. Such a difference matrix "maps" in all detail the differences of the adjustment methods to be compared.

The constraint related to the L vector is, however, a very serious one and in this way we can study mainly the effects of different weighting only.

If the L vectors of the adjustment methods under comparison are different, but otherwise the size of the related B_1 matrices and consequently also that of L are equal, then we can solve the problem introducing a so called transmitter matrix:

$$\bar{L}_{n,1} = T_{n,n} L_{n,1}$$

In the simplest case T will be a diagonal matrix and \bar{L} is called the vector of equivalent residuals (see F. R. Helmert 1924, and H. Wolf 1971). The least squares adjustment with \bar{L} can be performed now in the following way:

$$TA_x - T(L + v) = \emptyset \quad (3)$$

where v is the vector of the corrections. Then the normal equations with Q^{-1} are:

$$A^T TQ^{-1} TA_x - A^T TQ^{-1} TL = \emptyset$$

and the related filter matrix is:

$$\bar{B} = (A^T TQ^{-1} TA)^{-1} A^T TQ^{-1} T \quad (2a)$$

It is not so evident, however, how to determine the \bar{B} matrix for a non least squares adjustment method. In equation (3) the effect of the T matrix is similar to that of the special weighting technics introduced by F. R. Helmert, which is termed nowadays also for "homogenisation of the observation equations", but we call it here the Helmert premultiplication technic because of their dominant computational characteristics. Weighting is however a common procedure also for non least squares adjustment, and so the \bar{B} filter matrix can be computed here via simple weighting technics. For this reason we can make use from the so called Cholesky factorisation (or decomposition) of the Q^{-1} matrix:

$$Q^{-1} = Q^{-1/2} (Q^{-1/2})^T$$

and with the substitution

$$K = TQ^{-1/2}$$

we can write now:

$$\bar{B} = (A^T K K^T A)^{-1} A^T K K^T. \quad (2b)$$

It is easy to see that K and K^T work here as the Cholesky components of general weight matrix. When the relationship between \bar{L} and L is more complex that is the T matrix is no more a diagonal one, there is no restriction to use these weighting technics.

In the most general case - e.g. in the comparison of bundle and polynomial adjustment methods - the L vectors are entirely - also in size - different. The computation of the compatible B (resp. B_1) matrices via least squares leads us to the adjustment of correlated observations. This formally agrees with that of equation (3), but here we have a two-ways comparison procedure depending on the choice, which one of the different L vectors will be taken for base. So, it can occur, that the matrix-product KK^T results in a singular weight matrix and its use in connection with non least squares adjustments may cause some inconveniences. The alternative choice, however, produces always a unique \bar{B} matrix.

In the foregoing we dealt actually with the counterplay of the mathematical formulation of the aerotriangulation problem and weighting technics. It seems that a useful comparison method can be derived from these duality. The Helmert premultiplication technics and Cholesky factorisation are the basic mathematical tools in the numerical procedures of these proposed comparison strategy. Also for points not involved in the adjustment we can construct prediction filters. In such a case also the appropriate part of the B_2 matrix will be effective. Finally mention can be made, that least squares filters have always some optimum characteristics but it does not mean, that the coordinate estimates determined in this way are unbiased, i.e. the best ones.

REFERENCES

- Helmert, F. R.: "Die Ausgleichsrechnung nach der Methode der kleinsten Quadrate" Leipzig/Berlin, 1924.
- Bjerhammar, A.: "Theory of Errors and Generalized Matrix Inverses" Elsevier Scientific Publishing Company Amsterdam-London-New York, 1973.
- Jazwinsky, A. H.: "Stochastic Processes and Filtering Theory" Academic Press, New York-London, 1970.
- Wolf, H.: "Äquivalente und korrelierte Beobachtungen" Jeodezi Bülteni, 1971.

CONTRIBUTION TO A GENERAL STEREOSCOPIC BLOCK ANALYTICAL AEROTRIANGULATION

by E. Dorrer, Munich, Fed. Rep. Germany

SUMMARY

Elevation changes of the McCall Glacier, Brooks Range, Alaska, were to be determined from aerial photography flown in 1958 and 1971. Different photo scales, extremely low image contrast in the third generation 1958 photography, different object illumination and terrain snow coverage, however, made the identification of transfer points virtually impossible. Therefore, a method for connecting overlapping photographs not requiring transfer points was utilized, similar to the one published by Albertz (1972). Employing the coplanarity principle as fundamental condition, the method is based upon stereocomparator measurements in possibly all existing overlapping photopairs of a block.

Subsequent application of this method to a pilot project proved to be successful only partially, mainly due to the particular geometric configuration of the block. Modification of the original method by incorporating also transfer points significantly improved both the accuracy and the iteration convergence for the 2 by 3 photo block. Commencing with an analysis of the results of this project, the mathematical model of a general approach to block analytical aerotriangulation with or without transfer points is discussed.

INTRODUCTION

The purpose of this paper is twofold. Firstly, originating from a certain field of application, an uncommon photogrammetric method of aerial triangulation had to be utilized. Secondly, the mathematical background for the method used and for similar versions is described.

As part of its glaciological activities, the Geophysical Institute of the University of Alaska, Fairbanks, under Dr. G. Wendler, has carried out mass balance studies on a typical "cold" Arctic glacier. The selected McCall Glacier in the Brooks Range, Alaska, had been surveyed during the IGY 1957-58. From terrestrial and aerial surveys the glacier was mapped in 1 : 10 000, with 5 m contours on the glacier and 25 m contours elsewhere. This contour map, published by the American Geographical Society, was compiled from 1 : 24 000 aerial photography (USAF), and plotted on a Wild A-7 stereoplotter at the Ohio State University (Case, 1958).

The aerial photography was repeated in 1971 at the scale 1 : 20 000. Usually mass balance studies on glaciers are carried out by comparing two independently plotted contour maps (so-called topographic method). The only link between the two maps are common control points or parts of common bedrock contours or features. Having been determined to a large extent independently, such two plots yield statistically reliable results only if the glacier elevations changes are at least three times their standard error. As in the McCall Glacier project neither the old control points could be reestablished nor glacier surface changes larger than a few meters be expected, a purely analytical method was chosen. Its disadvantage, viz. giving singular points rather than lines, is largely outweighed by its higher accuracy.

OBJECTIVES AND PROBLEM DEFINITION

The objectives were therefore, to determine glacier height changes by analytical photogrammetric means, to establish a digital terrain model for each of the two epochs, and to compare the two models.

Theoretically, there would be no problem to combine all necessary aerial photographs from both epochs into a - whatever arranged - aerial block. Well identified pass or transfer points on non-glacier terrain (so-called bedrock or reference points) would be needed as well as some control points, in order to perform either a sequential or a simultaneous block adjustment. The raw digital terrain models would then be determined by spatial intersection of all measured glacier photo points.

The 1958 photography available was of third generation only, therefore image contrast proved to be extremely low. Together with the fact that the photographs of both epochs had different object illumination and showed completely different terrain snow coverage, identification of a sufficiently large number of well

distributed common transfer points was virtually impossible. It was therefore decided to make use of a method published by Alertz (1972) which deliberately propagates a solution for block triangulation without transfer points. This method requires stereo measurements in as many stereopairs as possible, i.e. in any combination of two mutually overlapping photographs. Merely by means of stereoscopic vision, corresponding places rather than points can be identified and visually correlated easier. Thus, point identification is strictly combined with point measurement.

A stereoscopic inspection in a Zeiss PSK showed the principal feasibility of this method. Figure 1 shows the geometric configuration of the 2 x 3 photo block measured. In total 11 stereo pairs were measured, viz. 2 pairs 1958, 2 pairs 1971 and 7 pairs 1958/71 combined. Ground control had been established in 1971 by a new field survey. Ten stations were signalized by 2 - 3 m crosses of fluorescent red material. The terrestrial network was subsequently adjusted in a local system and the coordinates of the stations were computed (Ameresekere, 1972). Final accuracy was 0.3 m in planimetry and 0.15 m for the elevations.

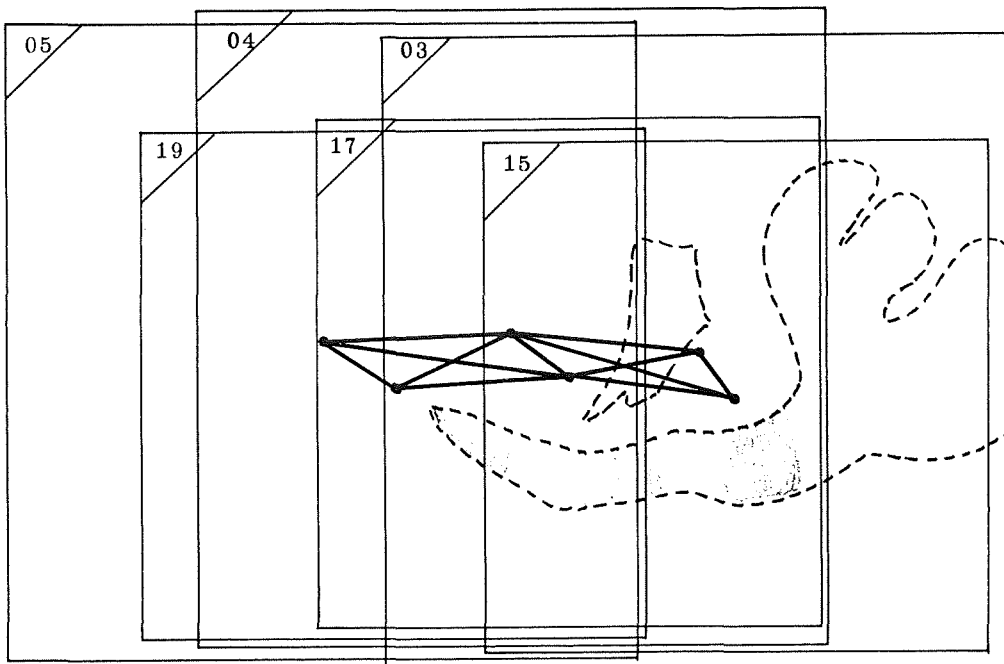


FIGURE 1 . Schematic photo coverage of McCall Glacier area for stereo block analytical triangulation.
1958 photographs 05, 04, 03 scale 1:24,000
1971 photographs 19, 17, 15 scale 1:20,000.

The entire problem was defined as follows:

- 1) Stereoscopic point measurements in all suitable stereo pairs.
- 2) Stereo-block analytical least squares adjustment of these measurements into the given ground control.
- 3) Establishment of digital terrain models for the two glacier epoch surfaces.
- 4) Comparison of the two digital terrain models.

In order to reduce possible local bias, common reference points on bedrock and along the periphery of the glacier had to be selected as well.

The purpose of this paper is to elaborate mainly on phase 2). First, the actual photogrammetric solution employed to the McCall Glacier project is briefly described, and the errors are analyzed. Finally an attempt is made for a general approach to a rigorous block analytical aerotriangulation, viz. with and/or without transfer points.

ACTUAL PHOTOGRAMMETRIC SOLUTION

When a decision had to be made whether a simultaneous or a sequential solution should be employed, the sequential solution received priority. This for the following reasons:

- 1) Developing the mathematical model and a corresponding computer program for a simultaneous solution would have taken a too long time. Both available man power and financial capabilities were far below a desirable figure.
- 2) The sequential solution provides a very valuable means of detecting errors after each phase.
- 3) For an as small block as the one of the McCall Glacier project, no significant loss of accuracy would have to be expected from a sequential approach.

Analogous to a single stereomodel the sequential solution adopted is based on a clear distinction between relative and absolute orientation. In the particular case of the McCall Glacier project, no information was available for the interior orientation of the 1958 photography. However, because of the extremely mountainous character of the terrain, the recovery of the interior orientation parameters could be combined together with the general relative orientation.

The block diagram in Figure 2 indicates the various phases involved in the sequential solution. Only the first six steps are typically photogrammetric.

STEP 1:

The comparator coordinates measured directly had to be transferred into photo coordinates via given fiducial marks. This transfer is necessary as the photographs cannot be centered and oriented in the PSK. The transformation is a simple planar rotation with translation.

STEP 2:

The first fundamental phase of the solution consists of a simultaneous relative orientation of all eleven stereo pairs measured. Basis for the mathematical solution is the coplanarity condition which must be applied to all pairs of corresponding image points (see Appendix A.1). For the McCall Glacier block consisting of $2 \times 3 = 6$ photographs, an auxiliary spatial reference system with origin in one of the photographs and parallel to its image system was chosen. Together with the 3 interior orientation parameters of the 1958 photography, a total of $3 + (6-1) \times 6-1 = 32$ parameters had to be determined. The unknowns were computed by linear least squares estimation, the mathematical model of which being established in the conventional straightforward manner by linearization of the nonlinear coplanarity equation. With a numerical convergence factor of 10^{-10} the solution of the linear equations converged to that of the nonlinear after 9 iterations. This comparatively large figure is caused by the specific block configuration (Figure 1) and the interior orientation parameters included.

STEP 3: (Appendix A.2)

With all internal and (relatively) external orientation parameters known, object space coordinates and parallaxes corresponding to the measured point pairs were established by spatial intersection (four linear equations each). In case the parallaxes of a point exceeded 3 times the RMS value determined from all parallaxes, this point was rejected as orientation point, and the relative orientation repeated. Four runs were required in the McCall Glacier project, causing a rejection rate of about 12 %. The points involved were either situated on the low contrast glacier surface, or measured in a stereopair consisting of photographs from different epochs and with mainly large vertical base component (pairs 05/19, 04/17, 03/15, in Figure 1). The result of step 3 is a digital multiple stereomodel consisting of orientation points, control points, glacier points, a few reference points.

STEP 4:

A control point measured in the 1971 photography should obtain unique model coordinates. If measured in several photopairs, the coordinates found by intersection were averaged. This procedure, however, entails inconsistencies of the solution, which is one of the main deficiencies of the adopted sequential method as compared to a simultaneous one.

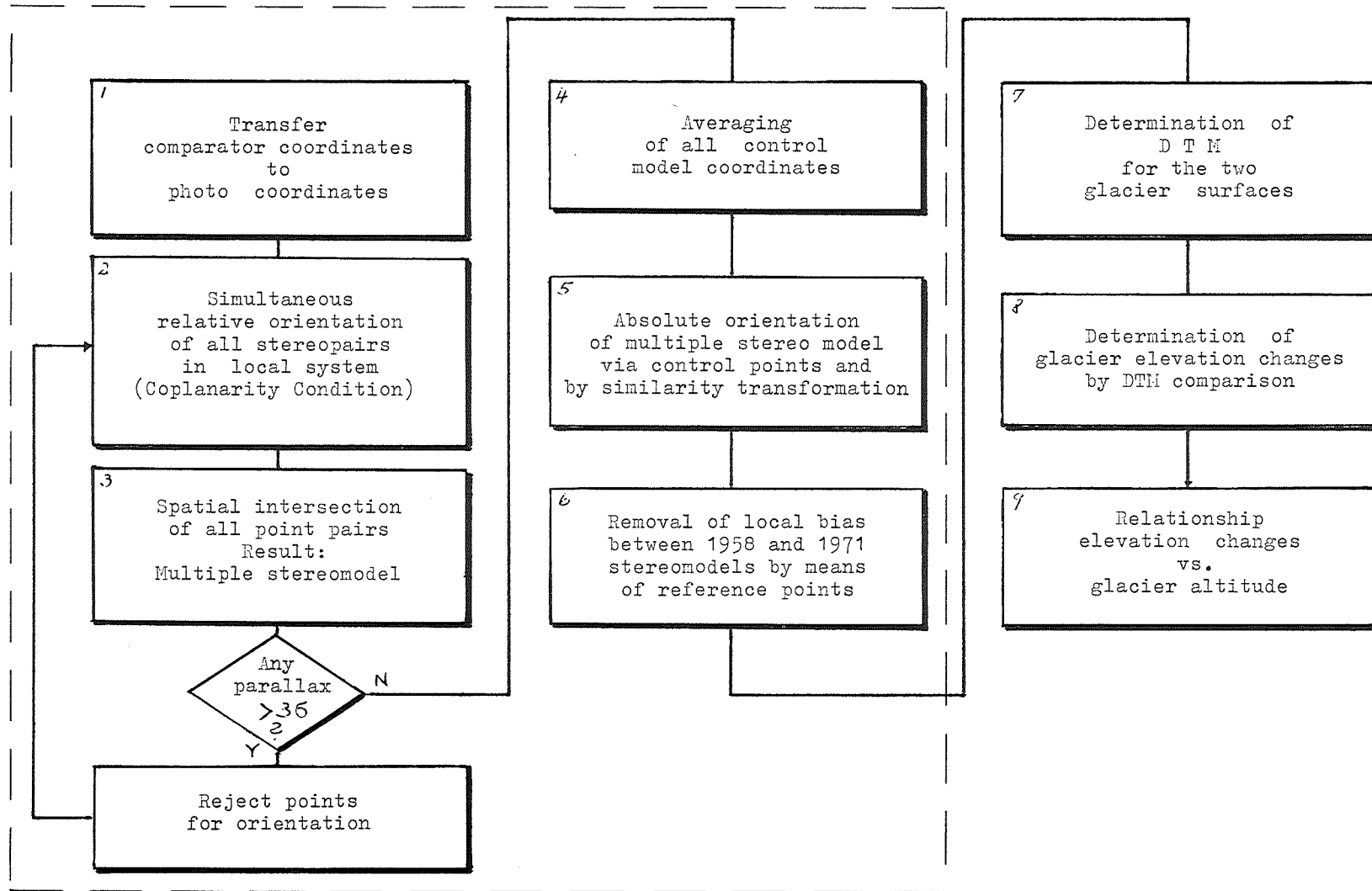


Figure 2. Block diagram of sequential solution

STEP 5:

The second fundamental phase of the method consists of an absolute orientation of the digital stereomodel, i.e. in a transformation of the model coordinates of all points into a given terrain coordinate system by means of control points. For a small block such as the one in the McCall Glacier project, a similarity transformation is sufficient. Larger blocks may require higher degree polynomials, unless a rigorous simultaneous solution is adopted. The actual transformation was carried out with the Stuttgart PAT-M43 computer program (Ackermann, 1970), although only one stereomodel was involved. The generality of PAT-M43 allows such a special case.

STEP 6:

Theoretically the previous steps should provide unique ground coordinates for the few reference points, i.e. points identical to both the 1958 and 1971 photography. Due to completely different systematic error patterns inherent in the two types of photographs, the expected value of the coordinate differences of these reference points cannot be considered zero. In order to reduce or eliminate this local bias, particularly relevant for the elevations Z' , Z'' , a correction surface must be computed for the height differences $\Delta Z = Z'' - Z'$ from all measured reference points. Each of the three glacier regions selected (Fig. 1) having its own set of reference points, three different local biases had to be determined. Due to the limited number of reference points, simple correction surfaces could be estimated only. The residuals are responsible for the final accuracy of the glacier surface elevation differences. A discussion of these is beyond the scope of the paper.

The method outlined above did not show very satisfactory results: too large a percentage of orientation points had to be rejected, and the coordinate differences of multiply measured points - control and pass points - frequently were larger than originally tolerated. A few control points having been misidentified, it was decided not to throw away the important information inherent in the measurements, but rather incorporate it as transfer information as done in ordinary block triangulation procedures. Therefore, step 5 was extended to include transfer points as well. For that reason the multiple stereo model was subdivided into two submodels with a few points in common, and PAT-M43 was applied. This resulted in a general decrease of the coordinate differences of common points by over 30 %, and the resulting RMS values seemed in agreement with the original expectations.

The computer program comprising steps 1 to 4 requires 100 Kbytes for compilation with the IBM FORTRAN IV-G compiler, and 110 Kbytes for the execution of 550 data points. The CPU-time on the IBM-System/370 of the University of New Brunswick was approximately 40 s for compilation and an average 240 s for execution of the data points in a single run of iteration.

ANALYSIS OF RESULTS

There are two kinds of analyses, one of intermediate, purely photogrammetric interest, mainly discussed in this chapter, the other of final glaciological interest.

A total of 516 points were measured stereoscopically on the PSK. This number can be subdivided into three tapes of stereo-models, as indicated in Table 1. It summarizes the RMSEs of residual y parallaxes, yielding, as measure for non-intersection of a pair of spatial rays, some indication of the stereomodel's accuracy. Obviously, standard errors in the 1958 photography were about twice those of 1971. A more detailed analysis shows that observations originated from highly normally distributed populations. An indication of how well the simultaneous relative orientation, including inner orientation for one set of photographs, performed, give the RMS values in Table 2. Photo 04 was kept fixed, thus all external orientation parameters are related to it. Recovery of the inner orientation parameters for the 1958 photography lead to the following result:

$$\begin{aligned}x_0 &= 0.17 \pm .14 \text{ mm} \\y_0 &= 0.12 \pm .08 \text{ mm} \\f &= 155.22 \pm .19 \text{ mm}\end{aligned}$$

Table 1. RMS errors of residual y parallaxes

Stereo Combination	Number of stereo pairs	Number of points	RMSE of py	Number of Measurements		
				1x RMS	2x RMS	3x RMS
1958/1958	2	154	.846 m	55	3	.
1958/1971	7	182	.627 m	60	8	.
1971/1971	2	180	.402 m	46	10	2

The absolute orientation as direct output of PAT-M43 showed RMS values of the coordinate residuals of photogrammetric model points, i.e. transfer and control points, as listed in Table 3. When reduced to image scale, the horizontal error is smaller than 15 μ m.

The standard coordinate errors turned out to be 0.30 m for planimetry and 0.22 m for the elevations. These values agree rather well with the a priori values of the terrestrial network adjustment (0.30 and 0.15 m). The result therefore indicates the validity of the statistical model used. For an average flying height of 3000 m above ground, the relative elevation error is below 0.5×10^{-4} ; this accuracy would never have been achieved by a purely topographic method.

Table 2. RMS values of orientation parameters after simultaneous relative orientation

E p o c h	1958	1971
Number of photographs	(2)	3
X_0	.8 m	3.4 m
Y_0	.7	1.9
Z_0	.4	4.7
ω	29"	53"
ϕ	42	57
κ	17	24

Table 3. RMS values of coordinate residuals

Coordinate	Photogrammetric model points	
	Transform. + Control	Control
X	0.12 m	0.15 m
Y	0.17	0.21
Z	0.10	0.14

From these results we may expect elevation errors mostly smaller than 0.30 m for well defined points. For glacier points, however, about two to three times this values must be considered, mainly due to difficult identification on the snow covered glacier surface.

From a photogrammetric point of view these achievements are rather satisfactory. For the glaciological investigation, additional errors revealed by reference points on bedrock around the glacier, must be considered. The photographs of both epochs yield different elevations for these reference points. The distribution of the elevation differences of corresponding reference points give an indication of the local bias still present in the computed glacier elevations. To reduce this bias, the following procedure was adopted. For each of the three glacier regions at least 4 reference points were carefully selected. The elevation differences ΔZ were used to interpolate a least squares bilinear trend surface. The elevations of glacier points were corrected prior to comparing the two glacier surfaces represented by unordered sets of spot heights. The standard error of glacier elevation change is a function of its position. Computed values for each region can be considered as representative for the final elevation changes shown in Table 4.

Table 4. Glacier elevation changes 1958-71 as determined by aerial photogrammetry.

R e g i o n	1	2	3
Mean altitude	1500 m	1715 m	1900 m
Elevation change ΔZ	4.5 m	2.9 m	2.0 m
Number of inter- polated spot heights (n)	6	8	5
Mean deviation	1.0 m	1.4 m	1.0 m
Number of reference points	5	7	4
σ_o	0.7 m	2.6 m	0.7 m
Regional average $\sigma_{\Delta Z}$	0.9 m	1.7 m	0.9 m
$\bar{\sigma}_{\Delta Z} = \sigma_{\Delta Z} / \sqrt{n}$	0.4 m	0.6 m	0.4 m

The standard errors $\sigma_{\Delta Z}$ are valid for a single elevation difference, averaged over each of the regions. Since for each region one elevation change ΔZ was determined out of several interpolated spot heights, the actual standard errors for the meaned height change must be smaller. Assuming no further bias, the standard errors of the mean of the determined elevation changes can be considered around 0.5 m (last line). This accuracy is completely satisfactory for glaciological purposes.

Due to unfavorable snow coverage of the glacier surface, only the three mentioned glacier regions could be chosen. Normally elevation changes should be determined for the entire length of the glacier. The McCall Glacier, however, was completely covered by snow from an altitude of 1950 m upwards. No information of the nevê region could therefore be obtained. As Fig. 3 shows, the normal trend of elevation change vs. altitude is clearly visible, and may be extrapolated beyond the observational region.

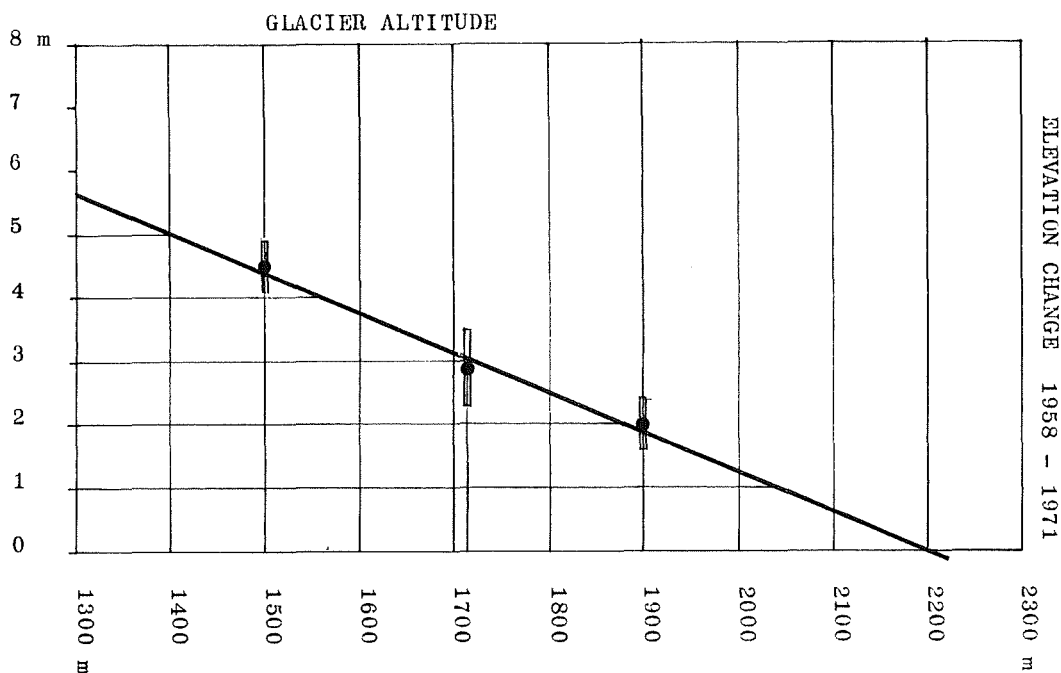


FIGURE 3 . McCall Glacier. Elevation change vs. glacier altitude obtained from aerial photogrammetry 1958 and 1971.

SPECULATIONS ON A RIGOROUS SOLUTION

Though consisting of ideas only, the following section nonetheless is of value for future consideration. The solution outlined in the previous sections has, besides its sequential character, the deficiency that either two different types of condition equations are to be used (Albertz, 1972) for orientation and control points, or a separation in relative and absolute orientation becomes necessary. The situation is further complicated if transfer points are to be included. Without a specific forcing condition, the common information inherent in transfer points cannot be utilized in a simultaneous solution. Since the ground system may be considered but another stereo model (0-model according to Ackermann, 1970) identical conditions can be used for control and transfer points.

It seems more adequate for a rigorous solution to describe the geometrical relationship between measured image coordinates and object coordinates by just one type of condition, viz. the collinearity condition. Which form one wants to use is immaterial. Appendix B.1 proposes an implicit form yielding a general least squares estimation problem.

The conventional least squares approach, i.e. if a differentiation is made between observations, unknowns, and fixed quantities (e.g. ground control coordinates), necessitates strict distinction between single points, transfer points and control points. This leads to a different consideration of each of these point types, a procedure that may easily be overcome by also considering ground coordinates as random variables (Brown, 1971). Such a solution, favored by the author, is discussed briefly in Appendix B.2. A rethinking of possible correlations between image coordinates of the same point when measured stereoscopically, seems desirable, though. This statement is particularly valid for statistical analyses.

CONCLUSION

The proposed rigorous stereo-analytical aerotriangulation procedure does not solve the point transfer problem. For an improved connection of individual stereomodels or bundles, Albertz' method should be included in the common triangulation and block adjustment procedures, and vice versa. The fundamental collinearity condition seems generally more applicable to all types of photogrammetric points than the coplanarity condition.

REFERENCES

- Ackermann F. et alii, 1970, "Ein Programmpaket für die Aerotriangulation mit unabhängigen Modellen", Bildmessung und Luftbildwesen 38, 218-224
- Albertz J., 1972, "Blocktriangulation ohne Punktübertragung" Bildmessung und Luftbildwesen 40, 38-40
- Ameresekere R.S.S., 1972, "Adjustment of the McCall Glacier Survey 1971" Fredericton N.B., Canada, University of New Brunswick, Master of Engineering Report, 128 pages
- Brown D.C., 1971, "Analytical Aerotriangulation vs. Ground Surveying", paper presented at 1971 Symposium on Computational Photogrammetry, San Francisco
- Case J.B., 1958, "Mapping of Glaciers in Alaska", Photogrammetric Engineering Vol. 14, 815-821
- Dorrer E., 1971, "Tensor Calculus in Computational Photogrammetry", paper presented at 1971 Symposium on Computational Photogrammetry, San Francisco
- Wendler G. and others, 1974, "The Climate of the McCall Glacier, Brooks Range, Alaska, in Relation to its Geographical Setting" Arctic and Alpine Research, Vol. 6, No. 3, 307-318

APPENDIX A

Analytical treatment of principle of sequential solution

1 - Coplanarity Condition - Relative Orientation

The coplanarity equation is the fundamental condition for relative orientation. It states that the base line between two exposure stations and the two object rays to an object point lie in the same plane. Consider, e.g. two mutually overlapping photographs p,q of a block. For a point i measured in the photopair (p,q) the coplanarity condition may be written in the following tensor form (Dorrer, 1971), $\lambda, \mu, \nu = 1, 2, 3$:

$$\epsilon_{\lambda\mu\nu} (C_{\lambda}^q - C_{\lambda}^p) u_{\mu}^{pi} u_{\nu}^{qi} = 0 \quad (A.1)$$

where

C_{λ}^s = object space coordinates of projection center of photo number s,

u_{μ}^{si} = image space coordinates (in a system parallel to the object space system) of a point i measured in photo number s.

(Note: Einstein's summation convention is adopted for subscripts only).

The image space coordinates u_{μ} are related to the actual photo coordinates $x_{\mu} = (x_1, x_2, 0)^T$ by the expression ($\kappa = 1, 2, 3$)

$$u_{\mu}^{si} = r_{\mu\kappa}^s (x_{\kappa}^{si} - c_{\kappa}^s), \quad (A.2)$$

where

$r_{\mu\kappa}^s$ = a 3x3 orthogonal rotation matrix of photo s,

x_{κ}^{si} = image coordinates of a point i measured in photo s, and

c_{κ}^s = photo coordinates of perspective center of photo s.

Equ. (A.1) and (A.2) combined define a non-linear condition for a measured point pair. All orientation parameters θ and image coordinates x combined yield a system of condition equations

$$f(\theta, x) = 0. \quad (A.3)$$

Linearization of equ. (A.3) by means of a Taylor expansion gives rise to the "design" matrix $A = \partial f / \partial \theta$, and the discrepancy vector $w = f(\theta^0, x)$, according to the least squares terminology. The stochastic model assumed was that all image coordinates have unit weight. Rather than make use of the combined adjustment case, a simplified parametric case was adopted, viz.

$$A d\theta + w = v \quad (A.4)$$

Here, the residuals v are referred to "pseudo-observations" w , i.e. to the coplanarity condition as random variable.

2 - Space Intersection

The purpose of space intersection is to determine the coordinates $X_\mu (\mu=1,2,3)$ of an object point by use of two (or more) photographs of known orientation. Fundamental equation is the collinearity equation which must be applied to both images, viz.

$$\begin{aligned} X_\mu &= C'_\mu + k' r'_{\mu\nu} (x'_\nu - c'_\nu) = C'_\mu + k' u'_\mu \\ X_\mu &= C''_\mu + k'' r''_{\mu\nu} (x''_\nu - c''_\nu) = C''_\mu + k'' u''_\mu \end{aligned} \quad (A.5)$$

The scalars k' , k'' can be eliminated by writing equ. (A.5) in the form ($\alpha = 1,2$)

$$\frac{X_\alpha - C'_\alpha}{X_3 - C'_3} = \frac{u'_\alpha}{u'_3}, \quad \frac{X_\alpha - C''_\alpha}{X_3 - C''_3} = \frac{u''_\alpha}{u''_3}$$

or

$$\begin{aligned} u'_3 X_\alpha - u'_\alpha X_3 &= u'_3 C'_\alpha - u'_\alpha C'_3 = s'_\alpha \\ u''_3 X_\alpha - u''_\alpha X_3 &= u''_3 C''_\alpha - u''_\alpha C''_3 = s''_\alpha \end{aligned} \quad (A.6)$$

Equ. (A.6) may be condensed by means of the 4th order Kronecker Delta, and by representing the primes by an additional index $\beta = 1,2$, viz.

$$\delta_{3\alpha\lambda\mu} u_\lambda^{(\beta)} X_\mu = t_{\alpha\mu}^{(\beta)} X_\mu = s_\alpha^{(\beta)}. \quad (A.7)$$

The components of t are entries of a 4x3 matrix; the three unknown coordinates X_μ may be estimated by parametric adjustment.

In order to estimate the achieved accuracy of the space intersection, the discrepancy was computed between an intersected object point and one of its determining object rays. The minimum distance d of a point X_μ and a vector u_ν originating from the projection center C_μ is given by

$$d^2 = (X_\mu - C_\mu)(X_\mu - C_\mu) - \frac{((X_\lambda - C_\lambda) u_\lambda)^2}{u_\nu u_\nu}. \quad (A.8)$$

The sum of the two minimum distances between a pair of object rays is the y parallax.

APPENDIX B

Analytical formulation of a rigorous solution

1 - Collinearity Condition

The collinearity equation is the fundamental projective condition between image coordinates and object coordinates. It may be applied to any block configuration and to any type of points. An implicit form of it may be written in the form

$$\delta_{3\alpha\lambda\nu} r_{\mu\lambda}^{p(s_i,\gamma)} (x_{\nu}^{ip(s_i,\gamma)} - c_{\nu}^p(s_i,\gamma)) (X_{\mu}^i - c_{\mu}^p(s_i,\gamma)) = 0 \quad (B.1)$$

where

- i = point number,
- s_i = any stereopair, in which point i occurs,
- p = photo number in stereopair s_i,
- γ = 1 for left photo of a pair, and
= 2 for right photo of a pair

$\delta_{\phi\sigma\kappa\lambda} = \epsilon_{\phi\sigma\nu} \epsilon_{\kappa\lambda\nu}$ is the fourth order Kronecker Delta
α, = 1,2; κ,λ,μ,ν, = 1,2,3.

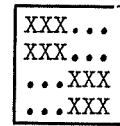
Equ. (B.1) contains the information for all point pairs or points measured in stereopairs or single photographs. For a point pair within a particular stereopair, equ. (B.1) simplifies to

$$f_{\alpha}^{i\gamma} = \delta_{3\alpha\lambda\nu} r_{\mu\lambda}^{\gamma} (X_{\mu}^i - c_{\mu}^{\gamma}) (x_{\nu}^{i\gamma} - c_{\nu}^{\gamma}) = 0. \quad (B.2)$$

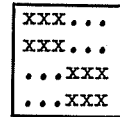
The partial derivatives of $f_{\alpha}^{i\gamma}$ with respect to the orientation parameters, i.e. c_{μ}^{γ} , θ_{κ}^{γ} (rotational parameters of $r_{\mu\lambda}^{\gamma}$), and c_{ν}^{γ} , show immediately the structure of the linear system of equations used for a linear least squares estimation.

Viz.

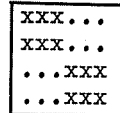
$$\frac{\partial f_{\alpha}^{i\gamma}}{\partial c_{\mu}^{\delta}} = -\delta^{\gamma\delta} \delta_{3\alpha\lambda\nu} r_{\mu\lambda}^{\delta} (x_{\nu}^{i\delta} - c_{\nu}^{\delta})$$



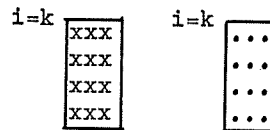
$$\frac{\partial f_{\alpha}^{i\gamma}}{\partial \theta_{\kappa}^{\delta}} = \delta^{\gamma\delta} \delta_{3\alpha\lambda\nu} r_{\mu\lambda}^{\delta} \cdot \kappa (X_{\mu}^i - c_{\mu}^{\delta}) (x_{\nu}^{i\delta} - c_{\nu}^{\delta})$$



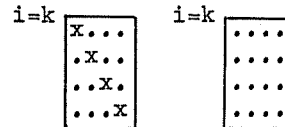
$$\frac{\partial f_{\alpha}^{i\gamma}}{\partial c_{\nu}^{\delta}} = -\delta^{\gamma\delta} \delta_{3\alpha\lambda\nu} r_{\mu\lambda}^{\delta} (X_{\mu}^i - c_{\mu}^{\delta})$$



$$\frac{\partial f_{\alpha}^{i\gamma}}{\partial X_{\mu}^k} = \delta^{ik} \delta_{3\alpha\lambda\nu} r_{\mu\lambda}^{\delta} (x_{\nu}^{k\delta} - c_{\nu}^{\delta})$$



$$\frac{\partial f_{\alpha}^{i\gamma}}{\partial x_{\beta}^{k\delta}} = \delta^{ik} \delta^{\gamma\delta} \delta_{\alpha\beta} r_{\mu\lambda}^{\delta} (X_{\mu}^k - c_{\mu}^{\delta})$$



2 - Least Squares Estimation

Equ. (B.1) applied to all measured image points gives rise to the following general system of nonlinear equations, written in matrix notation

$$f(\theta, X, x) = 0 \quad (B.3)$$

where θ = vector of orientation parameters
 X = vector of ground coordinates
 x = vector of image coordinates.

Independent of the fact what points are or are not known, the ground vector \mathbf{x} may be considered a random variable vector. If in addition to the covariance matrix K_x of the actual observables \mathbf{x} , also the covariance matrix K_X of the ground vector \mathbf{x} is known at least approximately, \mathbf{x} may be considered but another observation vector. With V and v representing the residuals to X and \mathbf{x} , respectively, the least squares condition

$$L = v^T K_x^{-1} v + V^T K_X^{-1} V = \min.$$

yields a linear system of condition equations with unknowns, viz.

$$A d\theta + B_x v + B_X V + w = 0.$$

With

$$M = K_w = B_x K_x B_x^T + B_X K_X B_X^T$$

the interesting parameters are

$$d\theta = -(A^T M^{-1} A)^{-1} A^T M^{-1} w,$$

$$v = K_x B_x^T t, \quad V = K_X B_X^T t,$$

where

$$t = M^{-1} (A (A^T M^{-1} A)^{-1} A^T M^{-1} - I) w$$

are the correlates (or Lagrange multipliers). The size of the largest matrix to be inverted is identical to the number of orientation parameters. For regular blocks this matrix has typical banded structure, and may be inverted by known numerical methods.

DEVELOPMENT OF A COMPUTER SIMULATION SYSTEM
CONCERNING THE ACCURACY OF PHOTOGRAMMETRIC OPERATIONS

by H. G. Jerie, Enschede, Netherlands

ABSTRACT

The objective of the paper is to give an introduction to a R and D project initiated by the ITC research group.

This research project concerns the development of a computer simulation system as a tool to meet various objectives, the most important being:

- a) Establishment of accuracy models for various photogrammetric operations;
- b) The evaluation of known and the development and evaluation of new data processing methods;
- c) Feasibility studies concerning new photogrammetric methods and equipment.

The computer simulation system is meant to replace practical integral experiments to a large extent and furthermore to yield a consistent system of accuracy models. Alternative methods to achieve the same objectives, i. e.:

- a) practical experiments and
- b) analytical derivation by application of the statistical laws of error propagation

require either much more effort (a) or are less capable to cope with the systematic character of the various error sources involved in photogrammetric operations (b). Past efforts to establish computer simulation systems are characterized by limited objectives and scope and were therefore not able to fully meet the above mentioned objectives.

In order to allow a universal as possible application of the computer simulation system, it will be constructed in a modular way. For specific applications the various relevant models will be combined by individual operating programmes, copying the actual flow of physical process to be simulated.

The main phases of a simulation programme are:

- a) Generation of photography (including generation of terrain elevation data);
- b) simulation of observation phase;
- c) data processing phase; and
- d) statistical processing.

Eventual new features of the simulation system will be a terrain elevation generator and furthermore the fact that the various error sources in the imaging and observation phase are generated sequentially and by random error functions. The total development project therefore consists of the task to design proper functional and statistical models for the various error sources and subsequently analyse a sufficiently large amount of experimental data, to verify the derived models for the parameters of the respective random functions.

While this paper only gives an overall description of the initiated simulation system, it is intended to describe the development of the various models in more detail in a series of papers to appear subsequently in the ITC Journal.

1. INTRODUCTION

The ITC research group has initiated a project which aims at the development of a triple purpose computer simulation system:

- a) For the establishment of accuracy models for various photogrammetric operations;
- b) as an efficient instrument for the development and evaluation of data-processing methods;
- c) for feasibility studies concerning new photogrammetric methods and equipment.

The necessity for accuracy models for various photogrammetric sub-processes employing different process-components which are currently available has already been explained in a preceding paper [1]. It is strongly felt that a computer

simulation system, being designed to simulate the functional and stochastic processes as realistically as possible in view of the intended applications, will yield a consistent system of accuracy models in the most efficient way.

With respect to the second objective, it is felt that for the development and evaluation of suitable data processing methods (e.g. adjustment procedures, gross error detection methods, etc.), data generated by a computer simulation system can be extremely useful. They can be produced with a fraction of the effort required for practical experiments, can be more representative as an individual test and contain complete data concerning "true values".

With respect to the third objective it will be quite obvious that a simulation system, being composed of all known information about possible sources of errors, will be a very convenient means of studying the probable effect of new concepts and designs, concerning methods and equipment. In this way a number of potentially good ideas which are never realized because of the required effort for practical testing might come to reality. On the other hand considerable effort which is currently spent on testing impracticable innovations might be saved. The literature contains a fair number of examples of both categories.

The objective of this paper is to give a general introduction to the problem and its various components and aspects and to serve as a basis for a series of papers to be published in this Journal, dealing in more detail with these components and eventually presenting results of the applications of the computer simulation system.

It will be obvious to the reader that the development of such a system is a tremendous task and cannot be completed within a short period. Indeed, it will never be complete as new data and information should be added continually. However, it is hoped that some useful results can already be produced by the system in the not too distant future, although in a provisional form.

2. COMPUTER SIMULATION VERSUS ALTERNATIVE APPROACHES TO THE PROBLEM

The development of a computer simulation system for the establishment of an accuracy model, in view of the considerable effort involved, is only justified if on the one hand the potential user of derived information can be persuaded to trust this information, and on the other hand if it can be proved that this approach is superior and more efficient than alternative approaches to the problem. Before attempting a comparative evaluation of the different approaches possible, let us first state the problem clearly:

Accuracy performance of photogrammetric operations is influenced

- firstly by the chosen process parameters and process components (e.g. type of camera, photoscale, measuring equipment and methods, control distribution, data processing methods etc.);
- secondly by error sources which in each individual case are mainly of a systematic nature, within individual photographs, models, strips or blocks, but differ to various degrees for different projects (e.g. irregular refraction, lens distortion, film flatness, film distortion, instrumental errors etc.);
- thirdly by errors mainly of a purely random nature such as observation errors;
- fourthly by indirect error generating influences which are themselves systematic in nature such as flight parameters, terrain deviations, accidental location of various points for measurement etc.

The planner of a project needs information concerning the accuracy performance of his choice of parameters and components. However, considering what has been stated above about the error generating influences (especially with respect to the random (unpredictable) nature of various systematic errors) it is evident that these are by no means constant, but can vary in a statistical sense. The planner therefore has to cope with this uncertainty. The degree of risk which he is willing to accept is a matter of policy, but it has to be known to him.

Let us now, in the light of this situation, analyse the value of accuracy information derived from individual practical experiments. Firstly they generally represent only one combination of project parameters and in most cases it is difficult, if not impossible, to determine the functional relationship between the various process parameters and the final accuracy performance. This means that

no useful information is derived for any situation with different process parameters. In order to achieve this it would be necessary to repeat the experiment under systematic variation of the different parameters. One can easily imagine that this would result in an inconceivable number of practical experiments. Furthermore, the individual experiment represents just one random combination of error generating influences and it is by no means certain that any independent repetition of the experiment would not lead to slightly or considerably different results (as a consequence of another combination of error generating influences). Hence to gain information concerning the character and range of this uncertainty, each experiment would have to be repeated many times under completely independent circumstances. Considering the high cost in time and money required for such integral tests, this method seems out of question.

How does the proposed approach by computer simulation now compare to integral practical experiments with respect to effort and achievements? This approach also requires practical experiments. However, the objective of these experiments is the establishment of comprehensive statistical data and stochastic models concerning the individual sources of errors. If this information can once be obtained then computer simulation can take over the role of practical experiments. The execution of a simulated project will take computer-minutes instead of many man-years. Only in this way will it be possible to allow not only for all possible variations in project parameters, but also for all possible variations in size and character of the different error sources.

The probability that the functional and stochastic models established and applied in the simulation process are not absolutely correct in each individual run, will in view of the unavoidable (i.e. natural) uncertainty of the outcome, play a negligible role. We have to balance this against the fact that practical experiments do not give any information concerning this uncertainty.

Let us now turn to another approach to the problem of establishing accuracy models: their analytical derivation by application of the statistical law of error propagation. Or, in other words: the establishment of functional and stochastic models (in the form of variance or covariance matrices of the stochastic quantities involved) and their formal processing analogue to the physical process in question in order to derive variance or covariance matrices of the final results.

Although the application of this approach in the past has contributed considerably to our knowledge, it suffers from a number of theoretical and practical short-comings, the effect of which on the results obtained is difficult to estimate. Considering past investigation of this type the following critical remarks can be made:

- a) In order to reduce the required computational effort various simplifying assumptions have to be made: Photographs, model, and strips are assumed in ideal positions. The same is true, e.g. with the position of orientation points, minor control points, tie-points, and ground control points.
- b) Investigations are not extended to include elevation differences of the terrain, although this must have some (possibly considerable) effect on the results. Not only do height differences in the individual model result in variations of the accuracy of relative orientation, but they also cause significant correlations between points in different photographs, models, and strips (because of the effect of systematic errors).

It is a generally accepted hypothesis in this approach that systematic errors (in a completely schematic configuration without terrain-deviations) cause systematic deformations within the strip which can easily be eliminated by the adjustment procedures. This assumption is, however, not longer true for irregular configurations and existing terrain elevations. In this case local errors and correlations are generated which have a pseudo random character within the whole block or strip.

- c) Although theoretically possible, in practice no correlations between observations or pseudo-observations are introduced in the computation process.
- d) Input- and output errors have to be considered to be normally distributed because the applied laws of error propagation are based on this assumption.

- e) No information can be given concerning the statistical spread of resulting variances. In some configurations, as for instance single strip triangulation, the variances of one individual strip can vary considerably from the mean values obtained through many repetitions. This is due to the high correlation existing within one strip which in turn is caused by the accidental effects of double summation.
- f) This approach does not allow the statistical investigation of the effects of "gross-errors".
- g) It would be extremely difficult using this approach to deal with various approximate methods because of the complex mathematical relationships involved (e.g. all kinds of smoothing processes), or the occurrence of systematic errors for which no suitable stochastic description can be defined.
- h) Finally - and this is in the eyes of the author the most serious shortcoming of the method (because of the necessity to make simplifying assumptions, and to use for different investigations different types of input in form of pseudo observations) - the results of different investigations are not compatible with each other. They do not form a consistent system, which allow the planner to judge for himself which results he can achieve under his specific circumstances.

The above discussion might appear to the reader to be too severe a criticism of the alternative methods, but it has been done in the desire to pave the way for discussion of an approach which appears to offer the only possibility of achieving a comprehensive and consistent system of information about accuracy performance. There will remain a limited necessity for the execution of integral experiments, partly in order to check and verify the results obtained by computer simulation and partly because there will still be people who will trust the "real thing" more. Computer simulation can, however, play a useful role in these also with respect to optimal designs of such experiments.

Last but not least it should be mentioned, that, to the author's belief, the value of the simulation system is only partly based on the possibility of evaluating processes and components already in use, but is even more important in that it offers the possibility of experimenting with new concepts before trying them out in practice. This, after all, is the proven advantage of the application of computer simulation and operational research in many other fields of technology.

3. COMPUTER SIMULATION IN THE PAST

Numerous examples of application of computer simulation are known from literature. However, most of these concern efforts of very limited scope and application, e.a. studies of the effect of control distribution on various adjustment procedures. Exactly this was also the purpose of a past development of the ITC (The ITC-test block [2], [3]) and of later developments (Doyle [4], Anderson [5]). The error models, applied for these developments were not sufficiently realistic to allow their applications for general investigations. This is certainly the greatest danger in developing such a simulation system. Cases are known, where authors reported enthusiastically about incredibly good results of new procedures, seeming completely forgetting the fact that this was only due to unrealistic assumptions concerning the input data.

The only serious effort to create a computer simulation system for more general use comes from P. Malinen [6]. However, as this author has left the photogrammetric profession, obviously no further development has taken place. However, all these efforts are characterized by considerable simplifications which were probably partly due to non-existence of relevant information, partly due to limitations in possible effect. The present project will have to stand on the shoulders of these predecessors. As the required knowledge concerning error models to a large extent does not yet exist, a considerable effort will have to be spent in acquiring this knowledge.

4. DESIGN PRINCIPLES AND SPECIFICATIONS FOR THE SIMULATION PROGRAMME

The objective to be achieved with the simulation programme, namely the possibility of establishing for various photogrammetric subprocesses accuracy models which are compatible with each other and form in themselves a consistent system, re-

quires a systems approach to the design and the operation of the simulation programme. A modular sequential form of data generating and processing will be chosen, which copies more or less exactly the actual flow of physical processes, which are to be simulated.

Simplifying assumptions will only be made as far as this is dictated by the limitations of available statistical data or as far as this is permissible in view of the inevitable uncertainty of the final results. We must always keep in mind that the ultimate objective of the exercise is to predict the obtainable accuracy for projects to be executed in the future, under governing circumstances which are partly of a random nature. With this in mind it could be unreasonable to consider small influences which have an insignificant effect on the final result.

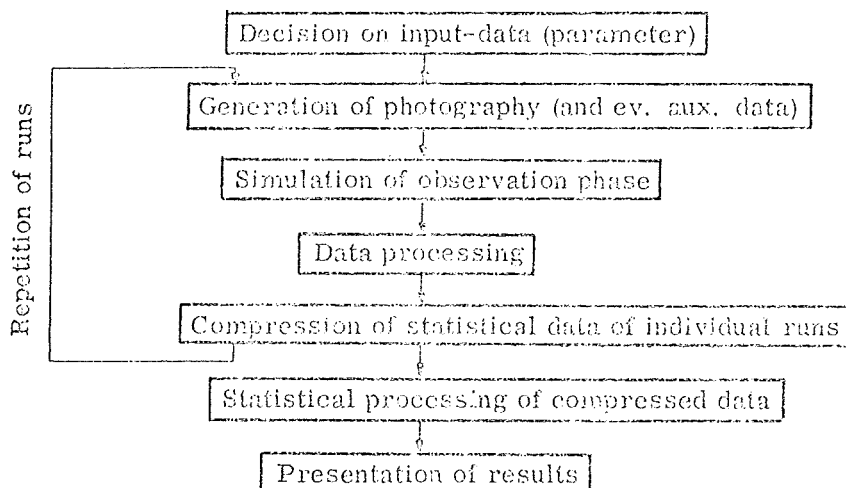
Considering the quite different applications of the simulation programme, it would not seem efficient or feasible, to endeavour to prepare one programme with possibilities for all these choices. It seems more reasonable to develop a set of sub-programmes for data generation, functional and statistical computation, which can be called on by operating programmes developed individually for each new type of application.

Four main phases can be distinguished in the total process of simulation:

1. Generation of "photography": This includes generation of terrain data (terrain elevation), flight parameters, and image coordinates of various categories of points: ground control, minor control tie-points, relative orientation points, scale transfer points, check points and, if required, auxiliary data also.
2. Simulation of "observation phase": Depending on the procedure (type of method and equipment) to be investigated, various stochastic influences, e.g. instrument errors and observation errors have to be simulated. The latter will partly depend on image quality (influenced by meteorological circumstances, optical quality of lens, flight speed and exposure time, granularity of photographic material, photographic processing, structure and contrast of terrain details, etc.) and human skill.
3. Data processing phase: This is identical to what happens in reality. Various methods of pre-processing and adjustment will be applied to the "observations" carried out in the second phase.
4. Statistical processing: Determination of those statistical indicators, by which the accuracy of results can be described, through comparison of the results of the third phase with the corresponding "true values".

As numerical simulation usually involves the execution of a large number of "runs" this means that a tremendous amount of data has to be generated and processed for each individual investigation. In order to reduce the amount of data to be stored the results of each individual run have to be suitably compressed to be used in the final statistical analysis of all runs.

The whole process is represented schematically below:



For the first and second of the above mentioned phases, the following components will have to be developed:

1. A terrain elevation generator: A number of typical terrain forms (landscapes) will be selected, and mathematical functions developed which simulate those properties of reality which are essential with respect to the accuracy of photogrammetric operations. These are in the first place height distributions and distributions of height differences in function of distance and mean elevations.

2. A generator for flight parameters (camera stations, tilts and crab): Depending on the flying height, stability of aircraft and navigational aids, different statistical populations for flight parameters will be made available for selection. Formal values for forward and lateral gain will be computed in function of the incidental terrain elevations encountered.

3. Generators for the approximate image coordinates of those points, which are in reality selected by the human operator, e.g. relative orientation points, minor control points, tie points, scale transfer points, in some cases ground control points. The formal position of these points depending on the flight parameters of the photographs involved and on ground elevations, will be perturbed by random values as analysed from real projects. These approximate image coordinates will be projected on to the "terrain" and thereby the "true ground coordinates" of these points determined.

4. Generators for "image errors": Several sources of errors will be generated in sequence:

4.1 - Influence of refraction: standard values will be perturbed according to assumptions concerning the statistical distribution of meteorological irregularities. In this way, correlations between image errors of ground points appearing in different photographs will be generated properly. The influence of turbulence under the camera window will be neglected for the time being, because of the lack of theoretical and statistical data. The same holds for the influence of front-plates, the influence of which will be considered at a later stage.

4.2 - Influence of lens distortion: of interest are of course not only the calibrated mean distortion functions (they are corrected for in most processes anyway, either by computational or physical means) but even more so the irregular radial and tangential distortions. In this respect it would be highly desirable to simulate gradual changes, as caused in reality by the influence of temperature changes on the lens during the flight.

4.3 - Influence of variation in film thickness: results of laboratory investigations on the possible variations will be used in appropriate functional and stochastic models for generation of resulting image errors.

4.4 - Influence of unflatness of film during exposure, caused by dust particles and incorrect working of suction devices, will be introduced by functional and stochastic error models, based on the findings of special investigations into the problem.

4.5 - Influence of regular and irregular film distortions, caused by mechanical influences at the moment of exposure, and during photographic processing. With such phenomena, large variations in the systematic deformations can be expected for different projects; smaller, gradual changes will occur with time during one flight mission (i.e. on the photographs of one film).

Both these large variations for different missions and the smaller gradual changes during one mission have to be simulated, because the former cause statistically large uncertainties for future projects, while the latter cause correlation of data within one strip or mission, which to a certain extent reduces the effect of the distortions on the final result of one individual project. Image distortions caused by the process of production of diapositives or paper prints will be of interest when investigations are made into the accuracy of plotting with approximate instruments.

5. In the "observations phase" we have to distinguish two sources of errors: The first are static and dynamic instrument errors, resulting in both systematic and random errors of observations. The second category concerns observation or measuring errors, which are influenced by many factors. They can partly be grouped together under the concept "image quality", resulting in systematic errors of individual points and in a basic uncertainty to which we have to add the effect of the observational skill of the human operator.

The foregoing analysis of the character of various error-sources should make it clear that the concept of purely random and independent "observation errors" is theoretically wrong. This can easily be proved by the fact that otherwise an increase of repetitions of observations should lead to each required level of accuracy.

For our intended purpose we have to consider two main aspects. The actual character of certain systematic errors can vary considerably, and cannot be predicted for future projects. It has in this respect to be treated as random. On the other hand, within one mission or parts of it, some of the systematic errors change only slightly and gradually in character, and this can cause accumulation as well as partial compensation of these error influences on the final accuracy results.

The extent to which these phenomena play a significant role, can only be established after actual application of the simulation system to different photogrammetric processes.

5. THE ESTABLISHMENT OF REALISTIC ERROR MODELS

To establish realistic error models for all the error sources mentioned in the foregoing paragraph will not be an easy task, and will require considerable effort. A consolation might be the thought that this will be only a fraction of the effort which would be required, if the general task were executed in an alternative way (e.g. by integral experiments). Different sources of statistical input data, like lens calibration data, reseau measurements, photogrammetric test field measurements, but also results from various laboratory tests (film thickness and unflatness) and even from other fields of sciences (like meteorology) will have to be suitably combined.

The results obtained in this way can be checked against results of practical experiments of different size and scope. Only after we can be satisfied that the results of previously executed practical experiments can be achieved by the simulation system in a significant manner, will it be applied to hitherto untested processes.

One of the difficulties encountered lies in the fact that although a large number of experiments and investigations has been carried out in order to establish the size of errors arising from different error sources, this has nearly always resulted in description by standard deviation. For error generation this is of course not sufficient, because the errors are in reality not normally distributed and independent.

For simulation purposes these errors must therefore be defined as functions (e.g. film distortion as a function of image-coordinates). For this purpose the complete set of measurements will be required in order to analyse their functional and stochastic characteristics. Each of the error-sources defined will be the subject of a specialized investigation. Reports on the results of these investigations can be expected in subsequent editions of this journal.

The author wishes to conclude this introduction to a research project, which it is hoped may be of considerable benefit to the photogrammetric community, by a request for assistance from his readers. The ITC will be extremely grateful for appropriate data in various forms, be it camera calibration data, test field photography or measurements, reseau photography and measurement, data concerning equipment calibration, observational accuracy etc., or any information concerning possible sources of such data.

REFERENCES

- |1| Jerie, H.G.: "PPP - An operations research programme for project planning"
ITC Journal 1973 - 3.
- |2| Jerie, H.G.: "A block of synthetic aerial triangulation strips"
ITC Publication A 27/28, Spring 1964.
- |3| Thorpe, J.A.: "Artificial block", M.Sc.thesis, ITC 1963.
- |4| Doyle, F.J.: "Fictitious data generator for analytical aerotriangulation"
Photogrammetria 1966.
- |5| Anderson, J.M. and Ramey, E.H.: "Summary of Working Group Reports,
(Simulated Test Data for Analytical Aerotriangulation)
I.S.P. Congress 1972 (Ottawa), Comm. III.
- |6| Malinen, R.P.: "Simulation in Photogrammetry"
The Photogrammetric Journal of Finland, 1969, no. 1.
- |7| Nasu, M., Kaji, K., Kamiya, R.: "An Experiment on Aerotriangulation by
Simulation", I.S.P. Congress 1968 (Lausanne), Comm. III.
- |8| Wolters, J.A.M.: "Accuracy of Analytics by Computer Simulation"
Photogrammetric Engineering 1968

CAMERA CALIBRATION BY PHOTOGRAPHING TEST FIELDS

by I. Hådem, Oslo, Norway

INTRODUCTION

An aerial camera is a precision instrument which gives numerical results to an accuracy of the order of one micron. However, unlike other precision instruments an aerial camera is not calibrated under real working conditions. The camera is ordinarily calibrated in laboratories, but other methods are also applied, e. g. photographing the horizon (in combination with angle measurements) or photographing from high towers [6]. In all cases, the conditions deviate from the real operational conditions, which are characterized by extreme temperature, humidity and air pressure.

It has been assumed that the large variation in temperature to which the camera is exposed under real working conditions might have a special influence on the camera calibration elements, especially the focal length. Investigations to verify or reject this assumption have, however, given contradictory results [4], [10]. The reason for this may be that in experiments in the air it is difficult to separate the influence of the temperature from the influence of other sources of error such as refraction and earth curvature, and in the laboratory (cold chamber) it is difficult to imitate the temperature conditions under which the camera operates.

In East Germany the temperature conditions in a camera were recorded during flight and then reproduced in the laboratory [17]. One conclusion was that both the extremely low outside air temperature and the large temperature gradient inside the lens might have a significant influence on the focal length (wide angle camera 11/18). However, no significant influence on the image quality and the characteristics of the distortion curve was found.

In this paper a survey of the possibilities of estimating and testing the inner orientation of aerial cameras from air photos of test fields will be given.

THE ESTIMATION OF PHYSICAL QUANTITIES IN PHOTOGRAMMETRY

The functional model of the aerial photograph is expressed by a) the condition equations which exist between the elements of the central perspective, and b) the correction formulae for the disturbances on the central perspective, viz. 1) refraction, 2) earth curvature, 3) lens distortion and 4) film shrinkage. Thus, the parameters of the functional model are:

$X_0, Y_0, Z_0, \phi, \omega, \kappa$: outer orientation
 X, Y, Z : terrain coordinates
 x, y : image coordinates
 x_0, y_0, c : inner orientation and
the coefficients of the correction formulae.

Traditionally these parameters are estimated as follows:

1. Refraction and earth curvature are estimated on the basis of physical data for a "normal" atmosphere and geodetic data for the dimensions of the earth.
2. Inner orientation including lens distortion is determined by camera calibration, ordinarily in laboratory.
3. Film shrinkage is determined from 4 or more fiducial marks.
4. The unknown terrain coordinates are estimated by an adjustment procedure regarding the inner orientation x_0, y_0, c and the known terrain coordinates as "constants", and the image coordinates, corrected for refraction, earth curvature lens distortion and film shrinkage, as independent "observations" usually with equal weights.

THE USE OF TEST FIELDS

By photographing a test field with height differences, it is possible to estimate and check inner orientation, distortion and even affinity, under operational conditions. However, in using a test field for this purpose, many difficulties are met:

A permanent network of signalized points, suitable for the flying heights in question, must be established. The points must be determined in the field with high accuracy ($m_x = m_y = m_h = 2$ cm or less). The network should be regularly located (preferably symmetrically) on the film.

The conditions under which the calibrated values are derived should be representative for the conditions under which these values are to be applied in later photogrammetric missions. However, the calibrated values derived from photographs over a test field reflect the particular physical conditions under which the calibration was performed. Photogrammetric missions might be carried out under quite different conditions, resulting in instability of the calibration data.

In mountainous terrain photogrammetric refraction is an important source of error. The atmospheric conditions of a test field with large height differences (which are necessary to determine the complete inner orientation) may not represent the operative conditions of the mission flights.

In addition, the temperature conditions in the operating camera and the physical conditions under which the film is handled, processed, stored and measured may be different.

It is difficult to find a test field with a terrain form that gives an accurate estimate and a powerful test of the errors in inner orientation. As known, these errors are compensated for, more or less, by other elements in the case of nearly flat terrain (correlation effect). A nearly sloping plane is also unfavourable in this respect. To give an idea of this problem, the accuracy of the elements has been derived on the basis of formulae (2), for theoretical cases of terrain forms, fig. 1. The result is presented in Table 1.

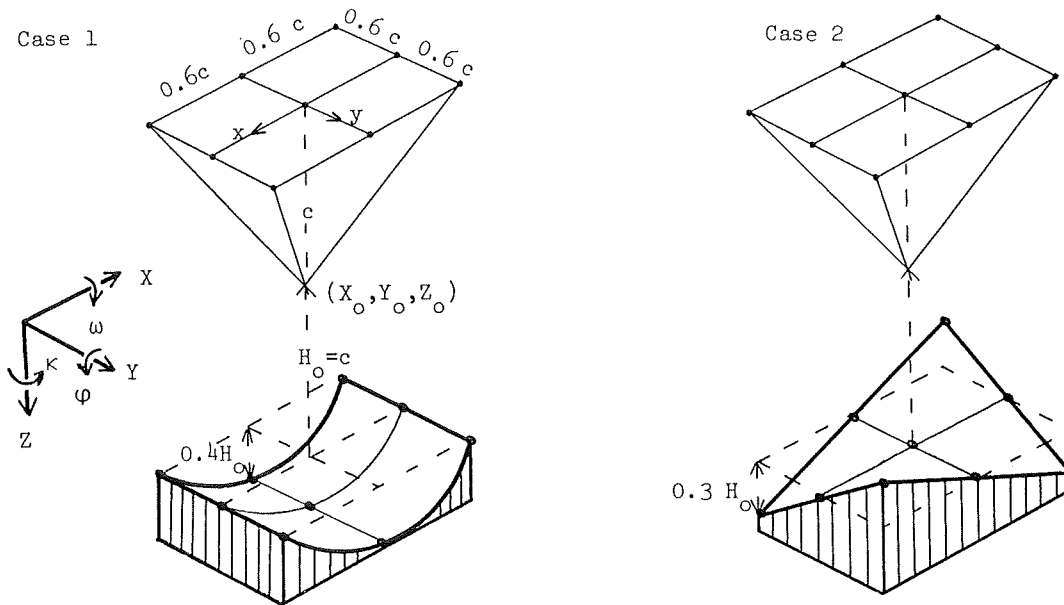


Fig 1. Theoretical terrain forms with 9 points

Thus, camera calibration from aerial photographs of test fields has many disadvantages in comparison with traditional calibration in the laboratory. The tendency towards analytical photogrammetry, which can take advantage of more specified camera calibration, has, however, made calibration under real conditions more justified than before. Further investigations into this field of photogrammetry are therefore desirable [18].

For the time being it may be said that because of the difficulties which are met in performing a complete camera calibration from air photographs it is doubtful whether this form of calibration can replace the traditional one. It should also be borne in mind that traditional analytical calibration (i.e. independent calibration of each element such as lens, cone, flatness of plates etc.) constitutes

Case 1

Case 2

	φ	ω	κ	X_o	Y_o	Z_o	x_o	y_o	c	m	β
φ	60u							54			
ω		90u			.58			-10			
κ			20u								
X_o				6			.83				
Y_o					2			.75			
Z_o						27			-98	.45	
x_o							1				
y_o								5			
c									22	-35	
m										50u	
β											40u

	φ	ω	κ	X_o	Y_o	Z_o	x_o	y_o	c	m	β
φ	190u	-40		.40	.83		.86	.70			
ω		190u		-83	.40		.70	.86			
κ			40u			.69			-66		-86
X_o				5			.80	.75			
Y_o					5		.75	.80			
Z_o						1			-96		-80
x_o							16				
y_o								16			
c									6.20	.77	
m										40u	
β											110u

$u = 10^{-12}$

Table 1. Weight numbers Q_{ij} and correlation coefficients $r_{ij} = \frac{Q_{ij}}{\sqrt{Q_{ii} Q_{jj}}}$ ($i \neq j$) of 11 parameters (2). The standard errors $\sigma_i = \sqrt{Q_{ii}} \cdot \sigma_0$ (in μ).
 σ_0 : the standard error of unitweight (=1 for all observations).

an important means of checking the result of the photogrammetric process [3]. Therefore, integral calibration by means of test fields should rather be considered as an additional form for checking the results as such calibration would check the performance of the whole procedure under operational conditions.

In the following a method of statistical investigation into the geometrical accuracy of air photographs taken over test fields will be outlined. Then a practical application will be reported.

DERIVATION OF THE BASIC EQUATIONS AND FORMULATION OF THE TEST

By photographing a test field with height differences it is possible to estimate the errors in the elements of inner orientation and also the residual affinity when the data from the calibration in laboratory and data for correction of refraction and earth curvature have been applied traditionally. The procedure for estimating these errors and testing their significance will now be formulated in agreement with the general theory of the Appendix.

According to the central perspective the image coordinates are non-linear functions f_x, f_y of the terrain coordinates and the orientation elements.

$$x = f_x(X, Y, Z, \varphi, \omega, \kappa, X_o, Y_o, Z_o, x_o, y_o, c) \tag{1}$$

$$y = f_y(X, Y, Z, \varphi, \omega, \kappa, X_o, Y_o, Z_o, x_o, y_o, c)$$

The terrain coordinates are assumed to be error free. Thus, expanding in a Taylor series we obtain, after neglecting terms of higher order and adding linear terms for the influence of residual affinity:

$$dx = dx_o - \frac{X'}{Z'} dc + \frac{c}{Z'} dX_o + \frac{X'c}{Z'^2} dZ_o - \frac{Y'c}{Z'} d\kappa + (1 + \frac{X'^2}{Z'^2})c d\varphi - \frac{X'Y'}{Z'^2}c d\omega$$

$$dy = dy_o - \frac{Y'}{Z'} dc + \frac{c}{Z'} dY_o + \frac{Y'c}{Z'^2} dZ_o + \frac{X'c}{Z'} d\kappa + \frac{X'Y'}{Z'^2}c d\varphi - (1 + \frac{Y'^2}{Z'^2})c d\omega$$

+ y dm + x dβ

where

$$X' = X - X_0$$

$$Y' = Y - Y_0$$

$$Z' = Z - Z_0$$

$$dx = x - f_{x_0}^0$$

$$dy = y - f_{y_0}^0$$

x, y = image coordinates transformed on the fiducial marks and corrected for lens distortion, refraction and earth curvature.

$f_{x_0}^0, f_{y_0}^0$ = given values being computed from the coordinates of the test field, the approximate values of the six orientation elements, and the values of the three inner orientation elements from laboratory calibration.

$d\phi, d\omega, d\kappa, dX_0, dY_0, dZ_0$ = corrections to the approximate values of outer orientation.

dx_0, dy_0, dc = corrections to the values of inner orientation.

$dm, d\beta$ = parameters of residual affinity, i.e. scale difference and lack of perpendicularity of the image coordinates, respectively.

The least squares' estimators $d\hat{c}, d\hat{x}, d\hat{y}, d\hat{m}$ and $d\hat{\beta}$ for the corresponding parameters in (2) can now be determined. These estimators reflect the errors in the inner orientation elements and residual affinity under operational conditions.

Investigations into whether these errors have a significant influence on the results can be carried out as a test of the null-hypothesis:

$$d\hat{c} = d\hat{x} = d\hat{y} = d\hat{m} = d\hat{\beta} = 0 \quad (3)$$

Thus, the test procedure given in the Appendix can be applied, with $r = 5$ and $s = 11$.

Residual distortion has not been regarded in the fundamental equations. Reliable determination of the distortion requires an appropriate control point distribution, which is difficult to achieve for a test field with large height differences.

EXAMPLE OF APPLICATION

The outlined procedure for integral calibration by means of test fields will now be demonstrated by a practical application.

The test field (about 1 km²) situated in Baerum community is characterized by a deep valley and a ridge parallel to this valley, with heights from 100 to 400 metres above sea level, see. Fig. 2

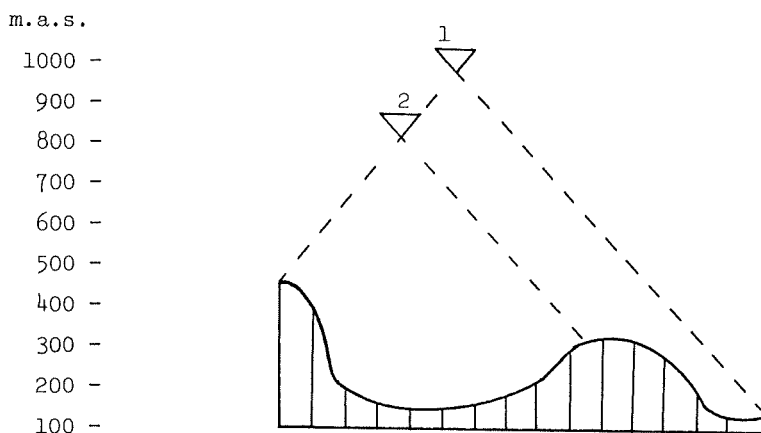


Fig 2. Cross-section through the test field

A geodetic network of about 30 control points was established in the field and signalized by yellow sheets of plastic, 30 x 30 cm. The test field was covered by two strips (c = 15 cm/ 23 x 23). The flying height H_0 above sea level and the base length B were as follows:

- Strip 1 : $H_0 = 1000$ metres, $B = 250$ metres
- Strip 2 : $H_0 = 850$ metres, $B = 200$ metres.

From each of the two strips, that photograph showing the most appropriate distribution of the imaged control points was selected for calibration. The two photographs selected in this way were copied on Cronaflex and measured in Zeiss Ascorcord monocomparator at I.T.C., Delft 1970.

Affine transformation on four fiducial marks and correction for lens distortion, refraction and earth curvature were carried out.

The test of the null-hypothesis (9) was performed for each of the two pictures independently. However, an equal σ_0 was assumed for these two cases (The assumption that σ_0 is independent of the flying height is in general justified when the flying heights do not differ too much). The result of the test is given in Table 2.

Case i	Flying height	Number of coordinates n_i	Square sum of residuals		1) $\hat{\sigma}_{0_i}$	2) F_i	3) f_i
			Under the 0-hypotesis Q_{H_i}	Under the alternative Q_{a_i}			
	metres				μ		
1	1000	24	1905	585	7.0	5.5	2.5
2	850	30	1655	921	6.9	3.0	2.5

Table 2. Test of the influence of inner orientation

1) $\hat{\sigma}_{0_i}^2 = Q_{a_i} / (n_i - s_a)$; $s_a = 11$

(the number of elements under the alternative).

2) $F_i = (Q_{H_i} - Q_{a_i}) / r \hat{\sigma}_0^2$; $r = 5$

(the number of elements being tested).

$$\hat{\sigma}_0^2 = \frac{\hat{\sigma}_{0_1}^2 (n_1 - s_a) + \hat{\sigma}_{0_2}^2 (n_2 - s_a)}{n_1 + n_2 - 2s_a}$$

($\hat{\sigma}_0^2$ is the weighted mean of $\hat{\sigma}_{0_1}^2$ and $\hat{\sigma}_{0_2}^2$).

3) f_i = the 95 %-value of the Fischer-distribution, with r and $(n_1 + n_2 - 2s_a)$ degrees of freedom.

Case	dc	dx_0	dy_0	dm	$d\beta$
1	237 μ	5 μ	-10 μ	0	-10 $\cdot 10^{-5}$
2	-22 μ	-40 μ	14 μ	-20 $\cdot 10^{-5}$	0

The estimated standard error of unit weight $\hat{\sigma} = 6.9\mu$

Table 3. Estimated calibration values

	Q_c	Q_{x_0}	Q_{y_0}	Q_m	Q_β
Q_c	193	70	88	$7 \cdot 10^{-6}$	$152 \cdot 10^{-6}$
Q_{x_0}		53	-35	0	$-66 \cdot 10^{-6}$
Q_{y_0}			56	$-31 \cdot 10^{-6}$	$60 \cdot 10^{-6}$
Q_m				$140 \cdot 10^{-12}$	$10 \cdot 10^{-12}$
Q_β					$310 \cdot 10^{-12}$

Table 4. Weight and correlation numbers in Case 1

It is seen from Table 2 that the null-hypothesis (3) has to be rejected in both cases.

A 95 % confidence interval of σ_o is

$$5.7 \mu \leq \sigma_o \leq 10.2 \mu.$$

The estimated calibration values are given in Table 3 and their correlation in Tables 4 and 5.

	Q_c	Q_{x_o}	Q_{y_o}	Q_m	Q_β
Q_c	44	13	-15	$-34 \cdot 10^{-6}$	$-47 \cdot 10^{-6}$
Q_{x_o}		16	-5	$-13 \cdot 10^{-6}$	$-46 \cdot 10^{-6}$
Q_{y_o}			14	$-13 \cdot 10^{-6}$	$16 \cdot 10^{-6}$
Q_m				$190 \cdot 10^{-12}$	$-20 \cdot 10^{-12}$
Q_β					$180 \cdot 10^{-12}$

Table 5. Weight and correlation numbers in Case 2

SOME COMMENTS AND ADDITIONAL REMARKS

1. The estimated values of the errors in the inner orientation and affinity are strongly correlated (tables 4 and 5). This circumstance, in addition to the fact that the abundance was moderate, did not justify testing the significance of each error independently by the t-test as mentioned in the Appendix.
2. Rejection of the null-hypothesis (3) indicates that other forms of checking the photogrammetric equipment, its function and its environmental conditions are desirable, such as independent calibration of lens, cone, filter, etc., or partial calibration by reseau photographs to check the integral effect of film shrinkage and unflatness from the moment of exposure. To check the atmospheric conditions and determine their influence would imply the difficulties referred to in the Introduction.
3. When many pictures taken with the same camera are calibrated by means of test fields the possibility of estimating and testing the variations in the calibration data exists (see 16). No conclusion has, however, been drawn in this respect from the two pictures taken of the Bærum test field.

APPENDIX - A short review of the theory of regression analysis

In mathematical statistics rigid methods have been derived for estimating unknowns x and testing hypotheses about x on the basis of observations of random variables Z , which are assumed to be independent and normal with expectations z being linear functions of x , i.e.:

$$\begin{aligned}
 z_1 &= y_{11}x_1 + y_{12}x_2 + \dots + y_{1s}x_s \\
 z_2 &= y_{21}x_1 + y_{22}x_2 + \dots + y_{2s}x_s \\
 &\dots \\
 z_n &= y_{n1}x_1 + y_{n2}x_2 + \dots + y_{ns}x_s
 \end{aligned}
 \tag{A1}$$

y : known values
 n : number of observations (Z)
 s : number of unknowns (x).

The fundamental equations (A1) express z explicitly. Thus, the problem of estimation the unknowns x and their reliability corresponds to "adjustment of indirect observed quantities" in the classical theory of adjustment. A procedure for testing hypotheses about x will be outlined since this procedure can be applied in checking the performance of the whole photogrammetric process under operational conditions (integral calibration).

For this purpose

$$(y_{i1}, \dots, y_{is}) : i = 1, 2, \dots, n$$

will be interpreted as different sets of values for the free variables:

$$y_1, \dots, y_s .$$

A procedure can now be derived for testing whether the variables

$$y_1, \dots, y_r, r < s$$

contribute to "explaining" the variation in Z. The null-hypothesis (H_0) is thus:

$$x_1 = x_2 = \dots = x_r = 0. \quad (A2)$$

To test this hypothesis the least squares' estimators $\hat{x}_1, \hat{x}_2, \dots, \hat{x}_s$ are firstly determined, giving the square sum of residuals

$$Q_a = \sum_{i=1}^n (Z_i - \sum_{j=1}^s (y_{ij} \cdot \hat{x}_j))^2 \quad (A3)$$

and the estimator of the variance:

$$\hat{\sigma}_o^2 = \frac{Q_a}{n-s} \quad (A4)$$

Then the least squares' estimators $x_{1+1}^0, x_{1+2}^0, \dots, x_s^0$ are determined under the conditions of (A2), giving a square sum of residuals

$$Q_H = \sum_{i=1}^n (Z_i - \sum_{j=r+1}^s (y_{ij} \cdot x_j^0))$$

An optimal test of H_0 is to reject H_0 when

$$F = \frac{Q_H - Q_a}{r \hat{\sigma}_o^2} \geq f_{1-\epsilon} \quad (A5)$$

where $f_{1-\epsilon}$ is the $(1-\epsilon)$ -value of the Fischer distribution with r and $n-s$ degrees of freedom. The theory of this test will be found in many testbooks on statistics

It can be found in the literature [2], [16] that in testing the influence of systematic errors $x_i (i = 1, 2, \dots, r)$ on the result of measurements in photogrammetry and geodesy a number of tests are carried out independently on the basis of the same square sum of residuals Q_a , given by (A3). Thus, for each of the elements $x_i (i = 1, 2, \dots, r)$ the null-hypothesis $\hat{x}_i = 0$ is rejected with a risk niveau of α when

$$t_i = \frac{|\hat{x}_i| \sqrt{(n-s)}}{\sqrt{Q_a} \sqrt{Q_{ii}}} \geq t_{1/2\alpha}$$

where $t_{1/2\alpha}$ is the $(1 - 1/2\alpha)$ -value of the t-distribution with $(n-s)$ degrees of freedom. Q_{ii} is the weight number of \hat{x}_i .

It should be remarked, though, that this approach is not theoretically correct when the t_i -values are algebraically correlated. If, however, the $x_i (i=1,2,\dots,r)$ are stochastically independent, at least approximately, and $(n-s) > 60$, the effect of the correlation between the t_i -values is negligible (how to deal with this problem when $(n-s) < 60$ is discussed in [14]).

SUMMARY

In the present paper some problems of camera calibration by means of a test field are discussed, in particular the estimation of errors in the inner orientation and tests of their significance. Attention is paid to analysis of regression, a statistical theory concept, and a numerical example of a practical application to camera calibration using a test field is given.

REFERENCES

- [1] Ahrend, M. "Analyse photogrammetrischer Fehler", Zeiss-Mitteilungen 4. Band 2. Heft, 1966
- [2] Berg, H. "Om kvalitetskontroll inom mättekniken", Svensk lantmäteritidsskrift, Nr. 1, 1966
- [3] Corten, F.L. "Cameras, Materials and Processing", Proceedings of the ITC-Post-Congress Seminar in Delft, ITC-Publications A 47, 1969
- [4] Hallert, B. "Results of Practical Investigations into the Accuracy of Aerial and Terrestrial Photographs", Svensk lantmäteritidsskrift, Nr. 1, 1960
- [5] Hallert, B. "Investigations of Weights of Image Coordinates in Aerial Photographs", Photogrammetric Engineering, 1961
- [6] Hallert, B. "Swedish Test Field for Aerial Photographs", The Photogrammetric Record, Oct. 1965
- [7] Hallert, B. "Notes on Calibration of Cameras and Photographs in Photogrammetry", Photogrammetria, No. 23, 1968
- [8] Hallert, B., Kaasila, P., Ottoson, L. Öhlin, K.A. "Quality Problems in Photogrammetry", Internat. Archives of Photogrammetry, Vol. XVII, 1969
- [9] Halonen, R.S. "Photogrammetric Test Fields", The Photogrammetric Journal of Finland, Vol. 3, No. 2, 1969
- [10] Halwax, F. "Über Zusammenhänge zwischen Aufnahmetemperatur, Kammerkonstanten und systematischen Fehlern der inneren Orientierung" Photogrammetria, No. 1, 1969/60
- [11] Härmälä, S. "The Camera Calibration Test Field of Tämijärvi", The Photogrammetric Journal of Finland, Vol. 3, No. 2, 1969
- [12] Hadem, I. "The influence of height differences on the accuracy of Aerial triangulation", presented paper to Commission III at the XII. Congress of Photogrammetry, Ottawa 1972
- [13] Morén, A. "The Geometrical Quality of Aerial Photographs", Stencil, Institutionen för fotogrammetri, Stockholm 1967
- [14] Ottestad, P. "Statistical Methods and their Experimental Application" Griffin's Statistical Monographs and Courses, No. 25, 1970
- [15] Salmenperä, H.: "Camera Calibration using a Test Field", Photogrammetric Journal of Finland, Vol. 6, No. 1, 1972
- [16] Torlegard, K. "On the Determination of Interior Orientation of close-up Cameras under Operational Conditions using Three-dimensional Test Objects", Treatise, Stockholm 1967
- [17] Zeth, U. "Thermische Einflüsse auf dem Kalibrierungszustand von Luftbildmesskammern", Int. Archives of Photogrammetry, Vol. XVII 1969
- [18] Ziemann, H. "Image Geometry Factors contributing to its Change", invited paper to Comm. III at the XIIth Congress of Photogrammetry, Ottawa 1972

TANGENTIAL AND ASYMMETRIC LENS DISTORTION, DETERMINED BY SELF-CALIBRATION

by O. Kölbl, Zürich-Birmensdorf, Switzerland

SUMMARY

The method of self-calibration is used for the determination of the asymmetric and tangential lens distortion. This method only applies the coplanarity condition for homologous rays and does not require any other references like ground control points. Therefore the computed parameters are free of systematic errors inherent to test fields or triangulation nets. The calibration procedure is applied to convergent and vertical photographs. A noticeable tangential distortion of 0.01 mm has been determined for an aerial camera. It should be possible to increase the accuracy in block triangulation by the incorporation of these calibration results.

1. INTRODUCTION

The increasing measuring accuracy in photogrammetry requires a continuous refinement of the mathematical model for the description of the imaging process. In general the atmospheric refraction and the symmetrical lens distortion are taken into account. Whereas there are only a few experiments in which the tangential and asymmetric lens distortion were incorporated in an analytical aerial triangulation [1]. The main reason for the omission of these factors seems to be the difficulty to determine the asymmetric components with sufficient accuracy.

The use of collimators or goniometers is of limited value, as the measurements occur along diagonals or half diagonals. The measurement along different diagonals requires a rotation of the lens. Small centring errors might cause a severe falsification of the asymmetric components.

Calibration with test fields has the advantage that the required photographs are taken under operational conditions. But the establishment of a test field is very costly and requires extremely high precision for the terrestrial point determination. The same objections hold for an experiment in which the tangential and asymmetric lens distortion are incorporated as unknowns in an analytical block triangulation [1]. As will be shown later these additional parameters cannot be determined in blocks with 30 % lateral overlap except control points are incorporated. This means that possible systematic errors in the control points are readily interpreted as errors of the inner orientation. It must be admitted that a better fit to the control points can be achieved in this way; only such approximations are not always desirable. The mentioned difficulties could be avoided by stellar-calibration. Although the star positions are known with high accuracy, the results of the camera calibration can be very limitedly transferred to other applications (close range or aerial photography). This is mainly due to the differences in atmospheric refraction.

In order to avoid these problems it was tried to determine the parameters of the decentring lens distortion by the method of self-calibration. A complete camera calibration is achieved by this method merely by the use of the coplanarity condition of homologous rays (cf. [3]). Convergent photographs would be required for the complete calibration; if the calibration is restricted to the radial and decentring lens distortion, then the calibration procedure can be applied to vertical photographs as well. This method should be of special interest for the analytical block triangulation in order to control systematic errors introduced by defects of the inner orientation.

In the following the mathematical model for the approximation of the lens distortion is briefly described and the limitations of the method are pointed out. The second part deals with the experimental results. The decentring distortion has been computed for various cameras under operational conditions but the presentation is mainly restricted to the calibration of aerial cameras with vertical photographs.

2. MATHEMATICAL MODEL

For a discussion of the asymmetric and tangential lens distortion it should be taken into account that these lens errors are mainly caused by manufacturing defects like small centring errors of the individual lenses. Therefore it is not

possible to calculate the asymmetric components from the design of a lens as it could be done, at least theoretically, for the symmetric distortion. Conrady [4] has tried to compare the asymmetric distortion with the deformation of a bundle of rays on a mince prism. This conception might be interesting for the construction of a compensation plate. For numerical calculations it would cause additional complications as the quality of the approximation should be tested beforehand.

For this reason no physical explanation was sought for the chosen mathematical model; but special attention is given to great flexibility of the formulae. Furthermore they should allow a differentiation between the tangential and asymmetric distortion. This differentiation is appropriate as the two components cannot be determined with the same precision. The asymmetric distortion can be affected by an insufficient film flatness. The deviation of the film in the camera from the ideal image plane will cause a shift of the image points in radial direction, similar to the radial displacement due to height differences in the terrain. Except for the film shrinkage a superposition with other errors can be excluded for the tangential lens distortion.

The specifications for the mathematical model are rather well met by mixed trigonometric terms. The following formulae have been used for the approximation of the radial lens distortion (1) and the asymmetric (3) and tangential (4) components of the distortion (cf. [1], [2], [5]).

$$\Delta r' = a_3(r'^3 - r'_0 \cdot r'^2) + a_5 \cdot r' \cdot \left(\sin \frac{r'}{r'_0} \cdot \pi\right)^2 + a_7 \cdot \sin \frac{r'}{r'_0} \cdot 2\pi \quad (1)$$

$$\text{with } r' = \sqrt{\bar{x}'^2 + \bar{y}'^2} \text{ and } \bar{x}' = x' - x'_0 - \Delta d'_x; \quad \bar{y}' = y' - y'_0 - \Delta d'_y \quad (2)$$

$$\Delta s' = \frac{r'^2}{r'_0{}^2} (s_1 \cos \alpha + s_2 \sin \alpha + s_3 \cos 2\alpha + s_4 \sin 2\alpha) \quad (3)$$

$$\Delta t' = \frac{r'^2}{r'_0{}^2} (t_1 \cos \alpha + t_2 \sin \alpha + t_3 \cos 2\alpha + t_4 \sin 2\alpha) \quad (4)$$

$$\alpha = \arctg \frac{\bar{y}'}{\bar{x}'} \quad (5)$$

a_3 , a_5 and a_7 are the parameters of the radial distortion, r' is the distance of an arbitrary image point from the principal point of symmetry and r'_0 fixes a second intersection of the distortion curve with the zero axis of the coordinate system. The image coordinates of the principal point of autocollimation are indicated by x'_0 and y'_0 ; $\Delta d'_x$ and $\Delta d'_y$ stand for a deviation of the principal point of autocollimation from the principal point of symmetry. This deviation can only be computed if the lens has a noticeable equation. In general such parameters should be set constant if the estimated mean square error outweighs the computed parameter.

The formula chosen for the radial distortion differs from the usual power series with only odd terms. Power series have the disadvantage that the individual coefficients are highly correlated, which might cause difficulties for the solution of the normal equations. This effect could be avoided by the use of orthogonal polynomials. But this orthogonality cannot be obtained for a complete calibration in a useful way. Therefore a formula was chosen which avoids the strong correlation of the power series. Furthermore the path of the distortion curve can be estimated from the coefficients of the trigonometric terms without computation (cf. [5]).

The pattern of the asymmetric and tangential lens distortion is shown in fig. 1. The parameters s_1 and s_2 would cause a shift of the principal point of symmetry equivalent to $\Delta d'_x$ and $\Delta d'_y$ and therefore are omitted for the following considerations.

The distance from the principal point (r') has been introduced in a quadratic form mainly to avoid a discontinuity in the origin. Actually the decentring distortion proved to be too small to test in which form the radial distance should be applied; r'_0 was used in formula (3) + (4) for a reduction of the parameters.

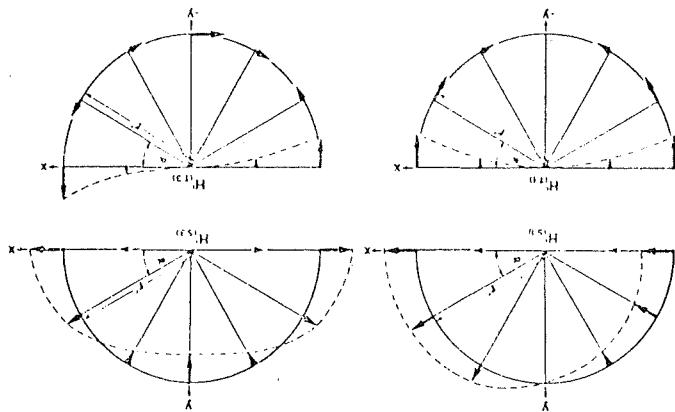


Fig. 1

Image displacement due to the decentering lens distortion as it is approximated by the formulae (3) and (4). The index of the principal point H' in the figure (S1, S3, T1 T3) refers to the parameters (s_1, s_3, t_1, t_3) in the formulae. The asymmetric distortion is shown in the upper part of the picture. The tangential components are shown in the lower part.

The further mathematical formulae for the calibration do not show any particularities. The correction equations for the adjustment were obtained from the coplanarity condition. The equations were linearized with the help of the quotient of the differences

$$\frac{\partial f}{\partial x} = \frac{f(x + \Delta x) - f(x)}{\Delta x}$$

The computed parameters were evaluated by their reproducibility in different blocks and by their mean square error and correlation coefficients estimated from the inverted normal equation.

When a certain parameter is not significantly different from zero it can be assumed that the optical or mechanical manufacturing is sufficiently high for this special component. Its determination in a special calibration procedure is then superfluous.

3. EXPERIMENTAL RESULTS

Various cameras have been tested by the method of self-calibration. Table 1 gives a survey of the calibration results. In general the tangential distortion remains within $\pm 2 \mu\text{m}$ for the controlled close range cameras as well as for the aerial cameras with picture size up to $9 \times 12 \text{ cm}^2$ and therefore can be neglected. In some cases an asymmetric distortion up to $5 \mu\text{m}$ has been determined which is due to a deformation of the image plane. For lack of space these experiments are not further discussed.

The procedure of self-calibration might be of special interest for the analytical aerialtriangulation. As already indicated convergent photographs are needed for a complete camera calibration. Vertical photographs can be used when the calibration is limited to the determination of the distortion. This limitation should not be very serious as the principal distance and the principal point for aerial cameras can be determined with high precision by laboratorial tests. A special advantage of the method would be that the photographs to be used are taken under operational conditions. The mathematical solution of the self-calibration is equivalent to a block adjustment according to the bundle method, but no control points are required.

Various triangulation blocks and triangulation strips have been used for the practical experiments. At last the triangulation blocks were reduced to a minimum size of only two strips with two pictures (60 % forward and lateral overlap - the two strips were flown in opposite direction). The photographs originate from the test block "Oberschwaben" of the OEEPE (camera: Zeiss RMK A 15/23 with Pleogon A2 1 : 5.6, $f = 153 \text{ mm}$). The measurements of the picture coordinates were taken on stereocomparators (Zeiss PSK and Wild STK). Fifty to hundred regularly distributed points have been measured in each model. In the measuring phase the floating mark is placed on the ground of the stereoscopic model and the transversal parallaxes are carefully eliminated. Point marking or sketching is obsolete as the individual points are only measured once.

Measurements were taken in all possible model combinations (df. fig. 2), in total 6 models were formed in a block with 4 pictures. The block size has been reduced to a minimum to keep the amount of time for the measurements and the computation as low as possible. The given results are based on two blocks in order to permit a control of the calibration date.

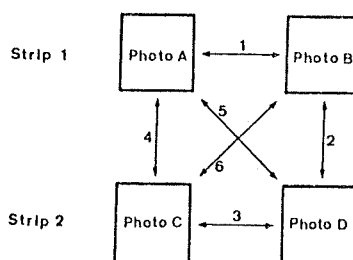
	close range photographs			aerial cameras convergent photographs		aerial cameras vertical photographs	
camera	Photo Theodolite	Linhof Tech nika	Hasselblad	Linhof Aero Technika	Hasselblad	Zeiss RMK	
lens	Orthoprotar	Symmar	Planar	Planar	Planar	Pleogon	
picture size [mm]	1:25/190	1:5.6/135	1:2.8/80	1:3.5/135	1:2.8/50	1:5.6/153	
focusing distance [m]	130 x 180	90 x 120	55 x 55	90 x 120	55 x 55	230 x 230	
emulsion base	4.5	3.5	3.5	∞	∞	∞	
number of tests	plate	plate	plate	film	film	film	
	2	3	3	1	1	1 (block 1)	1 (block 2)
m_p [μ m]	$\pm 2.9/\pm 3.5$	$\pm 3.2/\pm 4.2$	$\pm 2.9/\pm 3.0$	$\pm 6.9/\pm 7.8$	$\pm 5.3/\pm 6.4$	$\pm 4.8/\pm 5.6$	$\pm 5.1/\pm 6.9$
m_H [μ m]	$\pm 41/\pm 10$	$\pm 47/\pm 17$	$\pm 38/\pm 16$	$\pm 38/\pm 19$	$\pm 75/\pm 45$	-	-
m_c [μ m]	$\pm 38/\pm 25$	$\pm 29/\pm 20$	$\pm 21/\pm 15$	$\pm 136/\pm 103$	$\pm 83/\pm 74$	-	-
radial distortion							
$\Delta r'_S$ [μ m]	-2/-4	-10/-14	+29/+27	-10/-15	+20/+20	-4/-3	-3/-2
at r'_0 [mm]	50	30	20	40	20	100	100
$\Delta r'$ [μ m] for r' [mm]	-1/-6 80	+138/+136 60	-140/-139 30	+36/+70 60	-121/-123 30	-5/-4 120	-3/-3 120
point of symmetry							
$\Delta d'_x$ [mm]	-	-0.62 \pm 0.80	-0.15 \pm 0.20	+6.63 \pm 1.32	-1.02 \pm 0.78	-	-
$\Delta d'_y$ [mm]	-	-4.03 \pm 0.62	-0.19 \pm 0.14	+3.38 \pm 1.63	-0.72 \pm 0.47	-	-
asymmetric distortion							
s_3 [μ m]	-3.3 \pm 1.3	+2.9 \pm 0.5	-1.7 \pm 2.0	-4.2 \pm 1.8	+1.1 \pm 2.6	+3.1 \pm 5.9	+1.7 \pm 5.9
s_4 [μ m]	-0.5 \pm 1.0	+0.7 \pm 0.4	-1.6 \pm 2.7	+1.6 \pm 1.6	-3.0 \pm 1.9	+3.1 \pm 4.4	+0.7 \pm 4.3
tangential distortion							
t_1 [μ m]	-1.5 \pm 0.6	+0.9 \pm 0.5	-1.0 \pm 0.7	+0.5 \pm 2.2	+2.1 \pm 3.8	-10.3 \pm 1.1	-12.4 \pm 1.0
t_2 [μ m]	-0.9 \pm 1.8	+0.6 \pm 1.0	+0.8 \pm 0.9	-2.0 \pm 1.0	-7.4 \pm 3.7	-1.1 \pm 1.2	-1.8 \pm 1.2
t_3 [μ m]	+1.0 \pm 0.7	-0.6 \pm 0.3	-0.1 \pm 0.5	-1.6 \pm 1.9	+1.9 \pm 1.8	-1.4 \pm 2.0	+3.2 \pm 2.0
t_4 [μ m]	-0.4 \pm 1.0	-0.1 \pm 0.4	-0.8 \pm 0.6	+2.6 \pm 1.5	-1.1 \pm 2.2	+6.0 \pm 2.0	-0.1 \pm 2.0

Table 1

Calibration results of various cameras. The self-calibration has been computed with and without additional parameters for the decentring lens distortion (cf. values before and behind the slash). m_p stands for the root mean square error of the residual parallaxes, m_H and m_c for the root mean square error of the principal point and of the principal distance; $\Delta r'_S$ is the first maximum of the distortion curve which intersects the zero axis at a distance of r'_0 from the principal point; $\Delta r'$ gives a second point of the distortion curve at a distance of r' ; $\Delta d'_x$ and $\Delta d'_y$ indicate the deviation of the principal point of symmetry from the principal point of autocollimation. s_3 , s_4 , $t_1 \dots t_4$ are parameters of the asymmetric and tangential distortion, their values and the corresponding root means square errors are given.

Fig. 2

Model formation for the calibration of vertical photographs (60 % lateral and longitudinal overlap)



The computation was done in the data centre of the ETH Zürich (Eidgenössische Technische Hochschule) on a CDC 6500. A special program was set up for the computation. In this program the number of pictures used for the calibration is only limited by the capacity of the computer. The sequence of the calculated models is arbitrary, the point number is used to indicate by which pictures the individual models were formed.

An analysis of the computation results indicates that the asymmetric and tangential distortion as well as the coefficients (a_5, a_7) of the radial distortion are determined with high precision. The incorporation of the additional parameters leads to a reduction of the residual parallaxes of 20 to 30 %. Difficulties arise only for the determination of the coefficient a_3 of the radial distortion. Its precision estimated from the inverted normal equation is relatively low and would cause errors of the distortion curve of 30 to 40 μm . The estimated mean square error of the distortion curve is reduced to 0.5 to 1 μm when this coefficient (a_3) is set constant. According to the inverted normal equation this effect is due to a high correlation of a_3 with the angle of convergence ($\Delta\phi$ and $\Delta\omega$) of adjacent photographs. The high correlation between these parameters is noticed in triangulation strips as well as in blocks with 60 % sidelap. The correlation could be reduced by the use of convergent photographs as they are needed for a complete calibration (cf. fig. 3) or by a trivial solution, that means, one of the two correlated parameters is set equal zero or constant. As convergent photographs are excluded, an approximation must be found for one of the variables. For the tilt this could be done by the use of auxiliary data. The precision requirements would not be very severe for the special purpose of the determination of the decentring distortion and a mean square error of $\pm 0.5^\circ$ could be admitted.

If auxiliary data are not available then the coefficient a_3 of the radial distortion should be set constant. Its value could be taken from the calibration report of the camera. For the present computation a_3 has been set zero. In fig. 4 the computed radial distortion is compared with the values of the calibration report of the manufacturer. The distortion curves coincide rather well; the differences remain within $\pm 1 \mu\text{m}$ up to a distance of 100 mm from the principal point. Greater differences occur only at the edge of the pictures. This is partly due to the neglect of the third order term (a_3); a certain inaccuracy of the distortion curve results also from the limited number of points in this zone.

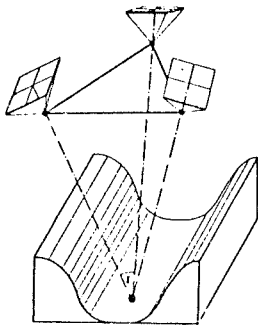
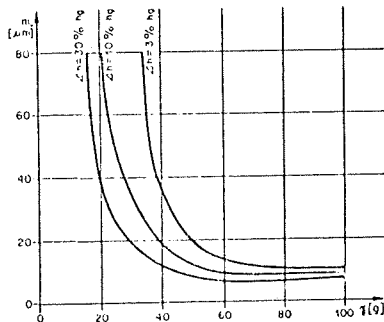


Fig. 3

Camera arrangement for a complete calibration of an aerial camera ($f = 150 \text{ mm}$, picture size $23 \times 23 \text{ cm}^2$) and the estimated mean square error of the principal distance (m_C). The photographs are simulated for different angles of convergency (γ). The block diagram indicates the assumed terrain shape. The computation was done for various height differences (Δh) in the terrain, h_g indicates the flying height. The mean square error of the residual parallaxes was set to $\pm 5 \mu\text{m}$.



The tangential distortion is very remarkable and larger than expected (cf. fig. 5). Its value rises up to 10 - 12 μm in the direction of the flight line at a distance of 100 mm from the principal point. The computed tangential distortion is highly significant as the corresponding mean square error remains within $\pm 2 \mu\text{m}$.

These values of the tangential distortion are described by the parameter t_1 (cf. formula 3). The other parameter of the tangential distortion as well as those of the asymmetric distortion are much smaller and not significant according to statistical tests. This means that an asymmetric distortion can not be detected.

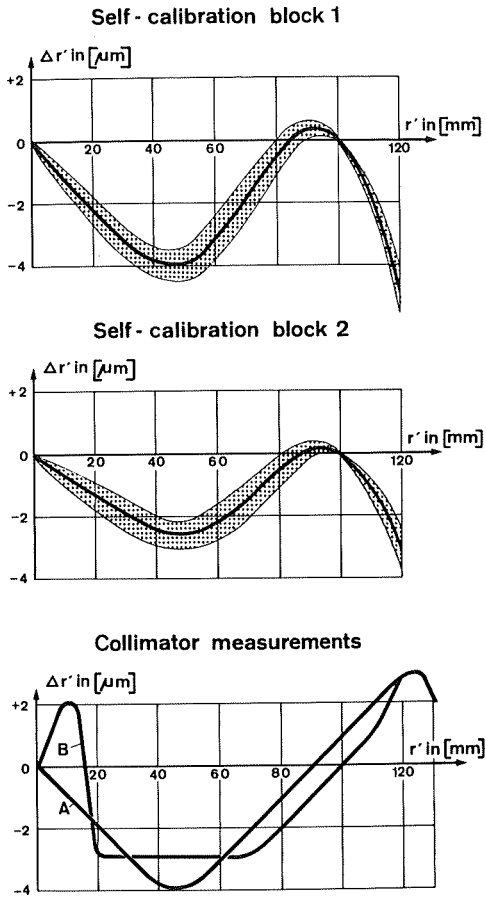


Fig. 4

Comparison of the radial distortion curves determined by self-calibration and collimator measurements. The last curves represent the mean of four half diagonals which have been measured. Curve A was taken from the calibration report before the flight, curve B after the flight. The first two curves are provided with the computed confidence interval (root mean square error).

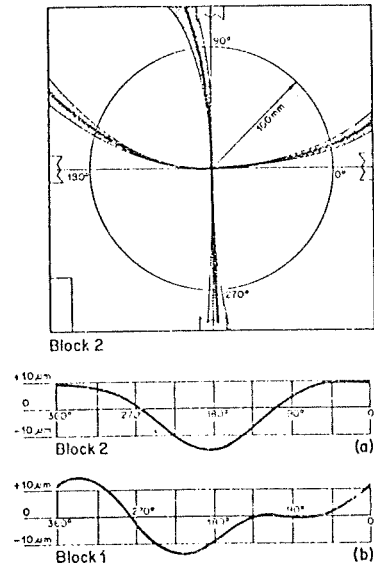


Fig. 5

Tangential distortion with confidence interval (camera Zeiss RMK A 15/23 with Pleogon A₂ 1 : 5.6, f = 153 mm).

The figures a and b represent the tangential distortion at a distance of 100 mm from the principal point. The mean square error of these curves is nearly constant and about + 2 μm . They are taken from different triangulation blocks.

The given calibration results are based on the two triangulation blocks with 60 % lateral overlap. The precision of the distortion parameters is considerably reduced if triangulation strips or blocks with less than 60 % sidelap are used. The calibration results of the two triangulation blocks coincide very well, but a further control is hardly possible. The camera calibration report of the manufacturer only states that the tangential distortion does not exceed $\pm 10 \mu\text{m}$.

Different results have been obtained in the investigation of Müller-Bauer [1], in which the material of the test block Oberschwaben has also been used. Various parameters for the decentring lens distortion and affine deformations have been introduced in this block adjustment. The differences might be due to systematic errors in the triangulation net of the ground control points or due to deformations of the national UTM projection system. As the block adjustment was done with pictures of only 30 % lateral overlap, the internal stiffness of the block is not sufficiently high to permit the determination of these additional parameters without the use of control points.

4. CONCLUSIONS

The application of self-calibration to vertical photographs shows that it can be recommended to extend the mathematical model for the decentring lens distortion and to make optimum use of the relations between adjacent bundles of rays. The camera calibration is achieved in this way without the use of ground control.

The results do not coincide with a block triangulation with additional parameters as systematic errors of the triangulation net originating from deformations of the national projection system might cause severe alterations of the assumed lens distortion.

It should be possible to increase the accuracy in block triangulation by the incorporation of the results of the self-calibration. As no special photographs are needed, the procedure could be included in routine triangulation work.

REFERENCES

- |1| Bauer, H. und Müller, J.: "Height accuracy of blocks and bundle adjustment with additional parameters", Int. Archives of Photogrammetry Ottawa 1972
- |2| Brown, D.C.: "Decentring distortion of lenses" Phm. Eng. 32, 444-462, 1966
- |3| Kölbl, O.: "Selbstkalibrierung von Aufnahmekammern" BuL 40, 31 - 37, 1972
- |4| Conrady, A.: "Decentring lens systems", Monthly Notices of the Royal Astronomical Society, Vol. 79, 384 - 390, 1919
- |5| Kölbl, O.: "Analytische Verzeichnungs-darstellung bei der vollständigen Kalibrierung", BuL 39, 169 - 176, 1971

EVALUATION OF SOME INTERPOLATION METHODS

by G. H. Schut, Ottawa, Canada

ABSTRACT

A recently published interpolation method is based upon the correlation theory of stationary random functions. This method is here discussed together with two others which are not overtly based upon correlation theory but employ its formalism and differ only in the choice of correlation function. In the case of a two-dimensional field of reference points, these methods perform the interpolation by the summation of surfaces and therefore they can be characterized as multisurface methods. A method of a different type which can be characterized as a moving surface method is presented here in a more general form than in earlier publications. Finally, results obtained with these methods are compared. The results tend to show that a multisurface method can give a better accuracy than a moving surface method but only with a fortunate choice of correlation function. The one measure which contributes most towards good results is the reduction of the data by a trend function.

INTRODUCTION

The theory of stationary random functions has become the mathematical basis for a method of interpolation and smoothing or, in other words and with a possibly somewhat different interpretation, prediction and filtering. This method is used in geophysics where it was introduced by Moritz (1963), and it was introduced in photogrammetry by Kraus (Kraus, 1972; Kraus and Mikhail, 1972) with an assumption that is not based upon the theory.

Recently also, two other interpolation methods have been published (Arthur, 1973; Hardy, 1971, 1972) which make use of the formalism of the theory. However, their authors do not refer to this theory but base their formulation upon other considerations. Therefore, these methods cannot properly be called prediction methods.

The present paper describes first the conditions under which the theory is applicable and the extent to which the three methods apply the theory. For this purpose, the following sections contain a summary of the so-called correlation theory of stationary random functions and an analysis of the three methods. As the analysis shows, the common characteristic of these methods is that in a two-dimensional field of reference points they perform the interpolation by the summation of fixed precomputed surfaces. Therefore, they may be called multisurface methods.

Very different from these methods is a method of pointwise interpolation and smoothing which has been developed by the present writer for specific cases of interpolation (Schut, 1970) and smoothing (Schut, 1972). A more general description of this method is given here. In the case of a two-dimensional reference field, it computes a surface for each point at which the interpolation is performed. When going from one interpolated point to an adjoining one, this surface continuously changes its position and possibly its shape and, therefore, this method may be called a moving surface method.

These four methods are applied to the interpolation of heights of points on a surface in three-dimensional space. For this application, a known analytical surface has been selected. This serves to compare the results of the methods and to obtain information on the degree to which in practical applications the specifications of correlation theory must be followed.

CORRELATION THEORY

A random function of one parameter, say x , is a function whose values are random variables (Yaglom, 1962). With such a function are associated distribution functions which specify the probabilities that the values of the function, individually and in sets of two or more, lie within specified ranges. The random function is called stationary if these probability distributions are independent of the value of x .

The correlation theory of these functions is based upon the first and second moments of the distribution functions. The first moment is the mean value of the

function. The second moment is a function, $B(\mu)$, of the separation μ in x of two values of the random function. $B(\mu)$ is called the correlation function or covariance function. The theory has been developed for the case where the first moment is zero.

To apply the theory to a given case where a number of function values at equally spaced values of x is given, the first moment is made zero by subtracting the mean from each value. Let μ be the number of spacings that two values of the random function are separated in x . The function $B(\mu)$ is now computed for each integer value of μ by taking the mean of the products of all pairs of values of the random function whose arguments are μ spacings apart. $B(0)$ is the mean square of all values of the random function. The correlation function can be normalized by dividing all its values by $B(0)$.

Because the correlation function is a statistical concept, it cannot be accurately determined if only a limited number of values of the random function is available. In such a case, if the correlation function is not known in advance, a correlation function must be assumed that agrees reasonably well with the values calculated from the available values of the random function. It must, among others, have the following properties based upon its statistical origin: it must be positive at $\mu = 0$, it must have its maximum absolute value at $\mu = 0$ and its graph must be symmetric with respect to $\mu = 0$. Further, if i and j are the sequence numbers of any two of the equally spaced values of x and $\mu = i - j$, the matrix B whose element b_{ij} equals $B(\mu)$ must be nonnegative definite.

According to (Yaglom, 1962) a correlation function which is often used in cases where precise information is not available is

$$B(\mu) = \exp(-a|\mu|); a > 0. \tag{1}$$

This function is always positive and with increasing values of μ it rapidly approaches zero. The correlation is not necessarily always positive; it can for instance have the character of a damped oscillation. In that case, a more suitable correlation function is

$$B(\mu) = (\exp(-a|\mu|))\cos(b\mu); a > 0, b > 0. \tag{2}$$

Let now the correlation function of a stationary random function be known and let the values ξ_j of the latter function at equally spaced values x_j ($j = -1, -2, \dots, -n$) have been measured. According to correlation theory, the best linear estimate of the random function at x_m ($m = 0, 1, 2, \dots$) is:

$$\xi_m = b_m^t B^{-1} \xi \tag{3}$$

Here, b_m^t is the row vector whose components are the values $B(\mu)$ for $\mu = m+1, m+2, \dots, m+n$; B^{-1} is the inverse of the above-mentioned matrix B whose elements have values $B(0)$ to $B(n-1)$; ξ is the column vector whose components are the values ξ_j of the stationary random function for the arguments x_j . Obviously, ξ_m is a linear function of the ξ_j with coefficients which depend upon the value of m . For economy of computation, the constant vector $B^{-1} \xi$ is computed first. Subsequently, for any value of m , the value ξ_m of the random function at x_m is computed as the scalar product of the two vectors b_m and $B^{-1} \xi$.

If the values ξ_j are affected by errors η_j , the actual observations are $\zeta_j = \xi_j + \eta_j$. Let it be assumed also that the errors η_j are elements of a stationary random function, that their mean value is zero and that the two random functions are not correlated. The correlation function of the actual observations is then the sum of the correlation functions of the two random functions:

$$B(\mu) = B_\xi(\mu) + B_\eta(\mu) \tag{4}$$

The best linear estimate of the value ξ_m of the random function at x_m is now obtained from

$$\xi_m = b_m^t B^{-1} \zeta \tag{5}$$

in which, as before b_m^t is the row vector whose components are the values of the correlation function $B_\xi(\mu)$ for $\mu = m+1, m+2, \dots, m+n$. However, the elements of the matrix B are now the $B(\mu)$ of eq. (4) for $\mu = +1, \dots, n-1$ and ζ is the vector whose components are the actual observations of the stationary random function.

Obviously, the formulas (3) and (5) can be extended to the case where m is not a nonnegative integer. If m is any rational non-integer number, the formulas serve for interpolation between the measured values or for extrapolation beyond them. Both these cases have been covered by the name prediction. If $m = -1, \dots, -n$, Eq. (3) reproduces the actual observations. Equation (5) gives here the best linear estimate of the values ξ_i of the random function. This has been called filtering.

INTERPOLATION IN TWO DIMENSIONS

Yaglom (1962) also mentions the concepts of a stationary random function in multi-dimensional space and the correlation theory of such a function. This random function is said to be homogeneous and isotropic if its correlation function is a function of only the distance between points in the space, not of location or direction.

Moritz (Moritz, 1963; Heiskanen and Moritz, 1967) has applied these concepts to interpolation in two-dimensional space. His ξ_i are the gravity anomalies in a given area. Assuming that the average product of two gravity anomalies is a function of the separation of their locations only, this average product again defines the correlation function. Moritz's interpolation formula is identical with Eq. (3) but it now has the following interpretation. The reference points, that is the points at which the gravity anomalies are determined, are ordered in an arbitrary sequence. The components of the vector ξ are the gravity anomalies, ordered in this sequence. The element b_{ij} of the matrix B is the value of the correlation function for the distance between the two points with sequence numbers i and j . The i -th component of the vector b_m is the value of the correlation function for the distance between the point at which the gravity anomaly is to be predicted and the point with sequence number i .

More recent publications (Moritz, 1972a, b, 1973) extend the interpolation and filtering to the case where the observations are the sum of a linear function of unknown parameters, a stationary random function, and measuring errors. The linear function contains the systematic part of the observations and may be called the trend function. If the trend function were known, its values could be subtracted from the observations and subsequently the correlation theory could be applied. In Moritz's formulation, however, the parameters in the trend function are computed simultaneously with the interpolation and filtering. Because the correlation function cannot be computed from the observations, a likely correlation function must here be assumed. Also the trend function must be a pre-determined type of analytical function of the spatial coordinates. For a further discussion of this see (Whittle, 1963).

KRAUS'S LINEAR LEAST-SQUARES INTERPOLATION

Kraus has adopted Moritz's (1963) formulation for his least-squares interpolation (Kraus, 1972). He makes use of Eq. (5) with the assumption that the random measuring errors are uncorrelated. This makes $B_\eta(\mu)$ non-zero only if μ equals zero.

In addition, he assumes that the most appropriate correlation function is a Gaussian curve. After normalization, this gives

$$B_\xi(\mu) = \exp(-a\mu^2); a > 0 \quad (6)$$

For this, there is no justification in the theory of random functions. When the first moment has been reduced to zero, for large values of μ the distribution function $B_\xi(\mu)$ is equally likely to have negative as positive values. This can be illustrated with practical examples. An experimentally derived correlation function in (Moritz, 1963) attains negative values. Also, the experimental data in Fig. 2 of (Kraus, 1972) can be fitted much better with a function that becomes negative for large values of μ . Finally, in a soon to be published investigation of film deformation by Dr. H. Ziemann of the Photogrammetric Research Section of NRC the experimental data produces a correlation function which with increasing point separations becomes unquestionably negative and remains so over a considerable range of separations before it returns to zero. In all these cases, the

experimental data can be fitted much better with a correlation function of the type

$$B_{\xi}(\mu) = (\exp(-a\mu^2))\cos(b\mu); \quad a>0, b>0. \quad (7)$$

Kraus (1972) states that this method of interpolation, which he applies here to film deformation correction, is independent of the type and structure of the systematic deformation. However, best results in the statistical sense are obtained only if the data is a realization of a random function with all the restrictions discussed in the preceding sections. This cannot be achieved by simply subtracting a constant from all observations to make the first moment equal to zero.

Recognizing this, in (Kraus and Mikhail, 1972) the concept of the trend function is utilized. As it is put here: relative to the trend function, the data must have positive and negative regions in a more or less random fashion. The trend function is assumed to have been determined first and the interpolation and filtering are performed after reducing the data by the trend function.

ARTHUR'S INTERPOLATION OF A FUNCTION OF MANY VARIABLES

Arthur (1965) has devised an interpolation method which makes use of Eq. (3). The correlation function used here is

$$B(\mu) = 1-\mu^2; \quad \mu = d/a, \quad (8)$$

in which d is the distance between two points and the parameter a is a constant distance. By making a larger than the largest distance between two points, $B(\mu)$ remains positive for all values of μ . For criticism of this method, the reader should refer to (Schut, 1970).

Arthur (1972), after having given a remarkably incorrect listing of this criticism, has changed his correlation function to a Gaussian curve. Based upon a desired closest possible approach to a linear interpolation in the case of two reference points only, he now chooses the correlation function

$$B(\mu) = \exp(-2.5\mu^2); \quad \mu = d/a. \quad (9)$$

Now, the parameter a is the average distance between adjacent reference points. As Arthur (1972) states that no interpolation method has a theoretical basis, he is apparently unaware that his method differs from the one derived in correlation theory only in the criterion used for selection of the correlation function.

HARDY'S INTERPOLATION WITH MULTIQUADRIC EQUATIONS

Hardy (1971, 1972), also, has developed an interpolation method which makes use of Eq. (3). The role of the correlation function is here assumed by one of the functions

$$B(d) = (d^2 + C)^{1/2} \quad (10)$$

and

$$B(d) = d^2 + C. \quad (11)$$

Here, d is again the distance between two points while C is a constant to which a value is assigned in advance.

Hardy (1971) has given the interpolation its geometrical interpretation. It is simply a summation of n functions. Each term of the scalar product of the vectors b_m and $B^{-1}\xi$ in Eq. (3) contributes one function to the summation. Each such function contains one adjustable parameter which is the component, say a_j , of the vector $B^{-1}\xi$. In a two-dimensional reference field, this function is a surface of revolution with its extreme at the i -th reference point and with $a_j B(d)$ as a vertical section.

Equations (10) and (11) appear to be unsuitable as correlation functions because $B(\mu)$ increases with increasing values of μ . However, Hardy reports reasonable-looking results in the use of his formulation for contouring. These results are obtained by carefully choosing the reference points at significant terrain points such as highs and lows. This seems to indicate that the form of the correlation function is not very critical, especially if a rather large number of reference points is used. Nevertheless, to avoid sharp peaks or dips at the reference points, one should avoid functions such as Eqs. (1) and (2), and Eq. (10) with $C = 0$.

In a more sophisticated version of the method (Hardy, 1971), a polynomial of low degree is added to Eq. (3). The coefficients of this polynomial are determined simultaneously with the components of the vector $B^{-1} \xi$. This means that here a trend surface is determined simultaneously with those components.

POINTWISE INTERPOLATION

As Eq. (3) and (5) show, the interpolated value ξ_m at any point is a linear function of the reference values ξ_j or ζ_j with coefficients which depend on the position of that point. Therefore, the interpolated value can be said to be a moving (weighted) average of the reference values.

Taking the case of the height interpolation over a given area, the interpolated value may be interpreted as the height of a horizontal plane. Therefore, for each interpolated point Eqs. (3) and (5) determine a horizontal plane and the height of this plane is taken as the interpolated value at the point.

The method of interpolation and smoothing developed in (Schut 1970, 1972) is a generalization of this concept. Taking again the case of the height interpolation the horizontal plane is replaced by a tilted plane or even by a curved surface. For each interpolated point separately, the surface is computed which best fits the reference heights in a specified sense and the height of the surface at that point is accepted as the interpolated value.

Let the equation of such a surface give its height as a linear function of its parameters and let the parameters be determined by the method of least squares. To compute the parameters, the observation equations generated by the reference points can be collected in the matrix equation

$$Ap = \xi \tag{12}$$

in which the components of the vector p are the parameters, the elements of the i -th row of the matrix A are the coefficients of the parameters in the observation equation for the i -th reference point, and the components of the vector ξ are the reference heights. This equation leads to the normal equation

$$A^t W A p = A^t W \xi \tag{13}$$

in which W is the diagonal matrix whose elements are the weights assigned to the reference points.

Because these weights will be functions of the location of the interpolated point they will be different for each such point. As a result, the matrix $A^t W A$ cannot be computed and inverted once for all, as the matrix B in the preceding methods, but the normal equations must be formed and solved for each interpolated point. Of interest is then only the height of the computed surface at that point.

This method is not restricted to the case of the interpolation of heights over a two-dimensional point field, as shown in (Schut, 1970). In its more general application, because of the necessity to form and solve normal equations separately for each interpolated point, this method may be referred to as the method of pointwise interpolation.

One important consideration in this method is the choice of the surface which is computed for each point. To save computation time, it should have only a few parameters. A simple formulation is a polynomial with respect to the planimetric coordinates. It need not have higher than first or second degree terms.

A second important consideration is the choice of the weights to be assigned to the reference points when determining a best-fitting surface. The weight should be a monotonically decreasing function of the distance between reference point and interpolated point. Because of this, the best-fitting surface varies slowly from any one interpolated point to immediately adjacent ones and for this reason this method may be called the moving surface method of interpolation. Further, the totality of interpolated points defines a continuous surface which cannot be given an analytical formulation. A rather sharp drop-off of the weight at small values of the distance produces a continuous surface which fits well at the reference points. A slower drop-off produces a smoothing effect.

In experiments with interpolation in planimetric block adjustment (Schut, 1970), the best results were obtained with the weight function

$$w = (1-r)^3 (1-r^2)^3/r. \quad (14)$$

Here, r is the ratio between the distance to a reference point and a fixed maximum distance beyond which reference points were not used. These results were obtained with a fixed distance which was somewhat larger than the largest distance in the block. For ratios smaller than 0.01, r was made equal to this value. This prevents the weight from rising to infinity when r approaches zero.

The use of maximum distance by which all distances are divided serves two purposes. Firstly, it makes it possible to specify a weight function which can be used independently of the size of the block and of the unit of measurement. Secondly, by making the weight function approach virtually tangentially to zero when the distance to a reference point approaches the maximum distance, discontinuities in the surface defined by the totality of interpolated points can be avoided without having to use all reference points for the interpolation of each point. In the case of a dense net of reference point, the proper choice of a maximum distance can save much computation time.

A weight function which proved to be suitable in a case where a strong smoothing was required (Schut 1972) is:

$$\begin{aligned} w &= 1 - 2r^2 \quad (r \leq 0.5) \\ w &= 2(1-r)^2 \quad (r \geq 0.5). \end{aligned} \quad (15)$$

Various other weight functions could be used. Arthur (1972) has suggested replacing the ratio r in the denominator of the weight function (14) by r^2 . This causes a considerably sharper drop-off in weight with increasing values of r than does an increase in the powers of $1 - r$ and $1 - r^2$.

A function which can be adapted to both interpolation and smoothing is

$$w = \exp(-ar^2). \quad (16)$$

If the constant a is equal to 14 or 20, this function varies from unity at $r = 0$ to less than 10^{-6} or 10^{-8} , respectively, at $r = 1$. The smoothing effect could be varied by varying either one or both of the constant a and the maximum distance. However, both these measures can affect the number of points that effectively participates in the interpolation. Rather, the degree of smoothing should be controlled by using the weight function

$$w = \exp(-ax^2); \quad x = r/(b + (1-b)r). \quad (17)$$

Here, a is a fixed value which may be taken to be 14 and b is a variable parameter. In the case of a fairly regular distribution of reference points and the use of a maximum distance which is about four times the average distance between adjacent reference point, the value $b = 0.2$ gives very little smoothing, $b = 1$ which reduces Eq. (17) to Eq. (16) gives a fair amount of smoothing, and $b = 2$ gives a very considerable amount of smoothing.

EXPERIMENTS

1. EXPERIMENTAL SURFACE

To evaluate and compare the results that can be obtained with these methods, they were applied to the height interpolation of points on a known analytical surface in three-dimensional space. This is the application in which the first three methods can be collectively called multisurface methods and the fourth method can be called the moving surface method.

The analytical surface was constructed by Dr. V. Kratky of the Photogrammetric Research Section for a non-topographic application of photogrammetry. Profiles in x -direction through this surface form a repeating wavelike pattern with a wavelength of about 125 mm while profiles in y -direction are 160 mm long and vary over one such wave from a straight line to a convex curve. A set of 17 x 5 reference points was selected in a grid pattern covering about 400 x 160 mm and

with a spacing of about 25 mm in x-direction and 40 mm in y-direction. The interpolation was performed on a set of 17 x 17 points in the centre of this area, covering about 125 mm in x-direction and the full 160 mm in y-direction. The maximum variation in height is about 26 mm and the mean height is zero.

This surface is clearly not a representative example of an isotropic stationary random function. Not only does it show systematic patterns, but the patterns in the x- and y-directions are different. Results obtained with this surface should be instructive because it corresponds to the situation often encountered in practical applications. For instance, heights in a digital terrain model can hardly be regarded as such a function.

2. MULTISURFACE METHODS

The multisurface method was first used with correlation functions of the type proposed by Kraus and by Arthur:

$$B(d) = \exp(-ad^2/b^2)$$

in which a and b are parameters whose values are specified in advance and d is the distance. This function actually has only one parameter, the ratio a/b^2 .

When first using this method with correlation functions of this type and with various values of the ratio, very poor interpolation results were obtained. This can be readily explained by the markedly anisotropic behaviour of the analytic surface and the geometric interpretation of the interpolation as a summation of surfaces of revolution.

Arthur (1972) remarked that the use of only distances in the correlation function is not very satisfactory if the distribution of reference points is markedly anisotropic and that the anisotropy should be eliminated by a preliminary affine transformation of the x,y coordinates. In the present case, this requires the reduction of the y-coordinates by a factor of about 0.62. With Arthur's specifications, the parameter a in the above equation equals 2.5 and b is the average distance between adjacent reference points. After the scale reduction of the y-coordinates and taking into account all directions, the average distance lies between 25 and 30 mm.

Accordingly, experiments were performed with various scale factors applied to the y-coordinates. Table 1 displays results obtained with the factors 0.62 and 0.25, and varying the ratio a/b^2 by varying b. With the factor 0.62, a local minimum of the RMS error is reached with Arthur's values (a = 2.5, b = 27 mm). However, if b is increased beyond 35 mm, the results improve very significantly until the value b = 100 mm is reached. At this last value, the inversion of the matrix B begins to deteriorate, even with the 15-digit double precision arithmetic that was used. This is demonstrated by the occurrence of non-zero errors at the reference points. Beyond this value, the deterioration becomes progressively worse, and finally the inversion process breaks down altogether.

As Table 1 shows also, the use of the scale factor 0.25 consistently gives much better results than that of the factor 0.62. This, again, can be explained by the geometric interpretation. In practical applications, however, it will often be difficult to provide a criterion that is better than the isotropic distribution of reference points and therefore in further experiments only the scale factor 0.62 was used.

When using the multisurface method with Hardy's correlation functions, the choice of unit for the distance d is important. The decimeter was chosen as the unit because this makes all distances roughly of the order of unity and avoids the occurrence of very large numbers in the computations. The correlation function of Eq. (10) gives no solution for negative values of C because this makes the elements on the main diagonal of the matrix B imaginary. The results that were obtained with nonnegative values are shown in Table 2. The inversion of the matrix begins to deteriorate at C = 0.6 and it breaks down at C = 1. The use of Eq. (11) did not produce any results because the inversion fails for all values of C.

Figure 1 shows the graphs of some of the above correlation functions. Evidently, good results can be obtained with very different correlation functions, provided that suitable values of the parameters in these functions are chosen. Best results were obtained with the choice of parameters that caused a near-breakdown

in the inversion of the matrix B.

Table 1 Results of multisurface method of interpolation with the Gaussian curve $\exp(-2.5 d^2/b^2)$ as correlation function (Kraus and Arthur); d is distance in decimeters, b is a constant.

value of b	y-scale factor 0.62		y-scale factor 0.25	
	RMS error	max. error	RMS error	max. error
0.20 dm	1.50 mm	5.3 mm		
0.25	0.61	2.4		
0.27	0.56	2.5		
0.30	0.61	2.5	0.43 mm	2.2 mm
0.35	0.69	2.5	0.25	1.1
0.4226	0.63	2.2	0.10	0.42
0.60	0.35	1.2	0.04	0.14
0.80	0.16	0.61	0.02	0.12;0.02*
1.00	0.12	0.35;0.06*	no solution	
> 1.00	rapid deterioration			

*Errors occur here at the reference points; the largest one is listed.

Table 2 Results of multisurface method of interpolation with Hardy's correlation function $\sqrt{(d^2 + C)}$ and y-scale factor 0.62; d is distance in decimeters, C is a constant.

value of C	RMS error	maximum error
< 0	no solution	
0	0.40 mm	1.35 mm
0.20	0.15	0.49
0.40	0.09	0.30
0.60	0.07	0.22;0.03*
0.80	0.17	0.45;0.18*
1.00	no solution	

*Largest error at the reference points.

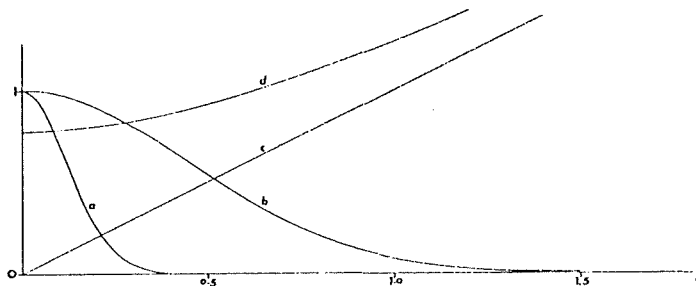


Figure 1 Correlation functions used in Tables 1 and 2

- a: $\exp(-2.5 d^2/0.27^2)$
- b: $\exp(-2.5 d^2)$
- c: d
- d: $\sqrt{(d^2 + 0.6)}$

It is interesting also to perform the interpolation with the actual correlation function of this analytical surface. Values of this function at 5 mm intervals were computed from the known heights of the interpolated points and normalized. For distances larger than 75 mm these values show increasingly larger discrepancies among each other and a smoothing is necessary. Over the first 100 mm, the computed correlation function can be approximated rather well by a function of the type of Eq. (7). From the value $-1/3$ at $d = 80$ mm and the first zero at $d = 45$ mm it follows that this function must have parameters $a = 1.6$ and $b = 3.5$. The value $b = 4.0$ gives a somewhat less good fit. The graphs of these functions are shown in Figure 2 and results are listed in Table 3. It is noteworthy that the function of Eq. (7) with $b = 3.5$ gives considerably better results than the computed correlation curve but that a small change in the parameter b is sufficient to make the results worse. Although the results obtained with these three functions vary and they are much inferior to the best results obtained in Tables 1 and 2, it appears that the danger of very large errors or non-existence of a solution has here been avoided.

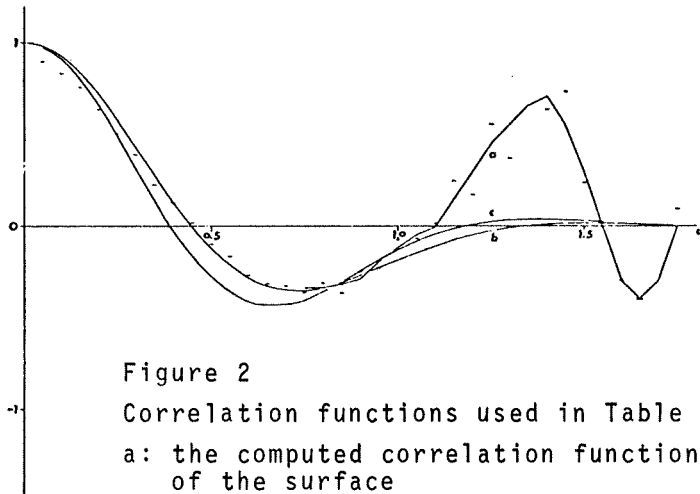


Figure 2
Correlation functions used in Table 3
a: the computed correlation function of the surface
b: $(\exp(-1.6d^2)) \cos(3.5 d)$
c: $(\exp(-1.6d^2)) \cos(4 d)$

Table 3 Results of multisurface method of interpolation using the actual correlation function and Eq. (7); y-scale factor 0.62, d is distance in decimeters.

correlation function	RMS error	max. error
actual correlation function (smoothed at $d > 0.75$ dm)	0.41 mm	1.35 mm
$(\exp(-1.6 d^2)) \cos(3.5 d)$	0.29	0.98
$(\exp(-1.6 d^2)) \cos(4.0 d)$	0.47	1.55

3. MOVING SURFACE METHOD

The interpolation was performed also by the moving surface method. A second-degree moving surface was used in combination with the y-scale factor 0.62. Figure 3 shows the graphs of the selected weight functions while table 4 lists results obtained with maximum distances of 75 and 100 mm. A smaller maximum distance tends to produce rather large errors in a few of the interpolated points and an increase in the variances of the interpolated values.

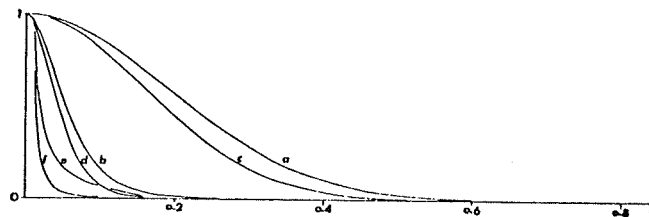


Figure 3
Weight functions used in Table 4
a: Eq. (17), $a = 14, b = 1$
b: Eq. (17), $a = 14, b = 0.2$
c: Eq. (17), $a = 20, b = 1$
d: Eq. (17), $a = 20, b = 0.2$
e: $(1-r)^3(1-r^2)^3/r$
f: $(1-r)^3(1-r^2)^3/r^2$

As the table shows, the selected weight functions produce varying degrees of smoothing. The selection of larger values of the maximum distance produces a much stronger smoothing. It is noteworthy here that over a large range of weight functions the results are better than those obtained with the multisurface method using the actual correlation function or its approximation by Eq. (7).

Table 4 Results of moving surface method of interpolation with a second-degree moving surface; the y-scale factor is 0.62, and r is the ratio of distance and maximum distance.

weight function	max. distance 75 mm			max. distance 100 mm		
	RMS error	maximum errors		RMS error	maximum errors	
Eq. (17) with $a = 14$, $b = 1$ (\equiv Eq. (16))	0.11 mm	0.30 mm	0.30 mm*	0.26 mm	0.81 mm	0.81 mm*
$b = 0.5$	0.12	0.33	0.04	0.14	0.33	0.25
$b = 0.2$	0.14	0.41	0	0.16	0.44	0.02
Eq. (17) with $a = 20$, $b = 1$ (\equiv Eq. (16))	0.11	0.30	0.11	0.15	0.46	0.46
$b = 0.2$	0.12	0.35	0	0.12	0.35	0
$(1-r)^3(1-r^2)^3/r$	0.12	0.35	0.01	0.19	0.51	0.06
$(1-r)^3(1-r^2)^3/r^2$	0.12	0.36	0	0.16	0.46	0

*Largest error at the reference points

4. TREND SURFACE

An additional measure that should be taken is to bring the data in a form that is more representative of an isotropic stationary random function. This can be done by means of the concept of referring the data to a trend surface, and not simply to the horizontal plane at mean height. Simple formulations for such a surface are polynomials and harmonic functions of low degree.

In the present case, the wavelike form of the analytical surface does not make it possible to fit a polynomial of low degree. A harmonic function could fit rather well but it would have required additional programming. As an interesting alternative, a trend surface was computed by the moving surface method. Moving surfaces of the first and second degree were used with a maximum distance of 100 mm and the weight functions of Eqs. (16) and (17).

After reduction of the data to a trend surface, the interpolation was performed with the multisurface method, using Eq. (6) with $a = 14$ as correlation function. Results are shown in Table 5. Comparison with the comparable case of $b = 42.26$ mm in Table 1 which has an RMS error of 0.63 mm shows that the introduction of a trend surface greatly improves the result of the multisurface method.

There is no reason why, after the reduction of the data to a trend surface, one should restrict oneself in the interpolation to the multisurface method. Interpolation with the moving surface method, and using the same specifications as for the construction of the trend surface, gives results which are shown also in Table 5. These results are not as good as those obtained with the multisurface method but, as the relevant cases in Table 4 show, they are an improvement upon the trend surface itself. Perhaps, different specifications with a reduced smoothing effect should be used for the interpolation.

Table 5 Results of interpolation after reduction of the data to a trend surface; y-scale factor 0.62.

Construction of moving surfaces with Eq. (17); max. distance 100 mm		Interpolation by multisurface method, correlation function $\exp(-14 d^2)$		Interpolation by moving surface method		
parameters	degree	RMS error	max. error	RMS error	maximum errors	
$a = 14, b = 1$	2	0.04 mm	0.11 mm	0.07 mm	0.21 mm	0.21 mm*
$a = 14, b = 0.5$	2	0.09	0.24	0.10	0.25	0.02
$a = 14, b = 1$	1	0.18	0.52	0.53	1.6	1.6

*Largest errors at the reference points.

CONCLUSIONS

The experiments show that the method of prediction and filtering which is based upon correlation theory can give excellent results even if the data has a very systematic character. The one measure which appears to contribute most towards this is the reduction of the data by a trend function. If this is not done, the method can give rather mediocre results even if the correlation function is properly derived from the data.

If the correlation function is not derived from the data one cannot properly speak anymore of a method of prediction and filtering. In this case, a method of height interpolation in a two-dimensional field of reference points may be called a multisurface method of interpolation. If here a Gaussian curve or the first one of Hardy's two functions is used, good results can be obtained if their parameters are well-chosen even though the use of a trend surface is omitted. However, with an unfortunate choice of parameters they may give poor results or even lead to no solution. Possibly, the best values of the parameters are here the extreme ones which do not or do hardly cause deterioration of the solution. Deterioration is here shown by residuals left at the reference points.

With the moving surface method of interpolation, it is not difficult to specify parameters that give reasonably good results and to obtain a desired degree of smoothing. However, in the experiments the results obtained with this method are not as good as the best ones obtained with the multisurface methods.

In these experiments, trend surfaces were computed by an interpolation method which employed considerable smoothing. A second interpolation method was then used for the actual interpolation. This procedure of using two successive interpolations may well be the procedure that should be followed to obtain the best results in practical applications.

References

- Arthur, D.W.G., 1965, Interpolation of a function of many variables, *Photogrammetric Engineering*, 31:2, pp. 348-349.
- Arthur, D.W.G., 1973, Interpolation of a function of many variables, II, *Photogrammetric Engineering*, 39:3 pp. 261-266.
- Hardy, R.L., 1971, Multiquadric equations of topography and other irregular surfaces, *Journal of Geophysical Research*, 76:8, pp. 1905-1915.
- Hardy, R.L., 1972, Analytical topographic surfaces by spatial intersection, *Photogrammetric Engineering*, 38:5, pp. 452-458.
- Heiskanen, W.A., and Moritz, H., 1967, *Statistical methods in physical geodesy*. W.H. Freeman and Company, San Francisco, California.
- Kraus, K., 1972, Film deformation correction with least-squares interpolation, *Photogrammetric Engineering*, 38:5, pp. 487-493.
- Kraus, K., and Mikhail, E.M., 1972, Linear least-squares interpolation, *Photogrammetric Engineering*, 38:10, pp. 1016-1029.
- Moritz, H., 1963, Statistische Methoden in der gravimetrischen Geodäsie, *Zeitschrift für Vermessungswesen*, 88:10, pp. 409-416.
- Moritz, H., 1972a, Neuere Ausgleichungs und Prädiktionsverfahren, *Zeitschrift für Vermessungswesen*, 98:4, pp. 137-146.
- Moritz, H., 1972b, *Advanced least-squares methods*. Department of Geodetic Science Report No. 175, The Ohio State University, Columbus, Ohio.
- Moritz, H., 1973, Determination of the gravity field by collocation, *Bollettino di Geodesia e Scienze Affini*, 32:1, pp. 1-13.
- Schut, G.H., 1970, External block adjustment of planimetry, *Photogrammetric Engineering*, 36:9, pp. 974-982.
- Schut, G.H., 1972, A computerized adjustment of APR strips, *The Canadian Surveyor*, 26:1, pp. 45-58.
- Whittle, P., 1963, *Prediction and regulation*. D. Van Nostrand Company, Inc., Princeton, New Jersey.
- Yaglom, A.M., 1962, *An introduction to the theory of stationary random functions*. Prentice-Hall, Inc., Englewood Cliffs, New Jersey.

EXTENSION OF STUTTGART CONTOUR PROGRAM TO TREATING TERRAIN BREAK-LINES

by E. Aßmus, Stuttgart and Vienna

During the last three years a program system for processing of digital height information has been developed at the Institute for Photogrammetry of the Stuttgart University by W. Stanger. This program, which was developed for large size computers starts with randomly distributed terrain points and interpolates the heights of a rectangular grid of high density. From this "digital height model" (DHM) the contour-lines are computed and stored on a magnetic tape for the subsequent automated plotting.

By the present program the terrain breaks are only considered to some extent. Therefore we have been working at an extended version. In this lecture I want to present the first results of our endeavours.

The structure of the old version has been published several times [1]; [2], [3]. For a better comprehension of the extended version the most important steps of the old program shall be repeated.

For computing the grid heights the map sheet is divided in rectangular computing units (figure 1). In order to avoid gaps additional overlapping zones are used for the interpolation of the grid heights in the computing unit itself. The computing unit is given such a size, that about 70 reference points are situated in each gross computing unit (= computing unit + overlapping zone).

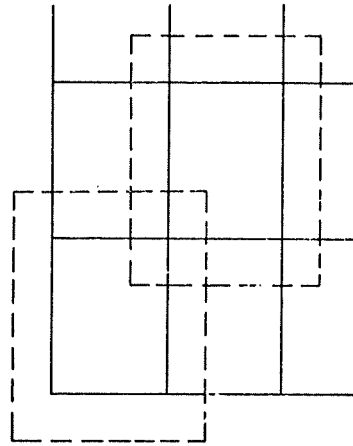


figure 1

Through these points an approximating polynomial surface of the first or the second order is fitted (figure 2). The remaining height-differences between the terrain and the polynomial surface are the reference values for the now following computation of the grid heights.

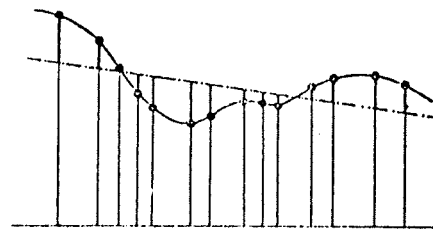


figure 2

The interpolation uses the method of the linear least-squares interpolation (= linear prediction) [4], [5]. For this statistical interpolation-method we must know the correlation (covariance) of the heights of any two points P_i and P_k (figure 3). In our program we assume that the covariance is only a function of the distance d between points. That means that in every interpolation area (= computing unit) homogenous and isotropic statistical conditions are presumed (independent of location and direction).

$$\text{Cov}(P_i, P_k) = f(d)$$

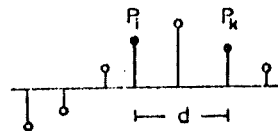


figure 3

The magnitudes of the covariances can be taken from a covariance function (generally a Gaussian function is used, see figure 4).

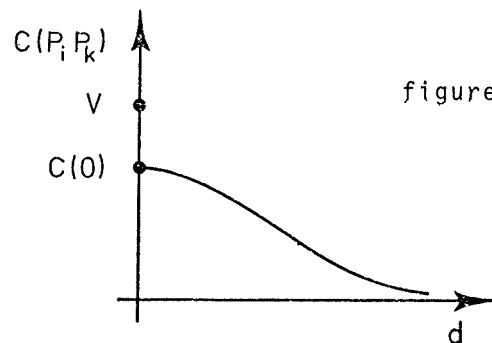


figure 4

By means of the above mentioned method of the linear least-squares interpolation the heights of the rectangular high density grid are produced for each computing unit (figure 5).

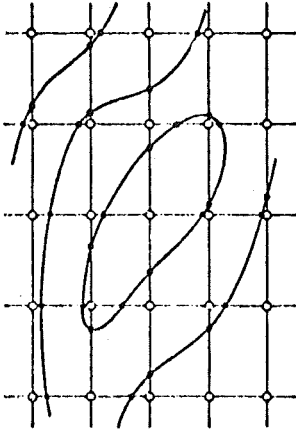


figure 5

The values of the polynomial surface are added accordingly. The resulting grid heights are arranged in the form of profiles over the entire map sheet and stored on a magnetic tape. This digital height model is the input for the interpolation of the contour lines. Contour points are computed between the grid points by linear interpolation. The points are sorted along the contours and stored accordingly. Later, during plotting, the automatic plotting table will connect the points by curves of third order.

We have been rather successful in computing and drawing quite a number of map sheets with this program. Our automatically produced contour lines are of about the same accuracy as the conventional contours, as various analyses proved. Figures 6 and 7 are to demonstrate the cartographic quality of our results.

Figure 6 shows a section of a contour map at a scale of 1 : 24 000. The given data for the whole map sheet which is about seven times the size of figure 6 are 12 000 reference points produced by photogrammetric profiling. 133 700 grid points and 153 000 contour points were computed.

HOEHENLINIENPLAN 1/1000

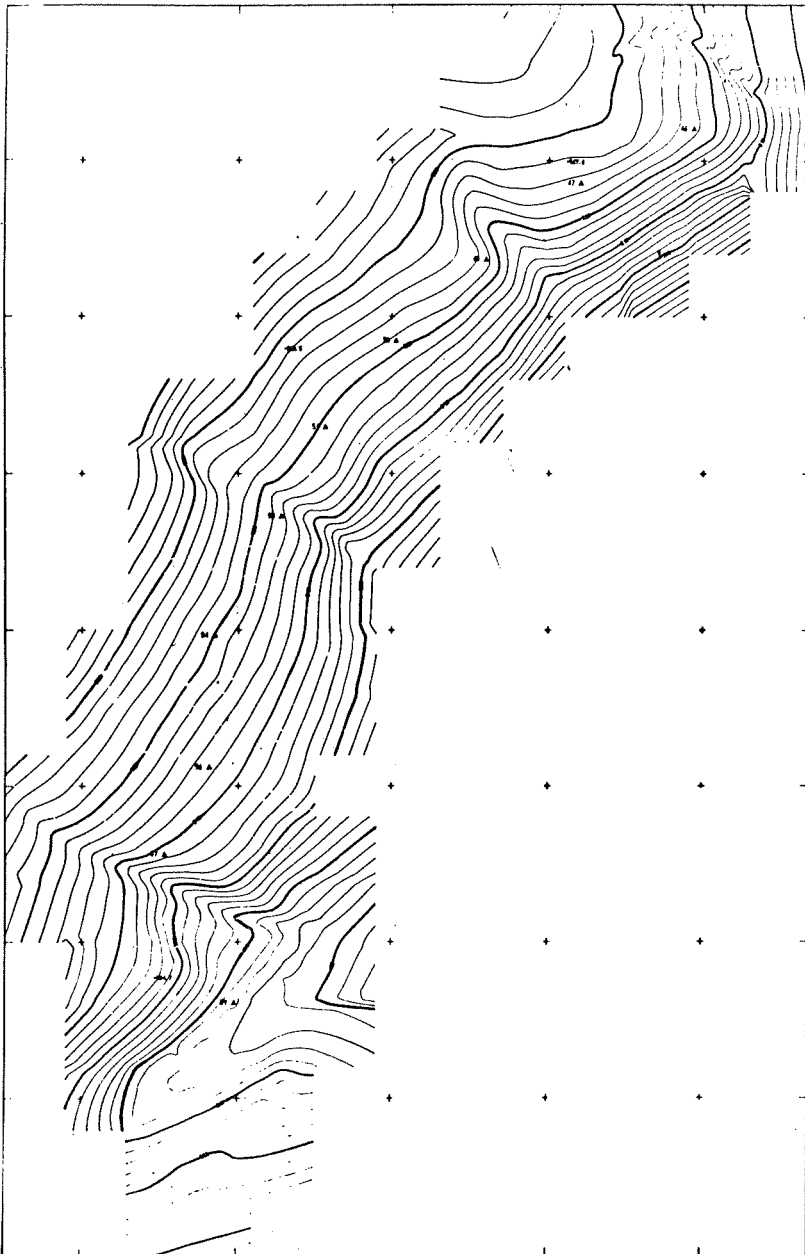


figure 7

ABmus 2

Figure 7 is an application for road construction (scale 1 : 1000). The input coordinates came from about 400 tacheometrically measured points. This example shows some units in which no contours were computed because of too low density of given points.

Both examples demonstrate the standard of contours reached by the present version of the program. They also show where improvements ought to be made, if highest cartographic demands are to be satisfied: in the latter example several erosion features can be seen, appearing somewhat smoothed out, although sequences of points were measured along the lines. Another example is to demonstrate better that our standard program can not yet meet all demands in a complicated area.

Figure 8 is a section from a "Deutsche Grundkarte" at the scale of 1 : 5000. The critical areas are the escarpments represented by linear hachures. In collecting the data by photogrammetric measurement, reference points were recorded along the lower and upper breaklines.

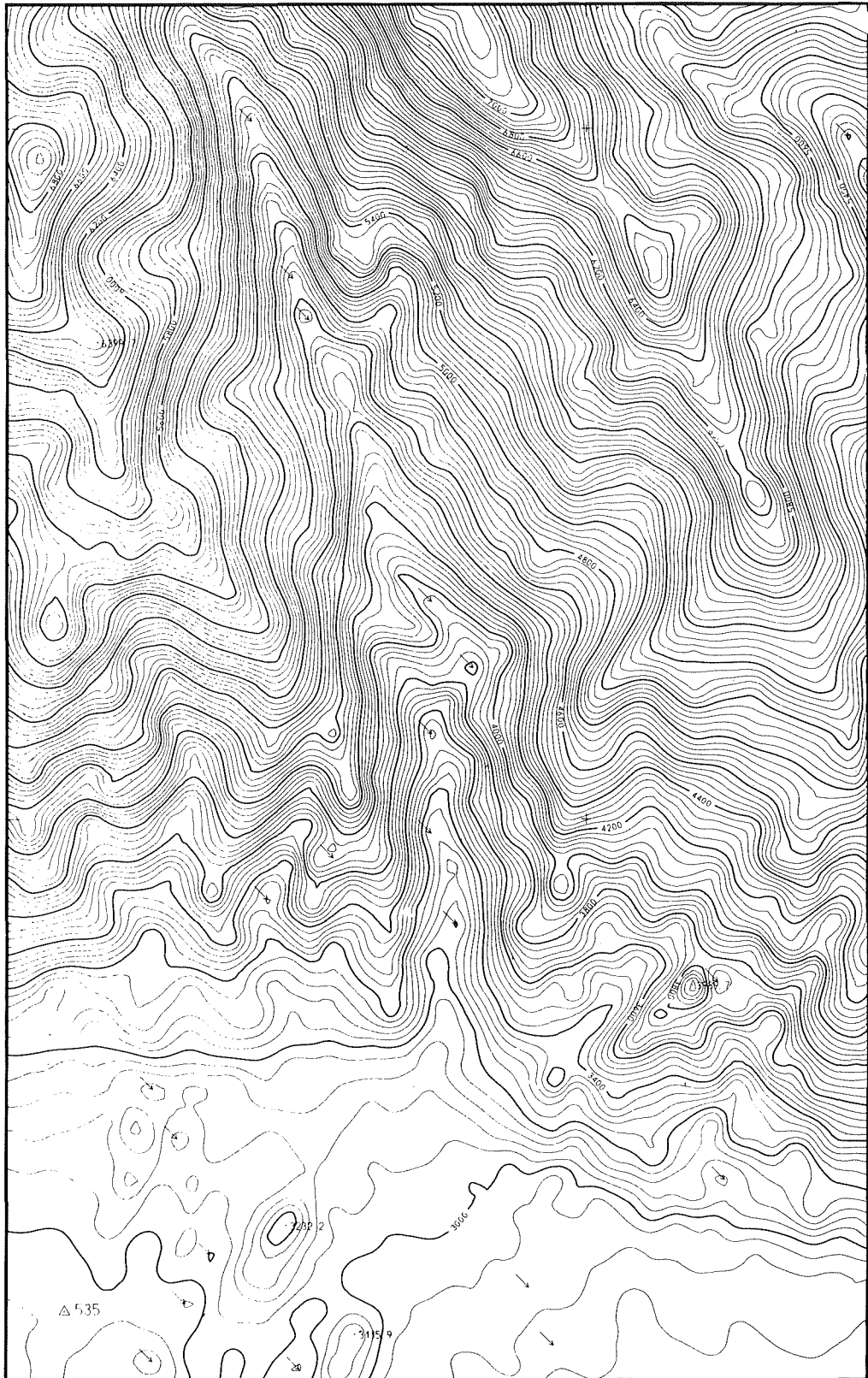


figure 6

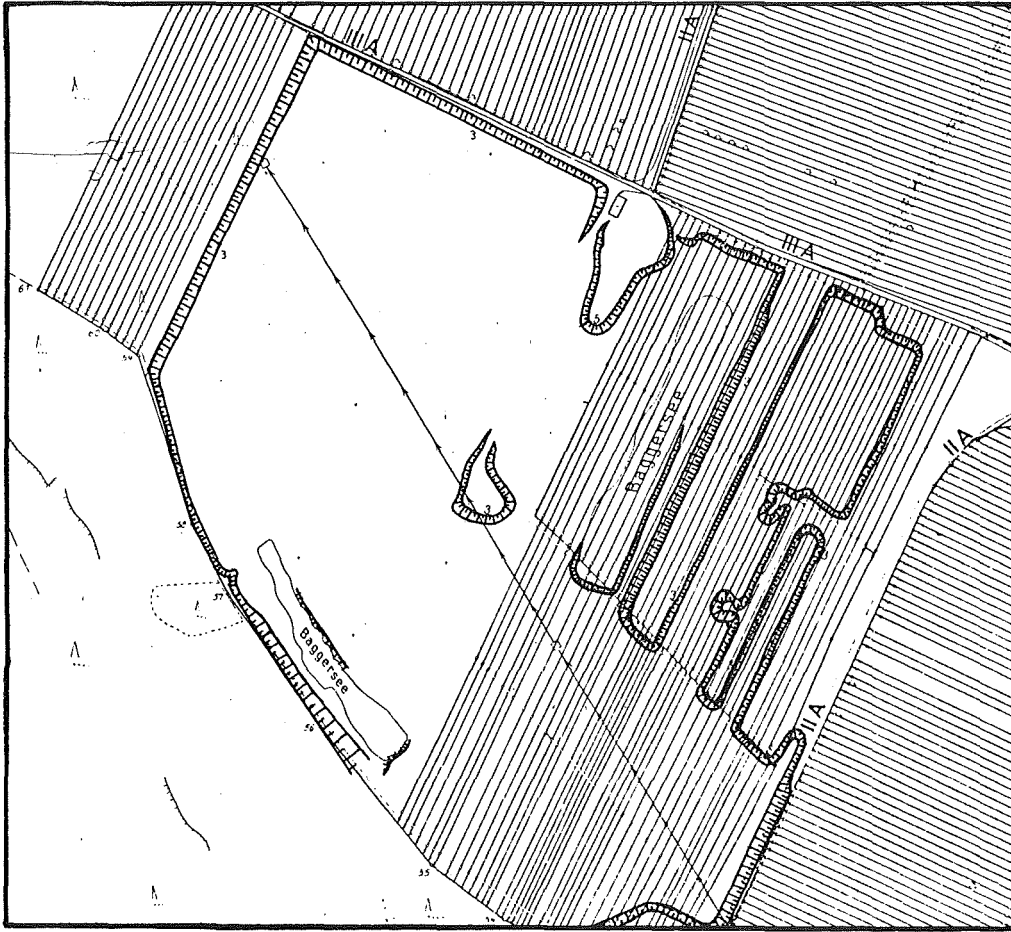


figure 8

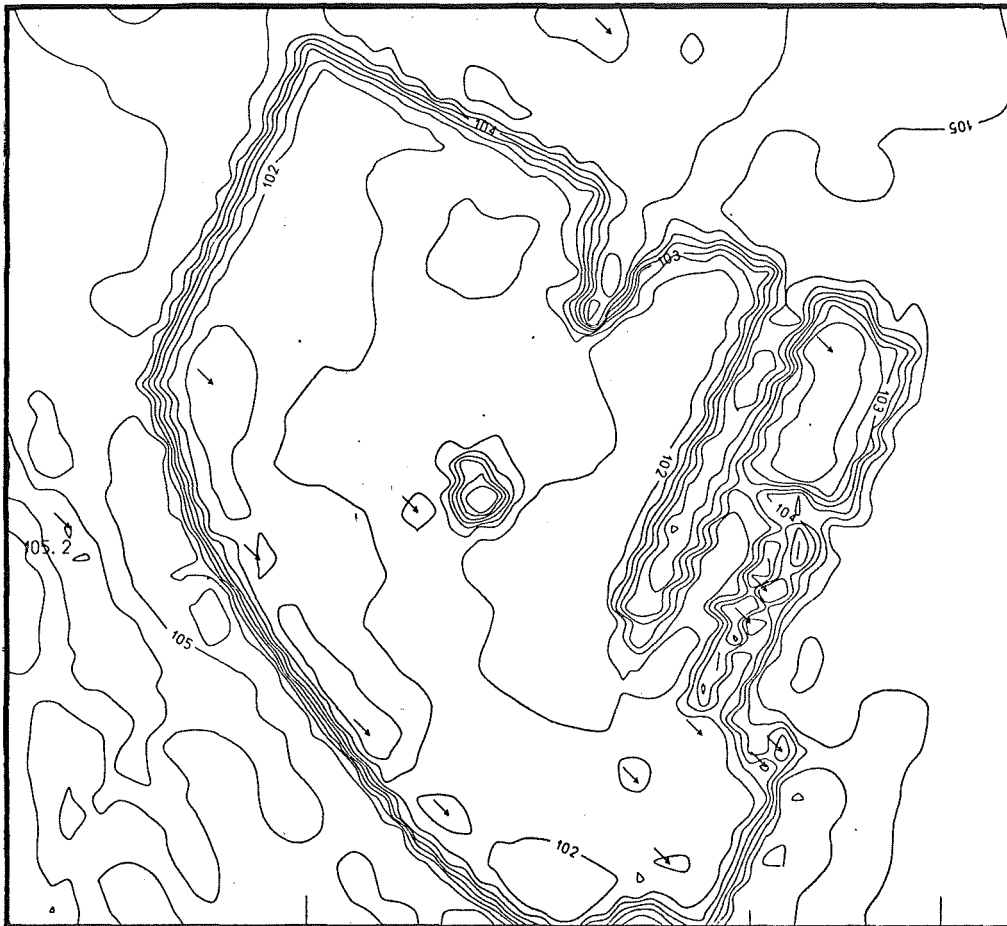


figure 9

The contours resulting from the standard program version are not satisfactory in the slope-areas (figure 9). The interpolation, based on a Gaussian curve as a covariance function, does not accommodate sufficiently break-lines in the terrain surface. Therefore the slope discontinuities are smoothed out. In addition it is evident that the points on the break lines are used as separate points without enforcing the edge conditions. As a result the contours appear oscillating.

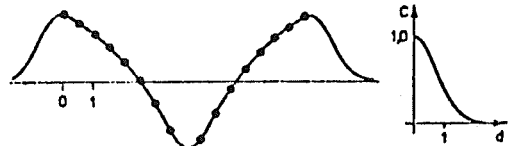


figure 10

In order to avoid such difficulties we expanded the standard contour program. The main alteration refers to the linear least-squares interpolation, according to a proposal of K. Kraus, Vienna, who designed originally the Stuttgart Contour Program [6]. The standard program version smoothenes out breaks, see figure 10 which represents a simulated vertical profile.

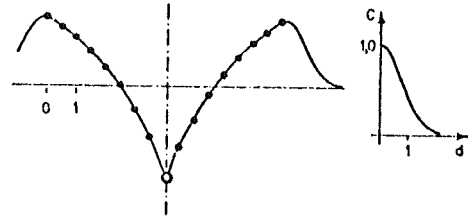


figure 11

The reason is that the covariance is treated only as a function of the distance d of any two points. In this example, however, the covariance depends on the location: two points on different sides of the break are less or even not at all correlated in comparison with two points on the same side.

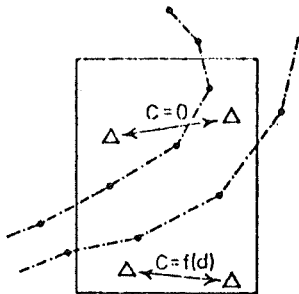


figure 12

Therefore in the well known equation of the linear prediction covariances between points which are separated by a break-line are set to zero (figure 11). In this way the inhomogeneity is taken into consideration and the smoothing of the break is prevented.

In the two-dimensional case (figure 12) the break-lines subdivide our computing units into separate regions. Between points from different regions the covariance is set to zero. Within a region the covariance is, as before, a function of the distance d .

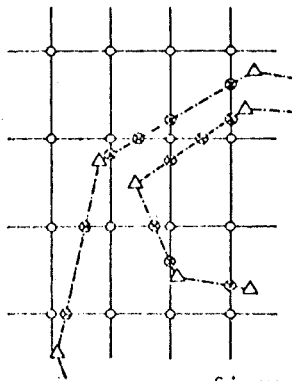


figure 13

According to this principle we interpolate the heights of the grid points (figure 13). However, we don't want to drop the geomorphological information given by the break-lines. So the density of points on the break-lines is increased by interpolating the intersections of these lines and the grid. The condensed point series of the break-lines are stored on the magnetic-tape directly after the grid heights. In this way the interpolation adheres very strongly and directly to the geomorphological features, therefore a grid with wide meshes is sufficient for the DHM.

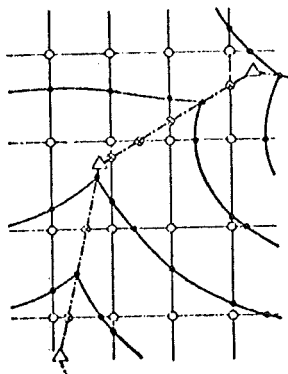


figure 14

The contour points are usually computed by linear interpolation between two neighbored grid heights (as it was done in the former program). In addition, break-lines intersecting the grid meshes are taken into account accordingly (figure 14).

Also contour points are interpolated on the break-lines.

The program has also been enlarged in that part which sorts the interpolated points by contour-lines. When a break-line is reached, the contour-line is interrupted, then restarted at the same point. Thus the plotter will produce the intended break in the contour.

During the last few weeks the first complete map sheet was computed with this new program. The data of the tacheometric survey, the result of which is shown in figure 7, were used once more. In figure 15 the new digital height model of one computing unit is presented (full lines = grid lines, dashed lines = break-lines). The interpolated surface clearly shows the required break.

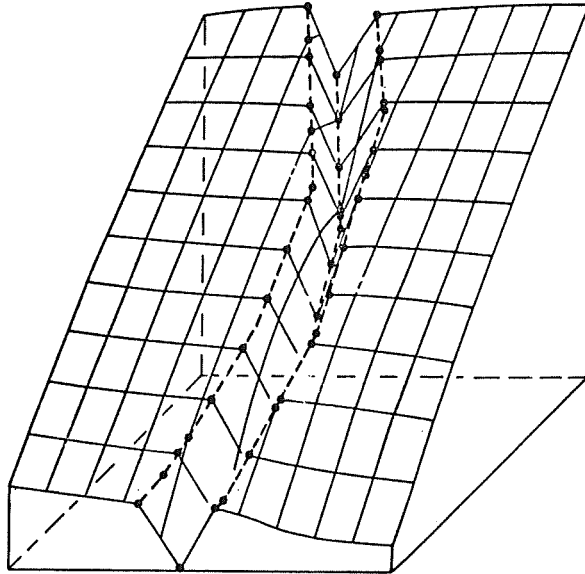


figure 15

Figure 16 shows a section of the map sheet composed of four computing units. The contour-lines break at the edges of the ravine as they ought to.

In figure 17 this new result is compared with the result of the standard contour interpolation in which the edges were disregarded (dashed lines).

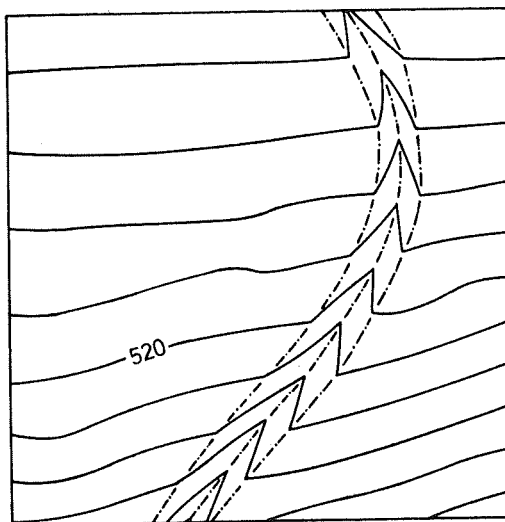


figure 16

Figures 18 and 19 show another section of the map sheet and the comparison with the standard interpolation.

The results of the first experiment prove that the extended program can properly present difficult geomorphological features. A striking increase of the quality of the computed contours is evident. Naturally the refined method requires slightly increased computing times.

In the following months the program will be completed and optimized.

It is felt that it will constitute a useful tool for the automatic production of contour maps of high cartographic quality.

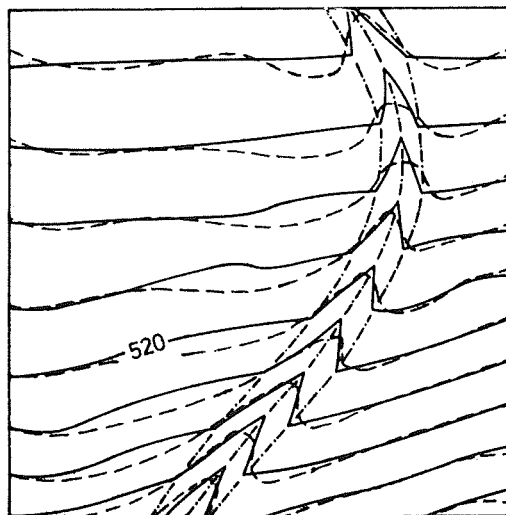


figure 17

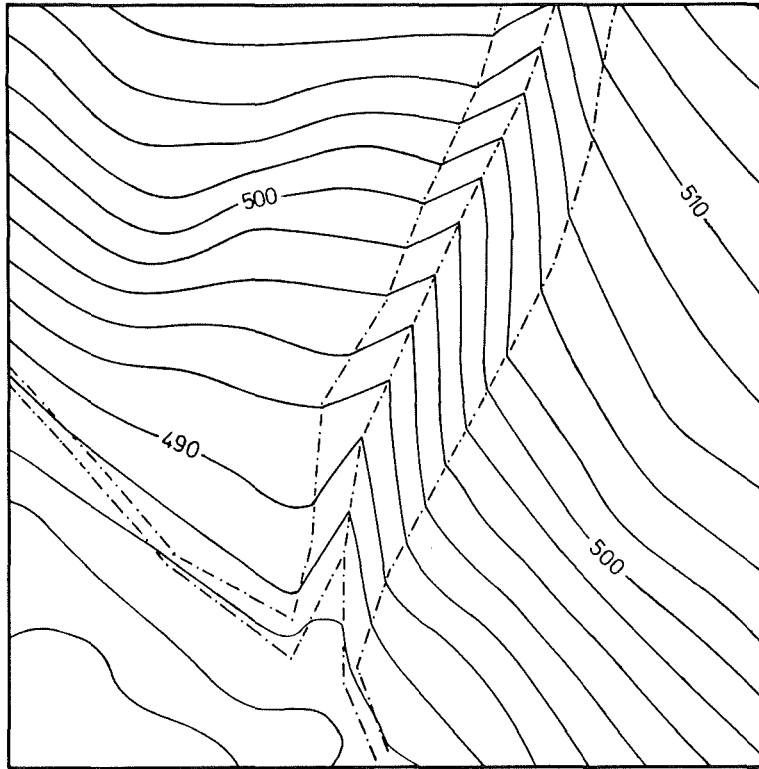


figure 18

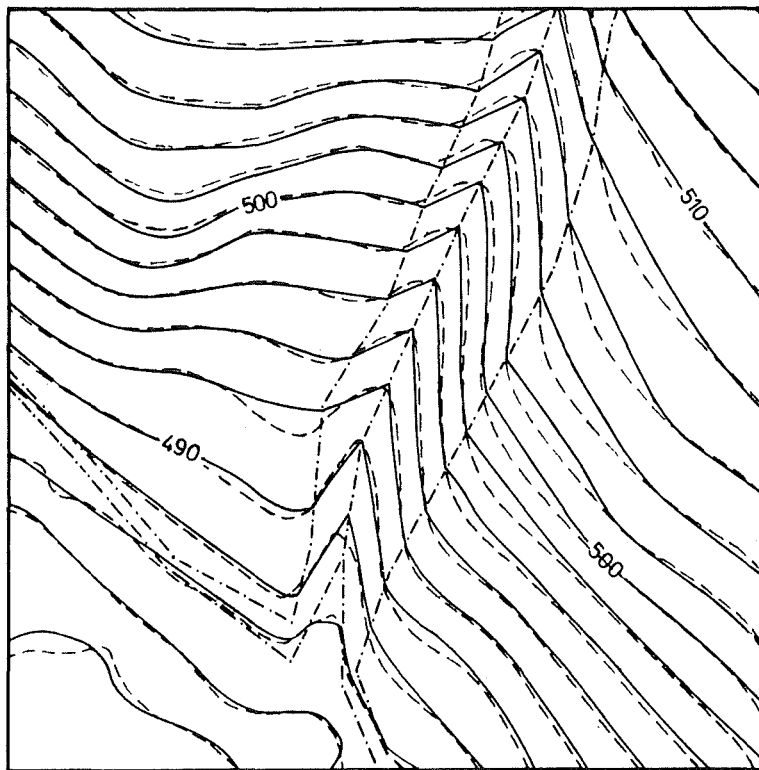


figure 19

REFERENCES

- |1| Stanger, W.: "Das Stuttgarter Höhenlinienprogramm - Beschreibung und Ergebnisse", Numerische Photogrammetrie von F. Ackermann, Sammlung Wichmann, Neue Folge, Band 5
- |2| Kraus, K.: "Ein allgemeines digitales Geländemodell - Theorie und Anwendungsmöglichkeiten", Numerische Photogrammetrie von F. Ackermann, Sammlung Wichmann, Neue Folge, Band 5
- |3| Kraus, K.: "Automatische Berechnung digitaler Höhenlinien", Zeitschrift für Vermessungswesen 96, S. 233 - 239, 1971
- |4| Moritz, H.: "Statistische Methoden in der gravimetrischen Geodäsie" Zeitschrift für Vermessungswesen 88, S. 407 - 416, 1963
- |5| Kraus, K.: "Interpolation nach kleinsten Quadraten in der Photogrammetrie" Bildmessung und Luftbildwesen 40, S. 3 - 8, 1972
- |6| Aßmus, E. und Kraus, K.: "Die Interpolation nach kleinsten Quadraten - Prädiktionswerte simulierter Beispiele und ihre Genauigkeiten" Deutsche Geodätische Kommission, Reihe A, Heft Nr. 76, 1974

THE THEORETICAL ACCURACY OF POINT INTERPOLATION ON TOPOGRAPHIC SURFACES

by E. Clerici and K. Kubik, Delft, Netherlands

1. INTRODUCTION

This report documents an investigation into the theoretical accuracy of point interpolation and volume computation for topographic surfaces. For this purpose the type and roughness of the terrain are described by a covariance function of exponential type (cf. Grafarend 1971, Koch 1973). Based on this model for the surface, the accuracy of interpolated points and of volumes is derived by the application of the law of propagation of errors.

The results of the investigation proved that the spacing of the control points and the roughness of the surface are the governing factors influencing the interpolation and volume accuracy. The method of interpolation is of minor importance for the accuracy as compared to the above mentioned factors. In the following sections, the model for the topographic surface is outlined, the problem of interpolation is defined and the interpolation and volume accuracies are stated for various interpolation problems.

2. A MATHEMATICAL MODEL FOR THE TOPOGRAPHIC SURFACE

During the last years it has been proved that a topographic surface can be properly described by a stochastic function $z = z(x,y)$, whose undulations and smoothness are characterized by its covariance function $K(i,j)$. The indices i and j define two values $z(x_i,y_i)$ and $z(x_j,y_j)$ of the function. Let us agree to call the variable z "height", although it may just as well represent depth, geophysical variables, etc.

The covariance function $K(i,j)$ measures, similarly to a covariance matrix, the variation of the heights about some mean level and their mutual correlation. The concept of the covariance function can be derived from that of the covariance matrix by allowing infinitely many stochastic variables z_i , which together define the surface $z(x,y)$.

figure 1
Characterization of surface profiles by the covariance function

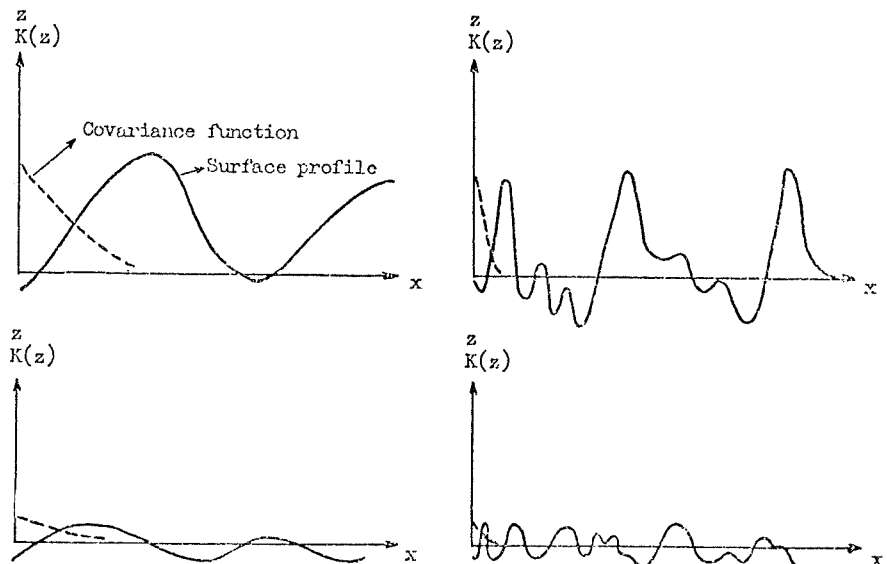


Figure 1 shows a number of examples of covariance functions for common surface profiles, it also demonstrates the ability of this covariance function to describe the properties of the profile. Smooth stochastic functions possess a covariance function, which slowly dampens out to zero, while with rough functions z,K will dampen out quickly.

The magnitude of the local undulations of z is represented by $K(i,i)$.

For our investigation we assume the covariance function to be of the type

$$K(i,j) = \sigma_0 e^{-d(i,j)/a} \tag{1}$$

with σ_0 and a denoting scalars and $d(i,j)$ denoting the planimetric distance between (x_i, y_i) and (x_j, y_j) . This assumed function is independent of the absolute position and of the azimuth of the pair of points. This type of covariance function can be used for local regions of the surface until its unsuitability for describing the topographic surface is proved ⁺).

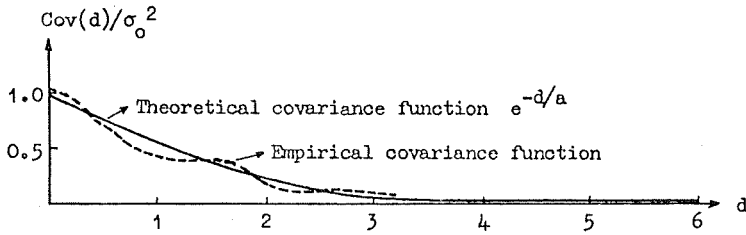


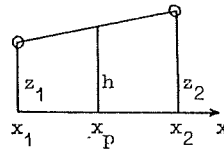
figure 2
Fitting of an exponential type covariance function to empirical data

Figure 2 demonstrates the suitability of this type of exponential covariance functions to describe the properties of actual topographic surfaces.

3. THE PROBLEM OF INTERPOLATION

In the interpolation problem a set of surface heights $z_\alpha = z(x_\alpha, y_\alpha)$ $\alpha = 1 \dots n$ (control points) is given, it is then the task to compute an approximation h for the surface height at a given position (x_p, y_p) . Various interpolation rules are possible, an example is given by the linear interpolation rule between two control points in a profile:

$$h = \left(1 - \frac{x_p - x_1}{x_2 - x_1}\right) z_1 + \frac{x_p - x_1}{x_2 - x_1} z_2 ;$$



or the local quadratic or cubic interpolation etc. All these commonly known interpolation rules may be formally written as

$$h(x_p, y_p) = A \cdot z_c \tag{2}$$

where z_c denotes the array of control heights, $z_c = |z_\alpha|^T, \alpha = 1 \dots n$ and A denotes an array with elements $|a_\alpha(x_p, y_p)|$ depending on the position (x_p, y_p) of the surface point to be interpolated. The error e of the interpolated height will be equal to

$$e(x_p, y_p) = z(x_p, y_p) - h(x_p, y_p) = z(x_p, y_p) - A \cdot z_c \tag{3}$$

and the variance of this error is equal to

$$Q_{ee} = K(p, p) + A \cdot K(\alpha, \beta) A^T - A \cdot K(\alpha, p) - K(p, \alpha) \cdot A^T, \quad \alpha, \beta = 1 \dots n \tag{4}$$

The accuracy formula (4) is used for the accuracy computations in the following sections.

⁺) Our assumption implies that the regions of similar surface type must be carefully selected based on geological information, and that a proper coordinate transformation may be necessary to ensure the independence of K from the azimuth.

⁺⁺) There exists an interpolation method which minimizes this variance, namely the method of prediction (cf. Wiener 1949). The coefficient matrix A for prediction interpolation is equal to

$$A = K(p, \alpha) K^{-1}(\alpha, \beta)$$

and the error variance equals

$$Q_{ee} = K(p, p) - K(p, \alpha) K^{-1}(\alpha, \beta) K(\beta, p)$$

The accuracy results listed in the following sections are based on the covariance function K, given in formula (1). The theoretical results can be readily applied to practical cases as is demonstrated in section 8 of this paper.

For studying the accuracy of interpolation the standard deviation $\sigma = \sqrt{Q_{ee}}$ of the interpolation error, its maximum σ_{max} and its mean $\sigma_{mean} = (\text{sum of all interpolated points } \sigma \text{ divided by the number of interpolated points})$ are used. The standard deviation σ is expressed in units of σ_0 .

4. THE ACCURACY OF POINT INTERPOLATION IN PROFILES

At first we will investigate the accuracy of height interpolation in profiles. We assume that the error free control points are located at equal spacings in a profile of the topographic surface, and intermediary points have to be interpolated.

The accuracy of the interpolated heights was computed for both linear and prediction interpolation. Since these two methods are expected to yield the lowest and highest accuracy among the commonly used interpolation methods, the interpolation errors of all these methods will be within the computed bounds.

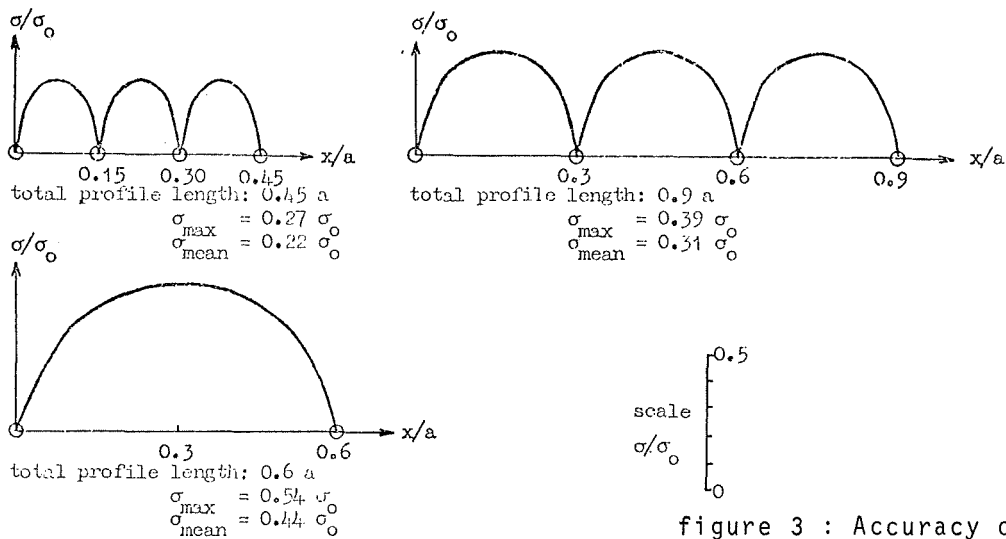


figure 3 : Accuracy of interpolated heights for linear interpolation

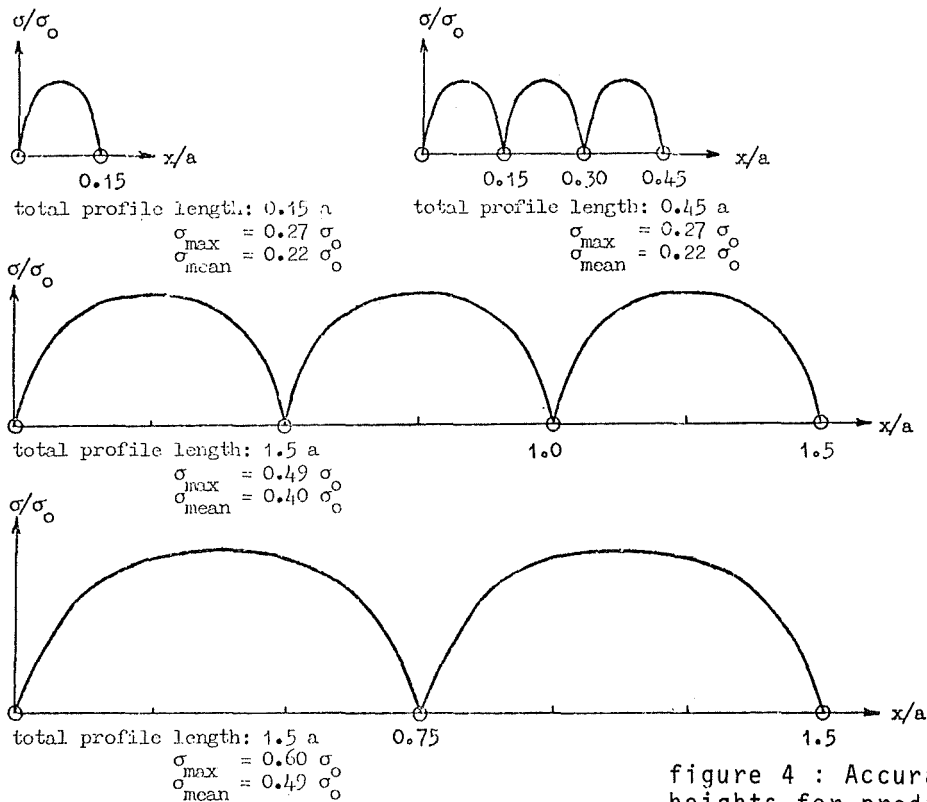


figure 4 : Accuracy of interpolated heights for prediction interpolation

Figure 3 shows the standard deviations σ for the interpolated heights for linear interpolation depending on the location of the points in the profile. Figure 4 holds for prediction interpolation. These figures show that the standard deviation of the interpolation error increases towards the centre of the interval between the control points, where it reaches its maximum value. This maximum σ_{max} is for linear interpolation independent, and for prediction interpolation practically independent of the length of the profile and the position of the interval in the profile, it is only dependent on the control spacing.

For both linear and prediction interpolation the standard deviations σ_{mean} and σ_{max} depend on the control spacing. The increase of both σ_{mean} and σ_{max} is relatively large for very short control spacings (cf. figure 5) and becomes increasingly smaller for larger control spacings. By approximation it holds

$$\sigma_{max} = \sigma_0 \sqrt{\frac{D}{2a}} ; \quad \sigma_{mean} = \sigma_0 \sqrt{\frac{D}{3a}} \quad \text{for small } D/a.$$

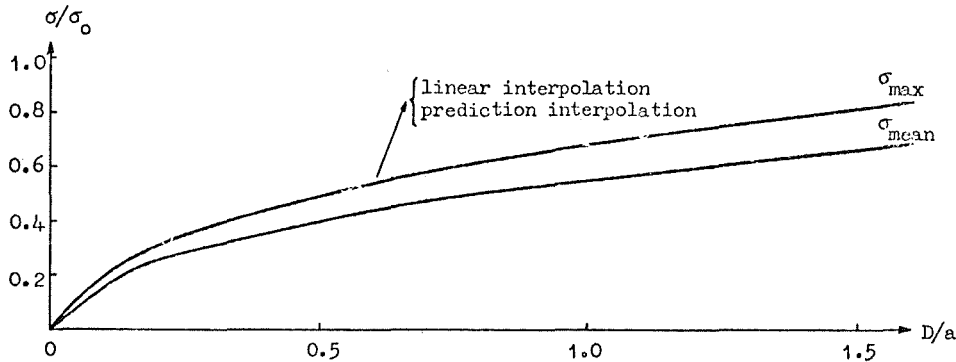


figure 5
Dependence of interpolation accuracy on control spacing for both linear and prediction interpolation

The accuracy results for prediction and linear interpolation are practically identical. This is a very important result indeed, because it tells us that - within the range of validity of our model - the accuracy of interpolation hardly depends on the interpolation method, which consequently may be selected according to other criteria, for example convenience and speed of computation.

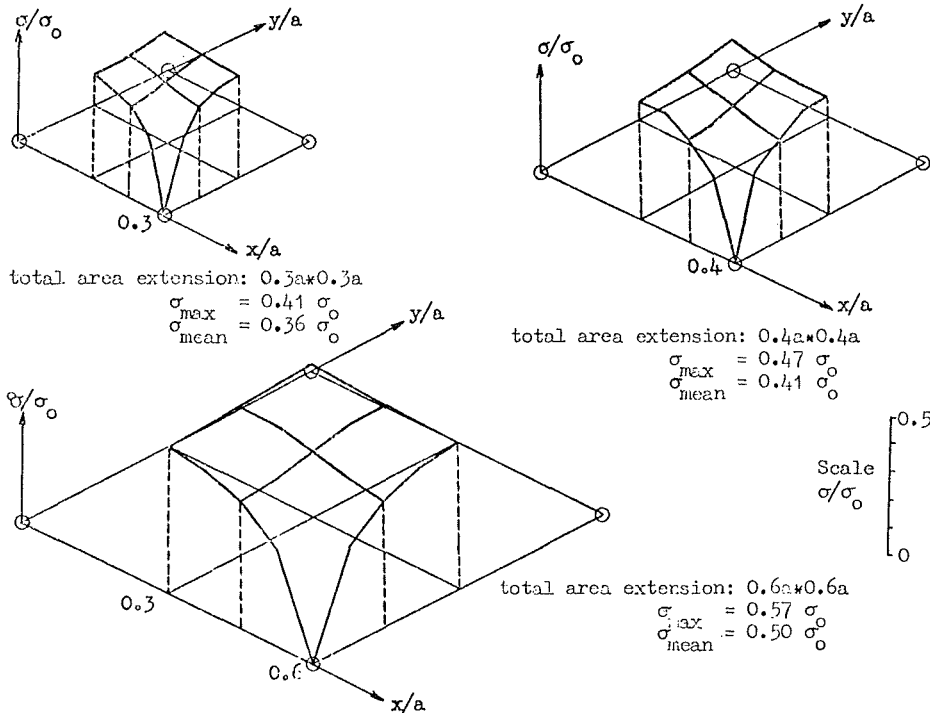


figure 6
Accuracy of interpolated heights for bilinear interpolation

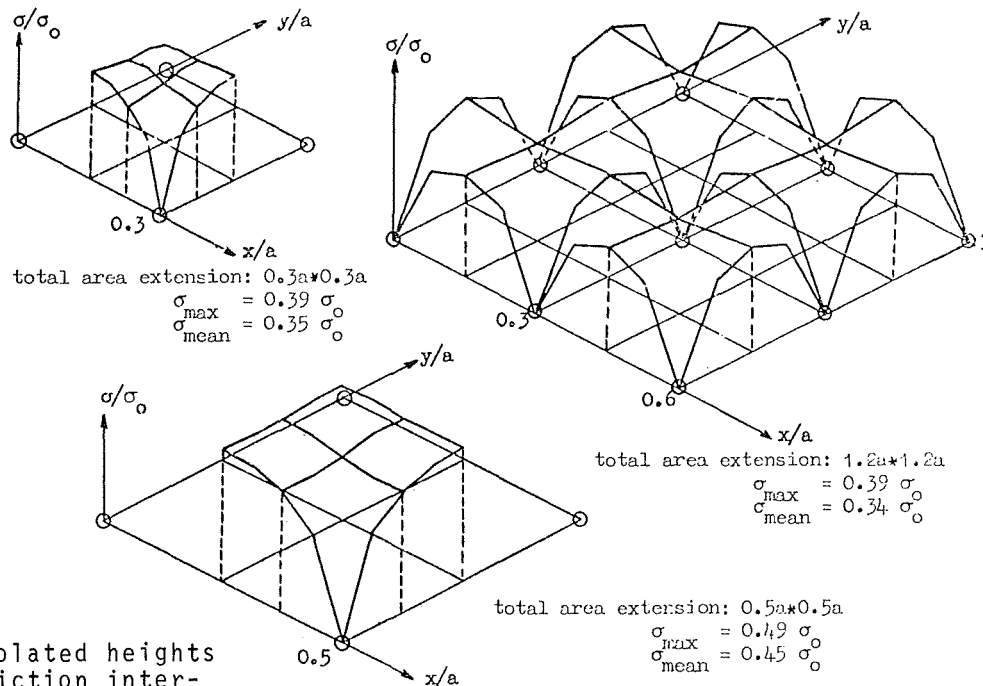


figure 7
Accuracy of interpolated heights for bivariate prediction interpolation

5. INTERPOLATION ACCURACY WITH GRIDS OF CONTROL POINTS

In this interpolation problem a grid of error free control is given, with equal grid spacing both in x and y direction. The accuracies were computed for bilinear and prediction interpolation in order to bound the accuracies of all commonly known interpolation methods. Figure 6 shows the accuracy results for linear interpolation, and figure 7 holds for prediction interpolation.

The figures show that local maxima of σ appear in the centres of the meshes. These maxima are, for both linear and prediction interpolation, practically independent of the extension of the grid and the position of the mesh in the grid.

The accuracy parameters σ_{mean} and σ_{max} increase with increasing control spacing in the same typical manner as we observed for profiles (cf. figure 8). Also with bivariate interpolation the difference in accuracy of linear and prediction interpolation is only marginal.

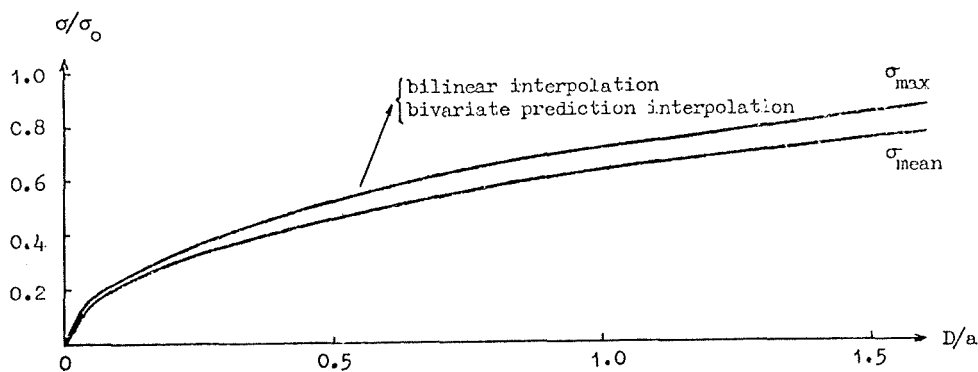


figure 8
Dependence of interpolation accuracy on control spacing for bivariate interpolation

6. EFFECT OF LOCAL POINT DEVIATIONS AT THE CONTROL POINTS

Local point deviations at the control points may be due to measuring errors or due to irrelevant local surface undulations. These local point deviations with standard deviation σ_D cause a decrease of the interpolation accuracy which is most significant in the surrounding of the control points. There the effect of these errors is fully superimposed on the results of interpolation (cf. figure 9).

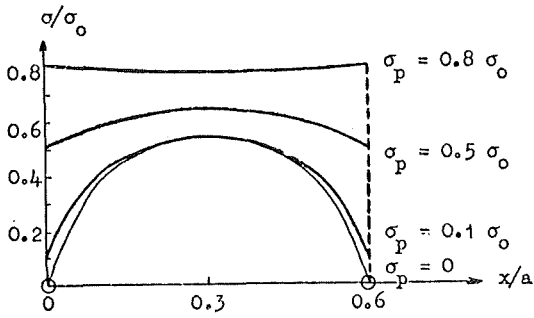
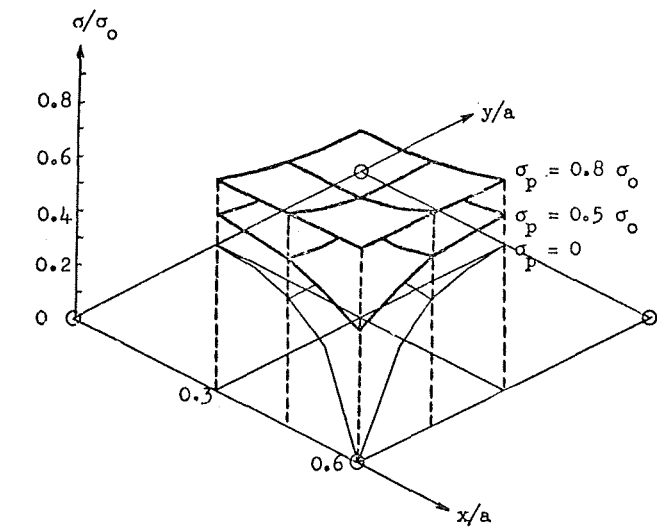
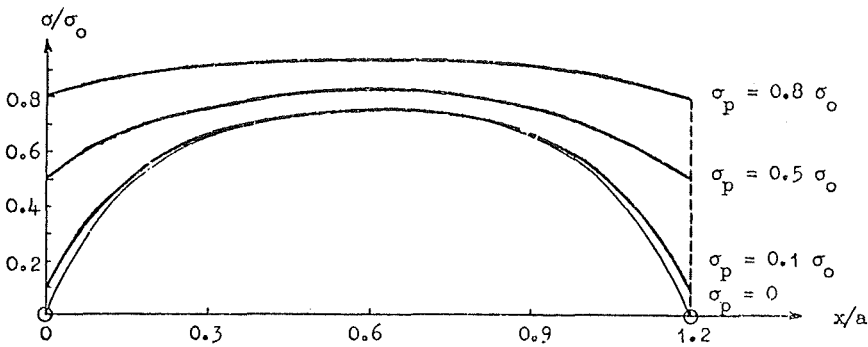


figure 9
Effect of local point deviations
at the control points



The influence is considerably smaller towards the centre of the control interval. For linear interpolation in the presence of points deviations the following accuracy relationship holds

$$\bar{\sigma}^2 = \sigma^2 + K \cdot \sigma_p^2$$

$\bar{\sigma}$ standard deviation of interpolated height in presence of local point deviations at control points

σ standard deviation of interpolated height in absence of local point deviations

K constant, $0.5 \leq K \leq 1$ for profile interpolation ($K_{\text{mean}} = 0.66$)

$0.25 \leq K \leq 1$ for surface interpolation (grid of control points; $K_{\text{mean}} = 0.36$)

7. VOLUME ACCURACY

In many applications also the volume has to be estimated between the surface $z(x,y)$ and the reference plane $z = 0$ for a pre-given, rectangular or square shaped area (block). For this purpose surface heights $h(x_p, y_p)$ may be interpolated in a regular grid of points in the block as shown in figure 10. The volume V then follows to

$$V = s.t. \sum_{p=1}^m h(x_p, y_p) = S.T. h_{\text{mean}} ; h_{\text{mean}} = \frac{\sum_{p=1}^m h(x_p, y_p)}{m}$$

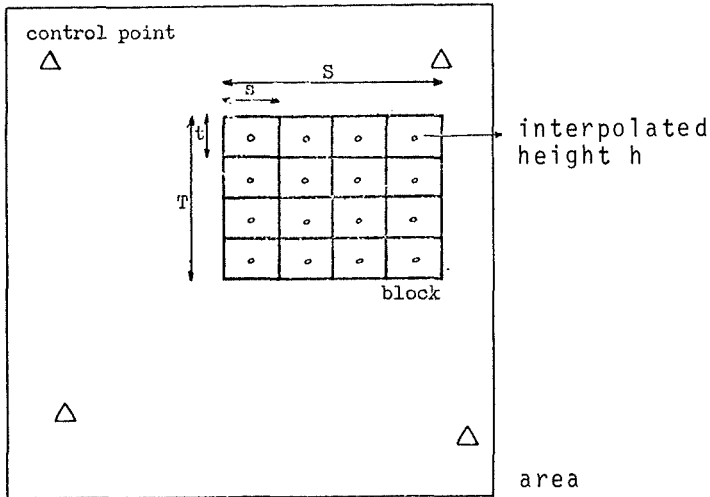


figure 10
Principle of volume computation

The standard deviations of the estimated volumes V and of the values h_{mean} were computed for a number of control point arrangements and block sizes, in an analogue manner as the interpolation accuracy. For studying the volume accuracy the standard deviation σ of the error in h_{mean} , its maximum σ_{max} and its mean σ_{mean} are used. Figure 11 shows some examples of the computations. This figure demonstrates that the magnitude h_{mean} becomes more accurate with denser control and with increasing block size (cf. figure 12). For a detailed discussion of the results cf. Dijkstra, Kubik 1974).

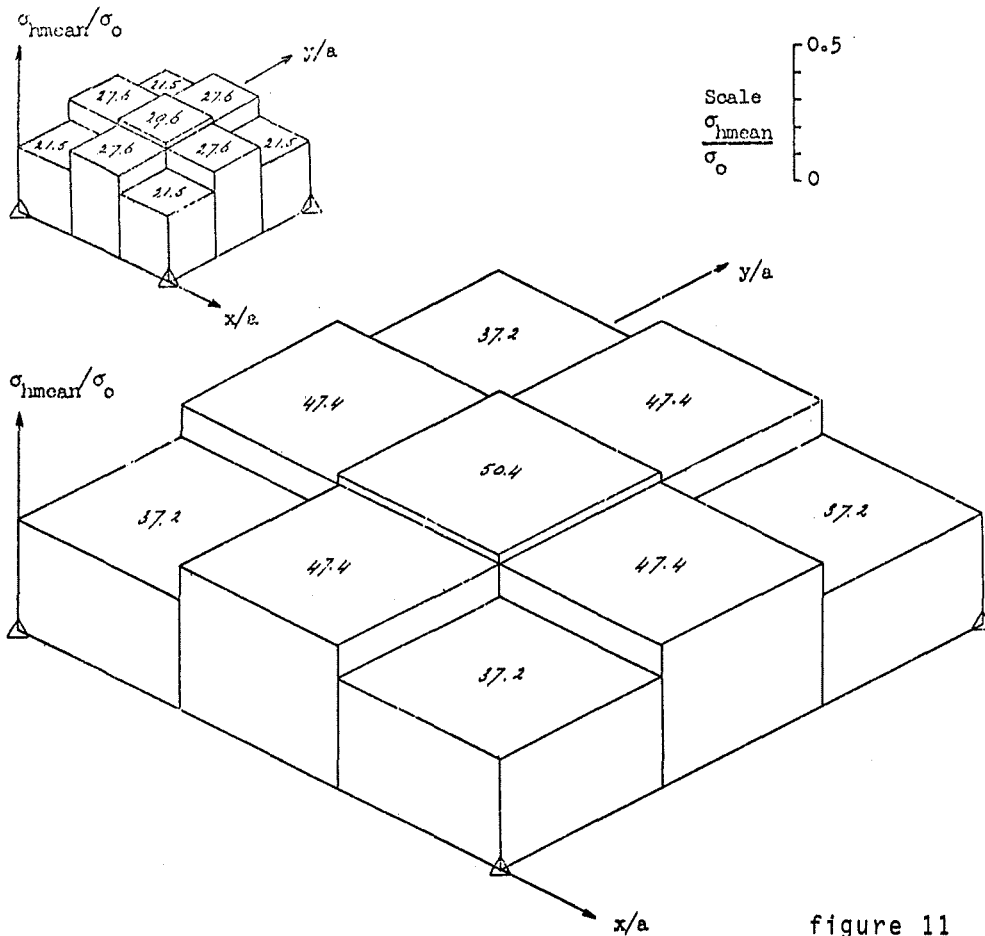
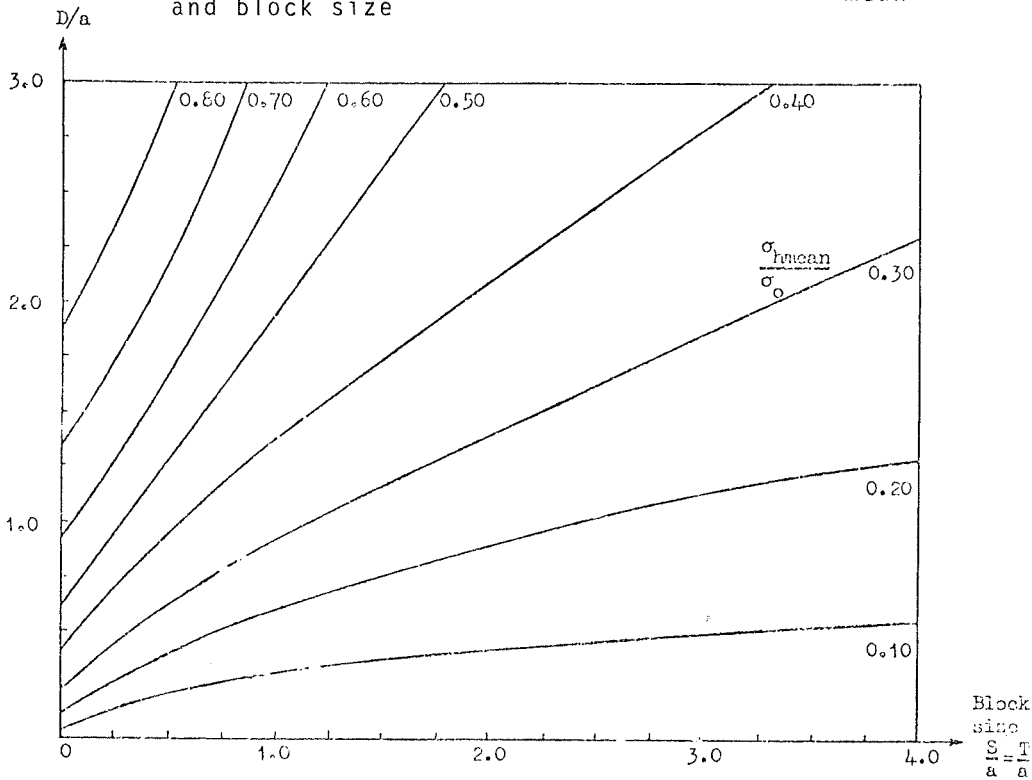


figure 11
Accuracy of volume determination

figure 12

Dependence of average standard deviation σ_{hmean} on control spacing and block size



8. CALIBRATION OF THE ACCURACY RESULTS FOR PRACTICAL USE

In order to be able to apply the above accuracy results to practical cases, the parameters σ_0 and a of the covariance function (1) must be estimated from the actual surface. For profiles the covariance function can be estimated from the formula

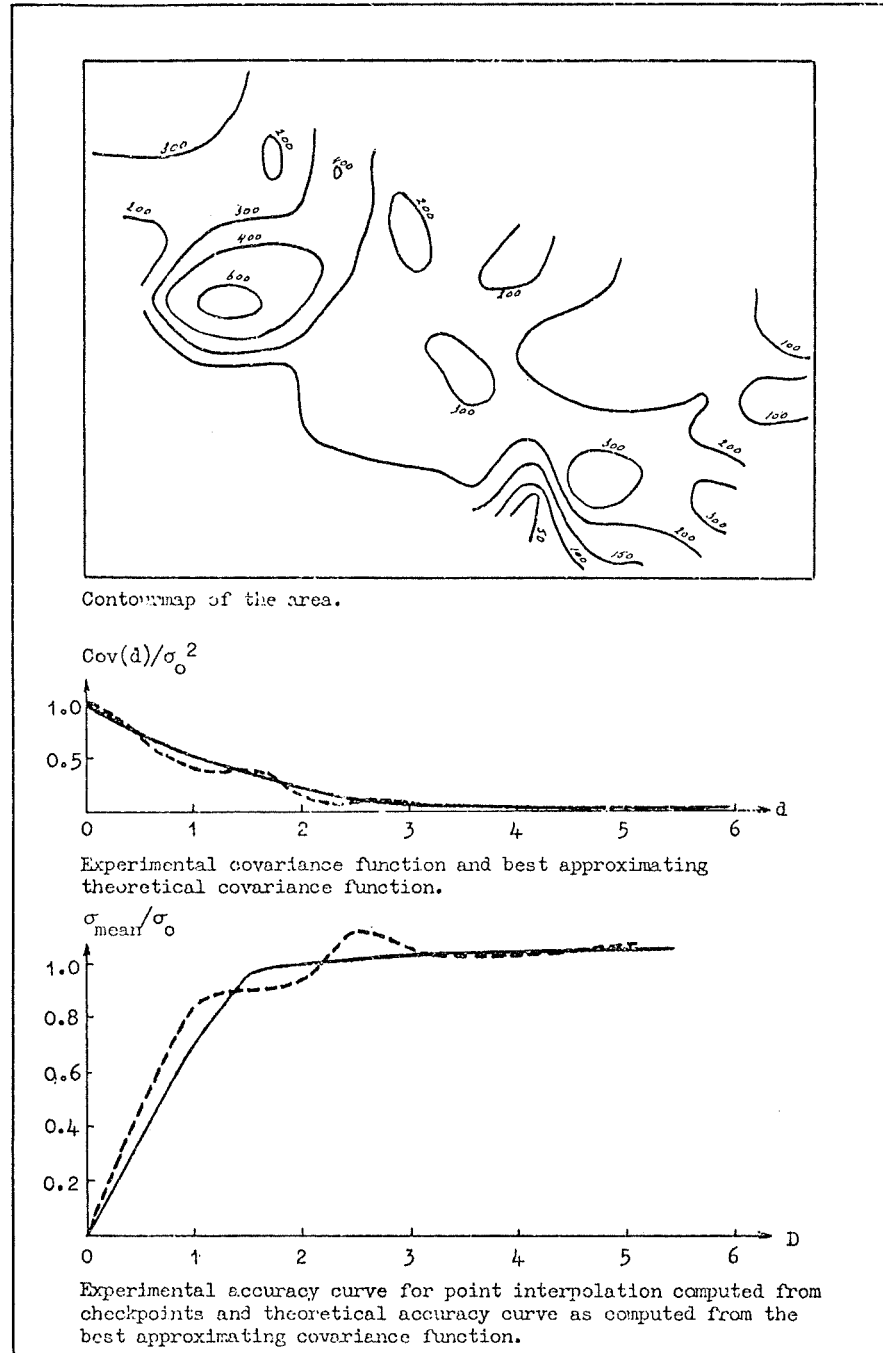
$$\hat{K}(d) = \frac{\sum (z_i - \bar{z})(z_{i+d} - \bar{z})}{n - d - 1}, \quad \bar{z} = \frac{\sum z_i}{n}; \quad i = 1 \dots n$$

This covariance function is then best approximated by the exponential function $\sigma_0 e^{-d/a}$ through a proper choice of σ_0 and a . Using the computed values for a and σ_0 , the interpolation accuracies σ_{mean} and σ_{max} may be obtained from the figure 5 for a given control spacing D .

Figure 13 shows an example of these computations while demonstrating the validity of the theoretically obtained data by comparison with experimental results.

The calibration of the theoretical accuracy results for bivariate interpolation proceeds along similar lines, but it is, however, somewhat more elaborate.

figure 13



REFERENCES

- Dijkstra, S., Kubik, K. "On the theoretical accuracy of volume determinations" to be published 1974
- Koch, K. R. "Digitales Geländemodell und automatische Höhenlinienzeichnung" Zeitschrift für Vermessungswesen Nr. 8, 1973
- Grafarend, E. "Statistische Modelle zur Prädiktion von Lotabweichungen" Vermessungstechnik 19, p. 66, 1971
- Wiener, N. "Extrapolation, interpolation and smoothing of stationary time series", New York, 1949
- Wolf, H. "Ausgleichsrechnung nach der Methode der kleinsten Quadrate" Dümmler Verlag, Bonn, 1968

APPROACH AND STATUS OF GEOMETRIC RESTITUTION FOR REMOTE SENSING IMAGERY

by G. Konecny, Hannover, Fed.Rep. Germany

INTRODUCTION

After declassification of military non-classical sensors, such as the infrared scanner and the side-looking airborne radar, remote sensing began to develop as a new field in the early 1960's principally through the interest created by the Remote Sensing Symposia at the University of Michigan and by the activities of the Remote Sensing Committee of the American Society of Photogrammetry.

The International Society of Photogrammetry adopted the topic during the congress period 1968 - 1972 in commissions I, II, IV, V and VII.

During the reorganization of commissions in 1972 the geometry aspects of remote sensing were allocated to commission III and a working group was established to work on geometric problems of remote sensing. The Stuttgart symposium 1974 offers the first opportunity to present the scope of the working group as well as preliminary results.

AIMS OF WORKING GROUP "GEOMETRY OF REMOTE SENSING"

The broad aims of the working group are to investigate geometrical aspects of non-classical remote sensing systems. There is no need to investigate classical remote sensors, such as aerial photography within the group, since this is already being done in several ISP commissions. Despite of this the task is still too large at the moment; therefore priorities must be set according to most urgent needs.

Table 1(a): sensor parameters

sensor	Film Size	Resolution Lines / mm	Angular view in x	Angular view in y	Angular resolution	ground pulse resolution	range of scale factors
aerial photography)	230 x 230 mm	20 to 60	-60°to+60°	-60°to+60°	0.1 mrad	-	1000 to 100 000
strip photography)	230 to 70 mm strip	20 to 60	strip	-60°to+60°	0.1 mrad	-	100 to 10 000
panoramic photography)	115 x 1140 mm	20 to 60	-40°to+40°	-90°to+90°	0.015 mrad	-	1000 to 100 000
television camera	25.4x25.4 mm enlarged to 230 x 230 mm	40 in enlargement	-5°to+ 5°	-5°to+ 5°	0.2 mrad	-	satellites > 1 000 000
multispectral scanner	70 mm strip enlarged to 230 mm strip	20 in enlargement	strip	-5°to+ 5°	0.5 mrad	-	satellites > 1 000 000
infrared scanner	70 mm strip	5	strip	-60°to+60°	3 mrad	-	1000 - 1 000 000
microwave scanner	70 mm strip	5	strip	semiannulus at constant angle	10 mrad	-	10 000-5 000 000
brute force radar	70 mm strip	20	strip	~45°to 60°	3 mrad in azimuth	25 m	100 000-1 000 000
coherent radar	70 to 2 x 70 mm strip	30	strip	~45°to 70°	2 mrad in azimuth	10 m	100 000-1 000 000
sonar	graph paper strip	5	strip	~45°to 70°	5 mrad in azimuth	1 m	1 000 - 10 000

	sensor	type	spectral band	spectral resolution	prinsipal use
passive systems	aerial photography	panchromatic	0.35 - 0.7 μm	0.4 μm	<u>aerial mapping</u> topographic features
		filtered color	within 0.35-1.2 μm	0.1 μm	
		false color	0.35 - 0.7 μm	0.2 μm	<u>photo-interpretation</u> object detection
		multi-lens	0.50 - 1.0 μm	0.2 μm	
	television	TV	0.35 - 0.7 μm	0.4 μm	satellite photography
		color-TV	0.35 - 0.7 μm	0.2 μm	
	scanners	MSS	0.3 - 3.0 μm	0.02 μm	object classification
		thermal scanner	3-5 / 8-14 μm	5 μm	<u>thermal mapping</u> measurement of heat balance
		spectral thermal scanner	within 8 - 14 μm	0.5 μm	
		microwave scanner	0.1 - 100 cm	10 %	
active systems	radar	real aperture	1 - 100 cm	0.5 %	<u>all weather mapping</u> object detection and mapping.
		synthetic aperture	1 - 100 cm	0.5 %	
	sonar		1 cm	-	underwater tool - object detection

Table 1(b): remote sensing tools

Table 1 shows:

- GEOMETRICAL ASPECTS:

- 1) Aerial photography and TV imagery are the only sensors resulting in a real-time two-dimensional image.
- 2) Platform movement and other time-varying calibration problems will cause deterioration of geometric accuracy for the remaining "dynamic" sensors.
- 3) Only the sensors in the visible range (photography, TV-imagery, scanning) have high angular resolution. They are therefore best suited for topographic object detection.
- 4) Since radar is a pulse system, it limits the resolution to a linear, not an angular value, more or less independent of the flying height. It fixes the image to a rather small scale (e.g. 1 : 400 000).
- 5) TV-imagery, panoramic photography, as well as multispectral scanning will despite of their inferior geometric characteristics be more suitable for mapping from satellites due to their extreme angular resolution.

- SPECTRAL ASPECTS:

- 6) The high spectral resolution of the multispectral scanner makes it preferable to filtered black and white or to color and false color photography as an object classification device.
- 7) Due to its simplicity in acquisition and in geometric presentation color aerial photography is a more preferred sensor product for object detection via photo-interpretation.
- 8) The thermal scanner can be seen in the light of a geophysical exploration or environmental monitoring tool.
- 9) Radar is the preferred sensor, where clouds fog and light conditions do not permit sensing in other spectral bands.

The photogrammetric tasks of direct concern to the working group must therefore lie in the following direction:

1. Geometric restitution for all cases where geometry is of primary importance: The prime requirement will therefore be in topographic mapping.
Since the primary tool, aerial photography, is not subject of the working group, the highest priority should therefore be directed to investigate radar as a mapping tool. It possesses acceptable ground resolution for small scale mapping requirements.
Panoramic photography is of interest to the military user; it could be of interest for mapping from space platforms. However, imagery is so far available only from lunar missions.
2. A second requirement is to produce geometrically correct thematic maps. These are important for graphical representation of earth resources surveys for a variety of purposes and disciplines (e.g. agriculture, land use, oceanography). Satellite uses have no doubt given a wider impetus to semiautomated and automated analysis, techniques, which were generally introduced through multispectral scanning. For this reason satellite imagery should also be investigated with high priority.
3. So that change detection becomes possible by semiautomated or automated analysis techniques it is necessary to refer spatially, spectrally and particularly temporally different images to a common geometric base beyond the limits of resolution. The topic of change detection should be next in the order of priorities.

STEPS OF PROGRESS

In pursuing the task of investigating the geometric aspects of remote sensing the following steps will be necessary:

- 1) An analytical analysis including the formation of a mathematical model and a controlled test in which image coordinates are measured and ground coordinates are determined by off-line digital computations to obtain sensor accuracies. The working group tests are principally in this stage.
- 2) Mapping of visually interpreted features either by digital off-line mapping from images (Rijkswaterstaat) or by analytical plotter restitution (TU Hannover, University of New Brunswick). This stage is in progress.
- 3) It may be appropriate to perform image gridding by digital-electronic/analog image processing, as this has been done for Nimbus 3 satellite images. It is possible to investigate the accuracy of this procedure (TU Hannover).
- 4) Differential rectification is the prerequisite for semiautomatic or automatic change detection operations. Geometric digital or hybrid corrections will no doubt in the future be part of any image processing system for non-classical remote sensors. The concern with these routines is within the scope of the working group (TU Hannover, Purdue University).
- 5) Automatic Image Correlation has been suggested as a mean to perform change detection without previous geometric restitution (IBM, TRW). The state of this work is too futuristic at the moment to be of serious concern to the working group now.

ANALYTICAL ANALYSIS

The analytical analysis requires the setup of an analytical model, the obtaining and the measurement of appropriate test imagery on a simple coordinate measuring device.

Already in 1970 strict analytical expressions were set up for conversion of ground coordinates to image coordinates for scanner and radar imagery. It has been shown that the orientation parameters and the image coordinates are functions of time. Only a line image is formed in real time [1], [2], [3], [4], [5].

Subsequently the formulations included instrumental parameters, such as squint for radar [6], or dealt with orientation procedures [7], and problems of intersecting corresponding vectors of overlapping scanner or radar images, or determining positions from direction and distance of a radar interferometer vector [8], [9].

A strict restitution becomes possible if the following parameters are known:

- 1) - for scanners
 - a) the 6 exterior orientation parameters (position and attitude) of the platform as functions of time
 - b) among the interior orientation parameters, timing marks to count and correlate the image coordinate along the film strips with time and to check the film velocity; film edge marks to count the image coordinate in perpendicular direction and to check mechanical translations of the film transport; the sensor constant.

The relations yield collinearity equations which may be used for space intersections in the usual way.

- 2) - for side-looking radar

usually a ground representation is used. The recorded image coordinate perpendicular to the direction of flight therefore not only becomes a function of the slant range, but also of the flying height set for the ground range reduction. In addition to this setting the following parameters must be known:

- a) 5 orientation parameters (ω has no influence on geometry)
- b) delay constants referring to electronically generated marks to count image coordinates in across flight direction and to check the functioning of the cathode ray tube
- c) timing marks to check the image scale and the film velocity in flight direction
- d) the squint angle

An intersection can be formed by two spheres of the intersecting radii resulting in a circle, which intersects with the antenna squint cone to give 2 points of intersection. The point with an elevation lower than the flying height is in general the proper point.

- 3) - The commercially not available radar interferometer permits to determine distance and direction to a point of determinable phase.

The knowledge of exterior orientation parameters, necessary for a restitution can be obtained by the following means:

- 1) by approximation; usually a uniform straight and level flight is assumed. This is the standard case of restitution at present,
- 2) by recording of orientation parameters; navigation devices permit to determine a continuous x-y record of the platform. An airborne profile recorder in conjunction with a statorscope may monitor the z-coordinate. The platform orientation may be traced with inertial systems. Recording of orientation parameters is costly; moreover difficulties are encountered for coherent radar; there the recording of attitude parameters may be irrelevant since the image is formed by a summation of Doppler-frequencies over a finite period.
- 3) by platform stabilization, the most convenient but most expensive solution may be obtained. Positional data are introduced to the autopilot; the attitude of sensor or antenna is maintained by an inertial platform. For radar (without interferometer) ω -stabilization is only required to improve resolution.
- 4) by orientation process; while an approximate relative orientation process for nearly flat terrain has been analyzed by Derenyi [7], a strict and more promising orientation possibility using a block adjustment using collinearity equations for transfer and control-point is being investigated by Dowdeit [10]. The orientation parameters may be expressed as Fourier-functions of time. Undesirable correlations existing between the chosen parameters may be appropriately constrained.
- 5) by interpolation; an interpolation procedure using polynomials, piece-wise polynomials or least squares interpolation in conjunction with a simplified mathematical model has been the standard application in previous tests and is continuing to be used.

TEST RESULTS OBTAINED BY ANALYSIS

While reference is made to the individual papers, wherever appropriate, a summary of test results obtained this far is given below:

A - RADAR

1) In 1972 results were obtained from an analysis of Westinghouse real aperture radar stereo imagery over New Guinea (scale 1 : 300 000, h = 6,5 km) at the TU Hannover [8]:

opposite side stereo
(R.M.S. values of check points)

same side stereo

$$\begin{aligned}\sigma_x &= \pm 68 \text{ m} \\ \sigma_y &= \pm 138 \text{ m} \\ \sigma_z &= \pm 240 \text{ m}\end{aligned}$$

$$\begin{aligned}\sigma_x &= \pm 130 \text{ m} \\ \sigma_y &= \pm 428 \text{ m} \\ \sigma_z &= \pm 1548 \text{ m}\end{aligned}$$

2) For opposite side imagery over Dutch flat terrain slightly better values were obtained in planimetry by Leberl [11]:

$$\sigma_x = \pm 62 \text{ m}$$

$$\sigma_y = \pm 76 \text{ m and}$$

3) at the Rijkswaterstaat [12]:

$$\sigma_x = \pm 48 \text{ m}$$

$$\sigma_y = \pm 70 \text{ m.}$$

The difference is most likely due to extreme elevation differences ($h = 1800 \text{ m}$) and interpretation difficulties in the Guinea imagery.

4) Within the working group a test has been carried out for coherent, synthetic aperture radar imagery flown with a Goodyear GEMS 1000-radar (scale 1:400 000, $h = 12 \text{ km}$) over Phoenix, Arizona.

This imagery consisting of 6 parallel strips has been made available to the group by Goodyear and the Aeroservice Corp. It was reproduced in Hannover and distributed to all working group participants. The US-DMA-TC provided 1 / 24 000 topographical maps of the area. On these 510 topographical features visible on the images were identified. The map coordinates of these points were measured with a digitizer. The selected points served as control or check points for the test. These values were distributed by the TU Hannover to 9 participants having shown an interest in the test. Results have so far been obtained from three institutions:

- at the Rijkswaterstaat (Clerici, Kubik) two section each in two strips were measured monocularly on a Kern PG-2. The measured data were subjected to a polynomial fit in planimetry:

Table 2: Phoenix Test Results obtained at the Rijkswaterstaat

strip no.	section no.	no of points measured	no of control points	no of check points	no of points rejected	residuals at control points		residuals at check points	
						σ_x	σ_y	σ_x	σ_y
						\pm	\pm	\pm	\pm
1	1	33	17	16	2	3,2 m	3,2 m	54,4 m	23,9 m
2	1	42	17	25	3	1,1 m	5,1 m	44,9 m	60,0 m
1	2	19	10	9	2	1,2 m	0,9 m	60,6 m	25,7 m
2	2	17	9	8	1	1,0 m	1,9 m	61,1 m	22,6 m

- at the University of New Brunswick (Derenyi [13]) two strips overlapping opposite were measured on a Zeiss PSK stereocomparator. Only well identifiable points were selected. They gave after polynomial transformation results of $\pm 27,4 \text{ m}$ in position and $\pm 30,7 \text{ m}$ in elevation.
- at the Technical University of Hannover 3 overlapping strips were measured as 4 image coordinate strips in a PSK stereocomparator. Strip 1 overlapped with strip 3 in the same direction; strip 1 overlapped with strip 2 in the opposite direction. Strip 1 was therefore measured twice. Radar parallaxes and radar shadow differences were larger in the combination of strips 1 and 2. The interpretation due to better stereoscopic viewing was better for strips 1 and 3. Considerable difficulty was encountered in proper identification of the chosen control. Street corner crossings, road forks, hill tops or creek bends chosen as control were sometimes misidentified. The 4 strips were subjected to a Helmert transformation in planimetry. Points with discrepancies larger than 3σ were rejected.

They mostly coincided with points, which during measurement already had been marked as uncertain. The results obtained so far are summarized as follows:

Table 3: Phoenix Test Results obtained at the Technical University Hannover

strip no.	no of points measured	no of points rejected	residuals after Helmert-Transform.	
			σ_x ±	σ_y ±
3	440	26	133 m	41 m
1	436	23	60 m	38 m
1	447	30	80 m	79 m
2	417	29	46 m	65 m

Further processing of these data with the Dowideit program [10] is intended for x, y and z.

5) Leberl undertook to investigate a 360 000 km² planimetric block flown with a GEMS 100 Goodyear coherent radar over Colombia. His residuals after planimetric adjustment described in [14] and converted into meters amount to

$$\sigma_x = \pm 220 \text{ m}$$

$$\sigma_y = \pm 280 \text{ m}$$

after adjustment with piecewise polynomials.

B - SCANNERS

1) An HRB-Singer Reconofax Infrared Scanner imagery test has been reported by the author in [8]. The flight data were: h = 1500 m, $2\theta = 120^\circ$, c = 28,5 mm. After space transformation, the following R.M.S. values were obtained at 36 check points:

$$\sigma_x = \pm 13 \text{ m}$$

$$\sigma_y = \pm 7 \text{ m}$$

$$\sigma_z = \pm 8 \text{ m}$$

2) The same imagery was remeasured with a larger number of points in a diploma theses at the TU Hannover (Liebig 1973):

Table 4: Infrared Scanner Test TU Hannover 1973

type	strip no.	σ_x	σ_y
single image	1	24 m	60 m
single image	2	23 m	62 m
model	1/2	16 m	12 m

An attempt to improve the accuracy by computing orientation parameters from control without imposing constraints on the orientation elements and then computing coordinates from these failed.

3) Investigations carried out at Purdue University with the University of Michigan multispectral scanner are reported in [15]. At $h = 1500$ m (ground resolution element 14 m) results of ± 36 m and ± 19 m respectively have been obtained, depending on the method of adjustment.

C - SATELLITE SCANNERS

Satellite scanner accuracy has also been tested.

- 1) A diploma thesis at the TU Hannover (Schuhr 1973) investigated the gridding accuracy of Nimbus 3-Satellite photographs. Using a photo covering Europe with 73 chosen control points a positional accuracy of $\pm 0,13$ mm was obtained (= ± 7 km; a resolution element is about 8,5 km).
- 2) Investigations on bulk ERTS satellite scanner imagery have first been carried out by Colvocoresses and McEwen [16], quoting check errors of $\sigma_{x,y} = \pm 145$ m after linear transformation.
- 3) Bähr and Schuhr from the TU Hannover [17] obtain comparable values.
- 4) The accuracy may be considerably improved using second degree polynomial-interpolation or least squares interpolation to about ± 50 to 60 m (Bähr [18]), below the nominal resolution of 79 m.

MAPPING

After an analysis has led to the improvement of the mathematical level to the stated accuracy, mapping of point and line detail becomes possible on-line by an analytical plotter system. Any analytical plotter may be used if it is programmed accordingly. (AS-11 A at US D.M.A.A.C.) (AP/C at University of New Brunswick, TU Hannover in progress). A special analytical plotter for the restitution of radar imagery has been built for the Engineering Topographical Laboratories of the US Army by Goodyear.

Another possibility is off-line plotting using a digitizer and an automatic drafting machine as used by the Rijkswaterstaat [12].

IMAGE GRIDDING AND DIFFERENTIAL RECTIFICATION

From the viewpoint of data handling or automatic processing it may be preferable to use geometrically annotated or corrected images as a product.

In order to make the operations of image gridding and differential rectification possible, as required for remote sensing, the images must first be available as scan records either in analog or preferably in digital form. This is possible by a scanning microdensitometer or a drum read-system (e.g. Optronics 1700), a CRT or a laser reader.

Satellite imagery or some multispectral imagery has the principal advantage that it can already be obtained in computer compatible tape form. Therefore one only needs to deal with the output. The output can be carried out by devices listed in table 5.

Satellite imagery, as well as multispectral scanner imagery is available to the user generally in already partially processed form, the so-called "bulk image".

Table 5: Digital image Output Devices.

Principle	Model	Resolution	Format	Grey Scale Values	Speed	Accuracy	Remarks
line printer	-	130 pixels per line	40 cm	4 to 13	1000 chars p. sec.	-	available
drum plotter	Optronics P - 1700 Prakla	12,5 m 10.000 elements	12,5 cm	128	480 RPM	0,02 %	relatively inexpensive
CRT	IBM 4481	4096 elements	2,5 cm	64	27 sec per element	0,5 %	fast
ink jet plotter	color jet A.B. Lund/Sweden	5 lines per mm	20 x 29,4 cm	3 colors	60 sec per picture	-	inexpensive reproduction
electron beam recorder	E.R.T.S.	6000 lines	5,7 cm	100	120 m/sec per image	0,3 %	very fast, analog use possible
laser beam recorder	R.C.A.	20.000 pixels	12 cm	30	0,6 cm per sec	0,005 %	extremely accurate

Therefore only the deviation from bulk to precision image (as derived from the analysis) needs to be corrected. The geometrical processing scheme carried out for ERTS satellite imagery may therefore be considered as a model for any remote sensing processing scheme:

1) Partial processing from the scanned records received is carried out according to the approximately known mathematical rectification model, as best as theory and known orientation or calibration data permit (for ERTS images this means correction by position and attitude data and eventually the figure of the reference surface through the electron beam recorder).

The rectification model should include the following options:

- a - transformation from ground reference system to ellipsoid to projection
- b - computation of image coordinates as a subroutine optionally for photography, scanning or radar
- c - the removal of image distortions known by calibration or reseau (timing) marks
- d - the removal of terrain displacements if a (digital) terrain model is known (e.g. by model scanning or by the contours of a map).

2) In the reconstituted bulk image recognizable features, whose ground coordinates may be determined from existing maps, standard aerial photographs or by ground measurements are identified (for satellite imagery the selection of such features may sometimes be difficult).

3) The image coordinates of these features are measured and compared with the ground coordinates. If the initial image is available in digital form it is of course possible to substitute the measurement operation by the counting of pixels. The Jet Propulsion Laboratory enhances in Mars Mariner photographs digitally every 25th pixels and thus obtains a superimposed grid on the image for the purpose of counting.

4) From differences between bulk image and ground coordinates correction functions may be derived:

- a - The simplest measure is to compute the coefficients of a correction polynomial.
- b - Other interpolation procedures such as least squares interpolation may be used.
- c - It is also possible to improve the orientation parameters of the imagery by an adjustment procedure.

- 5) According to the correction function the new positions of the image pixel centres are computed. The pixel center maintains the previous grey-scale value.
- 6) Grey-scale values must then be assigned to the rectangular output pixel grid. While the theory of image processing is still uncertain about the most suitable grey-scale assignment, a method more suitable than interpolation (maintaining contrast) appears to be the nearest neighbourhood assignment of grey-scale values:
Each output pixel obtains the grey-shade of the nearest rectified input pixel center.
- 7) The sequence of grey-values for the output pixels may be used for producing the precision image.

Programs of this nature are already in operation (IBM) or under development (LARS, TU Hannover).

CONCLUSION

The aims of the working group have so far principally been directed to analyze the potential of radar as a mapping tool. While standard photography yields accuracies of less than 1/3 of the resolution limit of aerial photography, the accuracies obtained in the Phoenix Radar test corresponded to about 3 times the resolution of radar images. While radar mosaics can be laid out to 1 : 250 000 mapping specifications, there is hope, at least geometrically, to map to higher specifications. Particularly the height accuracy obtained looks promising for applications in highly mountainous countries. For this special procedures need to be developed.

With respect to satellite imagery a restitution to resolution limit is possible using simple correction functions. Also for multispectral and infrared scanning geometric accuracy of 1 to 2 times the resolution is obtainable after interpolation to control. While this has been demonstrated in the analysis the implementation of change detection to that accuracy requires the setup of a processing system using digital differential rectification in which the determination of interior and exterior orientation parameters, the interpolation to control and the consideration of terrain displacement is included.

The development of these procedures will be the further aim of the working group.

REFERENCES

- [1] Derenyi E. and Konecny G.: "Geometry of Infrared Imagery", Canadian Surveyor 1964 (279-290)
- [2] Derenyi E. and Konecny G.: "Infrared Scan Geometry", Photogrammetric Engineering 1966 (113-118)
- [3] Case J.B.: "The Analytic Reduction of Panoramic and Strip Photography" Photogrammetria 1967 (127-141)
- [4] Leberl F.: "Metric Properties of Imagery Produced by Sidelooking Airborne Radar and Infrared Linescan Systems", ITC-Series A, No. 50, 1971 (125-151)
- [5] Konecny G.: "Metric Problems in Remote Sensing", ITC-Series A, No. 50, 1971 (152-177)
- [6] Leberl F.: "On model formation with remote sensing imagery", Österr. Zeitschrift für Vermessungswesen 1972 (43-61)
- [7] Derenyi E.: "Relative Orientation of Continuous Strip Imagera", Thesis, University of New Brunswick, 1970
- [8] Konecny G.: "Geometrical Aspects of Remote Sensing", Comm. IV, Internat. Congress of Photogrammetry 1972
- [9] Konecny G.: "Geometrische Probleme der Fernerkundung", Bildmessung und Luftbildwesen 1972/4
- [10] Dowideit G.: "Simulation and theoretical analysis of radar restitution", ISP Symposium, Comm. III, Stuttgart 1974
- [11] Leberl F.: "Untersuchung über die Geometrie und Einzelbildauswertung von Radarschrägaufnahmen", Dissertation, TU Vienna 1971 and ISP, Comm. II, 1972
- [12] Bosmann E., Clerici E., Eckhart D., Kubik K.: "Project Karaka", Bildmessung und Luftbildwesen 1972
- [13] Derenyi E.: "Topographic Accuracy of Sidelooking Radar Imagery", Bildmessung und Luftbildwesen 1975/1
- [14] Leberl F.: "Planimetric Adjustment of SLAR Block Proradam", Bildmessung und Luftbildwesen 1975/1
- [15] Baker J.R., Marks G.E., Mikhail E.M.: "Analysis of Digital Multispectral Scanner Data", Bildmessung und Luftbildwesen 1975/1
- [16] Colvocoresses A. and McEwen R.: "EROS Cartographic Progress", Photogrammetric Engineering 1973
- [17] Bähr H.P. und Schuhr W.: "Versuche zur Ermittlung der geometrischen Genauigkeit von ERTS Multispectralbildern", Bildmessung und Luftbildwesen 1974
- [18] Bähr H.P.: "Interpolation and Filtering of ERTS-Imagery", Bildmessung und Luftbildwesen 1975/1

GEOMETRIC PROBLEMS IN SIDE-LOOKING RADAR IMAGING

by L.C. Graham, Phenix, Arizona

PRINCIPLE OF OPERATION

This paper describes the operation of airborne synthetic aperture side-looking radar systems, with emphasis on the geometric properties of the imagery.

Side-looking systems produce images of terrain by transmitting short pulses of microwave energy through an antenna beam which is wide in the vertical direction and narrow in the horizontal direction, as shown in Figure 1.

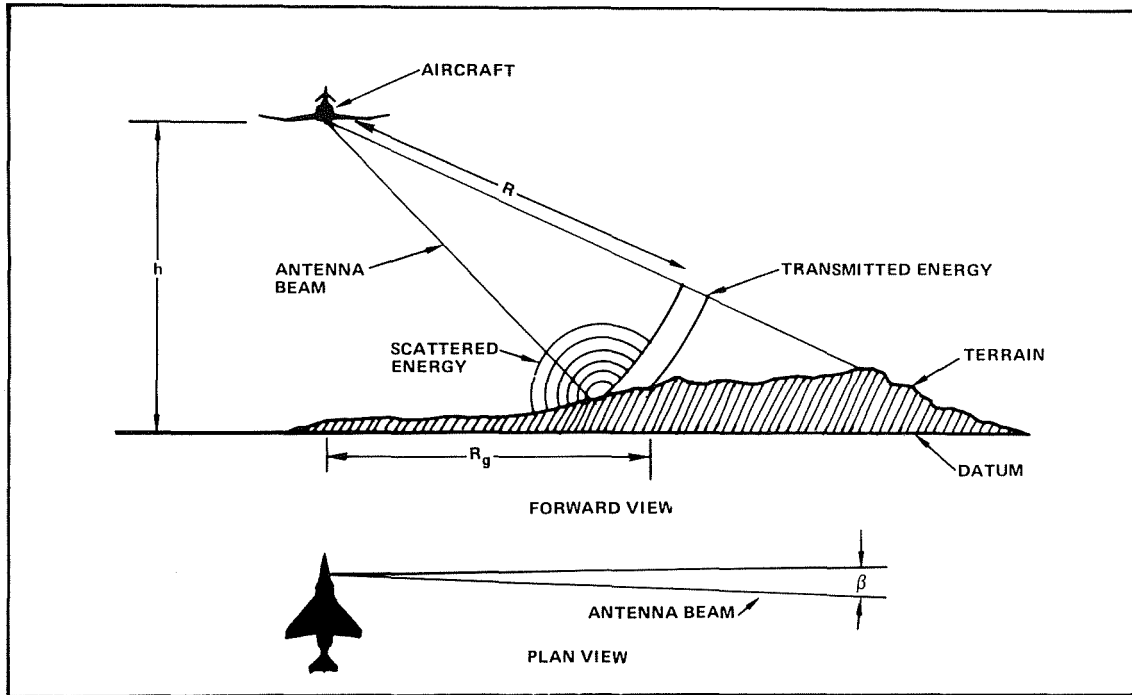


Figure 1 - Radar Operation

A portion of the energy scattered from the terrain is received back at the aircraft and used to construct a two-dimensional record of backscattered energy. For a given position of the aircraft the returns are plotted as a function of time from each transmitted pulse. The record is formed by causing the transmission of a photographic material to correspond to returned signal strength and thus terrain backscattering strength, as shown in Figure 2.

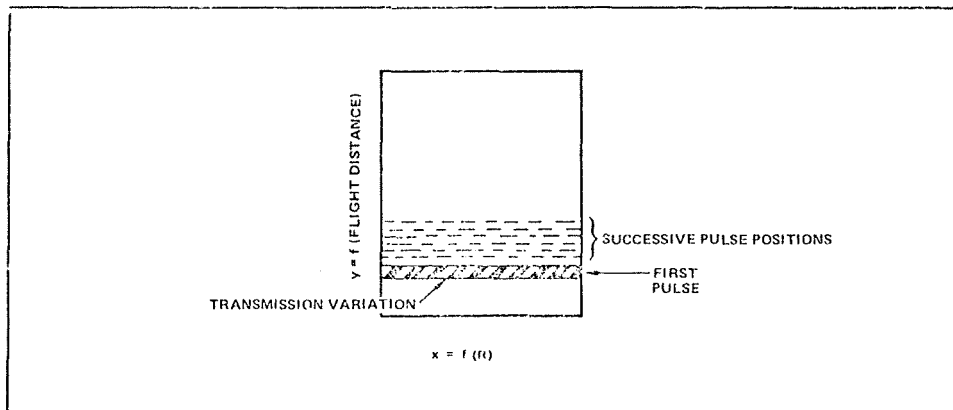


Figure 2 - Image Coordinates

Return data from each successive pulse are recorded alongside the data from the preceding pulses so that an area image is built up. Where the across-track time coordinate is linear, it is proportional to distance from the flightline R (slant range distance). If the velocity of propagation is c , then $R = ct/2$ and $x = pR = pct/2$, where p is the image scale and t is time measured from pulse transmission. In many applications, the across-track coordinate is made proportional to ground range R_g , the distance from the flight track in a horizontal reference datum plane.

In this case, the coordinate is $x = pR_g$. By triangulation,

$$R_g = (R^2 - h^2)^{1/2} = (c^2t^2/4 - h^2)^{1/2}$$

so that

$$x = p(c^2t^2/4 - h^2)^{1/2} \quad (1)$$

The along-track coordinate is made proportional to distance along the track, so that

$$y = pvt \quad (2)$$

where

- v = aircraft velocity
- t = time measured from start of imaging pass.

Image resolution is determined from radar technical parameters. The across-track resolution, measured always in the slant range direction, is proportional to the length of the transmitted pulse in nonchirped radars. Because of the two-way transmission, objects spaced greater than $\tau/2$ are separately discernible, so that

$$w_R = c\tau/2 \quad (3)$$

where w_R = slant range resolution and τ = time duration of transmitted pulse.

Usually, system bandwidth is made proportional to the band of signals required to form the pulse $\overline{BW} \approx 1/\tau$ so that

$$w_R = c/2 \overline{BW} \quad (4)$$

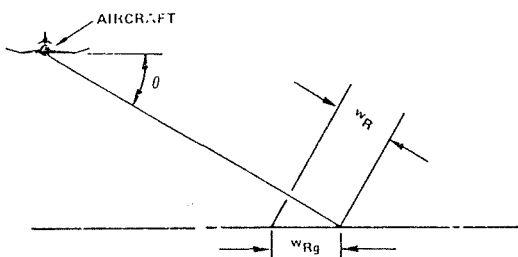


Figure 3 - Datum Plane Resolution

The resolution measured in the datum plane direction is degraded because objects spaced along the datum plane are separated less in the slant range direction as shown in Figure 3.

From the figure, where w_{R_G} = datum plane resolution and θ = depression angle,

$$w_{R_G} = w_R / \cos \theta \quad (5)$$

Along-track resolution in older radars is determined by the antenna beamwidth β and range as:

$$w_y = R\beta \quad (6)$$

The antenna beamwidth is determined by the length of the antenna L and signal wavelength λ by the rayleigh criterion $\beta = \lambda/L$. For wavelengths long enough to guarantee good weather penetration, i.e., longer than about 2 cm, fine resolution at usable ranges requires that antenna length be greater than that convenient to carry on an aircraft. Therefore, modern synthetic aperture systems store the signals received along the flightpath using a short physical antenna and sum them vectorially to synthesize a long antenna or aperture, L_s , as shown in Figure 4.

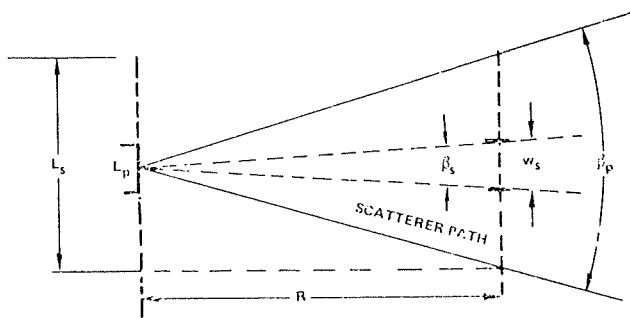


Figure 4 - Synthetic Antenna Formation

In Figure 4, the path taken by a scatterer moving through the physical antenna beam generates a synthetic antenna whose maximum length is

$$L_s = R\beta_p = R\lambda/L_p, \quad (7)$$

where L_p is the length of the physical antenna and β_p is its beamwidth.

The best achievable resolution of this synthetic antenna is

$$w_s = R\lambda/2L_s = R\lambda/2R\lambda/L_p = L_p/2. \quad (8)$$

The factor of 2 is included because, with the two-way path, the vectors in the signal summation have twice as much successive phase shift as for a system with a one-way path. This factor of 2 should not be used to compare real and synthetic antenna systems because a focused real antenna of length, L_s , would be used twice once each for transmitting and receiving, resulting in comparable resolution.

Also note that this values of half the physical antenna size is the diffraction limited, or theoretical best resolution. In practice, the limit is seldom reached for reasons which will be discussed later.

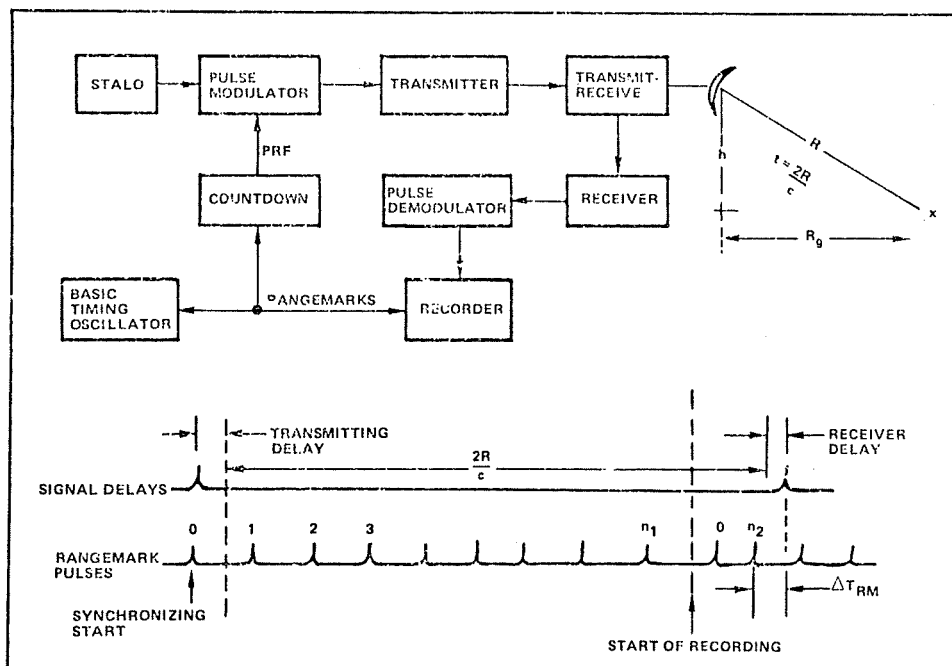
IMAGE GEOMETRY

- SLANT RANGE MEASUREMENT

The most accurate measurement made by the radar system is that of distance from the flightline to objects which appear in the image. This is basically a time measurement. A crystal-controlled oscillator generates rangemarks which are recorded along with the radar data and appear in the image. The basic measurement accuracy is on the order of the system resolution described earlier. In a particular system, such accuracy can be achieved only, however, if the internal time delays are calibrated (known). The relationship of the rangemark measurement to slant range distance is illustrated in Figure 5.

Figure 5

Range Measurement



As shown in Figure 5, the absolute distance to an image feature is determined as follows:

$$T_T + \frac{2R}{C} + T_R = n_1 T_{RM} + n_2 T_{RM} + \Delta T_{RM}$$

$$R = \frac{C}{2} (n_1 T_{RM} + n_2 T_{RM} - \Delta T_{RM} - T_R - T_C) ; \quad (9)$$

where

- n_1 = number of rangemark pulses before recording
- n_2 = number of rangemarks recorded before feature
- T_T = transmit delay
- T_R = receive delay
- T_{RM} = time between rangemarks
- ΔT_{RM} = interpolated time from rangemark to feature
- C = velocity of propagation
- R = distance to image feature in slant range.

In case the recording time base is linear, then the final image across-track coordinate is proportional to slant range distance from the flightpath, R , as described earlier; and the measurement accuracy is in that direction. The limiting accuracy in ground range is degraded according to Equation (5).

- ALONG-TRACK COORDINATE

The basic along-track coordinate is determined by driving the signal and image film at speeds proportional to the velocity of the aircraft so that $y = p$ (aircraft distance).

- IMAGE ERROR SOURCES

a - Aircraft Position

Because all measurements are made with respect to the airborne platform, uncertainties in its position and velocity result in errors in the final image. Therefore, accurate measurement requires the use of high quality navigation equipment in the aircraft. The basic navigation system normally used is the inertial navigation system (INS). This can be supplemented by doppler navigators, ground control, and/or radio navigation equipment such as SHORAN or HIRAN.

In addition to the fact that uncertainties in the aircraft horizontal position along the average flightpath determine the overall position in the final image, errors in altitude and variations of position along the average flightpath produce internal errors in the image.

b - Altitude Uncertainty

Equation (1) may be differentiated to produce

$$\frac{dR_g}{R_g} = -\frac{h^2}{R^2} \frac{dh}{h} = -\tan^2 \theta \frac{dh}{h} ; \quad (10)$$

where θ is the depression angle from the flightpath.

Thus, errors in aircraft altitude produce errors in across-track position which are small at shallow angles but large at steep angles. Errors of one-half percent or so are not uncommon in altitude measurement so that a nonlinear scale distortion of a percent or more might be expected. Of course, the rangemarks undergo the same distortion so that measurements with respect to them are not affected, except for a second order effect in interpolation accuracy. Rangemarks are normally spaced equally in slant range and this should be taken into account for accurate interpolation. Thus, altitude uncertainty need not affect accurate range measurement.

c - Elevation Displacement

Equation (10) also predicts the amount of elevation displacement to be expected from objects above or below the datum plane. As in photography, the differential displacement from noncolinear flightpaths can be used to measure the elevation of terrain features. The accuracy of such a measurement is limited by system resolution and the knowledge of flightpath position. Also, a visual model may be obtained by viewing two such images stereoscopically, but an apparent overall warping is observed because of the differences between radar and optical elevation displacement.

d - Along-Track Errors

1) Scale

Several possible error sources in the total system can contribute to an error in the along-track scale. The principal error is in the knowledge of aircraft velocity. Other possible sources are in converting this velocity to recorder signal film drive velocity and in synchronizing image film velocity to signal film velocity in the optical correlator. Of course, if sufficient ground control or accurate navigation data are available, this error can be removed in data reduction or in image correlation.

2) Pointing Errors

Probably the largest source of error in side-looking radar is the accuracy of pointing the synthetic beam with respect to the nominally straight line flightpath. Formation of a particular synthetic aperture, i.e., integrating the return over a flightpath distance long enough to produce the desired resolution, is equivalent to forming a parabolic surface in space which would cause plane wave energy (coherent light in the optical correlator) to focus to a point at the image.

Failure to achieve a straight line flightpath results in distortions in this parabolic surface resulting in various degradations to performance, depending on the nature and magnitude of the distortion.

Because the flightpaths achievable in practice are in general not sufficiently straight to ensure adequate system performance, deviations are sensed and corrections made to secure the performance desired. The levels of residual degradation after this correction, then, are the limiting performance parameters. Figure 6 shows the parabolic surface corresponding to ideal operation, an assumed surface, and a decomposition of the difference between actual and ideal surfaces.

As shown in Figure 6, a general error in generation (or correction) of this surface can be decomposed into a linear portion, a parabolic portion, and higher order portions. The linear error results in a pointing error, the parabolic in a focus error resulting in loss of along-track resolution, and the higher order terms cause noise. The linear errors are the ones of interest in the present discussion of accuracy and geometric fidelity.

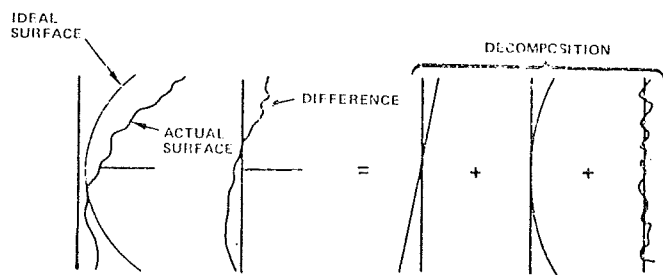


Figure 6 - Synthetic Aperture Degradations

Several kinds of equipment and techniques are available to effect corrections to the synthetic aperture errors. Antenna-mounted accelerometers measure the short term (high frequency) deviations from a straight line flightpath to maintain resolution and control noise and sidelobes. Usually, an inertial navigation unit is available to supply velocity signals and to stabilize the antenna in space. One or more antenna-mounted gyros may be used to supplement or replace inertial system stabilization signals. Doppler navigators sometimes perform some of these functions. Finally, the radar signals themselves can provide information about antenna pointing.

The use of the radar signals to provide synthetic antenna pointing depends on the fact that the radar can perform an accurate measurement of the doppler frequency shift of the signals caused by relative motion between the aircraft and terrain scatterers. As shown in Figure 7, the antenna beam will be in general misaligned by some angle θ . The doppler shift in the signal from a scatterer in the real antenna beam is $f_D = 2v/\lambda \sin\theta$. Electronic circuitry in the radar, referred to as a clutterlock system, effectively measures the energy in the signal having positive doppler shift and balances this against energy having negative doppler shift, providing a signal to either (1) drive the antenna so that the beam is aligned with the zero doppler line (normal to the flightpath) and/or (2) offset an electronic reference to receive and process signals in the center of the physical beam, thus steering the synthetic antenna.

A limitation to this technique is that the process generates a certain amount of noise because of both high and low spatial frequency variations of energy in the beam caused by the rough terrain. Therefore, the signals are averaged over several thousand feet of distance traveled. High frequency aircraft motions are corrected by signals from inertial components.

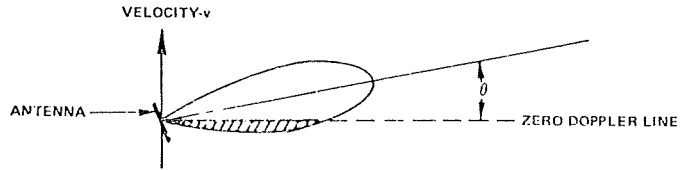


Figure 7 - Clutterlock

An example of the application of these techniques is illustrated in Figure 8, which is conceptual only and does not illustrate the actual complex interconnections between components.

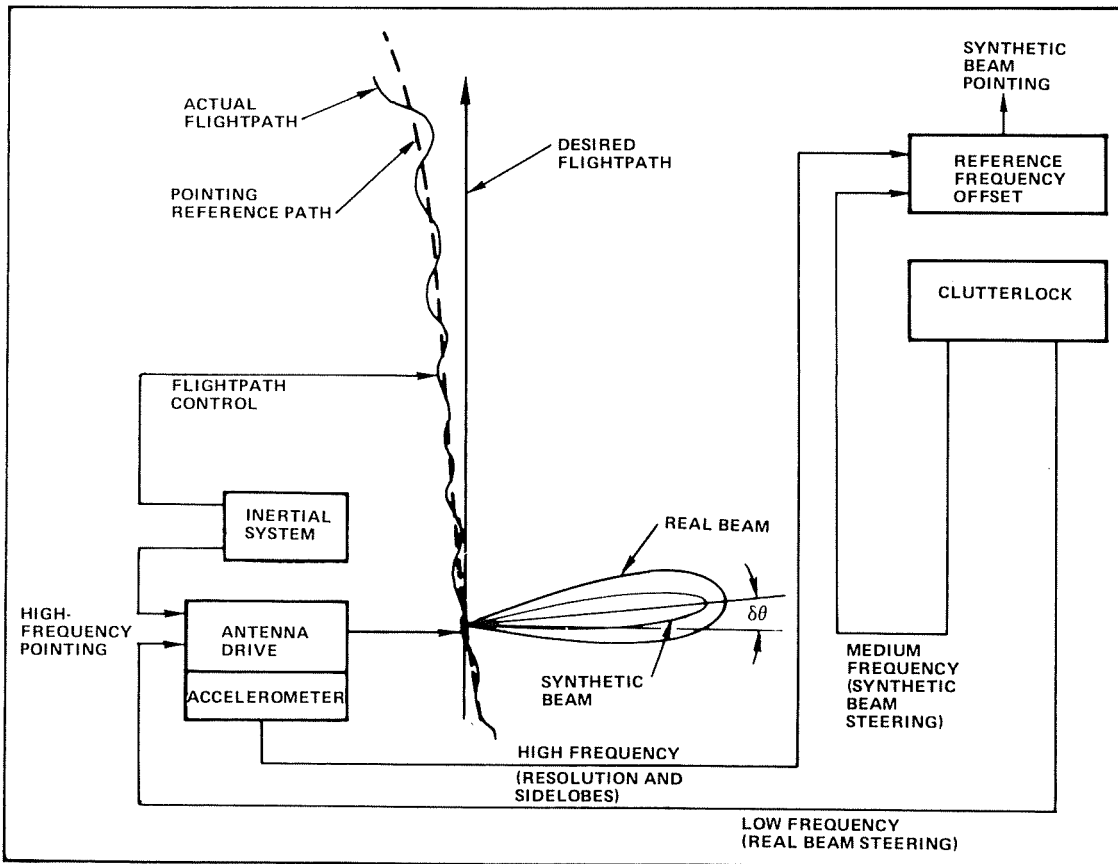


Figure 8 - Synthetic Antenna Pointing Methods

With the particular arrangement, both real and synthetic beams are steered by the clutterlock to be maintained at a right angle to the average flightpath achieved by the inertially guided aircraft. High frequency flightpath errors affecting system resolution and sidelobes are corrected by the antenna-mounted accelerometers.

Thus, flightpath deviations having spatial wavelengths on the order of several synthetic antenna lengths and shorter are corrected by the accelerometers. Deviations having wavelengths from a few synthetic antenna lengths to several miles are corrected by the clutterlock in steering the synthetic beam to match the real beam. Lower frequency errors are corrected by using clutterlock signals to steer the physical beam to the normal to the averaged flightpath.

Order of magnitude errors caused by the lack of precision of the components may be estimated as follows. If the inertial system performance is characterized by a velocity error on the order of δV , then an across-track error of $T\delta V$ can occur in a distance along track of vT . The resulting angular error of the flightpath between these points is $\delta\theta = T\delta V/vT = \delta v/V$. For example, a 4-NM/HR inertial system in a 400-NM/HR aircraft could generate angular errors on the order of 1/100 rad or 0.57 deg.

Clutterlock accuracies in beam steering are usually on the order of one-tenth the physical beam. For a one-deg beam, this amounts to about 0.1 deg.

If a more accurate measurement or control of the flightpath can be established by ground control or a ground navigation system such as SHORAN, the INS velocity error can be largely removed by data processing.

Both errors are RMS values averaged over a time period and may be exceeded for short periods. For example, the clutterlock errors can build up to be several times this value when land water boundaries or other large variations cause half the antenna beam to contain large scatterers compared to those in the other half. This can be minimized by proper choice of system time constants.

The residual error after corrections from the use of ground control and flightpath measurement data is seen to be on the order of one-tenth the physical beamwidth. In a system having a physical beam on the order of one degree, the linear along-track error at practical mapping ranges, say 50 kilometers, is then on the order of

$$\delta y = R\delta\theta = (50 \text{ km})(0.1)(\pi/180) = 90 \text{ m } (1\sigma). \quad (11)$$

This is strictly an order of magnitude value, and actual values will depend on the particular system, the kind of control, the roughness of the flight, and other variables.

If the flightpath is not horizontal momentarily, the synthetic beam will lie entirely ahead of or behind the normal to the average flightpath. This error is usually small compared to the others because the (pitch) angular error is of the same magnitude or smaller than the yaw error but the lever arm (altitude perhaps 10 kilometers) is much smaller than the maximum lever arm for yaw errors; i.e., maximum range of 50 kilometers. Thus, the error would not be expected to be as high as 20 meters.

Another error source which is normally small but occasionally must be considered is the fact that a clutterlock error or synthetic beam correction causes the synthetic beam to be on a doppler cone rather than in the vertical plane containing the radar and a terrain point. Because $f_d = 2v/\lambda \sin \theta$, the locus of constant f_d for $\theta \neq \theta_0$ is a cone whose axis is the flightpath and whose intersection with the datum plane is a hyperbola. The geometry is shown in Figure 9.

In the figure, line o-p is an element of the doppler cone whose semi-apex is $\alpha = \pi/2 - \theta_0$. Point p lies on a circle with center o at $y = y_p$ parallel to the x, z plane

$$x^2 + z^2 = y^2 \tan^2 \alpha, \quad (12)$$

which intersects the datum plane $z = h$, so that

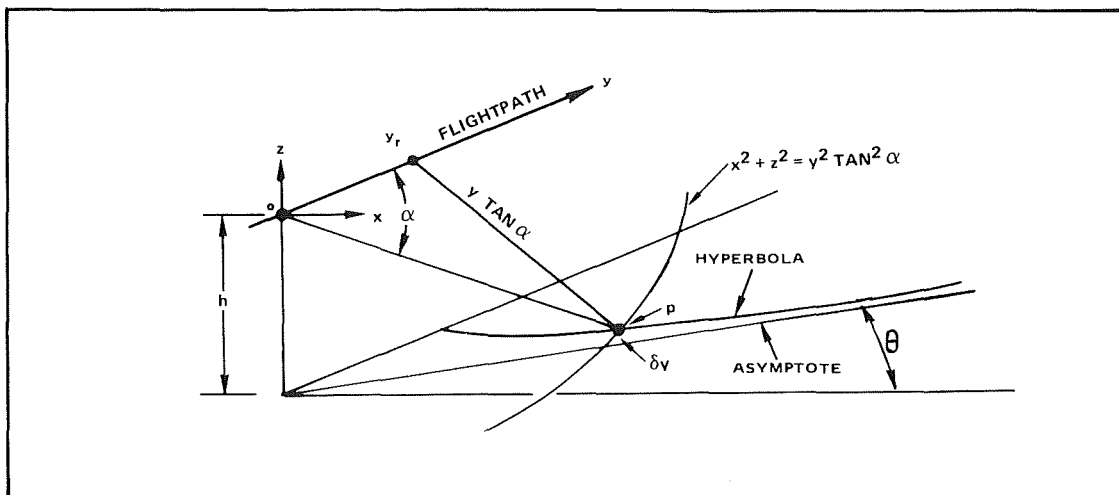


Figure 9 - Doppler Cone Geometry

$$y = (x^2 + h^2)^{1/2} / \tan \alpha \tag{13}$$

is a hyperbola in the datum plane.

For large x, the hyperbola is asymptotic to the line $y = x / \tan \alpha$, so that the error between the position of imaged point p and the assumed position in the plane $\theta = \text{constant}$ is

$$\delta y = (x^2 + h^2)^{1/2} / \tan \alpha - x / \tan \alpha \tag{14}$$

For example, for $h = x = 40\,000$ ft, $\alpha = 90 \text{ deg} - 0.1 \text{ deg} = 89.9 \text{ deg}$, so $\delta y = 28.9$ ft.

It should also be noted that elevated terrain having the same range R and doppler angle α as a point in the datum plane must also lie on the same circle so the elevation displacement is always toward the flightpath and in a direction normal to it.

CONCLUSIONS

Synthetic aperture radar systems are now available for exploration and mapping under adverse weather conditions. With proper care in navigation and ground control, accuracies of 100 meters or so over distances of 50 kilometers are realizable with equipment now available commercially. More precise measurements than those estimated here in connection with Equations (7), (8), (9) and (10) can be made by providing more precise measurement and control of flightpaths and antenna orientation. Improved performance can also be obtained by programming additional flightpaths to take advantage of the most accurate measurement made by the radar, i.e., slant range. Two flights at right angles can reduce the radar measurement error to the order of the range resolution for all points recognizable in both images.

RADARGRAMMETRIC POINT DETERMINATION "PRORADAM"

by F. Leberl, Enschede, The Netherlands

SUMMARY

PRORADAM (Proyecto Radargrametrico del Amazonas) is a Colombian reconnaissance type mapping project of about 360 000 km², using airborne sidelooking radar (SLAR). The paper deals with the procedures used and problems encountered in a planimetric adjustment of the block of SLAR image strips, making use of 44 ground control points. The adjustment was split into 2 steps: block formation and external adjustment. Accuracies obtained could be evaluated by comparing the adjusted block with independent ERTS-MSS images. Root mean square discrepancies between ERTS and SLAR amount to ± 1.5 mm at image scale 1 : 400 000.

INTRODUCTION

The present paper reports on the Colombian mapping project PRORADAM. This name stands for "Proyecto Radargrametrico del Amazonas" and refers to a reconnaissance type of mapping project using airborne sidelooking radar imagery, covering southern Colombia, about 360 000 km² (see figure 1). The prime cartographic product was to be a set of mosaics in the Colombian Gauss-Krueger projection at a scale of 1 : 200 000.



Figure 1: Project area PRORADAM within Colombia, covering nearly 400 000 km²

By now the entire Amazonas basin is covered by SLAR imagery. However, compared to the Brazilian, Venezuelan and Peruvian projects, the Colombian PRORADAM represented a novelty as for the first time the metric base for mosaicking was produced through a block adjustment with the SLAR imagery. In other projects, the Brazilian or Peruvian, precise auxiliary data (aircraft tracking by SHORAN) were considered to render such adjustment superfluous; or, as in Venezuela, mosaics were simply uncontrolled.

In Colombia the previously mentioned auxiliary data were not measured. But a 60 % sidelap between adjacent image strips, as well as the presence of 44 ground control points, made it very logical to attempt an adjustment. The work was carried out by the International Institute for Aerial Surveys and Earth Sciences (ITC, Enschede, Netherlands) under a contract with Aero Service Corp. of Philadelphia. This company acquired the imagery and prepared the mosaics.

In particular the paper will consist of an account of the procedures used and problems encountered in the adjustment. The procedures were chosen in view of a rather severe time constraint; this constraint resulted from the fact that an adjustment was not planned initially. The actual adjustment was split into an internal and external one, preceded by initial strip formation and correction of systematic image deformations.

IMAGE ACQUISITION

Goodyear's synthetic aperture radar was used in Aero Service's Caravelle jet. Image scale in this system is always 1 : 400 000. Flight lines were spaced 13,7 km, directed NS, and imaging was always in the same direction (see figure 2).

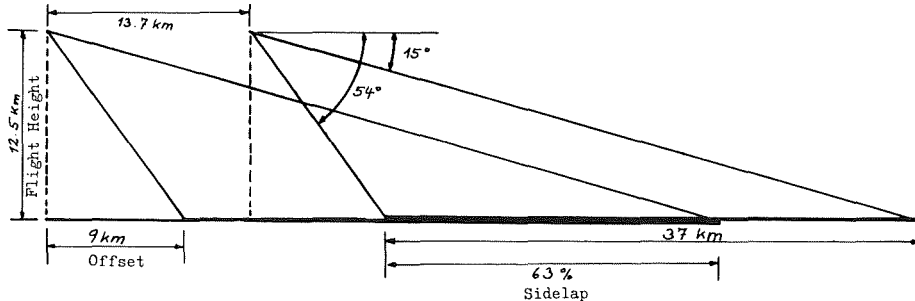


Figure 2: SLAR imaging geometry to obtain 60 % overlap

Flying height a.m.s.l. was 12.5 km. Seventy flight lines were planned but 30 re-flights were necessary (40 %!). These re-flights had to replace images with serious defects due to electronic failure, heavy rain or turbulence |3|.

Due to resolution of the CRT, each image strip is presented in two parts. This would correspond in aerial photography to photography cut into two pieces. There is, however, a slight overlap of 5 % between the pieces of an image strip. One piece corresponds to the range nearer the flight line, the other piece to the range farther from the flight line. Therefore, the 2 pieces are called "near range" and "far range view". Geometrically, the 2 pieces can be considered as one unit.

Apart from the NS flight lines, there were 3 EW transverse flights flown, producing so called "tie-lines". This was done at a time when it was expected that no ground control would be available. But in the progress of the project it turned out that the Inter-american Geodetic Survey was about to measure Doppler Satellite points in the mapping area. Consequently there were ground control points available for mosaicking as shown in figure 3.

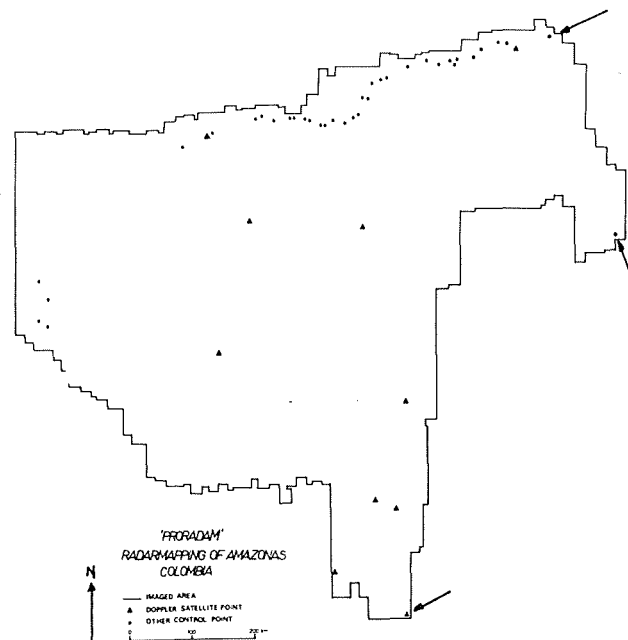


Figure 3: Distribution of ground control. The points marked by an arrow were only available in the ultimate phase of the computations. The figures 7a and 7b do not use information from these points.

STRIP FORMATION

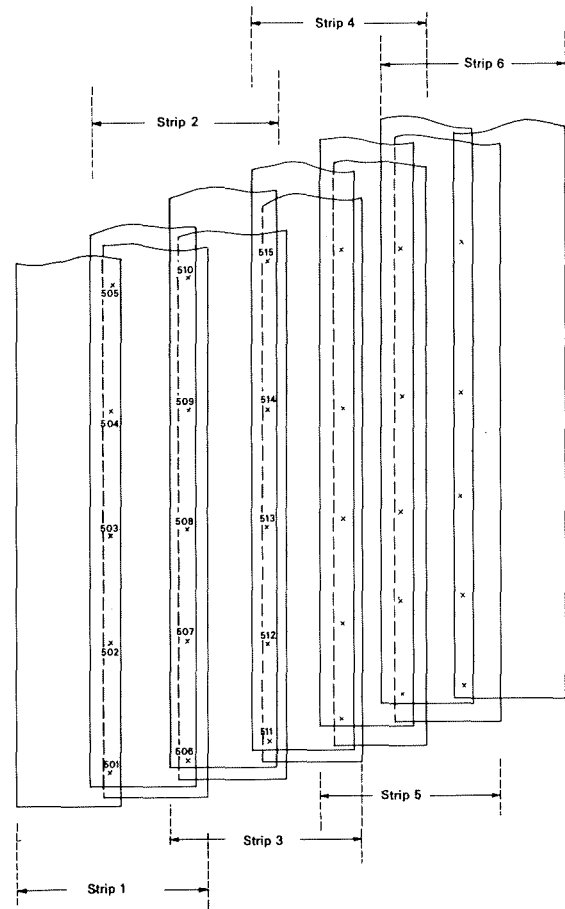
The purpose of the adjustment was to interpolate radargrammetric points in between the given ground control points as a basis for mosaicking. The basic unit for the adjustment is an image strip. Since the mapping area is flat, there was no requirement to form stereo models. Tie points had to be selected to connect the individual strips to form a block. These tie points had to be transferred stereoscopically, the ground control points identified, and all these image points measured.

A single SLAR strip, however, extends up to 250 cm. Measurement on a coordinatograph had therefore to be in parts. This and the fact that each strip was given as a near (NR) and far (FR) range view necessitated the initial step of "strip formation" in which all the piecewise measurements of a strip are transformed into a common strip system.

An effective selection of tiepoints was found to be in the small zone of 5 % overlap between NR and FR views of an image strip (see figure 4). Due to the 60 % overlap between adjacent strips, each tiepoint had to be measured at least 4 times.

Transformation of the piecewise measurements of a strip into a strip system was of course always overdetermined. This enables an estimate of the combined error of point transfer and measurement, showing a root mean square value of ± 0.33 mm at image scale.

Figure 4: SLAR strips with 60 % overlap, but split into near range and far range views through the use of 2 cathode ray tubes (CRTs). Indicated are the locations of tiepoints in the common overlap between the two views of a strip.



PREDICTABLE IMAGE ERRORS

Before block formation, it is essential to eliminate significant predictable image deformations from the individual strips. However, as the imagery of PRORADAM is in ground range presentation, and as the terrain is flat, the only predictable deviation of an image from a desired map projection is just due to this projection. This poses an interesting problem which is illustrated in figure 5.

Each SLAR strip represents an equidistant cylinder projection. The flight line is the reference meridian of the cylinder. Across track image lines represent great circles on the sphere with this reference meridian as an equator and the intersection of the great circles as a pole. Each SLAR strip however, represents a projection onto a different cylinder.

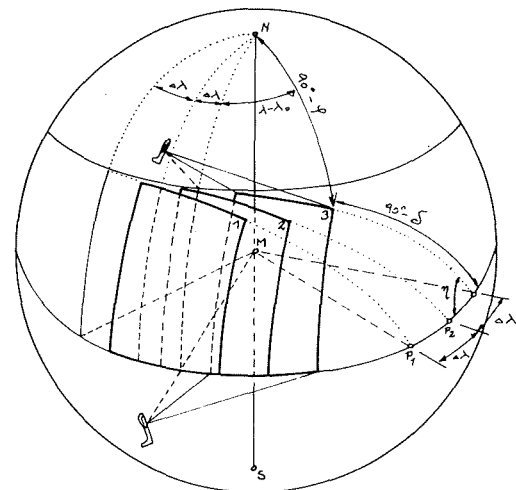


Figure 5: Projection deformation in SLAR imagery

Necessary conversion of alongtrack coordinate x and acrosstrack coordinate y into a Marinus projection with coordinates X, Y amounts to:

$$\begin{aligned} \delta &= k \cdot (x-x_0)/R & \tan(\lambda-\lambda_0) &= \tan\delta \cdot \cos\eta \\ \eta &= k \cdot (y-y_0)/R & X &= \phi \cdot R \\ \sin\phi &= \cos\delta \cdot \sin\eta & Y &= (\lambda-\lambda_0) \cdot R \end{aligned}$$

where

- k = scale factor
- R = radius of earth
- ϕ = longitude
- λ = latitude
- λ_0 = reference latitude
- x_0 = image x of equator
- y_0 = image y of flight line

Evaluation of these formulae reveals that corrections of SLAR image coordinates will always be less than 3 in 10 000.

INTERNAL ADJUSTMENT

Block formation, or internal adjustment should now produce a single pair of coordinates for each tiepoint, of which coordinates are at this point available in 3 adjacent SLAR strips. Due to unpredictable (random) image errors, there must be some discrepancies expected. Analysis leads to the conclusion that there are two main defects of image geometry: variation of along track scale and curvature of flight lines (see figure 6).

Block formation was done by starting from an initial image and transforming successively each adjacent image into the previous one. One thus progresses from the initial image throughout the whole block. One can compare this with photogrammetric strip formation where the role of individual models is taken over by the SLAR images.

The transformation was basically linear conformal, with correction terms for differential scale and curvature. The correction terms were set up as spline functions.

The fact that this block formation is sequential rather than simultaneous simplified numerical problems and was a consequence of the stringent time constraints. It is expected that simultaneous internal adjustment will produce a slightly superior block.

The result of the block formation can be evaluated to some extent from the discrepancies left in the tiepoints. These are shown as root mean square values in mm at photoscale (table 1). They represent discrepancies between internally adjusted tiepoints and transformed tiepoints.

Four computational alternatives were computed for the block formation: with and without correction of projection deformation and with or without splines in addition to linear conformal transformation of strips. Table 1 shows clearly that discrepancies are much smaller using spline corrections but that projection deformation is not significant.

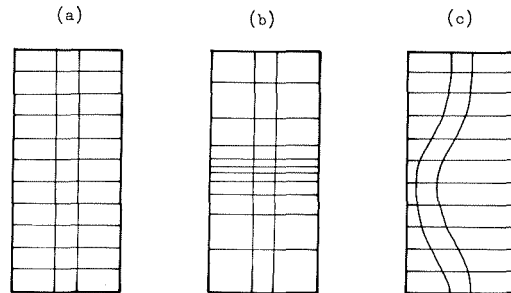


Figure 6: The grid of fig. (a) is deformed to (b) due to variations in along track scale, and to (c) due to a curvature of the flight line

		A 1	A 2	B 1	B 2
NS-LINES	RMSE X	1.12	1.13	0.66	0.65
	RMSE Y	1.17	1.18	0.68	0.68
TIELINES	RMSE X	1.20	1.20	1.30	1.30
	RMSE Y	1.40	1.50	1.40	1.31

Table 1: Internal root mean square discrepancies in mm at image scale, after block formation

A: without correction for projection deformation
B: with correction for projection deformation
1: without splines
2: with splines

An independent comparison of the block with the tielines shows that both are fairly consistent. It can be expected that the block deformation relative to ground control is of the same order of magnitude.

EXTERNAL ADJUSTMENT

Beginning external adjustment with a linear conformal transformation into the control point net reveals rather much larger block deformations than expected; and their order of magnitude does not vary, whether or not spline corrections or projection corrections are used (see table 2).

	A 1	A 2	B 1	B 2
RMSE X	4.07	3.93	4.89	5.15
RMSE Y	3.68	3.50	5.95	4.75

Table 2: External root mean square discrepancies in mm at image scale, after 4-parameter similarity transformation of SLAR block into geodetic control

An attempt to explain the obvious discrepancy between two independent evaluations of block deformation has initially and still focused on the fact that the complex inertial navigation was initialized at the airport of Bogota at 2700 m with rather unusual deviations of the local vertical. It is suspected that this led to a distorted frame for the inertial navigation above flat and low Amazonas. If this suspicion is correct, then this would explain why the tielines fit so well with the NS lines, and why, at the same time, the NS lines do not fit with the ground control.

Error vectors describing the block deformations appear to be largely systematic. This is confirmed by computing the covariance functions for deformations in northing and easting.

Correction of these deformations is an interpolation problem. Various methods can be and were used for the purpose. Only the results of two are presented here: of a polynomial, independent for errors of northing and easting; and of linear prediction. Application of linear prediction was by a combination of moving average and linear prediction proper. The moving average has the role of trend function in this application.

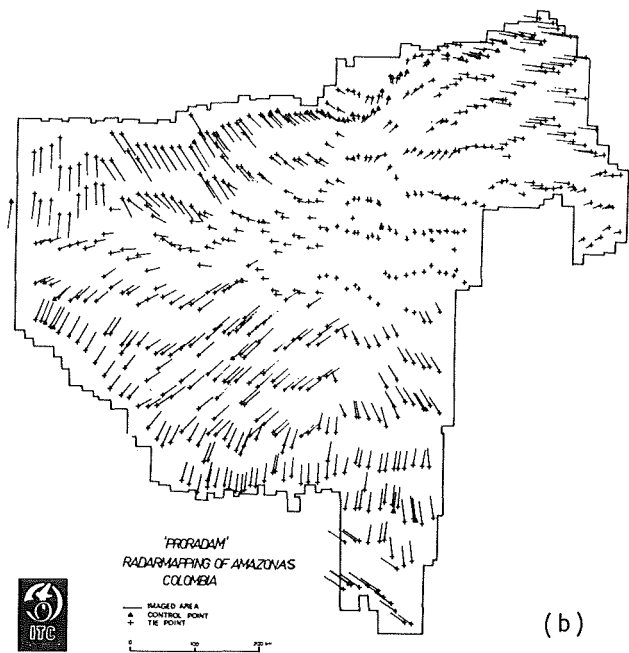
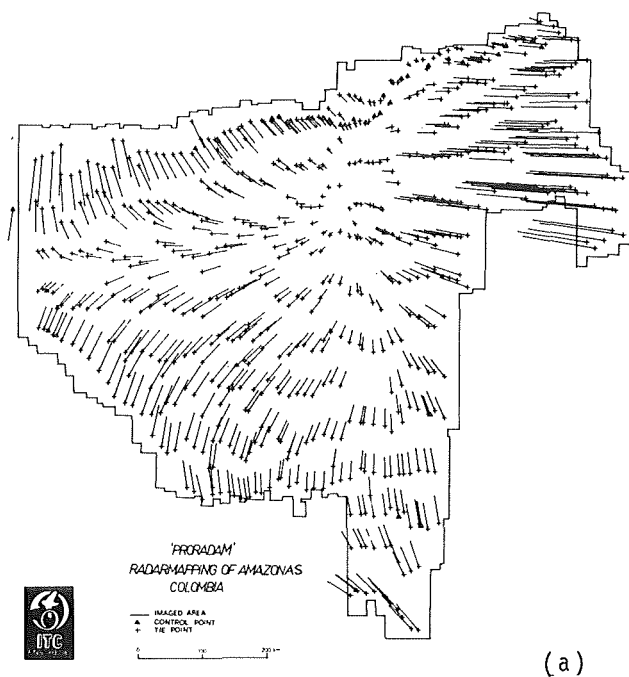


Figure 7: Corrections computed with polynomial (a) and linear prediction (b). In the North East and South West of the area, extrapolation leads to very large corrections with the polynomial]

Two vector diagrams show an essential difference of the applicability of the two methods for the purpose (figure 7). Diagram (a) refers to the interpolated corrections using a 10 coefficient polynomial (3rd order). The other (b) uses linear prediction. It is obvious that in certain areas corrections obtained from polynomials degenerate to very large values. This is in areas of extrapolation. With linear prediction, no degenerated corrections are obtained. Table 3 demonstrates that correction size is the same as of the original deformations in control points.

	A 1	A 2	B 1	B 2
RMSE X	0.56 (3.75)	0.55 (3.58)	0.56 (3.96)	0.59 (4.08)
RMSE Y	0.70 (3.39)	0.69 (3.25)	0.71 (4.52)	0.61 (3.65)

Table 3: Residuals at control points (without brackets) and corrections at radargrammetric points (in brackets), after external adjustment with linear prediction. Values in mm at image scale. Correlation function: $Gov(d) = 0.9/(1 + d^2/500^2)$.

ACCURACY OF SLAR BLOCK, EVALUATED WITH ERTS MSS IMAGERY

From table 3 reliable estimate is possible of the actual precision of radargrammetric points, but availability of ERTS-1-MSS imagery is used to obtain an independent estimate of this accuracy. ERTS images are available in about 50 % of the mapping area; only half of this is not covered by clouds. Therefore, only 25 % of the area is also shown on ERTS imagery. For the simple reason of lack of time, these remaining ERTS data were only used as a check rather than as control.

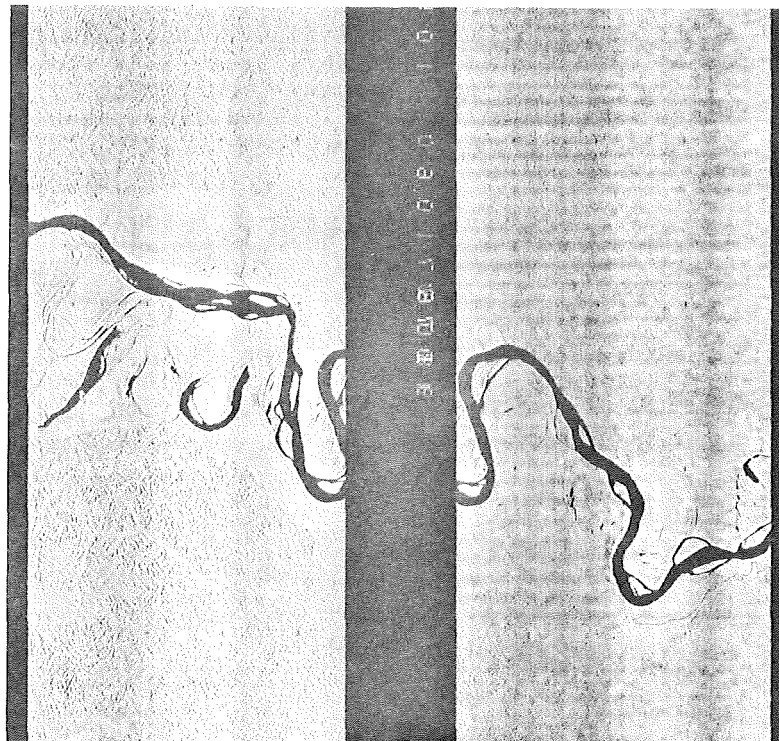
The check is only possible using drainage lines. From inspection of many ERTS images it can be concluded that at this state SLAR shows much more detail and for this reason is superior to ERTS imagery (see figure 8). The drainage lines are actually the only recognizable detail in most of the ERTS images of the Amazonas area but, due to a year's difference between taking ERTS and SLAR, some changes have occurred.

NR	RMSE X	RMSE Y	NUMBER OF POINTS	DATE OF ACQUISITION
1	1.06	0.51	9	Oct. 1972
2	0.80	0.69	10	Oct. 1972
3	2.77	2.85	11	Oct. 1972
4	1.32	1.26	7	Oct. 1972
5	1.08	0.71	18	Feb. 1973
6	2.29	1.35	12	Feb. 1973
7	1.15	1.35	22	Feb. 1973
Total	1.58	1.41	89	

Table 4: Root mean square discrepancies between ERTS-1-MSS images and SLAR block PRORADAM. Values in mm at scale 1 : 400 000. MSS-channel 7 used.



(a)



(b) far range

near range

Figure 8: Part of ERTS-1-MSS channel 7 (a) and of SLAR strip (b) at same scale. The images show the Rio Putumayo, at latitude S0 20, longitude W 72°

This might to some extent make the ERTS images of this area less reliable than in other cases. Reported ERTS image deformations are of the order of magnitude of 170 to 400 m (0.3 to 1 mm at SLAR image scale) (references |1| and |2|).

Table 4 shows the root mean square coordinate differences between seven ERTS images and the adjusted SLAR block. The overall root mean square discrepancy amounts to ± 1.5 mm, representing the sum of deformations of ERTS and SLAR.

This values allow the tentative conclusion that the relative accuracy of the adjusted SLAR block is about equivalent, or perhaps a little inferior, to ERTS accuracy. This suggests for future work the ERTS imagery in SLAR mapping projects should not be disregarded.

CONCLUSION

An internal and external block adjustment for planimetry was numerically carried out with SLAR imagery for the Colombian project PRORADAM. The mapping area consisted of the Colombian Amazonas Basin (400 000 km²). Forty-four ground control points were available.

Time constraint necessitated a rather simple solution for the problem. After sequential block formation, the consistent SLAR block was transformed into the set of ground control points. Residual block deformations at ground control points were used to interpolate corrections in radargrammetric points. The interpolation method was linear prediction.

Comparison of the adjusted SLAR block with independent ERTS-MSS-images reveals root mean square coordinate discrepancies of 1.5 mm at image scale.

The methods which were used for the adjustment were simple of necessity. It is expected that more rigorous methods of computation will improve results. ERTS imagery should be incorporated as external constraint in the adjustment.

REFERENCES

- |1| Bähr H.D., Schuhr W.: "Versuche zur Ermittlung der geometrischen Genauigkeit von ERTS Multispectral-Bildern", 1/1974
- |2| Colvocoresses A.D., McEwen R.B.: "EROS Cartographic Progress", Photogrammetric Engineering, 1973/2
- |3| Leberl F.: "Evaluation of SLAR Image Quality and Geometry for PRORADAM" ITC Journal 1974/4

A SIMULATION SYSTEM FOR THEORETICAL ANALYSIS OF RADAR RESTITUTION
AND A TEST BY ADJUSTMENT

by G. Dowideit, Hannover, Fed. Rep. Germany

ABSTRACT

Flight data are mostly not available together with radar-images for geometric tests. To make a statement about relationship between flight situation and geometric radar restitution it is necessary to procure those data or to simulate them together with radar image coordinates.

By use of Fourier-Series and Random Values the program SIMUL simulates flights and produces radar image coordinates.

The imagery equations used in SIMUL are the base for the error equations in the adjustment in the program SLARB (1). This (not well tested) program determines three-dimensional Gauss-Krüger-coordinates of unknown image points by using a few control points.

INTRODUCTION

In the last years the geometric restitution of unconventional Remote Sensing imagery got more importance, as more and more data is preserved for thematic and topographic mapping. The advantage to have those quick data collecting systems requires new and fast methods to handle all the mass of those material. Remote Sensing systems are measuring the radiation of the electromagnetic spectrum in different but typical ways and store these values in special manners. Especially in the case of Side Looking Radar (SLAR) the geometric problems are complicated by measuring-situation, influenced by time-varying parameters.

Many ways are possible to solve the reconstruction of terrain from the image-data. For example as BOSMAN, CLERICI, ECKHART and KUBIK did by using an approximate transformation for flat terrain [1] or DERENJY [3] or LEBERL [4] did by using polynomial fitting on single strips to get two-dimensional results. A more analog way had been done in Brasil by producing semicontrolled mosaics of the Amazon-Region (RADAM) [5].

To get three-dimensional results for mountainous terrain we used in Hannover some simple equations [6]. All those tests depend on a few Radar images flown by different conditions. The flight parameters are always unknown or respectively unused. In most cases mathematical models are used, which are different from the physical situation during the flights.

So it is possible to make a statement about the accuracy of results of each special test material by using those mathematical models. But it is not possible to make a statement about the relationship between the physical situation during the flight and the results of such models of mathematical approximation.

SIMULATION OF SIDE LOOKING RADAR IMAGE COORDINATES

- SIMULATION OF A FLIGHT PATH

To have a base for controlled test situations it is useful to simulate image flights over well known digital terrain-models. By definition, a straight flight path should be a loxodrome on a Gaussian Globe. The platform - (airplane) - coordinates are defined as a function of time (T_i):

$$(\lambda_{Fi}, u_{Fi}, R_{Fi}) = f(T_i) \quad (1.00)$$

By using a flight-starting-point $(\lambda_{Fo}, u_{Fo}, R_{Fo})_{T_0}$ the flight positions can be written as

$$u_{Fi} = u_{Fo} + S_{Fi} \cdot \cos(AZ) \quad (1.01)$$

$$\lambda_{Fi} = \lambda_{Fo} + S_{Fi} \frac{\sin(AZ)}{\cos\left(\frac{u_{Fo} + u_{Fi}}{2}\right)} \quad (1.02)$$

$$R_{fi} = R_{Fo} + k \cdot S_{Fi} \quad (1.03)$$

In which means

AZ = Azimuth, angel between the meridian and the flight path (loxodrome)

S_{Fi} = Spherical distance between $(\lambda_{Fo}, u_{Fo}, R_{Fo})_{T_0}$ and $(\lambda_{Fi}, u_{Fi}, R_{Fi})_{T_i}$ in degrees

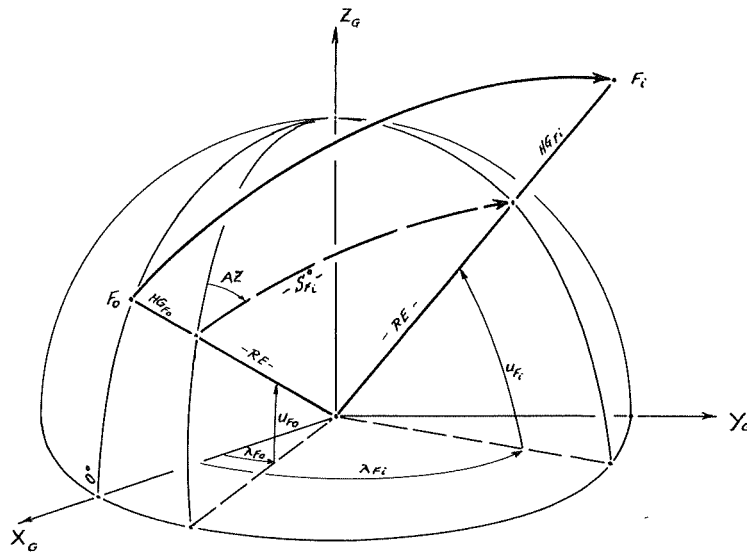
k = factor for variation of the flight path elevation.

With the known speed of the airplane over terrain the spherical distance can be written as

$$S_{Fi}^0 = \frac{VG \cdot (T_i - T_0)}{RE + HG} \cdot 90 \quad (1.04)$$

with

VG = speed of flight
 RE = radius of the globe
 HG = flight elevation above the surface of the globe



By dividing the spherical distance S_{Fi} into differential short pieces dS_i concerning to timestep dT and by using time varying expressions for the flight parameter

- $VG_{T_i} = f_1 (T_i)$ for flight speed changes
- $AZ_{T_i} = f_2 (T_i)$ for azimuth changes (for example readouts of a gyro)
- $\alpha_{T_i} = f_3 (T_i)$ for drift angel
- $k_{T_i} = f_4 (T_i)$ for elevation changes
- $\phi_{T_i} = f_5 (T_i)$ for pitch angel changes
- $\omega_{T_i} = f_6 (T_i)$ for roll angel changes and
- $\kappa_{T_i} = f_7 (T_i)$ for yaw angel changes

it is possible after defining these time functions to describe varying flight path with

$$K_{Ti} = AZ_{Ti} + \alpha_{Ti} \quad (1.05)$$

(direction of the assumed flight velocity)

and

$$dS_{Fi} = \frac{VG_{Ti} \cdot dT}{(RE + HG_{Ti})} \cdot \rho^0 \quad (1.06)$$

to write the flight positions as

$$u_{Fi} = u_{F0} + \int \cos (K_{Ti}) \cdot dS_{Fi} \quad (1.07)$$

$$\lambda_{Fi} = \lambda_{F0} + \int \frac{\sin (K_{Ti})}{\cos (u_{Fi})} \cdot dS_{Fi} \quad (1.08)$$

$$R_{Fi} = R_{f0} + \int k_{Ti} \cdot dS_{Fi} \quad (1.09)$$

(determination of the flight positions)

$$\phi_{Ti} = f_5 (Ti) \quad (1.20)$$

$$\omega_{Ti} = f_6 (Ti) \quad (1.21)$$

$$\kappa_{Ti} = f_7 (Ti) \quad (1.22)$$

(rotation of the airplane in each moment T_i).

The quality of approximation of a true flight with the additional aim of a controlled test situation depends on the definition of the time varying functions $f_1(T_i), \dots, f_7(T_i)$.

This could be done by Fourier-Series like

$$\begin{aligned} f_n(Ti) = & a_{n1} + a_{n2} \cdot \sin \left(2 \frac{(Ti - T_{0n})}{TP_n} \pi + b_{n1} \right) \\ & + a_{n3} \cdot \sin \left(4 \frac{(Ti - T_{0n}) \cdot \pi}{TP_n} + b_{n2} \right) \\ & + a_{n4} \cdot \sin \left(8 \frac{(Ti - T_{0n}) \cdot \pi}{TP_n} + b_{n3} \right) \\ & + \dots \end{aligned} \quad (1.23)$$

in which

$$\begin{aligned} a_{nk} &= \text{coefficients of amplitude} \\ b_{n(k-1)} &= \text{coefficients of phase and} \\ TP_n &= \text{length of the period time.} \end{aligned}$$

These functions $f_1(T_i) \dots f_7(T_i)$ should realize a mathematical model of the stochastic process of the flight parameters as good as possible.

This is a reason to generate the coefficients a_{nk} and $b_{n(k-1)}$ by a random generator with for example normal distributed values.

If k is the number of terms of the Fourier-Series, the values of the functions $f_n(T_i)$ could be characterized by the limitations of

$$a_{nk} \leq \pm \frac{1}{k} \cdot |A_{n \max}| \quad \text{and} \quad b_{n(k-1)} \leq \pm \pi$$

in which $|A_{n \max}|$ means the maximum value with a random probability of P %.

SIMULATION DER FOURIERKOEFFIZIENTEN AUS FLUGPA

SIMULIERTE AMPLITUDENHOEHEN FUER

V	H	ALPHA	KAPPA	PHI	OMEGA	KURS (AZ)
2.3882	2.4723	5.1759	8.2137	2.3897	9.3060	9.4078

LAGE DER PERIODENANFAENGE IN SEC NACH FLUGBEGINN TO FUER

V	H	ALPHA	KAPPA	PHI	OMEGA	KURS (AZ)
84.9618	30.3292	78.9442	28.6183	78.9442	94.7453	94.8069

SIMULIERTE PERIODENLAENGEN FUER

V	H	ALPHA	KAPPA	PHI	OMEGA	KURS (AZ)
49.8341	76.9859	2.2571	48.8374	60.3299	43.4115	74.1304

With a small loss of accuracy in approximation of a true flight path it is possible to use small real timesteps ΔT instead of the differential expression dT for computer-compatible equations (see example of simulated airplane rotations).

SIMULIERTE FOURIERREIHENKOEFFIZIENTEN

AV	AH	AAL	AK	APHI	AOM	AAZ
.1084	.1500	.2697	-.1455	.0928	-.6075	.2690
-.1304	.1293	.1057	-.2805	-.0194	.4621	.1604
-.1652	-.1868	-.2422	-.5488	-.0997	-.5781	-.1604
-.1781	-.1087	.3300	-.0052	-.1304	-.4610	-.1825
-.0110	-.0586	-.1022	-.3492	.1324	-.5308	-.4719
-.1370	.1062	-.1599	.5858	.0486	-.5403	-.5761
-.0545	-.1268	.1103	-.3121	.0756	-.2045	-.0802
.0217	.1047	-.0227	.4860	.0958	-.1909	.6594
-.1790	-.0305	-.1491	.0519	-.1816	-.1525	.3006
.1815	-.1581	-.3836	.1546	-.1349	.5026	-.5052
.0140	.0818	-.2642	.5458	-.1119	-.3645	-.1716
.0547	.1185	-.0016	.2037	.1686	.6373	.6259
.0526	.1545	.1653	-.2302	-.0515	.0219	-.4506

BV	BH	BAL	BK	BPHI	BOM	BAZ
-.1673	1.0909	.6274	-.5437	-.8397	-.7017	1.0194
-.3024	-1.4425	1.1337	.2273	.1001	-1.4797	-.3720
.2199	1.5161	-1.3188	.7616	.2253	-1.1990	1.3498
-.5210	-.0768	-1.4549	.5669	-1.2281	-.4099	-.6489
1.2566	-.3501	-.0800	-.2268	-1.3555	-1.1900	.9918
.7421	.0671	.4000	.1478	-.3792	1.3318	-.5253
1.1277	-.5000	.2220	.4172	.2755	-1.4221	1.2454
-.4139	.6550	.1961	1.3271	-.3319	.0413	-1.4877
1.2566	.1587	-.9277	-1.5509	-.2814	.3609	-.0911
-.4099	1.1468	-.2464	1.1686	-.4496	-1.2844	1.3612
-.3340	-.9050	.4173	1.2754	1.0470	-.2888	-.8219
-1.2747	.4647	.7167	1.4335	.2458	-1.2170	1.3315

- SIMULATION OF IMAGE COORDINATES

By using the definition of coordinate systems made by LEBERL in [2] combined with the FLIGHT-SIMULATION-System (λ_{Fi} , u_{Fi} , R_{Fi}) the RADAR-IMAGE-COORDINATES of a terrain-point could be determined by

$$\vec{s}_p = A \cdot B \cdot (D''_{Ti} \cdot D'_{Ti} \cdot (TF_P \cdot R_P - TF_{Fi} \cdot R_{Fi}) - \vec{a}) \quad (2.00)$$

$$SR = |\vec{s}_p| \quad \text{Slant Range}$$

$$\Delta t = \frac{2 \cdot SR}{c} \quad \text{Signal time} \quad (2.01)$$

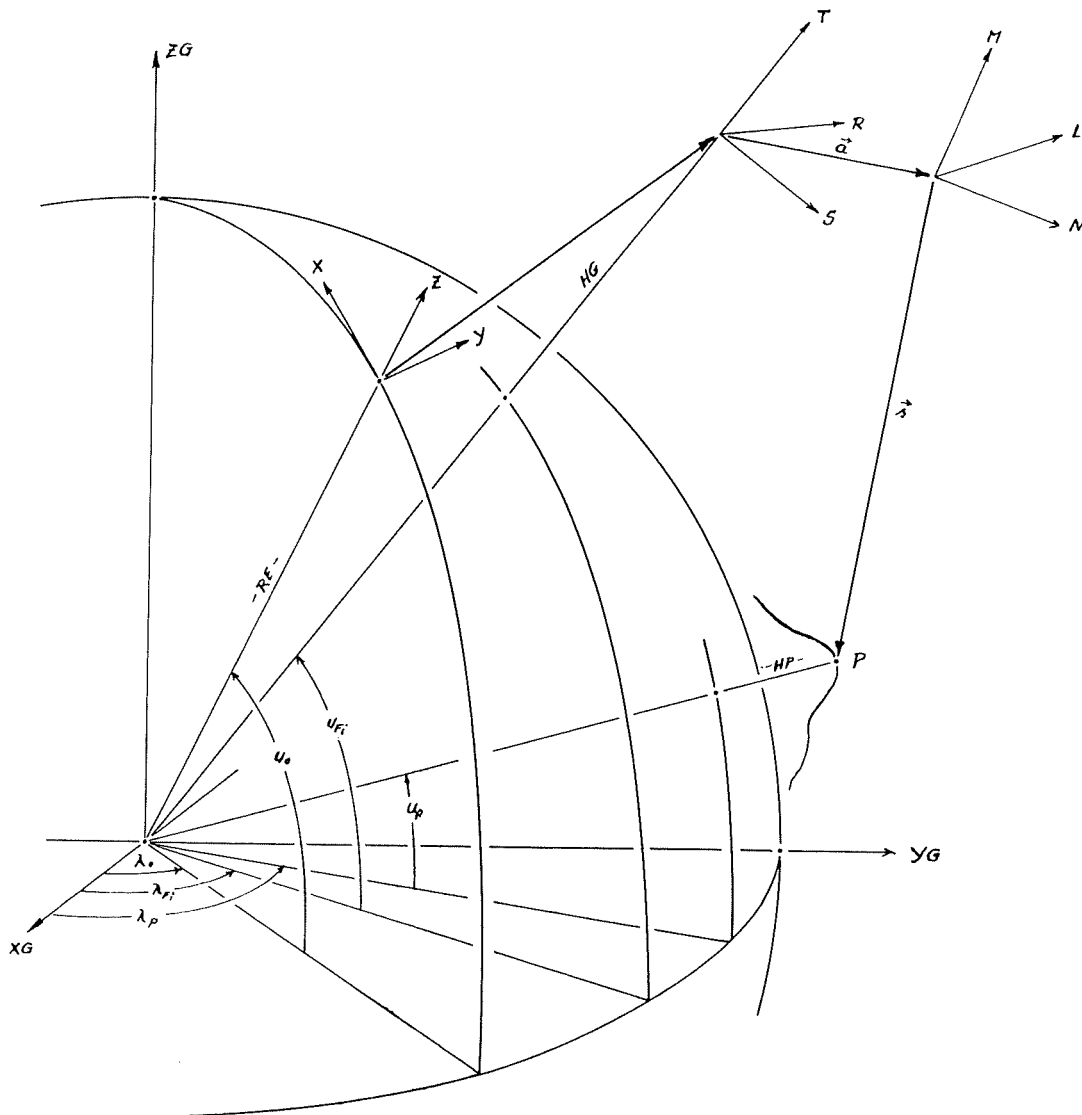
$$\Delta t_0 = \quad \text{time delay of CRT-display}$$

$$\Delta T = (T_i - T_0) \quad \text{flight time}$$

$$x' = m_{x'} \cdot \Delta T$$

$$y' = m_{y'} (\Delta t - \Delta t_0) \quad \text{for Slant Range Imagery} \quad (2.02)$$

$$y' = c \cdot m_{y'} \cdot \frac{(\Delta t^2 - \Delta t \cdot \Delta t_0)}{(\Delta t^2 - \Delta t_0^2)^{1/2}} \quad \text{for Ground Range Imagery}$$



Definitions to equation (2.00) :

$$TF = \begin{vmatrix} \cos \lambda \cdot \cos u \\ \sin \lambda \cdot \cos u \\ \sin u \end{vmatrix} = \text{trigonometric function vector of polar globe coordinates}$$

R = distance between the centre of the globe and a point (airplane or on terrain in the mean of the used index)

$(TF_P \cdot R_P - TF_{Fi} \cdot R_{Fi})$ = Vector between the airplane and the terrain point (in geocentric rectangular coordinate system)

D'_{Ti} = Rotation matrix of $(K_{Ti}, \lambda_{Ti}, u_{Ti})$ which rotates this vector into a flight path oriented rectangular coordinate system

D''_{Ti} = Rotation matrix of $(\phi_{Ti}, \omega_{Ti}, \kappa_{Ti})$ which rotates this vector into an airplane mounted rectangular coordinate system

\vec{a} = Translation between the origin of the airplane system into the origin of the sensor coordinate system

B = Rotations matrix of $(\phi', \omega', \kappa')$ to rotate the airplane system parallel to the sensor mounting system

A = Rotation matrix of $(\phi'', \omega'', \kappa'')$ to rotate the mounting system parallel to the sensor coordinate system

and the result

$$\vec{s} = \begin{vmatrix} L_P \\ M_P \\ N_P \end{vmatrix} = \text{Vector between the origin of the sensor and the terrain point P. (In a rectangular sensor coordinate system).}$$

The condition for imaging terrain point P is

$$\text{arc tan} \left(\frac{L_P}{(M_P^2 + N_P^2)^{1/2}} \right) = \phi \quad (2.03)$$

in the meaning that the L-axis is parallel to the axis of the radar beam cone produced by the Squintangle ϕ .

This condition can be used to determine the time ΔT of imaging:

$$(\phi - \Delta\phi) \leq \text{arc tan} \left(\frac{L_P}{(M_P^2 + N_P^2)^{1/2}} \right) \leq (\phi + \Delta\phi) \quad (2.04)$$

The limitation $\Delta\phi$ can be chosen as a function of the resolution W_{\max} in azimuth:

$$\Delta\phi = \frac{W_{\max}}{SR_{\max}} \cdot \rho^0 \quad (2.05)$$

Enclosing a routine to control the stabilization of radar antenna against yaw, pitch (and roll) and an additional random generator to simulate errors in measurement of image coordinates and point identification these formulars are programmed for a CDC-Cyber 76.

The executions time of these program SIMUL differs between 1 second for a straight flight with 60 image points and approximately 60 sec per image point by using extreme flight parameters and a high azimuth resolution of 5.0 meters.

An average execution time of 1 second per image point by simulation of a normal free varying flight can be expected.

RADAR EVALUATION TEST BY BLOCK ADJUSTMENT

- IMAGE EQUATIONS, ERROR EQUATIONS AND NORMAL EQUATIONS SYSTEM

The simulation program SIMUL was designed to supply controlled input data for the program SLARB. A just finished early test version SLARB (1) solves three-dimensional Gauss-Krüger-coordinates and corrections for some flight and imaging data.

On the base of the IMAGE EQUATIONS (2.00) (2.01) (2.02) the Error Equation coefficients are found by derivation.

These coefficients can be classified into three types:

- 1) coefficients corresponding to unknowns which are valid for all images with the same value as
 - a) correction of time delay Δt_0 and with some restrictions
 - b) correction of the two image scales m_x, m_y (interior orientation)
- 2) coefficients corresponding to unknowns which are valid for each image flight with an other value as for example
 - a) corrections of the flight starting point coordinates corresponding to the origin of the radar image (exterior orientation)
 - b) corrections of the airplane rotations ϕ and κ (exterior orientation).

In SLARB version (1) these corrections are realized in the meaning of average trend values, valid for the whole flights.

- 3) coefficients corresponding to the unknown point coordinates.

By using these classification system the ERROR EQUATIONS can be written as

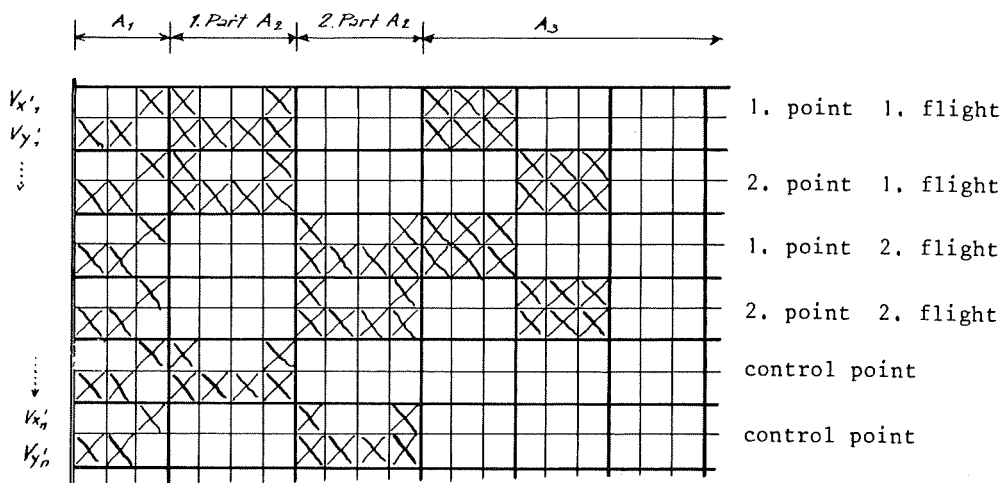
$$V = A_1 X_1 + A_2 X_2 + A_3 X_3 - L \quad (3.00)$$

This index numbers are equal to the type numbers.

It is necessary to orientate the system of equations by introducing control points. In this case the statement (3.00) has no term of type 3.

In SLARB (1) the used coefficient matrix A has the same structure

$$A = |A_1, A_2, A_3| \quad (3.01)$$



The resulting normal equation matrix is poor conditioned, so that the solution only could be found by iteratively repeated adjustments. As a test value to stop the repetition cycle the geometric average of the determined corrections of the unknowns should be less than a limitation value. In the actual program test phase of SLARB (1) this limitation value is set to 0.5. The test value is mainly influenced by the corrections of the unknown terrain point elevations, so we could say that the repetition stops in that moment when all height corrections are smaller than 0.5 meters.

- SOME RESULTS OF SLARB (1)

Though the program SLARB (1) is designed to process up to ten radar image strips with up to 60 terrain points and 140 unknowns, the just now finished tests depend on only two parallel simulated radar images with about 30 terrain points at a scale of 1 : 200 000.

The tests are made in three stages:

- 1) Program Test for SLARB (1) using exactly straight flights, correct input data for the necessary flight parameters and in different configuration three, four, six and eight control points.
- 2) Using the same straight flights with additional simulation of random measurement errors for the image coordinates ($\sigma = \pm 10\mu$ and $\sigma = \pm 20\mu$).
- 3) Using free simulated flights (flight parameters changes between $\pm 5,0$) with additional simulation of random measurement errors for the image coordinates ($\sigma = \pm 20\mu$).

Naturally, these results have no strong declarative meaning, because they are mainly produced as program tests for SLARB (1). But two statements could be made:

- 1) It is possible to determine three-dimensional point coordinates by using an adjustment for the image coordinates.

Under comparable conditions of flight path configuration nearly the same relations could be found as LEBERL [7] expected for the cofactors of the unknown point coordinates.

His declaration for scheme (b) by using $by = 10$ was:

	y = 1	y = 2.5	y = 5
Q_x	0.9	0.9	1.0
Q_y	1.2	1.0	0.8
Q_z	3.2	11.1	19.2

The comparable data produced by SLARB (1) are ($by = 11,5$):

	x = 1	y = 2.5	y = 5
Q_x	23	22	19
Q_y	1	1	1
Q_z	11	12	14

By considering the used equation system for adjustment with unknown absolute orientation of each flight path the differences in Q_x seemed to be clear. But in relation to the values of Q_y and Q_z the values of Q_x seemed to be contradictory. So we must say:

- 2) The actual version (1) of SLARB must be improved, because
 - a - repetition steps are converging too slowly,
 - b - the equation system is very sensitive against too large differences between the approximations of points coordinates and their true values,
 - c - the weights of the error equations had to be solved with more accuracy

for example by using the determined cofactors of the unknown and their functional connections as shown in expressions (2.00) (2.01) (2.02).

- d - it seems to be necessary to use a better test expression than the geometric average is to stop repetition cycle.
- e - the cofactors of Q_x seemed to be too large.

The results are shown in the table below:

Execution number	Test Stage 1				Test Stage 2			Test Stage 3	
	1.1	2.1	3.1	4.1	2.3	4.2	4.3	4.4	4.5
Flight Number	1,2	1,2	1,2	1,2	1,2	1,2	1,2	1,2	1,2
<u>SIMUL-INPUT-DATA</u>									
a) limits of flight parameters	± 0	± 0	± 0	± 0	± 0	± 0	± 0	± 5	± 5
b) simulated 25 of image coordinates	± 0	± 0	± 0	± 0	± 20 μ	± 10 μ	± 20 μ	± 20 μ	± 20 μ
<u>SLARB (1)- DATA</u>									
a) Differences between SIMUL-INPUT and SLARB (1)-INPUT									
a ₁) Flight starting point	0	0	0	0	0	0	0	$\Delta y/\Delta x/\Delta z$ 200/100/0	$\Delta y/\Delta x/\Delta z$ 200/100/0
a ₂) Speed of the aircraft	0	0	0	0	0	0	0	100/70/0	100/70/0
a ₃) delay-time	0	0	0	0	0	0	0	-7.5/+4.0	-7.5/+4.0
b) Simulated flight parameters are used in SLARB (1) (yes or no)	yes	yes	yes	yes	yes	yes	yes	no	no
c) Number of control points/unknown points	4/25	3/26	6/23	8/21	3/26	8/21	8/21	8/21	x ₁ : 7/20 x ₂ : 9/18
d) SLARB (1) repetition-limit	0.5	0.5	0.5	0.5	0.5	0.5	0.5	0.5	0.5
e) Number of repetitions	4	4	4	4	8	6	8	2	2
<u>Results of SLARB (1)</u>									
a) $\bar{\sigma}_0$ after adjustment	± 3 μ	± 3 μ	± 3 μ	± 3 μ	± 24 μ	± 10 μ	± 23 μ	± 7.0mm	± 6.9mm
b) Mean square errors of terrain coordinates (m)									
$\bar{\sigma}_y$	± 9.4	± 11.2	± 8.6	± 9.5	± 7.2	± 6.9	± 5.8	± 743.2	± 245.6
$\bar{\sigma}_x$	± 15.2	± 18.1	± 13.6	± 15.8	± 10.5	± 11.4	± 11.1	± 439.9	± 267.9
$\bar{\sigma}_z$	± 1.3	± 1.3	± 1.4	± 1.1	± 7.0	± 3.6	± 7.6	± 716.5	± 180.9
c) maximum Errors (m)									
Δy max	17.7	26.5	16.9	17.7	16.9	14.4	13.2	3222.0	609.6
Δx max	22.8	34.6	24.7	29.0	21.7	24.9	28.5	1615.9	546.8
Δz max	2.3	2.8	2.3	1.8	13.4	6.3	13.4	2630.0	613.3
Execution Time (sec)	~ 80	~ 100	~ 70	~ 60	~ 145	~ 85	~ 110	~ 60	~ 60
Costs (DM)	~ 265,-	~ 290,-	~ 240,-	~ 230,-	~ 530,-	~ 310,-	~ 400,-	~ 200,-	~ 200,-

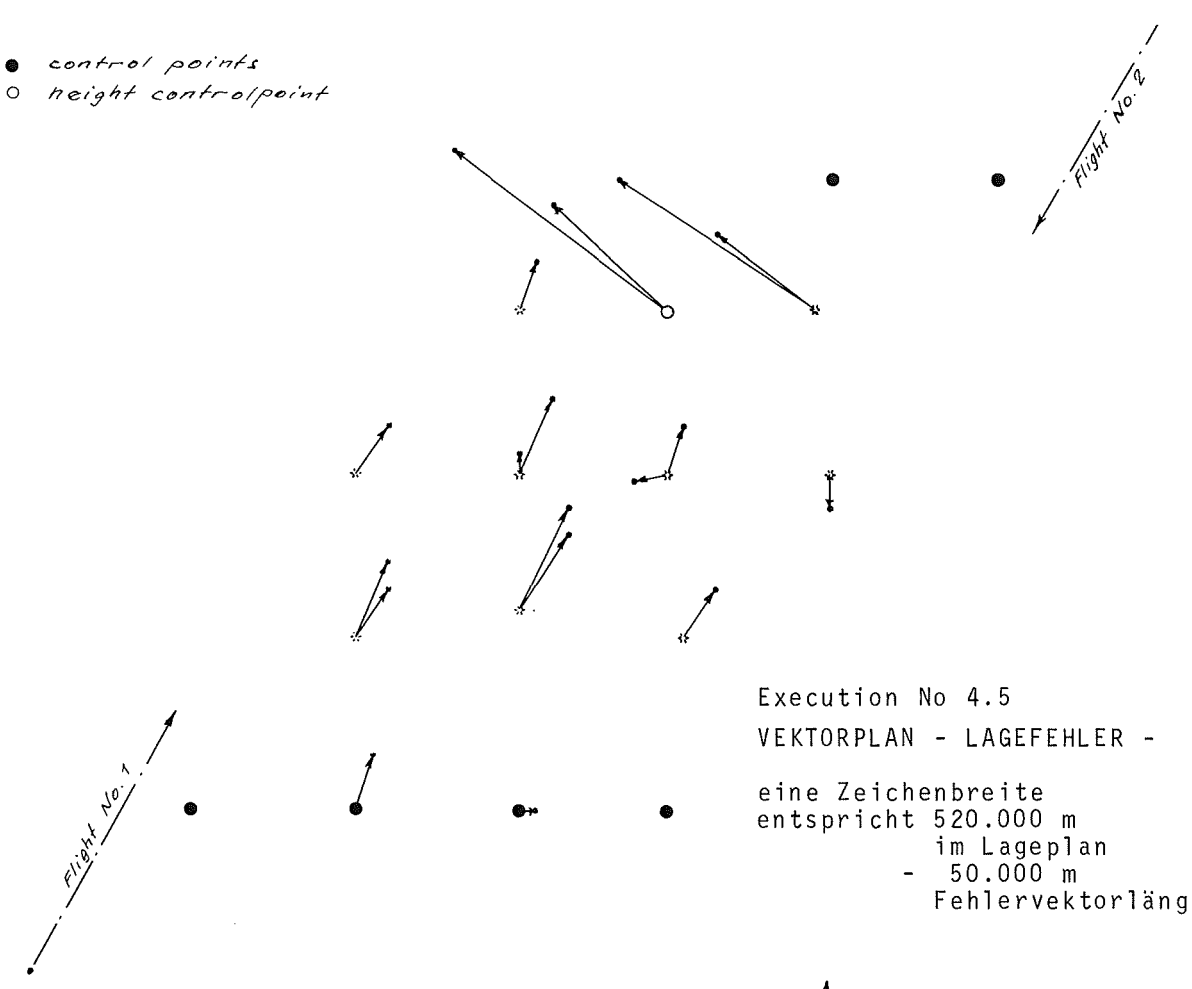
EXECUTION NO. 4.5

Results of adjustment

No.	Y	X	Z	Y	X	Z	Δy	Δx	Δz
59	520000.00	5825000.00	0.00	520000.00	5825000.00	0.00	0.00	0.00	0.00
49	515000.00	5825000.00	0.00	515000.00	5825000.00	0.00	0.00	0.00	0.00
50	515000.00	5825000.00	1000.00	515000.00	5825000.00	1000.00	0.00	0.00	0.00
47	515000.00	5820000.00	0.00	514390.37	5820456.04	613.32	609.63	-456.04	-613.32
48	515000.00	5820000.00	1000.00	514663.35	5820283.71	1378.36	336.65	-283.71	-378.36
37	510000.00	5820000.00	0.00	509361.66	5820546.78	0.00	638.34	-546.78	0.00
38	510000.00	5820000.00	1000.00	509639.11	5820379.29	1000.00	360.89	-379.29	0.00
45	515000.00	5815000.00	0.00	515035.36	5814882.18	-49.18	-35.36	117.82	49.18
27	505000.00	5820000.00	0.00	505061.38	5820175.60	-97.76	-61.38	-175.60	97.76
28	505000.00	5820000.00	1000.00	505055.46	5820174.73	887.55	-55.46	-174.73	112.45
35	510000.00	5815000.00	0.00	510089.30	5815200.22	-53.10	-89.30	-200.22	53.10
36	510000.00	5815000.00	1000.00	509890.85	5815081.96	1088.42	109.15	-81.96	-88.42
26	505000.00	5815000.00	1000.00	505123.10	5815261.98	984.57	-123.10	-261.98	15.43
25	505000.00	5815000.00	0.00	505012.10	5815160.56	78.55	-12.10	-160.56	-78.55
34	510000.00	5810000.00	1000.00	510136.06	5810205.52	951.46	-136.06	-205.52	48.54
33	510000.00	5810000.00	0.00	510128.07	5810213.35	-56.93	-128.07	-213.35	56.93
15	500000.00	5815000.00	0.00	500105.35	5815230.83	-33.23	-105.35	-230.83	33.23
23	505000.00	5810000.00	0.00	505165.54	5810337.11	-44.31	-165.54	-337.11	44.31
24	505000.00	5810000.00	1000.00	505151.68	5810313.56	946.12	-151.68	-313.56	53.88
31	510000.00	5805000.00	0.00	510000.00	5805000.00	0.00	0.00	0.00	0.00
13	500000.00	5810000.00	0.00	500138.68	5810255.25	-47.13	-138.68	-255.25	47.13
14	500000.00	5810000.00	1000.00	500120.72	5810235.10	954.25	-120.72	-235.10	45.75
21	505000.00	5805000.00	0.00	505064.69	5805029.93	-96.82	-64.69	-29.93	96.82
22	505000.00	5805000.00	1000.00	505000.00	5805000.00	1000.00	0.00	0.00	0.00
11	500000.00	5805000.00	0.00	500075.47	5805114.02	-50.64	-75.47	-114.02	50.64
12	500000.00	5805000.00	1000.00	500000.00	5805000.00	1000.00	0.00	0.00	0.00
1	495000.00	5805000.00	0.00	495000.00	5805000.00	0.00	0.00	0.00	0.00
				20	20	18	1206097.80	1435082.78	588803.66
				20	20	18	$\sigma_y = \pm 245.57$	$\sigma_x = \pm 267.87$	$\sigma_z = \pm 180.86$

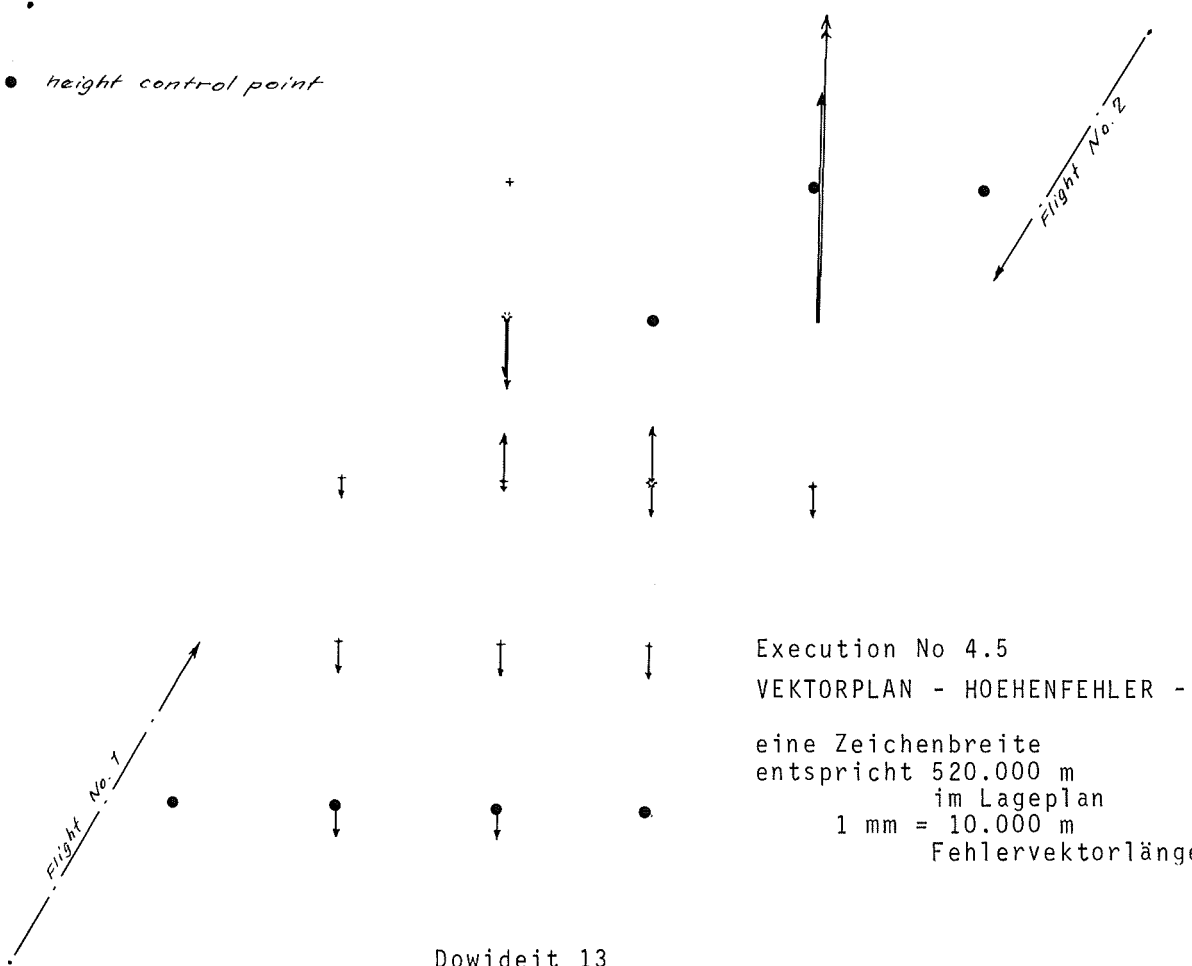
Dowdett 12

- control points
- height controlpoint



Execution No 4.5
 VEKTORPLAN - LAGEFEHLER -
 eine Zeichenbreite
 entspricht 520.000 m
 im Lageplan
 - 50.000 m
 Fehlervektorlänge

- height control point



Execution No 4.5
 VEKTORPLAN - HOEHNENFEHLER -
 eine Zeichenbreite
 entspricht 520.000 m
 im Lageplan
 1 mm = 10.000 m
 Fehlervektorlänge

REFERENCES

- |1| Bosman, E. R., Clerici, E., Eckart D., Kubik D., Delft: "Transformation of points from sidelooking radar images into the map system" BuL 4/1972
- |2| Leberl, F.: "Untersuchung über die Geometrie und Einzelbildauswertung von Radarschrägaufnahmen", Dissertation TH Wien und ITC Enschede, 1971
- |3| Derenjy, E. E.: "SLAR Geometric Test", Photogrammetric Engineering 1974
- |4| Leberl, F.: "Evaluation of Single Strips of SLAR images", Invited Paper of the Congress of the ISP, Ottawa 1972
- |5| Van Roessel, J. W.: "SLAR Mosaics for Project RADAM", Photogrammetric Engineering 1974
- |6| Konecny, G.: "Geometrische Probleme der Fernerkundung", BuL 4/1972
- |7| Leberl, F.: "On model formation with remote sensing imagery", Enschede

DEFORMATIONS OF SLAR IMAGERY - RESULTS FROM ACTUAL SURVEYS

by H. Jensen

This discussion relates to a system comprised of the following principal components:

- Caravelle Twin-Jet Transport
- GEMS-1000 Synthetic Aperture Side Looking Radar - manufactured by Goodyear Aerospace Corporation
- Litton LTN-51 Inertial Guidance System
- Stewart-Warner AN:APN-159 High Altitude Radar Altimeter System
- Lear-Siegler L-102 Auto Pilot
- RCA "SHORAN" Radio Positioning System

Fundamental to SLAR imagery is the fact that the two image components - along-track and across-track - are determined with complete independence. Consequently, it is evident that error studies must treat separately with the two components, and not mix them in statistical analyses as if the circumstances were isentropic.

This discussion will deal simply with the most prominent deformations, examining the consequences of system errors, noise, and resolution limits by following their effects upon a hypothetical square figure whose axis is parallel with the flight line, in a hypothetical level surface at ground level.

A synthetic aperture SLAR system, operating "perfectly" will seek the zero doppler line, which lies at right angles to the flight path, for the formation of the image elements. As a consequence, x and y , the cross-track and along-track components, will be orthogonal, and the transform of the ground square to image will result in a rectangular parallelogram (whose limiting shape will be a square).

Since the synthetic aperture SLAR system in commercial use (the Goodyear GEMS-1000 system) employs an excellently calibrated slant-range to ground-range conversion function; and since, as noted in Mr. Graham's paper ("Geometric Problems in Side Looking Radar Imaging" - GERA-2015, 1 August 1974), the most accurate aspect of SLAR imaging is the range (or x) component, it may be assumed, and our experience confirms, that the x measurement is of reasonably exact and constant scale (1 : 400 000) when the setting of the range conversion function reflects truly the difference in altitude of aircraft and ground (usually about 12 500 m).

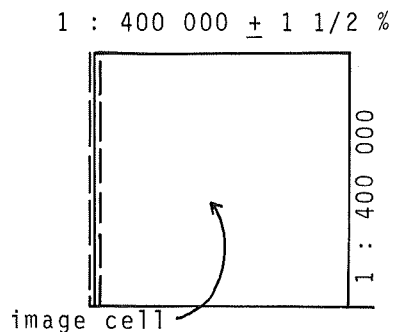
The y scale is determined by the rate of data film advance; and this, in turn, is determined by the velocity output derived from a Litton LTN-51 Inertial Navigation System.

Two time-dependent aspects of inertial systems affect the accuracy of this velocity input: (a) drift and (b) an 84-minute oscillation (the "Shuler Oscillation"). By manufacturer's specifications, the drift may not exceed a rate of one knot; and by selection of components and careful pre-flight adjustment, this performance can be improved to about one-half knot. Since the true airspeed under survey circumstances approximates 360 knots, it is evident that the drift error is of the order of one part in 720, or 0.14 %.

The 84-minute oscillation is a far more serious contributor to scale error. In a number of surveys in the past three years, the velocity as measured by the inertial platform has been continuously compared with the velocity indication of a Doppler navigator, to determine the magnitude of this variation. The basis for this comparison lies in the fact that, though the Doppler output is noisy, and is often interrupted by heavy rains, smooth water bodies, and so on, it has no time-related variation, and thus is a valid yardstick. It has been found that velocity variations of six knots or so occur with some frequency; and that variations of ten knots occur from time-to-time. These errors represent errors of more than ± 1.5 % of velocity indications when the true airspeed is of the order of 360 knots. The image scale variations of the y component are thus also often of the order of more than ± 1.5 %.

A simple diagram shows the consequences of the above discussion:

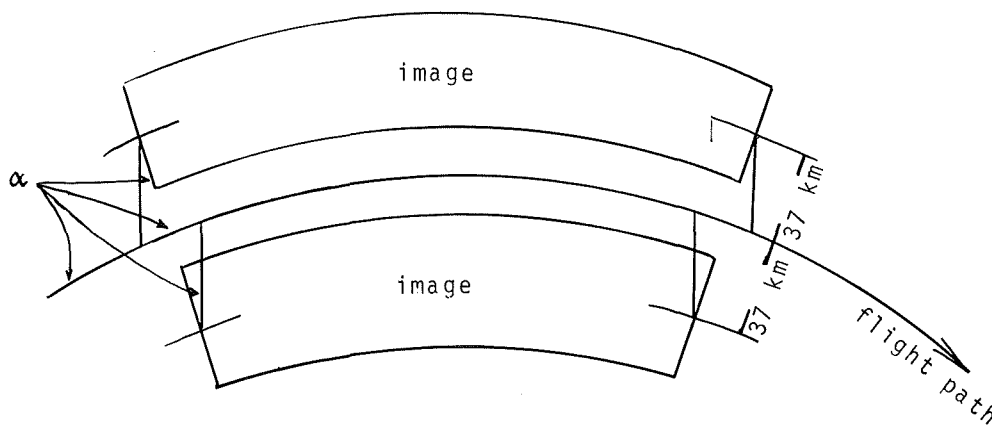
aircraft - appr. 360 knots \pm 6 knots error



CURVATURE

The 84-minute oscillation is random in its time and azimuth phases. Therefore, it imposes a cross-track cyclical error of the same magnitude as its along-track error; that is, an 84-minute sinewave of as much as six to an occasional ten-knot velocity. The cross-overs of maximum effect will, therefore, have an angle with the desired great-circle flight path of one to one-and-a-half degrees, et a ground separation of about 420 kilometers (the aircraft velocity approximates 10 kilometers per minute), representing a curvature roughly of two to three degrees per half-cycle (420 kilometers), or one degree per 140 to 210 kilometers.

Since the image is offset from the aircraft flight path, at its mid-point, by 28 to 37 kilometers, the effect of curvature will also impose a y error, by shortening or lengthening the offset path.



If the variation in direction is $\pm 1^\circ$, then it can be seen that the length of the mid-point of the image may be stretched or shortened by roughly $2 \times 37 \times \tan 1^\circ$, or approximately one kilometer in 420 as a consequence of the cross-track component of the 84-minute oscillation, or about $\pm 1/4 \%$.

VERTICAL OSCILLATIONS AND ERRORS

Vertical errors are great in SLAR surveys. In the first place, the area imaged is offset 18 to 55 kilometers from the aircraft path, so altitude or ground clearance measurements of the aircraft have inexact application to the trigonometry of image formation. In the second place, local variations of some extent will always exist on the ground surface. The trigonometric functions are relatively simple, and the variability of the assumption very great, so no attempt will be made here to examine the consequence of height error (which really means the consequences of an improper setting of the slant-range to ground-range conversion function for the area in question).

Instead of trying to outguess these matters, it seems more fruitful to minimize the functions. This can be done, in the case of stereo coverage, by mosaicking, whenever possible, the far-range imagery, which suffers distortion from these trigonometric functions to a far lesser degree than does near-range imagery. Integrated scale over the far-range will vary only by amounts approximating the following expression:

$$\frac{0.07 \times \Delta h}{18}$$

which, for a height error of 1 kilometer will equal:

$$\frac{0.07}{18} \text{ km} \approx 0.004 \text{ or } 0.4 \%$$

whereas, scale errors in the near-range for the same vertical error will be five to eight times as great.

Short-term oscillations of the aircraft path will, in general, be of the order of ± 10 to 15 meters, too small to affect scale significantly, or cause short-term variation of image forms. In general, aircraft angular motions have periods corresponding to about one kilometer of flight.

PROCESSING AS A SOURCE OF ERROR

Synthetic-aperture SLAR has two occasions for film travel in which there exist the possibility of film wander in the x-direction. The first occurs in the recorder itself, and the second in the correlator. In both cases, reduction of y scale by a factor of 72 to 1 will occur in the making of the image film, so that relatively long-epoch wandering of data film becomes short-epoch wander in the x direction on the image film. Careful engineering is reducing the amplitude of this variation, but films made so far have occasions of wander of as much as 0.5 mm. This variation appears, of course, as x-parallax, and it accounts for the "galloping" terrain often noted in SLAR stereo studies. If it occurs in the original recording, it cannot be removed; but if it occurs during correlation, re-correlation may well get rid of the difficulty.

AIRCRAFT GUIDANCE

Certain constraints are imposed on the aircraft flight profile which result in constraint on geometric errors possible in the final film. A firm realization of these constraints should simplify the analysis of image errors.

For example, aside from a possible start-up ramp which careful operations will avoid, there should be no cyclical y variation of a period shorter than 84 minutes, and no non-cyclical variations. Nor should a full cycle of cross-track effect on flight direction ever occur in less than 84 minutes.

The aircraft is controlled on its entire mission by auto-pilot linkage to the inertial guidance system, so the cause of deformations which can be caused by lateral variations of the flight path should always first be sought in the aircraft flight control. Cyclical or episodic variations of shorter periods should be sought in the "edge-wander" phenomenon, altitude control erratics, of internal hunting of the SLAR circuitry.

ACCUMULATION AND CORRECTION OF ERRORS

Since the cost of accurate radio-positioning of a single SLAR image strip would be economically infeasible, and since single strips are involved almost solely in reconnaissance for military targets or geologic evidence, it is evident that the positional errors on a single strip of synthetic-aperture SLAR are essentially trivial in the context of resolution limits, distortion due to elevation change, inaccuracy of location of control points, and other such errors. It is only when SLAR images are made over large areas and joined to make mosaics that the accumulation of errors causes difficulties which require either corrective measures or willingness to abandon all pretense of geometric exactitude.

A fundamental problem arises from the inability, by a one-step photographic process, to achieve individual scale changes in two orthogonal axes. If a succession of images displays a bias in scale relationship between x and y, this bias must express itself in a difference between the ultimate scales for x and y in the assembled mosaic.

For these, and other reasons, it would seem that the theoretical potential and the actual experience in the matter of assembling of SLAR imagery over large areas is far more indicative of the cartographic potential of SLAR images than would be the detailed examination of single strips.

The rather crude practices employed in mosaicking images contribute to the problem in a forceful way, whose consequences must be anticipated and corrected. For example, the most common practice in assembling photo mosaics is to expose dry photo-sensitive material on a paper base and then to process it by normal tray methods, after which the prints are made to fit a matrix of control, and while wet are glued with a water paste to a hard board substrate. Typically, this process results in a growth of the photo sensitive material of approximately 1 % in the direction of its grain and 2.5 % in the direction of cross grain. The residual bias approximates 1.5 %.

It will be evident that an assembly of such prints, carefully matched so that there are no gaps or overlaps at the print junctures, will accumulate a differential scale of 1.5 % if the input material is perfect and no corrective measures are made.

As noted in an earlier part of this discussion, there are also cyclical scale errors in the y direction of more than + 1 % as a consequence of the Shuler oscillation in the inertial platform. At scales of one-quarter million, or greater, it is possible to let the scale variations caused by the Shuler oscillation average itself out, as long as the paper shrink bias is corrected; but at scales of 200 000 or 100 000, this liberty cannot be taken, and corrections must be made for the cyclical variations as well as the bias.

Fortunately, in the synthetic aperture SLAR system the correlation process by which the data film is transformed to the ultimate image film includes a step in which differential scale changes of as much as + 5 % can be made. As a consequence of this anamorphic capability, it has become the practice of the user of the synthetic aperture system to incorporate a compensating bias in the correlation process, which anticipates the paper stretch bias and corrects for it. In other words, the standard correlation scale provides that the y dimension will be long by approximately 1.5 %, so that the assembled photographs which suffer from the paper stretch bias of 1.5 % will come out with equal scale.

The transverse component of the 84-minute oscillation can also be corrected by the ability to deform paper strips processed by wet chemistry to correct the curvature which is its consequence. Hence, it is clear that the capability exists within the synthetic aperture SLAR systems to correct for process system biases and cyclical variations of scale or path.

Practice has led to the conclusion that the improved photographic quality and the ability to achieve image fit which inhere in the conventional wet processing method provide more advantage than the manipulation of either pre-wet prints or stable base prints to avoid the stretch bias. Photographic quality usually suffers from these alternate methods, and the inflexibility of the paper prohibits the fitting which is a necessary attribute to mosaicking problems.

SCALE CONTROL

Two methods have been employed to achieve the knowledge of ground positions which correspond to the image, which is required to correct for the bias and cyclical scale variations. In Colombia, a matrix adjustment devised and carried out by Franz Leberl has been employed to prove a prescription to the correlator operator which permits a continuous variation of scale to achieve a fit with his matrix of interpolated points from a relatively sparse system of control. The scaled prints are then printed and mosaicked so that the set of positions will be met in coincidence by the corresponding mosaic images.

In Peru, the aircraft was monitored by a Shoran triangulation system such that its position was always known within 100 meters or so. Since the data-recording system was so arranged that the coordinates and positions were recorded on digital tape at 10-kilometer intervals, as sensed by the inertial navigator, it was a relatively-simple matter to instruct the computer to record the difference between the assumed 10 kilometers and the actual distance as measured by the Shoran. From this difference, a prescription for differential correlation scale could be made, which permitted continuous correction of the cyclical variations. Compilation in this case was achieved by matching "range marks" with their trigonometrically computed position.

SUMMARY

A synthetic aperture system flown over an ideal flat surface, with proper guidance, should have sufficiently good slant range-ground range correction to provide an almost perfect balance of scale, and produce a distortion-free image. Those distortions which arise from cyclical variations can be corrected in the correlation process in company with the opportunities for corrections, which lie in the mosaicking process itself.

It is suggested, therefore, that an analysis of scale and position errors in SLAR imagery should be made not solely from the raw strips, but instead from final mosaics, and in view of the correction potentials available in this process.

INTERPOLATION AND FILTERING OF ERTS-IMAGERY

by H. P. Bähr, Hannover, Fed.Rep. Germany

ABSTRACT

Least-squares filtering and interpolation is applied to an ERTS frame in channel 5 and 7. Covariance functions are determined from residual errors of 4-parameter fit. Though there is only a small number of reference points, results come out well. Results from least-squares interpolation are compared with residual errors from second-order polynomial interpolation.

INVESTIGATED IMAGERY

An ERTS-1 bulk photo from September 21st, 1972, showing parts of northern Germany lowlands was investigated (scale approx. 1 : 1 000 000). Though there is 40 % cloud cover, it is the most cloud-free photo available of this region.

Results by polynomial interpolation of this frame have been published (Bähr and Schuhr in [1]). Continuing these works, independent measurements have been carried out in channel 7 (0.8 ... 1.1 m) at 41 new points, which again are all related to water bodies. Additional observations were made at 20 points in channel 5 (0.6 ... 0.7 m) which nearly all are related to forest features. Interpretation of reference points was a sophisticated task, as they are of no symmetric shape; beside this, cloud cover in NE and SW and atmospheric haze prevent recording of more and better situated points. Image coordinates, measured at the Zeiss-PSK-Stereocomparator were related by a 4-parameter-fit ("Helmert-transformation") to terrain coordinates extracted from 1 : 50 000 scale maps.

Fig. 1 shows the result of this transformation for channel 7. All observations have been introduced as reference points. The root mean square errors, calculated from the residual errors, are

$$m_{x5} = \pm 109 \text{ m (channel 5)}$$

$$m_{y5} = \pm 127 \text{ m (channel 5)}$$

$$m_{x7} = \pm 131 \text{ m (channel 7)}$$

$$m_{y7} = \pm 136 \text{ m (channel 7)}$$

The vector diagrams show similar behavior of error distribution in both channels including the independent results from [1]. Finite regions indicate characteristic trends. Reasons for this may be effects from data processing, from atmospheric refraction or from inaccurate orientation data, i.e. parameters, which are identical for all channels at first-order approximation

DETERMINATION OF COVARIANCE FUNCTION

The results in Fig. 1 indicate presence of both correlated (l_s , "systematic") and uncorrelated (l_r , "observational") error components. Summation of these components give the vectors shown in Fig. 1

$$l_i = (l_s + l_r)_i$$

By least-squares filtering both parts can be separated; by least-squares interpolation, both parts can be predicted at any point, if suitable reference points are available.

To prepare filtering and interpolation, a covariance function is to be determined from residuals after the 4-parameter adjustment, where all 41 points were introduced as reference points (Fig. 1). This is the most appropriate way to find out the stochastic conditions of the ERTS-frame. After the covariance function is determined that way, it is used for all further calculations. Empirical determination of covariance functions interval by interval leads to discontinuous functions. They must be approximated by a continuous function.

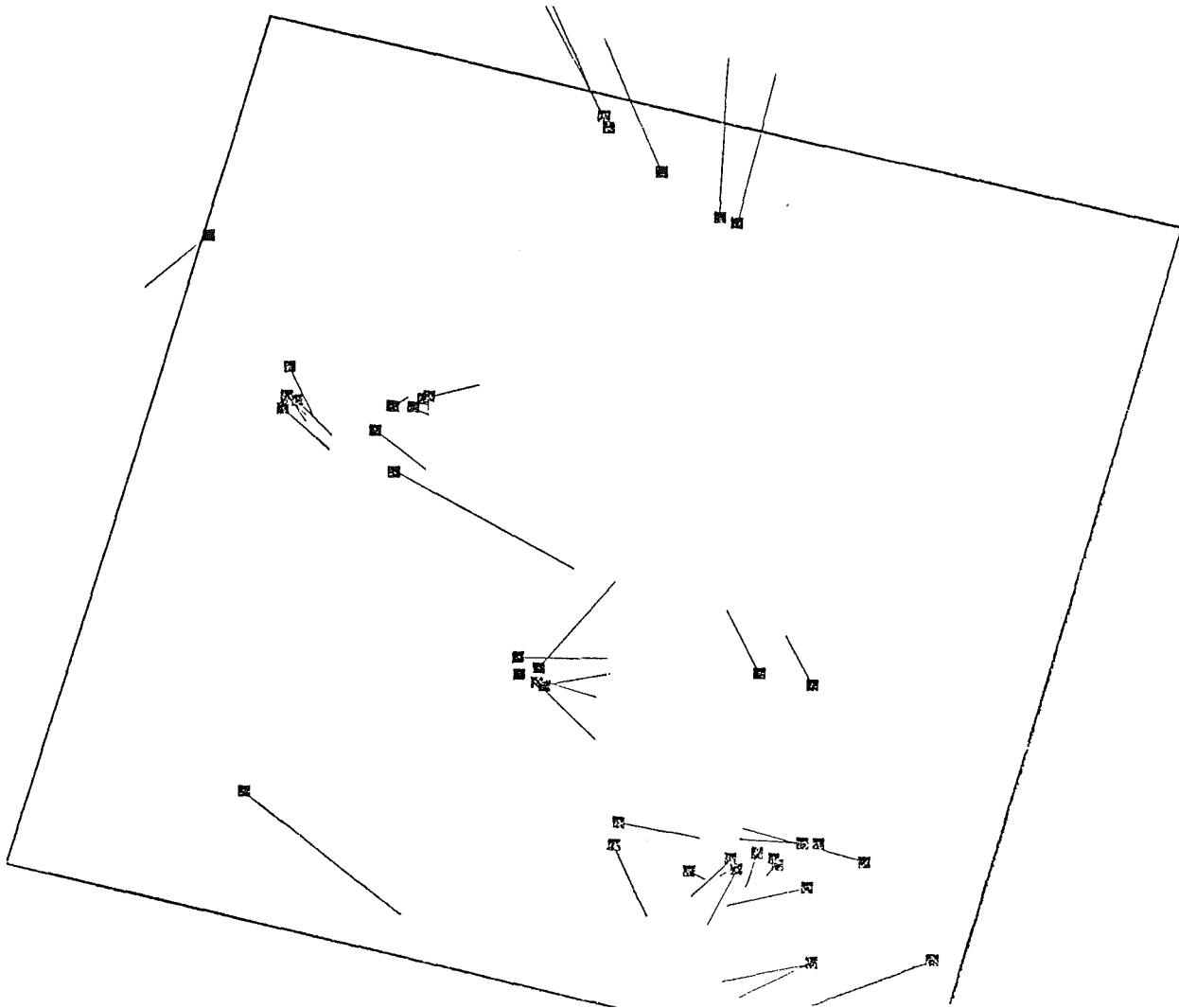


Fig. 1: ERTS Channel 7

Residual errors after 4-parameter-fit
Reference points shown by solid spots (41)

Variances of residual errors:

$$\begin{aligned} V_x &= 0,0171 \\ V_y &= 0,0185 \end{aligned}$$

Scale --- 10 km (situation)
100 m (vectors)

In Fig. 2 covariance functions have been found independent for x and y in terms of 1,0 cm- and 2,0 cm-intervals. Size of the ERTS-frame was 18 by 18 cm. Fig. 2 shows that the extend of interval size may be of importance for the function which has to be determined, because of the small quantity of points. Though it is not absolutely necessary, a Gauß function often is used to describe the covariance conditions:

$$C(\overline{P_i P_k}) = C(0) e^{-k^2 s^2}$$

Herein $C(0)$ and k^2 have to be determined. $C(0)$, vertex of the curve, represents the variance of the l_s -components V_s . Theoretically, V_s is smaller than the variance of the total error component V by the amount of V_r , variance of the l_r -components

$$\frac{1}{n} \sum_{i=1}^n (l_i \ l_i) = V = V_s + V_r$$

In Fig. 2 the amounts of V, which may be calculated from residuals after the 4-parameter adjustment, have been marked above the vertexes of the curves. The unit of the residuals is in kilometers. The k^2 -parameter influences on the "bandwidth" of the curve and indicates up to which distance s correlation between error components may be found.

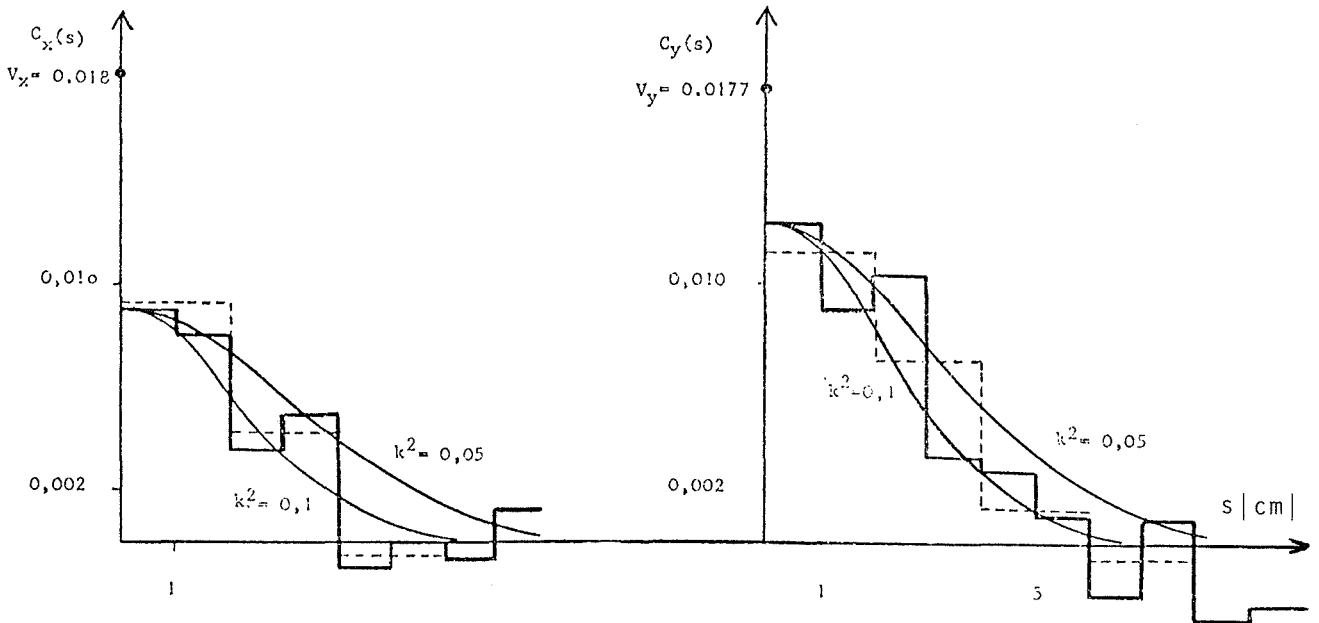


Fig. 2: Determination of covariance functions

The dashed lines represent values for a 2 cm-interval.
For $s > 10$ cm the values can show large discontinuities.

RESULTS FROM LEAST-SQUARES FILTERING AND INTERPOLATION

The covariance function includes the whole information of the error distribution. It allows to estimate the portion of l_s -components by following equations (see [3]):

$$l_{si} = c_i^t C^{-1} l$$

where

$$c_i = \begin{vmatrix} C \overline{(P_1 \ P_i)} \\ \vdots \\ C \overline{(P_n \ P_i)} \end{vmatrix}; \quad C = \begin{vmatrix} V & C \overline{(P_1 \ P_2)} & \dots & C \overline{(P_1 \ P_n)} \\ & V & \dots & C \overline{(P_2 \ P_n)} \\ & & \ddots & \vdots \\ & & & V \end{vmatrix}$$

The $C \overline{(P_i \ P_k)}$ elements may be calculated from the covariance function. This function must be continuous. If we use the covariance values calculated for certain intervals, we get identical lines in the C matrix, i.e. singularity in case that 2 points lie within the same interval.

V is known a priori from the residual errors in Fig. 1. Though the values for $l_i \ l_i$ differ from point to point, the mean square value V has been introduced into C . Its amount is about 0,018 for both x and y. As the determination of the covariance function out of 41 points, which configuration is poor, remains

uncertain, investigations with different parameters have been carried out:

$$C(\overline{P_i P_k}) = F V e^{-k^2 s^2}, \quad F V = C(0)$$

We call F the filtering coefficient. Regarding Fig. 2, we find $F_x \sim 0.5$ and $F_y \sim 0.7$. These numbers, empirically found, should give the best estimated values for l_s . If we use $F = 1.0$, we get larger l_s values: the whole l is interpreted as l_s -component and is filtered away. If F is smaller than the calculated values, we filter less than we should do. To improve the error distribution of the 4-parameter adjustment, we subtract the estimated l_s -components from the residual errors and get estimated random components l_{xr} , l_{yr} . Respectively, we have V_{xr} , V_{yr} and V_{xs} , V_{ys} for variances, which include values at the reference points.

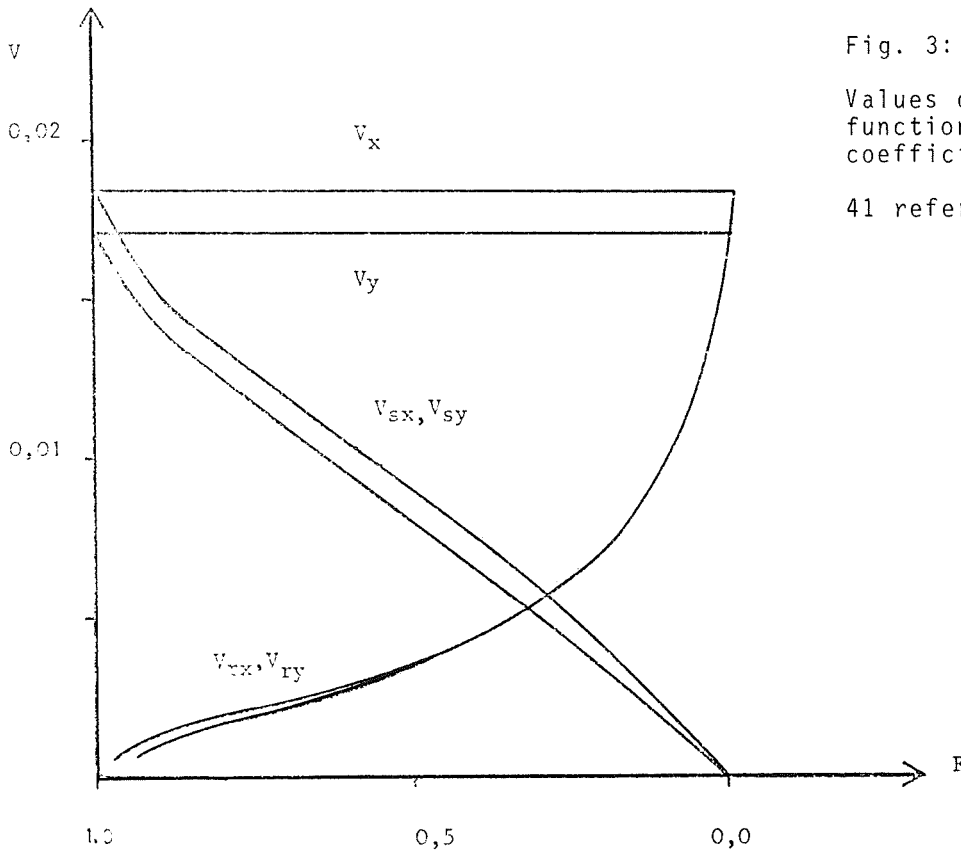


Fig. 3:
Values of variances as a function of the filter coefficient F
41 reference points

In Fig. 3 variances calculated that way show, that the behavior of errors is a function of F . In particular, we see the effect from $F = 1$, where $V_{rx} = V_{ry} = 0$ and the effect from $F = 0$, where $V_{sx} = V_{sy} = 0$. We find that the accuracy is not very sensitive down to values of $F = 0.5$ and does hardly differ in x and y . It is for this reason, that all examples for filtering and interpolation published here have been calculated with $F = 0.75$, both for x and for y . Beside this we read from Fig. 3, that V_r and V_s do not sum up to V as it should do theoretically. This will not happen, because the l_s -components have not been determined exactly, since the true variance-covariance conditions remain unknown (see [4]).

Fig. 4 shows the result after filtering the residual errors from Fig. 1 with $F = 0.75$. Fig. 5 gives the result from filtering and interpolation by 10 reference points for channel 7. The result shown in Fig. 5 is similar to Fig. 4, for there is not much change in error distribution if less than 41 reference points are introduced. However, this is not true for isolated points (see lower and upper left), which are hardly touched by the covariance function. For channel 5, we get the same variances V_r as in channel 7; this is because of accumulations of reference points. Error distribution after filtering is better in channel 7, where a larger number of points (41 versus 20) and a better configuration contributes to better stochastic conditions.

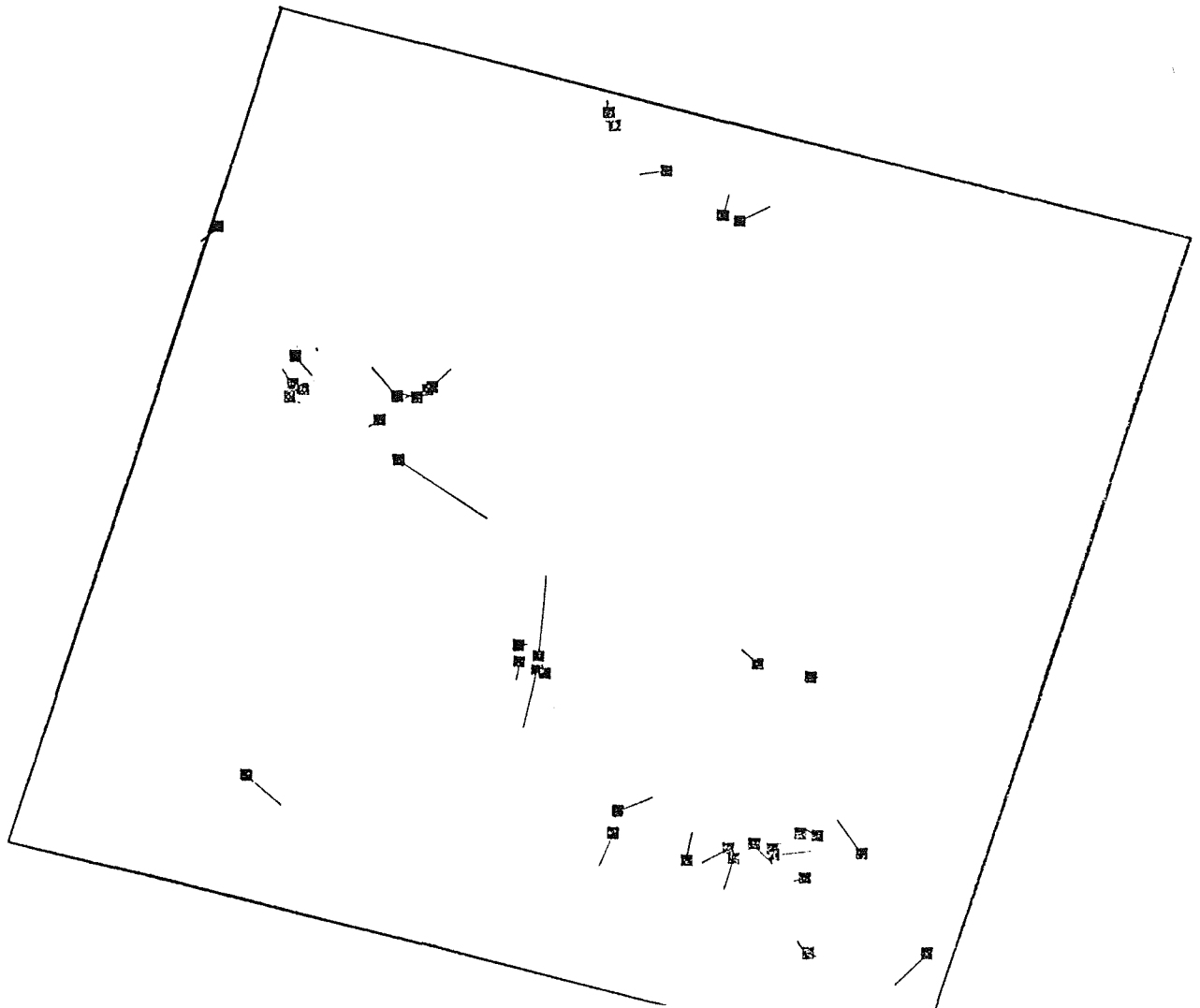


Fig. 4: ERTS Channel 7 - 1_r -components

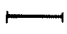
Reference points shown by solid spots (41)

$$V_2 = 0,018$$

$$K = 0,05$$

$$F = 0,75$$

$$\text{Variance of } 1_r: \begin{matrix} V_{xr} = 0,0025 \\ V_{yr} = 0,0021 \end{matrix}$$

Scale 

10 km (situation)
100 m (vectors)

In the diagrams, orientation is towards grid north, corresponding to the reference meridian of the 3rd Gauss-Krüger-System. Consequently, the ERTS frames appear in oblique sense.

To give a rough idea of the improved results, see Table 1. Here, residual errors from 4-parameter fit and from least-squares interpolation have been listed. We get the M values in meter by taking the roots of corresponding V values and by multiplication with 10^3 . Though they can not strictly be interpreted as root mean square errors, they indicate the magnitude of the residual errors.

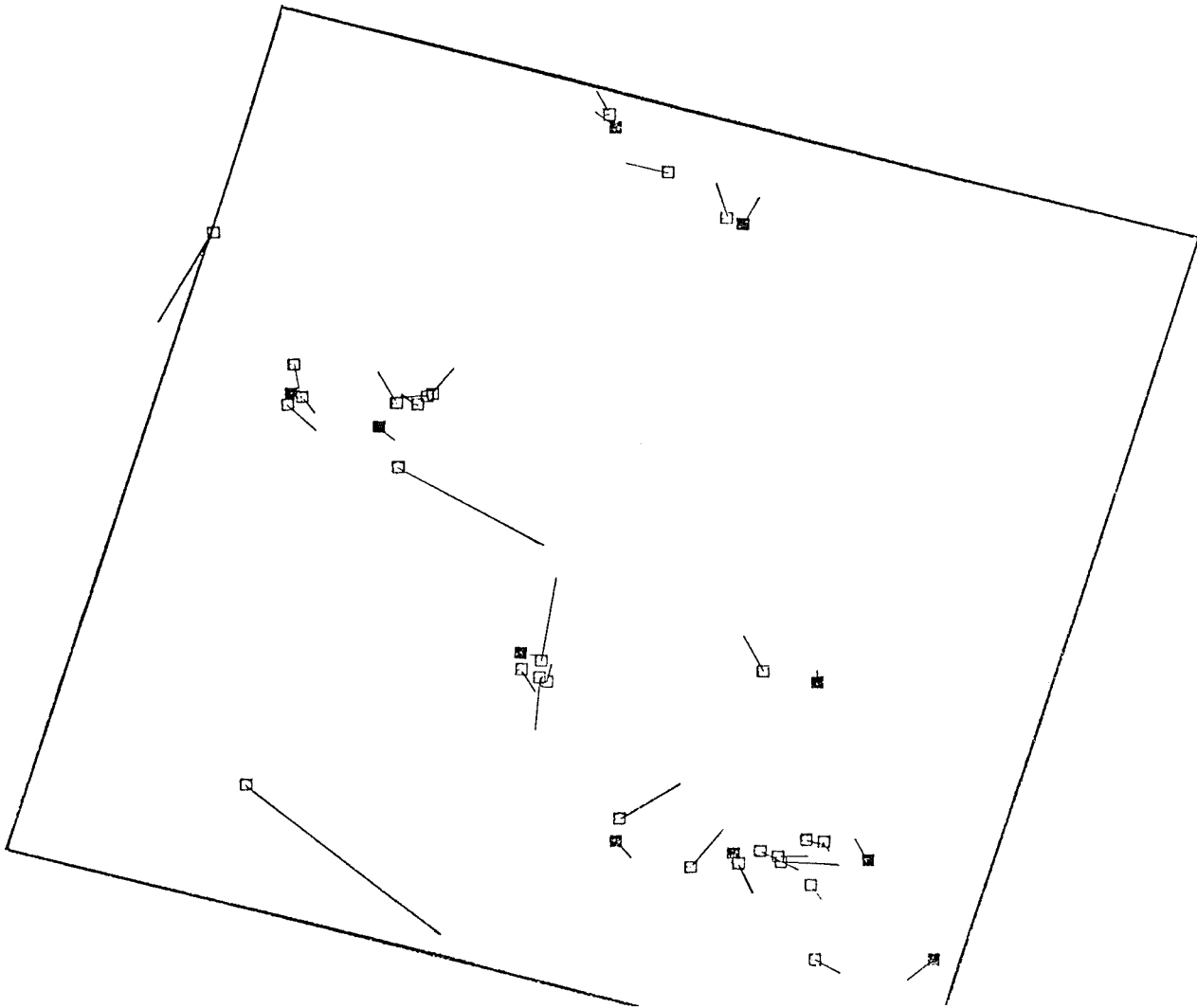


Fig. 5: ERTS Channel 7 - l_r -components
Reference points shown by solid spots (10)
 $V_2 = 0,018$
 $K = 0,1$
 $F = 0,75$
Variances of l_r : $V_{x_r} = 0,0063$
 $V_{y_r} = 0,0077$
Scale: ---
10 km (situation)
100 m (vectors)

First, M_x , M_y , i.e. residuals after 4-parameter adjustment, show the excellent quality of the ERTS image, which has a theoretical resolution of about 79 m per image point. The more reference points introduced, the better is the result, which lies about the value of theoretical resolution. An interesting detail is the influence of the k^2 parameter. For $k^2 = 0,01$ the M values go down a little bit compared with the value M from $k^2 = 0,1$. This is only because of the 2 isolated points at the left side of the frame. These points are improved if $k^2 = 0,01$, whereas they don't get corrections if $k^2 = 0,1$.

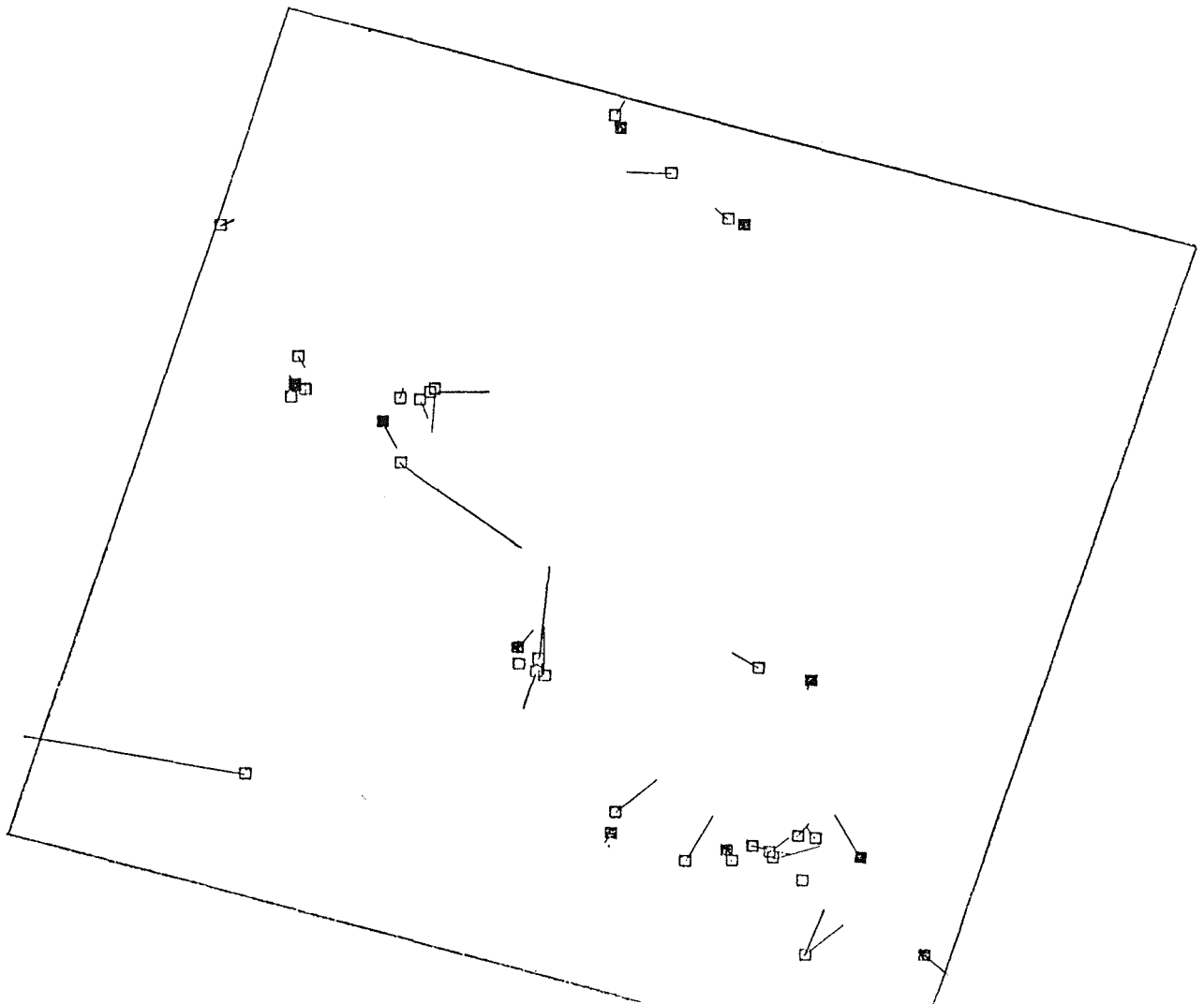


Fig. 6: ERTS Channel 7


Residual errors after second-order polynomial adjustment

Reference points shown by solid spots (10)

Variances of residual errors:

$$V_x = 0,00349$$

$$V_y^x = 0,00759$$

Scale: 

10 km (situation)
100 m (vectors)

INTERPOLATION BY POLANOMIALS

Least-squares interpolation is just one method for interpolation. In [1], polynomials have been successfully applied to evaluate ERTS imagery. Comparison of the results obtained by this two methods seems useful.

For interpolation, we take second-order polynomials:

$$x' = a_0 + a_1x + a_2y + a_3xy + a_4x^2 + a_5y^2$$

$$y' = b_0 + b_1x + b_2y + b_3xy + b_4x^2 + b_5y^2$$

with 6 unknowns for each coordinate. The result of the adjustment for channel 7 with 10 reference points is listed in Fig. 6. Comparison with results from the same point configuration after least squares interpolation in Fig. 5 show very good accordance. Differences can be observed at the 2 isolated points at the left side of the frame, where polynomials extrapolate, whereas least-squares interpolation does not transfer any information, if the covariance function is determined properly.

Channel	Reference points	Interpolated points	M_x [m]	M_{xr} [m]	M_y [m]	M_{yr} [m]	F	k^2
1	2	3	4	5	6	7	8	9
7	41	-	131	50	136	45	0.75	0.05
	31	10	134	57	134	58	0.70	0.10
	10	31	138	79 71	145	88 77	0.75	0.10 0.01
	5	36	134	91	141	101	0.70	0.10
5	20	-	109	41	127	60	0.75	0.02
	9	11	134	80	122	88	0.70	0.02
	4	17	152	103	126	96	0.70	0.02

Table 1

Table 2 lists the magnitudes of the residual errors after polynomial interpolation corresponding to Table 1 (r stands for "residual"):

Channel	Reference points	Interpolated points	M_x [m]	M_{xr} [m]	M_y [m]	M_{yr} [m]
7	10	31	138	59	145	87
5	9	11	134	59	122	77

Table 2

In conclusion we find that both interpolation methods give roughly the same results. However, polynomials are easier to process than least-squares interpolations. On the other hand, this method is more flexible and can be applied to a lot of further problems.

More sophisticated error analysis like Kraus suggests in [4] can not be carried out here because of small number and poor configuration of the reference points. Anyhow, the results obtained encourage to continue work into this direction.

REFERENCES

- |1| Bähr, H.P. and Schuhr, W.: "Versuche zur Ermittlung der geometrischen Genauigkeit von ERTS-Multispektral-Bildern", Bildmessung und Luftbildwesen 42, p. 22 - 24, 1974
- |2| Kraus, K.: "Interpolation nach kleinsten Quadraten in der Photogrammetrie" Bildmessung und Luftbildwesen 40, p. 4 - 12, 1972
- |3| Kraus, K. and Mikhail, E.M.: "Linear Least-Squares Interpolation", Photogrammetric Engineering 38, p. 1016 - 1029, 1972
- |4| Kraus, K.: "Untersuchung zur Genauigkeit der Interpolation nach kleinsten Quadraten", Zeitschrift für Vermessungswesen, p. 198-205, 1974

TOPOGRAPHIC ACCURACY OF SIDE-LOOKING RADAR IMAGERY

by E. E. Derenyi, Fredericton, Canada

ABSTRACT

The topographic accuracy of two strips of SLAR imagery, flown over Phoenix, Arizona by the Goodyear Mapping System at a scale of 1 : 400 000 was investigated. Linear conformal-, affine-, and polynomial transformations were employed to test the planimetric accuracy. The best results obtained for the root mean square error (RMSE) was 27.4 m. Polynomial was also used for the adjustment of heights. The smallest value attained for the RMSE was 30.7 m.

INTRODUCTION

The objective of this investigation was to ascertain the accuracy by which the planimetric position and elevation of points can be determined from side-looking airborne radar (SLAR) imagery. The test material used consists of two strips of SLAR imagery of Phoenix, Arizona and vicinity, flown by the Goodyear Mapping System 1000 (GEMS) at a scale of 1 : 400 000. The lines were flown in a North-South direction at an altitude of 12,040 m. The positions and elevations of ground control points were determined from 1 : 24 000 scale topographic maps at the Institute of Photogrammetry in Hannover.

These strips overlap in an opposite-side configuration. For Strip 1 the ground range delay is 5 nautical miles (9,266 m), while for Strip 2 it is 15 nautical miles (27,800 m). The first range marks appearing are those at 10.0 and 17.5 nautical miles (18,532 m and 32,431 m) slant range respectively. The spacing of the marks is 2.5 nautical miles slant range and the presentation is in ground range.

MEASUREMENTS AND PREPARATORY TESTS

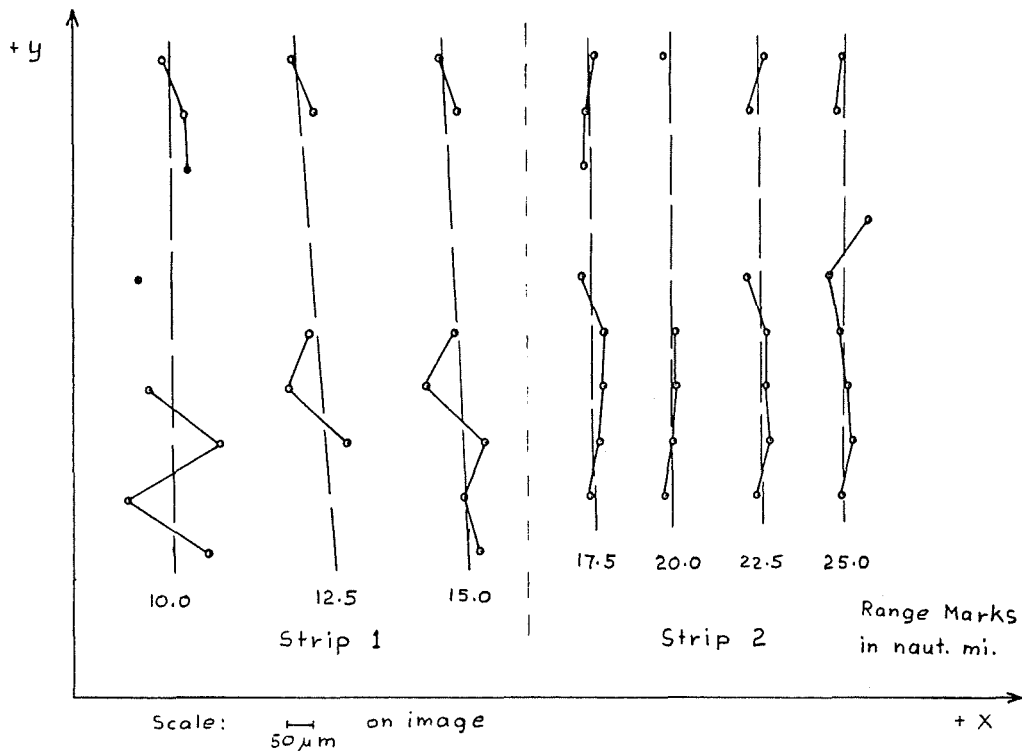
The image coordinates of the test points were measured in a Zeiss PSK comparator under 8 times magnification and in two independent sets. Stereo vision is extremely difficult on opposite-side overlaps, therefore, the measurements were performed monocularly. The standard error of one measurement as computed from the double measurements was 11 μ m and 15 μ m for the x coordinates, and 16 μ m and 18 μ m for the y coordinates in Strip 1 and Strip 2, respectively. This precision is regarded as entirely satisfactory, considering that the definition of the points was far less distinct than on conventional photographs.

On each strip the image coordinate system was defined by the row of range marks closest to the ground track. A straight line was fitted to these marks by least squares adjustment, which was then adopted as the direction of the y-axis. Straight lines were also fitted to the other rows of range marks in order to ascertain the accuracy of their alignment. Table 1 lists the standard deviation of the fit for each line and Figure 1 shows graphically the deviation of the individual marks from the fitted line.

TABLE 1 - STANDARD DEVIATION OF STRAIGHT LINE FIT TO RANGE MARKS

	Range mk. naut. mi.	σ fit in mm
Strip 1	10.0	0.066
	12.5	0.041
	15.0	0.035
Strip 2	17.5	0.024
	20.0	0.017
	22.5	0.010
	25.0	0.015

Figure 1: Straight Line Fit to Range Marks



In Strip 2 the fit is rather good and the deviations for the individual marks are in the range of the measuring accuracy of the image points. In Strip 1, however, the fit is poor and large deviations occur. Nevertheless, the lines are quite parallel to each other and the spacing between marks of adjacent lines remains remarkably constant. This systematic trend of the deviations is probably due to variations in the direction of the film movement during recording of the image.

Table 2: RANGE MARK SPACING AND SCALE FACTOR

	Range m. Interval naut. mi.	Average spacing in mm	Standard deviation in mm	Average scale factor
Strip 1	10.0-12.5	13.957	0.007	408 540
	12.5-15.0	13.004	0.008	404 891
Strip 2	17.5-20.0	12.246	0.007	403 469
	20.0-22.5	12.083	0.005	402 784
	22.5-25.0	12.039	0.003	400 116

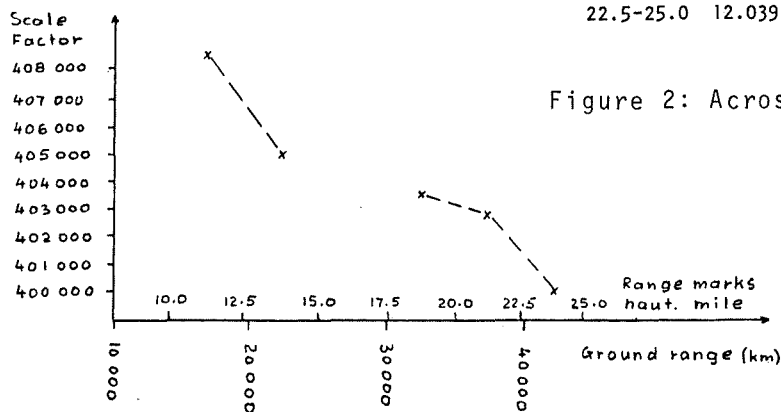


Figure 2: Across-track Scale Change

Next, the image scale was computed for each available range mark interval. For this purpose the corresponding ground distances were computed from the average flying height and the given slant range values of the range marks, based on the flat earth assumption. As expected from the fairly equal spacing between range marks, the average variation in the scale is only 0.05 % within adjacent rows of range marks. However, it shows a systematic decrease across-track towards the far range as illustrated by Table 2 and Figure 2.

TOPOGRAPHIC ACCURACY TEST

The preparatory tests on the quality of the imagery were now completed and the topographic accuracy was investigated next. Normally, an inertial navigation system, a radar altimeter and a statorscope are on board during SLAR survey flights. From the data provided by these devices the space position of the radar air stations could be determined at frequent intervals, then slant ranges could be interpolated for the measured image points in between range marks and finally the ground positions of the test points could be intersected. Data from the above mentioned sensors were not available for the test imagery, therefore the planimetric and height accuracy were investigated separately.

PLANIMETRIC ACCURACY

Essentially, the method of approach was to fit the radar record to planimetric control points by coordinate transformation. If the image is a faithful geometric representation of the terrain, in plan, then a good fit should result. Otherwise, large residuals will occur at the fitted points, but especially at the intermediate points. This approach, of course, disregards the effect of relief displacements and demonstrates the accuracy of single strips only.

First the image coordinates were transformed into the ground system by linear conformal transformation. Two widely separated points were employed for this purpose. At all other test points the discrepancies were formed between the ground coordinates and the transformed image coordinates and the root mean square error (RMSE) of the fit was computed. The results are listed in Table 3. Strip 1 shows a remarkably good fit, considering the simple transformation technique employed.

Table 3: ROOT MEAN SQUARE ERRORS OF DISCREPANCIES AT CHECK POINTS

Transform- ation	No. of check points	Strip 1				Strip 2			
		Ground Scale		Image Scale		Ground Scale		Image Scale	
		μX in m	μY in m	μx in mm	μy in mm	μX in m	μY in m	μx in mm	μy in mm
Conformal	314	27.8	30.2	0.069	0.075	69.0	58.2	0.174	0.146
Affine	300	27.4	30.3	0.068	0.075	31.4	46.4	0.079	0.117
Polynomial	300	27.6	29.5	0.068	0.073	29.1	45.9	0.073	0.116

Next a polynomial transformation was employed to improve the fit. The polynomials had the form

$$X = a_1 + a_2x + a_3y + a_4xy + a_5y^2 + a_6xy^2$$

$$Y = b_1 + b_2y + b_3x + b_4xy + b_5y^2 + b_6xy^2$$

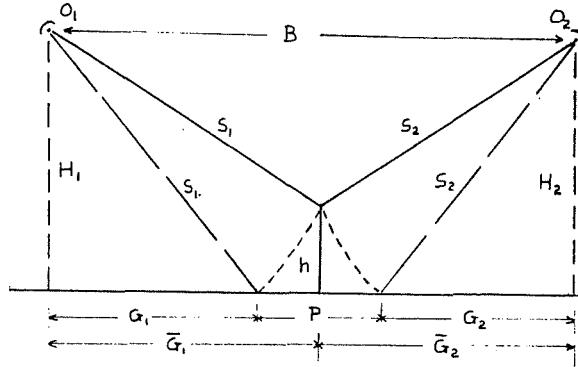
where X, Y are ground coordinates and x, y are image coordinates. These polynomials were designed to compensate for changes in the exterior orientation and to reduce the effect of certain interior orientation errors (Derenyi, 1974). Sixteen points distributed regularly over the strips were used to evaluate the coefficients. The RMSE of the discrepancies after transformation at the remaining, check points are listed in Table 3. The results obtained with the full length of the polynomials and when truncated at the third term, to form an affine transformation, are listed separately.

Affine transformation produced a marked improvement in the accuracy of Strip 2. The higher order terms in the polynomial, however, changed the RMSE only slightly. For Strip 1, on the other hand, very similar results were obtained by the three transformation techniques. It appears therefore, that affine transformation is a satisfactory method to derive ground coordinates from SLAR images.

HEIGHT ACCURACY

The geometry of the height determination is illustrated on Figure 3.

Figure 3: Geometry of Height Determination



It is assumed that the earth is flat and the two radar air stations are at the same height above the datum. Since the parallax was not measured directly, the heights were computed from the equation:

$$h = H - \frac{H^2 + G_1^2 - G_2^2}{2B}$$

where

$$G_1 = \frac{B^2 + G_1^2 - G_2^2}{2B}$$

or

$$h = H - \frac{H^2 + G_2^2 - G_1^2}{2B}$$

where

$$G_2 = \frac{B^2 + G_2^2 - G_1^2}{2B}$$

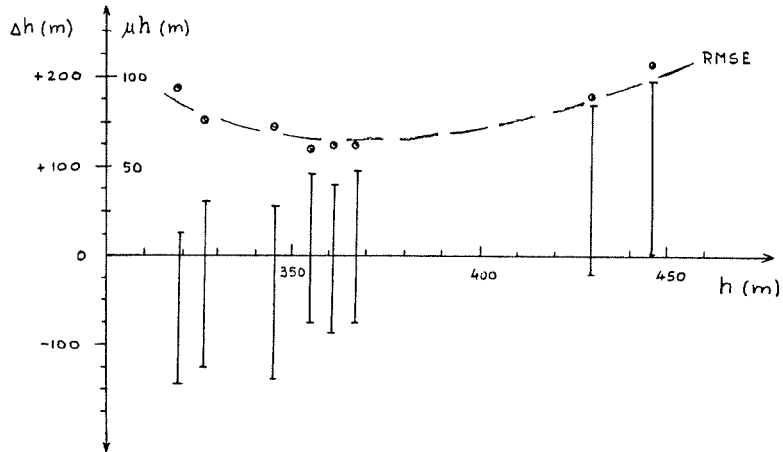
In the above equations, \$h\$ is the elevation of a point above the datum; \$H\$ is the elevation of the radar air stations above the datum; \$G_1\$ and \$G_2\$ are the ground ranges of a point as reduced from slant ranges, or obtained from ground range presentations, for flights 1 and 2 respectively; \$\bar{G}_1\$ and \$\bar{G}_2\$ are ground ranges to the projection of a point onto the datum plane, for flights 1 and 2 respectively and \$B\$ is the air base.

Some difficulties arose in finding the correct value for \$B\$, since the radar air stations coordinates were unknown. In conventional photogrammetry a change in the value of \$B\$ leads only to an overall scale change. Therefore, one can proceed by using an assumed value for \$B\$ to form model coordinates and perform the scaling later. For SLAR, however, the terrain height is a non-linear function of \$B\$ and an incorrect, or assumed value leads to severe model deformations.

One could determine \$B\$ as the sum of the two ground ranges of a point situated on the datum plane. However, the terrain elevation of the datum plane must be known, neither of which was available for this test. Therefore, the length of \$B\$ was derived by a trial and error procedure as follows.

Sixteen points, well distributed over the strip, were selected as a test sample. Eight of these points, which ranged in terrain elevation from 318 m to 446 m, were then chosen as datum points one after the other and the height of the remaining fifteen points was determined. Next, the discrepancies between the given and computed heights were formed and the RMSE calculated. When plotted, the RMSE's followed a second degree curve and reached a minimum value around one third of the way towards the high point from the low point. The range between the maximum and minimum discrepancies stayed approximately constant, but they were predominantly with a negative sign when the lowest point was used as the datum and all had a positive sign for the highest datum point. A near normal distribution was reached again close to the one third mark. Figure 4 illustrates these findings. Consequently, a point with an elevation of 344 m was selected as the datum point.

Figure 4: Effect of the Change of Datum Point on the Height Determination



The height of all 318 test points was now computed. The RMSE of discrepancies between the given and computed heights was 55.7 m, with the maximum error being 159 m. Thirty points had discrepancies larger than 100 m. However, the model still showed a somewhat systematic deformation as illustrated in Figure 5.

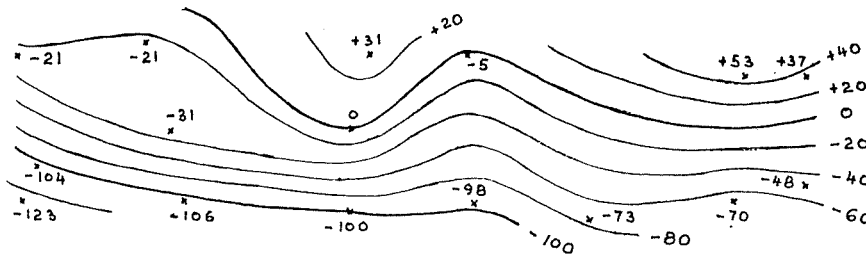


Figure 5: Model Deformations Before Adjustment

Therefore, four control points were selected near each corner of the model to evaluate the polynomial:

$$\Delta h = c_1x + c_2y + c_3xy + c_4x^2,$$

which then was employed to adjust the heights. Now the RMSE decreased to 30.7 m and the maximum value of the discrepancies to 77 m. The model deformation after adjustments is shown in Figure 6. It should be mentioned that a straight and level flight and parallel flight lines were assumed throughout the entire height computation process.

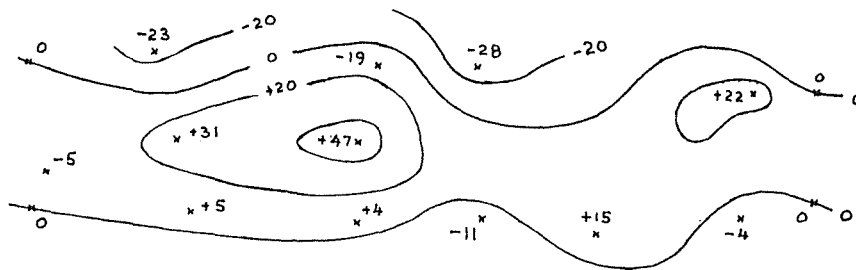


Figure 6: Model Deformations After Adjustment

CONCLUSIONS AND RECOMMENDATIONS

The procedures followed for the test are rather unsophisticated, as yet the results obtained are surprisingly good. For the scale of the image, the planimetric accuracy of both strips is well within the tolerances prescribed by map accuracy standards for Class A maps in North America, which states, that the standard error for the position of well defined features should not exceed 0.3mm at map scale. Even two to three times enlargements would meet the accuracy standards. In this respect, this study underlined earlier claims about the suitability of SLAR for planimetric mapping (see for example Von Roessel and de Godoy 1974).

For spot heights, the specifications for Class A maps require a standard error of not larger than one-third of a contour interval. Therefore, based on this test, it appears that 100 m contours are a definite possibility.

Another yardstick by which the results can be evaluated is a comparison with the accuracies attainable by conventional photography. A recent test indicates that the planimetric accuracy of orthophotos produced of low and moderate-relief terrain is 0.03 mm to 0.06 mm in terms of RMSE at the scale of the original photography (Fleming 1973). The same investigator indicates 0.056 mm to 0.120 mm for the planimetric RMSE in rectified photographs of the same terrain. In the light of these figures the planimetric accuracy of SLAR is excellent.

The absolute accuracy of heights obtained by conventional photogrammetric means ranges from 0.1 % to 0.4 % of the flying height. The 30.7 m RMSE obtained from the SLAR is equivalent to 2.5 % which is much larger than the above figures. One should note, however, that a flying height of 60,800 m would be required to produce a photography with a wide angle camera, at a scale of 1 : 400 000, whereby the 0.1 % - 0.4 % accuracy would become 6.1 m to 24.3m. Now the SLAR results look much more attractive.

Finally, the following recommendations are made to improve the topographic accuracy of SLAR:

- Data from the on-board navigation sensors should be made available. This would enable the computation of ground positions in a more rigorous manner.
- The use of crosses instead of dash lines for the range marks would provide control over the scale in the along-track direction and could serve as reference marks.
- Through a better understanding of the internal geometry, the observed image coordinates could be refined.
- Properly signalized ground control would remove the uncertainties in target identification.

In closing, it must be emphasized, that this investigation is being continued and extended to include more strips. Therefore, the results presented here should be regarded as preliminary.

REFERENCES

- Derenyi, E., 1974: "SLAR Geometric Test", Photogrammetric Engineering Vol. XL, No. 5, pp.597-604
- Fleming, E.A., 1973: "Quality of Production Orthophotos", Photogrammetric Engineering, Vol. XXXIX, No. 11, pp. 1151-1160
- van Roessel J.W. and de Godoy, R.C., 1974: "SLAR Mosaics for Project RADAM", Photogrammetric Engineering, Vol. XL, No. 5, pp. 583-595

ANALYSIS OF DIGITAL MULTISPECTRAL SCANNER (MSS) DATA

by E.M. Mikhail, J.R. Baker and G.W. Marks, West Lafayette, USA

ABSTRACT

Treatment of single (non-overlapping) digital MSS data is performed using both parametric and non-parametric techniques. Parametric methods are based on the collinearity equations and applying polynomials to express the behavior of the sensor exterior orientation elements. The resulting expressions may include the object point elevations if they are externally available.

Non-parametric procedures considered include: the arithmetic mean, the moving average, the meshwise linear transformation and linear least squares filtering.

The results are given for the purpose of comparison. The paper is concluded with a discussion of the specific characteristics involved in the reduction of digital data.

INTRODUCTION

Single MSS data coverage is a two dimensional representation of a generally three dimensional (object) space. Therefore, it is not possible to recover all three dimensions from such data. One either assumes that the object is a plane (i.e. flat terrain), or utilizes information external to the MSS data (e.g. point elevations). Both these possibilities have been analyzed in this research.

Methods for metric analysis of MSS data may be parametric where an attempt is made to functionally model the acquisition system, or non-parametric. Both groups of methods are considered hereafter.

PARAMETRIC TECHNIQUES

For every element in the MSS digital array a pair of collinearity equations may be written much the same as for a photogrammetric ray in frame photography. However, in the case of MSS the exterior orientation parameters vary from element to element because of being time dependent. Since it is impossible to determine a different set of sensor parameters for each data element, or for that matter for each scan line, some functional form is used to model the behavior of these parameters. Although there may be others, this study concentrated on the use of polynomials for that purpose.

There are two approaches to the use of polynomials: one is to rigorously apply the collinearity and substitute polynomials for differentials of the sensor parameters; and the other is to use simplified formulae similar to Hallert's, substitute for the sensor parameters, and continue to derive new polynomials. The first procedure is rigorous and relinearizations and iterations are applied. The second is simplified and is equivalent to multiple linear regression.

The difference between the two procedures was not significant, particularly in view of the computational efforts involved.

The collinearity equations are well known, and their form for MSS is given in [1].

Restitution Using General Polynomials;
the MSS differential formulae are

$$X = X_c + \delta X_c - h \delta \phi - h \tan \theta \delta \kappa \quad (1a)$$

$$Y = Y_c + \delta Y_c + h \tan \theta + \tan \theta \delta Z_c + h(1 + \tan^2 \theta) \delta \omega \quad (1b)$$

$$\text{with } h = Z_c - Z \quad (1c)$$

X, Y = restituted (or object) coordinates

X_c, Y_c, Z_c = sensor position

θ = scan angle

$\delta X_c, \dots, \delta \kappa$ = differentials of the sensor's six parameters.

Each of the six differentials in equations (1a) and (1b) can be expressed as polynomials of varying degree in x, the data (scan) line number. When this is done, element elevation Z which is implicit in h, can be either retained as a known value, or assumed as a constant. To illustrate, consider the case of using linear functions of the form

$$\delta P = A_p + B_p x \quad (2)$$

where P designates any one of the six sensor parameters. After substitution in equations (1a) and (1b) and rearranging, one gets for the case of constant Z:

$$X = A_1 + A_2 x + A_3 y + (A_3/3c^2)y^3 + A_4 xy + (A_4/3c^2)xy^3 \quad (3a)$$

$$Y = B_1 + B_2 x + B_3 y + (B_3/3c^2)y^3 + B_4 xy + (B_4/3c^2)xy^3 + B_5 y^2 + (2B_5/3c^2)y^4 + (B_5/9c^4)y^6 + B_6 xy^2 + (2B_6/3c^2)xy^4 + (B_6/9c^4)xy^6 \quad (3b)$$

In these equations $\theta = y/c$, with c being the effective panoramic recording radius and $\tan\theta$ was expanded to equal $\theta + (1/3)\theta^3$. If the system is roll stabilized, i.e. $\omega = 0$, the last six terms of equation (3b) will be zero.

The polynomials in equation (3) apply to the x and y values as panoramically recorded. If resampling, as explained in reference [1], is performed such that y is replaced by y' which is on an equivalent recording plane and c by c' which is an effective principal distance, these polynomials would be considerably simplified.

DATA SEGMENTATION

It is not practical to assume that a given polynomials equation will represent the behavior of a certain sensor parameter during the entire data record. Since higher order polynomials are not safe to use, it is preferable to select a lower order form and divide the data record into segments. When this is done, suitable constraints must be enforced at the boundaries between segments. When writing such constraints, one must be careful not to use dependent equations particularly in the case when Z is included in the general polynomials.

NON-PARAMETRIC TECHNIQUES

Unlike the parametric methods, non-parametric techniques do not seek to determine a fixed set of parameters for a given data record. Instead, they apply the assumption that the differences between unrestituted and restituted array points are realization values of a two-dimensional stochastic field. Several of these techniques have been applied by Leberl [2] to SLAR imagery. With regard to MSS data the following methods have been considered: Arithmetic Mean, Moving Averages, Meshwise Linear Transformation, and Linear Least Squares Filtering. Each will be briefly discussed.

ARITHMETIC MEAN

Common to all techniques, is having known values l_x, l_y at a specified set of reference points, on the basis of which values are to be estimated (either interpolated or filtered) at other points. In the present method, only interpolation is performed applying the equations:

$$\hat{l}_x = \frac{\sum_{i=1}^n w_i l_{xi}}{\sum_{i=1}^n w_i} \quad (4a)$$

$$\hat{l}_y = \frac{\sum_{i=1}^n w_i l_{yi}}{\sum_{i=1}^n w_i} \quad (4b)$$

where w_i are weight factors which are dependent on the distances between the interpolated point and the set of n reference points. Because the arithmetic mean is a linear algorithm, the raw data values must be preprocessed before interpolation. The preprocessing attempts to remove the panoramic effect and bring the

scale in both directions in the data to be nearly equal.

MOVING AVERAGES

This is a generalization of the preceding method, where the estimates are computed using polynomials or other functions. One such functional form is the linear affine:

$$\hat{l}_x = a_0 + a_1x + a_2y \quad (5a)$$

$$\hat{l}_y = b_0 + b_1x + b_2y \quad (5b)$$

The a_j , b_j coefficients are estimated once for every point to be interpolated, using weighted least squares and the values of l_x , l_y at the reference points. The weights are evaluated from selected functions which use the distances between the interpolated point and reference points as arguments.

It can be shown that if $l_x = a_0$, $l_y = b_0$ are used instead of (5a) and (5b), this method reduces to the arithmetic mean techniques.

MESHWISE LINEAR TRANSFORMATION

In this method the reference points are used to form a mesh of contiguous triangles. The three reference points forming the triangle, in which a point to be interpolated lies, are used to uniquely determine the coefficients of the affine transformation given by (5a) and (5b). A variation of the method would be to use sets of four reference points to form a mesh of quadrangles.

By comparison to the two preceding methods, this technique is less attractive for MSS work. This is because it requires having, as a minimum, reference points at the extreme corners of the data record, otherwise an extrapolation scheme will have to be applied. Furthermore, the formation of mesh units, and the search for the unit in which the point to be interpolated lies, makes it unattractive for automated reduction of MSS data.

LINEAR LEAST SQUARES FILTERING

In this method, each of the values l_x and l_y at each reference point, is considered to be composed of two components, one correlated s_x (and s_y) and the other uncorrelated r_x (and r_y). The latter components represent measuring errors or noise which can be filtered when computing an estimate at a new point. Details of this method may be found in reference [3].

EXPERIMENTAL RESULTS

Both parametric and non-parametric techniques were applied to two different MSS data strips. The particulars for the strip from flight No 208 are given in Table 1, and those from flight No 218 in Table 2. First, the collinearity equation method was used.

RESULTS FROM THE COLLINEARITY EQUATIONS

For four different cases, three solutions were carried out: the strip as a whole, two segments with constraints, and three segments with constraints. The results are summarized in Table 3 for both flights 208 and 218.

H = 5000' (1524 m) $\gamma = 0.006$ rad	H = 5000' (1524 m) $\gamma = 0.006$ rad
remote sensing unit (rsu) $\cong 40'$ (14 m)	rsu $\cong 40'$ (14 m)
$\lambda = 0.58 \mu\text{m} - 0.65 \mu\text{m}$ (Channel 6)	$\lambda = 0.58 \mu\text{m} - 0.65 \mu\text{m}$ (Channel 6)
Nominal Scale 1 : 58 000	Nominal Scale 1 : 54 000
Area 1591 lines x 222 columns 8 mi (13 km) x 1 mi (1.6 km)	Area 1439 lines x 222 columns 7 mi (11 km) x 1 mi (1.6 km)
Relief 700' (213 m) to 750' (229 m)	Relief 550' (167 m) to 850' (258 m)
Low ground cover	Area mostly wooded
Cross-identification 1 - 2 rsu	Cross-identification 2 - 3 rsu
No. of Control (Reference) Points: 39	No. of Control Points: 23
No. of Check Points: 60	No. of Check Points: 9

TABLE 1: Flight 208

TABLE 2: Flight 218

TABLE 3: Collinearity Analysis Results		Flight 208 Flat Terrain 60 Check Points			Flight 218 Hilly Terrain 9 Check Points		
		Number of Sections					
		1	2	3	1	2	3
Case 1							
Linear $\omega=\phi=0$	Reference Variance	5.80	2.56	2.16	8.69	6.12	5.44
	Positional Check Variance	6.63	3.53	2.88	5.98	4.81	4.15
Case 2							
Quadratic $\omega=\phi=0$	Reference Variance	2.48	1.76	1.33	6.75	4.38	3.00
	Positional Check Variance	3.25	2.53	1.94	5.05	6.80	6.75
Case 3							
Quadratic X_c, Y_c	Reference Variance	2.56	1.94	1.46	6.50	4.94	4.44
Linear Z_c	Positional Check Variance	3.30	2.67	2.05	5.50	5.13	4.22
$\omega=\phi=0$ κ -const.							
Case 4							
Quadratic X_c, Y_c	Reference Variance	2.48	1.82	1.28	6.62	4.88	4.06
Linear Z_c, κ	Positional Check Variance	3.27	2.63	1.99	5.15	4.84	4.47
$\omega=\phi=0$							

Extensive pairwise F-tests were performed with the following general remarks on the results obtained:

1. the primary factor yielding significant improvement was the segmentation of the data from one to three sections.
2. in general, significant improvement also resulted from the use of the quadratic polynomials over the linear case.
3. no significant difference was noted within the varying treatment of Z_c and κ in cases 2, 3 and 4, except those cases also involving segmentation of the strip from one to three sections.
4. the few check points in flight 218 resulted in no significant indications from the analysis of its data.

RESULTS FROM GENERAL POLYNOMIALS

In a similar fashion, four cases were considered for the whole strip, for two segments with constraints, and for three segments with constraints. The results are summarized in Table 4 for both flights 208 and 218.

TABLE 4: General Polynomial Analysis Results

		Flight 208 Flat Terrain 60 Check Points			Flight 218 Hilly Terrain 9 Check Points		
		Number of Sections					
		1	2	3	1	2	3
Case 1							
Linear	Reference Variance	7.91	3.29	2.87	10.20	7.94	6.80
Flat Terrain	Positional Check Variance	6.62	3.50	2.88	6.41	5.64	4.13
Case 2							
Linear	Reference Variance	7.92	3.29	2.86	9.11	7.02	6.33
Z included	Positional Check Variance	6.64	3.52	2.89	6.02	5.61	4.47
Case 3							
Second Degree	Reference Variance	3.16	2.41	1.82	8.88	5.52	4.19
Flat Terrain	Positional Check Variance	3.22	2.55	1.94	5.76	6.99	7.17
Case 4							
Second Degree	Reference Variance	3.16	2.40	1.83	7.78	5.07	3.56
Z included	Positional Check Variance	3.24	2.56	1.96	5.80	7.07	7.26

Extensive pairwise F-tests were also performed, the results of which led to essentially the same remarks as those for the collinearity method. In addition, the inclusion of the element elevations did not materially affect the results.

RESULTS FROM NON-PARAMETRIC TECHNIQUES

As mentioned previously, four non-parametric techniques were applied to the data from both flight lines. The initial feeling was that linear least squares filtering should lead to good results. However, a number of problems arose when the method was used. This led to more experimentation and analysis, but unfortunately with inconclusive results as of the time of this writing. Therefore in Table 5, only results from flight 208 are given for linear least squares filtering. In the mean time effort is continuing to find out how best to apply the method to remote sensing data in general, and to MSS arrays in particular.

Method	Flight 208 Flat Terrain 60 check points	Flight 218 Hilly Terrain 9 check points
Collinearity - First degree polynomials (ω, ϕ stabilized)		
one section	6.63	5.98
two sections	3.53	4.81
three sections	2.88	4.15
General Polynomial - First degree (Z included)		
one section	6.64	6.02
two sections	3.52	5.61
three sections	2.89	4.47
Arithmetic Mean	1.86	5.76
Moving Average	2.79	5.52
Meshwise Linear Transformation	3.26	6.05
Linear Least Squares Filtering (x separate from y)	1.92	(inconclusive - small sample size)

TABLE 5: Comparative Results Positional Check Variances (rsu^2)

To properly evaluate the results from the non-parametric techniques (each of which represents only one case), an appropriate case is included from each of the two parametric techniques, i.e. the collinearity and the general polynomials. The most obvious observation from Table 5 is that in general the results from flight 208 are better than those from flight 218. This should have been expected, since 208 is over flat terrain and the concern here is with single coverage data. Furthermore, the area recorded in 208 is relatively clear while that recorded in 218 contained a high percentage of ground cover which made the identification of control and check points relatively more difficult.

Another comment about the results in Table 5 concerns the relative accuracy of the different methods. Again, in general terms, the parametric methods yield results comparable to the non-parametric techniques only when the strip is divided in segments. This is more true for the relatively flat terrain in flight 208 than for flight 218. Finally, until more definitive results are obtained from linear least squares filtering, the simple arithmetic mean procedure seems to be an optimum non-parametric method.

DIGITAL DATA PROCESSING CONSIDERATIONS

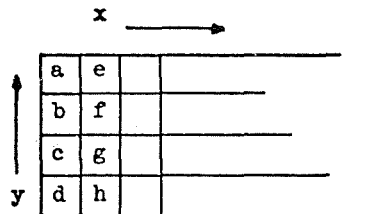
The nature of the digital MSS data is such that the arrays are expressed in integer units (rsu), both the original x,y sensor space data, and the restituted X,Y (object) space data. There are two possible procedures for transformation from one of these spaces to the other; one direct and the other inverse. Figure 1 is a schematic for both of these transformations.

DIRECT TRANSFORMATION

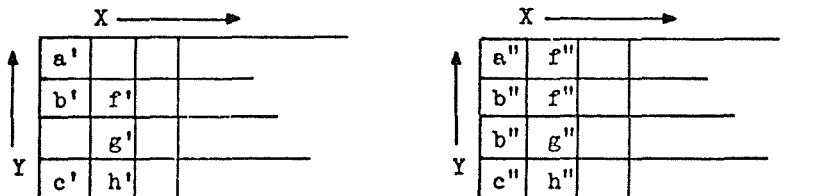
In this transformation, one computes X,Y for each pair of x,y as shown in Figure 1. Since in general the computed values of X,Y are no longer integers, some scheme is required to determine the proper element of the X,Y array in which the spectral values belonging to x,y should be stored. A possible scheme would be to roundoff simply to the nearest integer.

FIGURE 1

ARRAY TRANSFORMATION



UNCORRECTED ARRAY



DIRECT TRANSFORMATION

$$X = F_x(x,y)$$

$$Y = F_y(x,y)$$

GAPS

INVERSE TRANSFORMATION

$$x = F'_x(X,Y)$$

$$y = F'_y(X,Y)$$

DUPLICATION

Regardless of the scheme, it is likely that gaps may occur; that is, there will remain some X,Y array positions which will not have any spectral values stored. These gaps may be filled using either the nearest neighbor technique or an interpolation procedure. Other X,Y array elements may receive more than one set of spectral values. In that case, some selection technique is required, the simplest of which is to retain the last set stored.

INVERSE TRANSFORMATION

This transformation is performed by incrementing along X,Y and computing the corresponding x,y from which to obtain the set of spectral values. Since the computed x,y are again likely to be non-integers, either the nearest neighbor or line linear interpolation should be used to obtain a unique x,y for each X,Y position. This occasionally leads to having an x,y set of spectral values assigned to more than one position in the X,Y array as depicted in Figure 1.

Both types of transformation utilize a buffer area within the computer to handle either the position assignment of the spectral set in the direct method, or to search for the x,y in the inverse method. In the case of parametric restitution, the inverse approach would require more numerical effort. This is because the equations are not directly invertible and an iterative scheme is usually needed.

CONCLUSIONS AND RECOMMENDATIONS

The results of the analysis performed so far, though not extensive point out to the following remarks:

- 1 - Segmentation of data, coupled with constraints, yields in general, better results on check points.
- 2 - In general, the use of quadratic terms yielded better results than when linear polynomials were used. However, it is felt that one should not necessarily expect continued improvement with still higher order polynomials without proper investigation.
- 3 - The non-parametric methods applied to the data available gave results which were comparable to or better than the two parametric procedures.
- 4 - The arithmetic mean and linear least squares filtering, which assume isotropy, require preprocessing such as resampling and scaling.
- 5 - From the results obtained the arithmetic mean appears to be rather promising. Not only is it simple and computationally fast, but it also yields as good a result as any other method.
- 6 - The moving average method is similar to the arithmetic mean except that it does not require preprocessing. This is balanced, however, by the fact that the method requires more computational time due to estimating a new parameter set for each point interpolated.
- 7 - The meshwise linear transformation appears to be unsuitable for the restitution of MSS digital data.
- 8 - Linear least squares filtering is the only procedure attempted which allows for filtering of noise (measuring and other uncorrelated random errors). However, to the date of this writing the results obtained are so inconclusive that further research and experimentation is necessary. It would perhaps be better if testing is performed on simulated data, not only for this method but also on all other techniques which have proven feasible from the tests on real data.

REFERENCES

- |1| Mikhail E.M. and Baker J.R.: "Geometric Aspects in Digital Analysis of Multi-Spectral Scanner (MSS) Data", presented at the Annual Convention, American Society of Photogrammetry, Washington 1973
- |2| Leberl F.: "Untersuchung über die Geometrie und Einzelbilddauswertung von Radarschrägaufnahmen", Dissertation, Technical University, Vienna 1971
- |3| Kraus K. and Mikhail E.M.: "Linear Least-Squares Interpolation", Photogrammetric Engineering, October 1972

SPACE OBLIQUE MERCATOR - A NEW MAP PROJECTION OF THE EARTH

by A. P. Colvocoresses, Reston, Virginia, USA

ABSTRACT

The Earth Resources Technology Satellite (ERTS) Multispectral Scanner (MSS) is producing imagery of rather amazing geometric fidelity. The positional errors (rms) of points on a properly controlled image are less than the 80-meter instantaneous field of view (picture element) of the scanner. Such accuracy is attributed to the stability of the scanner and spacecraft and to the corrections that are being made by NASA before each image is printed. The image is in fact formed on a cylindrical surface in space which can be defined as a specific map projection which results in the mapping of the world (between the 82° parallels) every 18 days. Moreover the projection is mathematically definable and thus has the potential of developing into an automated mapping system in which the picture element (pixel) can be discretely related to its position on the figure of the Earth.

INTRODUCTION

Historically map projections have been based on static conditions. The figure of the Earth, perspective center (if there is one), and projection surface are all fixed with respect to one another. As long as the Earth is imaged by a framing camera that records a scene instantaneously, the static condition holds, and film returned from aircraft or spacecraft generally fits into this category. Moreover video systems that transmit recorded scenes such as those on the Lunar Orbiters and the Return Beam Vidicons (RBV's) on the Earth Resources Technology Satellite (ERTS-1), also represent the static mode, in which the image is considered to have been obtained instantaneously. In all such cases a perspective image of the Earth is recorded in a unique but definable form, and the image can then be fitted or transformed to one of the conventional map projections. However, we now have orbiting spacecraft equipped with scanning devices that are imaging the Earth scene continuously. Such satellites have mapping capabilities that open the door to an entirely new concept of map projections in which relative motion, and therefore time, becomes a mapping parameter. Thus the conventional static concept of map making is replaced by a dynamic concept. The basic conditions for this dynamic concept of mapping are found in the polar-orbiting weather satellites, such as Nimbus,ITOS, and DAPP (Data Acquisition and Processing Program, which utilizes U.S. Air Force weather satellites). Imagery from these satellites has so far not been defined with respect to the figure of the Earth with the precision expected of a map projection. The multispectral scanner (MSS) of the ERTS-1 satellite, however, creates an image of sufficient resolution and geometric fidelity to warrant definition as a true map projection.

DEVELOPMENT

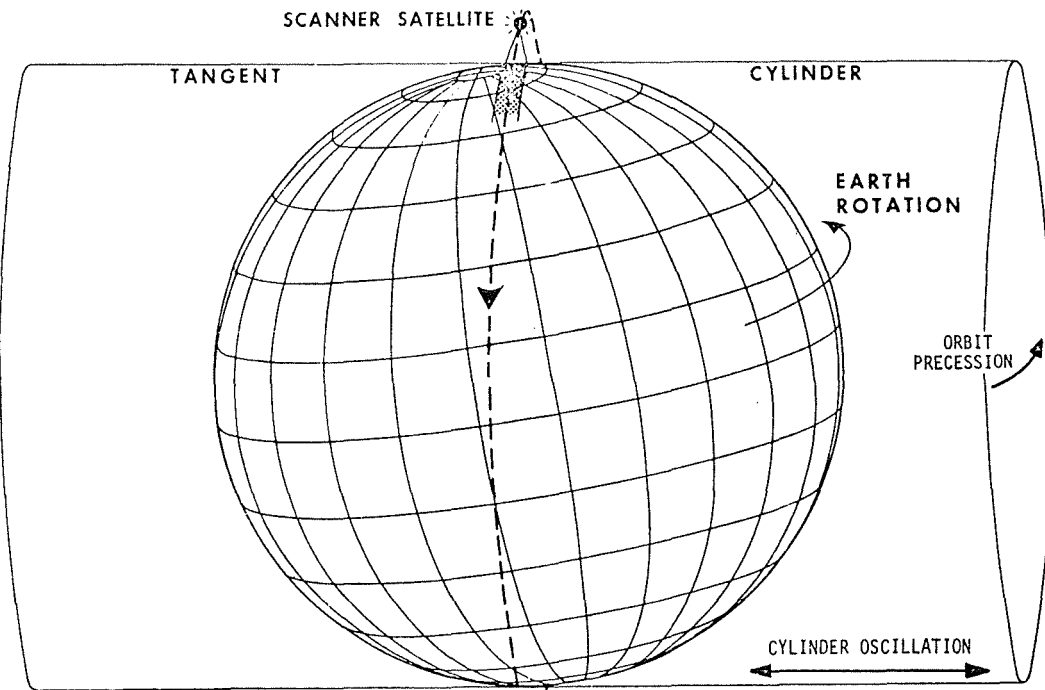
The ERTS-1 MSS has an instantaneous spot size (pixel = picture element) on the Earth of 79 m and therefore is considered a relatively low-resolution system for Earth sensing. The effective resolution (in optical terms) of ERTS is no better than 200 m. Nevertheless, ERTS imagery has high geometric fidelity, which results in cartographic products that have spatial errors on the order of 50 to 150 m (rms). This is the basic imagery, referred to by NASA as bulk or system-corrected which has in turn been related to the Earth's figure through ground control points (see [1]).

With such control and the application of appropriate procedures, geographics (lat/long) or a plane coordinate grid such as the Universal Transverse Mercator (UTM) can be fitted to the ERTS imagery. The UTM grid unit is not a true square when so fitted, but the deviations are so small that grid anomalies are not detectable when measurements are made with reference to the nearest lines of a nominal grid square. The procedure for gridding ERTS imagery was developed by the U.S. Geological Survey under NASA sponsorship, with the Ohio State University providing the initial computer programs (see [2]). The small size of the spatial anomalies observed when a geodetic grid was applied to the MSS imagery was the first indication that scanner imagery as corrected and printed by NASA is in fact on a continuous map projection of definable form. Further information relative to

the procedures used in grid fitting are available in reference [4]. The NASA ERTS Date Users Handbook (ref. [1]), pages G-17 and G-18, describes the 14 basic geometric corrections applied to ERTS MSS data before printout as bulk imagery. (Unfortunately these corrections have not, as yet, been applied to the digital computer-compatible tapes produced by NASA). When all 14 corrections have been applied, a pseudocylindrical map projection of rather curious characteristics results. Maximum distortions of the Earth figure due to the projection are on the order of only 1 : 1 000, which makes it acceptable for mapping purposes. The corrections were designed to give MSS imagery geometric characteristics similar to those of the ERTS RBV's, which are frame cameras and thus have perspective geometry. The MSS does have geometric fidelity comparable to that of the RBV's and thus warrants its own optimized map projection, which would have maximum distortions of only about 1 : 10 000. A further discussion of projections is contained in reference [5], in which a Space Oblique Mercator projection is described and recommended for ERTS-type imagery. The projection could have any one of several characteristics, but precise mapmakers generally consider the characteristic of conformality as dominant. Conformality retains equal scale locally in all directions and preserves angular relationships. The conformal cylindrical projection was conceived by Mercator and in this case is defined in Space and it is Oblique to the polar axis. Definition of the projection is given in non-rigorous but nevertheless geodetic terms in the following section.

GEODETIC CONSIDERATIONS

Conceptually one can start with a spherical Earth and then develop the elliptical modifications which - unfortunately - cannot be ignored. The diagram illustrates a cylinder defined by a truly circular ERTS orbit with the projection surface tangent to the Earth's spherical figure.



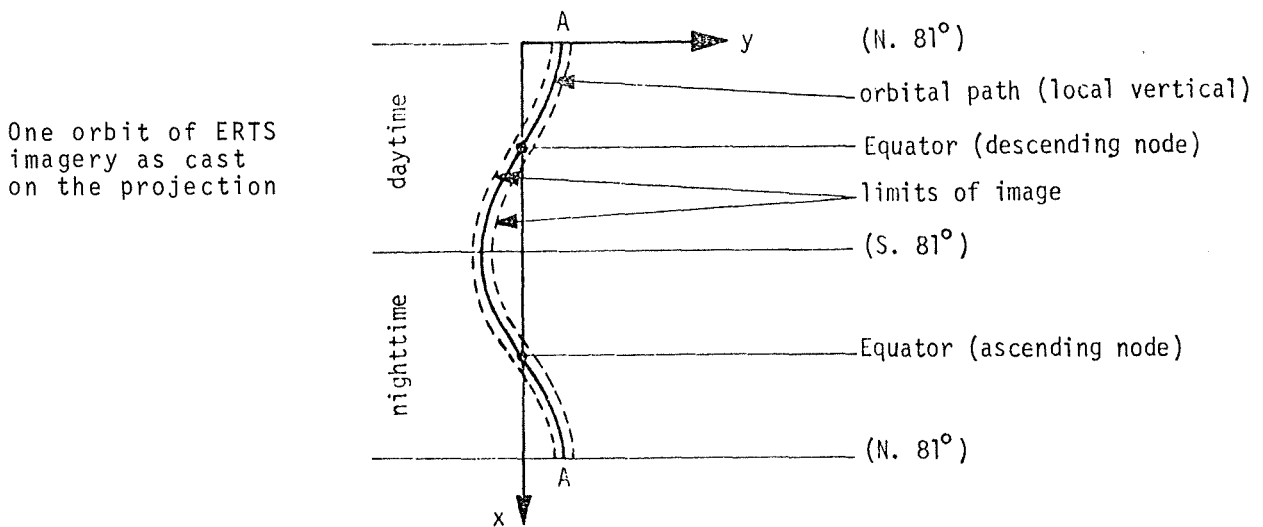
SPACE OBLIQUE MERCATOR PROJECTION

Images the Earth from N 82° to S 82° every 18 days

- MOTIONS INVOLVED
- Scanner sweep
 - Earth rotation
 - Satellite orbit
 - Orbit precession

Although four motions (scanner sweep, satellite orbit, Earth rotation, and orbit precession) are involved, the imagery can be recorded on the simple cylindrical surface - which, when developed into a continuous plane, is in fact a map projection. To keep Earth rotation from distorting the image, the cylindrical surface oscillates along its axis at a compensating rate which varies with latitude. Motion is otherwise uniform and symmetrical with respect to the orbit, and thus every orbit exactly repeats its path on the projection plane even though the Earth scene changes nearly 26° in longitude with each orbit. Thus the projection coordinate values are repeated each orbit even though a different portion of the Earth's surface is mapped on each successive orbital pass. This means that the Earth figure coordinates λ, ϕ are related to the projection coordinates x, y as a function f of time t . That is, $\lambda, \phi = f(x, y, t)$; t must expand through the 18 day system and then revert to zero for the next cycle.

The diagram (exaggerated) shows how the image (if continuous) is cast on the developed projection surface.



The fact that the orbit has precessed in space by a few minutes of arc with each revolution does not affect the projection surface, which is defined by the orbit. Orbit precession, which retains the orbit's angular relationship to the Sun, does slightly modify the effects of Earth rotation.

Since the Earth's figure is an ellipsoid instead of a sphere, several modifications must be considered. First, the Earth's polar radius is over 20 km less than the equatorial radius. An orbit which is at a fixed height above the Earth's figure and thus always images the Earth at the same scale would in fact have to have an elliptical orbit with two perigees which remain at the 81° points of maximum inclination, and this is contrary to the laws of physics. In practice, a truly circular or prescribed elliptical orbit is impossible to maintain, but NASA must (and does) consider the Earth's ellipticity as well as orbital ellipticity in computing satellite altitude.

A second consideration is that the scanner, controlled by horizon sensors, is referenced to the local geometric vertical rather than the direction to the center of mass of the Earth, which is the computational center for the orbit as well as the Earth's figure. The maximum difference between these directions approaches 12 minutes of arc. Since the orbit is only 9° off the pole, the angular difference is principally along track and thus slightly affects the time relationship of the satellite to the Earth's figure. The slight cross-track angle (3.6 min of arc maximum) between the local geometric vertical and the vector to the Earth's center does, in effect, deform the projection surface. The deformation constitutes a deviation from the concept of a uniform map projection and also disturbs the precise conditions of conformality in the projection. These considerations are probably academic and will never be found by the map user, but for the mathematician who defines the map projection in rigorous terms they are important. At 81° latitude the 3.6 minute of arc subtends nearly 1 km on the Earth's surface. As the orbit approaches the Equator, the cross-track deviation steadily decreases from 1 km to 0.

The actual path of the satellite on the Earth's figure as defined by the local geometric vertical is also of interest. To see this, we should first forget the Earth's rotation and merely consider the figure generated by the local geometric vertical from the orbit as it intersects a fixed figure of the Earth. This is not the true ellipse (great circle) that would result from passing a plane obliquely through the center of an ellipsoid, and it is not a geodesic - which is the shortest distance between two points on the elliptical Earth surface. Regardless of what the actual figure is, it must be defined in mathematical terms because it creates the locus of image centers. NASA probably could define ERTS imagery with respect to the direction to the center of mass of the Earth and thus simplify the computational problem. However, this solution would create a slightly tilted image with respect to the Earth's figure that is probably undesirable for any analog portrayal. Once a comprehensive mathematical analysis has been made, the various conditions stemming from the Earth's ellipticity can be fully evaluated. Only then can the decisions be made as to which conditions and terms must be considered or ignored.

SPECIFIC PARAMETERS

Certain parameters, assumptions, and nomenclature relative to the ERTS system must be defined before a mathematical model and transformation equations can be rigorously defined. Recommendations with pertinent values provided by NASA/Goddard are as follows:

- Earth figure (see diagram):

a = semimajor axis = 6,378,165 m

f = flattening of the ellipsoid = 1/298.3

R = nominal radius of curvature in the cross-track direction = 6,388,000 m

- Orbit, nominal:

Circular radius = 7,294,690 m

Altitude, computational = 918,592 m

Inclination = 99.092°

(This is the angle of the ascending node with respect to due East. The maximum latitude of the orbit is 80.968° . Imagery is taken on the descending (daytime) portion of the Sun-synchronous orbit).

Period = 103.267 minutes

Time of descending node (equatorial crossing) = 9:42 a.m. local Sun time

Coverage cycle duration = 18 days (251 revolutions)

Distance between adjacent ground tracks at Equator = 159,380 m

- Imaging System = Multispectral Scanner (MSS) (see following diagrams):

β = viewing angle of scanner with respect to nadir has a maximum value of 0.100749 rad, about 5.76° . The plane of the scanner motion is now defined as perpendicular to the plane of the orbit.

γ = angle of Earth curvature (max $\approx 0.83^\circ$)

f = effective focal length of scanner. Based on mirror size and f number this is 730 mm; however, this dimensions is immaterial with respect to the projection

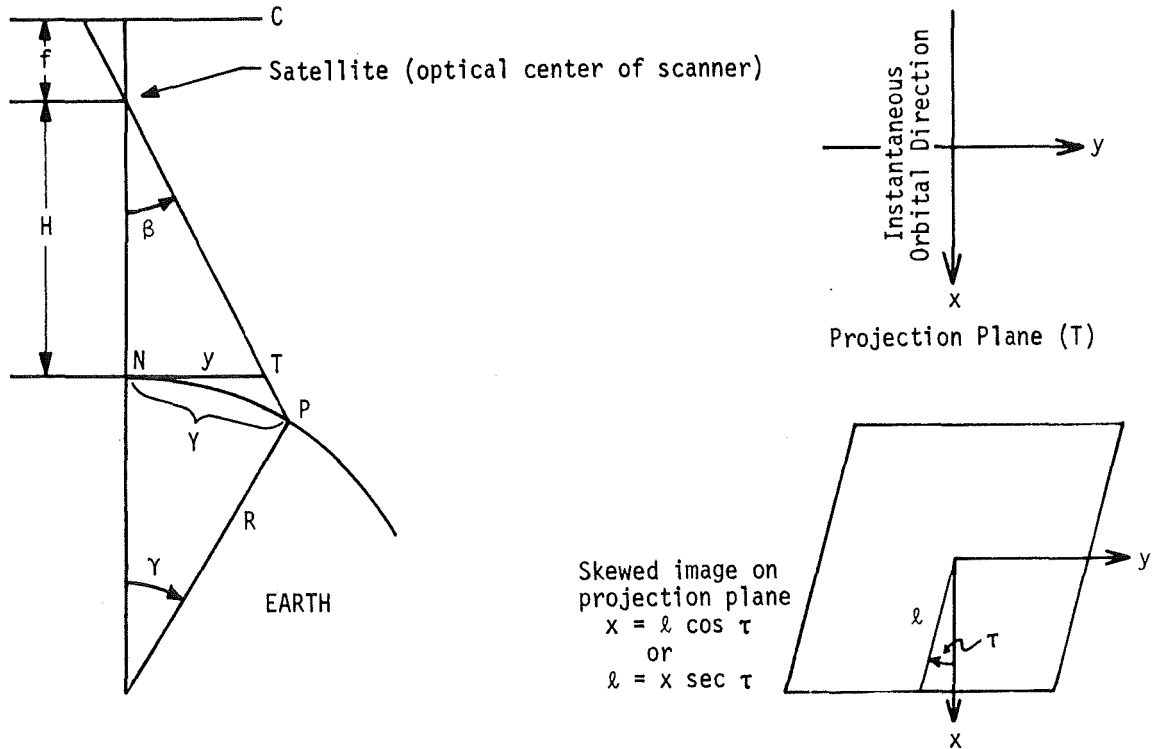
N = nadir point, based on local geometric vertical

P = point on Earth imaged by MSS sensor

C = cylindrical image surface, develops into image plane

T = cylindrical projection surface, develops into projection plane

Geometry of ERTS, MSS (orbital plane is perpendicular to plane on left).



X = distance in instantaneous orbital direction on Earth figure along orbital path +). This orbital path would be a great circle or orthodrome on a spherical nonrotating Earth

Y = distance normal to instantaneous orbital direction on Earth figure from nadir $Y = \gamma R$ +)

x = distance on projection plane in instantaneous orbital direction

y = distance on projection plane normal to x

l = actual orbital path as imaged

τ = skew angle (varies with latitude)

Space Oblique Mercator projection basic formulas (scale factor = 1):

$$x = X$$

and based on origin at nadir

$$y = R \int \sec \gamma \, d\gamma = R \log_e (\sec \gamma + \tan \gamma) = R \log_e \tan \left(\frac{\gamma}{2} + \frac{\pi}{4} \right)$$

y will generally contain another term to take care of the cylinder oscillation due to Earth rotation. A false value of perhaps 1 600 000 m should be given to the x axis as shown on page 3 in order to eliminate negative values of y .

-) If one disregards the small error introduced by Earth rotation during the scan sweep (the maximum displacement in the x direction is only about 200 m for the 185 km scan length), the y direction on the image is that of the scan lines (as now configured). However, the orbital path is skewed on the projection by as much as 40° with respect to the instantaneous orbital direction, again due to Earth rotation (see diagram p. 3).

THE PAYOFF

To make ERTS MSS-type imagery fully suitable for mapping, several steps must be taken, as follows:

- 1 - Parameters for the system must be set and adhered to within stated limits.
- 2 - The projection must be rigorously defined, and system corrections must be applied with results comparable to or better than those now being achieved with ERTS-1.
- 3 - The mathematical relationship between the projection (model) and the figure of the Earth must be rigorously defined.
- 4 - Image-identifiable control must be cataloged and used for system calibration. The density or form of the control is not known at present, but there are indications that spacing may be on the hundreds or even thousands of kilometers, with a few test sites of denser control (20 - 50 km spacing) for detailed system analysis.
- 5 - System corrections to be applicable to tapes as well as imagery.
- 6 - Precision (scene-corrected) processing to be of two forms:
 - a. Precise application of geodetic indicators (lat/long or UTM coordinates) to the system-corrected imagery (and perhaps tapes) without altering the system-corrected structure or projection.
 - b. Transformation of imagery (and perhaps tapes) to a conventional map projection, such as the UTM or polar stereographic, and addition of appropriate geodetic indicators. Transformation should be required for only a small percentage of the recorded imagery.

Steps 1 and 2 can be based on ERTS-1 performance as it is assumed that the performance of ERTS-1 can be equalled or exceeded on future ERTS-type space-flights. The mathematical problem (step 3) is of paramount concern. I suggest that NASA, with technical input from USGS (and others), take the lead. Here is a real challenge to the cartographic community. As geodesists and photogrammetrists, we must carefully examine the problems and the various solutions possible. Then, as mapmakers representing the map users of the world, we should spell out exactly what we need. A considerable and dedicated effort will still be needed to develop the mathematical model and associated computer programs. Since the programs thus developed could be applied to Earth imaging systems other than ERTS, the programs should have appropriate flexibility and precision.

Once the model and programs are developed, they should be tested against a variety of ground control arrays, and thus the requirements for control (step 4) can be defined. Steps 5 and 6 require the providing of appropriate processing at some centralized point. With these 6 steps made effective, we believe that ERTS-type images and tape in cartographic form and with geodetic precision can be produced in a matter of days after acquisition - particularly when the continuous and uniform Space Oblique Mercator projection is employed. Perhaps the era of automated mapping, based on Earth-sensing space systems, is not far off.

REFERENCES

- |1| NASA, Earth Resources Technology Satellite Data Users Handbook; prepared and maintained by General Electric Corporation, 1971 to date
- |2| Bender, L.E.: "An Algorithm for Gridding Satellite Photographs"; prepared by the Ohio State University for U.S. Geological Survey, 1970
- |3| Colvocoresses, A.P. and McEwen, R.B.: "EROS Cartographic Progress", Photogrammetric Engineering, Dec. 1973
- |4| Colvocoresses, A.P.: "Status of Positional Referencing of ERTS Imagery (EC-17-ERTS)", Memorandum submitted to NASA in part of an ERTS experiment, July 1973
- |5| Colvocoresses, E.P.: "Towards an Operational ERTS", to be published by NASA as part of the Third ERTS Symposium of Dec. 1973

Reference 5 contains the following additional references pertinent to this paper:

- a. Konecny, G. "Geometric Aspects of Remote Sensing", invited paper Comm.IV International Congress of Photogrammetry, Ottawa 1972
- b. Kratky, V. "Cartographic Accuracy of ERTS Images", Proceedings of the American Society of Photogrammetry, 30th Annual Meeting, Washington, March 1973
- c. Forrest, R.B.: "Mapping from Space Images", Bendix Technical Journal, Autumn 1970
- d. Colvocoresses, A.P.: "ERTS-A Satellite Imagery", Photogrammetric Engineering, June 1970
- e. Thomas, P.D.: "Conformal Projections in Geodesy and Cartography", Coast and Geodetic Survey Sp. Pub. No. 251, 1964

GEOMETRIC CALIBRATION OF CANADIAN ERTS PHOTOREPRODUCTION SYSTEM

by V. Kratky, Ottawa, Canada

ABSTRACT

Two photoreproduction instruments used in the Canadian production of ERTS photographs were experimentally tested to determine the magnitude and character of geometric image distortions caused by the reproduction process. Based on the results, a suitable analytical formulation was found, which was used for the system calibration. The implementation of the calibration procedure is described and relevant production aspects discussed together with an assessment of practical results.

INTRODUCTION

The Earth Resources Technology Satellite (ERTS) imagery is acquired by a four-channel Multispectral Scanner (MSS) which continuously covers a 185 km wide ground swath in a single orbit. The raw data, radio-received at a ground station, is recorded on video tape and transmitted to a data processing station where it is converted into photographs and computer compatible tapes.

In the Canadian ERTS image processing system [4] which is in many respects different from that adopted by NASA [3], the photographs are produced with the aid of two special reproduction instruments. An Electron Beam Image Reproducer (EBIR) converts the pictorial information from its digital record on video tape into a latent photographic negative on a 70 mm film. This is accomplished in the data processing facility of the Canada Centre for Remote Sensing (CCRS) in Ottawa. The exposed film is delivered to the National Air Photo Library (NAPL) reproduction centre where it is processed and enlarged to the final 1 : 1 000 000 photographs on a 230 mm film in a special Enlarger-Printer (E-P).

The MSS image is distorted due to several physical, instrumental and geometric factors which may affect the imaging, recording and reproducing process, as analyzed, e.g. in [2]. Most of the systematic distortions can be determined with the use of auxiliary information provided from satellite sensors, predicted from orbital parameters, obtained from geometric calibrations of instruments and also derived from suitable photogrammetric transformations based on the available ground control points. As a result, an analytical model of the distortions is derived, the parameters of which are used to control the reproduction process in the EBIR. Further details about the correction process developed for the Canadian ERTS program can be found in References [1], [2].

It is obvious that the performance of both reproducing units affects the geometric quality of ERTS photographs. It is, therefore, imperative to have these devices regularly calibrated, and to use parameters of the calibration, together with other correction parameters, for the control of the process. The present paper describes the way in which this is accomplished in the Canadian ERTS program in the CCRS.

DESCRIPTION OF REPRODUCING SYSTEM

The EBIR is a precision film recording device designed and built for CCRS by the Minnesota Mining (3M) Company. Basically, it is a modified cathode ray tube in which the face-plate is substituted by an ultra-fine grain film placed in a vacuum. Thus, the film is directly bombarded by electrons in a line-by-line mode reproducing the original line-scanning pattern of the MSS, retained in the video signal. A special unit, the EBIR controller, acts as an interface between a computer, and the EBIR, adding annotation, correction and calibration information which is provided by the computer, to the video signal. Data are directed from the video tape to the controller which controls the timing of the readout and the deflection of the electron beam in a way corresponding to the analytical model of those geometric corrections to be applied.

The Enlarger-Printer developed by the International Imaging Systems (I²S Company) provides an accurate optical scaling of images into the final format. The system is fixed to yield a 3.7x enlargement ratio and can be used in a semi-automatic mode to produce colour composite prints in different combinations of the four

available spectral images. For this purpose, a precision pin-registered framing mechanism is used to ensure an accurate image registration, identical to that in the EBIR, with respect to sprocket holes of the perforated film.

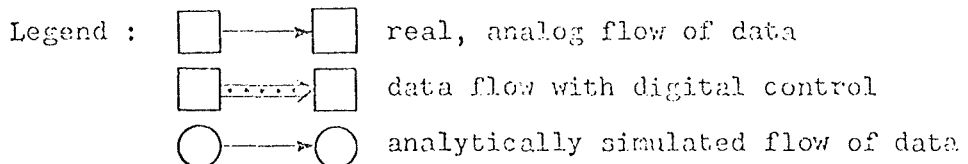
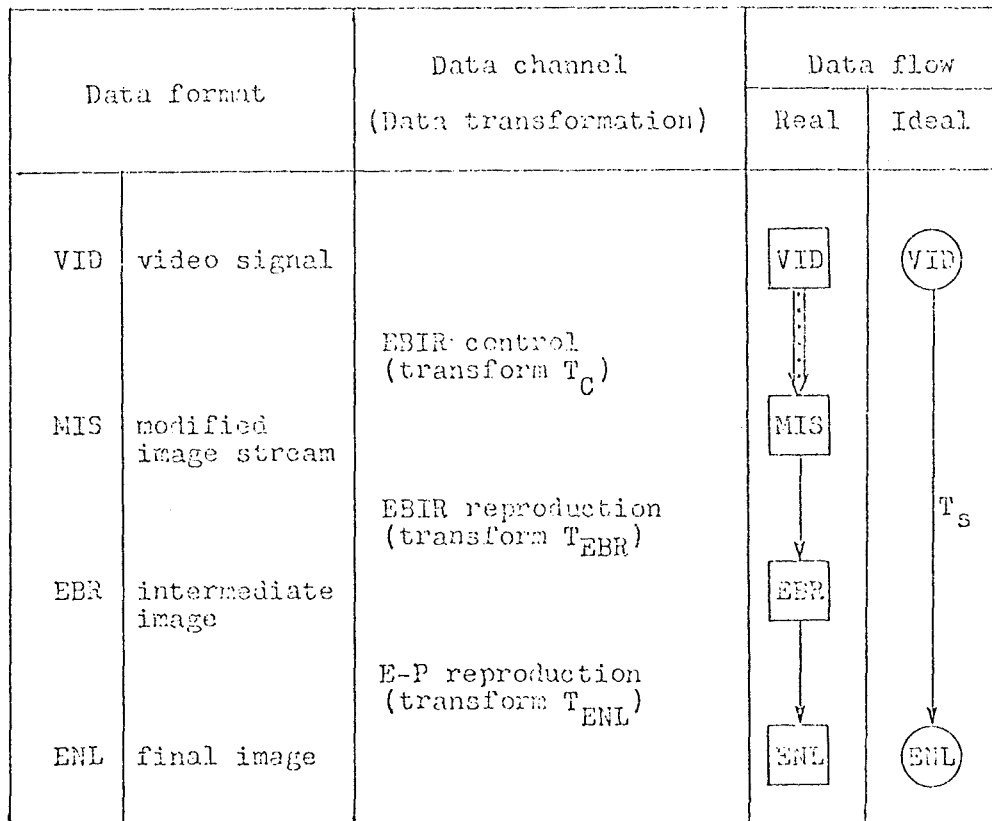
GEOMETRY OF PHOTOREPRODUCTION

Information flow

The analog video outputs from the MSS sensors are converted into a digital signal which is radio-transmitted and received at the ground station. The received data are digitally recorded on a video tape in separate channels for each spectral band. The MSS system preserves an inherent registration of data in all spectral bands, which means that their geometric distortions are identical. The physical flow and transformation of information in the reproduction phase is presented in Fig. 1 and described in the following steps:

- Digital video signal (VID) is input information; any geometric distortions caused by deviciencies in preceding operations are irrelevant to the calibration of the reproduction system and thus disregarded. The x,y-coordinates of any image detail are implied in the position of the corresponding pixel within the video image stream.
- Modified image stream (MIS) is derived by a transformation of the video signal (VID) in the EBIR controller. The effect of the control can be analytically described by a transformation T_C .

fig. 1: Information flow in the reproduction process



- The EBIR produces an intermediate photographic image (EBR). If the controller is set to support the standard printing function of the EBIR, without introducing any additional corrections, the image should ideally be a true geometric representation of the scan-line format of the video signal VID. Any deviation from this pattern represents geometric errors in the EBIR function, analytically characterized by a transform T_{EBR} .
- The final photographic image (ENL) is obtained by an optical enlargement of the intermediate negative in the Enlarger-Printer. The inherent inaccuracy of this process also affects the final image geometry. The analytical relationship EBR-ENL can be represented by a transform T_{ENL} .

Character of transformations

Transforms T_C , T_{EBR} , T_{ENL} represent analytical models of the individual phases in the photoreproduction process. In an ideal case the whole process should perform a simple scaling function simulated by a scalar transformation $T_S = sI$, where $s = 3.7$ and I is a matrix of identity transformation. The individual partial transforms would also be simplified to $T_C = T_{EBR} = I$ and to $T_{ENL} = sI$. In reality however, this can not be achieved and the above matrices are only crude approximations of more complex relationships for which linear transformations would not provide adequate definitions.

For an analysis of the reproduction geometry, the controlling function T_C is disregarded first, and the geometric change due to reproduction process is formulated by a transform T_R expressing the cumulative effect of transforms T_{EBR} and T_{ENL} .

Residual errors of the EBIR function are distributed in a fashion typical for the electronic geometric distortion [5], [6]. In general, a higher order polynomial transformation is considered suitable to represent the two-dimensional non-linear distribution of errors in this instance. The errors are subject to gradual changes with time, which affect both their magnitudes and the character of their distribution.

Proper functioning of the E-P is adversely affected by the optical distortion as well as by a mechanical misalignment of the system. The latter errors could be simulated by a projective transformation whereas the radial character of the lens distortion requires a polynomial formulation.

Analytical formulation

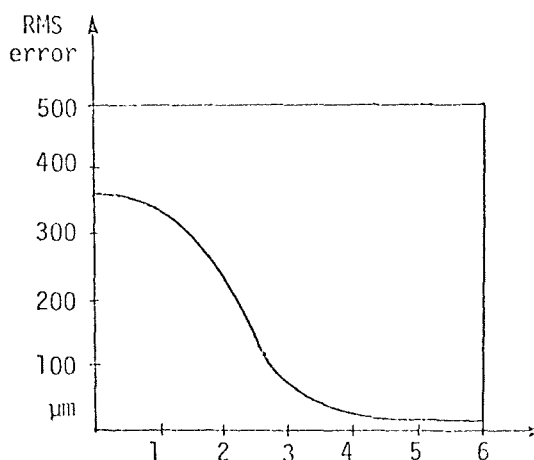
It is advantageous to describe both partial steps of the reproduction process as well as their cumulative effect with the same type of analytical formulation. Numerous experiments were performed at NRC and CCRS, utilizing an artificially generated video tape, which represented an image of a 9x9 or 18x18 réseau grid. The grid was reproduced through both EBIR and E-P, and after digitizing x,y-coordinates of individual réseau crosses in a Zeiss PSK stereocomparator, different analytical transformations were applied and statistically tested for the presence of systematic errors in residuals. The most useful polynomial formulation was found when keeping the maximum degree of a single coordinate even in mixed products $x^i y^j$, as in bilinear, biquadratic, bicubic etc. transformations. An $n \times n$ pattern of réseau crosses can accommodate a bi-polynomial transformation of $(n-1)$ -th degree, built up according to the following, gradually expanding scheme.

0° degree	1	Number of parameters
		1
1°	x xy y	4
2°	x ² x ² y x ² y ² xy ² y ²	9
3°	x ³ x ³ y x ³ y ² x ³ y ³ x ² y ³ xy ³ y ³	16
4°	x ⁴ x ⁴ y x ⁴ y ² x ⁴ y ³ x ⁴ y ⁴ x ³ y ⁴ x ² y ⁴ xy ⁴ y ⁴	25

This formulation with n^2 parameters gives complete freedom to express the errors in any row or column of the réseau grid with an independent x or y -polynomial of the n -th degree. The x - and y -errors are defined independently by separate polynomial functions.

Figure 2 shows the decrease of residuals, related to the increase in the degree of polynomials used to represent the T_{EBR} -transformation. The errors are expressed in the scale of the final, 3.7 times enlarged image corresponding to 1 : 1 000 000 ERTS photographs.

Fig. 2: degree of polynomial



Based on the results of the experiments the polynomial transformation of 4th degree was judged to provide the most useful definition of the reproduction errors. It can be conveniently defined with the use of a bilinear form

$$dx = u^T Av \quad , \quad dy = u^T Bv \quad (1)$$

where A, B are (5,5)-matrices of coefficients a_{ij} , b_{ij} associated with products $x^i y^j$, and vectors u, v are derived as

$$u^T = (1 \ x \ x^2 \ x^3 \ x^4) \ ,$$

$$v^T = (1 \ y \ y^2 \ y^3 \ y^4) \ .$$

CALIBRATION

General approach

Once the calibration video master is reproduced by both the EBIR and E-P instruments the polynomial formulation (1) can be applied to determine the transforms T_{EBR} , T_{ENL} , T_R as well as their inverse functions. Since the symbols T represent non-linear transformations, the inverses can be practically determined only by numerical fitting of available data sets in the reverse order, and not by analytical inversion of the functions. Figure 3 graphically shows the combinations in which the given and digitized data are used. So far, the three transforms T represent the distortions introduced by the system when the correction function of the EBIR controller is disregarded. This particular function can be determined indirectly when removing the effect of the reproduction errors from the hypothetical ideal scaling function of the system as illustrated in Fig. 3 and expressed in symbols by

$$T_s + T_R^{-1} \rightarrow T_C \ . \quad (2)$$

For the computation of T_C , the data set VID is fitted with the indirectly derived data MIS.

Practical calibration of the reproducing system calls for a physical implementation of the transform T_C , the coefficients of which can be supplied to the EBIR controller from the supporting computer. In this instance illustrated by a block diagram in Fig. 4, the composite effect of transformations T_C , T_{EBR} and T_{ENL} would cancel out all errors of the reproduction process, making the resulting performance of the system identical with the desired scaling function

$$T_C + T_{EBR} + T_{ENL} \rightarrow T_s \ . \quad (3)$$

Fig. 3: Calibration

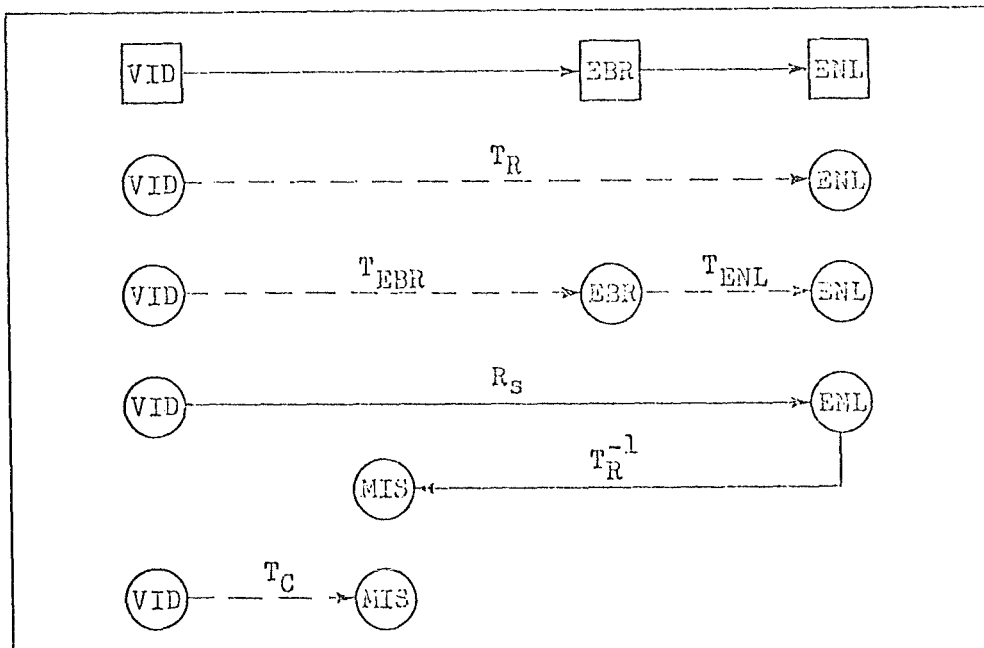
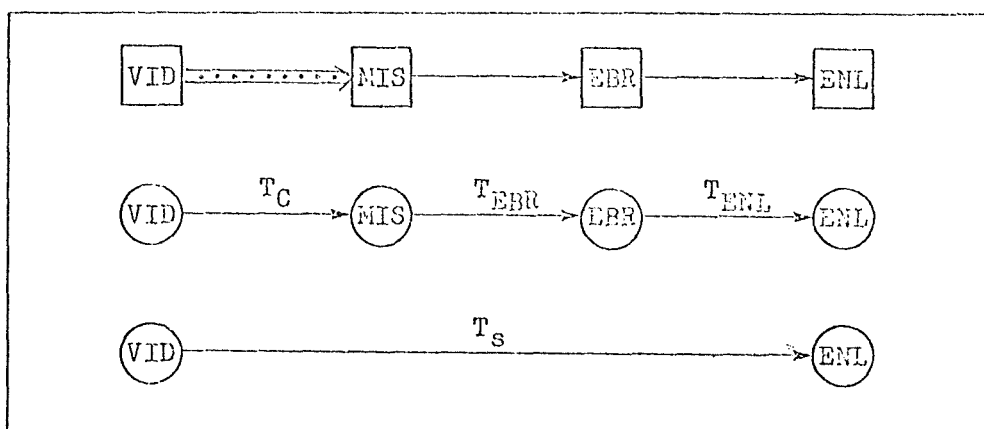


Fig. 4: Production



Practical considerations

Both the reproduction devices at CCRS were designed and built without any fiducial marks in their image fields. This introduces uncertainty into the transformations which are dependent on the choice of origins for the individual x,y-fields. Fortunately, this does not apply to the hypothetical plane of the video image VID where the origin is defined and preserved in an unambiguous way. However, the actual fitting involving EBR and ENL images becomes more complicated. For this reason, the fiducial marks missing in the intermediate photographs EBR are substituted in practical calibrations by appropriate details of the sprocket holes securing the registration of the film. Because the final enlarged photographs ENL do not contain projections of the film perforation, these images are always preoriented to the master grid with the use of a similarity transformation. A scaling change, which is one of the parameters, is omitted in the implementation of this auxiliary transformation to preserve the original dimension of the digitized image.

Coordinate sets in all the fields VID, EBR, ENL are numerically fitted using substitutions

$$x_2 = x_1 + dx \quad , \quad y_2 = y_1 + dy \quad (4)$$

where dx , dy are given in (1). The least squares fitting is performed in all combinations of fields and independently in both directions

$$(x,y)_1 \rightarrow (x,y)_2 \quad \text{or} \quad (x,y)_2 \rightarrow (x,y)_1$$

which yields transforms T as well as transforms T^{-1} .

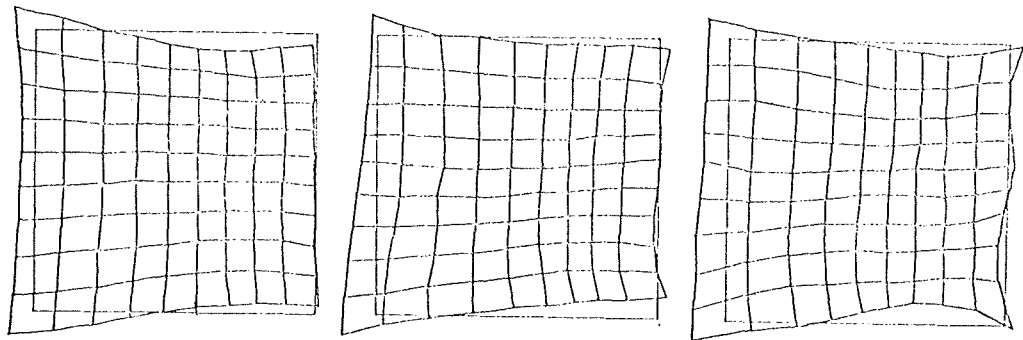
The calibration parameters are computed and stored in the computer memory for each of both EBIRs which are operational at CCRS, in combination with a single enlarger-printer. Regular updating of the parameters is required when a new set of MSS video tapes is handled.

For practical reasons, the calibration process can be simplified and restricted to the determination of the total reproduction distortion T_R without examining the contribution of the individual devices. This is particularly advantageous because the final ENL-image can be digitized in a faster and easier way with the aid of a Gradicon digitizer instead of using a stereocomparator. The digitizer is a part of the precision processing line at CCRS whereas a stereocomparator is not available. The accuracy of a Gradicon calibration is lower than that from a stereocomparator, but nevertheless still adequate for the purpose, as documented in the next section.

Discussion of results

The character of distortions within the reproduction process was studied in experiments extended over a period of more than one year. Although the values of distortion varied in the individual experiments, the basic distortion pattern remained stable for a period of a few months and was usually suddenly changed only by major maintenance adjustments. A typical example is shown in Fig. 5 where the distortion T_R is plotted at an exaggerated scale for three calibration tests performed one week apart. Each of the plots is based on two independent digitizations of test photographs. The example also indicates that the 4th degree transformation is really needed to compensate for the existing errors.

Fig. 5

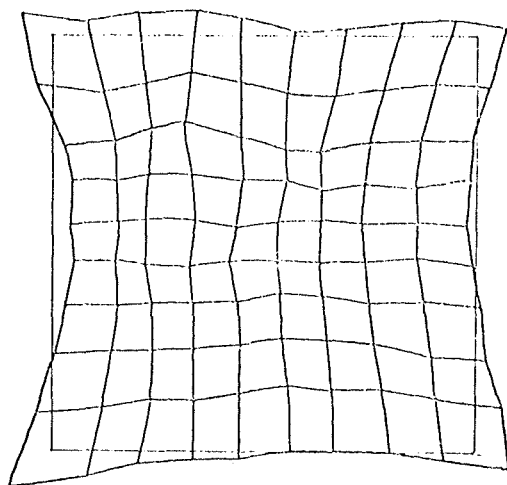


Not only does the full calibration distinguish between the errors introduced in the two basic phases of the reproduction, but it can also be used to separate the optical distortion of the E-P lens from the effect of mechanical misalignments. The latter effect can be numerically eliminated from the data by applying a projective transformation. The resulting data, such as shown in Fig. 6, can be accounted for by the lens distortion of the enlarger-printer. Here the maximum radial distortion of a 3.7 times enlarged image at the corners was close to $100\mu\text{m}$ whereas the RMS value of all x- and y-components were 27 and 25 μm , respectively. The RMS value for misalignment distortions amounted to 45 μm and the remaining random noise was 8 μm , for a coordinate measured in a PSK stereocomparator.

The same test was repeated with the Gradicon digitizer, yielding RMS errors of 26 μm for the lens distortion, 52 μm for the misalignment and 38 μm for the random residuals. The agreement in the systematic distortions, as assessed from PSK

and Gradicon measurements, is very satisfactory. The difference between the values for random errors is representative of results from numerous other experiments.

Fig. 6



In the long run of calibrations carried out at CCRS, the RMS values for the total reproduction distortion ranged between 300 and 400 μm . The RMS values of residual errors after transformation were always kept between 10 and 20 μm for PSK digitization and around 40 μm when digitizing with Gradicon.

REFERENCES

- |1| Kratky, V.: "Photogrammetric Aspects of Precision Processing of ERTS Imagery", Proceedings of the First Canadian Symposium on Remote Sensing, Ottawa 1972
- |2| Kratky, V.: "Photogrammetric Solution for Precision Processing of ERTS Images", Presented paper to XII International Congress of ISP Ottawa 1972
- |3| NASA: "Data User's Handbook", NASA Earth Resources Technology Satellite, Doc. No. 71SD4249, 1971
- |4| Strome, W.M.: "Canadian ERTS Data Handling System", Proceedings of the Canadian Computer Conference, Ottawa 1972
- |5| Wong, K.W.: "Fidelity of Space TV", Photogrammetric Engineering 36, 5; 1970
- |6| Wood, P.: "Television from Space", Photogrammetric Engineering 36,2; 1970

CONCLUSION of the Symposium (summary)

F. Ackermann

During the closing session an attempt was made to summarize the results of the presentations and discussions of the symposium and draw conclusions as to the future research and development activities of Commission III. Also the available information was given and some tentative schedule for the technical sessions of the forthcoming ISP-Congress at Helsinki were discussed.

Hereafter a summary is given of the views and recommendations which were expressed during the closing session about the technical and scientific situation of the various fields of interest of Commission III:

1st field of interest: Aerial Triangulation

- Efficient methods for numerical strip- and block-adjustment are developed and to some degree successfully established in practical application. The computational strategies have not been compared. Requirements and specifications for software packages and computers are not sufficiently established. There are no recent theoretical studies on the accuracy performance and comparison of the main methods of adjustment. Experimental results have raised new questions.

Self-calibrating adjustment systems have been and are still developed. Their results are very promising and receive great attention.

Similarly progress has been made with introducing auxiliary data into block-adjustment. The development and application of hybrid adjustment systems is still restricted to some special cases.

- It can be considered a major result of the symposium that the high accuracy capability of aerial triangulation has been confirmed and established. The experimental results prove, that the conventional error threshold of 10 μm has been lowered to the level of 5 μm and may reach 2 - 3 μm .

Theoretical tools and generalized adjustment methods have been developed to operate with and to realize such accuracy levels. The most promising progress is presently associated with the principle of self-calibration.

This development is of utmost practical importance. It will extend the range of application of photogrammetry.

- The question of mono- versus stereocomparator has not been discussed. It remains in its state of ambiguity.
- Regarding the practical side of aerial triangulation the problem of point transfer does finally receive some attention, although conclusive results cannot be claimed as yet. Also the importance of automatic blunder detection in aerial triangulation has been recognized. Solutions are still in a preliminary phase.

It is recommended to concentrate research activities on the following topics of immediate importance:

- Development and assessment of self-calibrating systems
- Tests and experimental analysis of systematic and correlated image errors
- Tests and experimental comparisons on the accuracy performance of aerial triangulation (integral and modular)
- Better solutions for the problems of tie points and point transfer
- Methods and programs for automatic blunder detection
- Application of aerial triangulation to cadastral measurements and to densification of geodetic networks.

- Increased use of auxiliary data for small scale aerial triangulation

In general the utilisation of advanced methods is recommended.

2nd field of interest: Digital terrain models, digital contour interpolation, digital mapping, data banks.

- This field is receiving renewed attention. The mathematical solutions and operations depend strongly on the data acquisition and on the intended tasks. For the time being the development towards complete automation seems not feasible. Interactive systems will be used.
- For the digital interpolation of terrain surfaces and of contours several methods have been developed. A number of computer programs are operational. Little is known about the relative merits of the various methods and programs.
- Although there are some studies systematic theoretical and/or practical investigations into the accuracy performance of interpolation procedures are still lacking.
- The relation of interpolation methods and data acquisition has not been sufficiently clarified. More practical experience is to be gained by operational systems.
- Digital Mapping of planimetry is emphasized. Commission III is only concerned, as far as mathematical and computational problems are involved.

It is recommended

- to continue the development of DTM- and contour interpolation procedures
- to continue the accuracy investigation and the comparison of interpolation procedures
- to encourage practical application and operational testing of digital interpolation and digital mapping procedures.

3rd field of interest: Geometric aspects of remote sensing.

The ranges and technical features of remote sensing are so very wide that concentrated research on certain aspects is warranted. Therefore a joint working group of the ISP Commissions III and VII has been established in 1972 to deal with the Geometry of Remote Sensing.

Attention is drawn to the report of Prof. Konecny, chairman of the working group. The experimental investigations concentrate at present on side-looking Radar and on Multi-spectral sensors, including scanners.

The investigations deserve and receive great interest. Accuracy performance models have been established and confirmed. They form a clear and necessary basis for the evaluation of remote sensing imagery and have encouraged practical application.

The working group is continuing its activities.

4th field of interest: Digital image processing, digital image correlation.

This symposium has not discussed topics of digital image processing. It is recommended to begin or to continue research in this field. It is expected that papers also on such subjects will be submitted for the forthcoming ISP-Congress in Helsinki.

SOME RESULTS CONCERNING THE USE OF AERIAL TRIANGULATION WITH INDEPENDENT MODELS, IN PRODUCTION

by Gherasim Marton, Rumania

1. INTRODUCTION

Aerial triangulation method with independent models is used in production, since 1970. Depending on the purpose in view, the method has been used in different variants; we can also see it from the concise description of the program. The method is chiefly used to up-to-date topographical maps at 1 : 25 000 scale. Photographs were taken with RC.8 11/18 wide angular Wild camera at 1 : 30 000 - 1 : 35 000 scale. PUG 4 instrument is used to mark and implement points. Unmarked aerial triangulation points and pass-points will be marked only on a photograph in the main zone, having triple overlapping, by using PUG 4 instrument. Photograph stereoscopic measurement including fiducial marks, is carried out on Zeiss Jena Stecometer.

A concise description of the aerial triangulation program facilities, some problems related to the precision of the input data for aerial triangulation computation and, finally, practical aerial triangulation results, coming out from the present production works, are presented in this paper.

2. AERIAL TRIANGULATION PROGRAMS

Aerial triangulation programs with independent models are set up in a library on magnetic disk of Felix C.256 computer. From the photogrammetric stand point, the library consists of three basic programs: computation program for aerial triangulation in strips with independent models, computation program to obtain aerial triangulation planimetric block with free strips and program of block-space adjustment.

A) - Aerial triangulation program in strips with independent models is the basic program. Irrespective of the chosen adjustment variant method or the instrument used in measurement, data processing begins with this program. Number of points in the model and the number of models in the strip is practically unlimited.

1)- during the first computation stage systematic errors are eliminated from the measurements made in comparators and they are transposed in the coordinate system established by the fiducial marks of the aerial camera. The relative orientation elements are then computed independently, for each pair of photographs. Independent model coordinates, including projection centres, are computed in two ways: using two photographs or three photographs. So far, independent models made up by considering three photographs were used. In this case, models have longitudinal and transversal overlapping like photographs and, at the same time, we can work without projection centres.

2)- Tie points among models in the same strip are checked during the second stage. In the same process, independent models are transformed by rigorous relation of the space orthogonal transformation within the first model system.

3)- When the aerial triangulation strips is not provided with control points necessary for adjustment, checked independent model coordinates are stored in file disk and the free strip coordinates are output on the punch card.

4)- When the aerial triangulation strip is provided with control points, the computation is going and the control points are tested. During this process, independent models are transposed in the coordinate system of the control points.

5)- Strip adjustment can be carried out in two ways: If the strip is provided with enough planimetric control points as well, the planimetric and height block adjustment is carried out. Otherwise only the height adjustment of the strip is accomplished. This last method is used more frequently in production.

6)- During the last stage, space orthogonal transformation of models is carried out and triangulated point coordinates are computed by averaging tie point coordinates. In this last stage, according to the choice made, we can make up the files of the adjusted model points on magnetic disk and the adjusted strip coordinates can be output on punch card.

B) - Program forming planimetric block with free strips is used when the aerial triangulation block is provided with a reduced number of planimetric control

points. Tie points among strips and control points in block are tested planimetrically, using this computation program.

Finally, approximate planimetric coordinates of the triangulated points in the coordinate system of the control points are obtained. Control points list within each strip is completed with those approximate planimetric coordinates and computations of the aerial triangulation in strips are resumed from point 4 and the height adjustment of the strip is carried out.

C) - Block space adjustment program is based in the simultaneous determination of the space orthogonal transformation parameters by planimetric and height iteration [1]. This program consists of two main stages:

1)- Rigorous check of the tie points among strips is accomplished during the first stage. Tie points which have not the required precision are considered, in succession, only within the strips in which they appear. This check is carried out using the points of the individually adjusted strips.

2)- Block-space adjustment is accomplished during the second stage of the program. When the block is not provided with enough planimetric control points, the adjustment is carried out using independently adjusted strips. When the block has enough planimetric control points, the adjustment is carried out using independent models coming out after strip independent adjustment is accomplished without considering, in our computation, tie points among strips which have not the required precision.

Adjustment method with independently adjusted strips is more frequently used in production, because of the method employed to establish control points.

3. THE PRECISION OF THE MEASURED POINTS

Usually, during aerial triangulation process, we consider three aspects regarding measurement precision of aerial triangulation data, namely: behaviour of the instrument used to measure photographs, measurement precision of the model coordinates and precision to establish control points.

1)- After each maintenance operation of Stecometer and at fixed intervals we make stereoscopic measurements of the control network in identical condition as for photographs. In our case, we use photographs taken with 11/18 wide angular cameras. In Table 1, we present the results of such control measurements for two models. They represent:

σ_o = the mean square error of weight unit, computed in relative orientation

$p_{y_{max}}$ = the maximum parallax of the stereomodel

σ = the mean square error of weight unit, computed in tie points after adjustment was accomplished

μ_x, μ_y, μ_z = mean square errors of coordinates computed considering absolute coordinate difference in all points of the network.

Table 1

Model	Results are in μm					
	σ_o	$p_{y_{max}}$	σ	μ_x	μ_y	μ_z
1	1,3	2,0	3,1	3,5	3,8	4,3
2	0,8	0,9				

Any operator doing common measurements can make this test; it is a general index of the instrument behaviour. Analysing results of many checks, we see that stecometer precision is of ± 3 to $\pm 5 \mu m$, in usual work condition.

2)- Obtaining homogeneous precision of model coordinates used in adjustment is a very important problem within the aerial triangulation process with independent models. This is done in three stages during aerial triangulation programs.

When determining relative orientation elements, at last iteration, point having maximum vertical parallax is eliminated and the iteration process is resumed if the maximum vertical parallax $p_{y_{max}}$ exceeds the value of the established maximum ϵ_{max} . Considering many production works, we can write the following ratio between ϵ_{max} and $\sigma_{o_{max}}$

$$\epsilon_{max} \approx 1,55 \sigma_{o_{max}} \quad (1)$$

Let $\epsilon_{max} = 20 \mu m$, the $\sigma_{o_i} < 13 \mu m$.

We present value groups of σ_{o_i} for $\epsilon_{max} = 20 \mu m$, $i = 1.025$, models, disposed in 16 aerial triangulation blocks situated in hill zones, up to 1 000 m height, in table 2.

Table 2

Number of the models	$\pm \sigma_o$ in μm		
	$\leq 7,5$	$7,5 - <10$	$10 - <13$
1.025	641	247	137

Maximum vertical parallaxes established by considering ordinate differences when independent model coordinate computation is done, always satisfy the condition:

$$p_{y_{max}} < \epsilon_{max} \quad (2)$$

Tie points among models of the same strip are tested during the second stage, using condition

$$(|x^i - x^{i+1}|, |y^i - y^{i+1}|, |z^i - z^{i+1}|) \leq 1,5 \epsilon_{max} \quad (3)$$

Checking photogrammetric measurements comes to an end when tie points among strips are tested. This problem is more difficult and we consider it is not well studied for the present production conditions. In the case of the works referred to in the introduction and if the control points are at a distance of 4 bases during the height adjustment with strips, we use the following condition to check tie points

$$|z^k - z^{k+1}| > 3 \epsilon_{max} \quad (4)$$

Points which do not satisfy condition (4) are eliminated from the adjustment computation as tie points among strips.

3)- The use of aerial triangulation with independent models emphasizes this method as having an internal, high and controlled precision. We may not say the same words about precision homogeneity of control points, established by different methods, instruments and operators, as well as other factors.

Up to now, the best results were got when height control points were established using spirit levelling and when pre-marked points of the state triangulation network were used for block-planimetric adjustment with strips.

4. PRACTICAL RESULTS

Practical results were obtained in an aerial triangulation block in the national photogrammetric test field and in 16 blocks in the current production.

1)- Aerial triangulation block within national test field consists of three strips of nine photographs each. Photographs were taken with RC.8 11/18 wide angular camera at 1 : 10 000 scale, 72 premarked points were uniformly located within the whole block. 12 points having complete X, Y, Z coordinates, spaced at 4 bases in each strip were used during the adjustment. All tie points among strips were premarked points. Measurements were made with stecometer. Independent models were made using three photographs. Obtained results were presented in Table 3. Mean square errors μ_x , μ_y and μ_z were computed, taking into account coordinate differences for the 72 pre-marked points. σ and μ values are in μm at photograph scale 1 : 10 000.

Table 3

Number of models within the block	σ	μ_x	μ_y	μ_z
3 x 7 = 21	11,3	13,8	12,6	15,9

2)- The 16 blocks used in production cover a 6 400 km² area. RC.8 11/18 wide angular camera was used to take photographs, at 1 : 33 000 scale. 45 points of the state triangulation network were premarked within the zone. Blocks consists of 5 - 6 strips each, having 12 - 14 photographs. Each strip had 8 - 10 height control points. Measurements were made using stecometer and independent models were made using three photographs.

We used the program presented in section 2.A to compute 85 free strips and program described in section 2.B to compute approximate planimetric coordinates. Approximate coordinate computation within coordinate system of the control points begins in blocks provided with 4 pre-marked points, at least, located in the four corners of the block. Tie point coordinates among computed blocks were used in the remainder of the block.

Height adjustment with independent models in each strip was carried out independently using those approximate coordinates and height control points. σ_H and μ_z values spaced at 5 μ m distance, at the photograph scale, for 85 photographs are shown in Table 4.

σ_H and μ_z values, at 1 : 33 000 scale, spaced at 5 μ m distance, were obtained during strip height adjustment.

Table 4

Interval in μ m	10-15	15-20	20-25	25-30	30-35	Total of strips
σ_H	15	33	26	11	-	85
μ_z	11	23	27	16	5	

Block-space adjustment with height previous adjusted independently strips was carried out to get a single row of coordinates within each block and final coordinates. In Table 5, we find σ_p , μ_x , μ_y and σ_H , μ_z . We should mention that the x,y coordinate values have distortion errors of the strip, as a result of successive model transformations during free strip computations. σ and μ values are in μ m, at a scale of 1 : 33 000.

Table 5

Number of the block	σ_p	μ_x	μ_y	σ_H	μ_z
1	35.6	49.5	26.3	24.6	29.3
2	41.6	32.1	38.6	14.6	20.1
3	33.4	43.4	41.2	18.3	19.8
4	39.9	45.7	31.8	18.8	21.2
5	35.8	55.5	26.7	15.2	18.1
6	38.1	45.6	27.3	24.2	26.3
7	29.4	21.7	32.7	12.5	17.2
8	39.8	46.2	41.2	14.8	19.5
9	35.1	38.3	29.5	21.2	24.7
10	41.3	48.5	36.9	22.1	25.3
11	37.4	46.2	38.8	20.2	26.1
12	41.2	49.5	52.3	27.1	31.2
13	32.5	41.8	38.1	16.4	19.3
14	39.4	38.5	37.6	15.7	17.8
15	35.1	42.6	43.7	19.4	23.9
16	36.7	42.8	47.3	23.6	27.5

Ground tests of the contour lines and of the heighted photogrammetric points prove the high height precision of the aerial triangulated points.

Two problems, however, are out of order in stereoplotting. On the first hand we cannot neglect the Δz coordinate differences in the control points if they exceed $20 \mu\text{m}$, at photograph scale; so we must do either control point rectifications after adjustment is accomplished or those deviation reductions using linear prediction method. The use of high weights for control points within the blocks is not a good solution because if $P = 1\ 000$, μz values are reduced a few and Δz differences in tie points can be doubled.

The second problem is related to the tie points among the strips. Z coordinate of the tie points is obtained as their averaging during block adjustment. Points located along the strip axes can be corrected even in a different way. In this case, after stereomodel absolute orientation, an artificial curvature of the model appears, which can not be corrected.

REFERENCES

- |1| Ackermann, F., Ebner, H. and Klein, H.: "Ein Rechenprogramm für die Streifen-triangulation mit unabhängigen Modellen" Bul 4, 1970
- |2| Ackermann, F.: "Ergebnisse kontrollierter Streifen- und Blockausgleichungen", AVN 4, 1973
- |3| Marton, G.: "Un pachet de programe de fotogrammetrie" Buletin de fotogrammetrie nr. 3, 1971

ACCURACY OF STATOSCOPE-DATA - RESULTS FROM THE OEEPE-TEST "OBERSCHWABEN"

by F. Ackermann, Stuttgart, Fed.Rep. Germany

1. INTRODUCTION

Auxiliary data have been known for a long time to be highly effective in aerial triangulation, [1] - [5]. Nevertheless they are not widely used in practice to this day.

Amongst auxiliary data especially APR and statoscope are most effective with regard to vertical accuracy of strips and blocks. When jointly included in simultaneous block-adjustment they are expected to improve accuracy and economy considerably beyond the present state of the technique [6].

There exists only scarce information about the accuracies of statoscope- and APR-data which are generally believed to be in the order of 1.5 m - 4 m, depending on altitude and circumstances. Therefore, the European Research Organisation OEEPE included an investigation of the accuracy of statoscope data in the research program of the controlled aerial triangulation test "Oberschwaben" [7]. This paper presents a summary of experimental results as completed up to now.

2. ACCURACY OF STATOSCOPE DATA

2.1 - The test field "Oberschwaben" covers an area of 40.0 km x 62,5 km. It contains 540 signalized trigonometric points to be used as control points and check points. For about 470 of them the heights (Z) are known. In addition all tie points were signalized (as double targets) whence pin point flying was asked.

Aerial photography was taken in spring 1969 by Firma Häussermann, with Aero Commander 560 F. The test field was completely covered by both wide-angle and super-wide-angle photography of scale 1 : 28 000 (with Zeiss RMK 15/23 and Zeiss RMK 8.5/23), each mission giving a block of 15 strips of 60 % lateral overlap and 25 models each, with simultaneous recordings of the Zeiss statoscope S 2 [8]. Thus, the statoscope investigation distinguishes 2 sets of data:

- 15 strips of 62.5 km (25 models) each; wide-angle photography; flying height $h_{rel} = 4\ 285\ m$, $h_{abs} = 4\ 990\ m$
- 15 strips of 62.5 km (25 models) each; super-wide-angle photography; flying height $h_{rel} = 2\ 380\ m$, $h_{abs} = 3\ 085\ m$.

There were 5 flying missions, on April 8th, 9th and May 12th for wide-angle-, on April 10th and 26th for super-wide-angle photography. Due to initial difficulties with pin point exposures the original photo-coverage had some gaps left. Reflying of 23 separate exposures was done without statoscope.

2.2 - Processing of statoscope data: The photographic statoscope recordings were read off paper prints of the aerial photographs, and converted to height differences Δh_{Stat} . The conversion factors, derived from the statoscope calibration and the reduction according to altitude, amounted to 1.05 m (w.a.) and 0.90 m (s.w.a.) respectively, per scale unit. Adding per strips a reference height H_0 gave preliminary statoscope-heights:

$$Z_{Stat} = H_0 + \Delta h_{Stat} \quad (1)$$

No further corrections were applied, in particular no Henry correction (due to lack of drift angle recordings).

The preliminary statoscope heights Z_{Stat} (1) still refer essentially to unknown isobaric reference surfaces. They are compared with the heights Z_{PC} of the perspective centres (camera stations) as obtained from independent model block adjustments which utilized all given points as control (about 3 per model). The differences

$$\Delta Z = Z_{PC} - Z_{Stat} \quad (2)$$

have been plotted for all strips separately, see examples in fig. 1

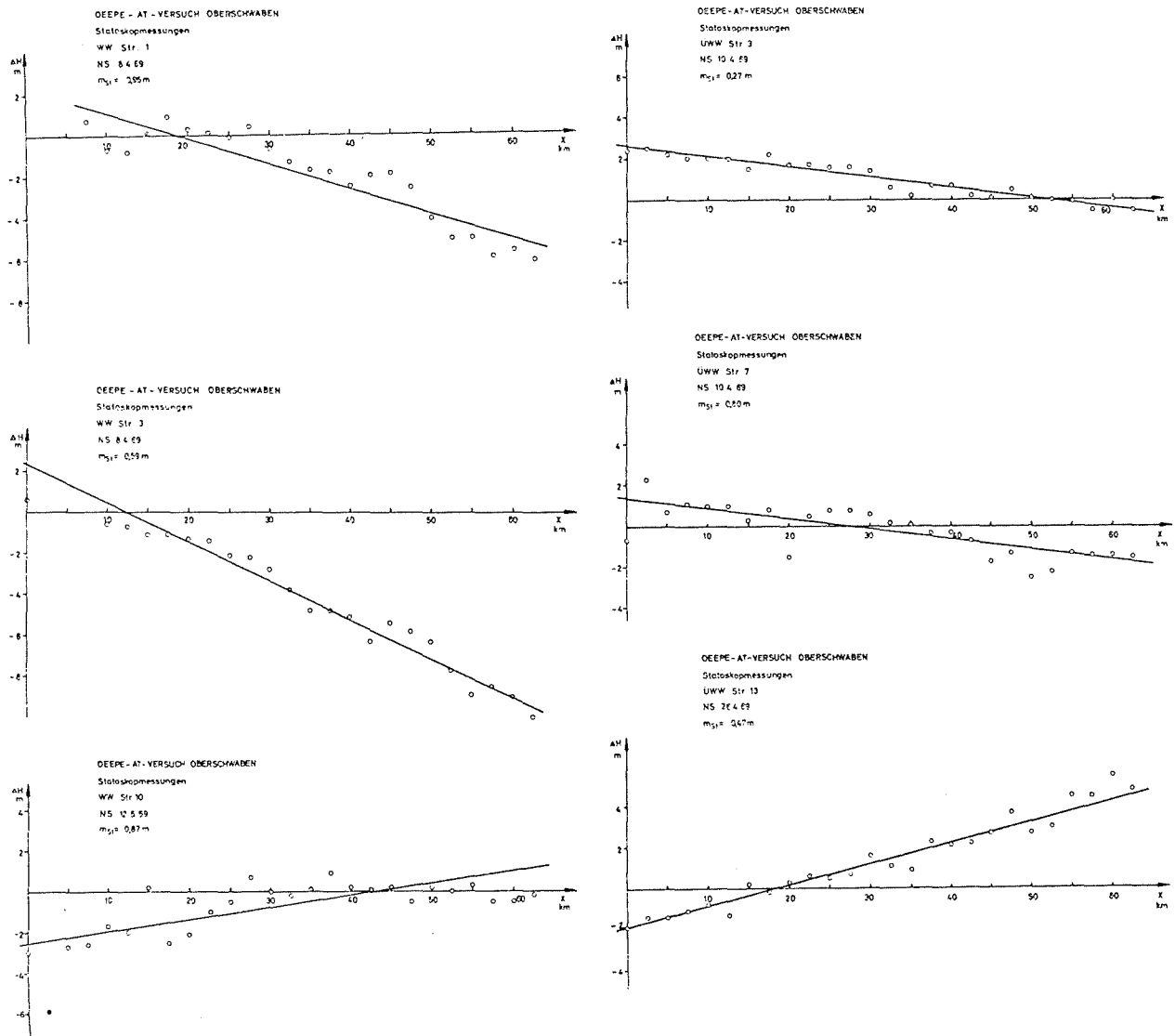


Figure 1 : OEEPE statoscope test "Oberschwaben" - Accuracy of statoscope data, 6 examples (Differences $Z_{PC} - Z_{Stat}$ and residuals against linear approximation to isobaric surface.)

2.3 - Accuracy results: To the graphs of ΔZ -values (2) straight lines were fitted graphically, see fig. 1. They each represent a linear approximation to the isobaric surface. The residuals between ΔZ -values and straight lines

$$dZ = \Delta Z - (a_0 + a_1 x) \quad (3)$$

are treated as errors of the statoscope measurements (against the isobaric reference), although they contain also the errors of the check-values Z_{PC} which are barely negligible. The residuals dZ are reduced per strip to root mean square values

$$m_{Stat} = \sqrt{\frac{[dZ \cdot dZ]}{n - 2}} \quad (4)$$

as collected in table 1. Altogether 23 values had to be excluded because of gross deviations, the causes of which are not known (such exclusion is permissible as gross errors would equally be detected in a practical case during the combined block-adjustment, see section 3).

The combined r.m.s. values of all strips amount to

$$m_{\text{Stat}} = 0.89 \text{ m (altitude 4 990 m, w.a.)} \quad (5a)$$

$$m_{\text{Stat}} = 0.79 \text{ m (altitude 3 085 m, s.w.a.)} \quad (5b)$$

The values (5) represent the direct experimental accuracies of the statoscope measurements with respect to isobaric surfaces. They refer to strip lengths of 62.5 km, and still contain possible error effects due to

- check heights of camera stations (!)
- non-linearity of isobaric profiles
- statoscope-calibration.

2.4 - Discussion of accuracy results: The first comment ought to point out that the obtained accuracy values are considerably better than originally expected. Also, they are rather representative, referring to 5 different flight missions, up to 5 weeks apart.

The accuracy results (5) correspond to 0.85 (w.a.) and 0.88 scale units (s.w.a.), respectively, of the statoscope recordings. Reduced to sea level the equivalent values are 0.59 m and 0.62 m. Thus the results are consistent with respect to altitude, and extrapolation seems to be permissible.

The accuracy results are close to the limits of resolution of the statoscope measuring system (involving stability of isobaric surface, pick-up of air-pressure, physical measuring process, registration and reading off dial). This is particularly true for some strips. 5 of the r.m.s. values m_{Stat} are equivalent to 0.3 (!) scale units. Consequently, in future, the measuring performance of statoscopes should be refined by, preferably, a factor of 2. Calibration values of less than 0.50 m/scale unit are desirable.

Linear approximations to isobaric surfaces have shown to be sufficiently representative, within the investigated distance range of 62.5 km. Although a few strips indicate a slight curvature in the order of 1 m there is altogether no significant evidence of curvature of an isobaric surface. This linear approximation is likely to be effective up to distances of at least 100 km.

The accuracy values m_{Stat} (5) spread over a rather wide range, for instance from 0.26 m - 1.30 m for the s.w.a. strips. 10 of the 15 s.w.a. strips have values between 0.26 m and 0.82 m, with a r.m.s. mean of 0.51 m. Clearly distinguished are the other 5 strips with values between 1.08 m and 1.30 m and a r.m.s. mean of 1.15 m. Thus we have obviously 2 sets of values, not belonging to the same population. According to a F-test the difference is significant on the 1 % level of significance. A similar disintegration, although not as marked, in 2 separate groups of accuracy results can be observed with the wide-angle strips. The total range of m_{Stat} values from 0.58 m - 1.30 m can be subdivided in a group of 12 values between 0.58 m and 0.94 m (r.m.s. mean 0.78 m) and 3 values between 1.18 m and 1.30 m (r.m.s. mean 1.23 m).

A variance analysis gave no significant relation of the 2 groups of poor values of m_{Stat} with any of the relevant flight parameters (date, flight direction, altitude). The only significance found relates to the observation that always the first two strips of the four main flight missions are disturbed. They show the largest or large values of m_{Stat} , see table 1. Omitting those 8 strips the r.m.s. means of the remaining values are:

$$m_{\text{Stat}} = 0.80 \text{ m} \hat{=} 0.76 \text{ scale units (altitude 4 990 m, w.a.)} \quad (6a)$$

$$m_{\text{Stat}} = 0.60 \text{ m} \hat{=} 0.67 \text{ scale units (altitude 3 085 m, s.w.a.)} \quad (6b)$$

In this case, only two strips with large values of m_{Stat} (1.16 m, 1.18 m) remain. The assumption seems valid that the statoscope was not sufficiently ready for measurement at the beginning of the flights, whatever the cause might have been. Consequently, results (6) can be considered realistic for experienced handling of statoscope-equipment.

A more detailed presentation of the accuracy results will be given in the complete OEEPE-report on the "Oberschwaben" statoscope investigation [9].

Table 1 : OBERSCHWABEN flight missions and accuracy results of statoscope data

strip no.	flight date (1969)	mission time ¹⁾	flight direction	no. of exposures reflown	statoscope reference height H ₀ [m]	investigation gross errors	accuracy m _{Stat} [m]
wide-angle, h _{abs} = 4990 m							
1	8.4.	12.09 ^h	N-S	3	4995		0.94
2	8.4.	12.30	S-N	3	4995	3	1.20
3	8.4.	13.04	N-S	3	4990	1	0.59
4	8.4.	13.30	S-N	5	4965	1	0.79
5	8.4.	13.54	N-S	1	4970	1	0.63
6	8.4.	14.24	S-N	1	5011	1	0.72
7	9.4.	12.54	N-S		5045		0.65
8	12.5.	12.11	S-N	5	5001	2	1.30
9	9.4.	13.18	S-N	1	4965	-2)	0.58
10	12.5.	12.34	N-S		5014	1	0.87
11	12.5.	14.07	S-N	1	4960	3	0.91
12	12.5.	13.00	S-N	1	5012	1	1.18
13	12.5.	14.27	N-S	2	4993	2	0.80
14	12.5.	13.21	N-S	4	4989		0.91
15	12.5.	14.47	S-N		4957	1	0.80
				30	4991	17	0.89
super-wide-angle, h _{abs} = 3085 m							
1	10.4.	11.29 ^h	N-S		3077	1	1.08
2	10.4.	11.50	S-N		3064	2	1.12
3	10.4.	12.12	N-S		3043		0.26
4	10.4.	12.33	S-N		3040		0.30
5	10.4.	12.54	N-S		3005		0.31
6	10.4.	13.16	S-N		3028		0.27
7	10.4.	13.36	N-S		3029		0.79
8	10.4.	13.58	S-N		3015		1.16
9	26.4.	11.40	N-S	1	3155	3	1.30
10	26.4.	12.00	S-N		3121		1.10
11	26.4.	12.20	N-S		3095		0.67
12	26.4.	12.40	S-N		3136		0.82
13	26.4.	12.58	N-S		3172		0.47
14	26.4.	13.17	S-N	2	3113		0.44
15	26.4.	13.36	N-S		3121		0.34
				3	3081	6	0.79

1) The times indicated refer to the first exposure of a strip.

2) Change of the reference height for the last 5 registrations by -28 m.

3. COMBINED BLOCK-ADJUSTMENT WITH STATOSCOPE DATA

3.1 - The method: In the second part of the investigation the original statoscope data are introduced into combined adjustment with the photogrammetric block, using minimum height control. Comparison with check points allows estimation of the resulting vertical accuracy.

The version S (statoscope) of the Stuttgart computer program PAT-M-43 for block adjustment with independent models has been used. It allows introduction of statoscope-data or APR-profiles (apart from level conditions of shore-lines) into the combined simultaneous adjustment. The method and the program have been described in [6]. It is expected to improve the vertical accuracy of adjusted blocks by extending bridging distances considerably. Adjustment results also allow analysis of corrections v to statoscope data and empirical weight determination.

Statoscope data are used as weighted observations, with the following observational equation for an exposure station i in strip k :

$$v_{ik}^{Stat} = - z_{ik}^{Stat} - (a_k + b_k x_{ik}) + z_{ik}^{PC} \quad (7)$$

The term $(a_k + b_k x_{ik})$ provides a constant shift and a tilt correction of the isobaric surface along the flight line k . a_k , b_k are unknown orientation parameters, to be simultaneously determined by the combined adjustment. The strips k can be subdivided in several separate lines.

The unknown heights z_{ik}^{PC} of the camera stations ik appear also as unknowns in the photogrammetric block-adjustment. They provide the connection of statorscope- and block-data in the combined adjustment.

3.2 - Results of controlled tests: A number of combined block-adjustments with statorscope data have been performed with the Oberschwaben material. The absolute vertical accuracy after adjustment is obtained from the check points of the test-field. The total research program has not been completed. The available test results are presented in table 2. They refer to 2 blocks of 200 models (one w.a., one s.w.a.), each of 8 strips with 20 % lateral overlap. Bridging distance is varied from 25 models (62.5 km, two chains of vertical control points) to 12.5 models (31 km, three chains) and 8 models (21 km, four chains).

The weights used for the combined adjustment were:

1 for z coordinates of model points and perspective centres; 0.11 = 1/9 for statorscope data; ∞ for terrestrial control; 0 for check points.

Table 2 : OEEPE statorscope test "Oberschwaben" - Vertical accuracy of combined block-adjustment (independent models + statorscope data)

vertical control	bridg.dist.i (base lengths)	n vert. contr.	n check pts.	n statorscope	ϵ_0 vert. adj. [cm]	\bar{v}^{Stat} [cm]	v^{PC} [cm]	μ_z check pts. [cm]	σ_h
Wide-angle-block Frankfurt									
8 strips, $q=20\%$, 200 models; 1:28.000, $h_{rel}=4285$ m, $h_{abs}=4990$ m									
2 chains	25	1)	18	434	180	23	38	12	84 0.20
+ 2 border pts.	25(12.5)	1)	20	432	180	23	38	12	69 0.16
3 chains	12.5	1)	27	425	180	24	39	12	67 0.16
3 chains	12.5	2)	27	425	180	23	36	11	55 0.13
+ 4 border pts.	12.5(6)	1)	31	421	180	24	42	12	58 0.14
4 chains	8	1)	36	416	180	24	41	12	53 0.12
4 chains	8	3)	36	416	180	23	34	11	45 0.10
+ 6 border pts.	8(4)	1)	42	410	180	24	42	12	50 0.12
Super-wide-angle-block The Hague									
8 strips, $q=20\%$, 200 models; 1:28.000, $h_{rel}=2380$ m, $h_{abs}=3085$ m									
2 chains	25	1)	18	414	193	21	35	16	58 0.24
+ 2 border pts.	25(12.5)	1)	20	412	193	21	35	16	57 0.24
3 chains	12.5	1)	27	405	193	21	36	16	55 0.23
3 chains	12.5	2)	27	405	193	21	34	16	57 0.24
+ 4 border pts.	12.5(6)	1)	31	401	193	21	37	16	52 0.22
4 chains	8	1)	36	396	193	21	37	16	52 0.22
4 chains	8	3)	36	396	193	21	32	16	53 0.22
+ 6 border pts.	8(4)	1)	42	390	193	21	37	16	52 0.22

- 1) linear isobaric correction - not subdivided, 62.5 km
- 2) linear isobaric correction - subdivided, 2 x 31 km
- 3) linear isobaric correction - subdivided, 3 x 21 km

The symbols of table 2 which need explanation are:

σ_0 : standard error of unit weight for the total (vertical) adjustment

\bar{v}_{Stat} , \bar{v}_{PC} : root mean square means of the adjustment corrections v_{Stat} of the statoscope data and v_{PC} of the z-coordinates of the perspective centres.

μ_z : r.m.s. mean of the residual height errors at check points = accuracy estimate of the adjusted block.

3.3 - Comment on the results: The results of table 2 demonstrate the effectiveness of the combined adjustment. With bridging distances of 25 models (62.5 km) and two additional control points at the open sides of the blocks absolute vertical accuracies of 69 cm (w.a., 0.16 ‰) and 57 cm (s.w.a., 0.24 ‰) have been reached, with photo scale 1 : 28 000. It is worth pointing out that the accuracy of the combined system is by 22 % and 28 % better than of the statoscope alone, if compared with (5).

The use of two additional control points has small effects, mainly by controlling tilts and twists of long strips.

Shortening the bridging distances to 12 and 8 models (31 km, 21 km) improved the accuracies to 58 cm (0.14 ‰) and 50 cm (0.12 ‰) for w.a. and to 52 cm (0.22 ‰) and 52 cm (0.22 ‰) for s.w.a., respect.

When the accuracy level is reached which the block has without statoscope, no further improvement can be expected. (Without statoscope data the height accuracies for 12.5 (6) and 8 (4) models bridging distance, respectively, are: w.a. 53 cm, 45 cm; s.w.a. 64 cm, 53 cm). For the same reason subdivision of the linear isobaric corrections gave no or only moderate accuracy improvements. Nevertheless, the accuracy of 45 cm / 0.10 ‰ of the wide-angle block, when bridging 8 models, is remarkable.

The corrections \bar{v}_{Stat} of the statoscope data, as obtained from the adjustments are of special interest. Their dependence on bridging distance indicates some systematic error effects. Nevertheless, the r.m.s. values of 38 cm (w.a.) and 35 cm (s.w.a.) although only given weight 1/9, confirm again the unexpectedly high accuracy capability of statoscope measurements. The corrections v_{Stat} , when checked closely, do not show marked evidence of systematic error effects, appearing rather random.

The tests will have to be completed before final conclusions are drawn. It is evident, however, that the accuracy capability of statoscope measurements is considerably higher than hitherto believed. Application for medium map scales (up to 1 : 10 000) seems feasible. Statoscope supported block-adjustments are now expected to bridge very long distances and still give vertical control accuracy sufficient for mapping with contour intervals of 10 m, 5 m, 10' and perhaps even 2 m. With regard to reduction of control the statoscope with combined block-adjustment may achieve a similar breakthrough for heights as perimeter control did for planimetry. Additional tests and practical applications have to verify whether the unexpectedly good results of the Oberschwaben statoscope test can be obtained regularly and repeatedly.

REFERENCES

- |1| Jerie, H.G. and Kure, J. "Data analysis and report on a investigation into the application of the airborne profile recorder to photogrammetric mapping" ITC Publications A 25/26, p.80, 1964
- |2| Jerie, H.G. "Theoretical height accuracy of strip and block triangulation with and without use of auxiliary data" Photogrammetria 23 p. 19 - 44, 1968
- |3| Kure, J. "APR-experience and applications (with special emphasis on the Saudi Arabia project), ITC journal 4, p. 618 - 639, 1973
- |4| Jerie, H.G. "Techniques, evaluation and applications of auxiliary data in Aerial triangulation" Invited Paper Comm. III, ISP-Congress Lausanne, 31 p., 1968
- |5| Zarzycki, J.M., "The use of auxiliary data in aerial triangulation" Invited Paper Comm. III, ISP-Congress Ottawa, 24 p., 1972
- |6| Ackermann, F., Ebner, H., Klein, H.: "Combined Block Adjustment of APR Data and Independent Photogrammetric Models", The Canadian Surveyor 26 / 4, p. 384 - 396, 1972
- |7| Proceedings of the OEEPE Symposium on Experimental Research on Accuracy of Aerial Triangulation (Results of Oberschwaben Tests); OEEPE, Official Publication No. 8, Frankfurt 1973, 350 p.
- |8| Meier, H.K.: "Ein neues Statoskop mit elektrischer Registrierung", BuL Sonderheft Stockholm, p. 60 - 69, 1956
- |9| Ackermann, F.: "Genauigkeit der Statoskopmessungen der Befliegung Oberschwaben", OEEPE Report, to be published.

SYSTEMATIC MODEL DEFORMATION OF THE OEEPE-TESTBLOCK "OBERSCHWABEN"

by M. Schilcher and E. Wild, Stuttgart, Fed.Rep. Germany

1. INTRODUCTION

Recent theoretical and empirical investigations have been concerned very much with systematic image errors and their influence on the accuracy of aerial triangulation. Several methods have been suggested for considering systematic errors during block adjustment both by the bundle and the independent model method (see [1], [2], [3], [4], [5]). There is, however, only very limited information available about the systematic errors occurring in practical cases, in particular about the types and magnitudes of such errors and their dependence on various factors.

In this paper the results are presented of an empirical investigation into the systematic model deformations of the testblock Oberschwaben, as appearing after block adjustment by independent models. It will be investigated whether systematic model deformations depend on the camera (wide-angle, super-wide-angle), flight direction, date of the flight mission and measuring instrument. Other points of interest are the influence of different distributions of control points on systematic model deformations and the question of how constant such errors are within certain areas of a block.

2. THE TEST "OBERSCHWABEN"

During spring 1969 aerial photographs were taken of 1 : 28 000 scale of the test area Oberschwaben which is located in southwestern Germany. The test area of 40 km x 62.5 km was photographed with a wide-angle camera Zeiss RMK 15/23 and a super-wide-angle camera Zeiss RMK 8.5/23, each coverage resulting in a block of 60 % longitudinal and lateral overlap with 15 strips of 25 models each. The strips run in north-south direction or vice versa.

For the restitution each of the two blocks was subdivided in two blocks of 20 % lateral overlap. The four separate blocks were given the names of the 4 centres which undertook the stereocomparator measurements:

- Wide-angle blocks: block Frankfurt, uneven strip numbers (1,3,5,...13,15),
8 x 25 = 200 models; block Vienna, even strip numbers (2,4,6,...12,14),
7 x 25 = 175 models.
- Super-wide-angle blocks: block The Hague, uneven strip numbers (1,3,...13,15),
8 x 25 = 200 models; block Delft, even strip numbers (2,4,...12,14),
7 x 25 = 175 models.

Aerial photography was taken on five different days by pin-point flying. Table 1 for wide-angle and Table 2 for super-wide-angle display date and direction of the flight strips. Within the test area 548 trigonometric points were signalized, to be used as control-points and check-points. For 480 of them also the heights are given. Pin-point flying was necessary because also the tie-points were signalized in the terrain by double targets, for test purposes. Therefore the models contain 6 x 2 signalized tie-points located in the 6 standard positions.

Stereocomparator measurements of the photographs were performed by 4 different photogrammetric centres (Zeiss PSK: Frankfurt, The Hague; Wild StK 1: Vienna, Delft). The image coordinates were corrected for radial symmetrical distortion, refraction, and earth curvature. Then independent models were computed, by analytical relative orientation. The independent models went into a number of block adjustments with the PAT-M-43 program the results of which have been published in [6]. The present study for systematic errors is based on the residual errors at tie-points and perspective centres as appearing after such block adjustments.

3. METHOD OF INVESTIGATION

The systematic errors of the independent models are represented by the average residual vectors at the 6 standard positions and at the two perspective centres of the models after block adjustment. In order to obtain the systematic errors the models, as appearing after the block adjustments, were transformed onto a nominal reference model, specified by giving the perspective centres of each model

the coordinates $x_1 = 0, y_1 = 0, x_2 = 2500 \text{ m}, y_2 = 0$ (2500 m was the base length according to the flight plan).

The residual errors of the tie-points were referred respectively to the ideally located standard positions of the reference model, see fig. 1. Then for each of the standard positions of tie-points and of the perspective centres the arithmetical means of all residual errors in x, y, z of all models were computed. The mean values represent the systematic planimetric and vertical model deformations.

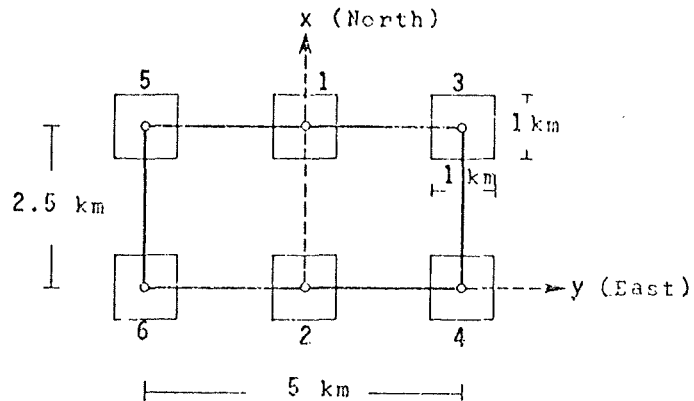


Figure 1: Reference model for representation of systematic model deformations.

The empirical investigation on systematic errors of independent models refers to the four separate Oberschwaben blocks of 20 % lateral overlap which include 200 and 175 models respectively. The following adjustments with different control versions are included:

Block Frankfurt (w.a.) and block The Hague (s.w.a.):

- version 0: all planimetric and vertical control points
- version 1: Planimetric control: perimeter, spacing $i=2$ base-lengths
Vertical control: chains, bridging distance $i=2$ base-lengths
- version 5: Planimetric control: 4 corner points
Vertical control: 3 chains, bridging distance $i=12.5(6)$ base-lengths, with 4 additional perimeter points (see [6]).

Block Vienna (w.a.) and block Delft (s.w.a.):

- version 0: all given planimetric and vertical control points.

Version 0 gives 2 - 3 control points per model. Therefore the adjustment is more or less equivalent to absolute orientation of single models. Version 0 will give the best estimation of the actual systematic model deformations. The versions 1 and 5 of the blocks Frankfurt and The Hague are intended to show the influence of control distribution on the apparent systematic errors.

4. RESULTS

The results of the investigation are summarized in the tables 1 - 4 and figures 2 - 5. The tables 1 and 2 present, separately for each of the 15 wide-angle and 15 super-wide-angle strips, the average residual coordinate errors at the 6 standard model tie-point positions, referring to the adjustment version 0 (all control points used). Table 3 presents the results of all adjustment versions treated of all 4 blocks, by summarizing the strips in groups by common flight direction. Table 4 displays accordingly the systematic residual errors at the perspective centres. In addition, the essential results are graphically represented in figures 2 - 5.

Table 1. OEEPE-Oberschwaben
Systematic model deformations after block adjustment by independent models.
Wide-angle strips: Control version 0; in units of μm

strip no.	1	2	3	4	5	6	7	8	9	10	11	12	13	14	15	
flight direction	NS	SN	NS	SN	NS	SN	NS	SN	SN	NS	SN	SN	NS	NS	SN	
flight mission	8.4.	8.4.	8.4.	8.4.	8.4.	8.4.	9.4.	12.5.	9.4.	12.5.	12.5.	12.5.	12.5.	12.5.	12.5.	
standard position																
x	1	+1.6	+0.6	+2.1	+2.1	+1.7	+1.0	+2.1	+1.6	+ 3.3	+2.7	+ 2.4	+2.0	+1.9	+0.3	+2.0
	2	-1.7	-0.8	-2.1	-2.1	-1.7	-1.0	-2.1	-1.7	- 3.3	-2.7	- 2.4	-2.0	-1.9	-0.3	-2.0
	3	-0.8	+7.7	+0.0	+6.4	-2.4	+6.7	+0.1	+4.0	+10.3	-4.2	+11.4	+5.8	-0.6	-5.4	+7.9
	4	+4.1	-3.7	+4.1	-2.7	+5.1	-4.5	+2.6	-4.5	- 6.2	+3.9	- 6.3	-6.1	+3.9	+5.4	-7.9
	5	+6.0	-3.4	+4.6	-4.1	+4.6	-4.4	+5.0	-2.7	- 3.5	+9.4	- 5.7	-2.1	+4.7	+7.1	-3.9
	6	-6.0	+3.9	-8.5	+0.0	-8.7	+1.5	-7.9	+0.7	+ 0.6	-9.2	+ 1.9	+2.4	-8.0	-6.2	+1.2
y	1	+2.8	+2.1	+3.4	+2.2	+2.7	+2.5	+3.0	+0.5	+ 2.0	-1.1	+ 2.6	-0.2	+1.5	-2.1	+1.7
	2	-2.7	-2.3	-3.4	-2.2	-2.7	-2.5	-3.0	-0.6	- 2.0	+1.1	- 2.6	+0.2	-1.5	+2.1	-1.7
	3	+0.4	+3.0	+0.8	+1.8	+0.4	+1.4	-0.6	+0.7	- 1.5	-2.8	+ 2.4	+0.4	-1.5	+0.5	+2.3
	4	-2.8	-5.6	-2.1	-4.8	-3.3	-3.4	-7.2	-1.5	- 2.8	-5.0	- 3.6	-0.7	-5.7	-0.3	-2.3
	5	+2.5	-0.1	+5.9	+3.8	+3.3	+3.3	+2.7	-1.0	+ 7.2	-0.2	+ 4.2	+1.5	+2.5	+0.6	+3.9
	6	-2.2	-0.2	-2.6	-0.7	-1.8	+0.2	-0.1	+3.0	+ 0.3	+0.6	+ 0.6	+6.3	-1.4	-0.2	+2.5
z	1	+2.6	+0.5	+3.5	-3.4	+3.4	-1.8	+3.8	-1.4	- 3.5	+2.7	- 0.8	-3.1	+0.2	+3.3	-1.1
	2	-2.4	-0.0	-3.5	+3.3	-3.4	+1.8	-3.8	+1.6	+ 3.5	-2.7	+ 0.8	+3.1	-0.2	-3.3	+1.1
	3	-1.2	-3.1	+0.0	-1.8	+0.1	+1.7	-1.5	-1.0	+ 2.8	-3.8	+ 0.1	-1.2	+0.0	-3.9	-0.1
	4	+0.1	+2.0	+1.3	-0.3	-0.0	-0.9	+2.6	+1.9	- 1.3	+3.8	- 0.9	-0.1	+0.9	+3.6	+0.1
	5	-2.1	+1.0	-0.9	+2.8	-3.3	+1.9	-2.3	+1.7	+ 1.6	+0.7	- 1.6	+1.8	+0.7	+1.7	-0.0
	6	+2.7	-0.7	+1.5	-2.2	+2.2	-0.1	+2.3	-2.4	- 2.2	-1.3	+ 0.3	-1.8	+0.1	-0.4	-0.6
r.m.s. differences of model-residuals against mean of strip																
σ_x		2.3	2.8	3.1	2.9	2.7	3.9	3.1	2.9	2.8	2.6	2.9	2.6	2.6	2.5	1.9
σ_y		3.3	3.0	4.5	5.1	3.3	4.1	3.8	2.8	4.1	2.8	3.7	2.8	2.9	3.3	3.2
σ_z		5.2	4.1	4.7	4.6	4.6	5.2	4.5	3.9	4.5	3.7	4.1	3.4	3.2	2.4	3.6

Table 2. OEEPE-Oberschwaben
Systematic model deformations after block adjustment by independent models.
Super-wide-angle strips: Control version 0; in units of μm

strip no.	1	2	3	4	5	6	7	8	9	10	11	12	13	14	15	
flight direction	NS	SN	NS	SN	NS	SN	NS	SN	NS	SN	NS	SN	NS	SN	NS	
flight mission	10.4.	10.4.	10.4.	10.4.	10.4.	10.4.	10.4.	10.4.	26.4.	26.4.	26.4.	26.4.	26.4.	26.4.	26.4.	
standard position																
x	1	+3.1	+1.4	+3.0	+ 3.5	+3.7	+2.9	+4.8	+ 4.3	+4.3	+1.8	+ 4.3	+2.8	+2.3	+1.2	+1.7
	2	-3.1	-1.4	-3.0	- 3.5	-3.7	-2.9	-4.8	- 4.3	-4.3	-1.8	- 4.3	-2.8	-2.3	-1.2	-1.7
	3	+6.3	-0.3	+8.5	+ 0.9	+6.9	+0.7	+5.9	+ 0.0	+8.7	-1.4	+ 8.8	-1.7	+8.2	-5.1	+5.1
	4	-4.9	+3.8	-5.3	+ 1.1	-4.4	+1.9	-4.3	+ 1.9	-4.0	+5.0	- 4.9	+4.8	-5.2	+4.8	-5.1
	5	-1.1	+7.1	-1.0	+ 5.8	-0.1	+5.6	+1.6	+ 8.0	+1.0	+6.0	- 2.8	+4.9	-3.9	+4.7	-2.4
	6	+1.1	-7.1	-0.9	-10.0	-2.5	-7.7	-3.0	-10.5	-2.6	-7.8	- 2.1	-8.0	-0.3	-8.3	+0.9
y	1	+1.0	+0.7	+3.0	+ 1.0	+2.0	+1.1	+0.7	+ 1.0	+1.9	+2.0	+ 4.5	+2.2	+1.8	+1.6	-0.0
	2	-1.0	-0.7	-3.0	- 1.0	-2.0	-1.1	-0.7	- 1.0	-1.9	-2.0	- 4.5	-2.2	-1.8	-1.6	+0.0
	3	-2.8	+1.9	-5.5	+ 1.4	-5.9	-1.1	-2.8	+ 0.5	-4.8	+2.9	- 3.4	+5.6	-2.2	+4.9	+0.7
	4	-2.0	-6.1	+1.2	- 7.6	-0.2	-4.5	-2.8	- 5.4	-0.8	-6.9	- 0.8	-8.6	-0.4	-4.8	-0.7
	5	+4.0	+0.4	+7.4	+ 4.2	+8.2	+5.0	+7.4	+ 2.7	+8.6	+4.1	+10.8	+0.4	+7.0	-0.2	+5.3
	6	-4.0	-0.4	-1.6	+ 0.6	-3.7	+0.9	+0.4	+ 2.8	-2.1	+0.6	- 3.7	+3.1	-2.6	+2.4	-2.8
z	1	+4.2	-4.3	+1.9	- 2.3	+2.2	-3.5	+3.5	- 2.9	+4.4	-3.8	+ 4.7	-3.0	+3.5	-1.9	+2.3
	2	-4.2	+4.3	-1.9	+ 2.3	-2.2	+3.5	-3.5	+ 2.9	-4.4	+3.8	- 4.7	+3.0	-3.5	+2.1	-2.3
	3	-1.5	+0.1	+0.9	- 1.2	+1.1	+1.5	-3.0	+ 0.6	-0.8	+1.6	- 1.0	+1.4	-1.3	+1.1	-2.2
	4	+1.4	+0.3	-0.1	+ 1.1	-0.5	-1.9	+2.4	- 0.1	+1.6	+0.2	- 0.3	-1.0	+0.5	-1.2	+2.2
	5	-0.8	+2.9	-0.8	+ 1.7	-0.4	+0.9	+0.8	+ 0.2	-0.2	+1.3	- 1.1	-0.7	+0.4	-0.5	+1.7
	6	+0.8	-2.8	+1.4	- 1.8	-0.1	-0.8	-0.8	+ 0.2	+0.8	-1.7	- 0.1	-0.4	+1.1	+0.6	-1.2
r.m.s. differences of model-residuals against mean of strip																
σ_x		2.8	3.3	4.0	3.6	3.8	3.9	3.8	3.2	3.4	3.9	3.8	3.6	3.7	3.3	3.5
σ_y		4.9	3.7	5.3	4.3	4.9	4.6	5.7	4.6	5.1	4.7	4.3	6.1	4.1	3.7	5.1
σ_z		3.6	3.5	3.9	3.2	4.5	3.3	3.9	3.2	4.4	3.3	4.0	4.6	3.1	3.2	3.0

Table 3. OEEPE-Oberschwaben

Systematic model deformations after block adjustment by independent models.

Dependence on flight direction and control version (in units of μm)

block	Frankfurt (w.a.)						Vienna (w.a.)		The Hague (s.w.a.)			Delft (s.w.a.)								
	0		1		5		0	0	0	1	5									
control version	0	0	1	1	5	5	0	0	0	1	5	0								
flight direction	NS	SN	NS	SN	NS	SN	NS	SN	NS	NS	NS	SN								
average of n strips	5		3		5		3		2		5		8		8		8		7	
x	standard position																			
	1	+1.9	+2.6	+1.6	+1.6	+0.1	-0.1	+1.5	+1.5	+3.4	+2.7	+0.2	+2.6							
	2	-1.9	-2.6	-1.6	-1.6	-0.1	+0.1	-1.5	-1.5	-3.4	-2.7	-0.2	-2.6							
	3	-0.7	+9.8	-1.2	+8.5	-3.9	+5.6	-4.8	+6.1	+7.3	+6.3	+3.0	-0.9							
	4	+4.0	-6.8	+4.0	-6.0	+3.9	-5.2	+4.6	-4.3	-4.8	-4.3	-2.8	+3.3							
	5	+5.0	-4.3	+4.9	-5.0	+4.3	-5.1	+8.3	-3.3	-1.2	-1.7	-2.9	+6.0							
6	-7.9	+1.2	-7.1	+2.3	-4.4	+4.8	-7.7	+1.7	-1.2	-0.1	+2.6	-8.5								
y	1	+2.6	+2.1	+2.2	+1.8	+0.3	+0.1	-1.6	+1.4	+1.8	+1.3	+0.0	+1.4							
	2	-2.6	-2.1	-2.1	-1.8	-0.3	-0.1	+1.6	-1.5	-1.8	-1.3	-0.0	-1.4							
	3	-0.1	+1.0	+0.4	+1.0	-0.3	+0.2	-1.2	+1.4	-3.4	-3.1	-2.6	+2.2							
	4	-4.2	-2.9	-2.8	-2.6	+0.3	-0.3	-2.7	-3.0	-0.8	+0.1	+2.7	-6.3							
	5	+3.4	+5.1	+2.9	+2.9	+0.4	-0.1	+0.2	+1.6	+7.4	+6.1	+3.2	+2.4							
	6	-1.6	+1.1	-1.1	-0.2	-0.3	+0.2	+0.2	+1.8	-2.5	-2.5	-2.9	+1.4							
z	1	+2.7	-1.8	+2.7	-1.7	+2.8	-1.8	+3.0	-1.9	+3.4	+3.5	+3.4	-3.1							
	2	-2.7	+1.8	-2.7	+1.7	-2.7	+1.8	-3.0	+1.9	-3.4	-3.5	-3.4	+3.1							
	3	-0.5	+1.0	-0.4	+0.7	-0.3	+0.6	-3.8	-1.0	-1.0	-0.9	-0.9	+0.7							
	4	+1.0	-0.7	+0.9	-0.7	+0.8	-0.6	+3.7	+0.5	+0.8	+0.8	+0.8	-0.3							
	5	-1.6	+0.1	-1.7	+0.4	-1.8	+0.5	+1.2	+1.8	-0.1	-0.2	-0.3	+0.8							
	6	+1.8	-0.8	+1.7	-0.8	+1.6	-0.9	-0.9	-1.4	+0.2	+0.2	+0.3	-1.0							

Table 4. OEEPE-Oberschwaben

Systematic errors of perspective centres after block adjustment by independent models.

Wide-angle-strips: Control version 0, in units of μm

strip no.	1	2	3	4	5	6	7	8	9	10	11	12	13	14	15
flight direction	NS	SN	NS	SN	NS	SN	NS	SN	SN	NS	SN	SN	NS	NS	SN
flight mission	8.4.	8.4.	8.4.	8.4.	8.4.	8.4.	9.4.	12.5.	9.4.	12.5.	12.5.	12.5.	12.5.	12.5.	12.5.
x	+7.7	+2.0	+2.1	+1.1	+7.6	+6.3	+6.2	+3.9	+4.3	+0.7	+4.6	+2.8	+5.1	+3.5	+5.0
y	-6.4	-2.0	-2.7	-1.9	-5.4	-2.2	-5.8	-1.6	-3.5	-0.3	-1.5	-0.3	-3.8	+0.9	-3.0
z	+1.5	-4.2	+2.7	-3.0	+0.8	-1.3	-0.1	-2.5	+0.1	+0.7	-2.1	-4.1	-0.3	+0.9	-2.4

Super-wide-angle strips: Control version 0; in units of μm

strip no.	1	2	3	4	5	6	7	8	9	10	11	12	13	14	15
flight direction	NS	SN	NS	SN	NS	SN	NS	SN	NS	SN	NS	SN	NS	SN	NS
flight mission	10.4.	10.4.	10.4.	10.4.	10.4.	10.4.	10.4.	10.4.	26.4.	26.4.	26.4.	26.4.	26.4.	26.4.	26.4.
x	+0.4	+0.7	-1.5	+1.3	+1.8	+3.5	-0.0	-1.7	-0.7	-0.2	-0.3	+1.8	+2.6	+3.3	+3.0
y	+0.7	-1.1	-0.8	-1.6	-2.2	-2.0	+0.7	-3.9	-1.2	-3.7	+0.1	-1.2	-0.7	-2.4	+1.7
z	+3.0	-3.2	+4.5	-3.0	+4.7	-0.6	+2.8	-2.4	+3.6	-3.1	+5.8	-4.5	+4.0	-3.3	+1.8

Dependence on flight direction and control version (in units of μm)

block	Frankfurt (w.a.)						Vienna (w.a.)		The Hague (s.w.a.)			Delft (s.w.a.)								
	0		1		5		0	0	0	1	5									
control version	0	0	1	1	5	5	0	0	0	1	5	0								
flight direction	NS	SN	NS	SN	NS	SN	NS	SN	NS	NS	NS	SN								
average of n strips	5		3		5		3		2		5		8		8		8		7	
x	+5.8	+4.6	+5.9	+5.0	+6.5	+5.9	+2.1	+3.2	+0.7	+1.4	+3.8	+1.3								
y	-4.8	-2.7	-4.2	-2.8	-2.4	-1.3	+0.3	-1.6	-0.2	+0.3	+1.6	-2.3								
z	+0.9	-1.4	+0.9	-1.6	+1.1	-1.8	+0.8	-3.0	+3.8	+3.6	+3.6	-2.9								

Figure 2: OEEPE Oberschwaben - Systematic model deformations after block adjustment by independent models
Dependence on flight direction
Planimetry: CP-version 0; 1 mm $\hat{=}$ 1 μ m

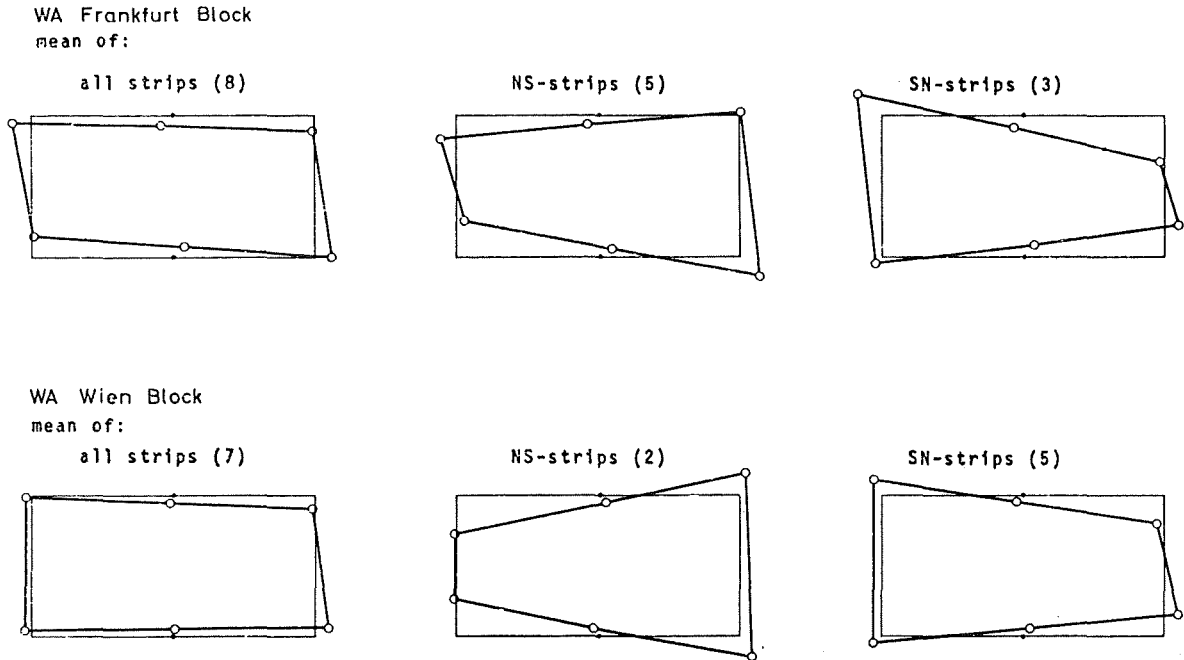


Figure 3: OEEPE Oberschwaben - Systematic model deformations after block adjustment by independent models
Comparison of wide-angle and super-wide-angle
Planimetry: CP-version 0; 1 mm $\hat{=}$ 1 μ m

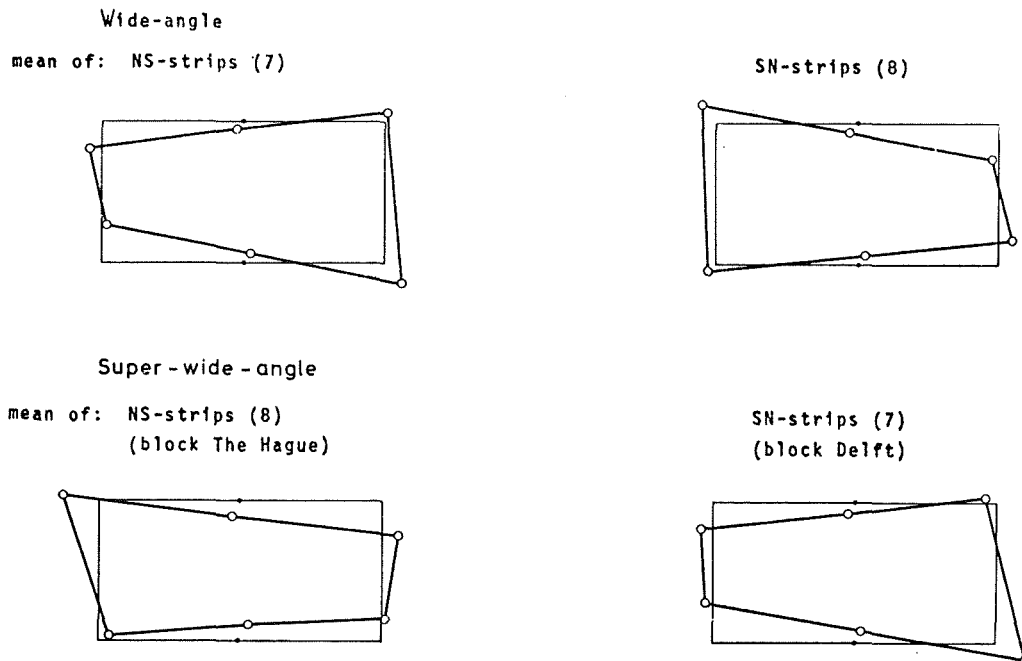
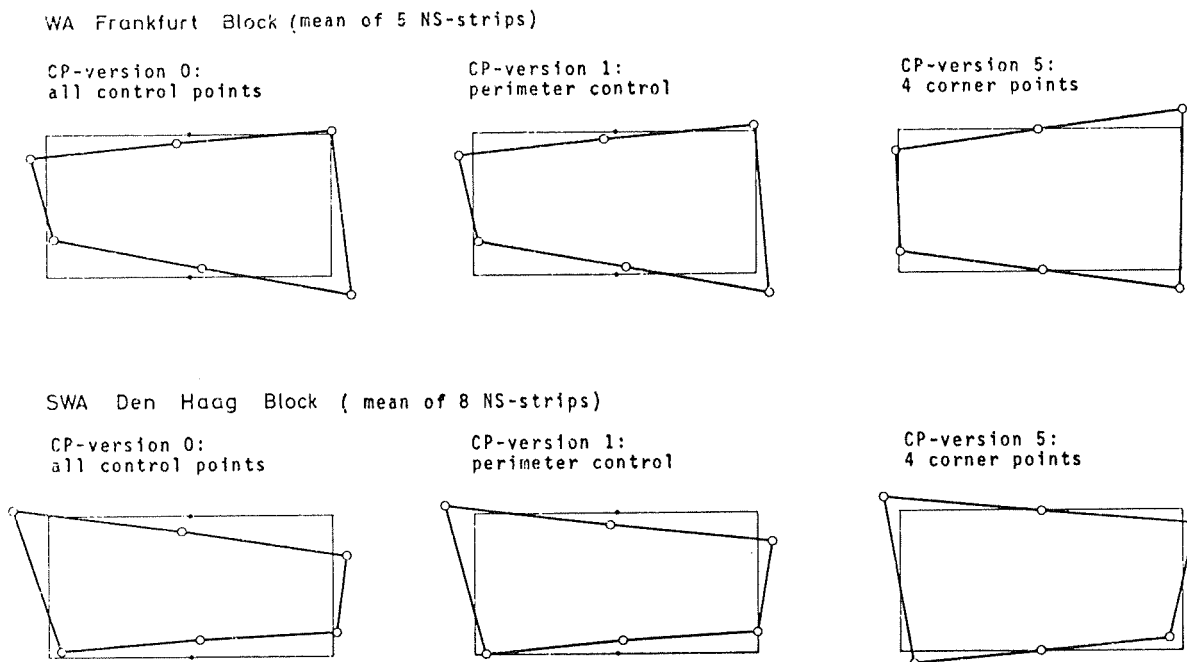


Figure 4 : OEEPE Oberschwaben - Systematic model deformations after block adjustment by independent models

Dependence on control versions:

Planimetry 1 mm $\hat{=}$ 1 μ m



5. DISCUSSION OF THE RESULTS

5.1 Magnitude and type of systematic model deformations

The results show clearly the presence of systematic errors, of considerable magnitude, at model points and perspective centres.

The maximum planimetric errors occur at model corners, the central points (1,2) being less affected. When judging the strips separately the maximum systematic coordinate errors are: Wide-angle 11.4 μ m in x, 7.2 μ m in y; super-wide-angle 10.5 μ m in x, 10.8 μ m in y. The respective maximum values at the central points 1 and 2 are only: w.a. 3.3 μ m and 3.4 μ m, s.w.a. 4.8 μ m and 4.5 μ m.

The average systematic errors of the separate strips are only slightly larger than the average systematic errors of groups of strips of common flight direction. Thus the systematic errors are, to a most remarkable degree, constant.

The root mean square values m_s of the planimetric systematic errors of the standard points are presented in table 5. They represent noticeable percentages of the values of σ_0 of the block adjustments.

Table 5: Comparison of standard errors of unit weight (σ_0) and r.m.s. values m_s of systematic errors; planimetry, control version 0.

block	Frankfurt w.a.	Vienna w.a.	The Hague s.w.a.	Delft s.w.a.
σ_0	20.3 cm 7.2 μ m	19.2 cm 6.9 μ m	25.1 cm 9.0 μ m	24.6 cm 8.8 μ m
m_s	11.1 cm 4.0 μ m	9.7 cm 3.5 μ m	10.9 cm 3.9 μ m	11.1 cm 4.0 μ m

The systematic vertical model deformations are, altogether, considerably smaller than the planimetric deformations. The maximum errors, occurring often at the central points 1 and 2, amount to 3.9 μ m and 4.7 μ m for wide-angle and super-wide-angle, respectively. The vertical errors at model corners are unexpectedly small.

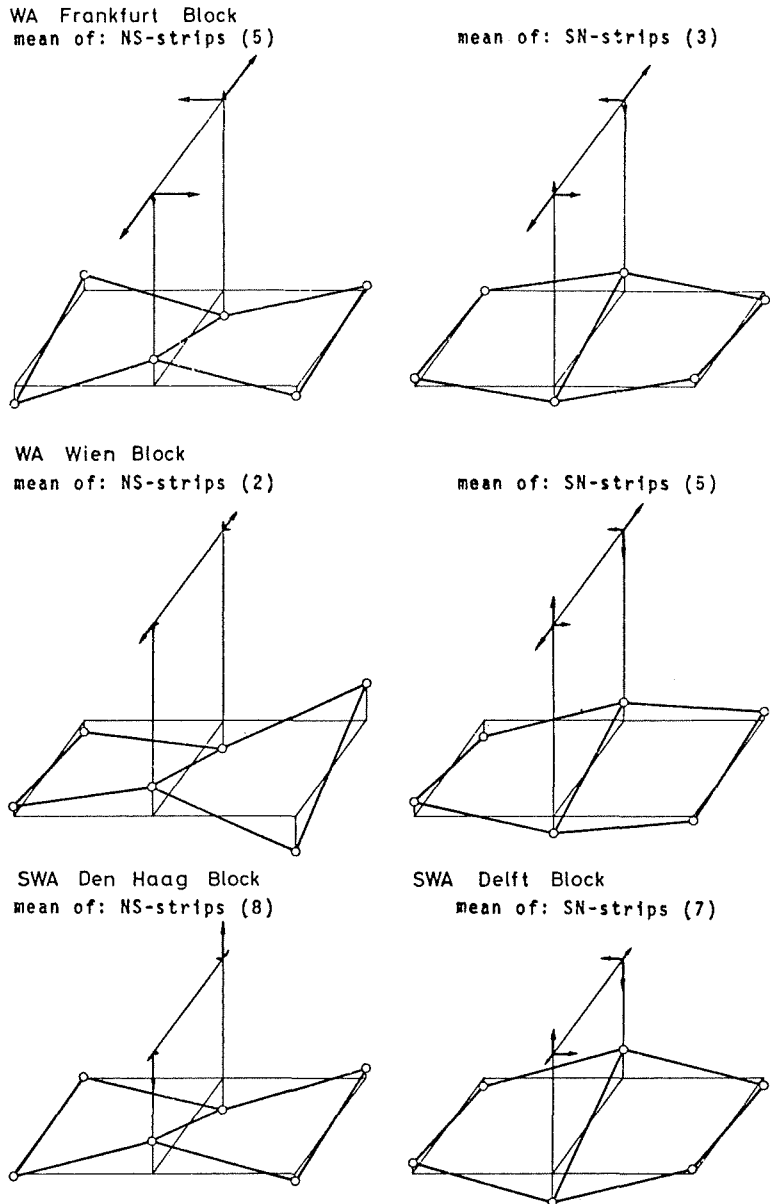
Figure 5:

OEEPE Oberschwaben - Systematic vertical model deformations and systematic errors of perspective centres

CP-version 0; 1 mm $\hat{=}$ 1 μ m

The systematic errors at the perspective centres are collected in table 4 and presented graphically in fig. 5. The values refer always to p.c. No. 1, the values of p.c. No. 2 being of exactly equal magnitude and opposite sign. In general, the planimetric errors at the perspective centres are smaller than of the model points, whilst the magnitude of vertical errors of the perspective centres compares with the vertical model deformations. The maximum systematic errors per strip, of the perspective centres amount in x, y, z, respectively, to 7.7 μ m, 6.4 μ m, 4.2 μ m (w.a.) and 3.5 μ m, 3.9 μ m, 5.8 μ m (s.w.a.), for control version 0.

Apart from the magnitude also the types of model deformations are of special interest. They are common for both w.a. and s.w.a. models as displayed in fig. 2 - 5.



The planimetric model deformations are trapeziform. Characteristic features are: Considerable scale difference between the short sides of the models; points 3-1-5 and 4-2-6, respectively, form straight lines; errors of points 1 and 2 have equal magnitude, reversed sign.

The typical features of vertical model deformations are: Little or no warping of the models; maximum height errors, of opposite sign, at central points 1 and 2 (arching and sagging).

It is only at the perspective centres that w.a. and s.w.a. behave somewhat different. In the first case (w.a.) symmetrical enlargement of the base and azimuthal rotation is predominant, in the second case (s.w.a.) the base is mainly tilted.

5.2 Dependencies of systematic model errors

With regard to possible corrections of systematic model deformations it is most important to investigate how constant they are and on what parameters they depend.

Flight direction, camera: The tables and graphs show clearly that the model deformations, as referred to the state coordinate system, depend in first instance on the flight direction. This is true for w.a. and s.w.a., see figures 2 and 3. After rotation by 180° the planimetric model deformations of the NS-strips match very well with those of the SN-strips. The dependence on flight direction is equally confirmed by table 3 and fig. 5 for vertical model deformations. It also holds for the perspective centres.

Fig. 2 shows that by taking the mean deformation of all models, without taking the flight direction into account, an entirely misleading type of model deformation would result. Only an affine deformation would be the result, the trapeziform deformation, related to the flight direction, being eliminated.

The important conclusion is, that the main systematic model deformations originate from the camera (all exposures were taken from the same airplane - Aero Commander 560 F; all strips were triangulated by stereocomparator in direction north-south; it is not known, how many film magazines were used during the flight missions). This is confirmed by the different planimetric model deformations of w.a. and s.w.a., although being of the same type. (The vertical deformations are, however, very similar in both cases, except for the perspective centres). It is also confirmed by the remarkable constancy of the deformations within each group, independent of the date of the flight missions which has no traceable effect.

The overall r.m.s. deviations of the individual residual errors of the models against the average systematic errors are for wide-angle $2.9 \mu\text{m}$ in x and $3.8 \mu\text{m}$ in y, for super-wide-angle $3.8 \mu\text{m}$ in x and $4.9 \mu\text{m}$ in y.

It is evident, therefore, that any method of correction of systematic errors by additional parameters, see [3], [5], has to consider the flight direction of strips. A different set of parameters per strip might be advisable.

Control version: According to table 3 and fig. 4, there is some influence of the Control version of the block adjustment on the apparent systematic model deformations. The effect is noticeable in planimetry only. The type of the effect is most interesting. With poor planimetric ground control the trapeziform type of planimetric model deformation is correctly indicated, with, however, additional affine deformation (scale and shear) superimposed. The additional affine deformation is rather small, however. The systematic planimetric model deformations differ with perimeter control (version 1) by less than $2 \mu\text{m}$, with 4 control points only (version 5) by less than $5 \mu\text{m}$ against the "true" model deformations as determined with all available control points (version 0). This effect is independent of camera or other flight parameters.

Restitution centre: There is a small systematic effect related to the 4 different centres of restitution, traceable again in planimetry only. The average planimetric model deformations, after duly considering the flight directions, differ for w.a. between block Frankfurt (PSK) and block Vienna (StK1) by $2.0 \mu\text{m}$, for s.w.a. between block The Hague (PSK) and block Delft (StK1) by $2.4 \mu\text{m}$. The respective maximum average differences are $4.2 \mu\text{m}$ and $2.2 \mu\text{m}$. Such systematic differences can be explained by the different sets of diapositives and systematic errors of the stereocomparators used.

6. SUMMARY AND CLOSING REMARKS

This paper presents the results of an empirical investigation into the systematic model deformations of the OEEPE test block Oberschwaben, as they are apparent from residual errors at tie-points and perspective centres after block adjustment by independent models. The results are most interesting with regard to magnitude and type of the model deformations and their relation to flight parameters:

- The magnitude of the systematic coordinate errors is considerable. In planimetry the deformations are trapeziform. The mean values range between $3.5 \mu\text{m}$ and $4.0 \mu\text{m}$, which amounts to a considerable percentage of the σ_0 values of the block adjustments (without correction of systematic errors), between $6.9 \mu\text{m}$ and $9.0 \mu\text{m}$. The vertical model deformations are rather small but also typical, with maximum values of opposite sign at the central points 1 and 2 of the models.
- The model deformations, as referred to the state coordinate system, are predominantly related to the flight directions. Thus, the main cause of the deformation is clearly the camera. Small systematic effects in planimetry have been found to be related to the density of ground control used for the adjustment and to the centre (instrument) of restitution. Other flight parameters have had no traceable influence on the model deformations.

The systematic model deformations have turned out, for a given camera, to be constant to a remarkable degree. Therefore it can be expected that suitable procedures for correcting the systematic errors during block adjustment will be highly effective and will extraordinarily increase the resultant accuracy of the adjusted block, possibly by a factor 2 or 3. It will be essential, however, to consider the flight direction when introducing additional parameters in a refined mathematical model.

REFERENCES

- |1| Kubik K.: "Systematic image errors in aerial triangulation", invited paper of Commission III, ISP-Congress Ottawa, 1972
- |2| Masson d'Autume G.: "Le Traitement des Erreurs Systématiques dans l'Aérotiangulation", presented paper of Commission III, ISP-Congress Ottawa, 1972
- |3| Bauer H.: "Compensation of systematic errors by analytical block adjustment with common image deformations parameters", OEEPE Official Publication No 8, 1973, p.319 - 334
- |4| Kraus K.: "Untersuchung zur Genauigkeit der Interpolation nach kleinsten Quadraten", Zeitschrift für Vermessungswesen 99, 1974, p. 198 - 205
- |5| Ebner H. and Schneider W.: "Simultaneous compensation of systematic errors with block adjustment by independent models", presented to the Symposium of Commission III/ISP, Stuttgart 1974
- |6| Ackermann F.: "Testblock Oberschwaben, Programm I. Results of block adjustment by independent models", OEEPE Official Publication No 8, 1973, p. 87 - 150

ON POLYNOMIAL METHODS FOR STRIP ADJUSTMENT

by Peter Waldhäusl, Vienna

INTRODUCTORY REMARKS

In 1972 ISP Commission III has recommended to continue with more research on the influence of systematic errors in aerial triangulation (AT). The author is well aware of the fact that strip adjustment is of minor importance for the future. But obviously many aersurvey organisations still operate with polynomial methods for strip- and strip-block-adjustment [1]. It was the idea to do retrospectively some thorough research on systematic errors based on the mathematical model of the polynomial formulae for strip adjustment. This paper is an extract from a much longer study published recently [2]. There, please, the complete list of references and more as well as more detailed formulae may be found. The practical sample 5.2 is published first in this paper.

FROM THE ROTATION MATRIX TO THE ADJUSTMENT POLYNOMIALS

Since the polynomial formulae for AT adjustment are based on the approximate rotation matrix the basic functional model of the polynomials is the very reason for some systematic "numerical deformations" of the strip coordinates. They are of measurable size (5µm, 10µm) as soon as the rotations to be corrected locally are bigger than maximum tolerances (40°, 60°). The numerical deformations are defined as the differences between the local transformations with the strict and the approximate formula for the orthogonal rotation matrix. The maximum tolerances for the absolute orientation of any part of a strip must therefore be smaller than the above given values.

Further systematic negligences follow from the polynomials used. Let us begin with the formulae for the approximate absolute orientation:

$$\begin{aligned} X - x &= x \, d m_x + \Delta x_0 - y \, d \quad + z \, d \\ Y - y &= x \, d \alpha + \Delta y_0 + y \, d m_y - z \, d \omega \\ Z - z &= x \, d \varphi + \Delta z_0 + y \, d \omega + z \, d m_z \end{aligned} \tag{1}$$

Six of the nine unknown coefficients are substituted by five "basic-polynomials":

$$\begin{aligned} d m_x &\dots\dots\dots \text{by} \dots\dots\dots \text{Pol}_x(x) \\ d m_y \text{ and } d m_z &\dots\dots \text{by} \dots\dots\dots \text{Pol}_y(x) \quad +) \\ d \varphi &\dots\dots\dots \text{by} \dots\dots\dots \text{Pol}_\varphi(x) \\ d \omega &\dots\dots\dots \text{by} \dots\dots\dots \text{Pol}_\omega(x) \\ d \alpha &\dots\dots\dots \text{by} \dots\dots\dots \text{Pol}_\alpha(x) \end{aligned} \tag{2}$$

The well known effect of the summation of all errors proportional x needs their integration. Thus (1) leads to the basic formulae for the most of the polynomial strip adjustment formulae used so far:

$$\begin{aligned} X - x &= \int_{x=x_0}^x \text{Pol}_x(x) dx + \Delta x_0 - y \text{Pol}_\alpha(x) + z \text{Pol}_\varphi(x) \\ Y - y &= \int_{x=x_0}^x \text{Pol}_\alpha(x) dx + \Delta y_0 + y \text{Pol}_y(x) - z \text{Pol}_\omega(x) \\ Z - z &= \int_{x=x_0}^x \text{Pol}_\varphi(x) dx + \Delta z_0 + y \text{Pol}_\omega(x) + z \text{Pol}_y(x) \end{aligned} \tag{3}$$

+) z-scale cannot be defined by ground control, normally

SELECTION OF BASIC POLYNOMIALS AND CLASSIFICATION OF STRIP ADJUSTMENT METHODS

The basic polynomials $Pol_i(x), i = x, y, \phi, \omega, \kappa$, normally are a selection out of the family $\pi(2)$, i.e. polynomials up to the second degree.

$$\begin{aligned} Pol_{(0)}(x) &= a \\ Pol_{(1)}(x) &= a + bx \\ Pol_{(2)}(x) &= a + bx + cx^2 \end{aligned} \tag{4}$$

The case $Pol_{(0)}(x)$ is trivial, because it leads back to formulae (1). The selection of polynomials out of (4) allows a simple classification of the most of the strip adjustment methods with polynomials. We just take the degree-numbers of the five basic polynomials following the same sequence as of i above.

We thus get a five digit type number. Two digits are set one above the other where independent basic polynomials are used for the two coordinates (sequence x, y, z , e.g. x (top), z (bottom), in the case of ϕ). Type digits in brackets indicate uncomplete polynomials (e.g. (2) for: $a + cx^2$). Whenever "flat terrain" has been assumed this will be indicated by "z = 0". Here we often find another typical source for systematic strip deformations by the polynomial adjustment methods. The negligences due to this assumption "z = 0" become greater very soon than 10 μ m in photo-scale: Let us allow for rotations locally somewhere along the strip up to 60c, then the above limit of 10 μ m is reached as soon as the height differences are greater than M in meters, where M is equal to one thousands of the photo-scale. And that is not very much.

Table (5) shows now a comparison of nine of the polynomial "methods" for strip adjustment. It is up to the reader to compare more of them. In (5) the coefficients are shown in a slightly changed order.

BASIC SPLINE FUNCTIONS INSTEAD OF BASIC POLYNOMIALS

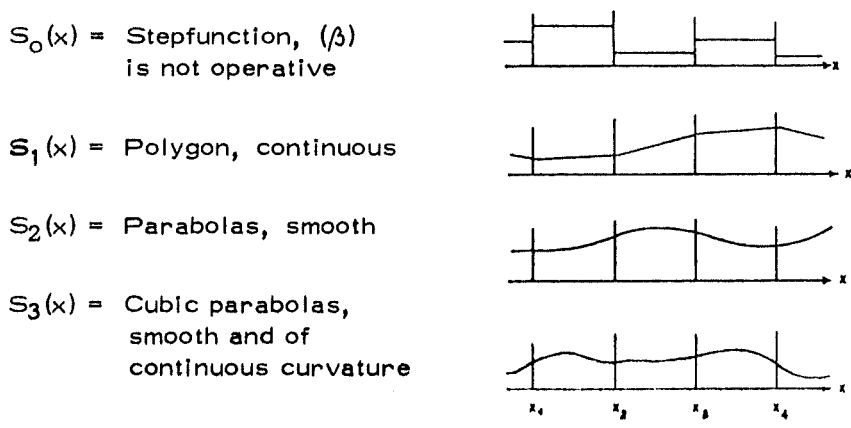
In order to increase the known limited flexibility of the functional model of polynomial strip adjustment formulae (3) spline functions can be introduced instead of the normal basic polynomials (4), see |2| and also |3| and |4|. Spline functions are not yet known too much in photogrammetry. Therefore a number of definitions shall follow.

1. DEFINITION OF SPLINE-FUNCTIONS

Given an increasing sequence of real numbers $(x_i), i = 1(1)n, x_i < x_{i+1}$.

- (α) A spline function $S_m(x)$ of degree m with the knots $x_i, i = 1(1)n$, is a function defined in each interval $(x_i, x_{i+1}), i = 0(1)n, x_0 := -\infty, x_{n+1} := +\infty$, by some polynomial of degree $\leq m$.
- (β) $S_m(x)$ and its derivations $S_m^{(j)}(x), j = 1(1)m-1$, are continuous (at least piecewise) everywhere.

Examples :



$$\Delta x = \Delta x_0 + (\text{Scale}) + (\alpha) + (\varphi)$$

$$\Delta y = \Delta y_0 + (\alpha) + (\text{Scale}) + (\omega)$$

$$\Delta z = \Delta z_0 + (\varphi) + (\omega) + (\text{Scale})$$

Method	1	x	$\frac{x^2}{2}$	$\frac{x^3}{3}$	y	xy	x^2y	z	xz	x^2z	Type
Vienna 1 (Long strips)	$\Delta x = \Delta x_0$	a_x	b_x	c_x	$-a_x$	$-b_x$	$-c_x$	a_φ	b_φ	c_φ	2 2 2 2 2
	$\Delta y = \Delta y_0$	a_x	b_x	c_x	a_y	b_y	c_y	$-a_\omega$	$-b_\omega$	$-c_\omega$	
	$\Delta z = \Delta z_0$	$-a_\varphi$	$-b_\varphi$	$-c_\varphi$	a_ω	b_ω	c_ω	a_y	b_y	c_y	
Vienna 1 (Short strips)	$\Delta x = \Delta x_0$	a_x	b_x	.	$-a_x$	$-b_x$.	a_φ	b_φ	.	1 2 1 2 1
	$\Delta y = \Delta y_0$	a_x	b_x	.	a_y	b_y	c_y	$-a_\omega$	$-b_\omega$	$-c_\omega$	
	$\Delta z = \Delta z_0$	$-a_\varphi$	$-b_\varphi$.	a_ω	b_ω	c_ω	a_y	b_y	c_y	
Vienna 2 (α independent)	$\Delta x = \Delta x_0$	a_x	b_x	.	$-a_{xx}$	$-b_{xx}$.	a_φ	b_φ	.	1 2 1 2 1
	$\Delta y = \Delta y_0$	a_x	b_x	.	a_y	b_y	c_y	$-a_\omega$	$-b_\omega$	$-c_\omega$	
	$\Delta z = \Delta z_0$	$-a_\varphi$	$-b_\varphi$.	a_ω	b_ω	c_ω	a_y	b_y	c_y	
v. d. Weele	$\Delta x = \Delta x_0$	a_m	b_m	c_m	$-a_x$	$-b_x$	$-c_x$.	.	.	2=2 2 1 2
	$\Delta y = \Delta y_0$	a_x	b_x	c_x	a_m	b_m	c_m	.	.	.	$z = 0$
	$\Delta z = \Delta z_0$	$-a_\varphi$	$-b_\varphi$	$-c_\varphi$	a_ω	b_ω	
Schwidefsky	$\Delta x = \Delta x_0$	a_x	b_x	1 1 1 1(1)
	$\Delta y = \Delta y_0$.	b_x	.	a_y	b_y	$z = 0$
	$\Delta z = \Delta z_0$	$-a_\varphi$	$-b_\varphi$.	a_ω	b_ω	
OEEPE / AB Gramastetten	$\Delta x = \Delta x_0$	a_x	b_x	.	$-a_{xx}$	$-b_{xx}$	1 1 1 1 1
	$\Delta y = \Delta y_0$	a_{xy}	b_{xy}	.	a_y	b_y	$z = 0$
	$\Delta z = \Delta z_0$	$-a_\varphi$	$-b_\varphi$.	a_ω	b_ω	
Zarzycki	$\Delta x = \Delta x_0$	a_x	b_x	.	$-a_{xx}$	$-b_{xx}$	$-c_{xx}$.	.	.	1 2 1 2 2
	$\Delta y = \Delta y_0$	a_{xy}	b_{xy}	.	a_y	b_y	c_y	.	.	.	$z = 0$
	$\Delta z = \Delta z_0$	$-a_\varphi$	$-b_\varphi$.	a_ω	b_ω	c_ω	.	.	.	
Neumaier (Formula 20)	$\Delta x = \Delta x_0$	a_m	b_m	.	$-a_x$	$-b_x$.	a_φ	b_φ	.	1=1 1 1 1
	$\Delta y = \Delta y_0$	a_x	b_x	.	a_m	b_m	.	$-a_\omega$	$-b_\omega$.	
	$\Delta z = \Delta z_0$	$-a_\varphi$	$-b_\varphi$.	a_ω	b_ω	.	a_m	b_m	.	
Maršik	$\Delta x = \Delta x_0$	a_x	b_x	.	.	$-b_{xx}$	1 1 1 1(1)
	$\Delta y = \Delta y_0$.	b_{xy}	.	a_y	b_y	$z = 0$
	$\Delta z = \Delta z_0$	$-a_\varphi$	$-b_\varphi$.	a_ω	b_ω	

Table (5): Comparison and classification of nine different polynomial strip adjustment formulae. References are given in [2] .

2. NATURAL SPLINE FUNCTIONS

A natural spline function has a finite number of knots $x_i, i=1(1)n$, in the interval (x_1, x_n) . In the interior of said interval the degree of the polynomials is odd, $\leq (2k-1)$, in both the end intervals $(-\infty, x_1)$ and $(x_n, +\infty)$ the degree is reduced to $\leq (k-1)$.

Example : $k = 2$

$$m_i = 2k - 1 = 3 \quad (i = \text{'interior'})$$

$$m_e = k - 1 = 1 \quad (3 = \text{'exterior' or 'end'})$$

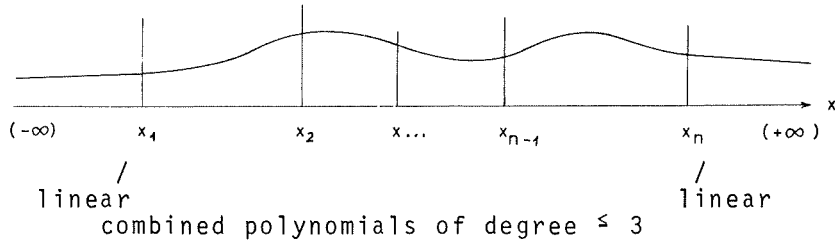


Fig. 6: Graph of a natural spline function $k = 2$.

The natural spline functions $\mathcal{N}_m(x_1, x_2, \dots, x_n)$ are known to be the smoothest interpolation from all possible functions

$f \in C^{k-1}[a, b]$ with at least piecewise continuous $f^{(k)}$, due to the definition

$$\delta(f) := \int_a^b |f^{(k)}(x)|^2 dx \rightarrow \min. \text{ with } n > k \geq 1.$$

It is of interest for us to know that this special class of smoothest interpolation functions is to be found among the spline functions.

3. SPLINE FUNCTIONS REPRESENTED BY TRUNCATED POWER FUNCTIONS

Each spline function $S_m(x) \in \delta_m(x_1, x_2, \dots, x_n)$, i.e. the family of all possible spline functions of degree m with the knots $x_j, j=1(1)n$, can be represented uniquely by truncated power functions.

$$S_m(x) = p(x) + \sum_{j=1}^n c_j (x-x_j)_+^m \quad \text{with } p(x) \in \pi_m \quad (7)$$

where π_m is the family of all polynomials of degree $\leq m$. The "+" simply indicates that

$$(x-x_j)_+^m = \begin{cases} (x-x_j)^m & \text{if } (x-x_j) > 0 \\ 0 & \text{if } (x-x_j) \leq 0 \end{cases} \quad (8)$$

Example:

$$y = c(x-x_1)_+^2$$

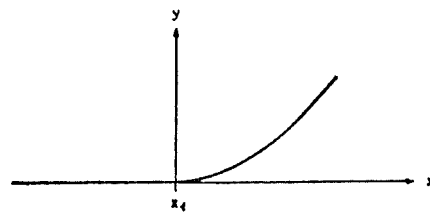


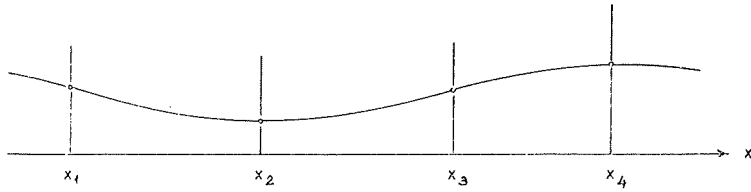
Fig. 9: Example of a truncated power function

4. INTERPOLATION, APPROXIMATION AND ADJUSTMENT OF STRIPS

Interpolation : $S(x)$ passes through the knots. The number of degrees of freedom of $S(x)$ equals the number of reference points (= pass points). We distinguish:

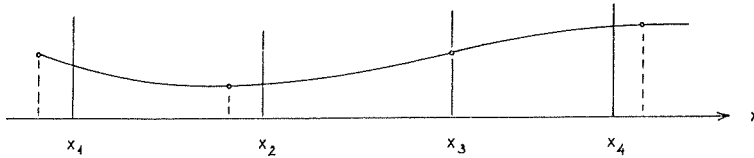
- (α) interpolation at the knots
- and
- (β) interpolation with reference points only near the knots.

(α)



$$\begin{aligned} x_V &= x_\phi & v &= 1(1)n & \text{knots} \\ n &= r & \phi &= 1(1)r & \text{reference points} \end{aligned}$$

(β)



$$\begin{aligned} x_V &\sim x_\phi & v &= 1(1)n \\ n &= r & \phi &= 1(1)r \\ x_\phi &< x_V < x_{\phi+m-1} & m &= \text{degree of } S_m(x) \end{aligned}$$

Fig.10: Interpolating spline-functions, for (α) and (β), see text.

Approximation: The number of degrees of freedom of $S_m(x)$ is reduced by only one condition ("smoothness-condition"):

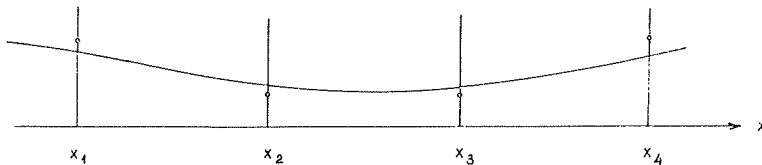
$$\bar{E}(u) = g_1 \sum_{i=1}^r p_i (X_m(x_i) - y_i)^2 + g_2 \int_a^b (S_m''(x))^2 dx \rightarrow \min. \quad (11)$$

where $\bar{E}(u)$ is the Euclidian norm of the vector of unknowns, and g_1, p_i and g_2 are variable weight numbers, $a \leq x_1$ and $b \geq x_n$ define the interval of interest $[a, b]$.

We again distinguish between

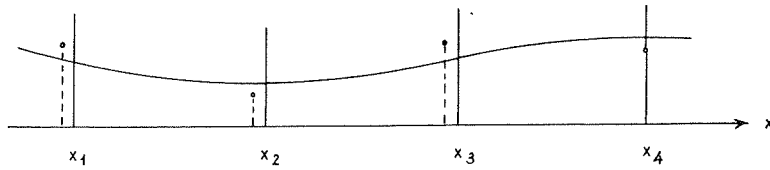
- (α) approximation at the knots
- and (β) approximation with references near the knots.

(α)



$$\begin{aligned} x_V &= x_\phi & v &= 1(1)n & \text{knots} \\ n &= r & \phi &= 1(1)r & \text{reference points} \end{aligned}$$

(β)



$$\begin{aligned}
 x_v &\sim x_\phi & v &= 1(1)n & \text{knots} \\
 n &= r & \phi &= 1(1)r & \text{reference points} \\
 x_\phi &< x_v < x_{\phi+m-1}
 \end{aligned}$$

Fig.12: Approximating spline functions, for (α) and (β), see text.

Adjustment: may be defined as the general case, where more reference points are given than knots and where - in general - a smoothness condition exists. g_2/g_1 in (11) may be 0. The reference points are situated also far away from the knots.

5. KUBIK'S PIECEWISE POLYNOMIALS

K. Kubik [4] introduced linear, quadratic and cubic parabolas for each interval (x_i, x_{i+1}) , $i = 1(1)n-1$. The formulae follow the presentation of Ahlberg [5] which represent a Hermite-interpolation between the knots. The parameters are the function values y_i , the first derivations y'_i and/or the curvatures $y''_{i,i+1}$. Comparable formulations are presented in [2], where Kubik's spline-version has been prepared for combination with formula (3). For exemplification the truncated power functions are easier to handle.

6. STRIP ADJUSTMENT WITH BASIC SPLINE FUNCTIONS

After introduction of basic spline functions formulae (3) read as follows.

$$\begin{aligned}
 X - x &= \int_{x=x_0}^x S_x(x) dx + \Delta x_0 - y S_{\mathcal{K}}(x) + z S_\varphi(x) \\
 Y - y &= \int_{x=x_0}^x S_{\mathcal{K}}(x) dx + \Delta y_0 + y S_y(x) - z S_\omega(x) \\
 Z - z &= - \int_{x=x_0}^x S_\varphi(x) dx + \Delta z_0 + y S_\omega(x) + z S_y(x)
 \end{aligned} \tag{13}$$

With the increasing number of knots x_i also the minimum number of ground control increases. The distribution and the number of pass-points shall not be evaluated by the number of unknown coefficients in the equations (3) or (13) only. Care should be taken that for the five different basic spline functions each the necessary information are functionally, geometrically well defined: the scales in x and y direction, the $tg_{\mathcal{K}}$, tg_φ and tg_ω . Due to the 3 integrations the relevant numbers of control are increased by one. The total number of equations required is always greater than the number of unknown coefficients. This results from the practical fact that nobody will measure x-pass-points, but only height-, plane- or full control, that not coordinates are required but scales and rotations.

Finally the minimum ground control distribution shall be shown for strip adjustment formulae (13) of the type S 22222, where all basic spline functions are of the order $m = 2$. σ_{max} shall not get greater than $2 \sigma_0$. Following [5], where Ackermann shows that

in models

$$\begin{aligned}
 \sigma_{max} &\approx 0,12 \sqrt{m^3} \sigma_0, \text{ we gain the maximum bridging distance} \\
 m &= 4,1 \sqrt[3]{\left(\frac{\sigma_{max}}{\sigma_0}\right)^2}
 \end{aligned} \tag{14}$$

Waldhäusl 6

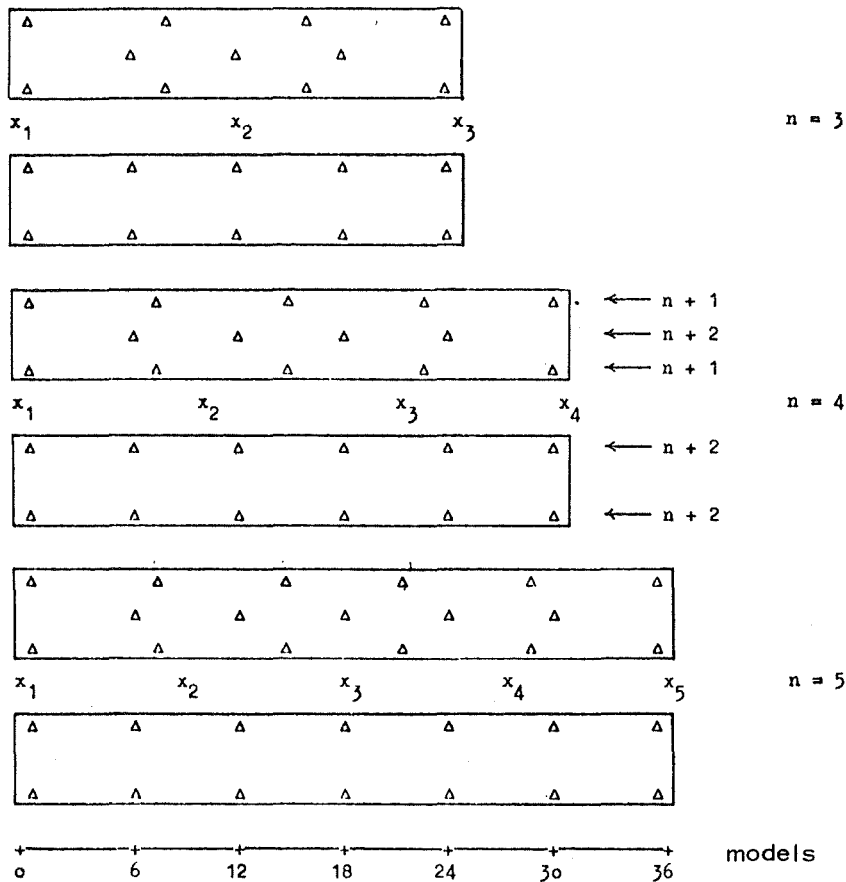


Fig.15: Minimum ground control for strip adjustment with type S 22222 with n knots x_v , $v = 1(1)n$, $x_v < x_{v+1}$. $\sigma_{max} = 2 \sigma_0$ for strip lengths of 24 to 36 models. Δ = Full control. For each of the three cases two possibilities are shown.

PRACTICAL EXAMPLES OF SPLINE STRIP ADJUSTMENT

For better demonstration of the improved flexibility of spline functions against normal polynomials a 19 models strip axis height-adjustment shall be demonstrated at first. The photo scale was 1 : 30 000, the A 7 machine scale 1 : 10 000. Two times three versions have been calculated.

- Case I : Only the minimum number of ground control has been used (4 - 7 points).
- Case II: All 20 height controlled nadir points have been used.

The three versions read:

$$\begin{aligned}
 A \quad v &= -\Delta z + \Delta z_0 + a(x-x_1) + b(x-x_1)^2 + c_1(x-x_1)_+^3 & (16) \\
 B \quad v &= -\Delta z + \Delta z_0 + a(x-x_1) + b(x-x_1)^2 + c_1(x-x_1)_+^3 + c_3(x-x_3)_+^3 \\
 C \quad v &= -\Delta z + \Delta z_0 + a(x-x_1) + b(x-x_1)^2 + c_1(x-x_1)_+^3 + c_2(x-x_2)_+^3 + c_3(x-x_3)_+^3 + c_4(x-x_4)_+^3
 \end{aligned}$$

Finally $|vv|$ has been computed, in all six cases from all 20 points. Table (17) shows that the spline functions B and C result in much smaller $|vv|$ than the normal cubic polynomial A.

	I	II
A	26,3	10,6
B	16,6	7,2
C	4,0	2,6

Table 17: The sums $|vv|$ for 20 height controlled nadir points after adjustment. For the six cases see test (v in meters).

The graphs Fig. 18 show the final corrections v in meters. We recognize that more ground control (4 → 20) cannot change the form of the strip, if an unflexible normal cubic polynomial has been used; compare IA and IIA.

The case IC (7 ground control points, spline function $\in \delta_3(x_1, x_2, \dots, x_5)$) gives a much better result than case IIA (20 ground control points, cubic polynomial).

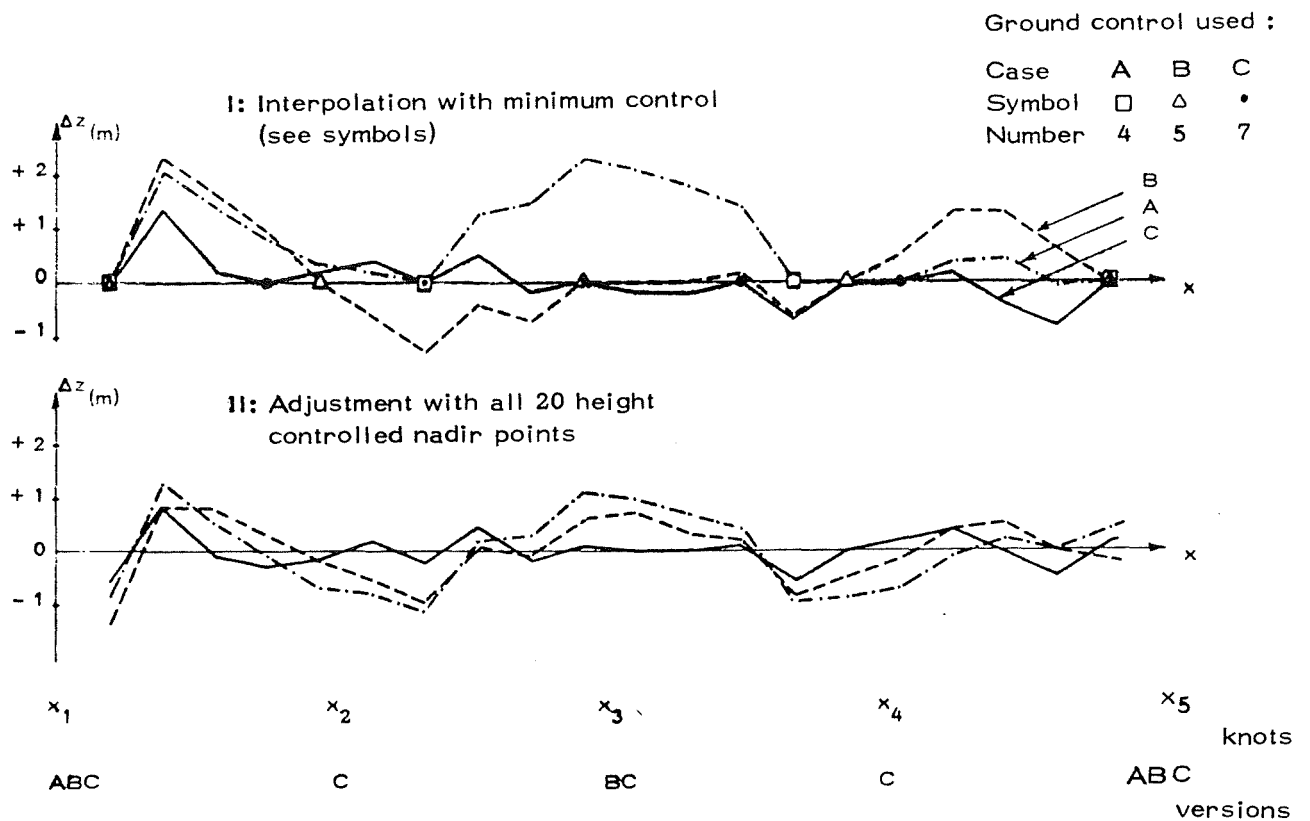


Fig.18: Final corrections $v = Z - z_{adj}$ for the six cases

21 models of the same strip have been adjusted with 3 corresponding versions:

- A : with formulae (3), type 22222, i.e. with quadratic basic polynomials ("knots" x_1, x_5)
- B, C: with formulae (13), type S 22222, i.e. with basic spline functions of second degree, again truncated power functions have been used.
 - B: 3 knots (x_1, x_3, x_5)
 - C: 5 knots (x_1, x_2, x_3, x_4, x_5)

Full control has been given to 8 pairs of control points (see fig.19) equally distributed over the 21 models.

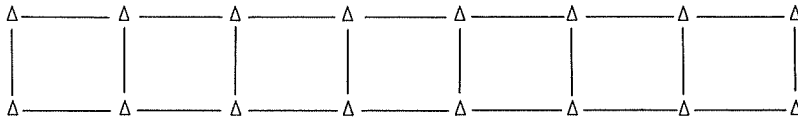


Fig.19: Full ground control and knots used for strip adjustment.

Version	[vv]	v_{max}	redundant
A	9,1	+ 1,06 (z) - 1,04 (z)	30
B	2,9	+ 0,58 (z) - 0,66 (z)	25
C	0,4	+ 0,20 (y) - 0,27 (y)	15

Table 20: Remaining defects $v = \xi_{terr} - \xi_{adj.}$, $\xi = x,y,z$,
after strip adjustment using 16 full control points.

From the remaining defects, see table 20, the conclusion can be drawn that a reasonable strip subdivision by spline-knots and adjustment with the more flexible basic spline functions leads to results which are remarkably better than those after adjustment with normal basic polynomials.

SUMMARY

In [2] a study has been made about systematic negligences in the functional model of polynomial strip adjustment formulae.

At first the functional model of the correction polynomials for aerial triangulation is rigidly derived from the rotation matrix. That is necessary in order to know that the rotations to be corrected locally in the strip are to be smaller than 60° . Greater values cause systematic "numerical deformations" $> 10 \mu m$ in photo scale.

The introduction of "basic polynomials" allows for a transparent classification of the most of the polynomial methods used so far.

Finally spline functions are used instead of the basic polynomials. This leads to polynomial strip adjustment formulae with controllable flexibility and constant quotient σ_{max}/σ_0 also for longer strips. In [2] the proposal has been made to compare such functionally more strict polynomial strip adjustment methods with single model- and bundle (strip) adjustment in order to find out the real progress made with the more analytical methods.

REFERENCES

- |1| Kubik K. and Kure J.: "ISP-Investigation into the accuracy of photogrammetric triangulation", Intermediate report Delft 1971
- |2| Waldhäusl P.: "Funktionale Modelle der Streifen- und Streifen-Block-Ausgleichungen mit einfachen und Spline-Polynomen für beliebiges Gelände", Sonderheft 26, Österreichische Zeitschrift für Vermessungswesen und Photogrammetrie, Wien 1973
- |3| Belling G.E.: "On the use of polynomials and sections in analytic block adjustment", Thesis ITC Delft 1963
- |4| Kubik K.: "Efficient methods for strip- and block-adjustment", Data Processing Department, Rijkswaterstaat Den Haag 1971
- |5| Ahlberg J.H. et alii: "The theory of splines and their applications" Academic Press New York-London 1967

EXPERIENCE WITH PHOTOGRAMMETRIC TRIANGULATION IN ASTRONOMY

by E. Clerici, K. Kubik and J. van Kuilenburg, Delft, Netherlands

ABSTRACT

This report documents the results of an application of photogrammetric bundle adjustment to an astronomical problem. In particular the application to the calibration of astronomical telescopes and the determination of proper motion of stars is treated.

INTRODUCTION

Determination of stars coordinates by photogrammetric block adjustment is becoming an established procedure in photographic astronomy. The astronomical problem however is a restricted version of the photogrammetric problem, since in astronomy the objects are at infinity while the cameras are effectively situated at one point.

Photogrammetry deals with the reconstruction of a three-dimensional object space observed with cameras at unknown location, while astronomy deals with a two-dimensional object space with cameras at known coincident locations. The geometrical adjustment procedure is, however, completely analogous and the formal solution methods can be the same. The computer program used for the application documented in this paper has been developed along the lines published by D. Brown (Brown 1958).

PLATE REDUCTION

Before the measured image coordinates (stars) can be transformed to object space, four problems have to be solved.

First of all a physical model of the imagery which isolates the distortions and points out the unknowns has to be developed. Secondly a reference frame has to be chosen to convert the measurements to some absolute system. Thirdly a statistical model has to be defined to describe the nature of the errors, their propagation and their interdependence. Only after these three problems are settled the fourth problem, concerning the choice of the reduction methods themselves, can be tackled. Only this last problem is explicitly treated in this study.

Most analysis of this reduction problem end up with the formulation of the least squares solution which operates iteratively, by improving a first order approximation. This repeated linearisation is fully justified in astronomy (and most other applications) since very good approximate values are generally available, in the approach used for this study, only linear reduction terms are used. It was hoped that systematic image errors after bundle adjustment would indicate higher order distortions. This procedure is justified as in the astronomical practice seldom terms of higher than third order are reported.

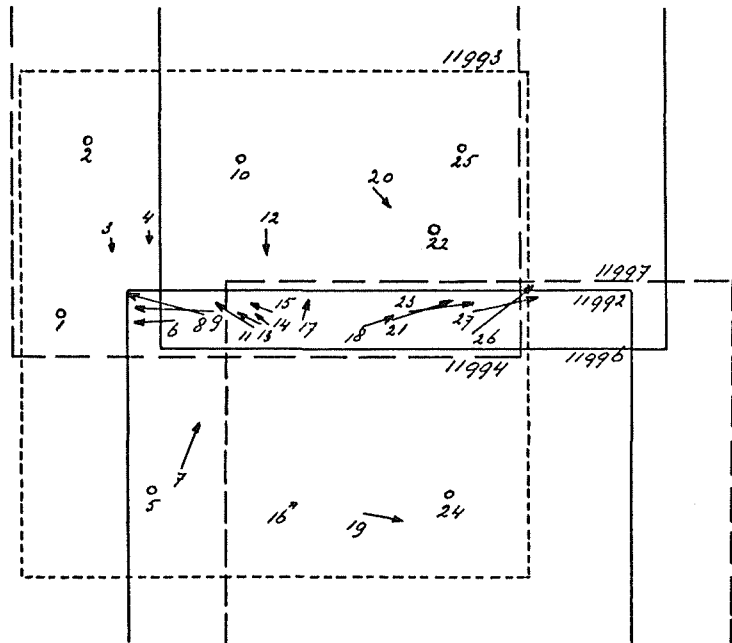
LEAST SQUARES ADJUSTMENT

The separate image coordinates and plate constants are adjusted and transformed into one system by the bundle adjustment method as developed by D. Brown (Brown 1958). This system is completely flexible and can accommodate the astrometric problem without major changes. In principle simultaneous adjustment can be performed to each of the three object coordinates (x, y, z) to each plate attitude and principal point ($\phi, \omega, \kappa, X_0, Y_0, Z_0$), and to each camera position and principle distance (x_0, y_0, c). The analysis starts from the conventional projective relationships.

In order to optimize the structure of the generated (sparse) normal equation system a careful analysis is needed, e.g. the numbering of points and plates is very important for the efficiency of the solution algorithm. The coefficient matrix organisation most used, shows a banded-bordered structure which can be solved with reasonable ease. Solutions of this type of matrices have been reported using up to one hundred plates and tens of thousands of stars. The separate problem of finding the proper weight matrix is still a matter of study.

Many applications for this technique are possible in astronomy, like improving photographically determined catalogues (Googe 1971, Lacroute 1971, Ebner 1970), radio-telescope calibration (Konefick 1971) and position determination (Vegt and Ebner 1972).

Residuals of individual stellar positions of the Praesepe area after a bundle adjustment using five plates and about thirty stars (residuals: 1 cm = 10 μ m).



PROCESSING OF THE PREASEPE AREA

To get some experience with this technique five overlapping photographic plates of the Praesepe area in the sky were obtained with the astrometric refractor of the Leiden Observatory (plate scale 40"/mm, field of view 105).

On the plates about 30 stars were measured on a monocomparator and adjusted along the lines pointed out in the former paragraph. The plate attitude angles found are consistent with those derived from the known telescope setting, and amount to the values tabulated in the table.

Plate	11993	11994	11992	11996	11997
φ	0	+ 0.56	- 0.71	- 0.62	- 0.64
ω	0	+ 0.10	- 0.34	- 0.68	- 0.64
κ	0	+ 0.50	+ 0.07	+ 0.01	+ 0.65

Adjustment Praesepe area; plate attitude angles as computed with reference to plate 11 993.

The resulting residuals, which certainly show a systematic trend, are depicted in the figure.

It is clear that when proper motions of stars have to be obtained from similar photographic measurements one has to take in consideration the effect of these systematic distortions.

In order to be able to correct these distortions the use of reseau telescopes is advisable.

REFERENCES

- Brown, D.C. (1958) "A solution to the general problem of multiple station analytical stereotriangulation" RCA Data Reduction Technical Report No. 43
- Brown, D.C. (1971) "Inversion of very large matrices encountered in large scale problem of photogrammetry and photographic astrometry" Conference on Photographic Astrometric Technique, Ed.H.Eichhorn, NASA CR-1825, p. 249
- Ebner, H. (1970) "Sternpositionsbestimmung mit Hilfe eines geschlossenen Kugelblockes, eine theoretische Genauigkeitsuntersuchung", Bildmessung und Luftbildwesen 3, p. 176
- Ebner, H. (1970) "Genauigkeitserwartung photographischer Sternpositionen bei geschlossener Blockausgleichung", Astron. Nachr. Bd. 292, H.2, p. 65
- Googe, W.D. (1971) "Photographic astrometry and overlap reduction techniques" Conf. on Photographic Astrometric Technique, Ed.H.Eichhorn, NASA CR-1825, p. 209
- Kenefick, J. (1971) "Ultra-Precise Analytics", Photogrammetric Engineering 1971, p. 1167
- Lacroute, P. (1971) "The overlap methods", Conf. on Photographic Astrometric Technique, Ed.H.Eichhorn, NASA CR-1825, p. 219
- de Vegt, C., Ebner H. (1972)
"Blockadjustment methods in photographic astrometry"
Astron. & Astrophys. 17, p. 276

ANALYTICAL TRIANGULATION - A SUGGESTED METHOD

by K. C. Saxena, Dehra Dun, India

ABSTRACT

Analytical triangulation using plate coordinates can be carried out by simultaneous solution of three consecutive photographs and then linking the groups of these three-three photographs, just as we connect models in Independent Model Triangulation. The method suggested by the author in the presented paper is far more simpler than the simultaneous solution of all the photographs which involves very heavy computations requiring fast computers. The problem has been further simplified by the use of transformation equations without 'f', i.e. Z coordinate of plate points.

INTRODUCTION

The author has already submitted two papers on the subject, for publication in the Photogrammetric Engineering. In the first paper titled 'Analytical Triangulation - a simplified approach' the use of a simplified mathematical model without 'f' for the transformation of plate coordinates into three dimensional system has been suggested. Simplified formulae have been worked out to facilitate computations on a desk calculator.

In the second paper titled 'Analytical Triangulation - a simplified solution' the author has outlined a method of analytical triangulation using plate coordinates which can be programmed on small computers.

In this method, instead of simultaneous solution of all the plates, the problem has been treated as sequential, solving three plates at a time and then linking the consecutive groups of three plates each sequentially to give strip coordinates. Coordinates of desired points are fixed up by intersection of three rays corresponding to their images in the three consecutive photographs.

In the present paper, the approach for the solution remains the same as laid down in the above mentioned papers. The algorithm has, however, been further simplified to facilitate programming on small computers. The suggested method will be found useful in the organisations where facilities for large computers may not be available.

MATHEMATICAL FORMULATIONS

The mathematical model without 'f' for transformation of plate coordinates into three dimensional system is as given below:

$$\begin{aligned} X &= a_0 + ax - by \\ Y &= b_0 + bx + ay \\ Z &= c_0 - cx + dy \end{aligned} \tag{1}$$

This can be written as

$$\begin{pmatrix} X \\ Y \\ Z \end{pmatrix} = \begin{pmatrix} x & -y & 0 & 0 & 1 & 0 & 0 \\ y & x & 0 & 0 & 0 & 1 & 0 \\ 0 & 0 & -x & y & 0 & 0 & 1 \end{pmatrix} \begin{pmatrix} a \\ b \\ c \\ d \\ a_0 \\ b_0 \\ c_0 \end{pmatrix} \tag{2}$$

$$\text{or } \begin{matrix} C_i &= & (a_{ij} D_I) & P_j & (4 \times 1) \\ (3 \times 1) & & (4 \times 3) & (3 \times 3) & Q_j & (3 \times 1) \end{matrix} \tag{3}$$

$$\text{or } C_i = a_{ij} P_j + D_I Q_j \tag{4}$$

Where $C_i = \begin{pmatrix} X_i \\ Y_i \\ Z_i \end{pmatrix}$ the coordinates of a point 'i'

a_{ij} = design matrix for a point 'i' falling in photograph 'j'

P_j = Parameters (a_j, b_j, c_j, d_j) scale and three rotations for photograph 'j'

$Q_j = (a_{oj}, b_{oj}, c_{oj})$ the three shifts for photograph 'j'.

If $\Delta_1, \Delta_2, \Delta_3$ are the three ground control points falling in the first two photographs 1,2 and C_1, C_2, C_3 are their known coordinates, then the condition equations for the ground control points are:

$$\begin{aligned} C_1 &= a_{11} P_1 + D_I Q_1 \text{ for point No. 1, in photo No. 1} \\ C_1 &= a_{12} P_2 + D_I Q_2 \text{ for point No. 1, in photo No. 2} \\ C_2 &= a_{21} P_1 + D_I Q_1 \text{ for point No. 2, in photo No. 1} \\ C_2 &= a_{22} P_2 + D_I Q_2 \text{ for point No. 2, in photo No. 2} \\ C_3 &= a_{31} P_1 + D_I Q_1 \text{ for point No. 3, in photo No. 1} \\ C_3 &= a_{32} P_2 + D_I Q_2 \text{ for point No. 3, in photo No. 2} \end{aligned} \tag{5}$$

The coordinates of tie points are taken as parameters and the observation equations for tie points are given by:

$$a_{ij} P_j + D_I Q_j - D_I C_i = 0.$$

Suppose C_4, C_5, C_6 are the unknown coordinates of tie points 04, 05, 06 falling in the first three photographs 1, 2 and 3, then the observation equations for these points are:

$$\begin{aligned} a_{41} P_1 - D_I Q_1 - D_I C_4 &= 0 \text{ for tie point No. 4, in photo No. 1} \\ a_{42} P_2 - D_I Q_2 - D_I C_4 &= 0 \text{ for tie point No. 4, in photo No. 2} \\ a_{43} P_3 - D_I Q_3 - D_I C_4 &= 0 \text{ for tie point No. 4, in photo No. 3} \\ a_{51} P_1 - D_I Q_1 - D_I C_5 &= 0 \text{ for tie point No. 5, in photo No. 1} \\ a_{52} P_2 - D_I Q_2 - D_I C_5 &= 0 \text{ for tie point No. 5, in photo No. 2} \\ a_{53} P_3 - D_I Q_3 - D_I C_5 &= 0 \text{ for tie point No. 5, in photo No. 3} \\ a_{61} P_1 - D_I Q_1 - D_I C_6 &= 0 \text{ for tie point No. 6, in photo No. 1} \\ a_{62} P_2 - D_I Q_2 - D_I C_6 &= 0 \text{ for tie point No. 6, in photo No. 2} \\ a_{63} P_3 - D_I Q_3 - D_I C_6 &= 0 \text{ for tie point No. 6, in photo No. 3} \end{aligned} \tag{6}$$

The observation equations (5) and (6) can be written as

$$L + V = AX \tag{7}$$

where

$$A = \begin{bmatrix} P_1 & P_2 & P_3 & Q_1 & Q_2 & Q_3 & C_4 & C_5 & C_6 \\ a_{11} & 0 & 0 & I & 0 & 0 & 0 & 0 & 0 \\ (3 \times 4) & & & (3 \times 3) & & & & & \\ (15 \times 9) & 0 & a_{12} & 0 & I & 0 & 0 & 0 & 0 \\ a_{21} & 0 & 0 & I & 0 & 0 & 0 & 0 & 0 \\ \text{Total:} & & & & & & & & \\ (45 \times 30) & 0 & a_{22} & 0 & I & 0 & 0 & 0 & 0 \\ a_{31} & 0 & 0 & I & 0 & 0 & 0 & 0 & 0 \\ 0 & a_{32} & 0 & 0 & I & 0 & 0 & 0 & 0 \\ a_{41} & 0 & 0 & I & 0 & 0 & -I & 0 & 0 \\ & & & & & & (3 \times 3) & & \\ 0 & a_{42} & 0 & 0 & I & 0 & -I & 0 & 0 \\ 0 & 0 & a_{43} & 0 & 0 & I & -I & 0 & 0 \\ a_{51} & 0 & 0 & I & 0 & 0 & 0 & -I & 0 \\ 0 & a_{52} & 0 & 0 & I & 0 & 0 & -I & 0 \\ 0 & 0 & a_{53} & 0 & 0 & I & 0 & -I & 0 \\ a_{61} & 0 & 0 & I & 0 & 0 & 0 & 0 & -I \\ 0 & a_{62} & 0 & 0 & I & 0 & 0 & 0 & -I \\ 0 & 0 & a_{63} & 0 & 0 & I & 0 & 0 & -I \end{bmatrix}$$

$$L = \begin{bmatrix} C_1 & (3 \times 1) \\ C_1 & " \\ C_2 & " \\ C_2 & " \\ C_3 & " \\ C_3 & " \\ 0 & " \\ 0 & " \\ 0 & " \\ 0 & " \\ 0 & " \\ 0 & " \\ 0 & " \\ 0 & " \end{bmatrix} \quad \text{total: } (45 \times 1)$$

$$X = \begin{bmatrix} P_1 & (4 \times 1) \\ P_2 & " \\ P_3 & " \\ Q_1 & (3 \times 1) \\ Q_2 & " \\ Q_3 & " \\ C_4 & (3 \times 1) \\ C_5 & " \\ C_6 & " \end{bmatrix} \quad \text{total: } (30 \times 1)$$

V represents the vector of residuals.

From the observation equations (7) we can form the normal equations as given below:

$$(A^T P^{-1} A) X = Y^T P^{-1} L$$

or $(A^T A) X = A^T L$ assuming weight matrix as identity.

$$\begin{array}{l}
 A^T A = \\
 \begin{array}{l}
 (9 \times 9) \\
 \text{total:} \\
 (30 \times 30)
 \end{array}
 \end{array}
 \left[\begin{array}{ccc|ccc|ccc}
 6 & T & 0 & 0 & 6 & T & 0 & 0 & T & T & T \\
 \Sigma_{i=1}^3 a_{i1} a_{i1} & & & & \Sigma_{i=1}^3 a_{i1} & & & & -a_{41} & -a_{51} & -a_{61} \\
 (4 \times 4) & & & & (4 \times 3) & & & & (4 \times 3) & & \\
 0 & 6 & T & 0 & 0 & 6 & T & 0 & T & T & T \\
 & \Sigma_{i=1}^3 a_{i2} a_{i2} & & & & \Sigma_{i=1}^3 a_{i2} & & & -a_{42} & -a_{52} & -a_{62} \\
 & (4 \times 3) & & & & (4 \times 3) & & & & & \\
 0 & 0 & 6 & T & 0 & 0 & 6 & T & T & T & T \\
 & & \Sigma_{i=1}^3 a_{i3} a_{i3} & & & & \Sigma_{i=1}^3 a_{i3} & & -a_{43} & -a_{53} & -a_{63} \\
 & & (4 \times 3) & & & & (4 \times 3) & & & & \\
 \hline
 6 & & 0 & 0 & 6 & I & 0 & 0 & -I & -I & -I \\
 \Sigma_{i=1}^3 a_{i1} & & & & (3 \times 3) & & & & (3 \times 3) & & \\
 (3 \times 4) & & & & & & & & & & \\
 0 & 6 & & 0 & 0 & 6 & I & 0 & -I & -I & -I \\
 & \Sigma_{i=1}^3 a_{i2} & & & & & & & & & \\
 & (3 \times 3) & & & & & & & & & \\
 0 & 0 & 6 & & 0 & 0 & 3 & I & -I & -I & -I \\
 & & \Sigma_{i=1}^3 a_{i3} & & & & & & & & \\
 & & (3 \times 3) & & & & & & & & \\
 \hline
 -a_{41} & -a_{42} & -a_{43} & -I & -I & -I & 3I & 0 & 0 \\
 (3 \times 4) & & & & & & & & \\
 -a_{51} & -a_{52} & -a_{53} & -I & -I & -I & 0 & 3I & 0 \\
 -a_{61} & -a_{62} & -a_{63} & -I & -I & -I & 0 & 0 & 3I \\
 \hline
 \end{array} \right]$$

$$\begin{array}{l}
 A^T L = \\
 \begin{array}{l}
 (9 \times 1) \\
 \text{total:} \\
 (30 \times 1)
 \end{array}
 \end{array}
 \left[\begin{array}{ccc|ccc}
 \Sigma_{i=1}^3 a_{i1} & C_i & & & & \\
 (4 \times 1) & & & & & \\
 \Sigma_{i=1}^3 a_{i2} & C_i & & & & \\
 " & " & & & & \\
 0 & " & & & & \\
 \hline
 \Sigma_{i=1}^3 C_i & & & & & \\
 (3 \times 1) & & & & & \\
 \Sigma_{i=1}^3 C_i & & & & & \\
 " & & & & & \\
 0 & " & & & & \\
 \hline
 0 & " & & & & \\
 0 & " & & & & \\
 0 & " & & & &
 \end{array} \right] = \left[\begin{array}{c}
 R_1 \\
 (12 \times 1) \\
 R_2 \\
 (9 \times 1) \\
 0 \\
 (9 \times 1)
 \end{array} \right] \quad (8)$$

On partitioning of the matrices $A^T A$ and $A^T L$ as shown above the normal equations can be written as:

$$\left[\begin{array}{ccc|ccc}
 D_1 & D_2^T & \alpha^T & P & R_1 \\
 (12 \times 12) & (12 \times 9) & (12 \times 9) & (12 \times 1) & (12 \times 1) \\
 D_2 & D_3 & E & Q & R_2 \\
 (9 \times 12) & (9 \times 9) & (9 \times 9) & (9 \times 1) & (9 \times 1) \\
 \alpha & E & D_4 & C & 0 \\
 (9 \times 12) & (9 \times 9) & (9 \times 9) & (9 \times 1) & (9 \times 1)
 \end{array} \right] = \quad (9)$$

BLOCK ADJUSTMENT WITH PROGRAMMABLE DESK CALCULATORS

by P. R. Datta, Hyderabad, India

A strip can be triangulated either by aeropolygon method, or by independent models (adjoining models sharing a common projection centre) or analytically (say, by Schut's program). A common characteristic of all these methods is that the projection centres are held fixed and are not burdened with residuals after adjustment. The scaling and rotation needed for adjustment are with reference to these projection centres. This is in contrast to block adjustment by independent models as units and by bundles, where the projection centres are also treated as stochastic variables. Our present discussion is in the context of the former case which in terms of accuracy is inferior but is sufficiently accurate for all photogrammetric production jobs. The object of this paper is to suggest a method of block adjustment with strips as units which can be programmed for desk calculators with extended memory (like Hewlett Packard 9100 A).

The deformations (δx , δy , δz) of a triangulated strip at a point can be deemed to be composed of three components. The first and the major component represents a trend of the error surface. It can be represented by expressing δx , δy , δz as continuous polynomial functions with strip coordinates x , y , z as arguments. The second component is a deviation from this trend which shows a systematic pattern locally - that is when only one or two adjoining models are considered - but is random when considered over the whole strip. The third and the least important component is a random error which is localised only at a particular point of observation and is caused by random observational or reading errors of strip coordinates or by random errors in the ground control used for check.

The errors of both first and second types can be explained as double summation effects of transfer errors from model to model as mentioned for the first time by Vermeir. As Zarzycky demonstrated, the polynomial trend can be viewed as the effect of a systematic and constant pattern of transfer errors while the quasi-random deformations of the second type can be deemed to be caused by a local deviation of the transfer errors from this systematic pattern and the irregularities of the model deformations caused thereby.

Determination of the trend surface can be looked upon as a problem of polynomial regression. If sufficiently close ground control data are available - say, one to two models apart - quasi-random errors of the second type can also be processed simultaneously by assuming covariance functions [1]. The covariance functions may have the magnitude of the distance between a pair of data points as arguments and may tend to '1' as the distance tends to '0' and tend to '0' as the distance tends to be large. A suitable covariance function is the normalised Gaussian frequency distribution function with the distance between any two data points as argument. It has, however, been observed that with favourable bridging distance, that is with ground control 5 - 6 models apart, the polynomial adjustment, without assuming any correlation, gives as accurate results as by any other method; and this is true also for block adjustment with deformed strips as units.

The formulae for the trend-polynomials can be deduced by assuming systematic and constant transfer errors. Alternatively, they can be deduced from the simple logic of strip deformation - characterised by three components, namely torsion, curvature and azimuthal error - being a linear function of strip length for shorter strips (about 10 - 12 models long), and a quadratic function of strip length for longer strips (15 - 18 models long). The formulae can be written (3) for shorter strips, as:

$$\delta x = a_0 + a_1x - b_1y + c_1z + a_2x^2 - 2b_2xy + 2c_2xz$$

$$\delta y = b_0 + b_1x + a_1y - d_1z + b_2x^2 + 2a_2xy - 2d_2xz$$

$$\delta z = c_0 - c_1x + d_1y + a_1z - c_2x^2 + 2d_2xy + 2a_2xz$$

It will be observed that according to the above formulae, the errors δx , δy , δz are correlated. Schut [4] has generalised the formulae by assuming errors in planimetry and height to be independent of one another and assuming the planimetric error propagation to be such that conformality is preserved in planimetry. His formulae for the shorter strip are:

$$\begin{aligned}\delta x &= a_0 + a_1x - b_1y + a_2(x^2 - y^2) - 2b_2xy \\ \delta y &= b_0 + b_1x + a_1y + b_2(x^2 - y^2) + 2a_2xy \\ \delta z &= c_0 + c_1x + c_2y + c_3x^2 + c_4xy + c_5xz\end{aligned}$$

The third option would be to treat δx , δy , δz as completely uncorrelated.

By practical experiments Ackermann [5] found that the accuracies obtained from the three options differ surprisingly little. In fact the difference was not more than 10 %. The third option can be adopted in cases where a planimetric absolute accuracy up to $\pm 75 \mu\text{m}$ and an altimetric accuracy up to 0.6 o/oo may be acceptable, and where only programmable calculators may be available.

In such cases, block adjustment with strips as units can be done in two stages. First, an internal adjustment can be performed by adjusting the strips one by one sequentially. The adjusted coordinates of the tie points from the lateral overlap with the previous strip can be used for adjusting the subsequent strip. Such an adjustment does not include a common projection centre unless the lateral overlap exceeds 50 %. But, the dominant trend of error propagation at right angles to the flight line can still be represented by a polynomial which includes y^2 and other second and third degree terms in y . For external block adjustment, therefore, the polynomials mentioned before have to be extended by including terms with y^2 and, in case of long blocks, with higher powers of y , line y^2x and y^2z . The y^2 term also covers the earth curvature. Also covered by this polynomial trend are curvature, torsion and azimuthal changes of the block, up to second degree, along cross-sections at right angles to the flight lines of the block.

It has been found in such cases that with a lateral overlap of about 20 %, and with tie-points along the lateral overlap on every model or every alternate model, the empirically adjusted block does not show any significant periodicity along the cross-sections. It may be mentioned here for clarification that the block is assumed to be regular without any cross-strips and is also preferably rectangular.

The real difficulty in handling such a block adjustment problem on a programmable desk calculator comes from the size of the matrices to be multiplied and inverted in a least squares solution. If a strip is to be adjusted with an adjoining strip with 'p' tie-points by a polynomial having 'n' parameters as coefficients, multiplication of a $n \times p$ matrix with a $p \times n$ matrix is involved three times, assuming that polynomials for x , y and z are not correlated. Also involved is the inversion of a coefficient matrix of normal equations of size $n \times m$.

To avoid the inversion of the matrix Gopalan [7] suggests the use of Orthogonal polynomials. By orthogonal polynomials is meant a set of polynomials,

$$\{P_i(x,y,z) \mid i=1 \text{ to } n\}$$

such that for all $i \neq j$

$$\sum_{\alpha=1}^m \{P_i(x_\alpha, y_\alpha, z_\alpha)\} \{P_j(x_\alpha, y_\alpha, z_\alpha)\} = 0.$$

The coefficients of the powers of x , y , z in the polynomials cannot be independent of the set of data points

$$\{(x_\alpha, y_\alpha, z_\alpha) \mid \alpha=1 \text{ to } m\}$$

as, otherwise, one of the polynomials would equate to zero identically. The technique of determining the coefficients of the polynomials is referred to as "generation of orthogonal polynomials". Householder's technique [6] of generating a set of orthogonal polynomials over a uni-variant data field is well known. We shall evolve here a technique of generating a set of orthogonal polynomials over a bivariate data field. The same technique can be extended to any number of dimensions.

Let us illustrate by the polynomial formula for ' δz ' for a short strip where there is not much relief (say $< 10 \%$):

$$\delta z = c_0 + c_1x + c_2y + c_3x^2 + c_4xy$$

Datta 2

This mathematical model involves 5 parameters - C_0, C_1, C_2, C_3 and C_4 . With the same number of parameters the polynomial can also be expressed as

$$\delta z = c_0\{P_0(x,y)\} + c_1\{P_1(x,y)\} + c_2\{P_2(x,y)\} + c_3\{P_3(x,y)\} + c_4\{P_4(x,y)\}$$

where P_0, P_1, P_2, P_3, P_4 are a set of orthogonal polynomials.

Now, if there is a set of 'n' orthogonal polynomials, it means that there will be $1/2 n(n-1)$ equations of the type

$$\sum_{\alpha=1}^m \{P_i(x_\alpha, y_\alpha)\} \{P_j(x_\alpha, y_\alpha)\} = 0$$

for $i \neq j$. Thus, the number of coefficients of these polynomial terms to be determined as functions of $\{(x_\alpha, y_\alpha)/\alpha = 1 \text{ to } m\}$ has got to be exactly $1/2 n(n-1)$, which in this particular case is 10.

Satisfying this condition, the polynomials can be formulated as follows:

$$P_0(x,y) = 1$$

$$P_1(x,y) = 1 + a_{11}x$$

$$P_2(x,y) = a + a_{21}x + a_{22}y$$

$$P_3(x,y) = 1 + a_{31}x + a_{32}y + a_{33}x^2$$

$$P_4(x,y) = 1 + a_{41}x + a_{42}y + a_{43}x^2 + a_{44}xy$$

where a_{ij} 's are functions of $(x_1, y_1), \dots, (x_m, y_m)$.

The observation equations in this case are:

$$z = c_0\{P_0(x_\alpha, y_\alpha)\} + c_1\{P_1(x_\alpha, y_\alpha)\} + c_2\{P_2(x_\alpha, y_\alpha)\} + c_3\{P_3(x_\alpha, y_\alpha)\} + c_4\{P_4(x_\alpha, y_\alpha)\},$$

$\alpha = 1 \text{ to } m.$

The coefficient matrix (N) of the normal equations would turn out to be a diagonal matrix:

$$N = \begin{bmatrix} \sum_{\alpha=1}^m |P_0(x_\alpha, y_\alpha)|^2 & 0 & \dots & 0 \\ 0 & \sum_{\alpha=1}^m |P_1(x_\alpha, y_\alpha)|^2 & \dots & 0 \\ 0 & 0 & \dots & 0 \\ \vdots & \vdots & \ddots & \vdots \\ 0 & 0 & \dots & \sum_{\alpha=1}^m |P_4(x_\alpha, y_\alpha)|^2 \end{bmatrix}$$

and this makes its inversion apparently very simple. But this apparent simplicity disappears when we have to evaluate the coefficients a_{ij} . The fundamental basis of least squares adjustment is not violated as the mathematical model still remains linear.

If the observation equations are weighted without correlation with ' w_α ' as the weight coefficient for the observation of the point ' α ' then w_α has to be included in the condition of orthogonality as

$$\sum_{\alpha=1}^m w_{\alpha} \{P_i(x_{\alpha}, y_{\alpha})\} \{P_j(x_{\alpha}, y_{\alpha})\} = 0 \text{ for all } i \neq j.$$

In that case, 'N' will still be a diagonal matrix but the diagonal elements will change to

$$\sum_{\alpha=1}^m w_{\alpha} \{P_0(x_{\alpha}, y_{\alpha})\}^2, \quad \sum_{\alpha=1}^m w_{\alpha} \{P_1(x_{\alpha}, y_{\alpha})\}^2, \quad \text{etc.}$$

Evaluation of the coefficients from the ten equations means, in terms of computer software, repetitive loops enclosing a few arithmetical statements or in FORTRAN terms, several DO loops, each loop being not very long. This point will be clear from the determination of the polynomials P_0 and P_1 as illustrations. From equation

$$\sum_{\alpha=1}^m w_{\alpha} \{P_0(x_{\alpha}, y_{\alpha})\} \{P_1(x_{\alpha}, y_{\alpha})\} = 0,$$

we can find

$$a_{11} = - \left(\sum_{\alpha=1}^m w_{\alpha} \right) / \left(\sum_{\alpha=1}^m w_{\alpha} x_{\alpha} \right).$$

From equation

$$\sum_{\alpha=1}^m w_{\alpha} \{P_0(x_{\alpha}, y_{\alpha})\} \{P_2(x_{\alpha}, y_{\alpha})\} = 0,$$

we have

$$a_{21} \sum_{\alpha=1}^m w_{\alpha} x_{\alpha} + a_{22} \sum_{\alpha=1}^m w_{\alpha} x_{\alpha}^2 = - \sum_{\alpha=1}^m w_{\alpha},$$

and from equation

$$\sum_{\alpha=1}^m w_{\alpha} \{P_1(x_{\alpha}, y_{\alpha})\} \{P_2(x_{\alpha}, y_{\alpha})\} = 0,$$

we have

$$\sum_{\alpha=1}^m w_{\alpha} (1 + a_{11}x_{\alpha}) (1 + a_{21}x_{\alpha} + a_{22}y_{\alpha}) = 0,$$

or

$$a_{21} \sum_{\alpha=1}^m w_{\alpha} (x_{\alpha} + a_{11}x_{\alpha}^2) + a_{22} \sum_{\alpha=1}^m w_{\alpha} (a_{11}x_{\alpha}y_{\alpha} + y_{\alpha}) = 0.$$

Thus, a_{21} and a_{22} can be evaluated by solving a pair of linear equations. To evaluate a_{41} , a_{42} , a_{43} , a_{44} , four linear equations will have to be solved. Further to avoid singular solutions at every stage of these linear equations, the origin will have to be kept out of the working area. Use of Orthogonal polynomials in this form therefore, has no special advantage over the normal method, where a 5×5 symmetric positive-definite matrix is to be inverted.

This is an extension to the bivariate case of the algorithm suggested by Gopalan [7] for a univariate data field. Apparently this does not lead to any simplification in computation. But there is a fallacy in this argument. The coefficients (a_{ij}) in the above case are the functions of '2m' real variables (x_j, y_j) $i=1$ to m . Hence, all the a_{ij} 's need to be considered independent of each other. This is evident from the recurrence algorithm developed by Householder in the univariate case for generating orthogonal functions (quoted by Forsythe [6]):

$$\begin{aligned}
 P_0(x) &= 1 \\
 P_1(x) &= xP_0(x) - \alpha_1 P_0(x) \\
 P_2(x) &= xP_1(x) - \alpha_2 P_1(x) - \beta_1 P_0(x) \\
 &\dots \dots \dots \\
 P_{i+1}(x) &= xP_i(x) - \alpha_{i+1} P_i(x) - \beta_i P_{i-1}(x)
 \end{aligned}$$

Here, α 's and β 's are functions of data set $\{x_\mu | \mu = 1 \text{ to } m\}$.

α_{i+1} is given by

$$\alpha_{i+1} = \left| \sum_{\mu=1}^m x_\mu \{P_i(x_\mu)\}^2 \right| / \left| \sum_{\mu=1}^m \{P_i(x_\mu)\}^2 \right|,$$

and β_i is given by

$$\beta_i = \left| \sum_{\mu=1}^m x_\mu P_i(x_\mu) P_{i-1}(x_\mu) \right| / \left| \sum_{\mu=1}^m \{P_{i-1}(x_\mu)\}^2 \right|.$$

In the bivariate case, the Gram-Schmidt orthogonalisation process [8] can be used to orthogonalise the column vectors of the $|x|$ matrix:

$$|x| = \begin{vmatrix} 1 & x_1 & y_1 & x_1^2 & x_1 y_1 \\ 1 & x & y & x^2 & x y \\ - & - & - & - & - \\ - & - & - & - & - \\ - & - & - & - & - \\ 1 & x_m & y_m & x^2 & x_m y_m \end{vmatrix}$$

The vectors after orthogonalisation are the column vectors:

$$|P_0(x_i y_i)|_{i=1 \text{ to } m}, |P_1(x_i y_i)|_{i=1 \text{ to } m}, \dots \dots \dots |P_4(x_i y_i)|_{i=1 \text{ to } m}.$$

The Gram-Schmidt algorithm is well known in mathematical literature and is clearly formulated by Thompson [8]. The algorithm is a recurrence algorithm in the sense that the value of $P_0(x_i, y_i)$ is used to calculate $P_1(x_i, y_i)$, the values of $P_0(x_i, y_i)$ and $P_1(x_i, y_i)$ are used to calculate $P_2(x_i, y_i)$ and so on. The inner product of the column vectors can be very easily handled in a computer by a loop.

Conformality can be enforced in planimetry by using complex variables $w = x + iy$ and $\delta w = \delta x + i\delta y$ and expressing ' δw ' as a power series in ' w ' with complex coefficients as parameters. Schut [9] uses the same formulation but carries out the computations in the real field by separating the real and imaginary parts of the variables. In a programmable calculator like Hewlett-Packard 9100 A or 9100 B, computations can be directly performed over the complex field, with the help of the hardware circuitry which transforms cartesian coordinates directly to polar and vice versa. For example, multiplication of two complex numbers w and w can be handled as

$$w_1 = r_1 e^{i\theta_1}, \quad w_2 = r_2 e^{i\theta_2} \quad \text{and} \quad w_1 w_2 = (r_1 r_2) e^{i(\theta_1 + \theta_2)}$$

To find correct normal equations for a least squares solution, from observation equations which are in the complex field, we must include the complex conjugate of the observation equation also. For example, for a point (i) if the observation equation is

$$\delta w_i = C_0 + C_1 w_i + C_2 w_i^2 + \dots$$

we must also include its conjugate

$$\overline{\delta w}_i = \overline{c}_0 + \overline{c}_1 \overline{w}_1 + \overline{c}_2 \overline{w}_2^2 + \dots$$

as an additional observation equation.

Using Householder's recurrence algorithm and substituting 'w' for 'x', orthogonal polynomials can be generated separately for the complex observation equations and their conjugates. The same orthogonal polynomials can be used for a combined set of equations including the complex equations and their conjugates, if there is no functional correlation between (c_0, c_1, c_2, \dots) and $(\overline{c}_0, \overline{c}_1, \overline{c}_2, \dots)$. In other words $c_0, \overline{c}_0, c_1, \overline{c}_1$, etc. are to be treated as independent parameters.

Householder's recurrence algorithm can be directly used for generating orthogonal polynomials over the real field when $(\delta x, \delta y, \delta z)$ are uncorrelated and functions of 'x' only. This may be the case when the flight lines are nearly straight and parallel and the tie-points are chosen on straight lines parallel to the flight lines.

It has not so far been discussed as to how $(\delta x, \delta y, \delta z)$ will be calculated for internal adjustment, at different points. Strip coordinates of every strip are transformed by a linear conformal transformation in planimetry only and the heights transformed by a scale change and datum shift, with reference to the coordinates of tie-points in the previous strip. No attempt is made to shift the origin to the centroid in any of the transformations. In case of (x,y) shift, the tie-point at extreme left of the strip is made to coincide with the same tie-point of the previous strip. For z-shift, the tie-points with minimum height are made to coincide.

The planimetric linear conformal transformation is calculated, not by least squares adjustment, but by two well-observed points at the end of the strips. The external block adjustment will have to be similarly proceeded by a planimetric linear conformal transformation followed by scaling and shift in z-direction.

REFERENCES

- |1| Kraus K. and Mikhail E.: "Linear Least Squares Interpolation", Photogrammetric Engineering, October 1972
- |2| Kraus K.: "A General Digital Terrain Model Theory and Applications"
- |3| Ackermann, F.: "ITC Notes on Aerial Triangulation Adjustments"
- |4| Schut G.H.: "A FORTRAN Program for the adjustment of Strips and Blocks by Polynomial Transformations"
- |5| Ackermann F.: "Experience of Block Triangulation by Independent Models"
- |6| Forsythe A.C.: "Generation and Use of Orthogonal Polynomials for Data Fitting with a Digital Computer", Journal of the Society of Industrial and Applied Mathematics, Vol. V, No. 5, June 1957
- |7| Gopalan N. "Use of Orthogonal Polynomials in Strip Adjustment", Indian Surveyor, July 1973
- |8| Thompson E.H.: "An Introduction to the Algebra of Matrices with some Applications", pp. 102 - 103
- |9| Copson E.T.: "Introduction to the Theory of Functions of a Complex Variable"

COMPARATIVE ACCURACY OF POINT DETERMINATION BY ABSOLUTE ORIENTATION AND BLOCK ADJUSTMENTS - A THEORETICAL ANALYSIS

by P. R. Datta, Hyderabad, India

The object of this analysis needs some clarification. Historically, block adjustment is an improvement over strip adjustment, by taking advantage of the connection at tie-points between stripes. As a result, requirements of ground control points could be relaxed as the connection at tie-points improved the overall accuracy of the block, and this is true irrespective of whether the block adjustment is done with deformed strips as units by polynomial transformation, or by similarity or affine transformation of models as units, or with photogrammetric bundles as units.

There was a time when, for very accurate work, every model of a block was independently controlled on the ground on the belief that coordinates determined by absolute orientation of a model with respect to ground-controlled points was more accurate than those obtained by aerial triangulation adjustments. In view of the development of efficient block adjustment programs, the time has come to examine this assumption critically especially, as a result of the extensive studies made by Ebner [6] and conclusions drawn by him. It could still be true that accuracy obtained by absolute orientation is better, when ground control is not dense. But, the question which needs to be answered is, for example, "Is the accuracy obtained by absolute orientation of one model with 1 : 20.000 scale photographs better or worse than those obtained by block adjustment of 4 models with 1:10.000 scale photographs?"

A good way of answering such a question is by testing the results from several sample observations with sample photographs. Another way is to simulate different sets of data with different patterns of distribution of random errors and work out the variances of the terrain coordinates from the sample of adjusted terrain coordinates at every point. However, results can also be predicted theoretically provided the variances and covariances of the observations are known. For a good A-7 instrument or A-8 instrument, the grid test should give us a standard deviation on the image plane of $\pm 5 \mu\text{m}$ or $\pm 6 \mu\text{m}$. In the case of an actual photograph, it could be $\pm 8 \mu\text{m}$, so that in either x or y direction it is about $\pm 6 \mu\text{m}$. In the case of stereoscopically observed y -parallax the accuracy on image scale has been found to be $\pm 2 \mu\text{m}$ from practical experiments. When the basic observations are the comparator coordinates measured on the image plane, the standard deviation on the image plane can be assumed to be $\pm 5 \mu\text{m}$ when we consider errors both due to comparator observations and point transfer. In each of x and y directions, the error can be assumed to be about ± 3.5 per μm . For all practical purposes, there is no correlation between x - and y -observations.

The approach to the problem here is similar to that of Ebner [6]. As pointed out by him in another paper [8], a theoretical study of this nature is sure to yield results which will agree with practical results within $\pm 20\%$. There are, however, two points of difference. First, every step of the working has been spelt out. Secondly - and this is a major difference - the variances of the observed model coordinates are not empirically assumed but have been statistically worked out. The investigations have still not been completed and as such I have outlined here only the method in detail and also, the results obtained for computed variances and covariances of the model coordinates from the basic assumptions of standard deviation on the image plane, and y -parallax on image scale.

To make a theoretical study of a problem like this, we need a mathematical model where the observed data are explicitly expressed as functions of parameters, and where the unknown terrain coordinates of a number of check points figure as parameters. Thus, a suitable mathematical model has to be found.

The polynomial model of error propagation along a strip is based on Vermeir's hypothesis of transfer errors from model to model and is strictly valid when the transfer errors are constant and systematic. It is at best a good approximation to the quasi-systematic error pattern actually generated by a double summation of the effects of random transfer errors, and indicates only the trend of deformation of the surface.

The inadequacy of the polynomial error propagation hypothesis was demonstrated by Ackermann [1] in a comparative study of the accuracies in x , y , z coordinates obtained from the STRIM program and from second and third degree polynomial adjust-

ments of strips. Thus, for the purpose of the present investigations, it would be legitimate to work with only two types of mathematical models:

- a) the mathematical model for block adjustment with models as units, and
- b) the mathematical model for bundle adjustment.

In case 1), a choice has to be made between affine transformations and similarity transformations.

Affine transformations [2], [3], [4] have the advantage of an easy and simple linear mathematical model at the cost of doubling the number of orientation parameters. Neither the transformation suggested by Oswal and Balasubramaniam [4] nor that of Blais [3] is an exact similarity transformation and the rotation matrix has been derived by constraining the affine transformation in both cases. This has been very clearly analysed by Schut [5].

In order to use an affine transformation to investigate the variances of the adjusted terrain coordinates, the variances and covariances of the parameters of transformation must be known. In a transformation of model-coordinates (x,y,z) into terrain coordinates (X,Y,Z) of the type

$$\begin{pmatrix} X \\ Y \\ Z \end{pmatrix} = \begin{pmatrix} a_{11} & a_{12} & a_{13} \\ a_{21} & a_{22} & a_{23} \\ a_{31} & a_{32} & a_{33} \end{pmatrix} \begin{pmatrix} x \\ y \\ z \end{pmatrix} + \begin{pmatrix} a_{14} \\ a_{24} \\ a_{34} \end{pmatrix}$$

$$\begin{aligned} &\text{var}(a_{ij}) \quad i=1 \text{ to } 3, j=1 \text{ to } 4, \text{ and} \\ &\text{cov}(a_{ij}, a_{i'j'})_{i,i'} = 1 \text{ to } 3, j,j' = 1 \text{ to } 4, \end{aligned}$$

can be either known directly from experience, or can be deduced from the knowledge of the variances and covariances of the basic observations. Direct experience in this field is not extensive, as affine transformations have not been extensively applied. Affinity in a model can be produced by incorrect principal distance and by affine deformation of the image plane due to elastic deformation of the base and emulsion of the photograph. We do not have complete knowledge of image deformations as yet and this factor alone should rule out consideration of block adjustment by an affine transformation of individual models. Besides, as pointed out by Blais [3] and although not explicitly mentioned by Das [2], there is the possibility of an indeterminacy creeping in when the (x,y,z-) and (X,Y,Z-) systems are sharing the same origin and the data points are coplanar with this origin. It is worthwhile to explain this point a bit.

If the origin is shared $|a_{14} \ a_{24} \ a_{34}|^T = 0$ and if the data points (x_i, y_i, z_i) $i=1$ to 3 and (X_i, Y_i, Z_i) $i=1$ to 3 are coplanar with this origin, then

$$\begin{pmatrix} x_1 & x_2 & x_3 \\ y_1 & y_2 & y_3 \\ z_1 & z_2 & z_3 \end{pmatrix} \text{ and } \begin{pmatrix} X_1 & X_2 & X_3 \\ Y_1 & Y_2 & Y_3 \\ Z_1 & Z_2 & Z_3 \end{pmatrix} \text{ are singular and } \begin{pmatrix} a_{11} & a_{12} & a_{13} \\ a_{21} & a_{22} & a_{23} \\ a_{31} & a_{32} & a_{33} \end{pmatrix} \text{ is indeterminate.}$$

However, if affine transformation is used for simultaneous block adjustment by independent models, this problem can be avoided by shifting the origin of the ground coordinated system from the centroid of the block to the level of the projection centres.

The mathematical model for transforming independent models should, therefore, represent similarity. If $|x,y,z|^T$ are the observed model coordinates, $|X,Y,Z|^T$ the unknown terrain parameters, and $|x_s, y_s, z_s|^T$ the parameters indicating the shift of the model in model space, then the mathematical model takes the form

$$\begin{pmatrix} x \\ y \\ z \end{pmatrix} = \lambda R^T \begin{pmatrix} X \\ Y \\ Z \end{pmatrix} - \begin{pmatrix} x_s \\ y_s \\ z_s \end{pmatrix}$$

Here, 'R' is a rotation matrix for the model space to be rotated into the ground space and the scale of the model. In Cayley's form

$$R^T = (1 + a^2 + b^2 + c^2)^{-1}$$

$$x \begin{vmatrix} 1 + a^2 - b^2 - c^2 & 2(ab + c) & 2(ac - b) \\ 2(ab - c) & 1 - a^2 + b^2 - c^2 & 2(bc + a) \\ 2(ac + b) & 2(bc - a) & 1 - a^2 - b^2 + c^2 \end{vmatrix}$$

where a,b,c are functions of the absolute tilts of the model and a:b:c = $\Omega:\Phi:\kappa$; s,a,b,c are the parameters of absolute orientation. (Ω,Φ,κ) are tilts of the model about the origin of (X,Y,Z) system; to minimise the values of X,Y,Z this origin is usually shifted to a point near the centroid of the block prior to least squares adjustment. It is also not necessary, for this theoretical investigation, to introduce the additional parameter (d), as done by Schut [5] as any swing of a model by about 180° can always be corrected by changing signs of model 'x' and 'y' coordinates.

For both least squares adjustment and calculation of variances, it is necessary to linearise the mathematical model, around certain approximate values of the mathematical model, around certain approximate values of the parameters. For every point, the linearized observation equations are

$$\begin{aligned} v_x + d_x &= \left(\frac{\partial X}{\partial s}\right)_0 ds + \left(\frac{\partial X}{\partial a}\right)_0 da + \left(\frac{\partial X}{\partial b}\right)_0 db + \left(\frac{\partial X}{\partial c}\right)_0 dc + \left(\frac{\partial X}{\partial X}\right)_0 dx \\ &+ \left(\frac{\partial X}{\partial Y}\right)_0 dY + \left(\frac{\partial X}{\partial Z}\right)_0 dZ + \left(\frac{\partial X}{\partial x_s}\right)_0 dx_s + \left(\frac{\partial X}{\partial y_s}\right)_0 dy_s + \left(\frac{\partial X}{\partial z_s}\right)_0 dz_s \\ v_y + d_y &= \left(\frac{\partial Y}{\partial s}\right)_0 ds + \left(\frac{\partial Y}{\partial a}\right)_0 da + \left(\frac{\partial Y}{\partial b}\right)_0 db + \left(\frac{\partial Y}{\partial c}\right)_0 dc + \left(\frac{\partial Y}{\partial X}\right)_0 dx \\ &+ \left(\frac{\partial Y}{\partial Y}\right)_0 dY + \left(\frac{\partial Y}{\partial Z}\right)_0 dZ + \left(\frac{\partial Y}{\partial x_s}\right)_0 dx_s + \left(\frac{\partial Y}{\partial y_s}\right)_0 dy_s + \left(\frac{\partial Y}{\partial z_s}\right)_0 dz_s \\ v_z + d_z &= \left(\frac{\partial Z}{\partial s}\right)_0 ds + \left(\frac{\partial Z}{\partial a}\right)_0 da + \left(\frac{\partial Z}{\partial b}\right)_0 db + \left(\frac{\partial Z}{\partial c}\right)_0 dc + \left(\frac{\partial Z}{\partial X}\right)_0 dx \\ &+ \left(\frac{\partial Z}{\partial Y}\right)_0 dY + \left(\frac{\partial Z}{\partial Z}\right)_0 dZ + \left(\frac{\partial Z}{\partial x_s}\right)_0 dx_s + \left(\frac{\partial Z}{\partial y_s}\right)_0 dy_s + \left(\frac{\partial Z}{\partial z_s}\right)_0 dz_s \end{aligned}$$

The least squares adjustment in this case is an iterative process. The linearised mathematical model can be assumed to be fully valid only in the case of the last iteration when further changes in parameter values are negligible; and in this case, since every model would be nearly levelled, we shall be entitled to treat planimetry and height to be uncorrelated.

(X,Y,Z) can be assumed to be reduced to mean model scale prior to adjustment computations, as is normally done in all programs. Then, the approximate values of the parameters s,a,b,c are $s \approx 1$, $b \approx 0$, $c \approx 0$, and

$$\begin{aligned} \left(\frac{\partial X}{\partial s}\right)_0 &= X, \left(\frac{\partial Y}{\partial s}\right)_0 = Y, \left(\frac{\partial Z}{\partial s}\right)_0 = Z, \left(\frac{\partial X}{\partial a}\right)_0 = 0, \left(\frac{\partial Y}{\partial a}\right)_0 = 2Z, \left(\frac{\partial Z}{\partial a}\right)_0 = -2Y \\ \left(\frac{\partial X}{\partial b}\right)_0 &= -2Z, \left(\frac{\partial Y}{\partial b}\right)_0 = 0, \left(\frac{\partial Z}{\partial b}\right)_0 = 2X, \left(\frac{\partial X}{\partial c}\right)_0 = 2Y, \left(\frac{\partial Y}{\partial c}\right)_0 = -2X, \left(\frac{\partial Z}{\partial c}\right)_0 = 0 \\ \left(\frac{\partial X}{\partial x_s}\right)_0 &= -1, \left(\frac{\partial Y}{\partial y_s}\right)_0 = -1, \left(\frac{\partial Z}{\partial z_s}\right)_0 = -1, \\ \left(\frac{\partial X}{\partial y_s}\right)_0 &= \left(\frac{\partial X}{\partial z_s}\right)_0 = \left(\frac{\partial Y}{\partial x_s}\right)_0 = \left(\frac{\partial Y}{\partial z_s}\right)_0 = \left(\frac{\partial Z}{\partial x_s}\right)_0 = \left(\frac{\partial Z}{\partial y_s}\right)_0 = 0, \\ \left(\frac{\partial X}{\partial X}\right)_0 &= \left(\frac{\partial Y}{\partial Y}\right)_0 = \left(\frac{\partial Z}{\partial Z}\right)_0 = 1, \\ \left(\frac{\partial X}{\partial Y}\right)_0 &= \left(\frac{\partial X}{\partial Z}\right)_0 = \left(\frac{\partial Y}{\partial X}\right)_0 = \left(\frac{\partial Y}{\partial Z}\right)_0 = \left(\frac{\partial Z}{\partial X}\right)_0 = \left(\frac{\partial Z}{\partial Y}\right)_0 = 0 \end{aligned}$$

(X,Y,Z) in this case are the approximate values of the terrain coordinates of the point, reduced to mean model scale and referred to a system of axes parallel to the ground system with its origin close to the centre of the block.

Using 'ij' as suffix to indicate point 'j' in model 'i' the linearized observation equations can be symbolically expressed as

$$(I) \dots v_{ij} + dU_{ij} = \begin{vmatrix} L_j \\ \vdots \\ I \\ \vdots \\ I \end{vmatrix} \begin{vmatrix} dP_j \\ \vdots \\ dQ_j \\ \vdots \\ dR_j \end{vmatrix}$$

where

$$U_{ij} \equiv \begin{vmatrix} x_{ij} & y_{ij} & z_{ij} \end{vmatrix}^T$$

$$P_i \equiv \begin{vmatrix} s_i & a_i & b_i & c_i \end{vmatrix}^T$$

$$Q_i \equiv \begin{vmatrix} x_s^{(i)} & y_s^{(i)} & z_s^{(i)} \end{vmatrix}^T$$

$$R_j \equiv \begin{vmatrix} X_j & Y_j & Z_j \end{vmatrix}^T$$

and

$$L_j \equiv \begin{vmatrix} X_j & 0 & -2Z_j & 2Y_j \\ Y_j & 2Z_j & 0 & -2X_j \\ Z_j & -2Y_j & 2X_j & 0 \end{vmatrix}$$

If there are 'm' models and 'n' observed points in the block, these equations will be valid for i = 1 to m and j = 1 to n, provided that there is no equation when 'j' is not a point observed in model 'i'.

For those points which are the ground control points additional observation equations will have to be added. If (GX_j, GY_j, GZ_j) are the ground control data for point 'j' reduced to mean model scale and referred to the centre of the block as origin, then these equations are

$$(II) \dots v_j^{(g)} + dX_j = 0.$$

All these observation equations can be symbolically represented by AX = B where 'X' is a vector of corrections which can be called pseudo-parameters and 'B' is the vector of pseudo-observations. If the adjustment is carried out without taking equations (II) into account, the standard error obtained would be a measure of the relative accuracy of the adjusted block. Absolute accuracy of the block cannot, however, be defined merely by including equations (II) in the adjustment, as absolute accuracy is to be found from the deviations at check points which are not used for adjustment.

The same set of observation equations as (I) and (II) may be used for digitally calculating the standard error of absolute orientation also. In that case, equations (I) will be only for one model. The accuracy obtained from a digitally performed absolute orientation is likely to be higher than that for absolute orientation performed on an analogue instrument, as in the latter case, it is a sequential process of scaling and levelling the model. However, digital orientation with simultaneous solution for all the orientation parameters is possible in a medium-sized computer and even in a desk calculator like Hewlett Packard's 9100 A with an extended memory. Thus, a digital absolute orientation is not only desirable but is also possible where only discreet points are required to be co-ordinated and no plotting in the dynamic mode is necessary.

The solution of the system of normal equations in this case can be symbolically represented by

$$X = (A^T P A)^{-1} (A^T P B)$$

where 'P' is the weight matrix. The variance - covariance matrix (Σ_X) of the adjusted parameters can be expressed as

$$\Sigma_X = (A^T P A)^{-1} \sigma_o^2 \text{ where } \sigma_o^2 = \frac{V^T P V}{n-u};$$

in this case, 'σ_o' is the standard error of unit weight, 'V' is the vector of residuals offer adjustment, 'n' is the total number of observation equations and

'u' is the number of parameters to be determined.

Since P is the weight matrix and not just the weight-coefficient matrix, it is the inverse of the variance-covariance matrix of the observations. If the observations are not correlated, then using usual notations,

$$p_{11} = \sigma_1^{-2}, \quad p_{22} = \sigma_2^{-2}, \quad p_{33} = \sigma_3^{-2}, \quad \text{etc.}$$

and

$$E \{V^T P V\} = p_{11} E\{v_1^2\} + p_{22} E\{v_2^2\} + p_{33} E\{v_3^2\} + \dots ;$$

hence

$$E \{\sigma_o^2\} = \frac{n}{n-u} .$$

The exact value of this ratio will depend on the layout of the block and tie-points. But, usually the number of redundant equations will be about 50 % of the number of parameters, and then we can assume

$$\Sigma_x = 3(A^T P A)^{-1} .$$

Our problem is now to find 'p' or, to be more precise, p^{-1} , which is the same as the variance covariance matrix of the model coordinate observations. Since, independent models are normally formed in analogue instruments, using rotational elements only, the variances and covariances of the elements ($\kappa I, \kappa II, \phi I, \phi II, \omega II$), have been first calculated on the basis of the standard deviation of the y-parallax observations. Using usual notations, $\sigma_{py} = + 2 \mu m$, on image scale. Using the same notations as in the previous paragraph, however, this time in a different context, where the 'p' matrix is identity, all parallax observations being of equal weight,

$$E\{\sigma_o^2\} = 6x (2\mu m)^2 .$$

The variance covariance matrix for the orientation elements is given by

$$(A^T A)^{-1} x\{6x(2\mu m)^2\}$$

where 'A' is the coefficient matrix for the parallax equations. If the number of points at which y-parallax is observed is increased to 9, then

$$E\{\sigma_o^2\} = 2.25 x 4(\mu m)^2 \quad \text{and the variance covariance matrix becomes} \\ (A^T A)^{-1} x(9x10^{-6}) \text{ mm}^2 .$$

For our investigation, we assume parallax observations at 6 points as usual. From the linear equations expressing model deformations ($\delta x, \delta y, \delta z$) at every one of the 6 points in terms of the rotational elements, the variance covariance matrix for the model deformations at the 6 points has been worked out. The parallax equations used are for a flat model and the photography is assumed to be normal wide-angle photography with 60 % endlap. To reduce the accuracy figures to a commonscale for comparison, the model scale has been assumed to be the same as the scale of photography. The base is assumed as 92 mm and the projection distance as 152 mm.

The complete variance covariance matrix is of size 18 x 18 and it is not possible to reproduce it here. But some of the main points are summarised below:

a) At the 2 neat model points vertically below the projection centres, there is no correlation between the 'x' and 'y' coordinates at the same point or between the two points; 'x' and 'z' coordinates of the same point are correlated to the extent of about 68 %.

b) At each of the other 4 neat model points on the wings 'x' and 'y' are correlated to the extent of about 50 % although correlation between 'x' and 'z' or 'y' and 'z' is negligible. The 'x' coordinates of the 4 points are correlated to the extent of about 50 %. There is no correlation in 'y' and the pattern of correlation in 'z' is not steady.

It would have been ideal to include the correlations in the 'p' matrix, if possible. Unfortunately in the programs known to me (till middle of 1973) this is not possible. Even differential weighting of the model coordinates depending

upon the position of the point on the neat model is not possible. The calculated average standard deviation on image scale of the neat model points are as below:

c) For points vertically below projection centre,

$$\sigma_x = \sigma_y = 10 \text{ } \mu\text{m}, \text{ and } \sigma_z = 27 \text{ } \mu\text{m}.$$

d) For other 4 neat model points,

$$\sigma_x = \sigma_y = 16 \text{ } \mu\text{m}, \text{ and } \sigma_z = 27 \text{ } \mu\text{m}.$$

For the purpose of the current investigation, no correlation are being assumed but different variances as calculated above are being assumed for model coordinates of different neat model points. The figures would have reduced to 1/3 of their value if 9 points were assumed for parallax observations.

We can assume a setting error of 4 μm on image scale for 'x', 'y' and 'z' and an additional 4 μm for pointing the floating mark in the z-direction. But this will not make any appreciable difference in the standard deviation figures.

DETERMINATION OF THE VARIANCES AND COVARIANCES OF THE PROJECTION CENTRE COORDINATES

Projection centre coordinates are normally determined by monocular observations on the same points on the dispositive at two different projection distances, usually 'f' and '2f'. If (X_0, Y_0, Z_0) are the projection centre coordinates and (x, y) and (X, Y) are the coordinates observed in the upper (3) and lower (z) projection planes, then (X_0, Y_0, Z_0) are determined from the simplified equations

$$X_0 = X - t(X - x)$$

$$Y_0 = Y - t(Y - y)$$

$$Z_0 = Z - t(Z - z)$$

and

$$t = \frac{X_2 - X_1}{(X_2 - X_1) - (x_2 - x_1)} = \frac{Y_2 - Y_1}{(Y_2 - Y_1) - (y_2 - y_1)} \approx 1.67$$

The projection centres are seldom determined by a rigorous least squares adjustment. The equations in differential form are

$$dX_0 = dX - t(dX - dx) - dt.(X-x)$$

$$dY_0 = dY - t(dY - dy) - dt.(Y-y)$$

$$dZ_0 = dZ - t.d(Z-z) - dt.(Z-z)$$

and

$$dt = \frac{(dY_2 - dY_1) |(Y_2 - Y_1) - (y_2 - y_1)| - (Y_2 - Y_1)(dY_2 - dY_1 - dy_2 + dy_1)}{|(Y_2 - Y_1) - (y_2 - y_1)|^2}$$

As the mathematical model is itself approximate, there is no point in calculating correlation. Here, $\sigma_x = \sigma_y = 8 \text{ } \mu\text{m}$ and $\sigma_x = \sigma_y = 16 \text{ } \mu\text{m}$; further,

and $x_2 - x_1 = y_2 - y_1 = 184 \text{ mm}$

and $X_2 - X_1 = Y_2 - Y_1 = 368 \text{ mm}$

and $\sigma_t = 3 \times 10^{-4}$.

We can also assume: $\sigma_z = \sigma(Z-z) = 5 \text{ } \mu\text{m}$. Since $X-x = Y-y \approx 184 \text{ mm}$, and $Z-z=f = 152 \text{ mm}$, we have

$$\sigma_{x_0} = \sigma_{y_0} = 65 \text{ } \mu\text{m} \text{ and } \sigma_{z_0} = 47 \text{ } \mu\text{m}.$$

If 't' is determined independently from x observations on 3 pairs of points and y observations on 3 pairs of points and the mean of 6 values accepted, then

$$\sigma_t = 1.2 \times 10^{-4}.$$

In this case, X_0 and Y_0 are determined from 6 observations each. The computed values of σ_{X_0} and σ_{Y_0} are in this case $\sigma_{X_0} = \sigma_{Y_0} = 16 \mu\text{m}$. With the revised value of σ_t , we have $\sigma_{Z_0} = 20 \mu\text{m}$.

CASE OF ANALYTICAL TRIANGULATION

The case of analytical triangulation arises when the observed input data are image coordinates observed on a comparator. It can be assumed that all known systematic and quasi-systematic errors like lens distortion and image deformations are eliminated by a pre-processing program which reduces the image coordinates to the principal point as origin. If a large computer system is accessible, sequential analytical triangulation should be followed by a simultaneous adjustment by bundles. For a theoretical study, therefore, the mathematical model based on collinearity condition used in adjustment by bundles can be accepted.

With usual notations and system of axes, and using Cayley's form of the rotation matrix, the equations of collinearity are:

$$x = -f \left| \frac{(1+a^2-b^2-c^2)(X-X_0) + 2(ab+c)(Y-Y_0) + 2(ca-b)(Z-Z_0)}{2(ca+b)(X-X_0) + 2(bc-y)(Y-Y_0) + (1-a^2-b^2+c^2)(Z-Z_0)} \right|$$

$$y = -f \left| \frac{2(ab-c)(X-X_0) + (1-a^2+b^2-c^2)(Y-Y_0) + 2(bc+a)(Z-Z_0)}{2(ca+b)(X-X_0) + 2(bc-y)(Y-Y_0) + (1-a^2-b^2+c^2)(Z-Z_0)} \right|$$

For approximate values $a \approx 0$, $b \approx 0$, $c \approx 0$ of parameters and assuming the ground scale to be the same as image scale (so that figures of accuracy refer to a common scale), we have the following relations:

$$\begin{aligned} \left(\frac{\partial x}{\partial X}\right)_0 &\approx -1, & \left(\frac{\partial y}{\partial Y}\right)_0 &\approx -1, \\ \left(\frac{\partial x}{\partial X_0}\right)_0 &\approx +1, & \left(\frac{\partial y}{\partial Y_0}\right)_0 &\approx +1, \\ \left(\frac{\partial x}{\partial Y}\right)_0 &\approx 0 \approx \left(\frac{\partial x}{\partial Y_0}\right)_0, & \left(\frac{\partial y}{\partial X}\right)_0 &\approx 0 \approx \left(\frac{\partial y}{\partial X_0}\right)_0, \\ \left(\frac{\partial x}{\partial Z}\right)_0 &\approx \frac{x}{f}, & \left(\frac{\partial y}{\partial Z}\right)_0 &\approx \frac{y}{f}, \\ \left(\frac{\partial x}{\partial Z_0}\right)_0 &\approx -\frac{x}{f}, & \left(\frac{\partial y}{\partial Z_0}\right)_0 &\approx -\frac{y}{f}, \\ \left(\frac{\partial x}{\partial a}\right)_0 &\approx -\frac{2xy}{f} & \left(\frac{\partial y}{\partial a}\right)_0 &\approx -2f\left(1 + \frac{y^2}{f^2}\right) \\ \left(\frac{\partial x}{\partial b}\right)_0 &\approx 2f\left(1 + \frac{x^2}{f^2}\right) & \left(\frac{\partial y}{\partial b}\right)_0 &\approx \frac{2xy}{f} \\ \left(\frac{\partial x}{\partial c}\right)_0 &\approx -2y & \left(\frac{\partial y}{\partial c}\right)_0 &\approx 2x \end{aligned}$$

These partial differential coefficients are the elements of the coefficient matrix 'A' for linearised observation (correction) equations for every point observed in every photograph. Correction equations for ground control points are the same as (II) in case of independent models. As in the case of block adjustment by independent models, $E\{\sigma_0^2\}$ can be assumed and variance covariance matrix of the parameters which include the corrections to the unknown terrain coordinates is 3 (ATPA)-1. The inverse of the 'p' matrix, in this case, is

$$p^{-1} = \sigma_x^2 I, \text{ where 'I' is the identity matrix and } \sigma_x = \sigma_y = 8 \mu\text{m}.$$

For orientation of a single model, we need consider only two photographs and the ground control. It can be directly treated as a simultaneous block adjustment by bundles and the same formulation as for block adjustment can be used.

REFERENCES

- |1| Ackermann, F.: "Experience of Block Triangulation by Independent Models"
- |2| Das, G.B.: "Aerotriangulation with Independent Models using Affine Transformation" paper presented to Ottawa Congress of ISP, 1972
- |3| Blais, J.A.R.: "Three-Dimensional Similarity", Canadian Surveyor, 1972
- |4| Oswal and Balasubramanian: "An Exact Solution of Absolute Orientation" Photogrammetric Engineering October 1968
- |5| Schut, G.H.: "Formation of Strips from Independent Models" N.R.C. Publication
- |6| Ebner, H.: "Theoretical Accuracy Models for Block Triangulation" Stuttgart University
- |7| Arur, M.G.: "Theory of Errors and Adjustment Computations" CST&MP (Survey of India) Publication
- |8| Ebner, H.: "The Theoretical Horizontal Accuracy of Adjustment of Blocks of upto 10 000 Independent Models" Stuttgart University
- |9| Ghosh, S.K.: "Theory of Stereophotogrammetry", Ohio State University Publication
- |10| Kraus K. and Mikhail E.M.: "Linear Least Squares Interpolation" Photogrammetric Engineering October 1972

AEROTRIANGULATION WITH INDEPENDENT MODELS AND ADJUSTMENT USING AFFINE TRANSFORMATIONS

by G.B. Das, V. Ramakrishnan, B.K. ManjappaRai, Hyderabad, India

ABSTRACT

In this paper a semianalytical method of aerotriangulation with Independent Models and adjustments is outlined using affine transformations for determination of perspective centre, linkage of models, absolute orientation and adjustments of strip and block.

INTRODUCTION

At present the normal methods of aerotriangulation with independent models use a similarity transformation expressed as the product of a scale factor and an orthogonal matrix. This orthogonal matrix is put in Cayley's form and approximate orientation elements are substituted. Such an assumption reduces the number of points required for linkage and orientation. However, the observations are not reduced because redundant points are observed and a least square fit is obtained. This procedure does not take care of any model deformation due to inaccuracy in relative orientation and other differential distortions due to film shrinkage etc., which are normally affine in nature.

It is therefore suggested that affine transformations of the type

$$\begin{aligned} x' &= a_{11}x + a_{12}y + a_{13}z + a_{14} \\ y' &= a_{21}x + a_{22}y + a_{23}z + a_{24} \\ z' &= a_{31}x + a_{32}y + a_{33}z + a_{34} \end{aligned}$$

be used instead of similarity transformations. Such a transformation will require four corresponding points out of which one may be selected as the origin for both the systems (x y z) and (x' y' z') so that $a_{14} = a_{24} = a_{34} = 0$.

Then the solutions of such equations can be conveniently handled on an electronic desk calculator with programming facility.

PERSPECTIVE CENTRE

As usual a grid or a diapositive is mounted with the plate kept horizontal. Three well distributed points are observed at two well separated levels L, L'. Then the coordinates in the two systems (x y), (x' y') are related by an affine transformation of the type

$$\begin{aligned} x' &= a_{11}x + a_{12}y + a_{13} \\ y' &= a_{21}x + a_{22}y + a_{23} \end{aligned}$$

After solving for a_{ij} the invariant point in the above transformation is obtained as solution of the characteristic equations

$$\begin{aligned} (a_{11} - 1) x_0 + a_{12} y_0 + a_{13} &= 0 \\ a_{21} x_0 + (a_{22} - 1) y_0 + a_{23} &= 0 \end{aligned}$$

(x_0, y_0, z_0) are the coordinates of the perspective centre, where x_0, y_0 are the solutions of the above equations and $z_0 = F.(L - L') + L'$, F being $(x' - x_0/x' - x)$. Following is an example worked out with data given in ITC exercise on independent model triangulation:

Point Nr.	x	y	x'	y'
3	381.35	411.78	385.22	520.71
4	498.27	410.23	605.28	517.88
5	373.19	192.13	369.86	107.41

$a_{11} = 1.88214$	$a_{12} = .0001$	$a_{13} = -332.53798$
$a_{21} = .00074$	$a_{22} = 1.88160$	$a_{23} = -254.37831$

Solution of equations

$$(a_{11} - 1) x + a_{12}y + a_{13} = 0$$

$$a_{21} x + (a_{22} - 1)y + a_{23} = 0$$

gives the x_0, y_0 coordinates of the perspective centre

$$x_0 = 376.97062$$

$$y_0 = 288.22522$$

The scale factor $F = 2.1338$ and $z_0 = f \times 140 + 10 = 308.74$. Hence the coordinates of the perspective centre are

$$(376.97, 288.23, 308.74).$$

LINK ORIENTATION

The linkage between successive models is achieved by a chain of affine transformations, the common perspective centre being the origin for both the systems of coordinates. The distribution of three pass points required should be such that two points will be on the flanks on one side and the third below the perspective centre on the other side. The longitudinal separation of this third point from the first two ensures a better linkage in the direction of flight.

Example:

With the input data from Schut's [7] example the following equations are obtained:

$$\begin{array}{rcl}
 (100) & -24.10 a_{i1} - 147.31 a_{i2} - 294.33 a_{i3} & = \begin{array}{l} -25.51 \\ -128.55 \\ -258.01 \end{array}
 \end{array}$$

$$\begin{array}{rcl}
 (47) & -1.68 a_{i1} + 5.33 a_{i2} - 291.44 a_{i3} & = \begin{array}{l} -2.62 \\ +4.83 \\ -255.65 \end{array}
 \end{array}$$

$$\begin{array}{rcl}
 (778) & -25.93 a_{i1} + 156.42 a_{i2} - 290.96 a_{i3} & = \begin{array}{l} -20.67 \\ +137.84 \\ -255.14 \end{array}
 \end{array}$$

Solving for a_{i1}, a_{i2}, a_{i3} $i = 1,2,3$ and substituting in (49)

$$-33.08 a_{i1} + 23.55 a_{i2} - 292.63 a_{i3}$$

the coordinates of point (49) are obtained as

$$-29.76, +21.47, -256.52$$

compared with the data

$$.29.77, +21.46, -256.51.$$

Whereas in Schut's example the residuals are as large as -0.27, -0.23 in height and 0.07, 0.08 in plan, in the affine solution, there are no errors and there is no scope for propagation of any due to residuals.

ABSOLUTE ORIENTATION

If there are four control points in the starting model, it can be oriented absolutely with respect to the ground by a set of affine transformations. If, however, the distribution is not good then the absolute orientation can be achieved after strip formation. For a good orientation, the four points should preferably be at the four corners of the model or strip. A fifth point in the centre of the area will be a good check for any systematic deformation.

Example:

The following is based on data from Schut's example. Instead of taking a single model the entire configuration of three models is considered. The points (1), (75), (217) and (195) are selected as control points and point (24) as the check point. The equations, with point (1) as origin, are

$$\begin{array}{rcl}
 (75) & - 4.31 a_{i1} + 263.95 a_{i2} - 4.92 a_{i3} & = \begin{array}{r} - 211.48 \\ -1564.72 \\ - 29.03 \end{array} \\
 (217) & +456.36 a_{i1} + 273.16 a_{i2} - 0.13 a_{i3} & = \begin{array}{r} -2911.63 \\ - 992.49 \\ - 17.95 \end{array} \\
 (195) & +425.35 a_{i1} - 41.02 a_{i2} - 1.19 a_{i3} & = \begin{array}{r} -2478.32 \\ + 624.60 \\ - 17.95 \end{array} \\
 \text{Check point:} & & \\
 (24) & + 69.61 a_{i1} + 122.37 a_{i2} - 2.10 a_{i3} & = \begin{array}{r} -521.49 \\ -661.10 \\ - 14.20 \end{array}
 \end{array}$$

agreed perfectly, whereas with similarity transformations this point had a residual error of the order of 0.15 in the transverse direction.

ADJUSTMENTS

For purposes of adjustments of strip or block it is assumed that affine parameters a_{ij} are continuous functions of the spatial situation. Further, if the number of bands of control points in a strip is n , then it is assumed that the affine parameters a_{ij} will fit into a curve of degree $n-1$, which is different for each a_{ij} .

Having obtained the transformation from model to ground the affine parameters for the models other than those in the control bands are corrected according to their situation in the strip.

In case the terrain is flatish or low undulating then the three dimensional affine transformation is not likely to yield stable solution and in such cases the two dimensional transformation in the planimetric coordinates will be found to be quite practical.

In photogrammetric plotting it is often found that with the control as supplied by aerial triangulation due to continuous transformation setting of individual models poses a problem. In view of this, for purposes of plotting the adjustments can be modified by polynomials in x and y where x may stand for strip and y for model and the block thus adjusted will be found to give consistency within each model separately.

Affine adjustment is recommended because in aerotriangulation with independent models there is no provision for correction of the various sources of errors and distortions and the minimum correction that can be assumed is of an affine nature. To assume a similarity transformation or conformal polynomial is to preserve the already introduced errors in angles because of the affine nature of distortion.

CONCLUSION

In normal strips and blocks one expects differential distortions and deformations which can be suitably corrected by assuming the transformations to be affine. With a medium sized computer or an electronic desk calculator affine transformations will be found quite handy and avoidable inaccuracies can be eliminated.

REFERENCES

- |1| Altenhofen R.E.: "Operational Use of Semi-analytical Aerotriangulation Programs", Symposium on Computational Photogrammetry, Gaithersburg, Maryland, USA, December 1967
- |2| Altenhofen R.E.: "Semianalytical Aerotriangulation in Quadrangle Mapping" Paper read at the 36th Annual Meeting of American Society of Photogrammetry, March 1968
- |3| Das G.B.: "Aerotriangulation with Independent Models by Monomorphic Transformations", Ohio State University, October 1970
- |4| Thosh S.K. and Morgan P.G.: "A Method of Block Triangulation with Independent Models", Ohio State University, July 1970
- |5| Inghilleri G.R.: "Further Developments of the Method of Aerotriangulation by Independent Models", Photogrammetria Vol. 22, No. 1, 1967
- |6| Klaver J.: "Semianalytical Aerotriangulation with the Kern PG 2" Symposium on Computational Photogrammetry, Gaithersburg, Maryland, December 1967
- |7| Schut G.H.: "Formation of Strips for Independent Models", Report AP-PR 36, N.R.C. Canada, July 1967
- |8| Thompson E.H.: "Aerial Triangulation by Independent Models", Photogrammetria Vol.19, No. 7, 1962 - 64

BUNDLE BLOCK ADJUSTMENT FOR BLOCKS OF LIMITED SIZE IN ORDER TO DENSIFY TRIGONOMETRIC NETS

by A. Verdin, Brussels, Belgium

SUMMARY

The "Institut Géographique Militaire" in Brussels (IGM) employs the numerical photogrammetry in order to determine planimetric and altimetric control points on the photographs used for the revision of the general map of Belgium at the scales of 1 : 10 000 - 1 : 25 000, or for special works at scales of 1 : 5 000 - 1 : 10 000.

This paper shows the adopted methods in relation with the typical conditions existing in the IGM. The density and the regular distribution of the trigonometric points in Belgium allows the use of little size blocks (30 photographs maximum).

Besides analogical models observed on stereoplotters, the IGM more and more employs observations of perspective bundles, made with the stereocomparator SOM. A cheap iterative procedure of bundle block adjustment has been programmed on the computer terminal of the IGM, for blocks of limited size with a regular density of 1 control point every two or three photographs (inside and on the borders of the blocks). In the future, this procedure will be completed by a direct method applied when the density of control is not sufficient to obtain a good convergency of the iterative procedure.

INTRODUCTION

L'activité de l'Institut Géographique Militaire de Bruxelles dans le domaine de la photogrammétrie numérique s'exerce en grande partie dans le cadre particulier de la révision de la carte de base de la Belgique aux échelles du 1/10.000 et 1/25.000.

Dans les régions en évolution rapide, il est souvent nécessaire de reconstituer en vue de la restitution un canevas de points de contrôle planimétrique complet. Certains travaux spéciaux demandent également la reconstitution d'un canevas de contrôle altimétrique valable.

PROGRAMMES DE ROUTINE HABITUELS

Autant que possible, ces nouveaux points de contrôle sont observés sur les clichés originaux de la première couverture photogrammétrique exécutée entre 1950 et 1968, dont les couples ont été préparés directement par voie topographique. Ces couples de clichés sont observés de préférence sur instruments analogiques. Les points nouveaux à déterminer sont obtenus en appliquant les formules classiques de transformation spatiale d'orientation absolue, calculées sur la base du canevas de préparation ancien.

Si la mise en place de ces clichés est devenue impossible sur les instruments analogiques disponibles (c'est le cas par exemple des clichés sur plaques SOM - 18 x 18 cm), la détermination se fait à partir des observations sur stéréocomparateur. Les observations corrigées des erreurs de distorsion, de courbure de terre et de réfraction permettent la reconstruction de modèles calculés, dont l'orientation absolue est effectuée à partir du canevas de points connus.

Ces solutions classiques donnent les meilleurs résultats. Les deux programmes d'orientation relative et d'orientation absolue ont été retranscrits en langage FORTRAN et sont couramment utilisés sur ordinateur IBM 370/155 à partir du Terminal IGM.

CONDITIONS DE TRAVAIL PROPRES A L'IGM

Il devient cependant de plus en plus difficile, vue l'évolution rapide de l'environnement de sélectionner avec certitude sur deux couvertures photographiques différentes d'une même région, des points de contrôle inchangés communs à deux prises de vues éloignées de plus de 15 ans dans le temps.

C'est pourquoi le procédé indiqué ci-dessus devient de plus en plus aléatoire. D'autre part, les coûts grandissants des travaux topographiques imposent de rechercher par voie photogrammétrique une solution avantageuse au problème de la

création ou de la densification d'un canevas de points de contrôle. Il importe donc de tirer parti au maximum des points connus du réseau géodésique et topographique. Ce réseau de points se présente très favorablement en Belgique. Outre le réseau fondamental de points trigonométriques constitué en général de points élevés utilisables pratiquement en photogrammétrie comme contrôle planimétrique seulement, les services terrain de l'IGM déterminent sur chaque feuille de la carte un réseau de points de contrôle au sol connus en plan et en altimétrie dont la répartition est en principe tout à fait homogène et dont la densité est de l'ordre de 1 pt par 10 km². Ces points peuvent être directement identifiés sur photographies, ou balisés avant la prise de vues. Ils permettent de plus le levé immédiat d'un détail photogrammétrique dans leur voisinage.

La densité et la répartition du type de contrôle permanent ainsi constitué sur la couverture photographique (1 point pour 1 photo et demie ou pour 2 photos) exigent l'utilisation des méthodes photogrammétriques numériques les plus précises pour la compensation des blocs de photographies. L'homogénéité dans la répartition des contrôles terrain permet de se limiter à des blocs photogrammétriques de faible dimension (30 photos au maximum pour les échelles couramment adoptées à l'IGM pour des surfaces de 16 x 10 km).

On évite ainsi le traitement de système d'équations d'observations démesurément grands et les solutions adoptées peuvent être envisagées suivant les routines de calcul IBM disponibles.

Les méthodes de compensation des blocs doivent être les plus générales et permettre l'emploi de points de contrôle connus en coordonnées (X, Y, Z), (X, Y) ou Z uniquement.

SOLUTIONS ADOPTÉES POUR LES OBSERVATIONS ET LA COMPENSATION DES BLOCS

- OBSERVATIONS

S'il s'agit de modèles analogiques, les observations sont effectuées soit par modèles indépendants sur A8, soit classiquement par bandes sur A7. On veillera à assurer aux couples observés une orientation absolue très approchée (en α seulement sur A8) en tenant compte du contrôle altimétrique tiré de la carte de base.

Si les observations sont effectuées sur stéréocomparateur, on procédera soit à l'observation cliché par cliché des faisceaux photographiques sur toute leur surface.

Les observations sont alors présentées et exploitées comme des observations sur monocomparateur, mais l'observation de chaque détail est faite en vision stéréoscopique, à moins qu'il ne s'agisse d'un point matérialisé au sol. Ce procédé d'observation est praticable sur le stéréocomparateur SOM de l'IGM ou sur comparateur Nistri à 3 plaques.

- COMPENSATION

La détermination d'un réseau de points planimétriques s'effectue, en général, à partir des observations sur instruments analogiques. L'IGM utilise un procédé de compensation calculé de bloc analogique planimétrique, similaire au procédé An-Block. Les systèmes d'équations d'observations sont résolus aisément sur l'ordinateur 370/155.

Pour la détermination d'un réseau de points planimétriques et altimétriques, l'IGM avait le choix entre la compensation de blocs de modèles indépendants ou la compensation par faisceaux perspectifs.

Sans exclure a priori le premier procédé, l'IGM s'est orienté particulièrement vers les faisceaux perspectifs pour les raisons suivantes:

- a) facilité et précision des observations par faisceaux sur le stéréocomparateur SOM;
- b) standardisation des procédés d'observation. Le service du cadastre belge demande également à l'IGM, pour ses besoins personnels, des observations de coordonnées instrument sur l'entièreté de la surface du cliché, en vue du relèvement spatial et du redressement perspectif calculé des clichés aériens.

Il va de soi que l'observation est aidée dans l'instrument par le pointé stéréoscopique de chaque détail;

- c) élimination sur la surface totale du cliché des erreurs de distorsion, de courbure de terre et de réfraction;
- d) disponibilité et précision de données terrain approchées fournies par la carte de base, avec un écart-type moyen planimétrique $\sigma_p = 2$ m, altimétrique $\sigma_z = 1$ m;
- e) faculté de réalisation d'un programme unique qui partant des coordonnées cliché observées, fournit directement la solution du block en coordonnées absolues terrain, sans stades intermédiaires de calcul;
- f) détermination de la précision de chaque point intersecté, à partir de 2 ou plusieurs sommets à chaque tour de calcul, en vue d'une élimination rapide des erreurs grossières du levé (voir programme A 50 ci-après).

PROGRAMMES PARTICULIERS DE COMPENSATION DE BLOCS DE FAISCEAUX PERSPECTIFS

- PROGRAMME ITERATIF A 50

Ce programme a été établi en suivant le programme itératif de l'IGN de Paris. Les données de départ sont constituées par les coordonnées cliché des points observés par faisceaux, après correction des erreurs de déformation du support de l'émulsion en fonction des données de calibration de la chambre de prise de vues.

Dans le programme A 50, les données de départ sont tout d'abord corrigées des effets de la distorsion, de courbure de terre et de réfraction. La partie itérative du programme se décompose comme suit:

- a) relèvement séparé de chaque gerbe perspective sur points terrain connus (contrôle) ou approchés, par le procédé IGN de Paris. On attribuera un poids beaucoup plus important aux équations d'observation relatives aux points de contrôle;
- b) calcul de la matrice spatiale de rotation propre de chaque gerbe perspective et application aux coordonnées cliché, de cette rotation autour des centres de projection;
- c) intersection de tous les rayons correspondants à un point commun à deux ou plusieurs gerbes perspective. Le procédé utilisé est basé sur la détermination du point dont la somme des carrés des distances à chaque rayon perspectif est minimale. Il a été programmé à l'IGM de Bruxelles à l'occasion du calcul des coordonnées des centres de projection d'un instrument analogique en vue de la triangulation par modèles indépendants;
- d) calcul en chaque point des distances à chacun des rayons utilisés pour l'intersection. L'examen de ces distances permet la détection rapide d'une erreur grossière commise sur l'observation d'un point sur un cliché déterminé et la correction ou l'élimination de cette erreur.

Les résultats du premier tour de calcul sont toujours imprimés. Pour passer aux stades suivants du calcul itératif, les coordonnées approchées des points utilisés pour les relèvements sont modifiées en utilisant les nouvelles valeurs trouvées par l'intersection des rayons perspectifs, tout en veillant à conserver inchangées les coordonnées des points de contrôle du bloc et l'on repart en par. a) pour le 2ème tour ou les suivants.

Pendant la compensation du bloc, appuyé sur un certain nombre de points de contrôle, on demande l'impression des résultats tous les 15 tours de façon à vérifier la convergence du procédé.

Ces résultats sont imprimés dans l'ordre suivant:

- matrices de rotation de chaque gerbe perspective,
- coordonnées des centres de projection,
- coordonnées cliché transformées après rotation dans un système local rapporté au centre de projection de chaque cliché,
- coordonnées des points intersectés et distances de ces points à chacun des rayons perspectifs utilisés pour l'intersection.

Le procédé est bien convergent, pour une densité suffisante des points de contrôle, par exemple, si la distance entre points de contrôle ne dépasse pas trois fois la longueur de la base des couples formés par les gerbes perspect-

ives se monte pour 46 itérations effectuées sur le terminal de l'IGM à environ 5 000 francs belges.

- PROCÉDE DIRECT

Il est nécessaire d'envisager le cas d'une densité des points de contrôle plus faible ou le cas des feuilles de la carte dont le canevas des points au sol n'a pas encore été réalisé. Le procédé itératif devra être remplacé par une compensation d'ensemble directe de tous les faisceaux perspectifs en bloc. Rappelons les limitations imposées à la dimension des blocs (30 clichés maximum) et la possibilité de disposer de valeurs approchées initiales valables ($\sigma_p = 2$ m, $\sigma_z = 1$ m).

L'IGM cherche à résoudre le problème du bloc, en généralisant un procédé d'orientation relative et absolu simultané expérimenté sur un couple de photographies. Le procédé est basé sur les relations de colinéarité des rayons objet et image dans chaque faisceau.

Si (X_p, Y_p, Z_p) sont les coordonnées approchées du point P, (x_p^i, y_p^i, z_p^i) les coordonnées cliché obtenues éventuellement après une rotation κ_0 approchée initiale, λ_p^i le facteur d'échelle relatif au rayon issu de P dans le faisceau d'ordre i, on obtient en attribuant des corrections (dX, dY, dZ) aux coordonnées terrain (dX_0^i, dY_0^i, dZ_0^i) aux coordonnées des sommets, $d\lambda_p^i$ aux facteurs d'échelle et une rotation élémentaire $(d\omega_i, d\phi_i, d\kappa_i)$ au faisceau i de sommet (X_0^i, Y_0^i, Z_0^i) :

$$\begin{vmatrix} X_p + dX_0 \\ Y_p + dY_0 \\ Z_p + dZ_0 \end{vmatrix} = \begin{vmatrix} X_0^i + dX_0^i \\ Y_0^i + dY_0^i \\ Z_0^i + dZ_0^i \end{vmatrix} + (\lambda_p^i + d\lambda_p^i) \begin{vmatrix} 1 & -d\kappa_i & d\phi_i \\ d\kappa_i & 1 & -d\omega_i \\ -d\phi_i & d\omega_i & 1 \end{vmatrix} \begin{vmatrix} x_p^i \\ y_p^i \\ z_p^i \end{vmatrix}$$

c.a.d., si on néglige les termes de 2ème ordre, un système d'équations linéaires d'observations relatives aux rayons de l'ensemble des deux gerbes perspectives:

$$\begin{vmatrix} v_x \\ v_y \\ v_z \end{vmatrix}_p^i = \begin{vmatrix} 0 & -\lambda_p^i z_p^i & \lambda_p^i y_p^i & -x_p^i \\ \lambda_p^i z_p^i & 0 & -\lambda_p^i x_p^i & -y_p^i \\ -\lambda_p^i y_p^i & \lambda_p^i x_p^i & 0 & -z_p^i \end{vmatrix} \begin{vmatrix} d\omega_i \\ d\phi_i \\ d\kappa_i \\ d\lambda_p^i \end{vmatrix} + \begin{vmatrix} dX_p \\ dY_p \\ dZ_p \end{vmatrix} - \begin{vmatrix} dX_0^i \\ dY_0^i \\ dZ_0^i \end{vmatrix} + \begin{vmatrix} X_p - X_0^i - \lambda_p^i x_p^i \\ Y_p - Y_0^i - \lambda_p^i y_p^i \\ Z_p - Z_0^i - \lambda_p^i z_p^i \end{vmatrix} \quad (1)$$

Pour fixer les points de contrôle terrain, on introduit, à côté du système (1) les équations d'observations suivantes pour chaque donnée terrain de contrôle (planimétrie et/ou altimétrie), en attribuant à ces équations un poids largement supérieur aux équations (1):

$$\begin{vmatrix} v_x \\ v_y \\ v_z \end{vmatrix}_p = \begin{vmatrix} dX_p \\ dY_p \\ dZ_p \end{vmatrix} \quad (2)$$

La solution d'ensemble des systèmes (1) et (2) fournit les corrections:

$(d\omega_i, d\phi_i, d\kappa_i)$, (dX_0^i, dY_0^i, dZ_0^i) , $d\lambda_p^i$ et (dX_p, dY_p, dZ_p) .

Adoptons les valeurs corrigées :

$$\begin{aligned} & \lambda_p^i + d\lambda_p^i, \\ & (X_p + dX_p, Y_p + dY_p, Z_p + dZ_p), \\ & (X_o^i + dX_p^i, Y_o^i + dY_o^i, Z_o^i + dZ_o^i) \end{aligned}$$

$$\begin{vmatrix} x_p^i \\ y_p^i \\ z_p^i \end{vmatrix}_{\text{cor}} = R_{\omega_i \phi_i \kappa_i} \begin{vmatrix} x_p^i \\ y_p^i \\ z_p^i \end{vmatrix}$$

Elles vérifient les relations de colinéarité si les matrices orthogonales $R_{\omega_i \phi_i \kappa_i}$ sont pratiquement identiques à leur forme linéarisée, c'est-à-dire si (ω, ϕ, κ) sont petits.

Il vient alors:

$$\begin{vmatrix} X_p \\ Y_p \\ Z_p \end{vmatrix}_{\text{cor}} = \begin{vmatrix} X_o^i \\ Y_o^i \\ Z_o^i \end{vmatrix}_{\text{cor}} + \lambda_p^i \begin{vmatrix} x_p^i \\ y_p^i \\ z_p^i \end{vmatrix}_{\text{cor}} \quad (3)$$

Si tel n'est pas le cas, c'est-à-dire si les données initiales angulaires ne sont pas suffisamment approchées, il faut prévoir une ou deux répétitions des calculs à partir des valeurs corrigées, ce qui en accroît fortement les coûts.

Une manière aisée d'obtenir des valeurs initiales très approchées pour les angles (ω, ϕ, κ) c'est-à-dire également pour les coordonnées (x_p, y_p, z_p) est d'effectuer un calcul préliminaire du bloc par le programme A 50 (10 itérations par exemple). Ainsi, on disposera de valeurs approchées précises pour toutes les inconnues du système, tout en se réservant la possibilité d'éliminer toute erreur grossière avant la compensation directe finale. On réalise ainsi une grosse économie de temps et d'argent.

Un bloc de 30 photographies comportant chacune environ 10 points observés ou un total de 100 points à déterminer conduirait à la compensation simultanée de 900 équations d'observation à environ 780 inconnues, à savoir

30 x 6 éléments des gerbes perspectives (coordonnées sommet et angles de rotation)

30 x 10 facteurs d'échelle λ_p^i

100 x 3 coordonnées (X, Y, Z) terrain.

Le procédé direct de compensation de bloc envisagé ci-dessus conduit à des systèmes comportant des équations d'observation plus nombreuses que les systèmes adoptés généralement puisque chaque point dans chaque faisceau donne lieu à 3 équations au lieu des 2 équations obtenues habituellement en traitant les coordonnées réduites $(x/z, y/z)$.

Cependant les équations sont par elles-mêmes beaucoup plus simples et comportent de nombreux coefficients égaux à l'unité.

Le procédé est en voie de programmation systématique pour les blocs limités traités à l'IGM.

PROGRAMMES DE PHOTOGRAMMETRIE NUMERIQUE DE L'IGM DE BRUXELLES

- a) Orientation absolue (procédé itératif
(procédé direct de Tienstra
- b) Triangulation analytique: orientation relative et enchaînement des modèles
- c) Bloc planimétrique analogique
- d) Triangulation par modèles indépendants - enchaînement des modèles par bandes
- e) Compensation de bandes par polynômes
- f) Programme A 50: calcul itératif d'un bloc de faisceaux perspectifs
- g) en cours de programmation, méthode directe de compensation d'un bloc de faisceaux perspectifs

BIBLIOGRAPHIE

- |1| Créhange, A.: "Théorie de l'aérot triangulation analytique", Ministère des Travaux Publics et des Transports, France
- |2| Ackermann, F., Ebner, H., Klein, H.: "Aérot triangulation mit unabhängigen Modellen" Bildmessung und Luftbildwesen, Juli 1970
- |3| Verdin, A.: "La relèvement dans l'espace et ses applications", Bulletin trimestriel de la Société Belge de Photogrammétrie No 103 Juin 1971
- |4| Verdin, A.: "Du relèvement spatial à la compensation de blocs de gerbes perspectives", Bulletin de la Société Belge de Photogrammétrie Mars-Juin 1974

INDEPENDENT MODEL TRIANGULATION WITHOUT USING PERSPECTIVE CENTRES COORDINATES

by R. C. Badjatia, Roorkee, India

Determination of coordinates of perspective centres of the instrument is known to be an important operation for performing independent model triangulation. In Kern PG-2, PG-3 and Planimat, it is possible to record the perspective centres coordinates directly with the help of certain special devices. However, in other instruments procedures like space resection etc. are to be followed which involve substantial increase in operation and computation time. In most of the cases perspective centres coordinates must be determined for each model or at least after an interval of 4 to 5 models, unless it is assumed that the coordinates of the perspective centres as determined for the first model do not change, and can be used for other models of the strip. In such cases also the base must be kept constant and the instrument system must remain undisturbed.

The above assumption also cannot hold if the cameras in the instrument do not rotate precisely about their corresponding perspective centres during relative orientation phase. Even if the coordinates of the perspective centres can mechanically be kept constant, it may become necessary to change the base intentionally in the case where the z-range of the particular instrument cannot accommodate large height differences.

The attempt of this paper is to study the possibilities of avoiding determination of perspective centres coordinates during independent model triangulation, thereby saving operation and computation time, avoiding restrictions of constant base and of constant instrument system.

Considering that relative orientation of models in independent model triangulation is achieved at its best and that no further analytical refinement is to be attempted, the important computational part is absolute orientation of one model with respect to the other model i.e. the connection of models. It is here that the use of perspective centres coordinates is made. It is generally considered that the connection of models will be weak if the common perspective centre is not used as one of the tie points. In other words the absolute orientation parameters will not be correctly determined without including perspective centre during model connection. It is desirable, therefore, to examine the determination of absolute orientation parameters during model connection viz determination of scale factor, rotation matrix and shifts.

During model connections the origins of both the model systems are shifted to a common control point in the two systems thereby eliminating the shifts. The common point is generally the perspective centres when this is used as a tie point. When perspective centre is not to be used any other control point will serve the purpose. Hence determination of shifts is not a problem. This leaves only the scale factor and the rotation matrix to be determined.

In a relatively oriented model produced from two consecutive photographs, the geometrical relations between points or lines on the model are exactly the same as between corresponding points or lines in the actual terrain e.i. the model is a rigid body scaled down by a certain factor. Determination of scale factor is possible without the use of perspective centre coordinates, by comparing distances between various control points in the two models and obtaining a mean value. In fact if one is not sure about the stability of the perspective centres in the instrument, its use for determining scale factor should be avoided. The scale factor determination, therefore, is also no problem when perspective centre is not to be included.

The orientation of a model can be changed at will, by the application of an orthogonal transformation, without including the perspective centres in the transformation. As such it does not appear necessary to use perspective centre as one of the tie points for determining the rotation matrix connecting the two models. If all the control points (three or four in number) are situated in the model space, Schut's method of absolute orientation [1] may be successfully used for determining the rotation matrix. The points should have a maximum separation in x, y and z. In the worst case, even if the points form a plane surface in the model space Schut's solution does not fail as is evident from one of the recent papers of Schut's [2]. In this paper it is shown that Oswal and Blais' methods fail to give solution when the control points form a plane surface, whereas Schut's method provides satisfactory results.

Model connection, an important process of independent model triangulation, can thus be carried out without using perspective centre coordinates. The three control points in this case lie in the model surface. It may be desirable to select four points for model connection symmetrically situated and forming a rectangle in the superlap area. The superlap area for model connection is quite sufficient to have a rectangle of four pass points located as far apart as possible. If the photographs have 60 % longitudinal overlap, the superlap area is about 33 % of the total overlap area. The size of rectangle of points is about $0.15 l \times 0.75 l$, if l is the format size. If the overlap of the photographs is 70 % the superlap will be about 57 % of model area and the rectangle size will be $0.33 l \times 0.75 l$.

To check the validity of above arguments experiments were conducted. Instead of independent model triangulation the procedure was first tested by performing analytical aerial triangulation of hypothetical strips.

Two strips of 13 photograms each (12 models) was triangulated. The strips were of hypothetical photograms [3] having following specifications:

- 1) - modestly rolling ground with height differences 5 % of flying height.
- 2) - mountainous terrain with height differences 25 % of flying height.

Format 18 x 18 cm, focal length = 115.0 mm, precision of image coordinates ± 0.01 microns, overlap longitudinal 65 %.

The image coordinates and other data for hypothetical photograms were available at the University.

Analytical relative orientation of various models was done using single centre method (Ordnance Survey). Model connection was done using Schut's method of absolute orientation [1] without using perspective centres coordinates. Four points were used in the model space forming a rectangle. Strip formation was done using ordnance survey method. The strip was transformed to the ground system by Schut's absolute orientation method using 6 ground control points. The strips required no further adjustment.

Necessary computer programmes were developed for computations on IBM 1620 and all the computations were done on the same. The results obtained were as follows:

	Mean standard error in microns		
	x	y	z
Strip I Hypothetical	7.3	5.9	3.9
Strip II Hypothetical	4.3	5.5	3.5

The results above indicate that the analytical aerial triangulation without perspective centres coordinates for model connection can be performed successfully. The experiments for performing independent model triangulation without using perspective centres coordinates are in progress but incomplete at the time of submission of this paper and could not be included here. The results are expected to be favourable.

REFERENCES

- [1] Schut, G.H.: "Formation of Strips from independent models", Photogrammetric Engineering, Vol. 34, No. 7, July 1968
- [2] Schut, G.H.: "Similarity Transformation and Least squares", Photogrammetric Engineering, Vol. 39, No. 6, June 1973
- [3] Oswal, H.L.: "Developments in analytical exterior orientation including the generation of analytical photogrammetric blocks", Ph. D. Thesis Civil Engineering Department, University of Roorkee, 1969

GEOMETRIC CORRECTION OF ERTS-1 MSS IMAGES

by R. B. Forrest, Southfield, Michigan, USA

ABSTRACT

ERTS-1 images have three levels of accuracy, corresponding to the effort applied to processing. All images are system corrected to give 750 meters circular standard error. A selected 5 to 10 percent are processed further, reducing the error to about 100 meters. Research indicates that the limiting error is less than 40 meters. ERTS image processing equipment and imaging models are discussed.

INTRODUCTION

This paper discusses the geometric accuracy of multispectral scanner (MSS) images collected by the first Earth Resources Technology Satellite, ERTS-1. The specific application may not be of particular interest to many who work with aerial imagery, since positional ERTS-1 errors of tens of meters are involved. However, many of the matters discussed are of fundamental concern to the metric use of line-scanner images.

The ERTS-1 satellite has been extensively discussed in both popular and technical media [1], [2], [3]. Only those aspects of special concern will be summarized here. The satellite orbit has an inclination of 81 degrees and is designed to remain in a sun-synchronous orbit - each southbound pass occurs at local solar midmorning. Passes repeat every 18 days (Figure 1). Images are collected by a four-channel Hughes multispectral line scanner (the MSS) and by an array of three spectrally filtered RCA return-beam vidicon (RBV) cameras. The MSS images a continuous strip of imagery 185 km wide, centered on the satellite ground track. The RBV cameras produce central-perspective framed images 185 km square with 10 to 15 percent overlap. Image sidelap between adjacent orbital passes is about 14 percent at the equator and increases with increasing latitude. The image data, together with other satellite performance data, are telemetered to ground receiving stations, where all data are recorded on magnetic tape. Images are reconstructed on photographic film later from the tape data. For some uses, magnetic tape is more desirable as a data medium.

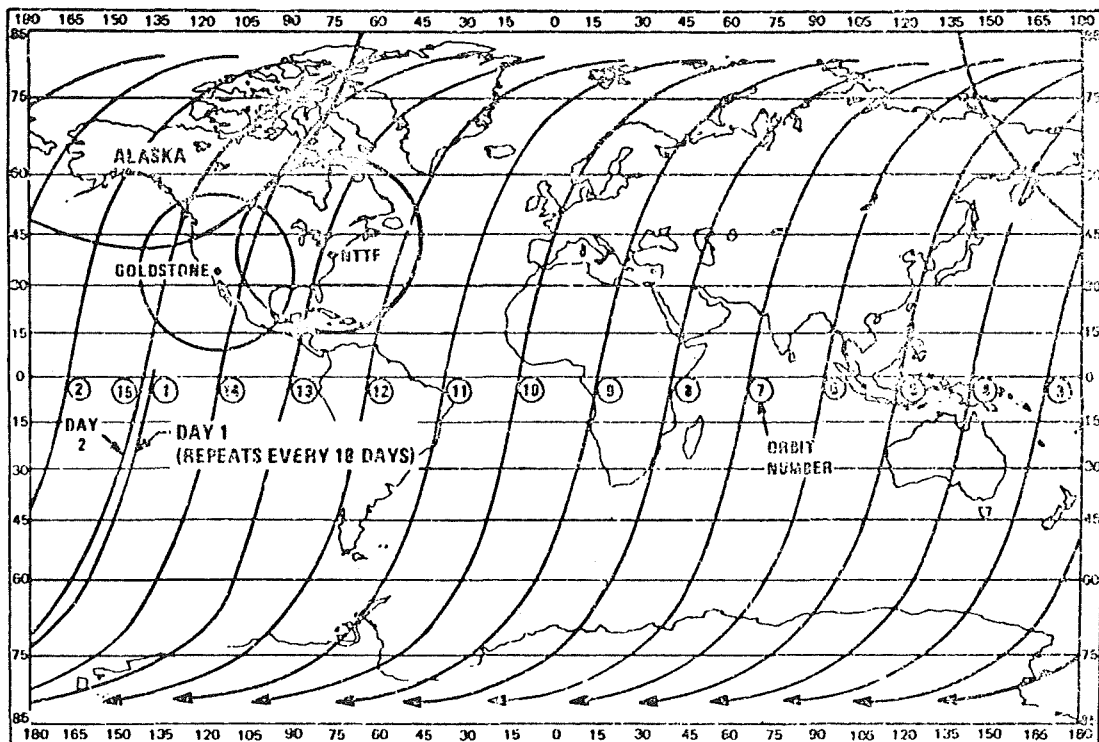


Figure 1: Typical ERTS Ground Trace for one day (only Southbound Passes shown)

Because of technical difficulties on board the satellite, the RBV camera array has not been used extensively; nearly all images have been obtained by the MSS sensor alone. This discussion will be largely limited to the MSS images. The MSS sensor has proven to be unexpectedly durable and stable, and has far surpassed all expectations for its performance. Tens of thousands of these images have already been collected by ERTS-1 during its two years of operation.

Each earth scene imaged by ERTS-1 includes four MSS images, one in each of four spectral bands. To perform multispectral analysis, the image data from all bands must be accurately registered. Much analysis is done using the data on magnetic tape, for which band registration is rigorously enforced by the geometry of the MSS sensor and the method of digital data processing. Some investigators use film images, often color composites of three spectral bands. Extreme care is needed during film recording to maintain image registration. Absolute positioning of the images on the earth's surface is also important. This permits temporal analysis using successive ERTS-1 images of the same locale, and also simplifies comparison of other types of source data with the ERTS images.

At the Goddard Space Flight Center NASA facility in the United States, thousands of MSS images each week are recorded on film from magnetic tape. Other facilities in Canada and Brazil perform similar operations, although their production is lower. As the images are printed on photographic film, systematic geometric and radiometric corrections are applied to that positionally accurate registered images of high radiometric fidelity are produced. All ERTS-1 images are processed in this way to give the basic film products, variously called production images, system-corrected images, or bulk-processes images. To obtain an image product with improved positional accuracy, a selected number of the bulk images can be given additional treatment with a sequence called precision processing. The procedure gives increased accuracy by using the geographic positions of map details which can be identified in the bulk images. The resulting film products are called scene-corrected or precision-processed images.

The precision images still contain on the order of 100 meters circular standard error. Recent research at Bendix Research Laboratories indicates that much of this error can be removed by more intensive processing techniques.

This paper is primarily concerned with the three different levels of geometric accuracy (bulk-processed, precision-processed, and intensive-processed), the equipment entailed, and the prospects for improvement. The discussion of film recording techniques applies in general to the NASA, Canadian, and Brazilian facilities, except as otherwise mentioned; specific details may differ slightly.

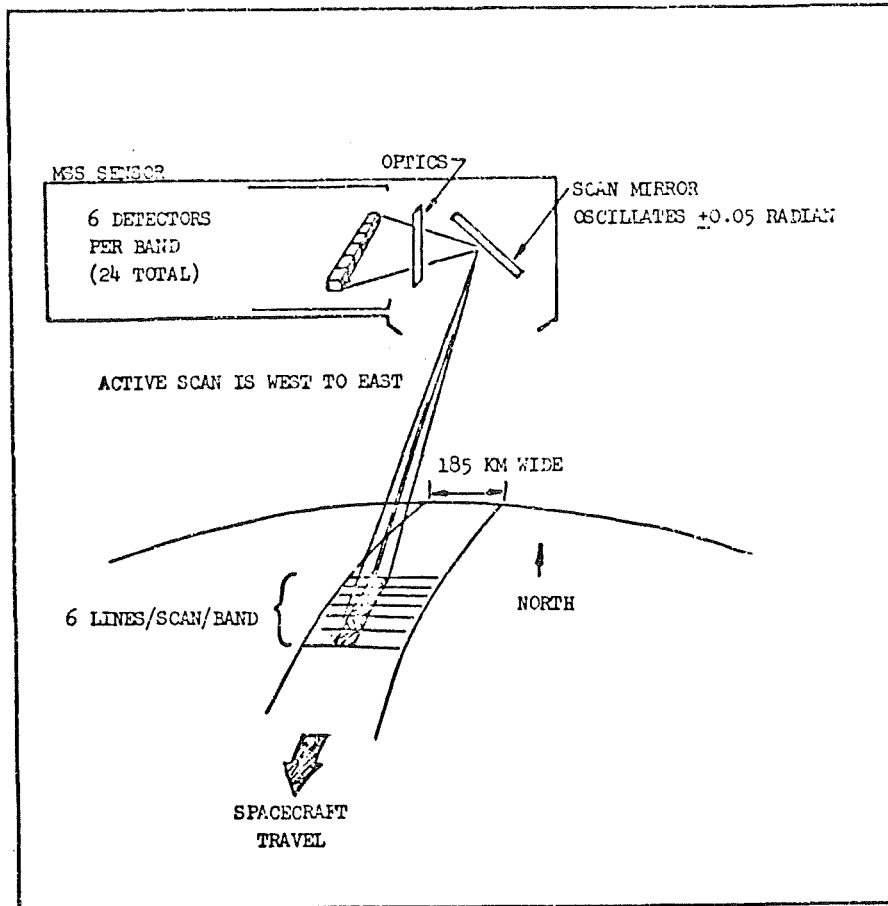
MSS SENSOR

Two of the four MSS spectral bands are in the visible, and two in the near infrared portion of the spectrum. The geometry of an aerial line scanner has been described previously by Derenyi and Konecny [4]. If provisions are made for earth curvature and rotation many of these same considerations are also valid for the ERTS-1 MSS scanner.

A single-line scanner by itself provides only one image dimension. Usually a rotating faceted mirror is used to perform the scanning of the earth image past the sensing element or elements. The ERTS-1 scanner [5] uses a single pivoted mirror, rocking back and forth through 0.1 radian 13 times per second. As shown in Figure 2, six consecutive scan lines are imaged in a single mirror sweep. Thus 24 separate sensing elements are needed in the image plane of the scanner, 6 detectors for each of the 4 spectral bands. On the ground, the instantaneous field of view for each detector element is a square 79 meters on a side. During a single west-to-east sweep of the mirror, the detected radiation at each detector is quantized at 1 of 64 values every 10 microseconds, corresponding to a ground translation of 56 meters in the direction of scan. Thus one mirror sweep collects a swath of six scan lines, covering 474 meters by 185 km and including about 20 000 picture elements or "pisels", 56 by 79 meters, for each of the four spectral bands. A single swath is collected in about 0.033 second.

The mirror velocity changes somewhat during the active part of the scan, and since the detectors are sampled at fixed time intervals a small nonlinearity of scan angle versus time is introduced. Although largely systematic, some changes have been noted during the operational life of ERTS-1.

Figure 2



The forward movement of the scanner platform provides the extended second dimension of a scanner image. Metrically, a satellite has an advantage over an aircraft as a scanner platform [6], because attitude and velocity changes are much smoother. The scanner image requires lower-order geometric adjustments over longer distances.

MSS images are not printed on film in continuous strips as they are obtained; instead they are recorded as individual frames 185 km square, with coverage and format chosen to match that of the RBV images. As will be seen, the geometry of an MSS frame is intentionally changed during film recording to be that of a secant-plane perspective projection (neglecting terrain relief effects) with mean scale of 1 : 3 370 000.

Theoretically, all spectral channels of the same scanner pixel are imaged and recorded at the same time. (This is not strictly true, but the delays are fixed and compensated during image processing). Geometrically, any one of the four spectral bands is like any other. Digital image data has inherent registration between spectral bands. When registering film images of different spectral bands (as would be done in making a color composite, for example), misregistration results from instabilities in film and film-recorder operation. These instabilities must be kept to a minimum for successful multispectral film analysis.

BULK IMAGE PROCESSING

Film Recorder

Over 1000 bulk ERTS-1 images can be produced daily by the NASA facility, converting the serial MSS sensor signals on magnetic tape into high-resolution film. All present ERTS-1 facilities create bulk images on 70 mm film using an electron beam recorder (EBR). This device operates in a basically analog manner: a high-energy electron beam exposes the film directly, scanning a series of lines across

the film. As it scans, the beam intensity is modulated by the sensor data stored on magnetic tape. The basic deflection pattern of the beam is supplied by the internal controller of the EBR. Additional deflection and intensity adjustments are applied through a special interface controlled by a digital computer. The adjustments provide desired geometric alterations, and are in part based on calibration measurements of previous bulk images. An important advantage of electron-beam recording over visible-light methods is the ease with which the beam can be rapidly deflected to make positional image corrections during printing. It is difficult to over-emphasize the tremendous significance of these transformation-printing techniques in image-data processing. The original image data can be re-mapped and presented in virtually any desired geometry.

The EBR also exposes the individual characters of annotation information which appear around the edges of the bulk image. Corner registration marks, geographic coordinate ticks, and alphanumerics are printed. Internal geographic coordinate intersections are not shown to avoid obscuring image information.

Bulk Image Geometry

Although it does not appear in the bulk image, positional reference is based computationally on a square image border. This border is considered to be centered on the earth's surface at a location determined from the satellite ephemeris and the telemetered satellite pitch and roll. The border is not oriented with north at the top, but at an azimuth determined by satellite heading plus the telemetered satellite yaw angle. For most ERTS-1 images the border is rotated east of north by 9 to 15 degrees. All MSS and RBV images in the same scene (a scene is an image set of the same 185 km square on the earth collected at the same time) use the same earth-surface location for the border. The border always is the same size on the earth, about 190 by 202 km. The additional dimensions allow individual images of the same scene to be slightly shifted during film recording to compensate for slight misalignments between the different image sensors. Registration is done by aligning border ticks or the four corner registration marks.

As the film recorder exposes an MSS image for one of the four spectral bands within the image border, extensive geometric corrections are applied to the scanning electron beam. Without such adjustments, each successive MSS six-line image swath would be exactly aligned with its neighbors to create a rectangular image. While the resolution and general appearance of such an image would be acceptable, it would be considerably distorted from the desired perspective projection.

The major distortion is caused by earth rotation. During the 28 seconds required to image 185 km along the satellite ground-track, the earth rotates 7 minutes of longitude eastward beneath the orbital plane. The earth-surface area covered by the resulting scanner frame is not a square, but approximately a rhombus (see Figure 3). Maximum deviation from orthogonality is about 4 degrees and occurs at the equator. To remove this distortion, the EBR must displace successive image toward the west edge of the image.

The correction is implemented by applying small correcting deflections to the electron beam during film recording. The magnitudes of these deflections are determined by the bulk-processing control computer, based on the spacecraft ephemeris and the known time at which the bulk image was sensed. The exact amounts of deflection are computed only for 81 image points, spaced uniformly inside the image border in a 9 by 9 grid, called the EBR image Correction (EBRIC) grid. When the bulk image is being printed, an interface between computer and EBR controls the application of the EBRIIC deflections. Beam deflection is linearly interpolated between points in the EBRIIC grid. All geometric adjustments use the grid, summing individual corrections to obtain the composite adjustment at each grid point. The attitude and altitude values at the center of the MSS frame are used as references. Away from the frame center, correcting deflections are added to the EBRIIC grid adjustments depending on the amount of change and the effect on EBRIIC grid-point location. The shapes of the different image distortions are shown schematically in Figure 3. The Canadian and Brazilian facilities use a much more dense EBRIIC grid, 32 by 32 points. The greater number of points followed from the desire to eventually apply terrain corrections to the images as they are printed, although this has not yet been realized.

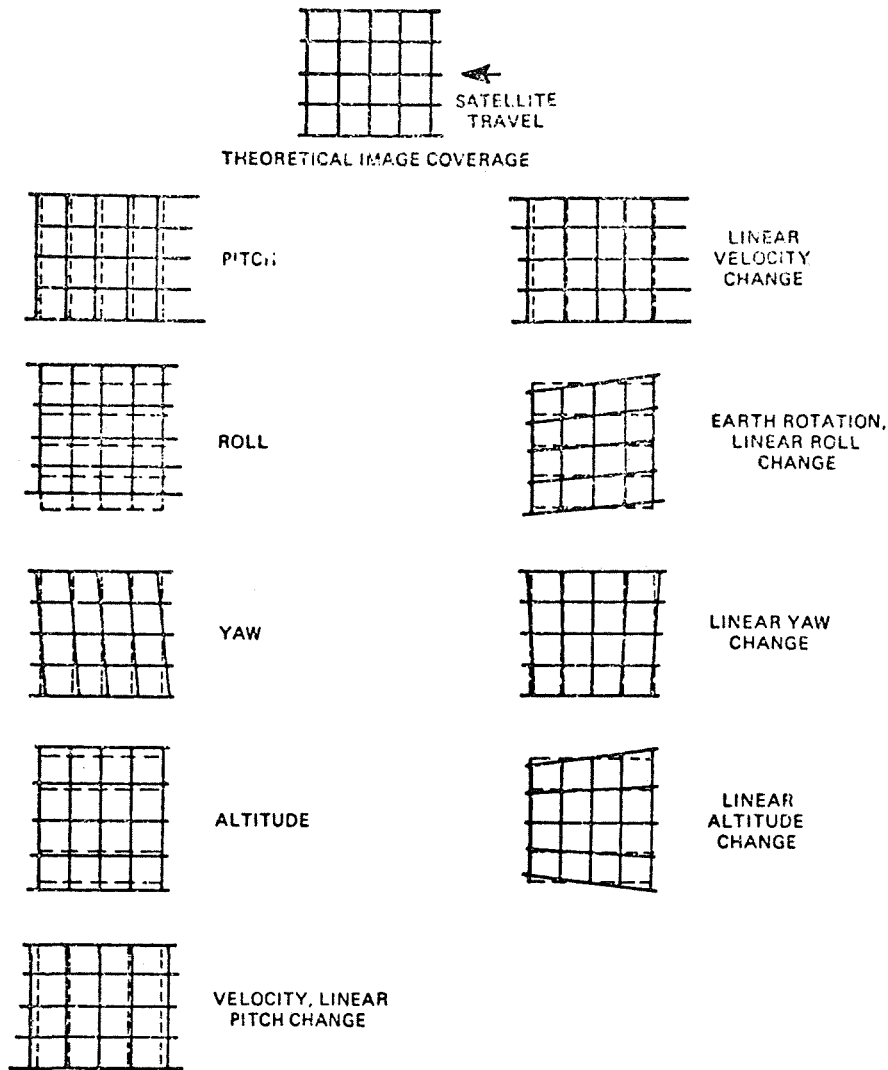


Figure 3 : Principal MSS Image Distortions

Each scan line is slightly elongated during bulk-image recording to adjust the geometry from the panoramic curved surface of the original scanner to the plane surface characteristic of a frame camera. Spacing between scan lines is decreased away from the center of the MSS frame to produce a perspective effect in that direction as well. These adjustments also are added to the EBRIC grid deflections. Colvocoresses [7] has questioned the wisdom of this latter adjustment. The rationale lies in the original desire to give the MSS images the same geometry as that of the RBV images.

Another EBRIC contribution results from the imperfect alignment of the MSS sensor in the satellite with respect to the attitude sensors. The entire MSS bulk image must be slightly rotated and translated with respect to the image border. The extent of this adjustment is determined as part of the precision image processing operation described below.

Earlier, it was mentioned that nonlinearities in the mirror sweep rate introduce spatial distortions in the sampling of pixels along a scan swath. This nonlinearity is monitored as part of precision image processing. The correcting deflections are supplied to the bulk-processing control computer as additions to

each of the 81 EBRIC grid points.

By its nature, the EBR equipment applies additional image distortions to the bulk images. Compensating corrections must be entered as EBRIC grid deflections to cancel these equipment errors. A calibrated film grid is periodically printed with the EBR and measured to update these equipment corrections if necessary.

In summary, bulk image geometry is not a simple unmodulated presentation of consecutive scan lines. A closed-loop control sequence exists with which bulk images are measured and the results used to improve subsequent bulk images. Once the systematic errors have been removed by this control loop, a continuous monitoring process is followed to ensure that accuracy is maintained. The net result is a complex and interrelated flow of information to remove errors caused by attitude and velocity differences, earth rotation effects, internal sensor geometry non-linearity, and EBR equipment drifts and distortions.

Bulk Image Accuracy

The film bulk images exhibit good registration between the different spectral bands. Circular standard error from early operations was about 150 meters; this has improved somewhat with time and is presently closer to 100 meters. But the circular standard error in absolute position remain at about 750 meters. By far the most significant component is caused by errors in telemetered spacecraft attitude. Internal image geometry is rather good; only a shift and rotation are needed to greatly improve absolute position. The only feasible way to achieve such improvement is through the use of ground control points: small details of known earth-surface position which can be measured in the ERTS-1 images. This leads us to the area of precision image processing and the second accuracy level of ERTS-1 images.

PRECISION IMAGE PROCESSING

The primary function of the precision image processing sequence is to produce special "precision" images with accuracy improved from that of the bulk images. In addition, information is obtained which can be used to monitor and periodically improve the corrections being applied by the bulk-image EBR at the 81 EBRIC grid points. To this extent, precision image processing improves the accuracy of all bulk images, not only those undergoing precision processing. An ERTS-1 precision image as produced by the NASA facility is printed directly on 240-mm roll film at 1 : 1 000 000 in a transverse Mercator projection. Except for the small effects of terrain elevation variations, the precision image is geometrically a map. Projection zones correspond to those used for the Universal Transverse Mercator system. Both geographic and UTM ticks are shown around the image border. Interior geographic or UTM ticks can be provided at the request of the user ordering the image.

Ground Control Points for ERTS

During the preliminary planning for ERTS, it became clear that satellite attitude data would not be adequate to meet the initial precision-image positional goal of 500 meters circular standard error. Image-derived data offered the only possible solution in the short time available, and the use of ground control points for positioning ERTS-1 images was studied. It was quickly apparent that, in addition to an increase in positional accuracy, ground control points offer other significant advantages for ERTS. Most important, failure of the attitude sensor is not a problem. Second, ground control points for ERTS are quite cost-effective because of the modest accuracies required: selected features on existing maps can be used.

A third advantage of the control-point application had important system design implications. A photogrammetric resection in space provides the image-sensor attitudes completely independent of the satellite attitude sensors. This permits the angular offsets between image and attitude sensors to be established more accurately than can be done by prelaunch alignment. Moreover, the offsets are measured after the satellite has undergone the rigors of launch and is established in orbit. When the effects of the attitude offsets are passed to the bulk-image EBR control computer via the EBRIC grid, all subsequent bulk images can be given compensating shifts within the image border during film recording. (Recall that the bulk-image border is placed on the earth solely from satellite data).

Control points have other advantages as well. When using more than the minimum number of points for a spatial resection, the redundant data gives information on the quality of the spatial resection and the individual control points. Image sensor performance also can be evaluated: for example, changes in MSS sweep non-linearity can be detected by analyzing control-point residuals.

All of these advantages were attractive enough to warrant further consideration of control points for ERTS-1 precision image processing. Several problems had to be worked out, largely a consequence of the heavy workload to be accommodated. The first of these was identification. Photogrammetric mapping experience with control points shows that misidentification is a frequent source of trouble. Often, this results when the point is not compared directly against a reference image. But storage of a world-wide network of reference control-point images for rapid access is a formidable problem. On the other hand, the digital information about a point: identification number, latitude, longitude, elevation, even the type of point, its average residuals and variances - all can be stored easily on tape or disk and accessed quickly and directly.

For ERTS- a second problem with control points was their visibility. There was considerable initial uncertainty as to what constitutes a good control point. In general, these have been resolved. Small bodies of water are consistently good control points; other man-made and natural features also are used, depending on the circumstances. Once a number of such control points have been selected in one image, they form a data base for all future images of the same area (orbit and data collection are adjusted so that subsequent scenes of the same earth area repeat to within about 30 km). Of course, the points may not be visible for the next orbital pass of the satellite. Clouds are the biggest problem. Seasonal change is another, although not as severe as was originally thought. Provision must be made for using supplemental control points for any single ERTS image.

The method finally devised to implement control point for ERTS-1 uses a film-chip control-point library on glass plates. A chip of film 5 mm square is cut from an extra copy of a 70 mm bulk image whenever a new control point is selected. Each chip covers 17 km square on the earth, and is approximately centered on the control point. The chips are fastened to 240-mm square glass plates as they are selected, adding them to previously fastened chips. Each plate is capable of holding up to 2025 chips in a regular 45 by 45 array. A special glue is used for a permanent film-to-glass bond. After a film chip is mounted on a chip plate, the plate coordinates of the exact control-point location are carefully measured. These coordinates are stored in a digital control data base, together with the other data needed for the point. The identification number for the control point is established by the plate number and the row and column numbers on the plate where the film chip is fastened. A total of 30 chip plates are used, corresponding to the 30 zones on the earth shown in Figure 4. Each zone covers a land area equivalent to a square between 1 900 and 2 400 km on a side, with the smaller zones used for areas of particular concern to ERTS-1 investigators. Duplicate control-point coverage is allowed for where zones join, and one consideration in selecting the zones was the minimization of land-area boundaries.

Where suitable maps are lacking or of questionable accuracy, relative control points can be used for positioning ERTS-1 images. The geographic location of a relative control point is defined at the time it is first selected, using only satellite data and the measured image coordinates of the point (terrain elevation is assumed equal to zero). Once selected, relative control points provide a stable reference to which subsequent images of the same area can be accurately temporally registered. Even the standard error in absolute ground position of 750 meters for relative control points may represent a real improvement in position determination for some areas of the world.

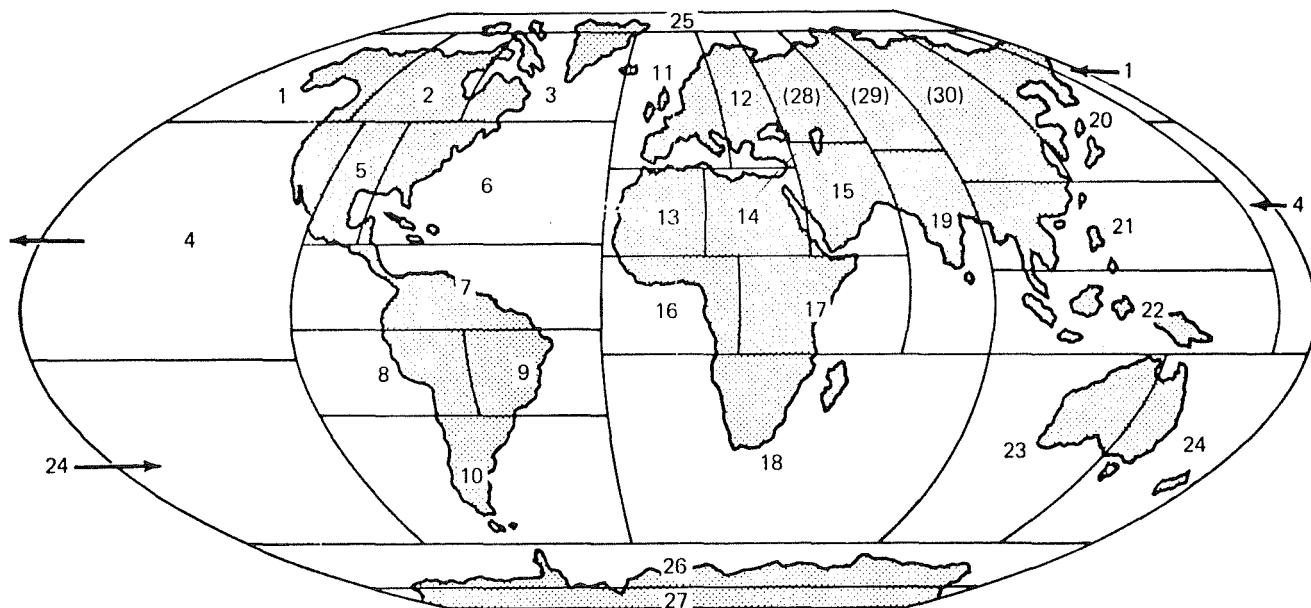


Figure 4 : Control Point Zones

Precision-Image Processing Sequence

The three parts of precision processing are shown schematically in Figure 5. Separate queuing is used for each part; all three functions normally occur simultaneously, but for three different ERTS-1 scenes. For each image to be processed, the processing instructions and satellite data are provided on a magnetic tape prepared elsewhere in the facility. The 70 mm bulk images also are provided. The precision-processing computer controls all subsequent operations.

During the Screening and Control Point Selection activity, existing ground control points are checked for visibility and new points are selected if needed. This operation uses conventional light tables, magnifiers, and a graphic digitizer for the maps.

The next two precision sequences are handled differently at the NASA facility than at the Canadian and Brazilian facilities. NASA operations are discussed first. The Image Measurement sequence in Figure 5 takes place at a Viewer/Scanner instrument, somewhat similar in appearance and capability to a computer-controlled stereocomparator. The bulk images are placed on one stage and a control-point chip plate on the other. Electronic image correlation is used to automatically match each control-point image detail on the bulk images with the same master control-point film chip on the glass plate. The entire operation is controlled by the precision-processing computer, and manual operator assistance in control-point matching also can be used. With all control points measured, the program calculates the transformation required to map bulk-image details into the necessary 1 : 1 000 000 transverse Mercator projection.

Image Conversion and Annotation at NASA takes place at the Scanner/Printer equipment, a second precision two-stage computer-controlled device. A flying-spot scanner converts the bulk-image information into a video signal; a cathode ray tube (CRT) re-images the adjusted video signal and prints the image back on film in its correct location, Figure 6 shows the basic concept. The image is scanned and printed in 64 separate blocks. On the printed precision image the blocks appear as adjoining squares; on the input bulk image these same squares are slightly distorted quadrilaterals. It is the task of the transform computation to determine the correct distorting adjustments to apply to the flying-spot scanner raster as it collects the image information for each print block. For each corner of the 64 print blocks the sequence of coordinate transformations is:

precision-image printing stage → UTM grid → geographic → Universal Space Rectangular → Local Space Rectangular → bulk-image coordinates → x,y stage coordinates at the Viewer/Scanner where control points were measured → x,y stage

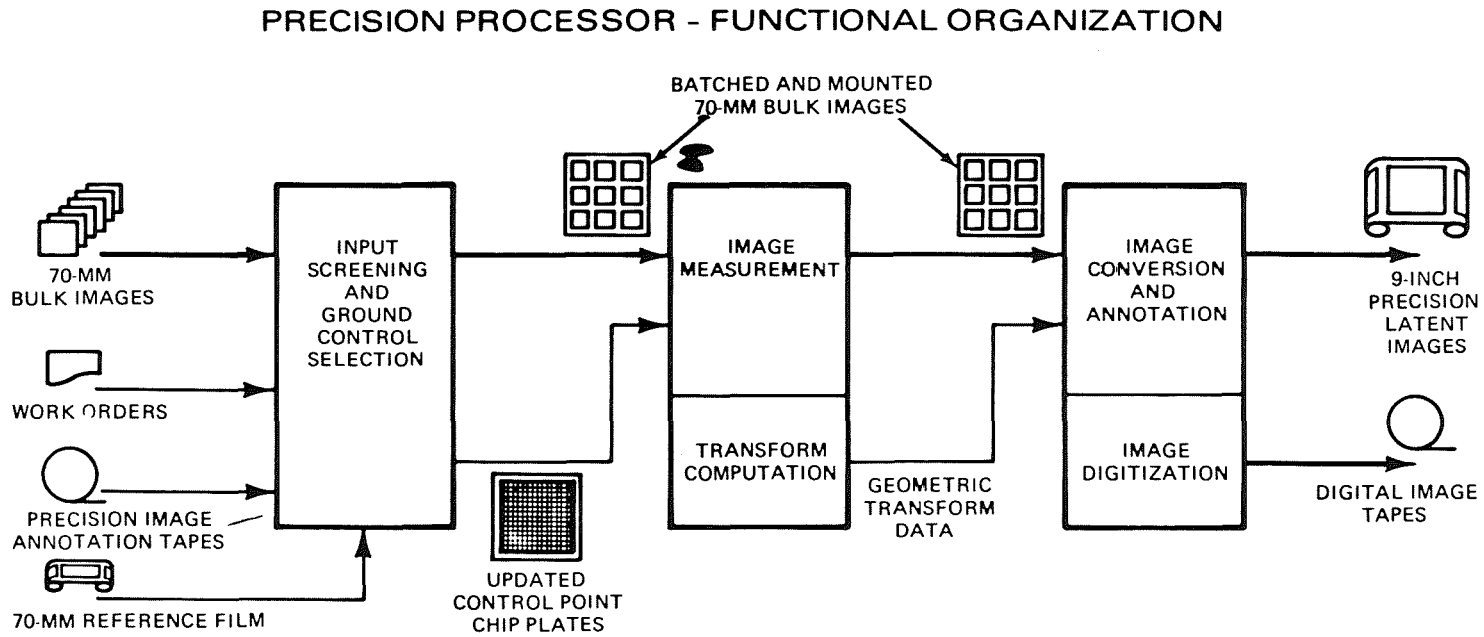


Figure 5

coordinates on the scanning stage of the Scanner/Printer where the image is mounted while being scanned. The spatial resection supplies only two transformations in this sequence. The others are determined from the established bulk-image border, the earth spheroid being used, a knowledge of the bulk-processing geometry modifications, and an image-to-stage orientation carried out at the Scanner/Printer.

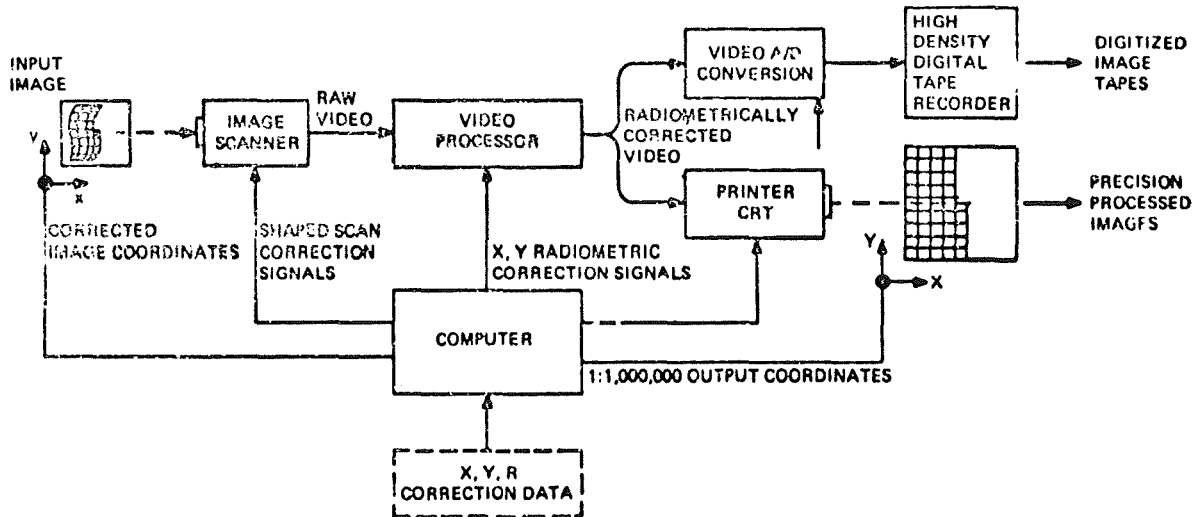


Figure 6 : NASA ERTS Image Transformation, Printing and Digitizing (RBV AND MSS)

Precision Image Geometry

The MSS spatial resection is somewhat different from the normal photogrammetric spatial resection with six unknowns. Eight unknowns are determined. As a result of unavoidable errors, the bulk images contain errors introduced by incorrect satellite attitude, altitude, attitude changes, altitude changes, and residual film-recorder scale and skew errors. To remove the composite effects of these errors, coordinate corrections dx and dy are determined for the measured x and y bulk image coordinates, where

$$dx = a_0 \left| 1 + \left(\frac{x}{H} \right)^2 \right| + a_1 x + a_2 y + a_3 xy$$

$$dy = b_0 \left| 1 + \left(\frac{y}{H} \right)^2 \right| + b_1 x + b_2 y + b_3 xy$$

in which H is the satellite altitude reduced to bulk-image scale, The a_1 and b_1 are the eight unknowns used in the spatial resection. These equations basically are those required to map any quadrilateral into any other quadrilateral, with an additional small term in the a_0 and b_0 terms to include some of the erroneous attitude effects introduced earlier when the bulk image was printed as a perspective projection. The terms correspond to the first-order effects of the residual errors, as shown in Figure 4.

In the resection, the approximate position and attitude data used to position the bulk image are considered errorless. The control-point geographic coordinates are transformed to those bulk-image coordinates where the control-point images would appear if the desired perspective transformation had been errorless. The differences between these computed coordinates and the image coordinates actually measured at the Viewer/Scanner equipment are the residuals used in the least-squares resection computation, solving for the a_1 and b_1 terms.

Only four control points are theoretically adequate to position each ERTS-1 scene. However, nine points typically are used, arranged in a three by three array which encloses as much of the image area as possible. The large redundancy

gives a significant reduction to that component of the precision-image error which is caused by random control-point errors. It has also been useful in partially compensating for the low skill levels of the personnel being used by NASA to control the operations.

EBRIC Update

About once a week, the Viewer/Scanner equipment is used to measure a special bulk image containing a rectangular grid. The results of this calibration are sent back to the bulk-processing operation in the form of a magnetic tape containing updated adjustments to be applied to the 81 EBRIC grid points during bulk-image film recording. This same measurement and control path has been useful on several occasions during ERTS-1 operation. The initial bulk-image shift and rotation (to correct for misalignment of image sensors and attitude sensor) was determined by precision processing and applied by an EBRIC tape. The MSS mirror sweep non-linearity has been modified using the same technique, based on analysis of control-point residuals.

Canadian and Brazilian Precision Image Processing

The NASA approach to precision processing uses a film bulk image as if it were the original data input. This input is scanned and re-recorded with the corrections and the annotations needed to improve locational accuracy. A valid objection to this approach is that the bulk film image presents considerable degradation from the original sensor data stored on tape. Scanning and reprinting degrades the information still further. Resolution is better if the precision image is produced directly from the original tape data, using the same film recorder device but with slightly different EBRIC adjustments to improve and modify the geometry. This approach was considered during the design of the NASA facility, but at the time there was considerable uncertainty as to the stability of the EBR as a recording device.

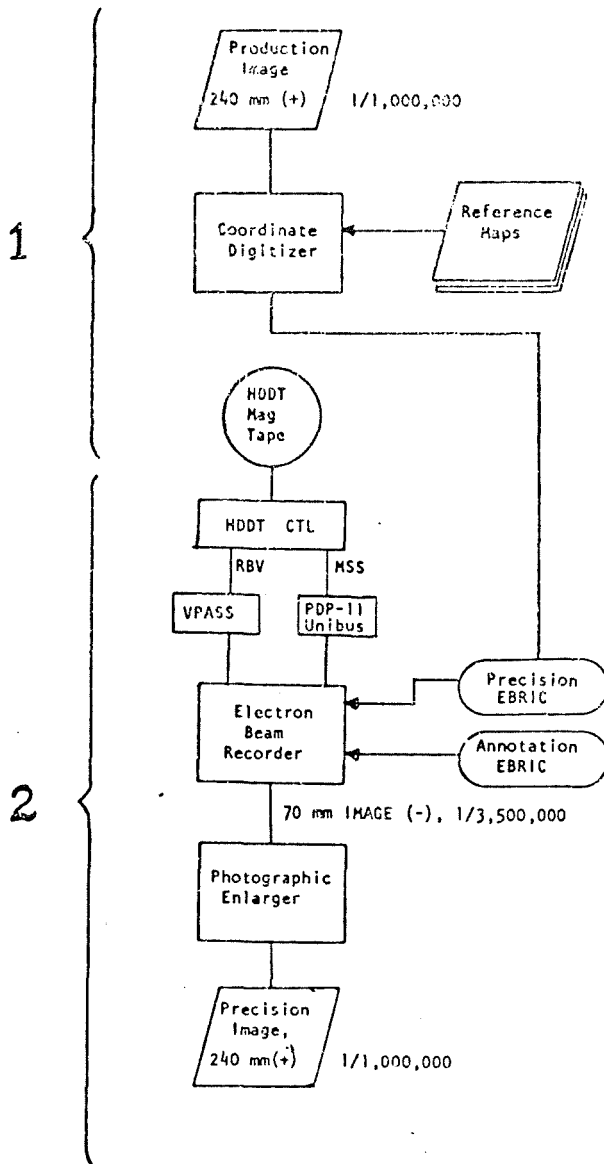
The Canadian and Brazilian precision-processing design proceeded along somewhat different lines, partly as a consequence of more modest production requirements. First, a slightly different type of film recorder was used. The NASA EBR requires the film to be in continuous motion forward as printing takes place, with consequent concern for the stability of the drive mechanism. And, since film exposure with electron-beam devices must take place under high vacuum, the problem was a difficult one to solve. The Canadian and Brazilian film recorders use a step-and-repeat technique, with the film stationary during printing. By using this same device for precision processing, the cost of a special additional Scanner/Printer can be eliminated, and this was the decision for the Canadian and Brazilian facilities. The stability of both types of film recorders has since proven to be quite good, verifying the advisability of this technique.

A second difference in the Canadian and Brazilian facilities concerns the control point measurement. The original 70 mm bulk image is enlarged in these facilities from a scale of 1 : 3 370 000 to a positive transparency at 1 : 1 000 000. Image coordinates of control points are measured on this transparency using a conventional graphic digitizer with a least count of 0.010 to 0.025 mm. Film chips are not used to provide a reference image of each control point, only available source maps. The technique permits the function of the Viewer/Scanner equipment to be replaced by a photographic enlarger and a conventional graphic digitizer. On the negative side, considerably more chance of point misidentification is introduced in this way, there is some loss in accuracy even with good identification, more time is needed, and higher skill-level operators are required.

Figure 7 shows the precision sequence schematically, starting with the bulk image. The flow segment labelled "1" represents the precision measurement sequence. Segment "2" is really only a repeat of the bulk-image production sequence, but with the substitution of a special set of "Precision EBRIC" correction grid points in place of the "Bulk EBRIC" corrections normally used. Notice that this sequence also enables EBRIC to compensate for the lens distortion introduced by the film enlarger. A variation of the precision sequence is used to update the bulk EBRIC grid points.

Figure 7 :

Canada/Brazil Precision Processing Sequence



POTENTIAL ACCURACY OF ERTS-1 MSS IMAGES

Intensive Processing

Early in the planning for the NASA ERTS-1 image processing facility, production rates became the dominant consideration. As a consequence, hybrid processing techniques were used, with the image data being transferred to film at analog rates, but with the geometry and density controlled digitally. Other techniques also merited consideration, including all-digital processing approaches. The chief disadvantage of such techniques at the time was the extensive processing and data handling time needed by very large computer systems to keep up with the data acquisition rates of the satellite. This is not difficult to understand when it is considered that one spectral band of one MSS image has over 7,000,000 pixels, each with a reflectance value from 1 to 64. Since early 1970, when the ERTS design took place, new digital processing methods have been developed which hold considerable promise for application to future earth resource satellites. Several new attitude sensors have also been developed. With such a potential, it is natural that there should be interest in finding how well ERTS-1 MSS images could be positioned, assuming unlimited ability to make corrections and monitor all the critical conditions.

Another concern is the technique used to locate control points on images in a production environment; some image presentation is needed other than photographic film with which to rapidly and precisely point to selected image details of control points. Still another area of interest is the fine structure in satellite relative attitude behavior. MSS images can provide valuable insight here. Some investigations at Bendix Research Laboratories have been carried out under contracts with NASA to find some answers to these questions [8].

Geometric errors in MSS images are caused by image sensor, satellite, and ground processing effects. Additional errors are introduced by attempting to point errorlessly and without bias to control-point image details. The interest for research is focused on only three of these four types of errors; ground processing effects are to be excluded. Thus, a substantial part of study effort must be concerned with removing the ground-processing error contributions. When this is done, it is possible to develop the systematic error components caused by the image sensor and the satellite. All of these could in theory be removed by a combination of modified MSS image sensor design, satellite attitude-sensor design [9], and the use of some number of control points. The remaining error when all this is done is called the limiting MSS geometric error in this discussion. The reduction of geometric errors to this level I call "intensive image processing".

The primary systematic error components in the present MSS images result from wobble of the scanning mirror normal to scan, scan sweep nonlinearity, and satellite attitude variation. All three could theoretically be removed from all image data: the mirror effects by careful inflight calibration, and the attitude variation by smoothing of telemetered high-resolution relative attitude data. Additional small systematic errors result from the placement of the individual signal detectors in the image plane of the scanner, and from the sampling-time delays for the different detectors. The limiting error is made up of random variations in the mirror during scanning - sweep rate and wobble - and of undetectable small image sensor attitude changes.

Intensive image processing is based on a variation of photogrammetric spatial resection, using a dense array of control points within a single ERTS-1 scene. In the work done to date, the control point images have been measured in each of several MSS image display media. Each medium is considered to be built up as a regular row-column array of adjacent MSS pixels. Row number and column number define a reference rectilinear image coordinate system. The resection mathematical model expresses the relation between the control points' locations in object space and the image column and row coordinates of the corresponding pixels. Model parameters are determined which give the best least-squares fit of the control-point data to the image coordinates. Residuals are analyzed for additional systematism not included in the current mathematical model. This systematism is added to the mathematical model and the procedure repeated. When no additional systematism is detected, the final residuals, less image pointing errors and control-point errors, are then considered to define the limiting MSS geometric error.

Image Display Media

A fundamental problem in pointing to image details is of concern in the study. To eliminate the effects of ground processing, the MSS image display must theoretically allow the original row-column pixel numbers of a control-point image detail to be determined directly. At the same time, the display must provide fractional pixel pointing precision; early in the study it was seen that the limiting geometric error is much smaller than one pixel; if only integer pixel row-column are used, a significant error source is introduced. These two requirements - direct pixel counting and fractional pixel pointing - conflict directly. When the image display medium is such that discrete pixels can be seen and counted, it is difficult to do fractional pixel pointing. Conversely, suppression of pixel boundaries creates a composite image that looks like a continuous-tone photograph; fine pointing can be done easily in such a display but the pixel rows and columns cannot be counted directly.

During the research thus far, three different image display media have been used in a search for the best compromise between fractional-pixel pointing and direct pixel counting. The first image form was a conventional ERTS-1 bulk image, a 70 mm film transparency. It contains the errors normally associated with such

Over 100 control points were selected for the initial research. Considerable effort was made to select points from symmetric image details: X road intersections, circular bodies of water, and three clearings. Nearly all of the points used were of this type. The source maps were at a scale of 1 : 24 000. The total circular standard error from the maps and the map-point measurement process was calculated to be 6.0 meters.

Imaging Models

Three different mathematical models were used in the course of the initial analyses. The most detailed simulates the entire MSS imaging process, in the same way discussed by Kratky [3]. The column and row pixel number measured for each control point, together with parametric values of scanner rate and duty cycle, establish the time at which the control point was imaged by the scanner. This fixes several time-dependent orientation elements - the unknowns in the model - which describe satellite position and attitude, from which pixel column and row numbers can be computed corresponding to control-point latitude, longitude, and elevation. If all orientation elements were correct, the computed and measured pixel numbers should be identical. Residuals indicate additional adjustment is required. A total of 13 orientation elements were established for the original imaging model. Several of these are very highly correlated, and only 9 of the 13 were originally carried as unknowns.

In the course of the analysis, 12 additional unknowns were added. These provide adjustments to the mirror sweep nonlinearity and higher-order attitude effects. Three terms each were used for separate east- and west-edge mirror effects. Separate adjustments to pixel row number and column number as third-order effects of time required the other six unknowns.

The detailed imaging model above is comprehensive in its geometric treatment of the imaging process, since it includes all known effects of the imaging process. However, it proved to be rather time-consuming for computer analysis of a great many control points. This was largely a consequence of using delta-process partial derivatives for 9 of the 21 unknowns, instead of explicit expressions. A second imaging model was developed which requires much less computer time. Results have since proven to be equivalent to those of the detailed model. Basically, the second model is a complete cubic polynomial representing image column and row pixels in terms of geographic coordinates. Latitude and longitude of each control point is modified initially by the cross-track terrain elevation displacement component. An additional term was added to the cubic, linearly varying as the row number within a six-line swath, to compensate for the swath nature of the scanning process and also for the average time difference between read-out of the six detectors in a single imaging swath. The total of 21 unknowns is the same as that used for the first imaging model described in the previous paragraph.

A third imaging model was used only for the ERTS-1 bulk image. Measurements in Pixel row and column numbers were not possible for this medium. Also, the bulk image already includes some geometric corrections, as seen above. The final equations for the third imaging model included 16 unknowns. The basic form is

$$\begin{aligned} dx &= a_0 + a_1x' + a_2y' + a_3x'y' + a_4(y')^2 \\ dy &= b_0 + b_1x' + b_2y' + b_3x'y' + b_4(y')^2 \end{aligned}$$

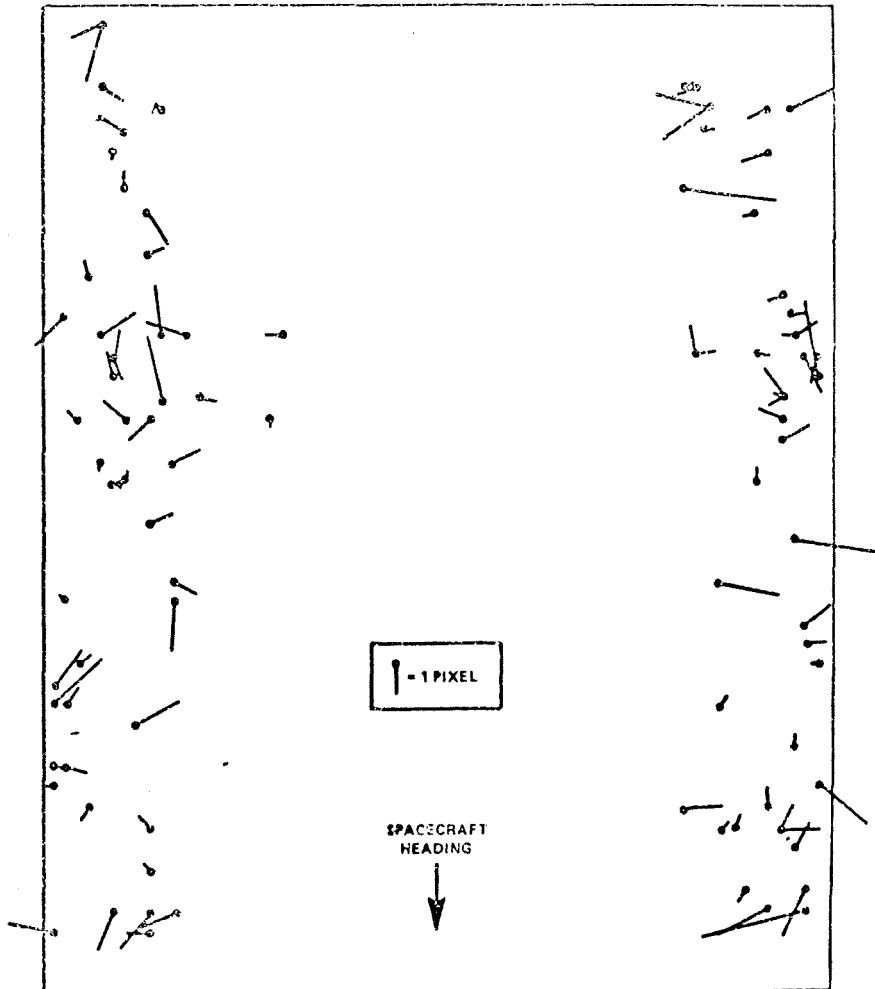
where x' and y' are the bulk-image coordinates as computed from a central-perspective projection of control-point coordinates, and dx and dy are added to x' and y' to obtain the measured bulk-image coordinates. Three additional terms also are used for separate second-order mirror sweep effects at the east and the west image edges.

RESULTS

The standard errors in the across-track (row) and along-track (column) dimensions were evaluated for the different image display media and imaging models. The results are summarized below in meters on the ground.

	Imaging model					
	1		2		3	
	Explicit (21 unknowns)		Polynomial (21 unknowns)		Bulk-Image (16 unknowns)	
	row	col.	row	col.	row	col.
CRT Film	45	57	--	--	--	--
Line Printer	57	54	36	46	--	--
Bulk Image	--	--	--	--	42	39

Figure 9 :
Control Point
Residuals from
CRT/Film Image
Measurement



For all of these values, the effects of image pointing and map error have been removed. The poor results of the CRT film image, shown in detail in Figure 9, appear to have resulted from high-order CRT distortions which could not be removed by the reseau spacing used. The line printer method shows considerable

promise for future analysis. But the standard ERTS-1 bulk image gave the best accuracy. This is all the more remarkable, since the image used was a third-generation positive copy. Also, none of the finer-structure corrections for MSS six-line swath scanning could be applied because of the impossibility of identifying discrete pixels. Based on these initial results, there is hope that the present errors of about 40 meters, or one-half pixel, can be further decreased with improved image display media.

The initial investigation indicated that:

(1) Using all available information, MSS circular standard errors can be reduced to about 40 meters, excluding the effects of terrain elevation displacement.

(2) The ERTS-1 satellite exhibits a relatively well-behaved regime of attitude variation over a single MSS image; variations could be largely compensated in production either by many (10 to 20) control points or by accurate relative attitude data and fewer control points. However, occasional anomalous spikes in the attitude behavior do appear to be present.

PRESENTLY PLANNED RESEARCH

Plans for additional investigations of ERTS-1 geometric accuracy will use a different image scene. For the utmost ease in interpreting some of the image display media which will be used, a test area is desired which has a large number of ponds and small lakes uniformly distributed throughout the scene (or alternatively, many small islands in a larger body of water). The entire test area also must be covered by accurate maps at scales no smaller than 1 : 50 000 for effective control-point selection. Finally, the area must be imaged in several different passes by the ERTS-1 MSS. Potentially satisfactory locations are found in New England, Florida, and several parts of the North Central United States.

With the scene selected, several hundred control points will be selected from the maps, with about 100 clumps of 3 to 5 points each distributed uniformly over the test area. Selection criteria will be: (1) general symmetry of the map feature for accurate centering both on map and image; (2) good visibility in the ERTS-1 image, preferably the 0.6 to 0.7 micrometer ("red") or the 0.7 to 0.8 micrometer ("IR₁") spectral band; (3) no evidence of change in shape between map and image.

A major task of the planned research will be to develop a discrete-pixel display which can be pointed with the same precision as a conventional aerial photograph. (Recall that sub-pixel pointing is mandatory). Three alternative techniques are planned for initial evaluation: (1) a high-resolution television screen, using direct operator pointing to scaled-up MSS display segments; (2) a line-printer digital image printout, with different overstruck alphanumeric characters (10) creating a grey-scale image from the individual MSS pixels; and (3) a line-printer digital printout with a single line-printer character for each of the 64 reflectance levels. The first two display media will create an image-line presentation, in which control point images can be pointed in the same way as a photographic image. The third format is intended for digital analysis, interpolating pixel row and column density centroids for the small symmetric control-point features. After using these three media for control-point measurements, the most promising will be selected for additional development. The merits of the second technique may require the use of a line-printer with different shades of grey as characters in contiguous blocks. Similar devices already exist for other applications.

Using the optimum image display format, the evaluation of limiting MSS geometric error can proceed, based on control-point measurements with small and well-known pointing errors associated with them. The results of the analysis will again be values for standard error in the MSS row and column directions, improved estimates of mirror behavior over a frame of scanning, and more definitive profiles of relative satellite attitude perturbations.

CONCLUSION

The ERTS-1 satellite has collected thousands of images over the past two years. These images have been applied to a great number of disciplines concerned with the earth's natural resources. Circular positional standard error of the ERTS-1 MSS images has three different levels; that associated with the bulk images of

about 100 meters, and the limiting value which can be attained of something less than 40 meters. Work is in progress to better establish the latter figure. The many investigators who must perform temporal registration of ERTS-1 images are asking for positional discrepancies of one-half ERTS-1 pixel or less. It is hoped that additional research will show a way to achieve such high quality consistently for images collected by the future earth resource satellites.

REFERENCES

- |1| Forrest, R. B.: "Geometric Processing of ERTS Images", Presented at the Fall Convention of the American Society of Photogrammetry, San Francisco, September 1971
- |2| Anon, R.: "Data Users Handbook", NASA Goddard Space Flight Center, Greenbelt, Maryland, September 1971
- |3| Kratky, V.: "Precision Processing of ERTS Imagery", Proceedings of the Fall Convention, American Society of Photogrammetry, San Francisco, September 1971
- |4| Derenyi, E. E. and Konecny, G.: "Infrared Scan Geometry", Photogrammetric Engineering, Vol. 32 (5), September 1966
- |5| Norwood, V. T.: "Optimization of a Multispectral Scanner for ERTS", Proceedings of the Sixth International Symposium on Remote Sensing of The Environment, University of Michigan, October 1969
- |6| Forrest, R.B.: "Mapping from Space Images", Bendix Technical Journal, Vol. 3 Summer/Autumn 1970
- |7| Colvocoresses, A. P.: "Space Oblique Mercator", Photogrammetric Engineering Vol. 40 (8), August 1974
- |8| Derouchie W.F. and Forrest, R.B.: "Potential Positioning Accuracy of ERTS-1 MSS Images", presented at the Spring Convention, American Society of Photogrammetry, St. Louis, March 1974
- |9| Bendix Research Laboratories, EOS Mapping Accuracy Study, Final Technical Report for Period April through August 1972, NASA Contract NASA-5-21727, March 1973
- |10| MacLeod, I.D.G.: "Pictorial Output with a Line Printer", IEEE Transactions on Computer, Vol. C-19, February 1971

M A R S - A PROCESSING SYSTEM FOR THE MAPPING OF REMOTE SENSING DATA

by E. Clerici, D. Eckhart and K. Kubik, Delft, The Netherlands

THE REMOTE SENSING PROBLEM AREA

- Image formation

In addition to the now classical methods of aerial photography several new techniques of taking images have been developed. These techniques have in common a very high rate of data acquisition. The different imaging methods, however, have all their rather particular geometry.

As a consequence of the strong data flow special processing as well as organisational efforts are required.

- Data preprocessing

In order to reduce the amount of data at the earliest possible stage data preprocessing methods have to be applied. It is interesting to note that also the human eye has a preprocessing task, namely to extract the most relevant features of the image before sending the signals to the brain.

For scanning methods a certain amount of data reduction is achieved via the photographic image registration. In fact an integration by overlapping scanlines is performed.

Even after preprocessing a vast amount of data is left, so that a very selective further processing is mostly indicated.

- Interpretation

Recognition is a most complex process as a large number of parameters is involved. Two general approaches may be mentioned: recognition via general shape and recognition via the spectral characteristics per point. The last procedure is easier for automatic treatment and is a typical microprocedure. Visual interpretation of photographs is mainly directed to recognition of macrostructures. Human interpretation and automatic treatment complement each other to a large extent, so that interactive processing may be a favourable proposition.

- Profit to "Waterstaat" as organisation

Clearly the purpose of applying remote sensing in an organisation with operational tasks must be profit oriented. Some promising application areas are listed in figure 1. The potential to achieve this, namely the data handling is illustrated summarily in figure 2.

Depending on the case, remote sensing may be the only applicable means or it may be one of several alternatives. For example it is the only means for synoptic determination of the temperature distribution over the surface of the sea or a river, whereas detection of oil pollution on the sea may also be performed by visual control.

<i>APPLICATION OF REMOTE SENSING TECHNIQUES AT THE RIJKSWATERSTAAT</i>	
<u>PROBLEM AREA</u>	<u>TECHNIQUE</u>
① <i>Detection of oil pollution of the sea.</i>	<i>SLAR, IRLS</i>
② <i>Detection of thermal pollution of inland waters.</i>	<i>IRLS</i>
③ <i>Studies of coastal water circulation.</i>	<i>IRLS</i>
④ <i>Marine traffic control.</i>	<i>SLAR</i>
⑤ <i>Detection of swell.</i>	<i>SLAR</i>
⑥ <i>Fast mapping of large areas.</i>	<i>SLAR</i>
⑦ <i>Mapping of the sea floor.</i>	<i>SSS</i>

Figure 1

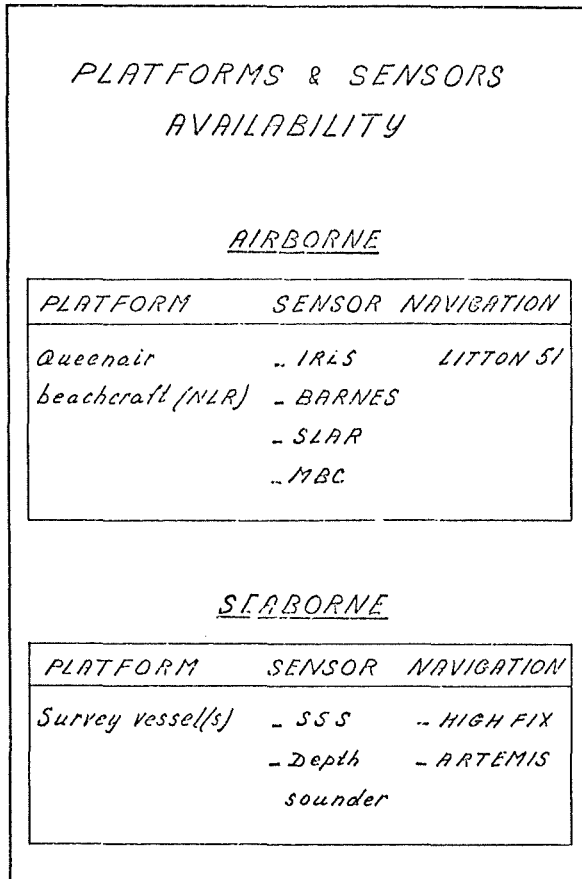


Figure 2

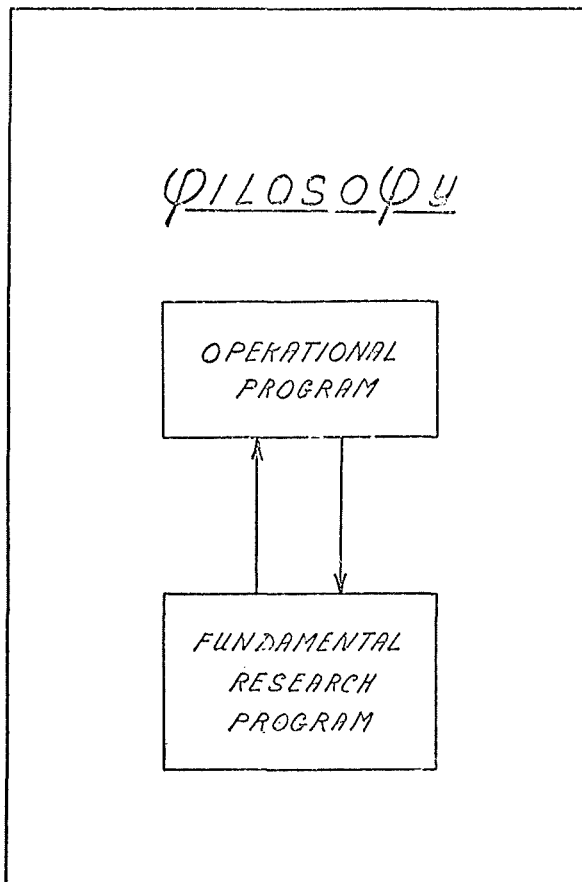


Figure 3

Using remote sensing methods however, the chances of detection are much higher; moreover one is not necessarily restricted by daylight or clear weather conditions. Early detection of oil pollution on sea may result in quite substantial savings in costs of clean up actions (in the order of millions of dollars) even without consideration to the ecological consequences of coastal pollution.

Of course an operational system has to be developed from a research programme directed to application, as most of the remote sensing techniques have only recently become available. Also basic research has to be performed in order to give proper support to the application research programmes (vide figure 3).

MARS

- Computer aspects

Central to MARS is a large computer system (P 1400) which includes a mini-computer (PDP 11), used mainly to control the hardware specially developed for processing remote sensing data. The software design of MARS is developed for a multiprogramming environment in order to make it accessible from terminals distributed over the country (vide figure 4).

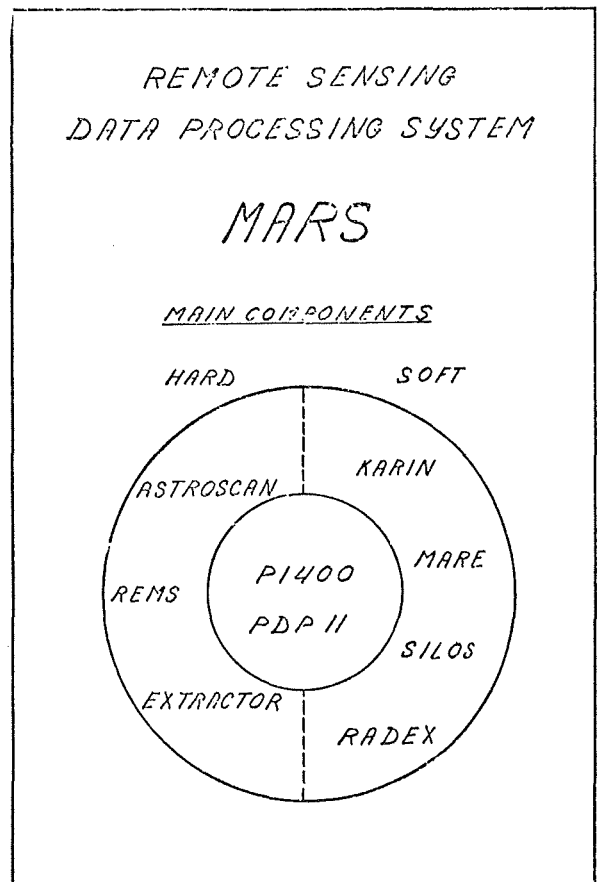


Figure 4

- Special purpose hardware

A - ASTROSCAN

This device is basically developed as a computer controlled densitometer of utmost flexibility. The mechanical part of it is a David Mann comparator made available by the Astronomical Institute of Leiden University, and modified by the effort of NIWARS and Rijkswaterstaat (vide figure 5).

B - REMS

REMS is an imaging device coupled to the PDP that can perform a rectification of scanner images recorded digitally. The rectification is a function of the available flight parameters, which are registered in parallel to the video signal.

The PDP allows quick look inspection of the recorded image by playing the tape on to a television display (vide figure 6).

C - RADEX hard

RADEX is the RADar EXtractor in development at the "National Physics Laboratory TNO" on commission by the Rijkswaterstaat. The hardware system is airborne. The purpose is detection of ships at sea using SLAR. Signals above a preset level

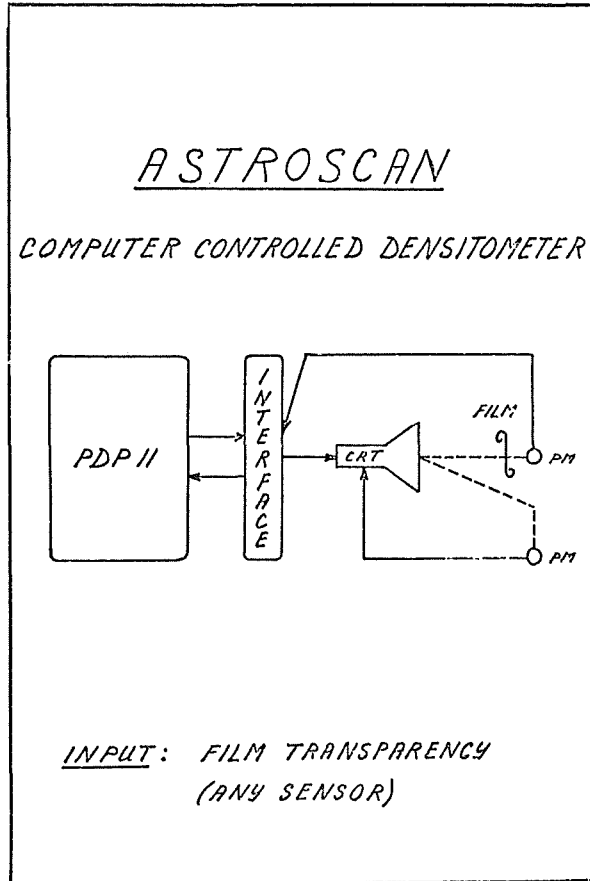


Figure 5

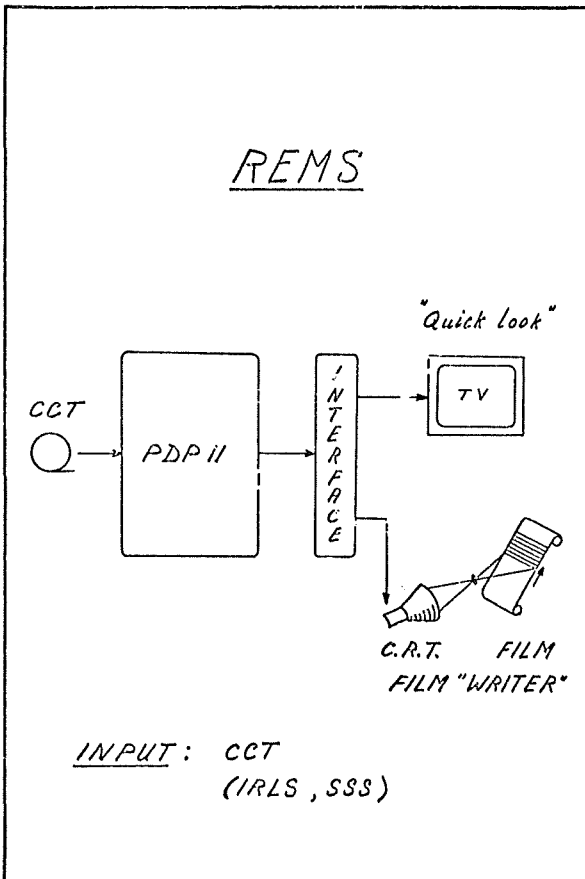


Figure 6

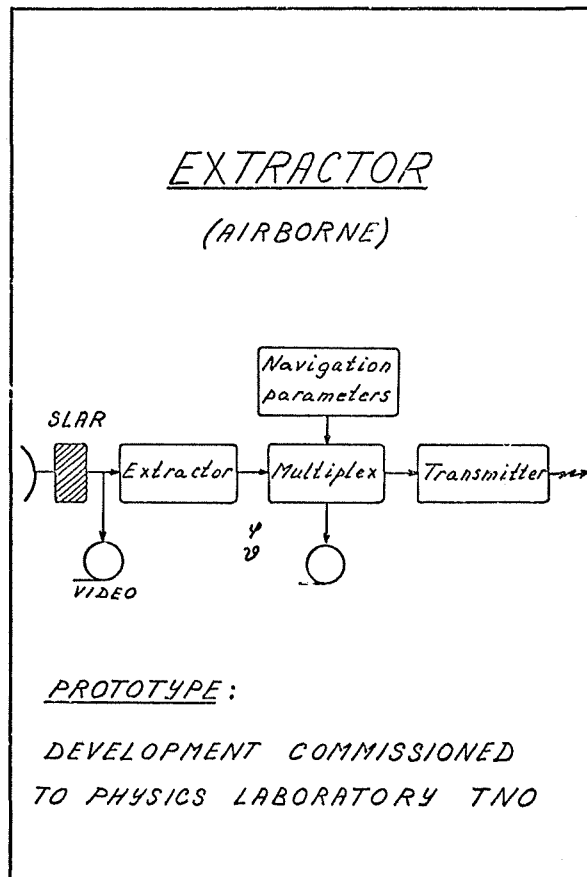


Figure 7

are accepted as representing a target and as such extracted from the scanlines and either recorded or transmitted to a ground station (vide figure 7).

- Application software
(vide figure 8)

A - KARIN

KARIN transforms selectively digitized image points to the map coordinate system. The transformation parameters are determined from a set of reference points. The output may take either the form of a coordinate list or of a line drawing.

B - MARE

This system was designed to produce temperature maps from digitized signals of IRLS. Typical is the feature that microstructure may be studied in an interactive way.

C - SILOS

This programme simply transforms selectively digitized features from Side Scan Sonar images into a suitable map system with the help of navigation parameters. A procedure is included to smooth the recorded navigation parameters which may be mixed with a high noise level.

<u>Program</u>	<u>Input</u>	<u>Output</u>
KARIN	Selectively digitized image points (SLAR, IRLS, MSS, ...) + control points	- Transformed coordinates - Line drawing
SILOS	Selectively digitized image points (SLS) + navigation parameters	- Line drawing
MARE	Digitized video signals from IRLS + ground truth	- Temperature map via line printer
FFT	Image density values along selected line on SLAR-image	- Power spectrum
RADEX*	Target range and "strength" + navigation parameters	- Target position (classification?)

Figure 8

ORGANISATIONAL ASPECTS

Figure 9 is showing how the "Remote Sensing Group Waterstaat" is composed of five different departments within the Ministry of Traffic and Public Works, and at the same time it summarizes the whole paper in one picture. The arms of the mill stand for basic dimensions of the remote sensing problem area whereas the sails supply the driving force to the problem solution effort, provided by

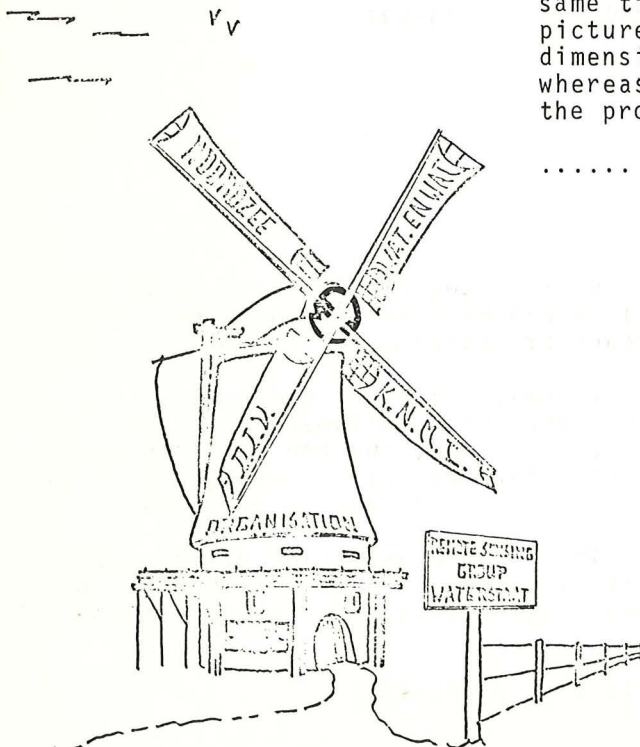


Figure 9

..... M A R S .

REFERENCES

- Bosmann E.R., Clerici E., Eckhart D. and Kubik K.: "KARIN - a program system for the mapping of remote sensing information", XIIth Congress Ottawa 1972
- Blansjaar P.W.H., Eckhart D., Geerders P.J.F., van Kuilenburg J. and Seyhan, M.E.: "A computer controlled comparator densitometer", XIIth Congress Ottawa 1972

FILM FLATNESS IN AERIAL CAMERAS - A MODEL FOR ITS COMPUTER SIMULATION

by K. Tempfli, Enschede, The Netherlands

ABSTRACT

A model for the simulation of the unflatness of aerial film in vacuum pack cameras at the moment of exposure has been developed, on the basis of investigations reported in literature.

The deterministic and stochastical models employed for the three components: unflatness of the vacuum platen, film thickness variations, and lack of contact between the vacuum back and the film, are described. The limitations of the present system and recommendations for further studies conclude this article.

(original paper published in: ITC journal 1973-4, p. 562-582)

DETERMINATION OF STOCHASTIC MODELS FOR OBSERVATION AND POINT TRANSFER ERRORS

by H. G. Jerie, Enschede, The Netherlands

ABSTRACT

This paper describes a comprehensive experimental programme aimed at establishing stochastic models for observation and point transfer errors as functions of their influencing factors.

An outline is first given of the various types of observations which have to be investigated and of their main influencing factors, namely the object quality, the image quality, the quality of the observation system, the quality of the human perception and the base-height ratio.

The concept of observation errors is then analysed, after which a detailed description is given of the required material, preparation, measurements, and data processing for each of the experiments.

(original paper published in: ITC journal 1974-2, p. 73-90)

INSTRUMENTAL ERROR ANALYSIS AND GENERATION

by B. Makarović, Enschede, The Netherlands

ABSTRACT

One of the inputs for the computer simulation of photogrammetric processes is the instrumental distortions. Such distortions can be generated hypothetically from real statistical data, collected by means of experimental tests.

The experimental test data can be analyzed systematically for different characteristic distortions. The results are distribution parameters of the typical distortions, correlations, residual distortions, and the corresponding standard errors. These data represent the input for generating the hypothetical distortions, generation being essentially the reverse process to analysis.

The analysis can be performed more efficiently if the acquisition of the experimental test data is standardized. For practical reasons it is expedient to combine this data acquisition with the standard routine tests for instrument performance.

(original paper published in: ITC journal 1974-2, p. 91-110)

ANALYSIS AND SIMULATION OF DEFORMATION

by K. Tempfli, Enschede, The Netherlands

ABSTRACT

A statistical analysis of réseau photography is suggested as a framework for a possible approach to the digital simulation of film deformation. "Film deformation" refers to the distortion of the image which is measured as compared to the image which is formed in the photographic emulsion at the moment of exposure. The simulation of this change of image geometry is one of the components of an extensive computer simulation system concerning the accuracy of photogrammetric operations to be developed at ITC. Existing réseau photography measurements are proposed as original data for a statistical analysis since they will represent a wide variety of what is happening in photogrammetric practice, if procured from various organizations. To obtain statistically representative data, laboratory experiments do not seem feasible when the large number of factors possibly influencing film deformation such as type of camera, cycle speed, kind of film, processing equipment and method, storage conditions, age of film, type of printer, and the kind of diapositives used are considered. A method is outlined for reducing the original data for the effect of the deviation of the emulsion surface from a plane and for the measuring error.

The analysis is designed in such a way that it will lead to the description of film deformation by a purely inductive procedure. An orthogonal transformation of the error surface forms the core of the trend analysis. For the variation of the trend coefficients throughout a film of consistent history the theory of stationary random functions is applied. The distortion remaining after subtraction of the trend will be defined within the framework of the correlation theory. A statistical comparison of the results obtained from films with different history has to reveal the inter-relations existing between a variation in any of the process parameters and the variation of the properties of film deformation.

(original paper published in: ITC journal 1974-2, p. 111-137)

ERTS COLOR IMAGE MAPS

by Robert B. McEwen, James W. Schoonmaker, Reston, Virginia, USA

ABSTRACT

The U.S. Geological Survey has prepared several experimental color image maps from Earth Resources Technology Satellite (ERTS-1) images. Examples are the gridded image of Upper Chesapeake Bay and the mosaic of New Jersey. Both were printed at a scale of 1:500 000 with a full UTM grid and placed on public sale in February 1974. A color mosaic of Florida is being prepared from 16 separate scenes. It also will be printed at 1:500 000 scale. The publication of satellite image maps has required the development of innovative procedures, combining computational photogrammetry, image geometric control, photomechanical mosaiking, and color lithography. These color image maps are the first to meet cartographic standards and to be lithographed for public sale at a nominal charge. The detailed procedures and equipment are described, along with some of the results.

(published in the Proceedings of 1974 Fall Convention of the ACSM, original paper published in Photogrammetric Engineering XLI, 4. 1975)

GRIDDING OF ERTS IMAGES

by William H. Chapman, Reston, Virginia, USA

ABSTRACT

The technique of converting an ERTS image into a map by fitting a common reference grid to the image has proven to be very useful for obtaining an inexpensive but precise cartographic product. Normally the details of a map are manipulated to fit the projection. Transforming ERTS images to fit a projection causes image quality to diminish to an unsatisfactory level. However, sitting the grid to the image relates image details to the ground coordinate system with no loss of image quality. Gridding an ERTS image requires (1) identifying on the image discrete points whose ground coordinates are known, (2) measuring the x and y values of the points on the image, preferably with a coordinatograph, (3) computing the transformation parameters to relate the image and the ground coordinate systems and computing the grid intersections in the image coordinate system, and (4) plotting the grid on an overlay which is precisely registered to the image.

(published in the Proceedings of 1974 Fall Convention of the ACSM)

SPACE CARTOGRAPHY - CURRENT ACCOMPLISHMENTS AND FUTURE PROSPECTS

by Frederick J. Doyle, U.S. Geological Survey, Reston, Virginia, USA

ABSTRACT

The paper gives a comprehensive review of the US and sovjet lunar space missions and of their cartographic achievements. Similarly the planetary missions for Mars, Jupiter, Venus, and Mercury and the earth orbiting missions are reviewed including the present state of information processing and mapping. Finally the author lists the planned future planetary missions and discusses the prospects for earth orbiting satellites for cartographic and related purposes.

(published in the Proceedings of the International Conference of Cartography, ICA, Madrid, Spain 1947)

